N72-12424

NASA CONTRACTOR REPORT

NASA CR-1830

NASA CR-1830

CASE FILE COPY

BASIC INVESTIGATION OF TURBINE EROSION PHENOMENA

by W. D. Pouchot, R. E. Kothmann, W. K. Fentress, F. J. Heymann, T. C. Varljen, J. W. H. Chi, J. D. Milton, C. M. Glassmire, J. A. Kyslinger, and K. A. Desai

Prepared by
WESTINGHOUSE ELECTRIC CORPORATION
Pittsburgh, Pa. 15236

for

NATIONAL AERONAUTICS AND SPACE ADMINISTRATION • WASHINGTON, D. C. • NOVEMBER 1971

1. Report No.	2. Government Accession No.	3. Recipient's Catalog No.
NASA CR-1830		

4. Title and Subtitle	5. Report Date
BASIC INVESTIGATION OF TURBINE EROSION PHENOMENA	November 1971
	6. Performing Organization Code

7. Author(s) W. D. Pouchot, R. E. Kothmann, W. K. Fentress, F. J. Heymann, T. C. Varljen, J.W.H. Chi, J. D. Milton, C. M. Glassmire, J. A. Kyslinger, and K. A. Desai

9. Performing Organization Name and Address
Westinghouse Electric Corporation
Westinghouse Astronuclear Laboratory
P. O. Box 10864
Pittsburgh, Pennsylvania 15236

8. Performing Organization Report No. WANL-TME-1977

10. Work Unit No.

11. Contract or Grant No. NAS7-390

12. Sponsoring Agency Name and Address
National Aeronautics and Space Administration
Washington, D. C. 20546

13. Type of Report and Period Covered: Contractor Report

14. Sponsoring Agency Code

15. Supplementary Notes

16. Abstract

The objective of the study reported herein is to provide an analytical-empirical model of turbine erosion that fits and explains experience in both steam and metal vapor turbines. Because of the complexities involved in analyzing turbine erosion problems, in a pure scientific sense, it is obvious that this goal can be only partially realized. Therefore, emphasis is placed on providing a useful model for preliminary erosion estimates for given configurations, fluids, and flow conditions.

The first section of this report describes the assembly of the overall erosion model, summarizes the component process models used and describes results of application of the model to several turbines. Section 2 covers detail computational procedures that may be used to follow the fluid-dynamic processes involved in erosion. Section 3 covers in detail experimental evidence and analysis thereof of the actual material removal by liquid impingement.

17. Key Words (Suggested by Author(s))
Turbine Erosion, Turbine Internal Flow, Wet Vapor Formation, Wet Vapor Collection, Drop Formation, Erosion by Drop Impact, Turbine Blade Wakes

18. Distribution Statement
Unclassified - Unclimited

19. Security Classif. (of this report)	20. Security Classif. (of this page)	21. No. of Pages	22. Price*
Unclassified	Unclassified	377	$6.00

*For sale by the National Technical Information Service, Springfield, Virginia 22151

FOREWORD

The work described herein was performed under NASA Contract NAS7-390, "Basic Investigation of Turbine Erosion Phenomena." The work was done under the supervision of Mr. W. D. Pouchot of the Systems and Technology Department at the Astronuclear Laboratory of the Westinghouse Electric Corporation in Pittsburgh, Pa. Mr. L. G. Hays of the Jet Propulsion Laboratory in Pasadena, California is the NASA Program Manager. Mr. S. V. Manson of NASA Headquarters in Washington, D. C. is the NASA Technical Director.

The work reported is the result of a team effort by personnel of the Westinghouse Astronuclear Laboratory, the Westinghouse Research and Development Center, and the Westinghouse Steam Divisions. Contributors are: W. D. Pouchot, R. E. Kothmann, W. K. Fentress, F. J. Heymann, T. C. Varljen, J. W. H. Chi, J. D. Milton, C. M. Glassmire, J. A. Kyslinger and K. A. Desai.

TABLE OF CONTENTS

Section			Page
	SECTION 1. INTRODUCTION & SUMMARY		
1.1	GENERAL		1-1
1.2	EROSION MODELS IN WET VAPOR TURBINES		1-1
	1.2.1	Erosion Locations of Turbine Rotor Blades	1-2
	1.2.2	Processes Involved in Erosion	1-3
	1.2.3	Turbines Used for Example Calculations	1-4
	1.2.4	Process Descriptions	1-6
1.3	RESULTS OF SEVERAL TURBINE EROSION ANALYSES		1-25
	1.3.1	Comparative Erosion Potential of NAS5-250 Cesium Turbine and Potassium Turbine Conceptual Designs	1-25
	1.3.2	Erosion Trends in Central Station Steam Turbines	1-27
	1.3.3	Erosion Potential of Sunflower Mercury Turbine	1-28
1.4	CONCLUSIONS AND RECOMMENDATIONS		1-30
	APPENDICES TO SECTION 1		
	A.	Row-by-Row Design Characteristics of Large Steam Turbines Used as Examples	1-31
	B.	References	1-33
	C.	Results of Detailed Fluid-Dynamic Analysis of Blade Passage Flows of NAS 5-250 Potassium and Cesium Turbines	1-35
	SECTION 2. FLUID-DYNAMIC COMPUTATIONAL PROCEDURES		
2.1	BACKGROUND		2-1
2.2	TURBINE PERFORMANCE WITH DETAILED HISTORY OF CONDENSATION		2-1
	2.2.1	Background	2-1
	2.2.2	Theory	2-1
	2.2.3	Method of Solution	2-10
	2.2.4	Sample Turbine Calculation Results	2-11
	2.2.5	Discussion	2-13
	2.2.6	Nomenclature	2-15
	2.2.7	References	2-16
	APPENDICES TO SECTION 2.2		
	A.	Listing of Computer Program	2-17
	B.	Listing of ICEADAMS Integration Procedure	2-33
	C.	List of Input Data	2-36
	D.	Program Flow Chart	2-37
	E.	Description of Input Control Variables	2-38
2.3	TWO-D AXISYMMETRIC FLOWS BEHIND BLADE ROWS IN WET VAPOR TURBINE		2-39
	2.3.1	Background	2-39
	2.3.2	Intent of Code	2-39
	2.3.3	Nomenclature for Input and Output of Modified Code	2-41
	2.3.4	Method for Calculation of Modified Parameters for Wet Vapor Turbines	2-44

Section			Page
	2.3.5	Possible Future Modifications to Code	2-47
	2.3.6	References	2-47
		APPENDICES TO SECTION 2.3	
	A.	Sample Problems Illustrating Use of Code	2-47
	B.	Listing of Code	2-68
	C.	Control Cards for WANL CDC-6600 Computer	2-141
2.4		BLADE SURFACE VELOCITY CALCULATIONS	2-142
	2.4.1	Background	2-142
	2.4.2	Calculation of G. E. Blade	2-142
	2.4.3	Discussion	2-143
	2.4.4	Conclusions	2-146
	2.4.5	References	2-146
2.5		COLLECTION OF CONDENSATE AND MOVEMENT OF CONDENSATE ON TURBINE SURFACES	2-146
	2.5.1	Nomenclature for Section 2.5	2-146
	2.5.2	Deposition of Moisture on the Surface of Blades	2-148
	2.5.3	Movement of Moisture on Blade Surfaces	2-155
	2.5.4	Collection on Turbine Casing	2-158
	2.5.5	References	2-161
2.6		TRANSPORT OF ATOMIZED DROPS BETWEEN STATORS AND ROTORS	2-162
	2.6.1	Background	2-162
	2.6.2	Analytical Model of Atomized Drop Transport	2-162
	2.6.3	Computer Model of Atomized Drop Transport	2-165
	2.6.4	Description of the ADROP Code Package	2-169
	2.6.5	Solution of an Illustrative Problem	2-179
	2.6.6	Summary	2-182
	2.6.7	Nomenclature	2-185
	2.6.8	References	2-186
		APPENDICES TO SECTION 2.6	
	A.	Calculated and Experimental Atomized Drop Velocities in Last Stage of Large Steam Turbines	2-187
	B.	ADROP Code Source Program Listing	2-189
2.7		ATOMIZATION OF COLLECTED CONDENSATE	2-206
	2.7.1	Background	2-206
	2.7.2	Stator Atomization Model	2-206
	2.7.3	Conclusions	2-215
		APPENDICES TO SECTION 2.7	
	A.	Primary Atomization Expressions	2-216
	B.	Analysis of Contract NAS 7-391 Results	2-221
	C.	References	2-225

Section		Page
	SECTION 3. TURBINE BLADE EROSION MODEL	
3.1	A SURVEY OF CLUES TO THE RELATIONSHIPS BETWEEN EROSION RATE AND IMPINGEMENT CONDITIONS	
	3.1.1 General Considerations Relating to the Interpretation and Correlation of Test Data	3-1
	3.1.2 Dependence on Impingement Angle	3-5
	3.1.3 Dependence on Drop Size and Shape	3-8
	3.1.4 Dependence on Impact Velocity	3-15
	3.1.5 Dependent Parameters Other Than Rate	3-28
	3.1.6 Summary and Conclusions for Section 3.1	3-30
3.2	THE VARIATION OF EROSION RATE WITH EXPOSURE TIME	3-32
	3.2.1 Observed Rate-Time Patterns	3-32
	3.2.2 Effect of Material Removal Mechanisms on Rate-Time Pattern	3-35
	3.2.3 An Analytic Model of the Erosion Rate-Time Relationship	3-37
	3.2.4 Mathematical Formulation of Model	3-43
3.3	HYDRODYNAMICS MODEL OF CORRELATION OF METAL REMOVAL RATES FROM REPETITIVE DROP IMPACT	3-47
	3.3.1 Background	3-47
	3.3.2 Review of Some Observations on Drop Impact Material Removal	3-47
	3.3.3 Possible Reasons for Drop Size Effects	3-50
	3.3.4 Correlation Model	3-53
	3.3.5 Temperature Effect in Drop Impingement Material Removal	3-61
	3.3.6 Summary	3-62
	3.3.7 Nomenclature	3-62
	3.3.8 Derivation of Expression for CEGB Apparatus Water Film Thickness	3-63
3.4	TURBINE BLADE DISSOLUTION IN LIQUID METALS	3-65
	3.4.1 Background	3-65
	3.4.2 Analytical Model	3-67
	3.4.3 Analysis of Last Rotor of a Potassium Turbine Design	3-70
	3.4.4 References	3-72
	SECTION 4. LOW SPEED CASCADE TESTS	
4.1	BACKGROUND	4-1
4.2	SYMBOLS	4-2
4.3	TEST APPARATUS & PROCEDURE	4-3
	4.3.1 Blade Description	4-3
	4.3.2 Test Rig	4-3
	4.3.3 Instrumentation	4-5
	4.3.4 Data Logging and Calculation	4-5
	4.3.5 Checkout Procedure	4-5
	4.3.6 Wake Traverse Tests	4-6

TABLE OF CONTENTS (CONTINUED)

Section		Page
4.4	RESULTS & DISCUSSION	4-6
	4.4.1 Theoretical Models of Flow	4-6
	4.4.2 Test Results	4-8
4.5	SUMMARY OF RESULTS	4-12
4.6	REFERENCES	4-13

LIST OF ILLUSTRATIONS

Figure		Page
1.2-1	Eroded Steam Turbine Blade	1-2
1.2-2	Rotor Blade Material Removal	1-3
1.2-3	WANL Turbine Blade Erosion Model	1-3
1.2-4	Yankee Steam Turbine	1-6
1.2-5	Cross Section of Six-Stage Potassium Turbine	1-6
1.2-6	Cross Section of Two-Stage Cesium Turbine	1-6
1.2-7	Thermodynamic Diagram of Vapor Turbine Expansion	1-7
1.2-8	Moisture Fracture in Divergent Portion of a Steam Nozzle	1-7
1.2-9	Pressure Data for Saturated Potassium Vapor	1-8
1.2-10	Moisture Content (Fraction of Equilibrium) as a Function of Pressure Ratio for Condensing Vapor in Two Sample Potassium Turbines	1-8
1.2-11	Steam Condensate Droplet Growth in Divergent Portion of Nozzle	1-9
1.2-12	Calculated and Experimental Turbine Moisture Collection	1-10
1.2-13	Relation of Moisture Particle Travel to Motion in Plane Normal to Axis of Rotation	1-10
1.2-14	Baker's Map of Two Phase Flow Regimes	1-13
1.2-15	Impingement on Rotating Blade	1-13
1.2-16	Wake Trough Velocity	1-14
1.2-17	Displacement of Drops to Breakup	1-14
1.2-18	Sunflower Turbine - Stage 3. Primary Drop Distance to Disruption	1-15
1.2-19	Bayshore No. 2 - Stage 7. Primary Drop Distances to Disruption	1-15

LIST OF ILLUSTRATIONS (Continued)

Figure		Page
1.2-20	General Solutions for the Terminal Velocity of Drops Traveling along Stator Wake Axis Streamlines	1-16
1.2-21	Sunflower Turbine - Stage 3. Drop Impact Velocities Relative to the Rotor Blade	1-17
1.2-22	Bayshore No. 2 - Stage 7. Drop Impact Velocities Relative to the Rotor Blades	1-17
1.2-23	Comparison of Impact Velocities on Sunflower and Bayshore No. 2 Turbines	1-18
1.2-24	Drop Distribution Functions	1-19
1.2-25	Temperature Dependence of α	1-21
1.2-26	Parametric Study of the Dissolution of Metals in Liquid Potassium	1-22
1.2-27	Stellite Erosion Rates - Data from CEGB; Reduced Normal Velocity ($V_n - V_{cd}$)	1-23
1.2-28	Correlation of CEGB Data by use of "Critical Velocity"	1-24
1.2-29	Threshold Velocity Correlation	1-25
1.3-1	Maximum Erosion Velocities at Last Rotor Blades of Central Station Steam Turbines	1-27
1.3-2	Damaging Moisture Impact Rates on Noses of Last Rotor Blades of Central Station Steam Turbines	1-27
1C-1	Potassium Sixth Stator Wake Pressure Side Velocity	1-39
1C-2	Potassium Turbine Sixth Stator Wake Suction Side Velocity	1-39
1C-3	Cesium Turbine Second Stator Wake Pressure Side Velocity	1-39
1C-4	Cesium Turbine Second Stator Wake Suction Side Velocity	1-39
1C-5	Potassium Turbine Portion Collected on Nose of Sixth Stator Blade	1-40
1C-6	Cesium Turbine Portion Collected on Nose of Second Stator Blade	1-40

LIST OF ILLUSTRATIONS (Continued)

Figure		Page
1C-7	Potassium Turbine Portion Collected on Concave Side Sixth Stator Blade	1-40
1C-8	Cesium Turbine Portion Collected on Concave Side of Second Stator Blade	1-41
1C-9	Maximum Impact Velocities on Six-Stage Potassium Turbine	1-42
2.1-1	WANL Turbine Blade Erosion Model	2-1
2.2D-1	Flow Diagram of the Condensation Code	2-37
2.2D-2	Flow Diagram of the Sonic Flow Section of the Condensation Code	2-37
2.3-1	Axial Station Velocity Nomenclature	2-45
2.3A-1	6th Stator Blade Exit Angles	2-54
2.3A-2	6th Rotor Blade Exit Angles	2-54
2.3A-3	6th Rotor Exit Jet Velocity	2-55
2.3A-4	5th Stator Exit Static Pressure	2-55
2.4.2-1	Third Stage Nozzle Mean Section	2-142
2.4.2-2	Geometric Data for the G.E. Blade	2-143
2.4.2-3	Surface Velocities Computed for the G.E. Blade	2-143
2.5.2-1	Knudsen Number Corrections	2-149
2.5.2-2	Collection Efficiency Ninth Stage Stator Nose Yankee Turbine	2-150
2.5.2-3	Portion Collected Ninth Stage Stator Nose Yankee Turbine	2-150
2.5.2-4	Collection of Moisture on the Concave Side of the Blade	2-150
2.5.2-5	Referred Collection Efficiency on the Concave Side of the Blade	2-152
2.5.2-6	Portion Collected; Concave Side, Ninth Stator Yankee Turbine	2-153

Figure		Page
2.5.2-7	Calculated and Experimental Turbine Moisture Collection	2-155
2.5.4-1	Baker's Map of Two-Phase Flow	2-159
2.5.4-2	Effect of Condensate Film Reynold's Number on Film Thickness	2-160
2.5.4-3	Effect of Vapor Reynold's Number on Film Thickness	2-160
2.6-1	Drag of Spheres and Liquid Drops	2-163
2.6-2	Analytic Solutions for the Bulk Flow Drop Impact Velocity	2-164
2.6-3	General Solutions for the Terminal Velocity of Drops Traveling along Stator Wake Axis Streamlines	2-164
2.6-4	Qualitative Representation of Vapor Wake Development Downstream of a Stator Blade Section	2-166
2.6-5	Drop Impingement Geometry	2-169
2.6A-1	Drop Velocity	2-187
2.6A-2	Secondary Drop Velocity	2-187
2.6A-3	Rotor Blade Impingement Locations	2-188
2.7-1	Drop Distribution Functions	2-213
2.7-2	Distribution of Drop Sizes in a Small Steam Turbine after Spies, Baughman, and Blake	2-213
2.7-3	Manipulation of Experimental Drop Size Distribution	2-214
2.7A-1	Average Drop Size, Primary Atomization	2-219
2.7B-1	Profile of Stator Blade 1-A	2-222
2.7B-2	Surface Velocities Computed for the Top Section of Rocketdyne Blade Shape 1-A	2-222
2.7B-3	Predicted Variation of Maximum Primary Drop Weber Numbers for the Rocketdyne Test Series with Blade Shape 1-A	2-223
2.7B-4	Variation of Drop Weber Number and Velocity with Distance along the Wake Axis Predicted for Rocketdyne Test 114A	2-223

LIST OF ILLUSTRATIONS (Continued)

Figure		Page
2.7B-5	Variation of Drop Weber Number and Velocity with Distance along the Wake Axis Predicted for Rocketdyne Test 114B	2-223
2.7B-6	Variation of Drop Weber Number and Velocity with Distance along the Wake Axis Predicted for Rocketdyne Test 114F	2-224
2.7B-7	Variation of Drop Weber Number and Velocity with Distance along the Wake Axis Predicted for Rocketdyne Test 113L	2-224
3.1-1	Various Interpretations of Same Hypothetical Erosion Data Points	3-2
3.1-2	Definition of Incubation Period, T_o, and "Steady-State" Erosion Rate, R	3-3
3.1-3	Hypothetical Erosion Curves	3-4
3.1-4	Rationalized Erosion Rate versus Normal Impact Velocity	3-5
3.1-5	Corrected Erosion Rate (E cos θ) versus Normal Impact Velocity (From Figure 5 of Reference 11)	3-6
3.1-6	Comparison of Erosion versus Angle Curves	3-7
3.1-7	Erosion versus Velocities	3-8
3.1-8	Arrangement of Nozzles for Water-Jet Tests	3-9
3.1-9	Erosion versus Jet Size (Adapted from Reference 1)	3-9
3.1-10	Erosion Rate versus Jet Diameter	3-10
3.1-11	Effect of Drop Size on Erosion Rate	3-10
3.1-12	Effect of Drop Size on Erosion Rate (Data Cross-Plotted from Figure 3.1-11). Dotted Lines are Based on Correlation of Figure 3.1-13.	3-11
3.1-13	Correlation of Data of Figure 3.1-11 by Use of "Critical Factor" $K_c \equiv (1-10^8/V^2D)$	3-12
3.1-14	Correlation of Data of Figure 3.1-11 by Use of "Critical Velocity" $V_{cd} \equiv \sqrt{10^8/D}$	3-12

LIST OF ILLUSTRATIONS (Continued)

Figure		Page
3.1-15	Critical Velocity versus Jet Diameter	3-13
3.1-16	Erosion-Velocity Relationships Plotted in the Manner of Fatigue Data	3-16
3.1-17	Loci of Constant Shear Stress S in Semi-Infinite Solid with Belt of Uniform Pressure P	3-18
3.1-18	Upper and Lower Loci for Various Values of Pressure/ Shear Stress Ratios	3-18
3.1-19	Area Between Surface and Lower Stress Locus	3-19
3.1-20	Impact Pressure Versus Velocity	3-22
3.1-21	Families of Hypothetical Erosion Versus Velocity Curves, According to Equations (3) through (7)	3-24
3.1-22	Erosion versus Velocity Curves, Computed from Data in Reference 2	3-25
3.1-23	The Data of Figure 3.1 -7b Plotted on Semi-Log Paper	3-25
3.1-24	Data of Hobbs in Reference 36, Plotted both versus V, (Curve "a"), and versus (V-270), (Curve "b")	3-26
3.1-25	Data of Figure 3.1-24a on Semi-Log Paper	3-27
3.1-26	Curves Based on the Data Points of Figures 3-1-13 and 14. Original Data from Reference 12)	3-27
3.1-27	Curves of Figure 3.1-26 on Log-Log Plot	3-27
3.1-28	Rationalized Incubation Periods at Various Drop Diameters and Velocities (Copy of Figure 7 of Reference 12)	3-29
3.1-29	Individual Curves for Different Drop Sizes, Based on Data Points of Figure 3.1-28.	3-29
3.1-30	A Comparison of Impact Failure with Failure by a Standard Fatigue Method for 304 Stainless Steel (Ripken et al, Reference 37)	3-30

Figure		Page
3.2-1	Characteristic Rate-Time Curve According to Thiruvengadam	3-33
3.2-2	Characteristic Rate-Time Curve According to Plesset, Hobbs, and Pearson	3-33
3.2-3	Typical Cumulative Erosion-Time Curves from Cavitation Tests, Adapted from Figure 7 of Reference 36. (Magnetostriction Device, in Distilled Water)	3-34
3.2-4	Cumulative Cavitation Erosion-Time Curves Which Begin at Maximum Rate, Adapted from Figure 24 of Reference 52. (Rotating Disc Device at 150 ft/sec)	3-34
3.2-5	Typical Erosion Rate-Time Curve Obtained in Westinghouse Steam Division Spray Impingement Facility During 1956-1959	3-34
3.2-6	Early Loss Measurements for a Titanium (6% Al, 4% V) Alloy Tested in the Westinghouse Steam Division Facility)	3-35
3.2-7	Typical Computed Erosion Rate-Time Curves from Preliminary Statistical Model, Using Normal Distribution Functions	3-38
3.2-8	Experimental Erosion Rate-Time Curves, Computed from Cumulative Erosion Curves Given in Reference 32	3-38
3.2-9	Computed Rate-Time Curves Based on Log-Normal Distributions, Showing Effect of Varying Dispersion, σ, with Median at Constant, M = 1.0	3-39
3.2-10	Computed Curves Based on Log-Normal Distributions, Showing Effect of Varying Dispersion, σ, with Mean at Constant, E = 1.0	3-40
3.2-11	Effect of Higher Median Value for "Unaffected" Surface (M_u = 3.0) than for Other Surfaces (M = 1.0). (Compare with Figure 3.2-9. Note Difference in Vertical Scale	3-41

Figure		Page
3.2-12	Examples of Computed "Surface Profile" Curves Showing the Uneroded Area as a Function of Level Below the Original Surface, At Various Values of Time: (a) - Corresponding to Figure 3.2-9 (b) - Corresponding to Figure 3.2-11 (c) - Corresponding to Figure 3.2-10	3-41
3.2-13	Computed rms Surface Roughness versus Mean Depth of Penetration (Cumulative Erosion) for Figure 3.2-12. The letters (a) (b) and (c) Correspond to the Similarly-Designated Cases in Figure 3.2-12	3-42
3.3-1	Model of Stages of Erosion After Pearson	3-48
3.3-2	CEGB 12% Chrome Incubation (Stage 1) Data	3-49
3.3-3	Stage 3 Erosion of 12% Chrome Steel (CEGB Data)	3-50
3.3-4	Configuration Diagram	3-55
3.3-5	Calculated Film Thicknesses, CEGB Apparatus	3-56
3.3-6	Threshold Velocity Correlation	3-58
3.3-7	Correlation of CEGB Data by Means of Equation 19	3-60
3.3-8	Referred Erosion Rates	3-61
3.3-9	CEGB Test Piece	3-63
3.4-1	Temperature Dependence of a	3-70
4.3-1	Cascade Test Rig	4-4
4.4-1	Wake Velocity Profiles at Various Downstream Positions	4-9&10
4.4-2	Change in Velocity in Core of Wake with Downstream Distance, 0 Deg. Incidence; 3.4×10^5 Reynolds Number	4-11
4.4-3	Increase in Wake Mixing Loss with Downstream Distance. 0 Deg. Incidence; 3.4×10^5 Reynolds Number	4-11
4.4-4	Increase in Wake Mixing Loss with Trailing Edge Thickness. 0 Deg. Incidence; 3.4×10^5 Reynolds Number	4-12
4.4-5	Increase in Loss Coefficient with Trailing Edge Thickness. 0 Deg. Incidence; 3.4×10^5 Reynolds Number	4-12

LIST OF TABLES

Table		Page
1.2-1	Comparative Data on Turbines Analyzed	1-5
1.2-2	Turbine Casing Flow Regime Parameters Six-Stage Potassium Turbine	1-13
1.3-1	Erosion Threshold Velocities	1-26
1.3-2	Last Rotor Blades Dissolution in a Potassium and a Cesium Turbine	1-26
1A-1	Rowe Yankee Atomic Steam Turbine Low Pressure End	1-31
1A-2	Toledo Edison Bayshore Number 2 Steam Turbine Low Pressure End	1-32
1A-3	Toledo Edison Bayshore Number 3 Steam Turbine Low Pressure End	1-32
1C-1	Condensation Results for Six-Stage Potassium Turbine	1-35
1C-2	Fog Particle Size Distribution for Six-Stage Potassium Turbine	1-35
1C-3	Condensation Results for Cesium Turbine	1-36
1C-4	Fog Particle Distribution at Exit from 1-S Cesium Turbine	1-36
1C-5	Cesium Turbine-Fluid Properties Along Height - Second Stage	1-37
1C-6	Potassium Turbine-Fluid Properties Along the Height of the Blade-Fifth and Sixth Stages	1-37
1C-7	Potassium Turbine-Calculated Boundary Layer Properties at the Trailing-Edge of the Blade	1-38
1C-8	Cesium Turbine-Calculated Boundary Layer Properties	1-38
1C-9	Potassium Turbine-Results of Blade Wake Calculation for Sixth Stator Blade, 3/4 Blade Height Position	1-39
1C-10	Cesium Turbine-Results of Blade Wake Calculation for Second Stator Blade, 3/4 Blade Height Position	1-39
1C-11	Six-Stage Potassium Turbine - Sixth Stage Moisture Inventory	1-41

Table		Page
1C-12	Two-Stage Cesium Turbine - Second Stage Moisture Inventory	1-41
1C-13	Secondary Atomization in Cesium Turbine -Suction Side Wake Streamlined at $Y/Y_o = 0.01$ Second Stator	1-41
1C-14	Secondary Atomization in Potassium Turbine - Suction Side Wake Streamlined $Y/Y_o = 0.01$ Sixth Stator	1-42
1C-15	Second Stage Rotor Drop Impingement Summary - Two Stage Cesium Turbine	1-42
2.2-1	Example Turbine Geometry for Three-Stage Potassium Turbine	2-11
2.2-2	Computer Output Summary Sheet for the Three-Stage Turbine Example	2-12
2.2-3	Nomenclature and Units for Computer Output	2-12
2.2-4	Computer Output Intermediate Summary Sheet for the Second Stator Exit	2-13
2.2-5	Nomenclature and Units for Computer Output	2-14
2.3A-1	Modified Parameters for Potassium Turbine	2-53
2.3A-2	Comparison of Potassium Turbine Data at Mean Diameter	2-54
2.4.2-1	Input	2-142
2.4.2-2	Sample of Item 4 Output	2-144
2.4.2-3	Sample of Item 5 Output	2-145
2.5.3-1	Yankee Turbine, Eighth Rotor Liquid Flow	2-156
2.5.3-2	Yankee Steam Turbine, Ninth Stator Liquid Flow	2-158
2.5.4-1	Moisture Collection on Turbine Housing Six-Stage Potassium Turbine	2-158
2.5.4-2	Moisture Collection on Turbine Housing Two-Stage Cesium Turbine	2-158

Table		Page
2.5.4-3	Estimated Condensate Film Depth on Turbine Housing Six-Stage Potassium Turbine	2-160
2.5.4-4	Estimated Condensate Film Depth on Turbine Housing Two-Stage Cesium Turbine	2-160
2.5.4-5	Mean Droplet Sizes From Sheet Atomization of Condensate on the Potassium and Cesium Turbine Housings	2-161
2.6-1	ADROP Input Namelist Definitions	2-171
2.6-2	Common Block Layout in Program ADROP	2-172
2.6-3	ADROP Input Data Cards for the Sample Program	2-180
2.6-4	ADROP Input Data Summary	2-180
2.6-5	Boundary Layer Input Data Summary	2-181
2.6-6	Detailed Boundary Layer Result Printout	2-181
2.6-7	Trailing Edge Boundary Layer Data Summary	2-183
2.6-8	Printout of Detailed Trajectory Results	2-183
2.6-9	Summary of Trajectory Results	2-183
2.6-10	Secondary Atomization Summary	2-184
2.6-11	Impact Geometry Data Summary	2-184
2.7-1	Relationship of D_3, D_{3-0}, D_m, and n	2-210
2.7-2	Tabulation from Reference 2	2-214
2.7A-1	Spray Liquid Volume Distribution Versus Drop Size	2-220
2.7A-2	Data on Stator Primary Atomization	2-220
2.7B-1	Rocketdyne Test Conditions Used in the Study	2-222
2.7B-2	Trailing Edge Boundary Layer Data Obtained for the Rocketdyne Test Series	2-222
3.1-1	Erosion Rate E for Different Specimen Velocities u and Jet Velocities v	3-7
3.1-2	Drop Size Correlation Attempts for Data of Figure 3.1-11	3-11

LIST OF TABLES (Continued)

Table		Page
3.1-3	Critical Values of V_{cd} and D_c Based on $(V^2D)_c = 10^8$	3-13
3.1-4	Data of Hobbs in Reference 36	3-26
3.3-1	Values of the Interface Angle β for Which Flow First Deforms the Surface	3-51
3.3-2	Critical Pit Diameters for Capillary Water Retention	3-57
3.4-1	Experience on Material Removal by Liquid Potassium	3-66
4.3-1	Test Blade Specifications	4-4
4.3-2	List of Tests	4-7

SECTION 1
INTRODUCTION & SUMMARY

1.1 GENERAL

The objective of the study reported herein is to provide an analytical-empirical model of turbine erosion that fits and explains experience in both steam and metal vapor turbines. Because of the complexities involved in analyzing turbine erosion problems, in a pure scientific sense, it is obvious that this goal can be only partially realized. Therefore, emphasis is placed on providing a useful model for preliminary erosion estimates for given configurations, fluids, and flow conditions. In terms of the prescribed effort level, this goal was given precedence over the more interesting but less immediately fruitful goal of precise and comprehensive mathematical definition of the processes contributing to erosion.

The first section of this report describes the assembly of the overall model of erosion, summarizes the component process models used and describes results of application of the model to several turbines. The model is used to estimate erosion depths or weight losses on the rotor blades of several turbines and the results are compared qualitatively to operating experience where it exists. Section 2 covers detail computational procedures that may be used to follow the fluid-dynamic processes involved in erosion, and compares typical calculated values with experience where it was found. Section 3 covers in detail experimental evidence and analysis thereof of the actual material removal by liquid impingement, and presents theoretical models for transferring this experience to calculations of material removal in turbines. Section 4 presents results of an experimental investigation of turbine stator blade wakes and compares these results with results from use of wake analysis procedures imposed in this report.

The qualitative aspects of the model follow, to a large extent, opinions on the erosion process in wet vapor steam turbines that are widely held within the steam turbine community at the present time. In respect to the quantitative aspects, the study is indebted to excellent previous studies by Gyarmathy and Gardner. It is a refinement and extension of these two previous works (more the former than the latter) based on later experience and substantial additional component process theory and computation.

An effort has been made to make this report adequate by itself to provide calculational understanding of the erosion model and its components. However in the light of the complexities of some of these processes, knowledge of the referenced material may be required for a comprehensive understanding.

1.2 EROSION MODELS IN WET VAPOR TURBINES

The analytical models of processes leading to turbine blade erosion outlined herein are chiefly organized and used to examine material removal from the nose and the leading edge of a rotor blade. When erosion is a problem in a wet vapor turbine of well-ordered flow, operated at or near design condition, the attack on the leading edges of the rotor blades is generally of greatest concern to the turbine designer and the turbine user.

Other locations of erosion are observed and some are mentioned in passing. In addition, many of the processes involved in producing rotor blade leading edge erosion are not specific to that location and process models can be recast to examine other locations of erosion in turbines.

1.2.1 Erosion Locations of Turbine Rotor Blades

In wet vapor turbines most of the material removal by condensate is from the turbine's rotor blades. (See Figure 1.2-1.) In steam or alkali metal vapor turbines, the primary mechanism of condensation is spontaneous nucleation in the bulk vapor flow to form a fog. In the latter turbines, damage is not done directly by the fog particles in the vapor. The fog is composed of submicronic diameter particles and only a small percentage ever impinge upon a surface. The impingement of this small percentage does, however, allow concentrations of liquid to build up on the various turbine surfaces and it is this liquid that can do damage. In mercury turbines, the end result is the same but the collecting mechanism is probably different. Mercury vapor is theoretically very slow to undergo spontaneous nucleation and there is probably no fog formation in most mercury turbines. Damaging liquid does seem to collect readily, however, by direct condensation on the turbine surfaces so that the locations and kinds of damage experienced are similar to those in fog turbines.

Principal locations of material removal from rotor blades are illustrated in Figure 1.2-2. This figure shows forward and aft views of a shrouded turbine blade and points out four types of material removal by liquid that are likely to occur on the rotors of wet vapor turbines.

In turbines, such as steam and mercury, where chemical dissolution of blade material does not occur to any extent, the material removal mechanisms is largely that of mechanical removal by the force of liquid impingement as at locations (1) and (2) or by cavitation induced by the circulating eddies as at (4). In potassium vapor turbines the impingement removal can be compounded by dissolution effects either directly in the impingement areas or by rivulets, as illustrated at location (3). These rivulets can occur at other locations on the rotor blades as well as the trailing edge. They are nearly radial lines because the centrifugal force component on the liquid deposited on the rotors is much higher than the vapor shear force.

Most of the liquid collects initially on the rotor and stator blades as they represent the bulk

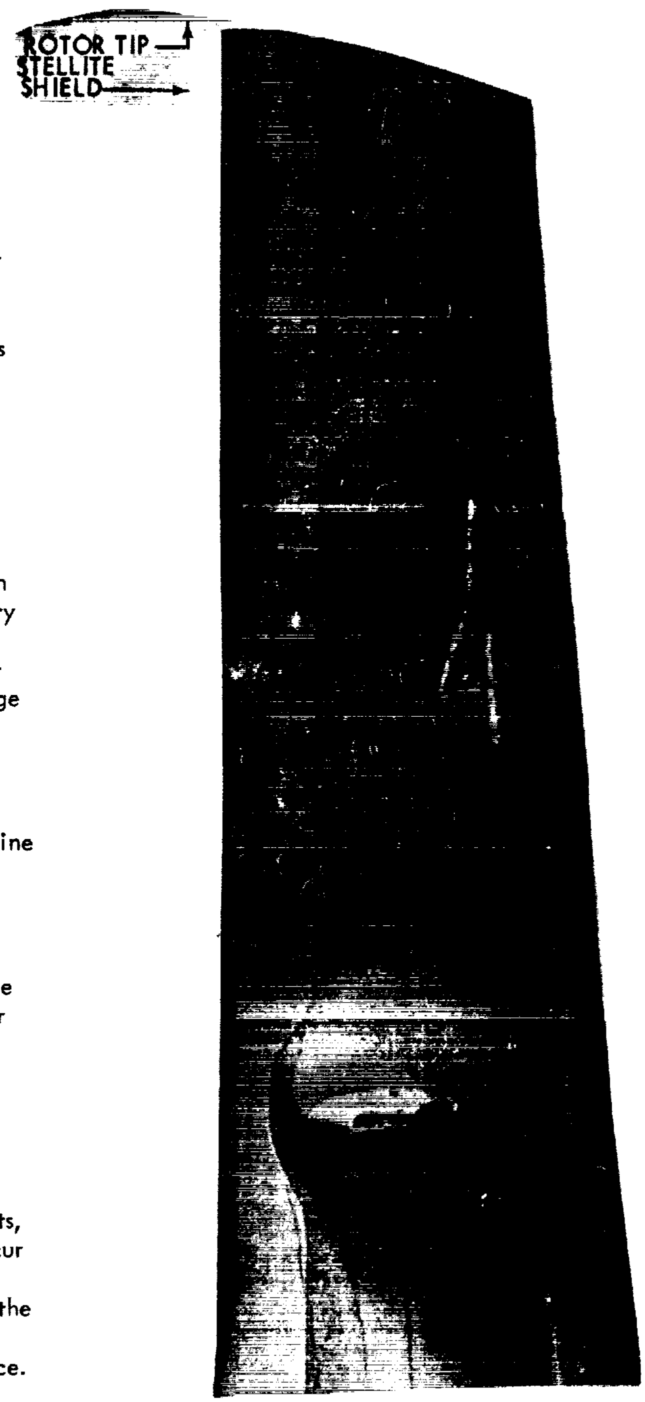

Figure 1.2-1 Eroded Steam Turbine Blade

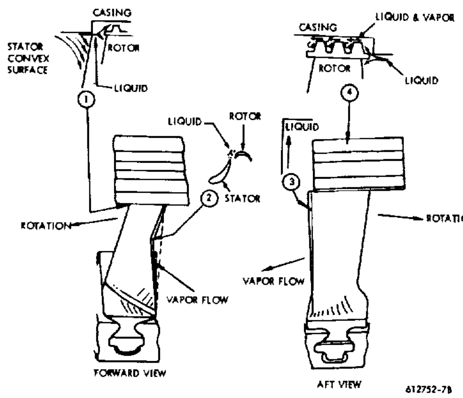

Figure 1.2-2 Rotor Blade Material Removal

of the turbine surface exposed to the main flow. As illustrated, damage can be done by casing and shroud liquid as well as liquid from or on the blades.

Liquid reaches the turbine casing primarily by being slung from the turbine rotors. It reaches the casing, secondarily, under urging of the vapor secondary flow from the pressure (concave) surface over the casing to the suction (convex) surface of the stator vanes. Other mechanisms, of less importance, are impingement and condensation from the bulk flow.

The casing-collected liquid, in addition to causing damage to shrouds and seals as indicated in Figure 1.2-2, tends to flow down over the stators on the convex side, as illustrated at location (1). This casing-collected liquid augments the liquid discharged from the stators that impacts the leading edges of the rotor blades. Since the highest normal impact velocities of collected liquid are with the leading edge of the rotor blades, increases in this liquid supply rate are obviously undesirable.

The classic means of controlling the damage that can be caused by the casing-collected liquid, as used by the steam turbine industry, is to remove this liquid periodically through suitable ports in the casing.

Even if all the casing liquid is removed, liquid which collects on the stator rotor blades of a given stage can cause material removal damage. The stator collected liquid can discharge from the stator blade trailing edges into the path of the rotor blades, causing rotor blade edge damage as at location (2) in Figure 1.2-2. The rotor blade collected liquid can run up the rotor blades, causing dissolution damage as indicated in the figure at location (3). In principle, this stator discharged liquid can be removed, as is done in the steam turbine industry, with casing-collected liquid. However, control of damage from stator discharged liquid without removal is the prevalent practice for steam turbines.

1.2.2 Processes Involved in Erosion

While erosion of rotor blading in turbines is a local phenomenon, numerical calculations of amounts of erosion either on a relative or absolute basis involve a nearly complete fluid-dynamic history of the turbine flow plus an accounting to the actual material removal phenomenon. A flow diagram of the analytical steps used in the erosion model is given in Figure 1.2-3.

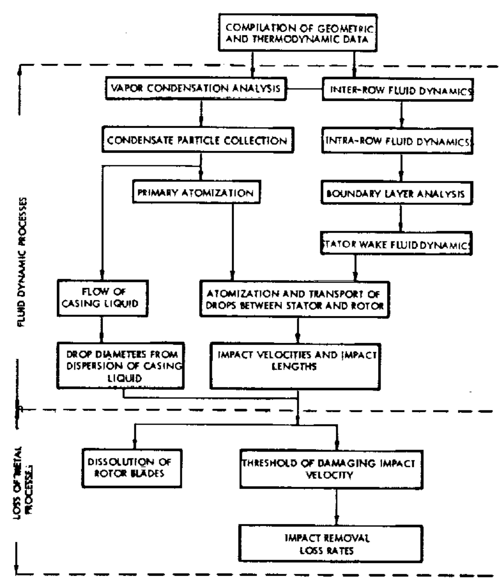

Figure 1.2-3 WANL Turbine Blade Erosion Model

In this section, procedures are discussed in outline, and characteristics calculated or experimental values of the various variables in turbines are given by example. Detail calculational procedures are given in Sections 2 and 3.

Detail methods for analyzing the material removal interaction of liquid with rotor blades is covered in Section 3. Caution in the use of the results from application of Section 3 methods is advised. The suggested procedures are based on reasonable hypotheses and are not established theory or practice.

Detailed methods by which the fluid-dynamic history may be traced are given in Section 2. The methods of fluid-dynamic analysis as given in Section 2 are generally based on widely accepted theoretical schemes. However, the actual implementation of the theories in a numerical sense in the computer codes and other computational procedures set forth in Section 2 assume that a highly efficient axial flow turbine of well-ordered flow in radial equilibrium is being analyzed for erosion. Further, these methods are basically ordered in terms of the flow path as the aerodynamic designer sees it before compromise with the mechanical design.

Most of the computer solutions of Section 2 require the insertion of a physical turbine geometry. The effective fluid-dynamic geometry rather than the real geometry should be used as input to these computer programs if possible. An attempt has been made in the bulk flow programs to adjust to a real geometry and less than ideal flow, but this range of adjustment is quite limited.

The bulk of the analysis carried out during this program was on turbines utilizing either steam or potassium vapors as the working fluids. As a result, the assemblage of analytical models proposed for carrying out an erosion analysis are most applicable to turbines using these readily fog forming low molecular weight working fluids.

The flow regime in high efficiency steam and potassium turbines is generally subsonic. Some analysis was carried out on the Sunflower mercury turbine and a cesium turbine conceptual design. Both these turbines have supersonic stator exit flow but the flow relative to the rotors is subsonic. The bulk flow analysis programs in Section 2 provide for calculations with supersonic stator flow but not for supersonic flow relative to the rotors. The local flow analysis procedures for boundary layers, wakes, and atomization are based on subsonic information and theory without correction for Mach number effects.

The computer programs cannot be treated as "black boxes" nor should the non-computerized procedures be treated as "cookbook" recipes. The erosion analyst will have to use a considerable amount of individual discretion with all the recommended procedures for good results.

1.2.3 Turbines Used for Example Calculations

A great many different turbines were analyzed with respect to erosion or erosion related processes during the course of this program. Calculations concerning these various turbines are scattered throughout the remainder of this section and Sections 2 and 3 as examples. Some overall characteristics and operating conditions of these turbines as used here are tabulated below. Further details on the various turbine designs created under government contract may be found in the references cited as a part of the brief descriptions given herein. Further details about the three large central station steam turbines sometimes used as examples may be found in Appendix A to this section.

TABLE 1.2-1

COMPARATIVE DATA ON TURBINES ANALYZED

	(Rowe Yankee Atomic) Steam Turbine Low Pressure End (Fig. 1.2-4 and Appendix A)	(Toledo Edison Bayshore No. 2) Steam Turbine Low Pressure End (Appendix A)	(Toledo Edison Bayshore No. 3) Steam Turbine Low Pressure End (Appendix A)	NASA Contract NAS 5-1143) Two Stage Potassium Test Turbine (1)	NASA Contract NAS 3-8520 Three-Stage Potassium Test Turbine (2)	NASA Contract NAS 5-250) Six-Stage Potassium Turbine Conceptual Design (Fig. 1.2-5)	NASA Contract NAS 5-250) Cesium Turbine Conceptual Design (Figure 1.2-6) (3)	(Sunflower) Mercury Turbine (4 and 5)	NASA Contract NAS 7-391) Small Steam Test Turbine (6)	NASA Contract NAS 3-10934 KTA Turbine Design* (7)
INLET PRESSURE (Psia)	59.2	48.56	60.097	38.2	30.82	178.6	411.0	240	Variable -10 psia 23	173.0
EXIT PRESSURE (Psia)	0.88	0.491	0.491	11.9	3.92	16.9	35.2	7	Variable -3 psia 10	5.44
INLET SUPERHEAT °F		301	327					~200		71
INLET MOISTURE (Percent)	<1			<1	<1	0	0		Variable 0.4-1.4	
EXIT MOISTURE (Percent)	15.2	7.71	8.36	8.5	14	15.4	16.7	3	Variable Unknown	11.3
NUMBER OF STAGES	9	7	6	2	3	6	2	3	2	10
FLOW RATE (Lb/sec.)	252	80.04	98.4	2.64	1.956	5.76	19.3	0.23	Variable 0.119 0.270	1.908
RPM	1800	3600	3600	19,200	18,250	24,000	24,000	40,000		19,208
TIP DIAMETER OF LAST ROTOR (Inches)	157.5	100.34	114.00	9.65	10.83	9.10	7.73	2.042		7.67
LAST ROTOR BLADE HEIGHT (Inches)	40.0	25.17	28.47	0.937	1.58	2.25	1.99	0.242		1.57

* Analysis carried out under subcontract to Contract NAS-3-10934

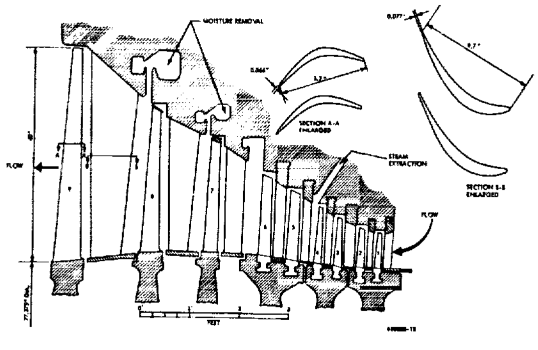

Figure 1.2-4 Yankee Steam Turbine

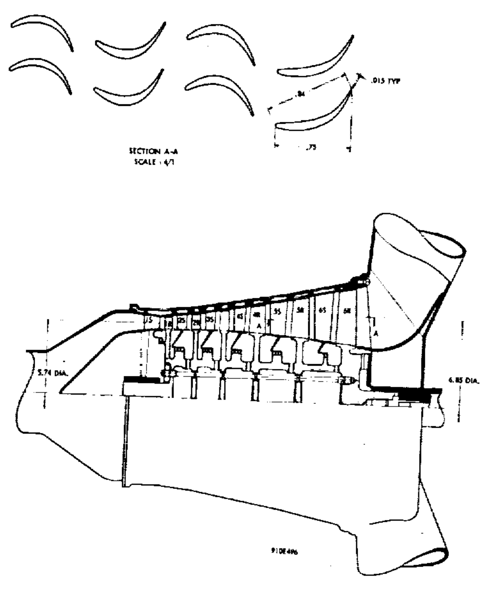

Figure 1.2-5 Cross Section of Six-Stage Potassium Turbine

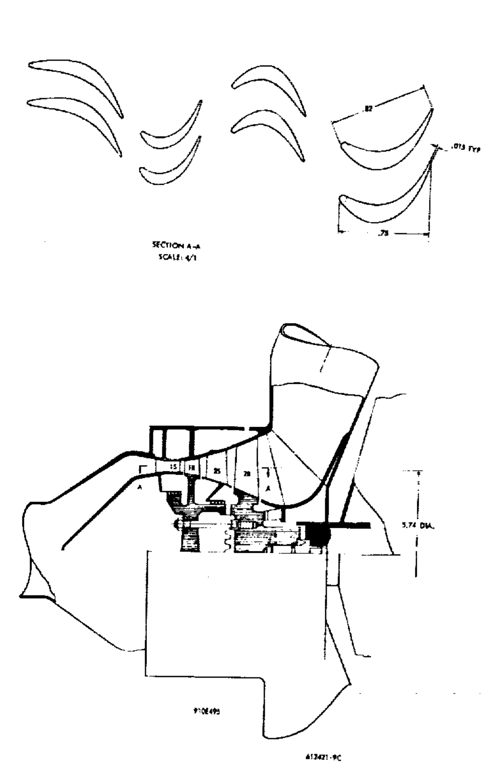

Figure 1.2-6 Cross Section of Two-Stage Cesium Turbine

1.2.4 Process Descriptions

1.2.4.1 Condensation

Nomenclature

P	Pressure
r	Fog particle radius
T	Temperature
Y	Moisture content of flow

Subscripts

Crit	Critical size for thermodynamic stability
IN	Nozzle inlet
L1, L2	Fog particle group

sat Thermodynamic equilibrium (ideal) saturated vapor condition

rev Reversion from supersaturated to near equilibrium vapor

1 Turbine inlet or local nozzle condition

0 Initial condition

E Equilibrium

t Total

w Wilson point

If a vapor such as steam or an alkali metal expands in a nozzle or turbine until the temperature of the vapor is reduced to that of equilibrium saturation, the vapor does not condense in any appreciable quantity immediately. Rather the vapor must be further cooled to produce sufficient supersaturation to cause rapid condensation. The thermodynamic condition at initiation of rapid spontaneous condensation* is called the Wilson point or line. At the Wilson line condensation takes place rapidly, and the moisture content quickly approaches equilibrium. Thereafter the expansion process follows with but slight lag an equilibrium expansion. This is illustrated thermodynamically in Figure 1.2-7. It is illustrated schematically in Figure 1.2-8. This latter figure is a calculated condensation path for the expansion of steam in the downstream section of a converging-diverging nozzle. This characteristic behavior of steam vapor upon rapid expansion is well established experimentally and theoretically [12].

That the same thing happens in potassium vapor expansions is illustrated by Figure 1.2-9, a plot taken from Goldman and Nosek[9]. In this plot the expansions in a converging-diverging nozzle initially follow along a line of chemical equilibrium expansion (n = 1.4). In the diverging section of the nozzle (after considerable expansion), the expansion crosses over to a nearly full chemical and thermodynamic equil-

* Calculations by Gyarmathy [8] show that compared to spontaneous condensation the other processes of condensation are of negligible importance in a wet vapor steam turbine. This is assumed to be true for alkali liquid metal vapor turbines on the basis that the casings can be thermally insulated if necessary.

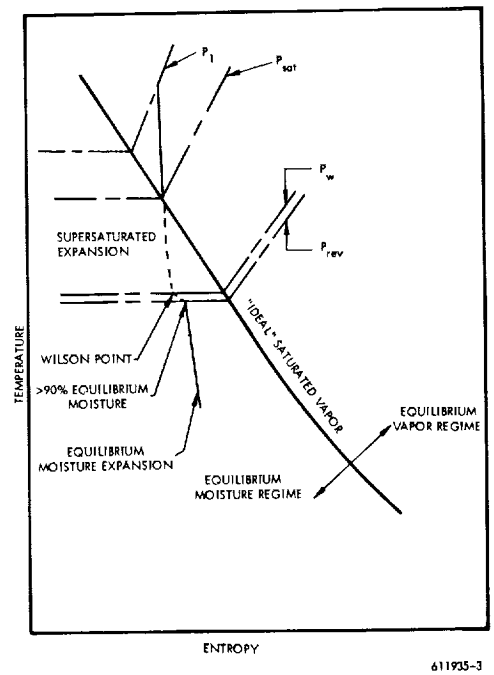

Figure 1.2-7 Thermodynamic Diagram of Vapor Turbine Expansion

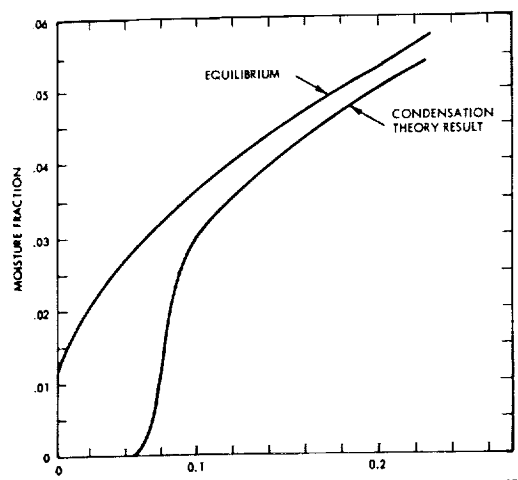

Figure 1.2-8 Moisture Fracture in Divergent Portion of a Steam Nozzle

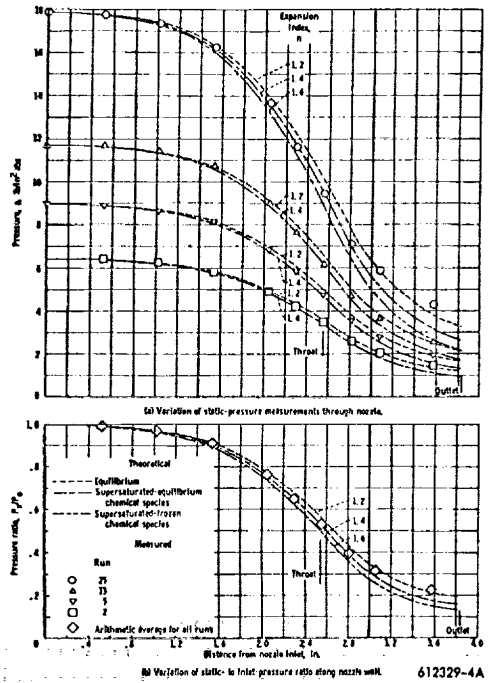

Figure 1.2-9 Pressure Data for Saturated Potassium Vapor

ibrium expansion (n=1.2). A potassium experiment similar to that of Goldman and Nosek is reported by Rossbach (10). Gyarmathy (11) has analyzed Rossbach's data and finds a degree of supersaturation in potassium similar to that evidenced by the Goldman and Nosek data.

Nucleation theory due to Katz, Saltzburg, and Reiss (13) coupled with vapor properties (after Ewing, et al) (14) and the energy, continuity, and momentum relations have been programmed for computer (See Section 2) in a form that can follow the expansion and nucleation process in detail as it proceeds through a turbine. Results of such calculations, for a three-stage potassium turbine and a six-stage potassium turbine, are shown in Figure 1.2-10 in the region of transition from supersaturated to thermodynamic equilibrium expansion. Also shown are points taken from the Goldman and Nosek results intersected, the expansion line, n=1.2, corresponds to 95 percent of full thermodynamic equilibrium.

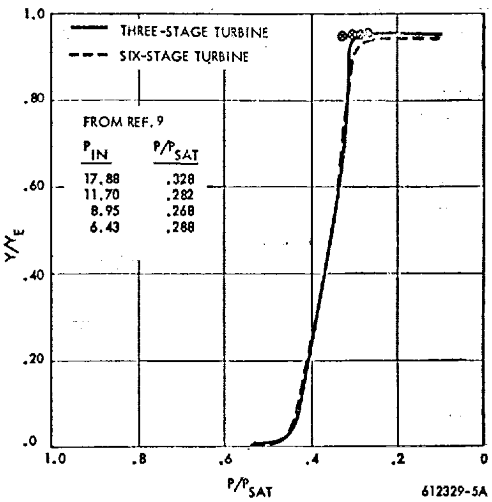

Figure 1.2-10 Moisture Content (Fracture of Equilibrium) as a Function of Pressure Ratio for Condensing Vapor in Two Sample Potassium Turbines

In examining Figure 1.2-10 it will be noted that there is little if any difference in the condensation expansion characteristics between the two turbines, even though the rate of expansion was much higher in the three-stage turbine than in the six. It will also be noted that the calculated pressure ratio for 95 percent of full thermodynamic equilibrium is in good agreement with the Goldman and Nosek results. Also, there is not much spread with pressure ratio for 95 percent of full equilibrium among the experimental results, even though the inlet pressures in the tests varied between approximately 18 psia and 6 psia. Examination of the original Goldman and Nosek publication also shows no consistent variation in condensation pressure ratio with inlet pressure conditions.

The original spontaneous nucleation creates sufficient surface area to allow further condensation to occur with minimal supersaturation. As originally formed, the condensation nuclei are extremely small (0.01 micron diameter) and are of relatively uniform size because of the short time period involved. The nuclei grow quite rapidly to about 0.2 micron diameter as the supersaturation potential created by the expansion in advance of spontaneous condensation is exhausted. Thereafter, a slower growth takes place as the droplets progress through the turbine. This sequence of events is shown in Figure 1.2-11 by a calculated history of the formation of condensation particles during the expansion of steam in a convergent-divergent nozzle.

The final condensate particle sizes exhausting from turbines examined during this program are on the order of 0.5 micron diameter. The calculated supersaturation in equivalent moisture to initiate spontaneous condensation in turbines is around 2.5 percent in steam, 7.5 percent in potassium, and 4.5 percent in cesium. No spontaneous condensation occurred during expansion calculations on the Sunflower mercury turbine.

1.2.4.2 Collection of Condensate Particles

Because of their small size*, the condensate particles are essentially locked to the vapor flow and most of them remain with the steam of their birth until turbine exit.** However, a small percentage of the condensate fog collects on surfaces because of the curvature of the flow passages and rotation of the moving blades. By calculation, the percentage collected per turbine row even in the wettest rows is on the order of 5 percent or less of the total fog present; generally, it is less.*** The collected moisture causes the erosion. The fog particles cause no erosion since they follow the vapor flow as it slices cleanly over the blading surfaces.

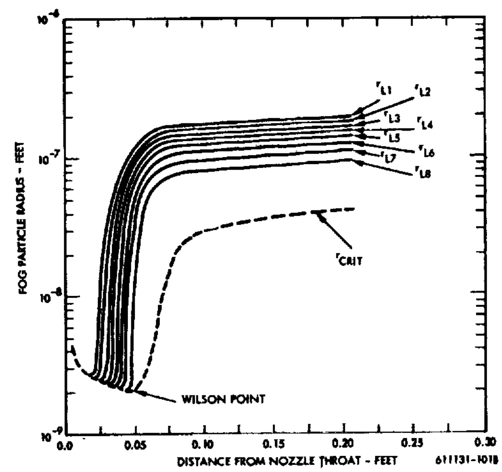

Figure 1.2-11 Steam Condensate Droplet Growth in Divergent Portion of Nozzle

It is hypothesized that the major mechanism in collection of these particles is by inertial impaction on the nose and concave surfaces of the turbine blades. Solutions for the equations governing measured collection by turbine blades by inertial impaction are given in Section 2.

The basis for using the inertial impaction hypothesis is that calculated collection using this assumption agrees reasonably well with measured collection in a steam turbine as reported by Smith[16]. Smith's tests were run on a four-stage machine with the water extraction between the third and fourth stages. The theoretical amount of moisture present at the exit of the third stage was varied by changing the amount of superheat in the vapor at the turbine inlet. Smith's data are shown as X-s in Figure 1.2-12. This is a plot of theoretical moisture against the portion of the theoretical moisture collected. Superimposed on this figure is a curve representing a theoretical calculation of the portion of moisture that would be collected by the Yankee steam turbine ninth stage stator if the turbine was operated to provide the varying amounts of theoretical moisture. In addition, the conditions and geometry are also adjusted to make the Wilson Point (at some location ahead of the ninth stator) occur at a value of $(1/P)\,dP/dt$ of 1100/sec, where P is the static pressure and dP/dt is the rate of change of this pressure with time at the Wilson Point.

---

* The particles are so tiny that the ratio of their diameters to the mean free molecular path places them in the slip-flow regime in most turbine flow streams.

** Normal secondary flows at hub and tip will modify this picture somewhat. There is also a negligible drift on the particles relative to the vapor in a radial direction due to the turbine centrifugal field.

***This calculation is in qualitative agreement with the observation that moisture removal devices in central-station-type steam turbines rarely remove as much as 25 percent of the total moisture present even though moisture is removed at a number of spots lengthwise along the turbine.

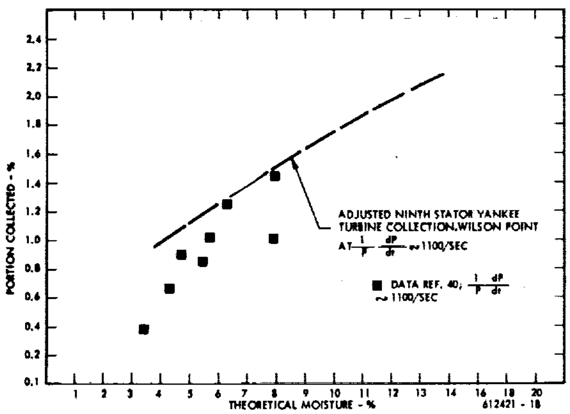

Figure 1.2-12 Calculated and Experimental Turbine Moisture Collection

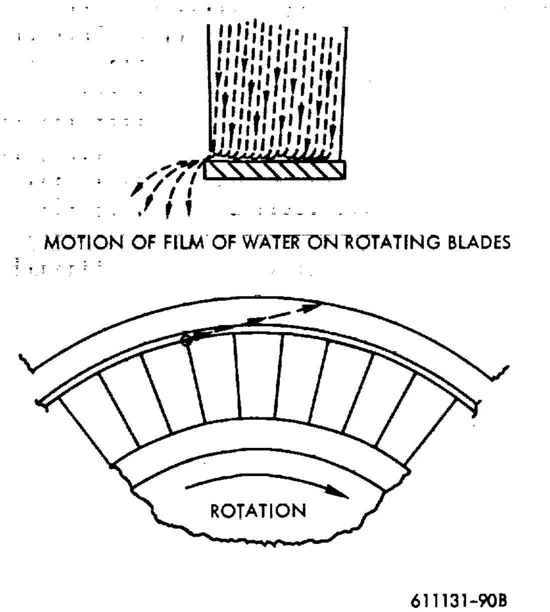

Figure 1.2-13 Relation of Moisture Particle Travel to Motion in Plane Normal to Axis of Rotation

If a line were drawn through Smith's data, it would be steeper than the theoretical line. However, the calculations are for collection on a single turbine row, whereas Smith's data represent collection on a varying number of turbine rows and fractions thereof. That is, the Wilson Point in Smith's turbine is moving toward the front end of the turbine as the amount of theoretical moisture available at the third stage exit rises. Therefore, the collecting surface area subject to the condensing region is increasing. The moisture collected at the drain port between third and fourth stages probably represents that collected on less than one row for 3 percent theoretical moisture, and on up to two or more rows for 8 percent theoretical moisture. This explains why the slope of the data points is substantially greater than the slope of the calculated line. If the drain ports in Smith's experimental turbine are catching nearly all of the moisture collected on the blades, and as the blade sections, spacing, and amount of turning of the experimental turbine rows are quite similar to that of the ninth stator of the Yankee turbine, then the theories of condensate spontaneous nucleation and deposition (taken together) somewhat over-estimate the actual amounts of moisture being collected in steam turbines. *

The calculated portion of the condensate particles caught by a given blade row in a small turbine is substantially greater than in a large turbine. For example, the last stator row of the NAS 3-8520 Three-Stage Potassium Test Turbine is estimated to collect 7 percent of the condensate particles in vapor of an 88.6 percent average quality; whereas by Figure 1.2-12, the Yankee Steam Turbine would collect only 2.3 percent in vapor of the same quality. The higher flow accelerations in the smaller turbine relative to the larger are the principal reasons for the difference.

1.2.4.3 Movement of Collected Moisture

The small percentage of fog particles collected form rivulets, films, and drops on the blading surfaces.

---

* The conclusion is still justified even though the basic comparison is between "apples" and "oranges" because the calculated single row moisture collection is greater than the measured multiple row moisture collection.

On the rotating blading, the predominant force over most of the blading surface is that of the centrifugal field of the blades. Under this force, the liquid collected on the rotors flows nearly radially outwards* and is thrown from the tips of the blades. The particle flow leaving the blade tips is essentially in the tangential direction, and the initial flow velocity is approximately the same as the peripheral speed of the blade. The tangential distance of travel in large steam turbines is often on the order of 5 inches. In models of cesium and potassium space turbines the tangential distances of travel may be as low as 5/32 inch.

A radial groove or grooves has been found to occur on the pressure surfaces just aft of the nose of the rotor blades in the NASA-G. E. two-and three-stage potassium test turbines after 1000 or 2000 hours operation [21, 22]. This can be taken as evidence of a strong liquid rivulet in this location. In the two-stage test turbine the presence of this

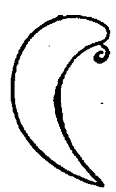

rivulet was ascribed[21] to a local flow separation eddy caused by negative flow incidence entering the rotor blades. During the course of this program, a number of surface velocity and boundary layer analyses of axial flow turbine blading were carried out (by the methods in Sections 2.4 and 2.5). In all cases, even at zero flow incidence, there was sufficient diffusion of the flow at the outer edge of the boundary layer just aft of the blade nose on the pressure surface to cause a local region of flow separation. This region of flow separation is quite local. The liquid atomization and trajectory analysis code (ADROP) developed under this program (Section 2.5) cannot handle a separated flow regime and the computations relating to atomized droplets discharged from the trailing edges of stator vanes must be started downstream of this local pressure surface flow separation to obtain droplet information from the code.

Due to the high peripheral velocity of the turbine rotor blade tips, the liquid flung from the tips is well atomized. An estimate of the characteristics of the spray discharged from the tips of the third rotor of the NAS 3-8520 Three-Stage Potassium Test Turbine has been made assuming that the discharge is similar to that from an underfed disc atomizer. These estimates give:

Maximum Drop Diameter - 76 $\pm$ 33 microns

Mass Mean Drop Diameter - 46 $\pm$ 23 microns

These drops are still large compared to the fog particles. Most of these atomized drops proceed in an almost undisturbed trajectory to impact the turbine casing at a very shallow angle. Even with a 5-inch path length, the time of flight is only about one-half millisecond at 800 ft/sec tip velocity. This time is too short for the vapor drag forces to produce any appreciable deceleration or acceleration of most of the flung liquid. A small percentage of the liquid is undoubtedly in the form of small drops (of sufficiently high surface to mass ratio) that are turned into the succeeding stator by the vapor stream. However, such drops will slice cleanly along the stators and cause no damage. For these reasons erosion at the inlet of stators* is seldom encountered in practice where moisture impinging on the casing is removed through suitable slots. **

* This is not so near the leading edge of a rotary blade as may be seen by examining the markings on the eroded blade of Figure 1.2-1. Results of an analytical study of moisture movement near the leading edges of rotor blades may be found in Gardner [20].

* Erosion at the exit of stators is sometimes observed and assumed to be caused by drops rebounding from the rotor blades.

** In steam turbines it is the practice to have a vapor flow into the slots. This tends to prevent any liquid splashes from returning to the main stream.

It is desirable not to have to incorporate internal moisture removal into alkali metal space turbines. If moisture removal slots are not incorporated, the liquid flung from the tips of the rotors will accumulate and run along the casing toward turbine discharge under the drag of the vapor flow. If unshrouded rotors are used and if the liquid remains on the casing as a film, it might not do much harm to turbine blading.

An analysis of turbine casing flows for the NAS 5-250 potassium and cesium turbine designs was carried out. This analysis is reported in greater depth in Section 2. By this analysis it is found that the casing flows towards the back end of the sixth-stage potassium turbine are unstable. That is, the film of liquid develops waves. These waves will grow to sufficient height to penetrate the vapor laminar sublayer and will be torn off as drops. Some of these drops will be upwards of 400 microns in diameter. Such drops are large enough to cause impact damage to rotor blade tips (and shrouds and seal strips if such are present). Since these drops may be formed anywhere along the casing, some of them will have insufficient time to break up before impacting the rotor blade tips or shrouds.

The stability of this casing liquid has been examined in terms of Baker's (17) two-phase flow map, and the Chien and Ibele (18) criterion for transition from annular to annular-mist flow of the form

$$(Re_V)\ (Re_L)^{0.3} = 1.2\ (10^6)$$

where

Re_V is the vapor Reynolds Number

Re_L is the liquid Reynolds Number

Both Reynolds numbers are based on mass velocity using the full cross-sectional area of the flow passage as constrained by the turbine blade row.

In addition, the technique of Wrobel and McManus (19) was used to estimate the wave height and its ratio to vapor laminar sublayer thickness. The degrees of casing liquid instability predicted by the three methods do not agree very closely. In addition the correlations were obtained using observations on pipe flows and their application to turbine casing flows has not been established.

The turbine casing flow regime parameters for the last two stages of the six-stage potassium turbine may be found in Table 1.2-2. The values given in Table 1.2-1 are outside the range of the Baker Plot shown in Figure 1.2-14 but a mental extrapolation of the plot indicates unstable flow. The Chien and Ibele factors are an order of magnitude greater than required to yield flow instability.

On the basis of the foregoing observations, it appears that casing moisture removal in potassium space turbines will reduce erosion.

On the stator blades, the primary force acting on the collected liquid is the drag force of the mainstream flow. Under this force the liquid flows to the rear of the stator where it collects until torn from the stator as rather large particles. In the model used it is assumed that the collected liquid follows the bulk flow streamlines and on a time average basis is uniformly distributed along a stator from hub to tip. Although the first assumption is of doubtful validity because of the secondary flows at blade hub and tip,* the second assumption is still reasonable, since the liquid displaced from the pressure surface of a particular stator will tend to flow over the casing or rotor hub and terminate on the suction surface of the companion stator.

The liquid, which is torn from or near the back edges of stator vanes, impinges on the following rotor blades. It may remove material by the force of impingement or by chemical dissolution of the rotor blade material or by a combination of these mechanisms. Initially, relatively large drops are

* There is an added force on the liquid stators, tending to move it from tip to hub in the form of the turbine radial pressure gradient. This force is considered to be of negligible importance.

TABLE 1.2-2

TURBINE CASING FLOW REGIME PARAMETERS SIX-STAGE POTASSIUM TURBINE

Exit of Blade Row	$Re_v \times 10^{-5}$	Re_L	$G \times 10^{-4}$ lb/hr-ft^2	L lb/hr-ft^2	$G/\lambda \times 10^{-4}$ lb/hr-ft^2	$L\lambda\psi/G \times 10^4$	$Re_v Re_L^{.301} \times 10^{-7}$
6K-4S	5.04	33.0	3.94	13.0	4.96	2.12	2.62
6K-4R	4.94	168.	3.32	56.1	4.11	11.2	2.56
6K-5S	4.95	321.	2.72	92.3	3.74	19.4	2.56
6K-5R	4.89	491.	2.19	120.	3.33	27.6	2.52
6K-6S	4.87	834.	1.87	181.	3.04	44.6	2.51
6K-6R	4.83	897.	1.54	164.	2.64	46.0	2.48

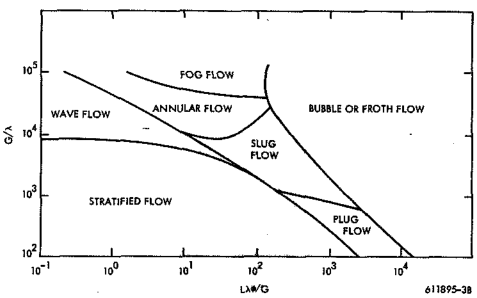

Figure 1.2-14 Baker's Map of Two Phase Flow Regimes

torn from the stators. Most of these drops undergo a breakup process and all undergo acceleration between stator and rotor. However, in the time available the drops do not attain vapor stream velocity, and because of the vector velocity difference can strike the nose and convex surfaces of the rotating blades with rather large normal velocity components. In turbines with high velocities of the liquid drops relative to the rotor blades, some of the larger drops strike with sufficient force to cause mechanical material removal by repetitive impact. This mechanical erosion of the rotor blades is confined to the nose and leading edge of the convex surfaces because of the shadow effect of companion blades. Because the blade speed is highest at the tip and hence the incident drop velocities are highest, the greatest degree of mechanical erosion occurs at the blade tips. (Dispersed casing liquid may also play a part if periodic removal is not performed.)

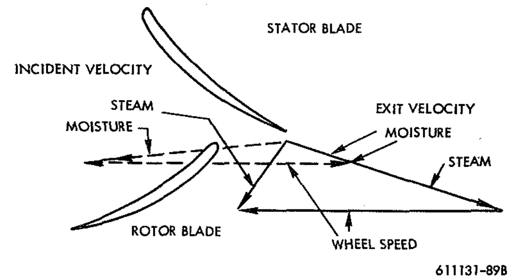

Figure 1.2-15 Impingement on Rotating Blade

As can be inferred from the preceding paragraphs, the mechanical impact intensity and the amount of mechanical erosion depend to a large degree on the extent to which the drops are accelerated and atomized in the space between the stator and rotor. In this respect the vapor density level as reflected in the vapor stream dynamic pressure is a most important parameter. The higher the pressure the more rapid the drop acceleration and the finer the atomization.

Because the vapor density levels in the potassium, cesium, and mercury turbines examined are high compared to those in a low pressure steam turbine of a central-station turbine complex, drop acceleration is much more rapid and atomized drop sizes much finer than in the low pressure steam turbine.

1.2.4.4 Atomization and Trajectories of Stator Discharged Liquid

Visual observations in steam turbines [6,23] reveal that the liquid collected on the stators is torn from the vicinity of the trailing edges of the stator vanes. Initially, this liquid is in the form of a distribution of sizes and fairly large drops. This stage of the process is called primary atomization. These large primary drops are caught up in the decaying wakes down-stream of the stators and accelerated by the vapor stream. Most of the primary drops are unstable under the aerodynamic conditions prevailing during this acceleration. Providing there is sufficient (time of flight) between stator and rotor, these unstable drops are broken down into smaller stable drops. This stage of the process is called secondary atomization. Completion of the secondary atomization process gives a relatively stable population of drops composed of a residual of primary drops that are small enough to be stable plus the secondary drops formed from shattered primary drops. In well designed turbines, it is this stabilized population of drops that impinges upon the rotor blades and can cause erosion damage.

There are at least four different mechanisms of primary atomization and two for secondary atomization that have been observed under conditions related to those in turbines. Primary drops have been observed to be formed by (1) tearing of masses of liquid from puddles of films (2) stripping of liquid in the form of pendant drops (3) tip bursting of pendant drops and (4) the coagulation of liquid on a surface into drops. Secondary drops can be formed either through stripping or bursting of primary drops. To trace the history of all these possible processes would be a formidable, if not impossible, task. Because of this the numerical procedures for atomization estimates given in Section 2.7 involve substantial simplification through gross description of droplet classes based in large part on empirical observations or empirical correlating relations commonly used in describing gas-atomized liquid sprays. Furthermore, almost all of the empirical observations used in preparing the numerical detail of the atomization model are taken from reference material where the reported tests were made using steam vapor or air atomization of water drops. Nonetheless, it is felt that observations on steam or air atomization of water drops, particularly observations in actual turbines or turbine-like cascades, are applicable to a broader spectrum of turbine working fluids (such as the liquid metals) of low liquid-viscosity and substantial surface tension.

As a conservative assumption, it is generally assumed that the bulk of the stator discharged liquid is concentrated in the trough of the stator blade wake and atomization and trajectory calculations are carried out using trough conditions. Although there are experimental observations [24] that a considerable amount of liquid rather quickly finds its way out of the wake into the bulk stream, there is no quantitative information on this point.

The wake velocities are calculated by the semi-empirical method of Lieblein and Roudebush[25].

Some experimental wake investigations were carried out during this program and results are reported in Section 4. If the trailing edges of the stator vanes are kept thin, the experimentally measured wake characteristics agree quite well with calculations using the Lieblein and Roudebush method. Evidence of this is given in Figure 1.2-16. It is also evident from this figure that the procedure will not give results as accurate for thicker trailing edges.

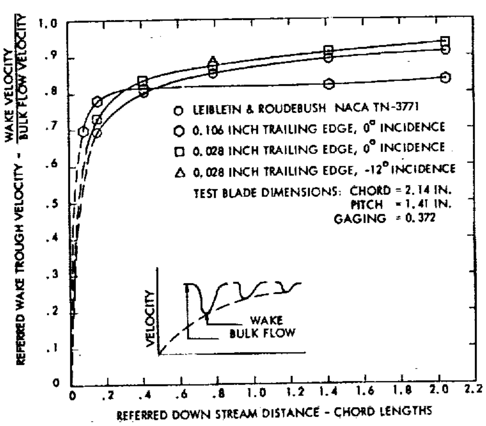

Figure 1.2-16 Wake Trough Velocity

- Distances Required to Complete Secondary Atomization

While the equations of motion concerning breakup and drop displacement cannot be solved rigorously in closed form, a reasonable approximate solution for large drops (that do not accelerate very much before breakup) can be obtained in closed form. The results of such a solution are shown in Figure 1.2-17.

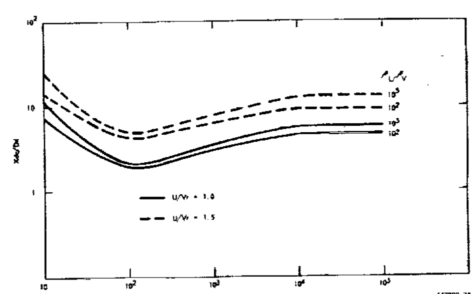

Figure 1.2-17 Displacement of Drops to Breakup

In this figure, the distance of travel before breakup (Xdc) is referred to the drop diameter (Dd) and this referred distance plotted as a function of initial drop Reynolds Number $(Re)_d$ based on the relative flow velocity between drop and vapor stream, drop diameter, and vapor density and viscosity. Parameters shown in this figure are U/Vr and ρ_L/ρ_V

where:

U is the vapor velocity relative to stator blade

Vr relative velocity between drop and vapor

ρ_L density of drop liquid

ρ_V density of vapor

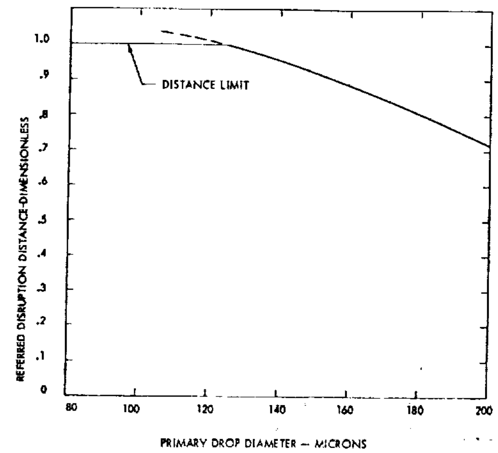

Figure 1.2-18 Sunflower Turbine - Stage 3. Primary Drop Distances to Disruption. Absolute Distances are Referred to the Maximum Possible Path Length

The maximum diameter primary drops discharged from stators (likely to be formed) in turbines may be assumed to have diameters about the dimension of the stator blades trailing edge thicknesses. For small potassium turbines this is about 250 microns. The initial drop Reynolds Numbers for such drops are in the order of 10^2 to 10^5, depending upon their position in the stator blade wakes. For such drops it can be seen that the maximum breakup distance is of the order of 10 diameters. Allowing a factor of two for conservatism, the distance between stator exit and rotor inlet can be as little as 5mm (0.2 in.) along the vapor flow path with the expectation that the primary drops will be broken up before impacting the rotor blades.

The ADROP computer code of Section 2.6, uses numerical means for calculation of the distances required to complete secondary atomization. Typical results are illustrated by calculations for the Sunflower Mercury Turbine (Figure 1.2-18) and for the Toledo Edison Bayshore No. 2 Low Pressure End Steam Turbine (Figure 1.2-19). The referral distances are 2mm for Sunflower and 112 mm for Bayshore No. 2. It will be noted that there is insufficient distance between stator and rotor of the Sunflower turbine to complete secondary atomization.

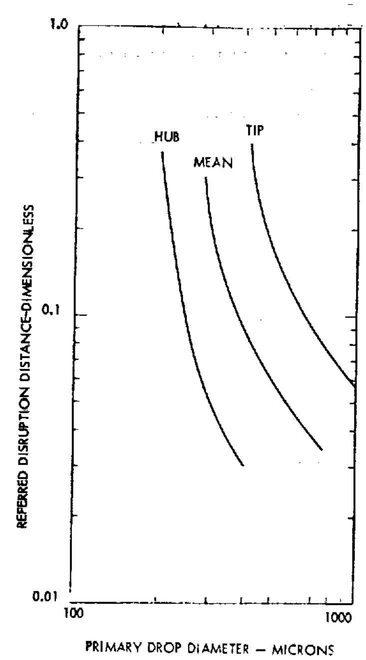

Figure 1.2-19 Bayshore No. 2 - Stage 7. Primary Drop Distances to Disruption. Absolute Distances are Referred to the Maximum Possible Path Length

• Velocities of Stator Discharged Liquid

The history of the acceleration of the liquid discharged from turbine stator vanes is a general case of motion with a variable local velocity field within the stator wake. A closed form solution does not seem possible because of the complexity of the resulting equation of motion. For this and other reasons the ADROP computer code of Section 2.6 was created to solve the complex equation of motion. A correlation of ADROP code solutions for drops traveling along a stator blade wake axis is given in Figure 1.2-20. These solutions are plotted as a function of drop velocity (Vd) to bulk stream velocity ratio in terms of a referred distance (X/C) along the wake axis in blade chords (c), with parameters of initial drop Reynolds Number (Re_o) and K_d an initial value of an inertial parameter. Where:

$$K_d = 3/4 \frac{\rho_v}{\rho_\ell} \frac{C_{do}}{D_d}$$

and

ρ_v vapor density

ρ_ℓ liquid density

C_{do} initial drop drag coefficient

D_d drop diameter — cm

Typical calculated values of V_d/U_o at the rotor inlet plane for four turbines are as follows:

	V_d/U_o
Sunflower, Mercury, 3rd Stator	0.05
Bayshore No. 2, Steam, 7th Stator	0.26
NAS5-250 6-Stage Potassium, 6th Stator	0.22
NAS5-250 2-Stage Cesium, 2nd Stator	0.72

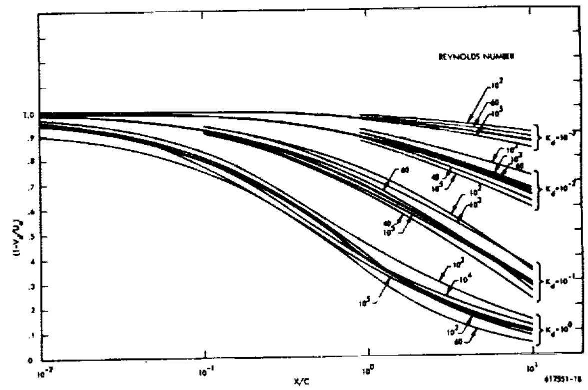

Figure 1.2-20 General Solutions for the Terminal Velocity of Drops Traveling along Stator Wake Axis Streamlines

A comparison of observed stator discharged liquid velocities in the low pressure end of a large English steam turbine and those calculated along the flow path between the 9th stator and rotor of the Yankee low pressure end, under similar conditions of jet velocity and pressure level, is given in Section 2.6, Appendix A. The observed velocities are 10 to 20 percent higher than the calculated velocities.

The velocities with which these stator discharged drops impact the rotor blades depend upon the turbine velocity triangles as illustrated by Figure 1.2-16. In all of the calculations of this program it has been assumed that the turbine is operating at design condition with zero vapor flow incidence into the rotor blades. Figures 1.2-21 and 1.2-22 give calculated values of impact velocity, W_d, with the last rotors of the Sunflower and Bayshore No. 2 turbine, respectively, as a function of drop terminal velocity, V_d. Of even more importance is the normal component, W_n, of the impact velocity for it is well established in impingement erosion experience that it is the normal component of drop impact velocities that is of primary importance. It will be noted that the normal velocities of drop impact of the Sunflower last rotor are, in general, substantially lower than the absolute velocities of impact; this is not so for the Bayshore No. 2 steam turbine. The reason is the Sunflower turbine is a relatively high hub to tip ratio impulse turbine and the inlets to the rotor blades are turned away from the direction of rotation. Bay-

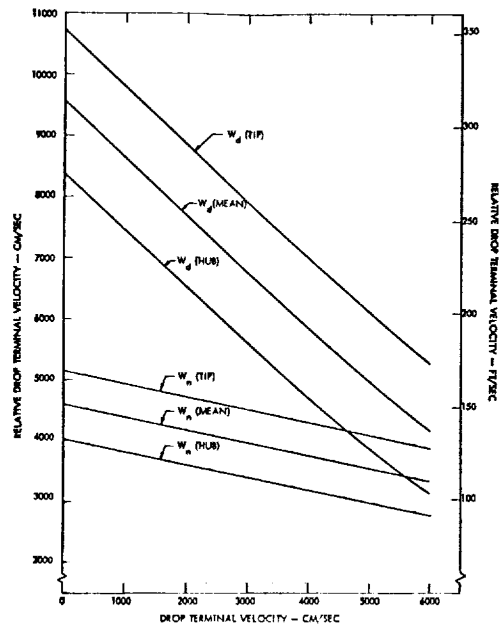

Figure 1.2-21 Sunflower Turbine - Stage 3. Drop Impact Velocities Relative to the Rotor Blade

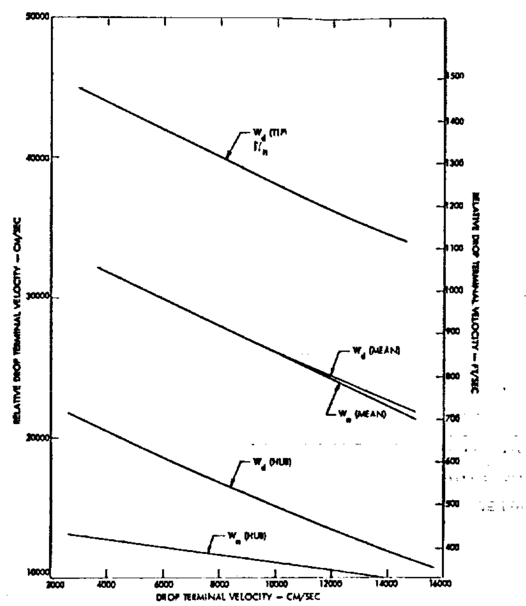

Figure 1.2-22 Bayshore No. 2 - Stage 7. Drop Impact Velocities Relative to the Rotor Blades

shore No. 2, is a relatively low hub to tip ratio turbine with a high degree of reaction at the blade tips. The inlets to the rotor blades, particularly at the tips, are turned in the direction of rotation.

The calculated drop impact normal velocities on the last rotor blades in potassium turbine designs are intermediate between those of the Sunflower and Bayshore No. 2 turbines and are in the range of 500 to 900 ft/sec. The calculated drop impact normal velocities on the last rotor blades of the NAS 5-250 two-stage cesium turbine are in the same range as those of the Sunflower turbine.

- Diameter of Drops Impinging on Turbine Rotor Blades

Two means of assessing the distribution of drop diameters impinging upon the turbine rotor blades have been investigated during this program. Both methods are discussed in Section 2.7. The first of these, of a semi-empirical nature, was used in the erosion analysis of the Yankee steam turbine low pressure end reported in Reference (26). The calculated drop diameter distribution produced is quite different from those reported by Christie [23,24] from actual observations in a large steam turbine. (See Figure 1.2-24.)

The second method is an empirical approach using an average distribution from those reported by Christie [23] applied to a calculated maximum drop

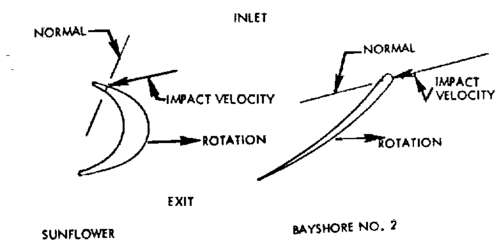

Figure 1.2-23 Comparison of Impact Velocities on Sunflower and Bayshore No. 2 Turbines

diameter of the stator discharged spray. The second method is presently preferred although it also (as discussed in Section 2.7)can yield quite inaccurate results with very small errors in determination of maximum drop diameter.

The maximum drop diameter of the stator spray is determined by use of the parametric time history of the drops in the stator wake covered in Section 2.6. It is assumed that the primary drops become entrained by a given wake streamline and the liquid represented remains with that streamline until rotor impact. The criteria for disruption of a primary drop is taken as the exceeding of a critical drop Weber Number at some point along the path between detachment from the stator to impact with the rotor. This assumes that there is time for the drop to disrupt, after the critical Weber Number has been exceeded, before it impacts the turbine rotor. All primary drops which experience a Weber Number greater than the critical are presumed to disrupt to smaller stable secondary drops.

Primary drops that experience local Weber Numbers in the wake less than the critical Weber Number are assumed stable and retain their primary configuration. The maximum size drop that will impact the rotor is the primary drop that just experiences, but does not exceed, the critical Weber Number anywhere between origin and impact with the rotor. This model uses Weber Number criteria because under local conditions at the time of break-up of the primary drops it is believed that the ratio of dynamic pressure force to surface tension force is the single most important criterion as to whether a drop is stable or not. Unfortunately, Weber Number alone is not sufficient to allow a prediction of maximum drop diameters in sprays even when the local conditions at disruption are known with reasonable accuracy. For this reason, Westinghouse has varied the numerical value of the Weber Number that has been used in analysis of turbines from turbine to turbine.

For small turbines, 1-inch chord, 1-2 inch high blades, the critical Weber Number used has been 13. For the large low pressure ends of central station steam turbines, the value used has been Weber Number = 22. The rationale is due to Gardner[20] who apparently drew on the work of Heinze. According to Spies, et al[6], Heinze shows that for a non-viscous fluid (the turbine working fluids are considered "non-viscous") the critical value of Weber Number is 13 for shock exposure of a drop to aerodynamic forces and this critical Weber Number increases to 22 for a steadily falling drop. This latter case is that of graduated application of aerodynamic forces to the drop. From trajectory calculations on both large and small turbines, it appears that the application of aerodynamic forces to the primary drops is quite abrupt or shock-like in the small turbine and quite gradual in the large central station steam turbine low pressure end. The selection of Weber Number = 13 for the small turbines and Weber Number = 22 are commensurate with the trajectory observations.

Since these values were selected, a considerable amount of actual observation in large steam turbines[23] and in a small steam turbine[6] built to simulate a space potassium turbine have become available. These data clearly show that from a conceptual point of view, the simplified two-valued scheme of this model is inadequate. However, in a numerical sense the selection of Weber Number = 13 for the small space turbines examined is a reasonable average value based on an analysis of the results of Spies et al[6] as given in Appendix B, Section 2.7. For a typical design such as the NAS3-GE 3-stage potassium test turbine, the procedure of Weber Number = 13 may err in estimating the maximum

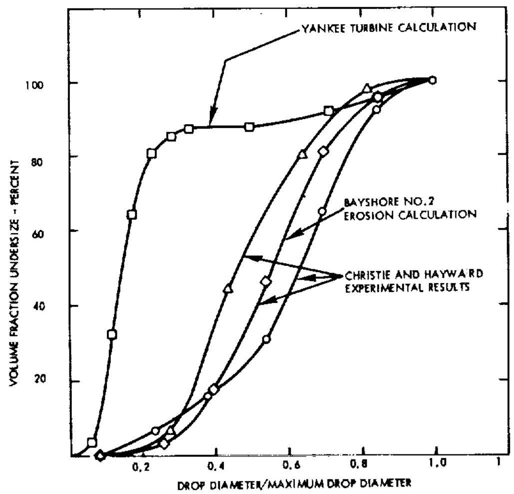

Figure 1.2-24 Drop Distribution Functions

size drop impinging on the rotor blades of that turbine by 30 microns. The maximum size drop is about 100 microns in diameter.

The selection of critical Weber Number = 22 for the low pressure ends of large central station steam turbines seems to be overly conservative in terms of steam stationary cascade tests as reported by Christie and Hayward[23] but not necessarily for actual turbines as reported by the same reference.

1.2.4.5 Material Removal

The liquid that is torn from the back edges of the stator vanes and impinges on the following rotor blades may remove material by the force of impingement or by chemical dissolution of rotor blade material or by a combination of these mechanisms. In the early days of steam turbines, it was postulated that chemical effects might play a part in the observed blade erosion. While the presence of such effects has never conclusively been disproved, it is not deemed important. The observed erosion in steam turbines can be adequately explained as a physical phenomenon without recourse to chemical explanations. It is believed that this is also true of mercury turbines.

The chemical situation in alkali liquid metal turbines is not as clear. Because of the elevated operating temperatures and the nature of the fluids involved in alkali liquid metal turbine systems,all proposed structural materials have a substantial degree of solubility in the working fluid. In pure fluid systems, such as can be maintained with reasonable state-of-the-art technology with alkali metal working fluids, it is thought that dissolution of the blade materials is the main chemical possibility for material removal and that present limited quantitative data can be extrapolated to other similar systems for rough, predictive comparisons.

• Chemical Dissolution

The stator discharged liquid impacts the rotor blades along a relatively narrow portion of the leading edge of the convex surface and is assumed to flow in a nearly radial direction to discharge at the blade tips. It is assumed that impacted moisture forms a continuous film, and the fluid impacts uniformly along the blade impaction zone. The concern of this analysis is the chemical dissolution of the blade material associated with the flow of this film in potassium or cesium vapor turbines.

Because the film of liquid formed on the rotor blades is at most a few micrometers thick and is violently stirred by the incoming drops, it is assumed that the rate controlling step, in the dissolution process, is that of the rate of dissolution for the blade material into the liquid at the liquid-solid interface. This is different than for dissolution of solids into liquids in pipe flow. In pipe flow, the rate controlling step is often the rate of diffusion of the dissolved solute across the solvent boundary layer into the bulk flow of solvent in the pipe.

According to Epstein[27], the rate of dissolution of a pure metal into a pure liquid solvent at the metal-liquid interface is given by

$$S = S_o \left[1 - \exp\left(-\frac{aAt}{V_\ell}\right)\right] \qquad (1)$$

where

- A is the surface area in contact with the liquid - cm^2
- S_o is the saturation solubility of material in the solvent - dimensionless
- S is the solute concentration in the solvent at time t - dimensionless
- V is the volume of liquid in contact with the metal for time t - cm^3
- t is the contact time between liquid and metal along surface A - sec
- α is the solution rate constant - cm/sec

Under steady-state conditions, such as in a turbine operating at design, it can be shown (Section 3.4) that Epstein's equation implies that the rate of blade metal thickness removal is:

$$\dot{\delta}_m = \alpha S_o \left(\frac{\dot{m}_a}{\dot{m}_a + \rho_\ell \alpha} \right) \qquad (2)$$

where the added variables are:

- $\dot{m}_a$, rate of liquid deposition per unit area per unit time - $gm/cm^2/sec$
- $\dot{\delta}_m$, rate of metal thickness removal - cm/sec
- ρ_ℓ, liquid density - gm/cm^3

The discussion so far has assumed a pure metal dissolving into a pure liquid. The latter assumption, pure liquid, is probably reasonable since turbine system operators go to some length to keep a pure liquid in the system. However, turbine blade materials are alloys composed of materials of differing solubility and probably chemical activity. In advanced high temperature Rankine cycle liquid metal systems, the turbine blade materials are likely to be refractory alloys such as TZM and TZC. These are molybdenum alloys with small amounts of titanium, carbon, and zirconium. The alloying materials such as Ti and Zr are more soluble than the base material; while present in concentrations of only 1 to 2 percent they tend to collect at the alloy grain boundaries where they may be more readily leached from the surface than if they were uniformly mixed. In addition, if there is preferential leaching at the grain boundaries, this may so weaken the material that a considerably greater amount of material may be lost than that which simply dissolved.

At the present time, there are insufficient experimental results or theory to judge these factors adequately. Nevertheless, it is worthwhile to delineate these areas of uncertainty by the application of multiplicative correction factors to Equation (2), as:

$$\dot{\delta}_s = k_1 \dot{\delta}_m = k_1 k a \alpha S_o \left(\frac{\dot{m}_a}{\dot{m}_a + \rho_\ell k a \alpha} \right) \qquad (3)$$

where

- a is the activity level of a readily dissolvable constituent of the alloy in the alloyed form relative to the constituents dissolvability in pure form - cm/sec
- k is the ratio of the effective surface area from which the constituent is dissolving to the total surface area of the alloy - dimensionless
- k_1 is the ratio of total alloy removal rate to dissolving constituent removal rate - dimensionless
- $\dot{\delta}_s$ is the thickness removal rate for the alloy surface as a whole - cm/sec

Results of a chemical dissolution examination of the sixth rotor of the NAS5-250 six-stage potassium turbine, and the second rotor of the NAS5-250 two-stage cesium turbine are reported in Section 3.0. Because of the doubtful basis for chemical dissolution examination of the NAS5-250 turbine designs, a parametric examination of chemical dissolution is presented in this section. In both these examinations, it is assumed that:

$$k = 1/k_1 \text{ and } a \sim 1. \tag{4}$$

Hence,

$$\dot{\delta}_s = a\, S_o \frac{\dot{m}_a}{\dot{m}_a + \rho_\ell\, k a} \tag{5}$$

$$\delta_s = a\, S_o\, \Delta t$$

Also, it has been assumed that k (the effective surface area ratio) is equal to the ratio of dissolving constituent volume to total alloy volume.

If it is assumed that $\dot{m}_a \gg \rho_\ell\, a$ and a is time independent, Equation (4) is readily integrated to give:

$$\delta_s = a\, S_o\, \Delta t$$

where

- δ_s is the total thickness of material removed from a metal surface in time of exposure (Δt) - cm
- Δt is the total time of metal surface exposure to the liquid metal - sec

With present knowledge, there are no experimental values of dissolution rate constant (a) available on the dissolving of solid metals under turbine blade conditions into the alkali liquid metals. There are values for Fe dissolving in Na[27] and 304 SS dissolving in Li[28], as illustrated in Figure 1.2-25 for low velocity pipe flow kind of conditions but their applicability to turbine blade dissolution is undemonstrated. However, in the dissolution examinations reported in subsequent Section 3.0, it is assumed that data for 304 SS dissolving in Li is applicable to the turbines examined(this is pure assumption).

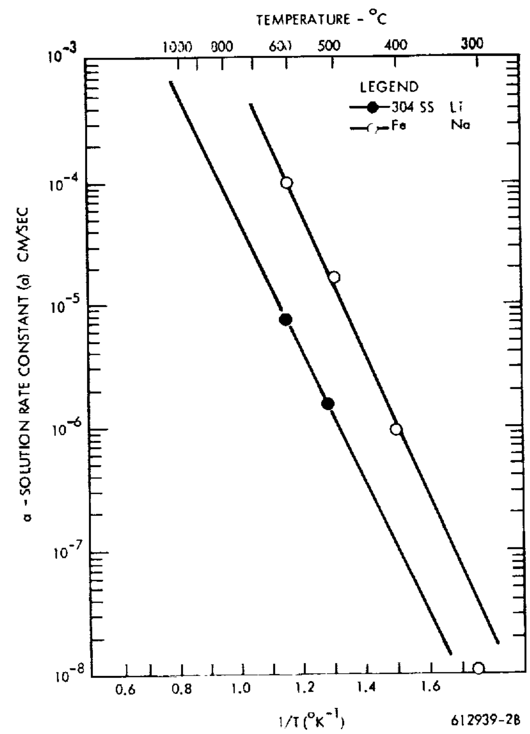

Figure 1.2-25 Temperature Dependence of a

Using the saturation solubilities from Table 1.2-3, Equation 5 has been used to calculate the material thickness dissolved as a function of variation in a for Fe, Ti, Zr, Cb, and Mo dissolving in 1400°F liquid potassium. The time of exposure to liquid potassium is held constant at 10,000 hours. The results of this parametering are given in Figure 1.2-26.

- Mechanical Removal by Liquid Impingement

The CEGB has run experiments and published data[31,32] on the rates of removal of material by repetitive impacts of water drops on several steam turbine blading materials. This information has been analyzed and some simple correlations formed. The first set of correlations does not include the physical properties of the impinging drop fluid or of the impacted metal as variables. It may be used in the examination or prediction of erosion in steam turbines,

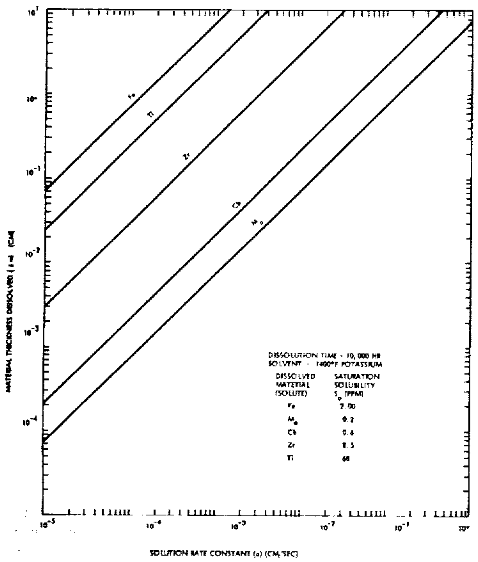

Figure 1.2-26 Parametric Study of the Dissolution of Metals in Liquid Potassium

provided, of course, the blade material or erosion shields are made from one of the materials reported upon by the CEGB. The second set of correlations attempts a broader interpretation of the CEGB steam turbine materials erosion data by factoring into the resulting correlations physical properties of fluid and metal. This is done through the use of a hypothetical mechanical erosion damage model. Neither the damage model or the resulting correlations have been checked experimentally at this time. Calculations relating to mechanical erosion of potassium, cesium, and mercury turbine blades were carried out using this second set of correlations based on the hypothetical damage model. A brief discussion of the resulting correlations follows: The study resulting in the correlations is covered in depth in Sections 3.1 and 3.3 of this report, WANL-TME-1977.

Neglecting fluid and metal properties, erosion rates are still a function of perhaps 11 or 12 independent variables. However, only three of these seem to be of first order importance, with respect to steam turbine erosion. These are (1) velocity of impact, (2) angle of impact, and (3) impacting drop size.

One of the greatest difficulties in interpreting and correlating erosion test data is not the multiplicity of the independent variables, but the identification of the dependent variable(s) for characterizing erosion. All would be well if, under given conditions, erosion proceeded at a constant rate and could be unmistakably characterized by a uniform slope of cumulative weight loss versus time curve. Since erosion rates are not constant with time, erosion can be only approximately characterized by a simplified time independent approach.

The most accepted view is that the first stage in erosion shows little or no weight loss and represents plastic deformation of the surface and initiation of fatigue cracks. This stage is followed by a second stage in which material loss appears and increases rapidly with time. This second stage merges into a third stage in which the rate of weight loss is at a maximum and relatively uniform over a period of time. This, in turn, merges into a later stage (or stages) in which the erosion rate diminishes and can or cannot tend toward another uniform value. Whatever the precise cause of this decrease in erosion rate may be, it is usually associated with rather general and severe damage to the surface, which through geometrical effects alone may result in an effective alteration of the impingement conditions.

It is assumed that the uniform rate of the third stage is the most meaningful in predicting the total erosion in the steam turbine. This assumes that the bulk of the erosion of the blades takes place during this third stage. The time periods of the first and second stages are short compared with the total operating time. Turbine designs which demonstrate severe enough erosion rates in the third stage to become fourth stage terminal cases will suffer from a lack of customer interest and disappear. In any case, from a design point of view, using a third stage rate is a conservative assumption.

CEGB[21] has measured the erosion from samples of Stellite 6 and 6B (an erosion shield material often used in steam turbines) subject to multiple stage of erosion rates for these Stellites and other steam turbine materials in the form:

$$\frac{\Delta W_m}{\Delta W_w} = k\,(V_n - V_{cd})^n \sec\theta \qquad (6)$$

where:

$\frac{\Delta W_m}{\Delta W_w}$ is the mass of material removed per unit mass of impinging water

V_n is the component normal to the impacted surface of velocity of impact

V_{cd} is a critical or threshold velocity below which erosion is negligible

θ is the angle between the impact velocity vector and the normal to the surface

k, n are empirical constants

CEGB data [32] for Stellite 6 and 6B are plotted in Figure 1.2-27. The sec θ correction is ignored because the angles of impact at which the data were taken were always within 30 degrees of the normal to the surface. The correlation of Figure 1.2-28 thus gives the erosion in terms of two out of three of the independent variables of primary importance.

A correlation for the third independent variable, drop size, is also derived from CEGB data. This correlation uses the observation that the threshold velocity of normal impact below which erosion is negligible appears to be a regular function of drop size.

Assume that:

$$V_{cd} \propto \sqrt{\frac{1}{D}}$$

where D is the diameter of the impinging drops. As shown in Figure 1.2-28, the correlations are good.

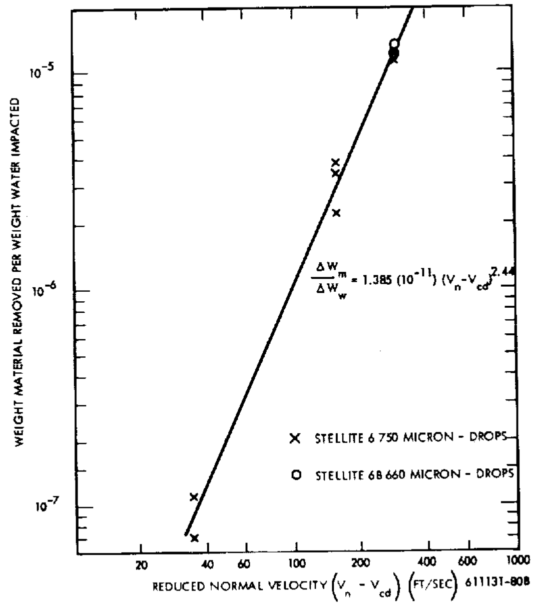

Figure 1.2-27 Stellite Erosion Rates - Data from CEGB; Reduced Normal Velocity $(V_m - V_{cd})$

The data of Figure 1.2-28 were taken using a stainless steel. Since there is insufficient spread to attempt a similar correlation in drop sizes in the data reported for the Stellites, it is assumed that the form for the Stellites would be approximately the same as for stainless steel with a different empirical constant relating the proportionality between V_{cd} and $D^{-1/2}$. This yields the expression:

$$V_{cd} = \sqrt{1155/D}$$

where:

D = drop diameter, ft

V_{cd} = threshold velocity, ft/sec

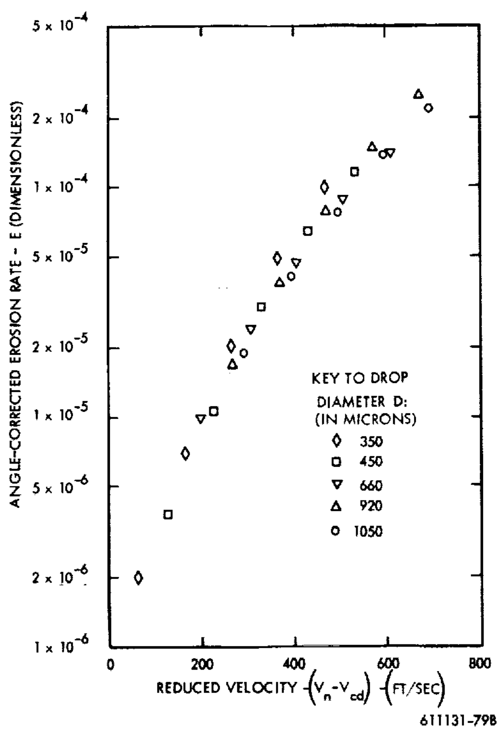

Figure 1.2-28 Correlation of CEGB Data by use of "Critical Velocity"

The foregoing expression used in conjunction with Figure 1.2-27 is then arithmetically sufficient to calculate material removal rates from Stellite 6B in steam turbines, if the states of the impacting fluid are known.

To our knowledge there are no data giving structural material removal rates by repetitive impact of drops of alkali metals or mercury that are quantitatively useful in terms of the impingement of stator-collected liquid on the rotor blades of metal vapor turbines. Therefore, correlating functions of the CEGB steam-water data have been extended to include the physical properties of liquids and a structural material strength by use of a hypothetical impact and damage model.

The basis of the model is hydrodynamic. It assumes that in multiple impact tests of the type reported by the CEGB (and in turbines subject to multiple impact damage) that the impacted material is covered by a thin liquid layer. It presumes that this layer accounts for the changes in threshold velocity that cause erosion (on a given structural material) observed as a function of impacting drop diameter and accounts for the increases in rate of material removal with an increase in velocity above a threshold velocity. The liquid layer may accomplish this through the protective nature of a film overlaying the surface and/or by providing a lubricated surface whereby the liquid outflow from the impact can occur more readily. This latter action will allow an earlier release of the impact pressure on a wet surface than on a dry surface. The model treats the eroded material as a black box characterized by its Vickers Hardness, but does not answer the question as to why, relative to their Vickers Hardness, cobalt and titanium base alloys are generally more erosion resistant than iron or nickel base alloys, and these in turn are more resistant than cemented carbides.[33] The erosion rates used here are the maximum rates of erosion observed in what is normally called the third stage of erosion when erosion is depicted as a four-stage process.

The equations developed are as follows:

$$\frac{m_m}{m_\ell} = \left(\frac{\epsilon}{17}\right)\left(\frac{\rho_m}{\rho_\ell}\right)\left(\frac{\rho_\ell U_n^2}{2S}\right)\left(\frac{U_n}{C_o}\right)^{2}\left(1-\frac{U_{cd}}{U_n}\right)^{n}$$

$$U_{cd} = K\left(\frac{S}{\rho_\ell C_o}\right)\left(\frac{\delta_{cd}}{D}\right)^{n}$$

For the particular CEGB apparatus the correlating film thickness δ is given by:

$$\delta = \sqrt{\frac{3\mu D_s}{4\pi\rho_\ell U_s}}$$

where

C_o is the acoustic velocity in undisturbed drop liquid - ft/sec

D_s is the effective diameter of the erosion sample, assumed equal to blade height for small space turbines examined - ft

D is the impinging drop diameter - ft

m_m is the mass material eroded - slugs

m is the mass of liquid impinged - slugs

U_n is the normal velocity of drop impact - ft/sec

U_w is the blade or erosion sample average peripheral velocity - ft/sec

U_{cd} is the threshold velocity of normal impact to cause erosion - ft/sec

S is the material hardness as measured by the Vicker's Diamond Point method. (Note: Vicker's Hardness, VPN or DPN, is normally given in kg/mm^2. For use in these equations it should be converted to the system of units being used. In the case of Figure 1.2-29, the units are ρ in slugs/ft^3, C_o in ft/sec, δ in ft, d in ft, U_{cd} in ft/sec, and VPN in kg/mm^2.)

δ is the depth of the liquid layer over the eroded material - ft

ϵ is the effectiveness of impingement process - dimensionless

ρ_ℓ is the density of the undisturbed liquid - slugs/ft^3

ρ_m is the density of the eroded material prior to erosion - slugs/ft^3

μ is the viscosity of the undisturbed liquid - lb-sec/ft^2

Based on the CEGB data[32] for iron and nickel base alloys, $\epsilon \sim 0.45$; for cobalt base alloys of the stellite type $\epsilon \sim 0.12$. The threshold velocity correlation for the same materials is given in Figure 1.2-29.

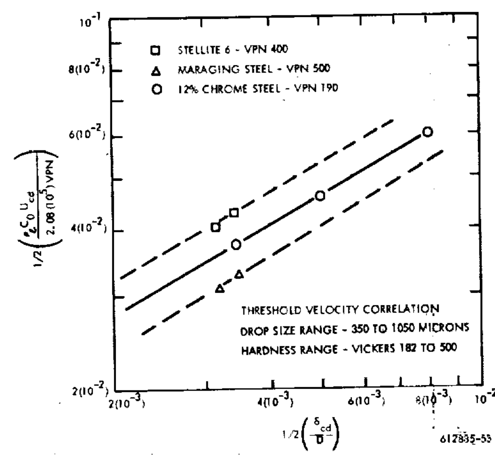

Figure 1.2-29 Threshold Velocity Correlation

1.3 RESULTS OF SEVERAL TURBINE EROSION ANALYSES

1.3.1 Comparative Erosion Potential of NAS5-250 Cesium Turbine and Potassium Turbine Conceptual Designs

The two wet vapor turbine conceptual designs were originally created under contract NAS5-250. These turbines are (1) a two-stage turbine for cesium working fluid and (2) a six-stage turbine for potassium working fluid. Both turbines were designed to produce about 1 MW shaft output at 24,000 rpm when exhausting to a 1420°F temperature condenser. Discussion of the original design criteria and design implementation is in Reference 3. Cross-sectional views of the turbines are shown in Figures 1.2-5 and 1.2-6; and information on design operating conditions is given in Paragraph 1.2.3. The comparative erosion analysis is confined to the last rotors of the two turbines since vapor moisture content is highest at the back end of the turbines.

1.3.1.1 Potential for Mechanical Removal from Last Rotor Blades

The conditions of impact on the last rotors were estimated by the methods outlined in Section 1.2.0. The results of these various fluid-dynamic calculations for the two turbines are given in Appendix 1C.

To use the Section 1.2.4.5 correlation of CEGB material removal data, the thickness of the liquid films on the nose and leading edges of the rotor blades must be estimated. Undoubtedly, these films of liquid are not uniform over the surface of the region of maximum impingement but vary from essentially a residual film thickness up to rivulets. For purposes of these calculations, it is assumed that the film is essentially a residual film. (This is a conservative assumption since the thinner the film, the lower the threshold velocity for mechanical material removel.) This is the basis of the film thickness calculation used in establishing the correlation of the CEGB data. By analogy with the correlation calculation

$$\delta = \sqrt{\frac{3 \mu h}{4 \pi \rho_\ell U_w}}$$

where

h is the blade height from hub to tip-ft

U_w is the blade tip velocity - ft/sec

and

ρ_ℓ and δ are as previously defined.

For the turbines examined the film flow using the thicknesses calculated from the foregoing equation is less than 20 percent of the total flow rate of impacting moisture. Table 1.3-1 gives the threshold velocities and film thicknesses calculated for the potassium turbine sixth rotor blade tips and the cesium turbine second rotor blade tips. It is assumed that the material of the blades has a VPN = 260. This is a characteristic value for TZM, which is often mentioned as a candidate structural material for alkali metal vapor turbine blades. The values are for the drops of maximum diameter calculated to hit these rotors. Also given are the expected maximum impact velocities of these drops with the rotor blades.

TABLE 1.3-1

EROSION THRESHOLD VELOCITIES

	Sixth Rotor Potassium Turbine	Second Rotor Cesium Turbine
Drop Diameter, micron	100.	5.
Film Thickness, micron	2.9	1.95
Threshold Velocity, ft/sec	1400.	>4000.
Maximum Normal Impact Velocity, ft/sec	800.	338.

From Table 1.3-2, it can be seen that for both turbines the calculated threshold velocity to cause mechanical damage is substantially above the estimated maximum normal impact velocities of the largest drops. Therefore, it is concluded that mechanical erosion damage to the rotor blades of these turbines is not likely to be a problem. The margin for error in this statement is considerably greater for the cesium turbine than it is for the potassium turbine.

TABLE 1.3-2

LAST ROTOR BLADES DISSOLUTION IN A POTASSIUM AND A CESIUM TURBINE

	NAS 5-250 Potassium Turbine Sixth Rotor	NAS 5-250 Cesium Turbine Second Rotor
Bulk Fluid Temperature - °K	1060°K	1045°K
Solution Rate Constant (a) - (cm/sec)	$1.1 (10^{-4})$	$0.95 (10^{-4})$
Deposition Rate on Rotor Blade Noses ($\dot{m}a$)-gm/cm²/sec	0.079	0.098
Rotor Blade Material	TZM	TZM
Average Solubility of Ti and Zr, ppm	63.	63.
Volume Fraction Ti & Zr (k)	0.0124	0.0124
Density of Liquid - gm/cm³	0.658	1.415
$k\, a\, \rho_\ell$ -gm/cm²/sec	$9 (10^{-7})$	$1.67 (10^{-6})$
δ_s (based on Ti & Zr) mils/1000 hour	9.6	8.5
Average Solubility of Mo, ppm	0.2	0.2
Volume Fraction Mo (k)	0.987	0.987
$k\, a\, \rho_\ell$ - gm/cm²/sec	$7.1 (10^{-5})$	$1.33 (10^{-4})$
δ_s (based on Mo) mils/1000 hour	0.03	0.027

1.3.1.2 Potential for Rotor Blade Dissolution

The chemical dissolution of material from the last rotor blades of the two NAS5-250 turbines has been calculated using Equation 4 and Figure 1.2-25 of Section 1.2.4.5. This method assumes that the rate of material loss is controlled by the rate at which material can cross the solid-liquid interface and that if selective leaching of the more soluble alloy constituents occurs, erosion surface regression will be at the rate set by selective leaching along grain boundaries. Other assumptions are (1) blade material is TZM, (2) the dissolution rate constant, a, is the same as that of 304SS into lithium as given by Figure 1.2-25 for both cesium and potassium, and (3) the solubility of the alloy constituents is the same in cesium as potassium. Substantiation of these assumptions has not been demonstrated.

The results of these calculations are shown in Table 1.3-2. In this table there are two sets of thickness removal (δ_s) values. The first set assumes that the soluble trace constituents, Ti and Zr, leach preferentially at grain boundaries, and the weakened structure resulting is immediately broken off by the impinging liquid to the depth of trace element removal. The second set assumes that the trace elements are held in place by the principal constituent molybdenum, and that the rate of surface regression is controlled by the rate of dissolution of molybdenum. The 300 fold difference between δ_s values for the two sets is unfortunately indicative of the uncertainty in absolute dissolution rates in potassium or cesium turbines on a calculation basis.

1.3.2 Erosion Trends in Central Station Steam Turbines

The low pressure ends of present day central station steam turbines are designed so that some stator discharged drops impact the rotor blades near the tips at velocities sufficient to cause erosion damage. This is particularly true of the last rotor blades. There is considerable economic incentive to use higher and higher tip speeds in these low pressure ends. For this reason it has been of interest to estimate the probable change of erosion in central station turbines last rotor blades with increase in tip speed.

The results of such an investigation are shown in Figures 1.3-1 and 1.3-2. This is a generalized investigation using a stylized turbine and is not intended as design information. To produce these two curves, estimates of moisture collection, drop diameters, and impact velocities of the drops hitting

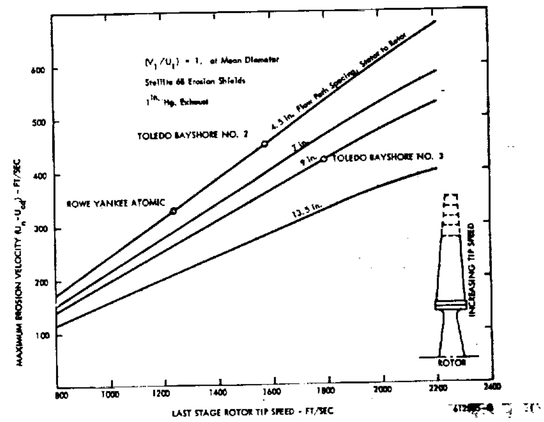

Figure 1.3-1 Maximum Erosion Velocities at Last Rotor Blades of Central Station Steam Turbines

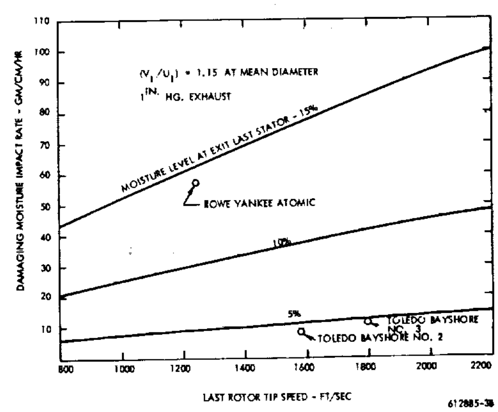

Figure 1.3-2 Damaging Moisture Impact Rates on Noses of Last Rotor Blades of Central Station Steam Turbines

the last rotor blades were made using the methods of Section 1.2. In addition, it has been assumed that the threshold velocity for stage 3 erosion moves in a regular way with drop diameter and film thickness as correlated in Section 1.2.4.5, even though the absolute velocities of drop impingement in the postulated turbines are substantially higher than in the CEGB tests and the impinging drops are on the whole substantially smaller in diameter.

Figure 1.3-1 is a plot of maximum erosion velocity versus last rotor tip speed with parameters of the spacing between stator and rotor along the path of the vapor flow. The turbines are all designed to have a mean diameter ratio of stator spouting velocity to a rotor blade speed of 1.0. The maximum erosion velocity is defined as the maximum normal impact velocity of the maximum diameter drop discharged from the stators minus the calculated stage 3 erosion threshold velocity for the maximum diameter drop.

Figure 1.3-2 is a plot of damaging moisture impact rate per unit of blade length versus last rotor tip speed with parameters of the bulk flow moisture level at the exit of the last stator. The damaging moisture is that fraction of the stator collected and discharged moisture contained in drops of sufficient diameter to have a calculated stage 3 threshold velocity below the normal impact velocity of these drops on the rotor blade at the tip. Also, it is assumed that only that moisture directly collected by the stator row is available for discharge from the stators. All moisture collected by the upstream rows of the turbine has been removed at the moisture removal parts prior to the inlet of the last stator row.

In these two curves are plotted three points representing actual steam turbines in service. While these are actual turbines, the points are still calculations and not measurements. These turbines are not identical to the stylized study turbines but are close enough for discussion purposes. All three turbines experience an acceptable level of last rotor blade erosion damage. The field reports on these turbines are qualitative in nature. It appears that Toledo Bayshore No. 3 has the lowest erosion rates of the three. Probably the Rowe Yankee Atomic Turbine has the highest rates of the three. This is consistent with Figures 1.3-1 and 1.3-2. Toledo BayshoreNo. 2 and No. 3 turbines have substantially lower damaging moisture impact rates than does Rowe Yankee Atomic. This should be more than enough to compensate for the higher maximum erosion velocities calculated for Toledo Bayshore No. 2 and No. 3 versus Rowe Yankee Atomic. A reduction in erosion rate between Toledo Bayshore No. 2 and No. 3 can be accounted for by a decrease in maximum erosion velocity through greater stator to rotor spacing along the flow path direction.

It can be said, on the basis of Figures1.3-1 and 1.3-2, that if very wet vapor turbines for nuclear power plants of the Yankee Atomic type are to operate at last rotor blade tip speeds of the order of 2000 ft/sec that: (1) the flow path spacing between last stator and rotor will have to be increased substantially, or (2) almost all the the moisture directly collected on the last stator blades will have to be removed before it can discharge into the path of the rotor blade tips, or (3) a more erosion resistant material than Stellite 6B will have to be employed, or (4) some way of providing better atomization of stator discharged liquid will have to be found.

1.3.3 Erosion Potential of Sunflower Mercury Turbine

The Sunflower turbine is a small mercury vapor turbine developed by TRW for NASA as a part of the Sunflower space power plant. A brief tabulation of design point parameters for the Sunflower turbine is given in Section 1.2.3.

In the overall study, the Sunflower turbine examination was the most interesting of all. The model of erosion created during the study is largely based on experimental information on the behavior of water and water vapor in apparatus of appropriate size for large central station steam turbines. The Sunflower turbine operating experience afforded an opportunity to check the reasonableness of the model in terms of a very tiny turbine operated on a vapor and liquid with physical properties quite different from those of water.

The most interesting observation made during the Sunflower analysis arose out of the size of the turbine. The nominal stator to rotor axial spacing in this turbine is only 0.6 mm (or 2mm along the path of flight of the stator discharged liquid). In addition the axial spacing tolerance band for these turbines is $\pm$ 0.3 mm, or from turbine to turbine the axial spacing could vary from 0.3 mm to 0.9 mm. From the analysis this is a significant variation. As illustrated in Figure 1.2-18 at the nominal axial spacing of 0.6 mm, there is not, on a calculated basis, sufficient time for all the third stator discharged primary drops that are unstable (those > 90 microns) to breakup before reaching the rotor inlet plane. If the axial spacing is reduced to 0.3 mm (0.5 referred disruption distance) the maximum diameter drop impacting the third rotor will more than double in size.

As shown in Figure 1.2-18, at the nominal 0.6 mm axial spacing all drops with diameters greater than about 120 microns will break up into small drops. An erosion threshold velocity calculation for the Sunflower last (third) rotor blade tips has been carried out using this 120 micron drop diameter. The calculation used the threshold velocity correlation of Figure 1.2-28. The presumed liquid film thickness at the rotor blade tips was calculated in the same manner as the erosion comparison of the NAS5-250 potassium and cesium turbine designs.

The result is given in the following table and is compared to the ADROP code calculated maximum normal impact velocity. The Sunflower rotor blade material is Ph 15-7 M. A handbook value of hardness for this material has been used in the calculation.

SUNFLOWER TURBINE MAXIMUM DIAMETER DROP
EROSION THRESHOLD VELOCITY

Maximum Drop Diameter, microns	120.
Film Thickness, microns	3.9
Threshold Velocity of Normal Impact (to cause erosion,) cm/sec; VPN = 500 (RC = 48)	5320.
Maximum Normal Impact Velocity, cm/sec	4980.

As can be seen the threshold velocity and the maximum normal impact velocity of the largest and slowest (highest rotor impact velocity) drops predicted to impact the Sunflower turbine last stage rotor blades are about the same. This indicates that little erosion was to be expected in the Sunflower turbine if the axial spacing between stator and rotor was equal to or greater than the nominal value of 0.6 mm.

The experimental observations with respect to erosion of the Sunflower turbines indicates a marginal situation in agreement with the model calculations. For example, a photograph [35] of the third (last) rotor blades of Sunflower CSUI-3 indicates average erosion depths on the blades leading edges as great as 1/64 inch and one blade appears to be cut back at the tip by as much as 1/32 inch. This was after only 2,348 hours of operation. On the other hand, visual observation [4] of the third stage rotor blades of Sunflower CSUI-3A after 4,329 hours of operation did not reveal erosion.

TRW[35] ascribed the improvement between CSUI-3 and CSUI-3A to (1) reductions in boiler-carryover and reductions in inlet nozzle plenum condensation and (2) redesign of the third stage nozzle to reduce mismatch. The third stage nozzle exit area of CSUI-3 is reported to have been 25 percent oversize. This oversize nozzle would lead to flow separation. In terms of the erosion model one can view this as an effective increase in the trailing edge thickness of the stator vanes. Because the nominal stator to rotor axial spacing in this turbine is only 0.6 mm, only a few mils increase in the stator effective trailing edge thickness is required to cause a dead space extending to the rotor inlet. Such a dead space will prevent secondary breakup of stator discharged drops. As a result, drops considerably larger than the 120 microns predicted here would impact the rotor blades. In addition the rotor on CSUI-3 might have been as close to the stator as 0.3 mm. Even without flow separation this tight spacing would have largely suppressed the secondary atomization process.

It seems possible that if the axial spacing had been a millimeter longer, the erosion of the CSUI-3 third rotor blades could have been as negligible as it was on CSUI-3A.

1.4 CONCLUSIONS AND RECOMMENDATIONS

An analytical model has been constructed that follows, step-by-step, the history of the condensation, collection, movement, impingement, and material removal by moisture in wet vapor turbines. The equations of the model are sufficiently detailed to allow calculation of numerical values of the erosion of turbine rotor blades.

The model has been used to examine the erosion in steam, mercury, and potassium turbines on which there is operating experience. With respect to steam and mercury turbines, where the primary mechanism of material removal is mechanical, the estimated erosion can be considered to be in agreement with observed erosion. For steam and mercury turbines, the overall model appears to be adequate for at least order of magnitude turbine erosion estimation in absolute terms and to be quite accurate where relative comparisons between turbines are concerned. With respect to potassium turbines, where it appears likely that the primary mechanism of material removal is chemical dissolution, the material removal calculation step in the erosion model is uncertain by, at least, two orders of magnitude. Unfortunately, the experimental results from operation of different potassium turbines are equally ambiguous.

Cesium vapor turbines will be less prone than potassium vapor turbines to material removal by the mechanical aspects of impingement erosion. However, in neither cesium nor potassium turbines should the purely mechanical aspects be of any great concern provided the liquid flowing along the turbine's casings is removed periodically. There should be little difference in blade erosion by chemical dissolution between cesium and potassium turbines designed for equivalent duty.

Three general rules in wet vapor turbine design that should be followed to minimize blade erosion are: (1) the turbine aerodynamic design should give well ordered flow with no gross separation in any of the turbine passages; even small local separations such as those associated with trailing edges of blades should be minimized, (2) the spacing between the stator and rotor rows of a turbine must be large enough to permit the complete atomization of stator discharged liquid, and (3) build-up of liquid flowing along the turbine casing should be minimized by periodic removal of this liquid.

It is recommended that further experiments in atomization of liquids from turbine stators be conducted. These experiments should be aimed at characterizing the total sprays so produced rather than in an examination of the detail processes as such.

It is recommended that additional experiments on material removal rates by liquid drop impact be done. The experimental information should be obtained under widely varying but carefully controlled and accurately reported velocities, angle of impingement, liquid and target temperatures, and impinging drop diameters for selected candidate turbine blade materials and comparison working fluids. Tests using the alkali liquid metals as the impinging fluid are particularly recommended. These investigations should be more oriented toward obtaining empirical engineering information of quantitative use to the turbine designer, rather than to a fundamental understanding of the complex material removal processes.

TABLE 1A-1

ROWE YANKEE ATOMIC STEAM TURBINE LOW PRESSURE END

YANKEE STEAM TURBINE ROW BY MEAN DIAMETER DATA *

ROW NUMBER	9th ROTOR	9th STATOR	8th ROTOR	8th STATOR	7th ROTOR	7th STATOR	6th ROTOR	6th STATOR	5th ROTOR	5th STATOR	4th ROTOR	4th STATOR	3rd ROTOR	3rd STATOR	2nd ROTOR	2nd STATOR	1st ROTOR	1st STATOR	INLET
EFFECTIVE BLADE HEIGHT, (Inches)	40.00	37.44	27.23	24.46	21.01	19.47	15.07	14.04	12.77	11.81	10.57	9.98	9.15	8.47	7.42	6.84	6.49	6.30	7.55
EFFECTIVE MEAN DIAMETER (Inches)	117.50	118.40	110.64	109.41	106.01	104.78	100.13	98.54	96.77	95.25	93.50	92.51	91.35	90.27	89.28	88.64	88.35	88.10	89.35
AVERAGE GAUGING	0.600	0.421	0.433	0.341	0.341	0.279	0.330	0.291	0.270	0.266	0.300	0.286	0.278	0.274	0.277	0.268	0.248	0.231	---
EXIT FLOW ANGLE (degree)	37.0	25.0	25.6	20.0	20.0	16.2	19.2	16.9	15.7	15.4	17.5	16.6	16.1	15.9	16.1	15.5	14.4	13.4	
STATIC PRESSURE, (psia)	0.88	1.515	2.313	3.411	5.072	6.573	8.745	10.695	13.331	16.367	19.386	22.748	26.473	30.521	34.852	39.679	45.345	51.931	59.2
MOISTURE CONTENT	0.152	0.140	0.130	0.120	0.108	0.100	0.0911	0.0846	0.0768	0.0693	0.0630	0.0560	0.0500	0.0440	0.0380	0.0310	0.0240	0.0170	0.0100
TEMPERATURE °F	97.5	115.9	131.5	146.5	162.8	174.1	187.0	196.4	207.1	217.5	226.3	234.9	243.2	251.3	259.0	266.8	274.9	283.4	292.0
SPECIFIC VOLUME, (Cpff)	318.9	194.5	131.9	92.6	64.7	51.19	39.59	33.03	27.11	22.56	19.39	16.81	14.68	12.93	11.50	10.25	9.11	8.08	---
JET VELOCITY, (fps)	1133.	1057.	1016.	1026.	857.0	905.7	779.8	811.5	800.0	744.2	727.3	709.7	700.6	686.5	692.7	699.0	705.4	689.1	---
MEAN WHEEL SPEED (fps **)	922.8	929.9	869.0	859.3	832.6	823.0	786.4	773.9	760.0	748.1	734.4	726.6	717.5	709.0	701.2	696.2	693.9	692.0	---
TIP WHEEL SPEED, (fps)	1237.0	1224.0	1082.8	1051.4	997.6	975.9	904.8	884.2	860.3	840.8	817.9	805.0	789.3	775.5	759.5	749.9	744.9	741.4	---
INLET FLOW ANGLE TO NEXT ROW, (degrees)	90.0	86.27	83.92	73.32	95.34	79.52	97.74	89.62	87.36	98.72	100.5	103.1	103.1	104.8	100.94	97.2	93.7	97.8	90.0
INLET VELOCITY TO NEXT ROW (degrees)	690.	456.	453.	378.	297.	266.	265.	242.	222.	203.	224.	210.	202.	196.	198.	192.	180.	165.	---
BLADE REYNOLDS NO. $\times 10^{-5}$ ***	1.5	5.9	2.2	7.9	3.4	8.2	5.7	6.1	7.6	6.4	5.3	6.3	5.2	11.6	8.4	8.2	9.5	14.7	---
STEAM FLOW (pph $\times 10^{-3}$)	801.1	801.1	801.1	801.1	801.1	801.1	801.1	801.1	801.1	801.1	904.9	904.9	904.9	904.9	904.9	904.9	904.9	904.9	904.9
CENTRIFUGAL FORCE, G's MEAN DIAMETER / TIP DIAMETER	5400. 7220.																4050.		
AXIAL SPACE STATOR EXIT TO ROTOR INLET (inches)	1.9		1.7		1.1		0.6		0.5		0.5		0.5		0.5		0.5		
TRAILING EDGE THICKNESS (Inches)	0.066	0.077	0.065	0.063	0.060	0.055	0.045	0.015	0.045	0.015	0.038	0.0125	0.037	0.010	0.038	0.010	0.033	0.010	
BLADING MATERIAL	12% Chromium Steel																		
STELLITE SHIELDS	Yes		Yes		Yes		Yes		Yes		Yes		No		No		No		No

* Generally, values are for exit of blade rows

** Stator blade "wheel speed" is that speed equivalent to a rotor of the same diameter

*** Reynolds Number based on the blade chord and exit velocity

TABLE 1A-2

TOLEDO EDISON BAYSHORE NUMBER 2 STEAM TURBINE LOW PRESSURE END

BAYSHORE UNIT NO. 2

ROW NO - MEAN DIAMETER SECTION	7th ROTOR	7th STATOR	6th ROTOR	6th STATOR	5th ROTOR	5th STATOR	4th ROTOR	4th STATOR	3rd ROTOR	3rd STATOR	2nd ROTOR	2nd STATOR	1st ROTOR	1st STATOR	INLET
INLET EDGE RADIUS, (inches)	0.075	0.100	0.105	0.068	0.225	0.256	0.135	0.0966	0.150	0.077	0.201	0.1509	0.1509	0.1509	
EXIT EDGE RADIUS, (Inches)	0.025	0.031	0.035	0.032	0.027	0.032	0.021	0.005	0.016	0.005	0.016	0.005	0.005	0.005	
BLADE WIDTH, (Inches)	2.993	4.5	2.265	3.816	1.618	3.077	1.213	1.25	1.25	1.0	1.0	0.75	0.75	0.75	
AXIAL SPACE, (Inches)	1.5	3.3	1.0	1.0	0.8	0.9	0.6	0.438	0.438	0.438	0.438	0.438	0.438	0.438	
NO. OF BLADES PER ROW	120	72	122	78	154	70	169	130	138	148	146	204	215	242	
MAXIMUM THICKNESS (Inches)	0.371	0.762	0.340	0.630	0.341	0.882	0.412	0.5432	0.331	0.435	0.510	0.382	0.382	0.382	
CHORD LENGHT (Inches)	3.82	6.23	2.82	5.017	2.000	3.80	1.60	1.70	1.40	1.35	1.35	1.0	1.0	1.0	
BLADE SECTION	TS-8906	S-894	T-6246	S-845	T-388-a	S-620-a	T-477-a	6620	T-475	6600-a	5600 cl	5580-a	5580-a	5580-a	
BLADE WIDTH (ft) (Axial)	0.2494	0.375	0.18875	0.318	0.1348	0.25642	0.10108	0.10417	0.10417	0.08333	0.08333	0.0625	0.0625	0.0625	
PITCH (Inches)	1.968	3.243	1.765	2.705	1.289	2.804	1.115	1.424	1.318	1.209	1.200	0.8471	0.7969	0.7024	

TABLE 1A-3

TOLEDO EDISON BAYSHORE NUMBER 3 STEAM TURBINE LOW PRESSURE END

BAYSHORE UNIT NO. 3
FULL LOAD
MEAN DIAMETER CALCULATION

ROW NO.	6th ROTOR	6th STATOR	5th ROTOR	5th STATOR	4th ROTOR	4th STATOR	3rd ROTOR	3rd STATOR	2nd ROTOR	2nd STATOR	1st ROTOR	1st STATOR	INLET
TIP DIAMETER	114.00	109.828											
EFFECTIVE MEAN DIAMETER	85.526	84.170	75.354	73.663	68.578	67.080	66.099	65.134	64.650	63.973	63.668	63.293	
AVERAGE GAUGING (percent)	46.4	29.44	33.60	24.2	33.0	32.6	31.0	30.2	29.5	28.5	26.6	25.2	
EXIT FLOW ANGLE (degree)	33°06'	17° 10'	19° 38'	14° 0'	19° 16'	19° 02'	18° 04'	17° 35'	17° 09'	16° 34'	15° 26'	14° 30'	
EXIT STATIC PRESS, (psia)	0.491	1.457	2.632	4.468	7.386	10.430	14.168	18.645	24.140	30.792	39.128	48.596	60.097
MOISTURE CONTENT	0.0886	0.0477	0.241	0.0013	0.0	0.0	0.0	0.0	0.0	0.0	0.0	0.0	0.0
TEMPERATURE °F	79	114.7	136.4	157.5	227.9	282.6	334.7	383.4	431.6	479.3	528.2	574.3	621.6
SPECIFIC VOLUME (cf/lb)	597.9	222.8	130.9	81.6	55.1	42.1	33.2	26.8	21.8	18.0	14.9	12.57	
JET VELOCITY (fps)	1708.2	1376.2	1335.4	1346.9	1193.9	1133.8	1121.4	1108.1	1108.1	1105.6	1078.5	1056.9	
MEAN WHEEL SPEED (fps)	1343.46	1322.16	1183.7	1157.1	1077.2	1053.7	1038.3	1023.1	1015.5	1004.9	1000.1	994.2	
TIP WHEEL SPEED (fps)	1792												
INLET FLOW ANGLE	91°	80.6°	65.3°	82.8°	86.5°	18.1°	84.9°	90.01°	80.6°	82.4°	84.1°	90.0°	
INLET VELOCITY NEXT ROW (fps)	936	407	453	361	394	374	374	339	332	316	292	265	
STEAM FLOW (pph)	311181	311181	318932	318932	333607	333607	333607	333607	354364	354364	354364	354364	354364
EFFECTIVE BLADE (height -inches)	28.474	25.658	15.474	13.663	8.538	7.080	6.040	5.134	4.591	3.973	3.609	3.293	
LEADING EDGE RADIUS (Inches)	0.075	0.125	0.075	0.075									
EXIT EDGE RADIUS (Inches)	0.030	0.030	0.0225	0.025									
BLADE WIDTH (Inches)	3.50	5.00	2.414	3.560									
AXIAL SPACE (Inches)	2.5												
NUMBER OF BLADES PER ROW	120	78	120	80									
MAXIMUM THICKNESS (Inches)	0.377	0.852	0.423	0.585									
CORD LENGTH (Inches)	4.395			5.560									

APPENDIX 1B

REFERENCES

1. Rossbach, R.S. and G. C. Wesling, General Electric Co., "Two-Stage Potassium Test Turbine, "NASA Contractor Report NASA CR-922, Feb. 1968, Vol. I, Fluid Dynamic Design and Performance, Contract NAS5-1143

2. Rossbach, R. J., G. C. Wesling, and W. F. Lemond, General Electric Co., "Three-Stage Potassium Test Turbine," NASA Contractor Report NASA CR-72749, Final Design - Volume I - Fluid Design, Contract NAS3-8520

3. Blinn, H. O., et al, "Space Power Plant Study," Final Report, NASA Contract NAS5-250, Westinghouse Electric Corp., Astronuclear Laboratory, Report WANL-PR(B)-009, December 31, 1963

4. Thompson - Ramo - Wooldridge Inc., "Sunflower Turboalternator CSU1-3A, 4329 - Hour Test Summary Report," NASA CR-169, April 1965, Contract NAS5-462

5. Szanca, E. M., "Sunflower 1 Turbine Design Report," Thompson - Ramo - Wooldridge Inc., ER 4368, May 1, 1961, Project 512-108131-08

6. Spies, R., J. R. Baughman, J. E. T. Blake, "Investigation of Variables in Turbine Erosion, Influence of Aerodynamic and Geometric Parameters, "Rocketdyne Div. North American Rockwell Corp. R-7650, Dec. 1968, Contract NAS7-391

7. A1 Research Mfg. Co., "Potassium Turboalternator Preliminary Design Study, " Phase II Presentation, APS-5312-R, Jan. 21, 1969, Contract NAS3-10934

8. Gyarmathy, G., "Bases for a Theory for Wet Steam Turbines," Juris - Verlag, Zurich 1962

9. Goldman, L. J. and S. M. Nosek, "Experimental Nozzle Expansion and Flow Characteristics of Potassium Vapor," NASA TND-3209

10. Rossbach, R.J., "Critical Flow of Potassium Vapor Through Instrumented Converging-Diverging Nozzle," ASME Preprint 65-GTP-22, presented at the Gas Turbine Conference and Product Show, Washington D. C., Feb. 28 - Mar. 4, 1965

11. Gyarmathy, G., "Summary of Turbine Erosion Meeting Held at the Jet Propulsion Laboratory," Dec. 29 - 30, 1966 (Ed. L. G. Hays), Section II, p. 145-157, JPL Tech Memo 33-354, June 15, 1967

12. Gyarmathy, G. and H. Meyer, "Spontaneous Condensation Phenomena - Parts I and II," CEGB Information Services, C. E. Trans. 4160

13. Katz, J. L., H. Saltsburg and H. Reiss, "Nucleation in Associated Vapors," North American Aviation Science Center, SCPP-65-32, May 18, 1965

14. Ewing, C. T. et al, "High Temperature Properties of Potassium," U. S. Naval Research Laboratory, Report NRL 6233, September 24, 1965

15. Linhardt, Hans D., "Potassium Erosion Experiments," from "Summary of Turbine Erosion Meeting Held at the Jet Propulsion Laboratory, Dec. 29 - 30, 1966," (Ed. L. G. Hays) Section 9, p. 115-127, JPL Tech Memo 33-354, June 15, 1967

16. Smith, A. "The Influence of Moisture on the Efficiency of a One-Third Scale Model Low Pressure Steam Turbine," Institution of Mechanical Engineers, Thermodynamics and Fluid Mechanics Convention, Paper 10, Liverpool (Gr. Brit.), April 13-15, 1966

17. Baker, O., "Simultaneous Flow of Oil and Gas," The Oil and Gas Journal, July 1954, pp 185-195

18. Chien S. and W. Ibele, "Pressure Drop and Liquid Film Thickness of Two-Phase Annular and Annular Mist Flows, "Trans. ASME, J. Heat Transfer Paper No. 62-WA-170, 1962

19. Wrobel, J. R. and McManus, H.N., "An Analytical Study of Film Depth, Wave Height, and Pressure Drop in Annular Two-Phase Flow," Developments in Mechanics, Vol. I, Proc. 7th Midwest Mech. Conf.; Sept. 6-8, 1961, Plenum Press Inc.

20. Gardner, G. C., "Events Leading to Erosion in the Steam Turbine," Proc. Inst Mech Engrs, 178, Pt 1, No. 23, pp 593 to 623, 1963-1964

21. Zimmerman, W. F. and R. J. Rossbach, "Limited Impact Erosion and Metal Losses in Two-Stage Potassium Turbines, "Section 3, "Summary of Turbine Erosion Meeting Held at the Jet Propulsion Laboratory Dec. 29-30, 1966" (Ed. L. G. Hays), JPL Tech Memo 33-354, June 15, 1967

22. Rossbach, R. J., loc cit: Three-Stage Potassium Test Turbine Review Meeting, General Electric Co., Evandale, Ohio, Oct. 15, 1968

23. Christie, D. G., and G. W. Hayward, "Observation of Events Leading to the Formation of Water Drops which Cause Turbine Blade Erosion," Phil. Trans. Roy Soc London, Series A, No. 1110, Vol. 260, pg. 183-192, 28 July 1966

24. Christie, D. G., "Experimental Investigations of Internal Flow in Turbines," Section 12 "Summary of Turbine Erosion Meeting Held at the Jet Propulsion Laboratory Dec. 29-30, 1966" (Ed. L. G. Hays), JPL Tech. Memo 33-354, June 15, 1967

25. Lieblein, S. and W. H. Roudebush, "Low-Speed Wake Characteristics of Two-Dimensional Cascade and Isolated Airfoil Sections," NACA-TN-3771, October 1956

26. Pouchot, W. D., W. K. Fentress and R. E. Kothmann, "Analytical Investigation of Turbine Erosion Phenomena," Section 2, "Summary of Turbine Erosion Meeting Held at the Jet Propulsion Laboratory December 29-30, 1966" (Ed. L. G. Hays), JPL Tech Memo 33-354, June 15, 1967

27. Epstein, L. F., "Static and Dynamic Corrosion and Mass Transfer in Liquid Metal Systems," Chem. Engr. Prog. Sym. Series, Vol. 53, No. 20, p. 67 (1952)

28. Gill, W. N., et al., "Mass Transfer in Liquid Lithium System," A. I. CHE. Jour., Vol. 6, No. 1, p. 139 (1960)

29. Swisher, J. H., "Solubility of Fe, Ni, and Co in Liquid Potassium and the Effect of Oxygen Gettering Agents, "CONF-650411, AEC-NASA Liquid Metals Information Meeting, p. 43, April 1965

30. Ginell, W. S. and R. J. Teitel, "Determination of the Solubility of Transition Elements in Molten Potassium," Douglas Aircraft, SM48883, 1965

31. Baker, DWC, K. H. Jolliffe, and D. Pearson, "The Resistance of Materials to Impact Erosion Damage," Phil. Trans. Roy Soc London, Series A, No. 1110, Vol. 260, pp 193-203, 28 July 1966

32. Pearson, D. "A Summary of the M. E. L. Experimental Data on Erosion," Marchwood Engineering Laboratories, CEGB, RDD/M/MIB, Job No. 30023, Nov. 1964

33. Smith, Allen, R. P. Kent, and R. L. Armstrong, "Erosion of Steam Turbine Blade Shield Materials," ASTM Special Technical Publication No. 408, March 1967

34. Brun, R. J., W. Lewis, P. J. Perkins, and J. S. Serafini, NACA Report 1215, 1955

35. Winder C., "Turbine Erosion During Mercury Rankine Turbo-Alternator Endurance Tests," Summary of Turbine Erosion Meeting Held at the Jet Propulsion Laboratory, Dec. 29-30, 1966, (Ed. L. G. Hays,) JPL Tech Memo 33-354, Section 8, June 15, 1967

APPENDIX 1C

RESULTS OF DETAILED FLUID-DYNAMIC ANALYSIS OF BLADE PASSAGE FLOWS OF NAS5-250 POTASSIUM AND CESIUM TURBINES

1.0 CONDENSATION

1.1 Potassium Turbine

The results of the condensation performance calculations for the six-stage potassium turbine are shown in Table 1C-1. In this case the inlet vapor is superheated and remains superheated through the first stator row. The Wilson point occurs just before the exit of the third rotor blade row at approximately 7.3 percent moisture content. The expansion rate $\frac{1}{P}\frac{dp}{dt} = \dot{P}$ at the Wilson point is approximately 5000/sec. P is pressure and t is time. The expansion process approaches full thermodynamic equilibrium in the fourth stator row and remains in equilibrium through the fifth stator. These calculations were, therefore, terminated at the fifth stator row.

The rapid expansion at the Wilson point produces relatively small droplet sizes as shown in Table 1C-2. The mean droplet radius at the exit of 5-R and 6-S are estimated on the basis of equilibrium condensation to be 0.238 and 0.243 microns, respectively. In this turbine there is no appreciable difference in mass flow rate between the condensing and equilibrium flow calculations. The condensation calculation is sensitive to the values of liquid surface tension used. A calculation for this turbine, using a 25 percent increase in surface tension values, shifted the point of initial condensation to the fifth rotor row.

The results of the present calculations can be compared in a qualitative manner with the results of Goldman and Nosek,[9] in which saturated potassium vapor was expanded in a convergent-divergent nozzle. Although their results are somewhat inconclusive, it appears that condensation occurred when the ratio of pressure to initial saturation pressure was between 0.31 and 0.33 at an axial distance of about 3 inches from the nozzle inlet. In the present calculations, condensation was predicted at a pressure to initial saturation pressure ratio of 0.4. The axial distance from the inlet was about 3.5 inches. The somewhat earlier condensation, in terms of pressure ratio, in the turbine as compared to the supersonic nozzle is to be expected because of the lower expansion rate.

The droplet size results can be compared with those obtained by Linhardt.[15] His analysis predicts a droplet radius of 0.05 microns for 10 percent exit moisture in his test No. 4. Test Numbers 2, 3, and 4 had the same stagnation condition and the same nozzle except for length. With critical flow in the nozzle, the conditions at the condensation point would be unchanged due to the additional length of the nozzle. Thus, for the same conditions at the Wilson point, the droplet radius at the nozzle exit would be expected to be proportional to $(y_e)^{1/3}$, where y_e is the moisture fraction at the nozzle exit. Viewed in this way, the results of Linhardt's Test No. 3 corrected to 10 percent moisture would give a radius of 0.06 micron; Test No. 2 would give a 0.26

TABLE 1C-1

CONDENSATION RESULTS FOR SIX-STAGE POTASSIUM TURBINE

	Static Pressure (lb/in^2)	Static Temperature (°R)	Axial Velocity (ft/sec)	Equilibrium Moisture (lb/lb)	Condensed Moisture (lb/lb)
Inlet	171	2543	358	Superheated	-
1 - S	144	2442	404	Superheated	-
1 - R	121.5	2348	417	0.014	0
2 - S	102.7	2261	415	0.029	0
2 - R	86.2	2176	413	0.046	0
3 - S	72.2	2093	417	0.058	0
3 - R	59.0	2017	409	0.073	0.001
4 - S	47.0	2093	443	0.086	0.079
4 - R	36.8	2037	460	0.105	0.100
5 - S*	28.5	1977	466	0.125	0.120

TABLE 1C-2

FOG PARTICLE SIZE DISTRIBUTION FOR SIX-STAGE POTASSIUM TURBINE

Group	Number (drops/lb)	Radius (microns) 3 - R	4 - S	4 - R	5 - S
1	2.7×10^{11}	0.186	0.297	0.31	0.32
2	5.2×10^{11}	0.173	0.288	0.30	0.31
3	1.6×10^{12}	0.157	0.277	0.29	0.30
4	3.7×10^{12}	0.142	0.267	0.28	0.29
5	7.3×10^{12}	0.127	0.257	0.27	0.28
6	2.2×10^{13}	0.110	0.246	0.26	0.27
7	5.8×10^{13}	0.089	0.235	0.25	0.26
8	1.5×10^{14}	0.066	0.222	0.236	0.247
9	3.9×10^{14}	0.040	0.209	0.224	0.235
10	1.3×10^{15}	0.0015	0.189	0.206	0.218
	Mean Radius	0.065	0.200	0.215	0.229

N total = $1.92\ (10^{15})$/lb

* Calculations discontinued.

micron radius. The present calculations fall between these limits, but again are not directly comparable due to differences in the expansion rate and initial conditions.

1.2 Cesium Turbine

The results of the condensation calculations for the cesium turbine are given in Tables 1C-3 and 1C-4. The Wilson point occurs just before the exit of the first stator. The equivalent moisture at the Wilson point is approximately 0.046, and the expansion rate P is 1.9×10^4/sec.

TABLE 1C-3

CONDENSATION RESULTS FOR CESIUM TURBINE

	P (lb/in.^{2})	T (°F)	Velocity Relative to Blade (ft/sec)	y_e Equilibrium Moisture (lb/lb)	y Condensed Moisture
Stagnation	411.	2440	0	200°F superheat	-----
Static Inlet	399.	2415	216.5	177°F superheat	-----
Exit 1 - S	171.5	1822	1147.	0.045	0.021
0.024 inch into 1 - R	176.	1878	592	0.043	0.039

TABLE 1C-4

FOG PARTICLE DISTRIBUTION AT EXIT FROM 1-S CESIUM TURBINE

Group	N (drops/lb)	Drop Radius (microns)
1	3.4×10^{10}	0.089
2	1.2×10^{11}	0.087
3	3.6×10^{11}	0.085
4	1.7×10^{11}	0.082
5	6.2×10^{12}	0.079
6	1.9×10^{13}	0.076
7	6.5×10^{13}	0.072
8	2.1×10^{14}	0.068
9	7.7×10^{14}	0.063
10	4.5×10^{15}	0.055
11	7.1×10^{15}	0.048

$N_{total} = 1.27 \times 10^{16}$/lb
Mean Radius = 0.052 micron

It is seen that the drops are quite small due to the rapid expansion. The drop size is also relatively uniform and will become more uniform as the condensation proceeds. The thermodynamic description of the flow used resulted in critical flow occurring at approximately 1000 ft/sec, a slightly lower value than results for equilibrium flow. The mean droplet radii at the exit of 1-R and 2-S are estimated to 0.089 and 0.097 microns.

2.0 AXISYMMETRIC FLOW DOWNSTREAM OF THE BLADE ROWS

The fluid conditions such as pressure, temperature, density, velocity, and angle of flow with respect to blade height for the last or latter stages of the two turbines are given in Tables 1C-5 and 1C-6. Table 1C-5 covers the last stage of the two-stage cesium turbine. Table 1C-6 covers the fifth and sixth stages of the six-stage potassium turbine.

It will be noted in Table 1C-5 that there is recompression in the second-stage rotor of the cesium turbine at the hub of the blade. The pressure level at the inlet to the rotor hub is 26.74 psia and increases to 34.99 psia at the exit. In the turbine erosion analysis, the flow disorder (flow separation at the trailing edge of the rotor blade at the hub) is of no concern since there are no stages downstream of the second stage in the cesium turbine.

However, this same recompression at the hub was present in the fifth stage of the original conceptual design of the potassium turbine as set forth in Contract NAS 5-250. (This is not to be taken as a criticism of the work under Contract NAS 5-250. The designs were more than adequate as representative descriptions of potassium and cesium turbines for the nuclear Rankine cycle power system studies conducted.) Since our calculations indicate that there will be collected moisture as early as the fourth stage of the potassium turbine, the original design has been modified to increase the hub-to-tip ratios in the latter stages. This gives a slight fluid expansion at the hub, as will be noted in Table 1C-6. Elimination of flow separation in the fifth stage is necessary to protect the sixth stage from erosion difficulties.

TABLE 1C-5
CESIUM TURBINE-FLUID PROPERTIES ALONG HEIGHT - SECOND STAGE

ROW	Second Rotor Exit					Second Rotor Inlet*					Second Stator Exit									
APPROX. SECTION	h	1/4	m	3/4	t	h	1/4	m	3/4	t	h	1/4	m	3/4	t	h	1/4	m	3/4	t
DIAMETER (inches)	3.71	4.87	5.74	6.61	7.77	4.34	5.14	5.74	6.34	7.14	4.34	5.14	5.74	6.34	7.14					
GAUGING	0.5281	0.4652	0.4248	0.3905	0.3526	---	---	---	---	---	0.3834	0.3834	0.3834	0.3834	0.3834					
EXIT FLOW ANGLE (degrees)	31.88	27.72	25.01	22.98	20.65	24.25	20.67	19.42	18.79	18.50	29.42	25.45	24.00	23.24	22.85					
STATIC PRESSURE (psia)			34.99			26.74	37.14	44.10	50.22	57.12	27.94	37.60	44.10	49.87	56.42			82.2		
TEMPERATURE °F			1420.										1477.					1640.		
SPECIFIC VOLUME (cpff)	3.338	3.321	3.314	3.311	3.310	4.139	3.138	2.716	2.434	2.184	3.988	3.106	2.716	2.448	2.206					
JET VELOCITY (fps)	490.7	554.2	605.6	658.2	728.7	1136.3	1002.2	920.2	852.0	776.1	1119.7	996.7	920.7							
AXIAL VELOCITY (fps)	259.1	257.8	257.3	257.0	257.0	466.7	353.8	306.2	274.4	246.2	550.1	428.4	374.5							
WHEEL SPEED (fps)	388.1	509.8	601.1	692.4	814.1	454.5	538.3	601.1	663.9	747.7	454.5	538.3	601.1							
INLET FLOW ANGLE TO NEXT ROW (degrees)	83.72	94.28	101.6	108.6	117.2	38.74	41.54	48.89	62.54	92.72	46.57	49.87	57.35							
INLET VELOCITY TO NEXT ROW (fps)	260.7	258.5	262.6	271.2	288.9	745.7	533.5	406.4	309.3	246.5	757.5	560.7	444.8							

* Discharge characteristics of unbladed axial gap between stator blade trailing edges and rotor blade leading edges.

TABLE 1C-6
POTASSIUM TURBINE-FLUID PROPERTIES ALONG THE HEIGHT OF THE BLADE-FIFTH AND SIXTH STAGES

ROW	Sixth Rotor Exit					Sixth Rotor Inlet*					Sixth Stator Exit					Sixth Stator Inlet				
APPROX. SECTION	h	1/4	m	3/4	t	h	1/4	m	3/4	t	h	1/4	m	3/4	t	h	1/4	m	3/4	t
DIAMETER (inches)	4.54	5.70	6.85	8.00	9.16	4.82	5.82	6.82	7.82	8.82	4.75	5.75	6.75	7.75	8.75					
GAUGING	0.6396	0.5694	0.5154	0.4698	0.4308	0.4488	0.4782	0.5091	0.5394	0.5684	0.4737	0.5046	0.5363	0.5673	0.5965					
EXIT FLOW ANGLE (degrees)	39.77	34.71	31.02	28.02	25.52	26.67	28.57	30.60	32.64	34.64	28.28	30.30	32.43	34.57	36.62					
STATIC PRESSURE (psia)			16.90			17.37	18.76	19.69	20.35	20.83	17.43	18.79	19.69	20.33	20.80			22.04		
TEMPERATURE °F			1422.										1454.					1477.		
SPECIFIC VOLUME (cfpp)	23.81	23.79	23.79	23.79	23.81	23.19	21.70	20.81	20.23	19.82	23.13	21.67	20.81	20.25	19.85					
JET VELOCITY (fps)	637.8	715.8	790.6	867.6	946.8	1025.9	900.6	811.7	744.5	692.5	1021.0	898.3	811.7	746.5	696.2					
AXIAL VELOCITY (fps)	407.9	407.5	407.5	407.6	407.9	460.4	430.7	413.2	401.6	393.6	483.7	453.3	435.3	435.3	415.3					
WHEEL SPEED (fps)	475.4	596.9	717.3	837.8	959.2	504.8	609.5	714.2	818.9	923.6	497.4	602.1	706.9	811.6	916.3					
INLET FLOW ANGLE TO NEXT ROW (degrees)	87.94	91.13	95.58	100.06	104.40	48.17	67.16	92.15	115.56	131.96	50.29	69.06	92.86	114.93	130.72					
INLET VELOCITY TO NEXT ROW (fps)	408.2	407.6	409.4	414.0	421.1	617.8	467.4	413.5	445.2	529.3	628.8	485.3	435.9	467.0	548.					

ROW	Fifth Rotor Exit					Fifth Rotor Inlet*					Fifth Stator Exit									
APPROX. SECTION	h	1/4	m	3/4	5	h	1/4	m	3/4	t	h	1/4	m	3/4	5	h	1/4	m	3/4	t
DIAMETER (inches)	5.02	5.84	6.66	7.47	8.29	5.11	5.81	6.51	7.21	7.91	5.09	5.79	6.49	7.19	7.89					
GAUGING	0.4841	0.4625	0.4438	0.4266	0.4104	0.3875	0.3950	0.4059	0.4189	0.4330	0.4032	0.4109	0.4222	0.4356	0.4500					
EXIT FLOW ANGLE (degrees)	28.95	27.55	26.35	25.25	24.23	22.80	23.23	23.95	24.77	25.67	23.78	24.26	24.97	25.82	26.74					
STATIC PRESSURE (psia)			22.04			24.57	26.78	28.51	29.89	31.01	24.62	26.81	28.51	29.87	30.97			37.04		
TEMPERATURE °F			1477.										1534.					1592.		
SPECIFIC VOLUME (cfpp)	18.77	18.75	18.73	18.73	18.72	17.01	15.80	14.98	14.38	13.94	16.95	15.79	14.98	14.39	13.95					
JET VELOCITY (fps)	949.5	992.5	1033.5	1074.8	1117.2	1280.7	1167.2	1076.5	1001.6	939.0	1278.0	1160.0	1076.5	1002.6	940.9					
AXIAL VELOCITY (fps)	459.7	459.0	458.7	458.5	458.5	496.3	461.0	437.0	419.6	406.6	515.3	479.1	454.5	436.7	423.4					
WHEEL SPEED (fps)	525.7	611.6	697.4	782.3	868.1	535.1	608.4	681.7	755.0	828.3	533.3	606.6	680.0	753.2	826.6					
INLET FLOW ANGLE TO NEXT ROW (degrees)	56.45	59.68	63.46	67.52	71.79	37.56	44.82	55.34	69.80	87.46	391.01	46.39	56.94	71.14	88.15					
INLET VELOCITY TO NEXT ROW (fps)	551.5	531.8	512.7	496.2	482.7	814.2	653.9	531.2	477.1	407.0	818.7	661.7	542.3	461.5	423.6					

*Discharge characteristics of unbladed axial gap between stator blade trailing edge and rotor blade leading edge

3.0 VAPOR BOUNDARY LAYER ON SURFACES OF BLADES

Calculated values for the potassium turbine are shown in Table 1C-7 for the boundary layer thickness and form factor at the trailing edge of the sixth stator blade row, 3/4 blade height position. Values are also shown for the Reynolds No. based on chord length, the momentum thickness, the skin friction coefficient, and the shearing stress. These quantities are local blade surface values for the trailing edge position and are based on conventional turbulent boundary layer relationships.

Similar calculations performed on the second stator blade row of the cesium turbine are tabulated in Table 1C-8. The Reynolds No. and shearing stress (τ) are much higher in the cesium turbine due in large part to the high vapor density, roughly twelve times that in the back end of the potassium turbine. The low boundary layer thickness in the cesium turbine, approximately half the thickness in the potassium turbine, is associated with the high Reynolds Number 4.

TABLE 1C-7
POTASSIUM TURBINE-CALCULATED BOUNDARY LAYER PROPERTIES AT THE TRAILING-EDGE OF THE BLADE

	Sixth Stator Blade at 3/4 height position Pressure Side	$D = 7.75$ in. $\ell = 0.77$ in. $R_{e\ell} = 0.8 \times 10^5$ Suction Side	Total
θ/ℓ	0.0009096	0.0050094	0.0059190
H	1.300	1.825	
δ^*/ℓ	0.0011825	0.0091422	0.103247
δ/ℓ	0.009066	0.31303	0.40369
δ (in.)	0.006981	0.024103	0.031084
n	6.666	2.424	
$R_{e\theta}$	162.	892.	
C_f	0.0083	0.00233	
τ (ppsf)	3.57	1.00	

where $R_{e\theta} = V\rho\theta/\mu$; $n = 2/(H-1)$; $R_{e\ell} = V\rho\ell/\mu$; and $C_f = \dfrac{\tau}{\dfrac{\rho V^2}{2}} = 2 \times 0.123 \times 10^{-0.689H} \times R_{e\theta}^{-0.268}$

Here, θ, δ^* and δ are the momentum thickness, displacement thickness, and full thickness of the boundary layer at the trailing edge of the blade and ℓ is the projected chord length of the blade.

4.0 DOWNSTREAM WAKES

Calculated results for the sixth stator blade of the potassium turbine and for the second stator blade of the cesium turbine are shown in Tables 1C-9 and 1C-10. As shown, the wake properties quickly change downstream of the trailing edge, where there is little change beyond $0.20x/\ell$. Note also that while the wake thickness (δ) continues to increase

TABLE 1C-8
CESIUM TURBINE-CALCULATED BOUNDARY LAYER PROPERTIES

	Sixth Stator Blade at 3/4 height position Pressure Side	$D = 6.34$ in. $\ell = 0.703$ in. $R_{e\ell} = 10.8 \times 10^5$ Suction Side	Total
θ/ℓ	0.0004357	0.0025562	0.0029919
H	1.315	1.665	
δ^*/ℓ	0.0005729	0.0042561	0.0048290
δ/ℓ	0.0042105	0.0170562	0.0212667
δ (in.)	0.00296	0.01199	0.01495
n	6.349	3.008	
$R_{e\theta}$	470.	2750.	
C_f	0.00606	0.00220	
τ (ppsf)	28.2	11.3	

where $R_{e\theta} = V\rho\theta/\mu$; $n = 2(H-1)$ $R_{e\ell} = V\rho\ell/\mu$; $C_f = \dfrac{\tau}{\dfrac{\rho V^2}{2}} = 2 \times 0.123 \times 10^{-0.678H} \times R_{e\theta}^{-0.268}$; and

θ, δ^* and δ are the momentum thickness, displacement thickness of the boundary layer at the trailing edge of the blade, ℓ is the projected chord length of the blade.

All values are point values for the trailing edge position; e.g., C_f is the local skin friction coefficient at the trailing edge position.

beyond $2x/\ell$, the velocity within the wake, V(y), is nearly the same as that of the free stream since

$$V(y) = V(x) \left(\frac{y}{\delta}\right)^{1/n}$$

where

$$\left(n = \frac{2}{H-1}\right) \gg 1$$

Thus, the downstream flow is roughly axisymmetric from about 20 percent of the chord length distance downstream of the blade by this model of the process. The low wake thickness of the cesium turbine, about half that of the potassium turbine, is associated with the high vapor density, high Reynolds No., and low boundary layer thickness at the blade trailing edge.

Wake calculation results are also shown in Figures 1C-1 through 1C-4 in slightly different form. These curves give the wake velocity with respect to the distance, and normal to the distance, along the streamline downstream of the blades. These curves are used to estimate the atomization and acceleration of the moisture particles in the interval (both time and distance) between the stator and rotor. To compensate for the finite trailing edge thickness in these calculations, the trailing edge wake is treated mathematically as a dead space 4.8 trailing edge thicknesses in length, joined to a zero trailing edge thickness wake at a discontinuity and represented by a vertical line on the curves.

TABLE 1C-9

POTASSIUM TURBINE-RESULTS OF BLADE WAKE CALCULATION FOR SIXTH STATOR BLADE, 3/4 BLADE HEIGHT POSITION

x/ℓ	H	$\hat{\theta}$ $\frac{\theta}{\ell}$	a°	θ (inches)	n $\frac{2}{H-1}$	$\delta = \frac{\theta(1+n)(2+n)}{n}$ (inches)	V (x) (ft/sec)	V (y) (ft/sec)
Pressure Side								
0. (t.e.)	1.300	0.00250	36.1	0.000700	6.66	0.00698	767.	$V(y) = V(x)(y/\delta)^{1/n}$
0.039	1.169	0.00251	34.9	0.000702	11.82	0.01059	755.	
0.078	1.130	0.00251	34.6	0.000702	15.40	0.01305	749.	
0.156	1.095	0.00251	34.6	0.000702	21.0	0.01700	746.5	
0.234	1.078	0.00251	34.6	0.000702	25.6	0.0202	746.5	
0.312	1.067	0.00251	34.6	0.000702	29.8	0.0231	746.5	
0.394(rot. inl.)	1.060	0.00251	34.6	0.000702	33.3	0.0256	746.5	
Suction Side								
0. (t.e.)	1.825	0.01380	36.1	0.00386	2.424	0.0241	767.	
0.039	1.390	0.01393	34.9	0.00391	5.13	0.0332	755.	
0.078	1.285	0.1393	34.6	0.00391	7.01	0.0403	749.	
0.156	1.202	0.1393	34.6	0.00391	9.90	0.0503	746.5	
0.234	1.162	0.1393	34.6	0.00391	12.32	0.0606	746.5	
0.312	1.140	0.1393	34.6	0.00391	14.30	0.0680	746.5	
0.394(rot. inl.)	1.122	0.1393	34.6	0.00391	16.40	0.0764	746.5	

TABLE 1C-10

CESIUM TURBINE-RESULTS OF BLADE WAKE CALCULATION FOR SECOND STATOR BLADE, 3/4 BLADE HEIGHT POSITION

x/ℓ	H	$\hat{\theta}$ $\frac{\theta}{\ell}$	a°	θ (inches)	n $\frac{2}{H-1}$	$\delta = \frac{\theta(1+n)(2+n)}{n}$ (inches)	V (x) (ft/sec)	V (y) (ft/sec)
Pressure Side								
0. (t.e.)	1.315	0.002142	25.9	0.0003063	6.35	0.00296	876.	$V(y) = V(x)(y/\delta)^{1/n}$
0.0426	1.171	0.002160	23.8	0.0003089	11.70	0.00460	863.	
0.0854	1.128	0.002160	23.2	0.0003089	15.62	0.00576	856.	
0.171	1.093	0.002160	23.2	0.0003089	21.50	0.00759	856.	
0.256	1.078	0.002160	23.2	0.0003089	25.65	0.00888	856.	
0.342	1.066	0.002160	23.2	0.0003089	30.30	0.01030	856.	
0.480(rot. inl.)	1.055	0.002160	23.2	0.0003089	36.35	0.01217	856.	
Suction Side								
0. (t.e.)	1.665	0.01253	25.9	0.001792	3.01	0.01199	876.	
0.0426	1.320	0.01270	23.8	0.001816	6.25	0.01738	863.	
0.0854	1.238	0.01270	23.2	0.001816	8.40	0.02112	856.	
0.171	1.169	0.01270	23.2	0.001816	11.83	0.02725	856.	
0.256	1.138	0.01270	23.2	0.001816	14.50	0.03202	856.	
0.342	1.117	0.01270	23.2	0.001816	17.10	0.03669	856.	
0.480(rot. inl.)	1.097	0.01270	23.2	0.001816	20.63	0.04304	856.	

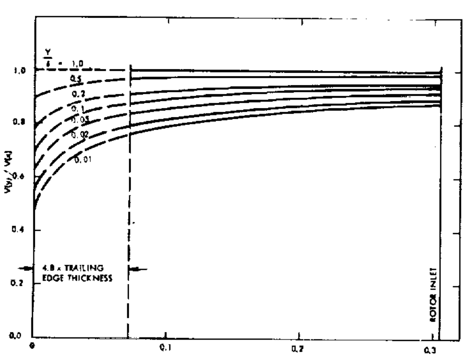

Figure 1C-1 Potassium Sixth Stator Wake Pressure Side Velocity

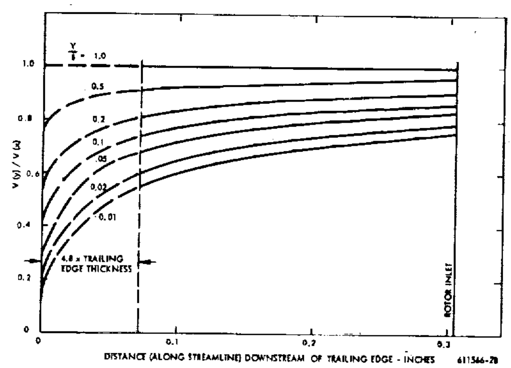

Figure 1C-2 Potassium Turbine Sixth Stator Wake Suction Side Velocity

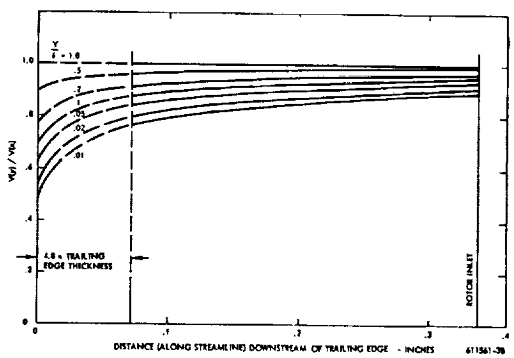

Figure 1C-3 Cesium Turbine Second Stator Wake Pressure Side Velocity

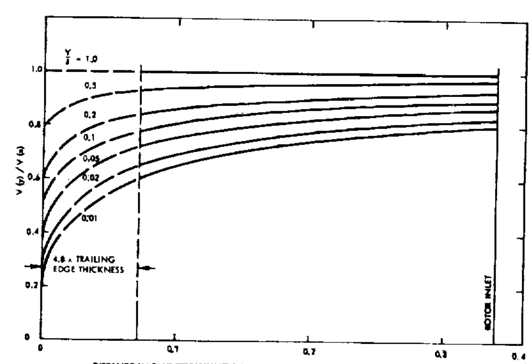

Figure 1C-4 Cesium Turbine Second Stator Wake Suction Side Velocity

5.0 DEPOSITION OF MOISTURE ON THE SURFACE OF BLADES

5.1 Inlet Edge Deposition

The calculated portion of drops collected on the nose of the sixth stator blade row of the potassium turbine is given parametrically in Figure 1C-5. Two methods of calculation are used that do not agree. In the summary of collected moisture for the two turbines the curve used is that generated from Gyarmathy's data,[8] because his data gives reasonable agreement with steam turbine collection information presented by Smith, et al.[16]

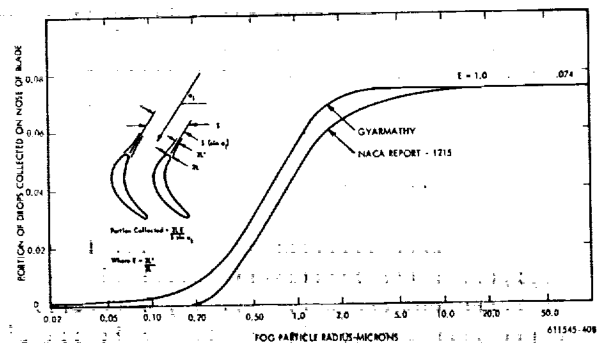

Figure 1C-5 Potassium Turbine Portion Collected on Nose of Sixth Stator Blade

For a 0.48 micron radius fog particle, the NACA[34] curve gives 2 percent collection on the inlet edge compared to 2.8 percent collection by the Gyarmathy curve. Also, by the NACA curve, fog particles of less than 0.2 micron radius are not collected.

Similar calculations performed for the second stator blade of the cesium turbine are shown in Figure 1C-6. Similar to the potassium turbine results, fog particles of less than 0.2 micron are not collected according to the NACA curve, but by the Gyarmathy curve 1 percent of the fog particles are collected for the 0.2 micron radius size.

In the cesium calculation, Figure 1C-6, there is a greater difference with respect to the NACA curve and the Gyarmathy curve than in the potassium calculation, Figure 1C-5. This is due to the fact that the NACA data account for the change in Stokes' Law drag with Reynolds No. while the Gyarmathy curve does not. As the Reynolds No. is higher in the cesium turbine, a larger difference is shown by the curves.

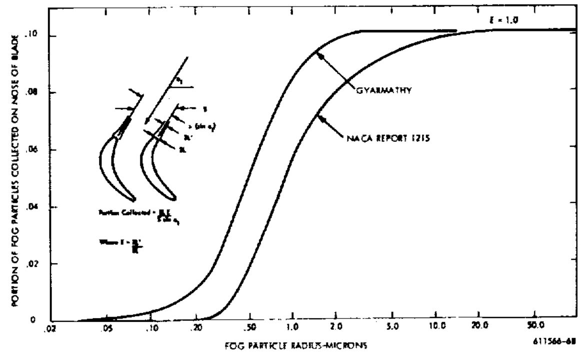

Figure 1C-6 Cesium Turbine Portion Collected on Nose of Second Stator Blade

5.2 Concave Surface Deposition

The calculated results for concave surface deposition on the sixth stators of the potassium turbine are shown parametrically in Figure 1C-7. Similar results for the second stators of the cesium turbine are shown in Figure 1C-8. These figures give the portion of the moisture present in the bulk flow that is collected as a function of condensate particle radius. As shown by the curve sketches, the portion collected is specified by the inlet width of the band (ζ), within which all particles impinge on the blade with respect to the blade pitch. The band width cannot exceed the space between blades (pitch minus inlet edge blockage) which accounts for the breaks in the curves. For equal condensate particle radii, a somewhat higher portion of moisture will be collected by the cesium turbine than by the potassium turbine.

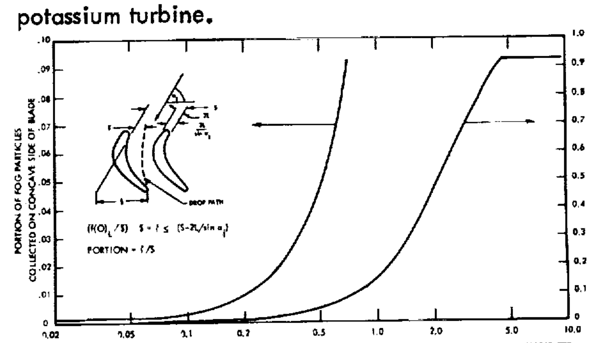

Figure 1C-7 Potassium Turbine Portion Collected on Concave Side Sixth Stator Blade

5.3 Quantity of Damaging Moisture Impacting Last Row Rotor Blades

As a first approximation, it will be assumed that the only potentially damaging moisture that will

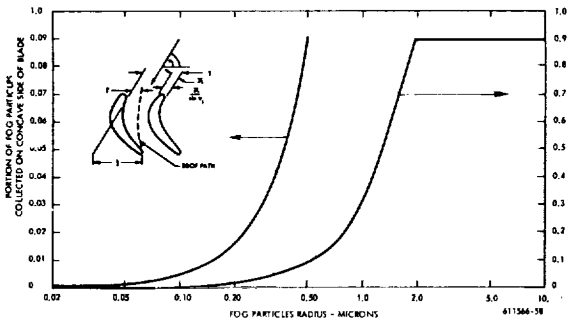

Figure 1C-8 Cesium Turbine Portion Collected on Concave Side of Second Stator Blade

impact the last rotor blades of these turbines is that collected by the last stator. The calculated amount of moisture collected by the sixth stator blades and subsequently impacting the sixth rotor blades of the six-stage potassium turbine is given in Table 1C-11. Similar information is given for the last (second) stage of the cesium turbine in Table 1C-12.

TABLE 1C-11

SIX-STAGE POTASSIUM TURBINE - SIXTH STAGE MOISTURE INVENTORY

Flow (Vapor Plus Liquid)	9100 kg/hr
Bulk Moisture Sixth Stator	14.3%
Bulk Moisture, Average Fog Particle Radius	0.24 micron
Portion of Bulk Moisture Collected, Sixth Stator	2.6%
Collected Moisture Impacting Sixth Rotor	34 kg/hr
Average Local Rate of Impact of Collected Moisture	167 gm/cm/hr
Average Local Collected Moisture Impact Rate/10,000 Hours	1670 kg/cm

TABLE 1C-12

TWO-STAGE CESIUM TURBINE - SECOND STAGE MOISTURE INVENTORY

Flow (Vapor Plus Liquid)	31,500 kg/hr
Average Bulk Moisture, Second Stator	12.8%
Bulk Moisture, Average Fog Particle Radius	0.093 micron
Collected Moisture Impact Rate, Second Stator	26.2 kg/hr
Collected Moisture Impact Rate	294 gm/cm/hr
Local Collected Moisture Impact Rate/10,000 Hours	2940 kg/cm

It is useful to compare these results with those calculated for the Yankee Atomic Plant steam turbine, where the calculated average local moisture impactior rate per 10,000 hours was 802 kg/cm for the last stage of the low pressure turbine.

6.0 STATOR BLADES COLLECTED MOISTURE ATOMIZATION AND TRAJECTORIES

The moisture potentially damaging to the rotor blades collects from the bulk stream, runs to the aft edge, departs this edge as primary drops, and is caught up in the wake of the stators where additional atomization takes place and acceleration is to a fraction of bulk stream velocity.

6.1 Atomization

The primary drops that have the best chance to survive the passage between stator and rotor are those deep in the suction side wake. Given in Table 1C-13 are the time of flight, the initial Weber Number, the time to droplet destruction, and the mass mean diameter of the resulting secondary drops for a range of primary drops departing the second stator of the cesium turbine. Information about the primary drops leaving the sixth stage of the potassium turbine is given in Table 1C-14.

It can be concluded from these results that no drops greater than 5 microns in diameter will reach the second rotor and most, if not all, of the drops will be under 3 microns in diameter. In the case of the potassium turbine a few drops reaching the sixth rotor could be as large as 100 microns in diameter.

TABLE 1C-13

SECONDARY ATOMIZATION IN CESIUM TURBINE - SUCTION SIDE WAKE STREAMLINED AT Y/Y_o = 0.01 SECOND STATOR

Primary Drop Diameter (microns)	Time of Flight (μ sec)	Weber Number (max.)	Time to Complete Droplet Destruction (μ sec)	Mass Mean Diameter of Secondary Drops (microns)	Remarks
2	43	10	---	-----	No disruption
5	58	24	1.3	0.490	"
10	67	49	2.5	0.533	Disruption
25	82	122	6.6	0.600	"
50	99	244	13.0	0.658	"
100	120	488	26.2	0.721	"
200	148	976	52.2	0.822	"
300	161	1464	78.4	0.880	"
400 (max)	173	1952	104.6	0.922	"

However, most, if not all of the drops will be under 60 microns in diameter. The average mass mean diameter drop calculated for the atomized liquid of the sixth stator of the potassium turbine is 40 microns.

TABLE 1C-14

SECONDARY ATOMIZATION IN POTASSIUM TURBINE - SUCTION SIDE WAKE STREAMLINED Y/Y_o = 0.01 SIXTH STATOR

Primary Drop Diameter (microns)	Time of Flight (μ sec)	Weber Number (max.)	Time to Complete Droplet Destruction (μ sec)	Mass Mean Diameter of Secondary Drops (microns)	Remarks
10	98	2.2	6.6	-----	No disruption
20	118	4.4	13.	-----	"
50	149	11.1	32.	-----	"
75	165	15.2	48.	-----	(?)
100	179	22.2	64.	-----	(?)
200	212	44.4	128	-----	Disruption
400 (max)	255	88.4	256	-----	"

* Y is the distance measured from the wake centerline; Y_o is the width of the wake.

7.0 DROP IMPACT VELOCITIES RELATIVE TO THE ROTOR BLADES

Table 1C-15 summarizes impingement results on the second stage rotor blades of the cesium turbine for drop diameters of 0, 2, and 5 microns. Two representative wake positions (Y/Y_o) and blade heights were investigated for the suction and pressure sides of the second stators. The values given in Table 1C-15 are at the rotor inlet; V_d is drop velocity relative to the preceding stators, and W_d is the velocity relative to the rotor blades. In this turbine, the velocity W_d, somewhere on the radius of the rotor blade nose is a normal velocity of impact. As can be seen the maximum normal drop impact velocities are quite low and cover only a narrow range of velocities. This is because the drops are accelerated to a very substantial fraction of the stator discharge vapor velocities.

TABLE 1C-15

SECOND STAGE ROTOR DROP IMPINGEMENT SUMMARY - TWO STAGE CESIUM TURBINE

Wake Position Y/Y_o		Drop Diameter (microns)	3/4 Blade Height		Blade Tip	
			V_d(fps)	W_d(fps)	V_d(fps)	W_d(fps)
Suction	0.01	0	685	273	632	296
		2	665	268	614	300
		5	560	267	517	338
Suction	0.2	0	796	321	735	294
		2	780	313	720	292
		5	665	268	614	300
Pressure	0.01	0	753	299	695	291
		2	740	293	683	291
		5	625	263	576	311
Pressure	0.2	0	822	338	758	299
		2	810	330	747	296
		5	700	278	646	293

Figure 1C-9 shows maximum impact velocities of drops colliding with the nose of the blades of the sixth rotor of the six-stage potassium turbine for representative drop diameters of 25, 50, and 75 microns. The impact velocities are plotted as a function of blade height fraction where the height fraction is 0 at the hub and 1.0 at the blade tips. As for the cesium turbine, somewhere on the nose these impacts are normal to the blade surface. In the potassium turbine, these maximum velocities occur for drops accelerated along the wake streamline at Y/Y_o = 0.01 of the suction side of the sixth-stator wake.

For comparison purposes the maximum impact velocities calculated for 400-micron diameter drops impacting the ninth rotor of the low pressure end of the Yankee Atomic Plant steam turbine are also shown in Figure 1C-9. A 400-micron diameter drop is about the largest expected to impact the ninth rotor of the Yankee turbine. As can be seen, the maximum drop diameters and impact velocities are much larger in the steam turbine than in either of the alkali metal vapor turbines.

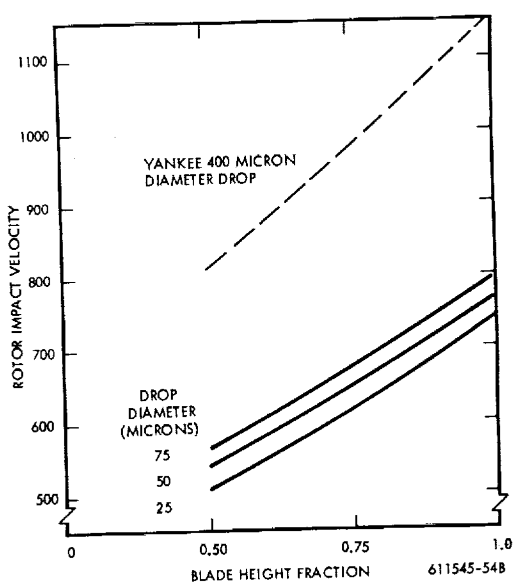

Figure 1C-9 Maximum Impact Velocities on Six - Stage Potassium Turbine

SECTION 2

FLUID-DYNAMIC COMPUTATIONAL PROCEDURES

2.1 BACKGROUND

As reported elsewhere in this report, while erosion in wet vapor turbines takes place locally, the conditions leading to the erosion involve the total thermodynamic and fluid-dynamic history of the working fluid from the time it enters the turbine. The many processes that require analysis are given, again, in block diagram form in Figure 2.1-1. This Section 2 gives an account of the basis of analysis and analytical procedures used in examining the detail fluid-dynamic process leading to the erosion. The processes covered in this Section 2 are indicated in Figure 2.1-1.

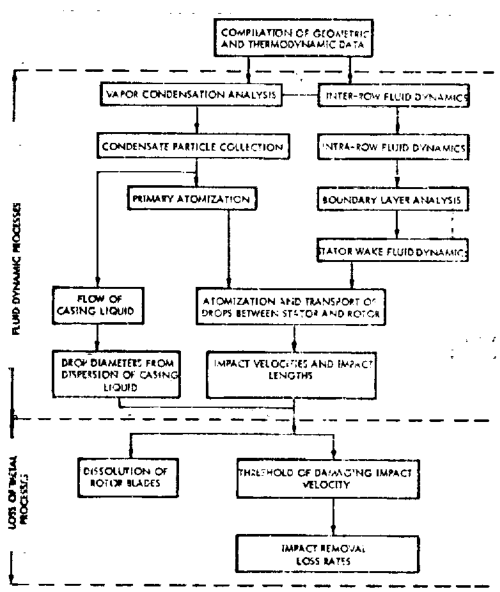

Figure 2.1-1 WANL Turbine Blade Erosion Model

2.2 TURBINE PERFORMANCE WITH DETAILED HISTORY OF CONDENSATION* (NUDROP Condensation Code)

2.2.1 Background

The purpose of this condensation study is to analytically predict the condensation point in wet vapor turbines and to determine the drop size distribution, including effects of molecular association on the condensation and flow processes. The approach is similar to that first developed by Oswatitish[1] and improved by others.[2, 3] The method consists of simultaneous solution of the continuity, energy, momentum, and state equations written for the turbine geometry, including a description of nucleation and growth processes to determine moisture content and drop size. The present study provides the thermodynamic description of the flow process by using the virial equation of state and enthalpy relations derived by Ewing, et al.[4]

The numerical solution is by an ALGOL computer code which has been used on a Burroughs B-5500 computer.

2.2.2 Theory

- Nucleation*

The nucleation theory due to Katz, Saltsburg, and Reiss[5] is used to describe the nucleation

* R. E. Kothmann, Supervisor, Power & Propulsion, Westinghouse Research Laboratories, Churchill Borough, Pa.

The change in moisture due to growth of a particular group of drops is

$$\frac{dy_i}{dz} = 4\pi \rho_L N_{ri} r_i^2 \frac{dr_i}{dz} \qquad (24)$$

The total rate of change of moisture fraction, including surface condensation and atomized drops originating by surface condensation, is

$$\frac{dy}{dz} = \frac{dy_N}{dz} + \sum_{\text{all groups}} \frac{dy_i}{dz} + \frac{dy_b}{dz} + \frac{dy_{bo}}{dz} + \frac{dy_{abs}}{dz} \qquad (25)$$

The liquid temperature is taken as the weighted average of the drop temperature of the various groups, or

$$T_L = \frac{1}{y} \sum_{\text{all groups}} y_i \, T_{ri} = T + \frac{\Delta T}{y} \sum_{\text{all groups}} \left(1 - \frac{r_{crit}}{r_i}\right) y_i \qquad (26)$$

The energy equation includes the rate of change of liquid temperature. Rather than by differentiating Eq. 26, the rate of change is obtained from the present and previous values of liquid temperature obtained in the integration process. This approximation is justified since the moisture energy change is small compared to the total energy change.

- **State Equations**

From the work of Ewing, et al, (4, 7) it appears that an accurate equation of state can be obtained either by use of the virial equation or by an association model. The virial equation of state was chosen since it is generally available for use in obtaining the thermodynamic properties of wet vapors. In the case of cesium and potassium the state equations (References 4 and 7) fit the experimental PVT data with an average deviation of + 0.26 percent. The virial equation of state has the form

$$\frac{PV}{R_o T} = 1 + \frac{B}{V} + \frac{C}{V^2} + \frac{D}{V^3} + \frac{E}{V^4} \qquad (27)$$

where B, C, D and E are functions of temperature only. These functions have the form

$$\log_{10} \left| B \right| = B_1 + B_2/T + \log_{10} T, \; B<0 \qquad (28)$$

$$\log_{10} C = C_1 + C_2/T + C_3/T^2 \qquad (29)$$

$$\log_{10} \left| D \right| = D_1 + D_2/T, \; D<0 \qquad (30)$$

and

$$E = E_1 = \text{Constant} \qquad (31)$$

where B_1, B_2, C_1, C_2, C_3, D_1 and D_2 are constants for a particular vapor. It is convenient to express the equation of state in terms of the compressibility, which gives

$$Z_c = 1 + \frac{B}{V} + \frac{C}{V^2} + \frac{D}{V^3} + \frac{E}{V^4} \qquad (32)$$

- **Property Equations**

The various physical and thermodynamic properties required in the flow and nucleation calculations are computed from the following equations.

The saturation pressure equation developed in References 4 and 7 has the form

$$\log_{10} P_s = a_1 + a_2/T + a_3 \log_{10} T \qquad (33)$$

where a_1, a_2, and a_3 are constants for a given metal vapor. By rewriting this equation for the saturation temperature corresponding to the vapor pressure P, subtracting the two equations and linearizing, the following approximate relation between supercooling, supersaturation pressure ratio, and temperature can be obtained:

$$\Delta T = \frac{-\Lambda_o T}{\Lambda_o - a_3 + \dfrac{a_2}{T \log_{10} e}} \qquad (34)$$

Surface tension of the liquid is correlated by an equation of the form:

$$\sigma = \sigma_o \left(1 - \frac{T}{T_c}\right)^{1.25} \qquad (35)$$

The liquid density at saturation pressure is correlated in References 4 and 7 by

$$\rho_L = \rho_o - \rho_1 (T-460) - \rho_2 (T-460)^2 \quad (36)$$

The enthalpy of the vapor derived from the virial equation of state in References 4 and 7 is

$$h_g = h_g^o - \frac{R_o T}{MJ} \left\{ \frac{1}{V} \left[B - T \left(\frac{dB}{dT} \right) \right] - \frac{1}{V^2} \left[C - \frac{T}{2} \left(\frac{dC}{dT} \right) \right] - \frac{1}{V^3} \left[D - \frac{T}{3} \left(\frac{dD}{dT} \right) \right] + \frac{1}{V^4} \left[E - \frac{T}{4} \left(\frac{dE}{dT} \right) \right] \right\} \quad (37)$$

where

$$h_g^o \; hg_o - hg_1 T - hg_2 \exp(-hg_3/T) \quad (38)$$

with hg_o, hg_1, hg_2, and hg_3 constants.

For calculating the enthalpy of vaporization the enthalpy of saturated liquid is expressed (4,7) by

$$h_L = h_{L0} + h_{L1} T + h_{L2} T^2 + h_{L3} T^3 \quad (39)$$

The enthalpy of vaporization of the super-saturated vapor is obtained by

$$h_{fg} = h_g - h_L \quad (40)$$

The specific volume of the vapor mixture is approximated by

$$v_m \cong xv = \frac{xV}{M} \quad (41)$$

The specific heat at constant pressure is given in References 4 and 7 by

$$C_{pv} = C_{pv}^o - \frac{R}{MJ} \left(1 - X_{C1} + \frac{TX_{C2}}{V} \right) \quad (42)$$

where

$$X_{C1} = \frac{\left(Z_c + T \frac{\partial Z_c}{\partial T} \right)^2}{\left(1 + \frac{2B}{V} + \frac{3C}{V^2} + \frac{4D}{V^3} + \frac{5E}{V^4} \right)} \quad (43)$$

$$X_{C2} = \left\{ \left(T \frac{d^2B}{dT^2} + \frac{2dB}{dT} \right) + \frac{1}{2V} \left(T \frac{d^2C}{dT^2} + \frac{2dC}{dT} \right) + \frac{1}{3V^2} \left(T \frac{d^2D}{dT^2} + \frac{2dD}{dT} \right) \right\} \quad (44)$$

$$C_{pv}^o = C_{po} + C_{pi} \exp\left(-C_{p2}/T \right) \quad (45)$$

- <u>Association</u>

The discussion of association is in terms of a method which successfully handled the association of cesium and potassium vapors. The molecular compositions of cesium and potassium are deduced from PVT data in References 4 and 7. The data indicate that potassium vapor consists primarily of monomer, dimer, and tetramer species, whereas cesium probably also contains species of still higher order. The molecular species reactions are represented by a series of independent equilibria of the type

$$iK = k_i \quad (46)$$

and the equilibrium constants are defined by

$$k_i = \frac{N_i}{N_1^i \left(\frac{P}{P_a} \right)^{i-1}} \quad (47)$$

Of the total vapor molecules, the fraction $\overline{N}_1$ exists as a monomer, and the remainder $1 - \overline{N}_1$, is assumed to exist as a dimer. The partial pressure of the monomer is the mole fraction $\overline{N}_1$ times the mixture pressure, or

$$P_1 = \overline{N}_1 P \quad (48)$$

The association is evaluated at both actual pressure and saturation pressure to obtain the ratio of partial pressure required in the nucleation expressions. The equilibrium constants k_2 and k_4 are expressed as functions of temperature in References 4 and 7 as follows:

$$\log_{10}(k_2) = k_{20} + k_{21}/T \quad (49)$$

and

$$\log_{10}(k_4) = k_{40} + k_{41}/T \quad (50)$$

The apparent equilibrium constant of dimerization $\overline{k}_2$, when all association is taken to be dimerization, can be expressed as a power series in terms of pressure and the true equilibrium constants:

$$\overline{k_2} = k_2 + \frac{2k_3 P}{P_a} + \frac{3k_4 P^2}{P_a^2} - \frac{2k_2 k_4 P^3}{P_a^3} + \dots \quad (51)$$

Then, the fraction of total atoms which remains as the monomer $\bar{N}_1$ is obtained from

$$\bar{k}_2 = \frac{\bar{N}_2}{\left(\bar{N}_1\right)^2 \left(\frac{P}{P_a}\right)} \tag{52}$$

where

$$\bar{N}_2 = 1 - \bar{N}_1 \tag{53}$$

Solution for $\bar{N}_1$ from these two equations gives

$$\bar{N}_1 = \frac{-1 - \sqrt{1 - \frac{4P\bar{k}_2}{P_a}}}{\left(\frac{2P\bar{k}_2}{P_a}\right)} \tag{54}$$

- Flow Equations

The flow through the turbine is described by one-dimensional flow equations. The flow is assumed to have uniform velocity and pressure across the flow area; thus curvature of flow path and radial pressure gradients due to rotation have been neglected. The description is intended to describe the mean diameter flow conditions. The differential form of the continuity, energy, and state equations are as follows:

$$\frac{1}{A}\frac{dA}{dz} + \frac{1}{W}\frac{dW}{dz} - \frac{1}{v}\frac{dv}{dz} + \frac{1}{x}\frac{dy}{dz} = 0, \tag{55}$$

$$\frac{W^2}{Jg}\left(\frac{1}{W}\frac{dW}{dz}\right) + x\frac{d}{dz}\left(h_g(V,T)\right) - h_{fg}\frac{dy}{dz} + y\,C_{pL}\frac{dT_L}{dz} = 0, \tag{56}$$

and

$$\frac{1}{P}\frac{dP}{dz} + \left(1 - \frac{V}{Z_c}\frac{\partial Z_c}{\partial V}\right)\left(\frac{1}{v}\frac{dv}{dz}\right) - \left(1 + \frac{T}{Z_c}\frac{\partial Z_c}{\partial T}\right)\left(\frac{1}{T}\frac{dT}{dz}\right) = 0 \tag{57}$$

It should be noted that the enthalpy change cannot be described by the form $C_p\,dT$ since enthalpy is pressure or volume dependent due to association reactions. The extra terms in the state equation arise from the use of the virial equations of state where the compressibility Z_c is a function of T and V. For an ideal gas, $Z_c = 1$ and the partial derivatives of Z_c are zero.

The momentum equation for a stream tube can be written as

$$\frac{W}{g}\frac{dW}{dz} = -v_m\frac{dP}{dz} - v_m F \tag{58}$$

where F is the friction force per unit volume of the flowing mixture. For an isentropic flow the change in enthalpy is $dh_s = v_m dP$. If it is assumed that irreversibilities (friction losses) are proportional to isentropic enthalpy change, the expression

$$-v_m F = (1 - \eta_p)\frac{dh_s}{dz} = (1 = \eta_p)\left(v_m\frac{dP}{dz}\right)$$

is obtained, and the momentum equation becomes

$$\frac{W}{g}\frac{dW}{dz} = -\eta_p\, v_m\frac{dP}{dz} \tag{59}$$

For a given value of η_p the description is that of a constant local condition expansion process; namely, for each increment in isentropic enthalpy drop, the fraction $(1 - \eta_p)$ appears as a friction loss which is converted to heating of the flow, and the remaining fraction η_p is the net gain in kinetic energy.

In the solution of the flow equations the quantities P, T, v, and W are treated as dependent variables with other quantities as independent variables. Simultaneous algebraic solution of the flow equations for the changes in P, T, v, and W gives the following:

$$\frac{1}{W}\frac{dW}{dz} = \frac{\Delta_W}{\Delta_o} \tag{60}$$

$$\frac{1}{v}\frac{dv}{dz} = \frac{1}{W}\frac{dW}{dz} + \frac{1}{A}\frac{dA}{dz} + \frac{1}{x}\frac{dy}{dz} \tag{61}$$

$$\frac{1}{P}\frac{dP}{dz} = -\left(\frac{W^2}{g}\right)\left(\frac{1}{W}\frac{dW}{dz}\right)\Big/\left(P\,x\,v\,\eta_p\right) \tag{62}$$

and

$$\frac{1}{T}\frac{dT}{dz} = \frac{\frac{1}{P}\frac{dP}{dz} + \left(1 - \frac{V}{Z_c}\frac{\partial Z_c}{\partial V}\right)\left(\frac{1}{v}\frac{dv}{dz}\right)}{\left(1 + \frac{T}{Z_c}\frac{\partial Z_c}{\partial T}\right)} \tag{63}$$

where

$$\Delta_o = P\,x\,v\,\eta_p\left[\frac{W^2}{Jg}\left(1 + \frac{T}{Z_c}\frac{\partial Z_c}{\partial T}\right) + x\,\phi\right] - \frac{W^2}{g}\,x\,T\frac{\partial}{\partial T}\left(h_g(V,T)\right) \tag{64}$$

$$\phi = T\left(1 - \frac{V}{Z_c}\frac{\partial Z_c}{\partial V}\right)\frac{\partial}{\partial T}\left(h_g(V,T)\right) + V\left(1 + \frac{T}{Z_c}\frac{\partial Z_c}{\partial T}\right)\frac{\partial}{\partial V}\left(h_g(V,T)\right) \tag{65}$$

and

$$\Delta_W = P\,x\,v\,\eta_p\left[\left(1 + \frac{T}{Z_c}\frac{\partial Z_c}{\partial T}\right)\left(h_{fg}\frac{dy}{dz} - y\,C_{pL}\frac{dT_L}{dz}\right) - \phi\left(\frac{1}{A}\frac{dA}{dz} + \frac{1}{x}\frac{dy}{dz}\right)\right] \tag{66}$$

- Turbine Description

The turbine geometry is required to compute the flow cross-sectional area. The passage for each blade row is described as the annular area between concentric truncated cones, with modification to account for blade thickness and blade angles. The axial cross-sectional area is

$$A_a = \frac{\pi}{4}\left(d_2^2 - d_1^2\right)\left(1 - \frac{t_b}{t_{bs}}\right) \quad (67)$$

The diameters and blade thicknesses are given by

$$d_1 = d_{1i} + (d_{1o} - d_{1i})\ z/L \quad (68)$$

$$d_2 = d_{2i} + (d_{2o} - d_{2i})\ z/L \quad (69)$$

and

$$t_b = t_{bi} + (t_{bm} - t_{bi})(1 - \frac{z}{L})\ \frac{4z}{L} \quad (70)$$

The blade shape is assumed to have a parabolic contour so that the local angle is

$$\cot\beta = \cot\beta_1 + (\cot\beta_o - \cot\beta_1)\ z/L \quad (71)$$

and the local gauging is

$$\sin\beta = \frac{1}{\sqrt{1 + \cot^2\beta}} \quad (72)$$

The cross-sectional area normal to the local flow direction is

$$A = A_a \sin\beta \quad (73)$$

The flow velocity relative to the blade is

$$w = U_a / \sin\beta \quad (74)$$

The changes in area with axial position are obtained by differentiating the above expressions.

- Approximation Method for Supersonic Exit Velocities

Special techniques are required to continue stepwise numerical integration of the flow equations through the transition from subsonic to supersonic flow due to the singularity in the flow equations at the critical point. An approximate method is derived which permits computation to proceed for flow through the throat of a convergent-divergent passage. Briefly, the method is to continue the numerical calculation until the critical point approaches some arbitrary amount, say $W = 0.95\ C_{crit}$. At this point special equations are employed to obtain the flow properties at the critical point and at some point just past the throat where the flow is supersonic. The stepwise integration can then be continued.

The following assumptions are made to extrapolate the flow variables from the subsonic to the supersonic state.

1) The enthalpy change of the condensate is neglected.

2) The value of η is maintained at the original value for the particular nozzle.

3) The condensation can be calculated from the supercooling at the beginning and end points.

4) Certain vapor properties during the extrapolation are defined by their effective values at the starting point of the extrapolation.

The flow equations described in a previous section can be integrated in a manner similar to the case of isentropic expansion of an ideal gas except that condensation terms are also included.

The critical point occurs when the denominator of the solution for $\frac{dw}{dz}$ is equal to zero, namely when $\Delta_o = 0$, as defined by Eq. 64. Rearranging the expression for Δ_o and setting $\Delta_o = 0$ to find the critical speed gives

$$Px^2 v \eta_p \phi \left(1 - \frac{W^2}{C_{crit}^2}\right) = 0 \quad (75)$$

where

$$C_{crit}^2 = \frac{R_o \gamma_\eta gT}{M} \quad (76)$$

and

$$\gamma_\eta = \frac{M x}{R_o}\left[\frac{V_z \frac{\partial h_g(V,T)}{\partial T} + \frac{VT_z}{T}\frac{\partial h_g(V,T)}{\partial V}}{\frac{T}{P v \eta_p}\frac{\partial h_g(V,T)}{\partial T} - \frac{T_z}{J}}\right] \tag{77}$$

Thus, the critical point is reached when $W = C_{crit}$, where C_{crit} is defined by Eq. 76 and where γ_η is assumed to be a constant calculated from the properties at the initial state point of the extrapolation. The symbols V_z and T_z are defined by equations 80 and 81.

For smooth flow transition through the critical point, the numerator in the solution for $\frac{dw}{dz}$ must be zero simultaneously with $\Delta_o = 0$. This requires that $\Delta_w = 0$, which from Eq. 66 is found to occur when

$$\frac{1}{A}\frac{dA}{dz} - \left(\frac{T_z h_{fg}}{\phi} - \frac{1}{x}\right)\frac{dy}{dz} = 0 \tag{78}$$

Since $\frac{dy}{dz}$ is positive during an expansion and the term in parentheses is also positive for x near 1, the critical point must occur at a location where $\frac{dA}{dz}$ is positive, that is at some point past the throat of the passage. For the present work the assumption is made that the critical point occurs at the throat, so that the minimum area is taken as A*.

The flow equations will now be integrated by defining a number of pseudo properties which are held constant during the extrapolation. From the first assumption (page 2-7) above, the term $\frac{dT_L}{dz}$ is set equal to zero in the energy equation 56. Eliminating $\frac{dP}{dz}$ and $\frac{dW}{dz}$ from the momentum, energy, and state equations 56, 57, and 59 gives

$$\frac{1}{T}\frac{dT}{dz} + \left(\frac{\phi_V - V_z}{\phi_T - T_z}\right)\frac{1}{v}\frac{dv}{dz} + \left(\frac{J h_{fg}}{P v \eta_p (\phi_T - T_z)}\right)\frac{1}{x}\frac{dx}{dz} = 0 \tag{79}$$

where

$$V_z = \left(1 - \frac{V}{Z_c}\frac{\partial Z_c}{\partial V}\right) \tag{80}$$

$$T_z = \left(1 + \frac{T}{Z_c}\frac{\partial Z_c}{\partial T}\right) \tag{81}$$

$$\phi_V = \frac{V J \frac{\partial h_g(V,T)}{\partial V}}{P v \eta_p} \tag{82}$$

and

$$\phi_T = \frac{J T \frac{\partial h_g(V,T)}{\partial T}}{P v \eta_p} \tag{83}$$

Defining

$$k_\eta - 1 = \frac{\phi_V + V_z}{\phi_T - T_z} \tag{84}$$

and

$$\lambda_\eta = \frac{J h_{fg}}{P v \eta_p (\phi_T - T_z)} \tag{85}$$

and assuming k_η and λ_η are constant during the extrapolation of their initial values, Eq. 79 can be integrated to give

$$\frac{v}{v_1} = \left[\frac{T}{T_1}\left(\frac{x}{x_1}\right)^{\lambda_\eta}\right]^{\frac{1}{1-k_\eta}} \tag{86}$$

where the subscript 1 refers to values at the starting point of the extrapolation.

Also assuming T_z and V_z are constant during the extrapolation, the state equation 57 can be integrated to give

$$\frac{P}{P_1} = \left(\frac{T}{T_1}\right)^{T_z}\left(\frac{v}{v_1}\right)^{-V_z} \tag{87}$$

Integration of continuity equation 60 gives

$$\frac{A}{A_1} = \frac{\left(\frac{v}{v_1}\right)\left(\frac{x}{x_1}\right)}{\left(\frac{W}{W_1}\right)} \tag{88}$$

Substituting the expression for $\frac{1}{v}\frac{dv}{dz}$ from Eq. 79 into the energy equation 56 yields

$$\frac{W}{Jg}\frac{dW}{dz} + C_\eta \frac{1}{T}\frac{dT}{dz} + h_\eta \frac{dx}{dz} = 0 \tag{89}$$

Complex conjugate of A = A

where

$$C_\eta = x\left[T\frac{\partial h_g(V,T)}{\partial T} - \frac{V}{(k_\eta - 1)}\frac{\partial h_g(V,T)}{\partial V}\right] \quad (90)$$

and

$$h_\eta = h_{fg} - \frac{\lambda_\eta}{k_\eta - T}\left(V\frac{\partial h_g(V,T)}{\partial V}\right) \quad (91)$$

By assuming the values of C_η , and h_η to be constant at their initial values, Eq. 89 can be integrated to give

$$\frac{W^2}{2gJ} + C_\eta T + h_\eta x = \frac{W_1^2}{2gJ} + C_\eta T_1 + h_\eta x_1 \quad (92)$$

At the critical point, $W^2 = C^2_{crit} = C_\eta R_o g\, T/M$.

Then, denoting the temperature at the critical point by T*, the energy equation at the critical point gives

$$\frac{T^*}{T_1} = \frac{1 + \frac{W_1^2}{2gJC_\eta T_1} + \frac{h_\eta}{C_\eta T_1}\left(x_1 - x^*\right)}{1 + \frac{\gamma_\eta R_o}{2MJC_\eta}} \quad (93)$$

Equations 86, 87 and 76 written at the critical point then give

$$\frac{v^*}{v_1} = \left[\frac{T^*}{T_1}\left(\frac{x^*}{x_1}\right)^{\lambda_\eta}\right]^{\frac{1}{1-k_\eta}} \quad (94)$$

$$\frac{P^*}{P_1} = \left(\frac{T^*}{T_1}\right)^{T_z}\left(\frac{v^*}{v_1}\right)^{-V_z} \quad (95)$$

and

$$W^* = \sqrt{\lambda_\eta g \frac{R_o T_1}{M}\left(\frac{T^*}{T_1}\right)} \quad (96)$$

The critical area ratio can then be found from

$$\frac{A^*}{A_1} = \frac{\left(\frac{v^*}{v_1}\right)\left(\frac{x^*}{x_1}\right)}{\left(\frac{W^*}{W_1}\right)} \quad (97)$$

Provided x* is known, Eqs. 94, 95, 96, and 97 define the conditions at the critical point in terms of those at the start of the extrapolation.

An iteration technique is required to determine x* to complete the description of the critical point conditions. It is assumed that the condensation rate is proportional to the supercooling rate for the drops that already exist and no new drops are formed. Let the supercooling at the start of the extrapolation be ΔT_1, and at the critical point, ΔT^*. The average supercooling rate is

$$\overline{\Delta T} = \frac{1}{2}\left(\Delta T_1 + \Delta T^*\right) \quad (98)$$

and the average condensation rate is

$$\left(\overline{\frac{dy}{dz}}\right) = \left(\frac{dy}{dz}\right)_1\left(\frac{\overline{\Delta T}}{\Delta T_1}\right) \quad (99)$$

Integrating and expressing the results in terms of x gives

$$x^* = x_1 - \left(\frac{dy}{dz}\right)_1\left(\frac{\overline{\Delta T}}{\Delta T_1}\right)\left(z^* - z_1\right) \quad (100)$$

From the geometry, z* is known as the location of A_{min}. A value of ΔT^* is assumed and x* is calculated. Then T*, v*, and P* are calculated and the value of ΔT^* is found from Eqs. 33 and 34. When ΔT^* matches the assumed value, the critical point is specified. Then, it is necessary to compare the value of A* with the actual minimum area A_{min}. If A* and A_{min} are not within a specified tolerance, the inlet velocity is corrected and calculations begin anew at the turbine inlet. When A* and A_{min} agree, the extrapolation is continued to a point past the throat in the case of a convergent-divergent passage, or the extrapolation ends at the throat for a convergent passage. Let A_2 be the area at this point to which the extrapolation takes place. The Mach number at this position is estimated by approximate expression to start the iteration, or

$$M_2 = \sqrt{\frac{2\left(A_2 - A_{min}\right)}{A_{min}\left(3 - k_\eta\right)}} \quad (101)$$

Then x_2 is found from

$$x_2 = x^* - \left(\frac{dy}{dz}\right)\left(z_2 - z^*\right) \quad (102)$$

The values of T_2, v_2, P_2, W_2 and A_2 are then found with Eqs. 93, 94, 95, 96, and 97 rewritten in terms of conditions at position 2. Thus,

$$\frac{T_2}{T_1} = \frac{1 + \frac{W_1^2}{2gJC_\eta T_1} + \frac{h_\eta}{C_\eta T_1}\left(x_1 - x_2\right)}{1 + \frac{M_2^2\left(\gamma_\eta R_o\right)}{2MJC_\eta}} \quad (103)$$

$$\frac{v_2}{v_1} = \left[\frac{T_2}{T_1}\left(\frac{x_2}{x_1}\right)^{\lambda_\eta}\right]^{\frac{1}{1-k_\eta}} \qquad (104)$$

$$\frac{P_2}{P_1} = \left(\frac{T_2}{T_1}\right)^{T_z}\left(\frac{v_2}{v_1}\right)^{-V_z} \qquad (105)$$

$$\frac{W_2}{W_1} = \sqrt{\gamma_\eta\, g\, \frac{R_o T_1}{M}\left(\frac{T_2}{T_1}\right)} \qquad (106)$$

and

$$\frac{A_2}{A_1} = \frac{\left(\frac{v_2}{v_1}\right)\left(\frac{x_2}{x_1}\right)}{\left(\frac{W_2}{W_1}\right)} \qquad (107)$$

If A_2 does not agree with the desired value, M_2 is corrected until A_2 converges. These properties are then used as inputs to continue the stepwise integration process. Each type of moisture, including surface condensate, is assumed to increase in the same proportion during the extrapolation, and these new values are also required as inputs for continuing stepwise integration.

- Expansion from Stagnation to Static Inlet Conditions

The inlet to the turbine is specified by the stagnation temperature T_o, and the axial velocity U_{ao} at the first stator inlet. In the case where the inlet is supersaturated, the inlet temperature T_o is obtained from its value corresponding to the equilibrium state as P_s and T_s and moisture fraction y by using the relationship:

$$T_o = T_s - \frac{y\, h_{fg}}{C_{pv}} \qquad (108)$$

The expansion from stagnation to static conditions at the inlet is evaluated by the same technique used in the extrapolation. The values of C_η and k_η are evaluated at the inlet stagnation state, which is analogous to state point 1 in the extrapolation. The static temperature is obtained from

$$T = T_o - U_{ao}^2 \Big/ \left(2\, g\, J\, C_\eta \sin^2 \beta_1\right) \qquad (109)$$

The specific volume is obtained from

$$v = v_o \left(\frac{T}{T_o}\right)^{\frac{1}{1-k_\eta}} \qquad (110)$$

and the pressure from the state equation using the values of v and T to evaluate the compressibility.

2.2.3 Method of Solution

The numerical solution to the problem consists of integrating the continuity, energy, state, and momentum equations 60, 61, 62, and 63 for the area change obtained from the turbine geometry and the rate of change of condensate as determined by the nucleation and growth expressions. A stepwise integration is performed using the ICEADAMS integration procedure listed in Appendix B. Basically, the order of calculation is as follows. Knowing the properties T, P, v, and the velocity W at a point, the property equations are used to calculate

$$Z_c, \frac{\partial Z_c}{\partial T}, \frac{\partial Z_c}{\partial V}, C_{pv}, h_g, \frac{\partial h_g}{\partial V}, \frac{\partial h_g}{\partial T}, h_{fg}, \rho_L, \sigma_L, P_s, \Lambda_o, \Delta T, T_s, r, \text{ and } T_{rec}$$

The association expressions are then used to obtain k_2', P_1, P_{1s}, and A_1. The turbine description gives $\frac{dA}{dz}$. The nucleation expression gives $\dot{J}$ and $\frac{dN_i}{dz}$ for the group of droplets being formed at the present value of z. The droplet growth and surface condensation expressions are evaluated to obtain $\frac{dr_{Li}}{dz}$, $\frac{dT_L}{dz}$, and $\frac{dy}{dz}$. These calculations then provide the required data to calculate $\frac{dT}{dz}$, $\frac{dP}{dz}$, $\frac{dv}{dz}$, and $\frac{dW}{dz}$ which are used to obtain the new values at the end of the integration step. This brief description is intended only as an overall view of the calculation routine.

A listing of the computer code is given in Appendix A. The list of input quantities is given in Appendix C in the order required by the code. A flow chart for the code, showing the major control and logic, is provided in Appendix D. The correspondence between the code symbols and the text symbols is given in the nomenclature. Appendix E gives a description of the function and use of the control variables not included in the text.

2.2.4 Sample Turbine Calculation Results

The computer code was run for a three-stage potassium turbine. The numerical input data used are listed in Appendix C, except for the turbine geometry description which is presented in Table 2.2-1. The stagnation inlet state is defined by $T = 2010^{\circ}R$, $P_o = 30.2$ psia $= 4349$ lb/ft^2, and $x = 0.99$. The inlet is assumed to be supersaturated, and the inlet temperature corrected for moisture content by Eq. 108 is $T_o = 1982.9^{\circ}R$. The summary of calculation results provided by the computer printout is shown in Table 2.2-2, and the output nomenclature when the mean radius is in feet and units are given in Table 2.2-3. A typical printout is shown in Table 2.2-4 for the conditions at the exit of the second stator with corresponding nomenclature and units given in Table 2.2-5.

The value of y_e calculated by the computer program requires correction due to variable specific heat between supercooled and saturated state points. The value of y_e is obtained from

$$y_e = y + \frac{\Delta T \, C_{pv}}{h_{fg}}$$

where y_e is the equivalent moisture, and C_{pv} is the specific heat at the supersaturated state. The correction to be applied is

$$y_e' = y + \frac{(y_e - y)}{2} \left[1 + \frac{\left(C_{pv}\right)_{sat}}{C_{pv}} \right]$$

The value of C_{pv} is obtained from the computer printout and $\left(C_{pv}\right)_{sat}$ may be obtained from any suitable source of thermodynamic property values for the specific turbine fluid. For this particular example, see Reference 4. In Table 2.2-2, the value of C_{pv} is 0.36 Btu/lb-$^{\circ}$R, and $\left(C_{pv}\right)_{sat}$ is found to be 0.28. Thus, the corrected equilibrium moisture content is 0.102 and the tabulated value is 0.105. The correction is larger when greater supercooling exists. The correction required on the value of y_e does not affect any other calculations in the program.

TABLE 2.2-1

EXAMPLE TURBINE GEOMETRY FOR THREE-STAGE POTASSIUM TURBINE

Row	1	2	3	4	5	6
Inlet Mean Diameter (In.)	7.693	8.080	8.17	8.68	8.80	9.22
Inlet Blade Height (In.)	0.605	0.772	0.66	1.076	1.04	1.59
Outlet Mean Diameter (In.)	8.08	8.17	8.68	8.80	9.22	9.31
Outlet Blade Height (In.)	0.772	0.66	1.076	1.04	1.59	1.53
Expansion Efficiency (η_p)	0.95	0.80	0.95	0.80	0.90	0.80
Axial Length (ft)	0.1166	0.081	0.0955	0.0903	0.101	0.0983
Inlet Angle (degrees)	90	26.41	124.72	30.19	121.32	47.70
Outlet Angle (In.)	14.5	154.65	16.70	152.14	21.55	146.95
Blade Pitch (In.)	0.653	0.41	0.572	0.455	0.641	0.557
Edge Blade Thickness (In.)	0.012	0.0125	0.012	0.012	0.012	0.012
Blade Velocity (ft/sec)	0	641	0	689	0	734
Maximum Blade Thickness (In.)	0.12	0.166	0.100	0.154	0.120	0.125

The Wilson point occurred at $z/L \cong 0.63$ inch in the second stator row at a corrected equivalent moisture content of 7.4 percent. The expansion rate at the Wilson point was approximately $P = 2500$/sec.

The Wilson point occurred at a supersaturation pressure ratio of 2.32. With all other parameters fixed, the classical nucleation theory would predict a critical supersaturation ratio of about 2.13. In the present case this will shift the Wilson point slightly within the second stator.

The turbine geometry used has a diffuser-type section in the first part of the second rotor, causing the flow to return to the saturation state. The condensation zone in which nuclei growth occurred was located in this portion of the second rotor and the flow remained near the saturated state throughout the remainder of the turbine.

The results of the present calculations can be compared in a qualitative manner with the results of Goldman and Nosek[8] in which saturated potassium vapor was expanded in a convergent-divergent nozzle. Although their results are somewhat inconclusive, it appears that condensation occurred when the ratio of pressure to initial saturation pressure was between 0.31 and 0.33 at an axial distance of about 3 inches from the nozzle inlet. In the present example, condensation is predicted at a pressure/inlet saturation pressure ratio of 0.324.

TABLE 2.2-2

COMPUTER OUTPUT SUMMARY SHEET FOR THE THREE-STAGE TURBINE EXAMPLE

SUMMARY OF RESULTS OF CONDENSATION CALCULATIONS

ROW	T	P	VV	W	UA	YE	YS	Y	RMEAN	NTOTAL
0	1970.7	4324.7	16.03	333.4	333.4	0.00000	0.00000	0.00000	0.0000E+00	0.0000E+00
1	1786.4	2765.9	22.19	1375.5	343.3	0.06189	0.00000	0.00000	0.0000E+00	0.0000E+00
2	1731.1	2336.8	25.28	1056.7	452.4	0.07921	0.00000	0.00000	9.9317E-08	1.4163E+12
3	1685.1	1360.9	44.28	1484.4	426.6	0.10519	0.00000	0.06805	9.9459E-07	4.2736E+14
4	1712.8	1114.3	56.52	1146.3	533.9	0.11004	0.00000	0.10182	1.1401E-06	4.2736E+14
5	1666.5	784.0	79.06	1232.3	452.6	0.13338	0.00000	0.12930	1.2300E-06	4.2736E+14
6	1601.4	554.1	107.95	1146.7	624.0	0.15442	0.00000	0.14664	1.2762E-06	4.2736E+14

TABLE 2.2-3

NOMENCLATURE AND UNITS FOR COMPUTER OUTPUT

Title	Code Symbol	Text Symbol	Units
RØW	S	Blade row index	---
T	T	T	°R
P	P	P	lb/ft^2
VV	VV	υ	ft^3/lb
W	W	W	ft/sec
UA	UA	U_a	ft/sec
YE	YEQUILIB	y_e	---
YS	YSURFACE	$y_b + y_{bo} + y_{abs}$	---
Y	YSUM	y	---
RMEAN	RMEAN	$\bar{r} = \left(\frac{3y}{\rho_L 4\pi \Sigma N_{ri}}\right)^{1/3}$	ft
NTØTAL	NTØTAL	ΣN_{ri}	lb^{-1}

An earlier condensation in terms of pressure ratio, in the turbine as compared to the supersonic nozzle, is expected due to the lower expansion rate.

According to Linhardt, condensation in his tests occurred upstream of the nozzle throat. This would imply a ratio of condensation point pressure to inlet saturation pressure ratio greater than 0.5. This is contrary to the Goldman and Nosek experiment and theoretical calculation.

The droplet size results can be compared with results obtained by Linhardt[9]. His analysis of his experiment predicts a droplet radius of 0.05 microns for 10 percent exit moisture in his test No. 4. His tests 2, 3 and 4 had the same stagnation condition and the same nozzle except for length. With critical flow in the nozzle, the conditions at the condensation point would be unchanged due to the additional length of the nozzle. Thus, for the same conditions at the Wilson point the droplet radius at the nozzle exit is expected to be proportional to $(y_e)^{1/3}$, where y_e is the moisture fraction at the nozzle exit.

TABLE 2.2-4

COMPUTER OUTPUT INTERMEDIATE SUMMARY
SHEET FOR THE SECOND STATOR EXIT

COUNT	STEP SIZE H	Z
22	2.5000000E-04	9.5500000E-02

P	T	SP. VOL.-V	W	U-AXIAL	Z-COMPRESS	
1.36086E+03	1.68511E+03	4.42755E+01	1.48440E+03	4.26557E+02	9.04912E-01	
DP	**DT**	**DV**	**DW**	**-(DP/DT)/P**	**AREAA**	**DA/A**
-1.14633E+05	-2.49928E+04	2.98666E+03	9.73836E+04	3.59311E+04	2.87259E+01	-3.58485E-01
DELTAT	**TLIQUID**	**LAMBDA0**	**LAMBDA1**	**JOUT**	**RCRITICAL**	**DN/DZ**
8.64861E+01	1.77101E+03	5.16223E-01	4.72843E-01	1.35274E-07	6.93401E-09	1.30937E-08
K2	**K4**	**K2PRIME**	**HFG**	**CPVD**	**CPV**	**SIGMA**
1.95664E-01	1.02667E-02	2.07326E-01	8.40427E+02	1.27000E-01	3.60882E-01	4.21801E-03
TOTAL MOISTURE	**PARTIAL P1**	**QUALITY**	**MEAN RADIUS**	**TOTAL DROPS**	**K2PRIME SAT**	**SINBETA**
6.80549E-02	1.21603E+03	9.31945E-01	9.94586E-07	4.27356E+14	1.99970E-01	2.87361E-01
Y-EQUILIB	**HG**	**HL**	**HFG**	**DELU**	**DELW**	**1-M*2**
1.05192E-01	1.15772E+03	3.17295E+02	8.40427E+02	1.62210E+06	1.06417E+08	5.94087E-02
YB=Y BLADE	**YBD=Y CASE**	**YABS=YATOMIZED**	**YSURFACE**	**NATOMIZE**		
0.00000E+00	0.00000E+00	0.00000E+00	0.00000E+00	0.00000E+00		

GROUP	MOISTURE	NUMBER	RADIUS	DMOISTURE	DNUMBER	DRADIUS
1	1.2972271E-03	1.4163227E+12	1.7819811E-06	1.4155714E-02	0.0000000E+00	6.4818298E-06
2	3.0755897E-03	3.5449487E+12	1.7500804E-06	3.4690616E-02	0.0000000E+00	6.5799160E-06
3	1.2008010E-03	3.2210567E+12	1.3206145E-06	2.2539314E-02	0.0000000E+00	8.2627470E-06
4	2.0584719E-03	6.5642729E+12	1.2466311E-06	4.2816629E-02	0.0000000E+00	8.6433924E-06
5	4.1815108E-03	1.5990821E+13	1.1733818E-06	9.6821046E-02	0.0000000E+00	9.0563797E-06
6	9.0587305E-03	4.2679487E+13	1.0945474E-06	2.3704503E-01	0.0000000E+00	9.5472175E-06
7	2.1244067E-02	1.3342308E+14	9.9453654E-07	6.5696240E-01	0.0000000E+00	1.0251852E-05
8	2.5938509E-02	2.2051609E+14	8.9905601E-07	9.5454880E-01	0.0000000E+00	1.1028555E-05
9	0.0000000E+00	0.0000000E+00	0.0000000E+00	0.0000000E+00	0.0000000E+00	0.0000000E+00
10	0.0000000E+00	0.0000000E+00	0.0000000E+00	0.0000000E+00	0.0000000E+00	0.0000000E+00

Viewed in this way, the results of Linhardt's test 3 corrected to 10 percent moisture would give a radius of 0.06 microns while Linhardt's test 2 would give a 0.26 micron radius. The present calculations indicate a mean radius of 0.35 microns at 10 percent moisture. The larger size is consistent with the lower expansion rate.

2.2.5 Discussion

The results obtained by the condensation code have been in general agreement with the limited experimental data available for comparison. The variable with the greatest influence on the location of the Wilson point is the surface tension. It appears that the correlation used provides satisfactory agreement and is suggested for use until further experimental data are available.

The computer code performance has been satisfactory for subsonic turbine analysis. On occasion, choking flow conditions have been encountered in turbines designed for subsonic flow. This difficulty is due to the relatively simple blade profile and blade thickness expressions which are not general enough to give the same flow area as an actual blade when the actual blade thickness is used in

TABLE 2.2-5

NOMENCLATURE AND UNITS FOR COMPUTER OUTPUT

Title	Code Symbol	Text Symbol	Units
CØUNT	CØUNT	Steps since last output	---
STEP SIZE H	H	Step size	ft
Z	Z	z	ft
P	P	P	lb/ft^2
T	T	T	$^\circ R$
SP. VØL.-V	VV	v	$ft^3/16$
w	W	W	ft/sec
U-AXIAL	UA	U_a	ft/sec
Z-CØMPRESS	ZC	Z_c	---
DP	DP	dP/dz	lb/ft^3
DT	DT	dT/dz	$^\circ R/ft$
DV	DVV	dV/dz	ft^2/lb
DW	DW	dW/dz	1/sec
-(DP/DT)/P	PDØT	1/P dP/dt	1/sec
AREAA	AREAA	A_a	$in.^2$
DA/A	DA	1/A dA/dz	---
DELTAT	DELTAT	ΔT	$^\circ R$
TLIQUID	TLIQ	T_L	$^\circ R$
LAMBDA0	LAMBDA0	Λ_0	---
LAMBDA1	LAMBDA1	Λ_1	---
JDØT	JDØT	$\dot{J}$	$1/ft^3$ sec
RCRITICAL	RCRIT	r_{crit}	ft
DN/DZ	NEU	$\dot{J}v/U_a$	1/lb ft
K2	K2	k_2	1/atm
K4	K4	k_4	$1/atm^3$
K2 PRIME	K2 PRIME	k_2	1/atm
HFG	HFG	h_{fg}	Btu/lb
CPV0	CPV0	C^{o}_{pv}	$Btu/lb^\circ R$
CPV	CPV	C_{pv}	$Btu/lb^\circ R$
SIGMA	SIGMA	σ	lb/ft
TØTAL MØISTURE	YSUM	y	---
PARTIAL PI	PI	P_1	lb/ft^2
QUALITY	X	x	---
MEAN RADIUS	RMEAN	$\bar{r} = \left(\frac{3y}{4\pi\rho_L \Sigma N_{ri}}\right)^{1/3}$	ft
TØTAL DRØPS	NTØTAL	N_{ri}	1/lb
K2 PRIME SAT	K2PRIMES	k_2 at saturation	1/atm
SINBETA	SINB	$\sin\beta$	---
Y - EQUILIB	YEQUILIB	y_e	---
HG	HG	h_g	Btu/lb
HL	HL	h_L	Btu/lb
HFG	HFG	h_{fg}	Btu/lb
DELØ	DELØ	Δ_o	Btu ft/lb
DELW	DELW	Δ_w	Btu/lb
1 - M*2	DELØS	$1-W^2/C^2_{crit}$	---
YB = YBLADE	YB	y_b	---
YBØ = Y CASE	YBØ	y_{bo}	---
YABS = YATØMIZED	YABS	y_{abo}	---
YSURFACE	YSURFACE	$y_b+y_{bo}+y_{bs}$	---
NATØMIZE	NATØMIZE	Number of atomized drops	1/lb
GROUP	I	Index denoting group	---
MOISTURE	Y [I]	y_i	---
NUMBER	NL [I]	N_{ri}	1/lb
RADIUS	RL [I]	r_i	ft
DMØISTURE	DY [I]	dy_i/dz	1/ft
DNUMBER	DNL [I]	dN_{ri}/dz	1/ft - lb
DRADIUS	DRLD [I]	dr_i/dz	---

the expressions. This difficulty is overcome by decreasing the blade thickness. The blade heights used should also correspond to the actual flow areas.

In the present version of the program, the inlet angles to blade rows are modified to line up with the relative velocity vector at the inlet to the blade row. The incidence angle effect could be approximated by assuming that an additional blade row exists between each actual blade row to provide the expansion or compression effect of non-zero incidence.

The code has a provision for extrapolating through the critical point from subsonic to supersonic flow. After one such extrapolation, subsequent blade thicknesses must be modified to accommodate the flow, since no provision for shock waves is included. The code has a provision for automatically adjusting blade thickness; however, the code did not converge in the case of a cesium turbine analysis.

The subsonic-supersonic transition worked smoothly when the correct blade thickness was supplied as input. Careful description of the flow areas at the throat and exit of a supersonic blade row is required to obtain a desired exit velocity since an increase in Mach number from 1.00 to approximately 1.10 will occur for a change in the exit-to-throat area ratio from 1.00 to 1.01.

In summary, the code has performed satisfactorily for subsonic turbines but requires careful input to obtain desired area ratios for turbines having supersonic flow.

2.2.6 Nomenclature

Test Symbol	Code Symbol	Definition - Units
A	-	Flow cross-sectional area, (ft^2)
A_a	AREAA	Axial cross-sectional area, (ft^2)
A_1, A_2	A1, A2	Flow cross-sectional area at points 1 and 2, (ft^2)
A_{min}	AMIN	Minimum flow cross section, (ft^2)
A^*	-	Critical minimum flow cross section, (ft^2)
a_1, a_2, c_3	APS, APS1, APS2	Constants describing saturation pressure, (ft^3/lb mole)
B, B_1, B_2	B, B1, B2	Constants in virial equation of state, (ft^3/lb mole), (-), (^oR)
C, C_1, C_2, C_3	C, C1, C2, C3	Constants in virial equation of state, (ft^3/lb mole)^2, (-), (^oR), ($^oR^2$)
C_{crit}	CCRIT	Critical speed of mixture, (ft/sec)
C_{pL}	CPL	Specific heat of liquid, (Btu/lb^{o}R)
C_{pv}	CPV	Specific heat of vapor, (Btu/lb^{o}R)
$C_{p\dot{v}}$	CPV	Temperature dependent term in expression for C, (Btu/lb^{o}R)
C_{p0}, C_{p1}, C_{p2}	ACP0, ACP1, ACP2	Constants defining C_{pv}^o as a function of T, (Btu/lb^{o}R), (Btu/lb^{o}R), (^oR)
C_η	CETA	Effective specific heat (Btu/lb^{o}R)
D, D_1, D_2	D, D1, D2	Constants in virial equation of state, (ft^3/lb mole)^3, (-), (^oR)
d_1, d_{1I}, d_{1O}	DIA1, DIA1I, DIA1Ø	Hub passage diameter, at stage inlet, at stage outlet, (ft)
d_2, d_{2I}, d_{2O}	DIA2, DIA2I, DIA2Ø	Tip passage diameter, at stage inlet, at stage outlet, (ft)
E, E_1	E, E1	Constants in virial equation of state (ft^3/lb mole)^4
F	-	Friction force per unit volume of flow, (lb/ft^3)
g	G	Acceleration of gravity, (ft/sec^2)
h_{abs}	HABS	Heat transfer coefficient, atomized moisture, (Btu/sec ft^2 ^oR)
h_{amb}	HAMB	Heat transfer coefficient, casing to ambient, (Btu/sec ft^2 ^oR)
h_b	HB	Heat transfer coefficient on blade surface, (Btu/sec ft^2 ^oR)
h_c	-	Heat transfer coefficient, (Btu/ft^2 ^oR)
h_{fg}	HFG	Latent heat of vaporization, (Btu/lb)
h_g	HG	Enthalpy of vapor, (Btu/lb)
$h_g^{\cdot}$	HG0	Enthalpy of monomer species, (Btu/lb)
h_{g0}, h_{g1}, h_{g2}, h_{g3}	AHG, AHG1 AHG2, AHG3	Constants defining temperature dependence of hg^o, (Btu/lb), (^oR Btu/lb), (Btu/lb), (^oR)
h_L	HL	Enthalpy of saturated liquid, (Btu/lb)
h_{L0}, h_{L1}, h_{L2}, h_{L3}	AHL, AHL1, AHL2, AHL3	Constants defining temperature dependence of h_L, (Btu/lb), (Btu/lb^{o}R), (Btu/lb^{o}R^2), (Btu/lb^{o}R^3)
h_η	HETA	Effective heat of vaporization, see Eq. 91, (Btu/lb^{o}R)
J	J	Mechanical equivalent of heat, (ft-lb/Btu)
$\dot{J}$	JDØT	Nucleation rate, (1/ft^3sec)
K	-	Chemical symbol for potassium
k_i	K2, K4	Equilibrium constants for species i = 2, 4(atm)$^{i-1}$
$k_{i,0}$, $k_{i,1}$	AK2, AK21, AK4 AK41	Constants defining temperature dependence of k, (-), (^oR), (-), (^oR)
k_2	K2PRIME	Apparent equilibrium constant, (atm)$^{-1}$
k_v	KV	Vapor thermal conductivity (Btu/sec ft ^oR)
k_η	KETA	Effective polytropic exponent, (-)
ℓ	-	Length along chord, (ft)
L	LENGTHB	Axial length of blade row, (ft)
$\dot{m}$	-	Mass flow rate, (lb/sec)
M	M	Molecular weight of monomer vapor, (lb/lb mole)
M_2	M2	Mach number at point 2, (-)
N_0	N0	Avogadro's number, (molecules/lb mole)
N_i	-	Molal concentration of species i, (-)
$\bar{N}_i$	N1PRIME	Apparent molal concentration of species i, (-)
N_{ri}	NL [I]	Droplets per pound in group i, (1/lb)
P	P	Static pressure, (lb/ft^2)
P_a	PATM	Atmospheric pressure conversion constant, (lb/ft^2/atm)
P_1	-	Partial pressure of species i, (lb/ft^2)
P_{eff}	PEFF	Pressure term in nucleation equation, (lb/ft^2)
$\dot{P}$	PDØT	Expansion rate defined by $\frac{1}{P}\frac{dP}{dt}$, (1/sec)
P_o	PØ	Inlet stagnation pressure, (lb/ft^2)
P_{1s}	P1S	Partial pressure of monomer at saturation pressure corresponding to vapor temperature, (lb/ft^2)
P_r	PRANDTL	Prandtl number, (-)

Nomenclature (Continued)

P_s	PS	Saturation pressure at vapor temperature, (lb/ft^2)
$\dot{Q}$	-	Heat transfer rate to blade surface, (Btu/sec)
R_o	R0	Universal gas constant, (ft-lb/lb mole^{o}R)
r	RECF	Recovery factor, (-)
$\bar{r}$	RMEAN	Radius of mean droplet, (ft)
r_{abs}	RABS	Atomized drop radius, (ft)
r_{crit}	RCRIT	Critical radius, (ft)
r_i	RL [I]	Droplet radius of group i, (ft)
S	-	Perimeter of flow passage, (ft)
T	T	Vapor temperature, (^oR)
T_{amb}	TAMB	Ambient temperature, (^oR)
T_c	TC	Critical vapor temperature, (^oR)
T_L	TL	Condensate temperature, (^oR)
T_o	TEMPØ	Inlet stagnation temperature, (^oR)
T_{rec}	TREC	Adiabatic recovery temperature, (^oR)
T_{ri}	-	Temperature of droplets in group i, (^oR)
T_s	TSAT	Saturation temperature at pressure P, (^oR)
T_z	TZ	Parameter, see Eq. 81, (-)
T^*	-	Temperature at critical point, (^oR)
T_1, T_2	ØLDT, T2	Temperature at point 1, 2, (^oR)
ΔT, ΔT^*, ΔT_1, $\Delta\bar{T}$	DELTAT, -, ØLDDELTAT, TDS	Supercooling, at critical point, at point 1, average during extrapolation, (^oR)
t	-	Time, (Sec)
t_b, t_{bi}, t_{bm}	THICKB, THICKBØ, THICKBMAX	Blade thickness, at stage inlet, maximum blade thickness, (ft)
t_{bs}	BLADESPACE	Blade spacing at mean diameter, (ft)
t_f	-	Thickness of flow channel, (ft)
U_a, U_{ao}	UA, UAØ	Axial velocity of vapor, at inlet, (ft/sec)
v, v_m	VV, -	Specific volume of vapor, of mixture (ft^3/lb)
v^*	-	Specific volume of vapor at critical point (ft^3/lb)
v_1, v_2, v_o	OLDVV, V2 -	Specific volume of vapor at point 1, 2, at inlet stagnation (ft^3/lb)
V	V	Molal specific volume of vapor, (ft^3/lb mole)
V_z	VZ	Parameter, see Eq. 80, (-)
W, W_1, W_2	W, ØLDW, W2	Stream velocity relative to blade, at point 1, 2 (ft/sec)
w_{crit}	-	Weight of critical size droplet, (lb)
x, x_1, x_2, x^*	X, ØLDX, X2 XSTAR	Vapor quality, at point 1, at point 2, at critical point, (lb/lb)
X_{C1}, X_{C2}	XC1, XC2	Abbreviations, see Eqs. 43 and 44, (-), (ft^3/lb mole)
y	YSUM	Moisture fraction, (-)
y_{abs}	YABS	Moisture fraction atomized from blade, (-)
y_b, y_{bo}	YB, YBØ	Moisture fraction on blades, casing, (-)
$\dot{Y}_b$	-	Rate of condensate formation on blades, (lb/sec)
Ye, Ye'	YEQULIB, -	Equivalent equilibrium moisture, corrected value, (-)
y_i	MY [I]	Moisture fraction of group i, (-)
y_N	-	Moisture fraction due to formation of stable droplets, (-)
Z_1	Z1	Parameter in nucleation expression, (-)
Z_c	ZC	Compressibility, (-)
z, z_1, z_2, z^*	Z, ØLDZ, Z2, ZMIN	Axial coordinate, at point 1, at point 2, at critical point, (ft)
β, β_i, β_o	BETA, BETAI, BETAØ	Blade angle, at inlet, at exit, (degrees)
γ_η	GETA	Effective specific heat ratio, (-)
Δ_o	DELØ	Abbreviation, see Eq. 64, (Btu ft/lb)
Δ_W	DELW	Abbreviation, see Eq. 66 (Btu/lb)
η_p	ETAP	Local expansion efficiency, (-)
Λ_o, Λ_1	LAMBDA0, LAMBDA1	Logarithmic supersaturation pressure ratio, for monomer, (-)
λ_η	LETA	Exponent in extrapolation, see Eq. 85, (-)
ν_v	NEUV	Kinematic viscosity of vapor, (ft^2/sec)
μ	-	Absolute viscosity, (lb/ft-sec)
ρ_L	RHØL	Density of saturated liquid, (lb/ft^3)
ρ_{Lo}, ρ_{L1}, ρ_{L2}	ARHØ, ARHØ1, ARHØ2	Constants defining temperature dependence of ρ_L, $\frac{lb}{ft^3}$, $\frac{lb}{ft^3\,{}^oF}$, $\frac{lb}{ft^3\,{}^oF^2}$
σ	SIGMA	Surface tension, (lb/ft)
σ_o	SIGMAØ	Constant in surface tension correlation, (lb/ft)
ϕ	PHIØ	Abbreviation, see Eq. 65, (Btu/lb)
ϕ_T	PHIT	Abbreviation, see Eq. 83, (-)
ϕ_V	PHIV	Abbreviation, see Eq. 82, (-)

2.2.7 References

1. Oswatitsch, K., and Z. Angew, Math. U. Mech., Vol. 22, pp. 1-14 (1942).

2. Hill, P. G., H. Witing, and E. P. Demetri, "Condensation of Metal Vapors During Rapid Expansion," Trans. ASME (Heat Transfer), Vol. 85, Part C, pp. 303 to 314, November 1963.

3. Gyarmathy, G., "The Basis for a Theory of the Wet Steam Turbine," Juris-Verlag Zurich, 1962.

4. Ewing, C. E. et al, "High Temperature Properties of Potassium," U. S. Naval Research Laboratory, Report NRL 6233, September 24, 1965.

5. Katz, J. L., H. Saltsburg, and H. Reiss, "Nucleation in Associated Vapors," North American Aviation Science Center, SCPP-65-32, May 18, 1965.

6. Eckert, E. R. G., and R. M. Drake, Jr., Heat and Mass Transfer, McGraw-Hill, New York, N. Y., 1959, pp. 211, 257-260.

7. Ewing, C. T., et al, "High Temperature Properties of Cesium," U. S. Naval Research Laboratory, NRL 6246, Sept. 24, 1965.

8. Goldman, L. J., and S. M. Nosek, "Experimental Nozzle Expansion and Flow Characteristics of Potassium Vapor," NASA TN D-3209.

9. Linhardt, H. D., "Potassium Condensate Droplet Size Determination," Aeronutronic Division, Philco Corporation, U-3709, August 1, 1966.

APPENDIX 2.2A

LISTING OF COMPUTER PROGRAM

```
09:17:23 THURSDAY, SEPTEMBER 28, 1967

BEGIN
COMMENT       STUDY OF CONDENSATION OF ASSOCIATING VAPORS IN TURBINES;
   FILE OUT PRINT 4(2, 15);
   FILE IN READER(2, 10);
   REAL ARRAY ROTOR, DIAMI, HEIGHTI, DIAMO, HEIGHTO, BETAIN, BETAOUT,
    BSPACE, ETAPI, LI, UB, THICKBOI, THICKBMAXI[0:18];
   REAL ARRAY OLDF, OLDCASE[0:54];
   INTEGER COUNT, EQNS, GROUPS, GROUPMAX, GROUPO, GROUPPRINT, I, S,
    STAGES, N, N2;
   REAL ARRAY JS, MY, DTL, DRLD, DNL, DMY, RL, RLD, RLO, WR, NL[0:25];
   BOOLEAN WILSON, WILSONO, RESTART;
   LABEL LABELV, EXIT, SKIPV;
   LABEL NEWSTAGE;
   BOOLEAN EXTRAPOLATED;
   REAL ARRAY ASAVE[0:100];
   REAL ARRAY F[0:54];
   INTEGER ARRAY CASE[0:25];
COMMENT DECLARATIONS;
   LABEL ENTERICE, INITIAL;
   LABEL LABELICE;
   LABEL CHECKSTAR;
   REAL ARRAY DT, DP, DVV, DW, DUA, DYE, DYS, DY, DRMEAN, DNT[0:18];
   REAL ACPO, ACP1, ACP2, AREAA, AHFG, AHFG1, ARHO, ARHO1, ARHO2, AK2,
    AK21, AK4, AK41, B, B1, B2, BDOT, BDDOT, BPRIME, BPPRIME,
    BLADESPACE, APS, APS1, APS2, BETAI, C, C1, C2, C3, CPL, CPV, CPVO,
    COTB, COTBI, COTBO, CDOT, CDDOT, CPRIME, CPPRIME, COSB, CALLCD,
    JOLD, D, D1, D2, DDOT, DDDOT, DA, DIA2, DIA2I, DIA2O, DIA1, DIA1I,
    DIA1O, DAREAA, DBETADZ, DELO, DTLIQ, DPRIME, DPPRIME, DZDT, DZDV,
    DELTAT, DYSUM, DELW, DW, DP, DT, DVV, CALLC, HMIN, HMAX, DELOS, DMF
    , PHIV, PHIT, PHIP, KETA, CETA, PHIG, GETA, CCRITSQ, OLDW, OLDVV,
    OLDP, OLDT, OLDZ, OLDDELOS, OLDDHGDV, OLDPXVN, OLDDHGDT, OLDVZ,
    OLDTZ, OLDX, OLDV, OLDAREA, AMIN, ZMIN, PP, OLDGROUPS, TSTART,
    VSTARV, WSTARW, ASTARA, ERRORA, M2, T2, W2, VV2, A2, Z2, ZF, TSAT,
    PRANDTL, RECF, TR, TAMB, HAMB, SOA, REYNOLDS, HB, DYB, DYBO, RABS,
    YABS, DYABS, HABS, YB, YBO, YSURFACE, NATOMIZE, TF, SOAO, E, E1, G,
    GAMMA, H, HFG, J, JDOT, JCRIT, JINC, HG, HGO, HL, DHGDOT, DHGDT,
    DHGDV, YEQUILIB, AHG, AHG1, AHG2, AHG3, AHL, AHL1, AHL2, AHL3, LETA
    , HETA, TD, TDS, DYDZ, XSTAR, PSTARP, ERRDT, PHIO, AA1, X2, OLDHFG,
    OLDDYDZ, OLDDELTAT, SUSPEND, NOSURF, JD1, JD2, KV, K2, K4, K2PRIME,
    K2PRIMES, LENGTHB, LNPA, LAMBDAO, LAMBDA1, M, ML, MACH, NO, NEU,
    NEUV, NEFF, N1PRIME, N1PRIMES, NTOTAL, P, P1, PI, PS, PDOT, PATM,
    P1S, PEFF, PXVN, PO, RELB, ABSB, PHI, RO, RI, RHOL, RCRIT, SINB,
    SIGMA, SIGMAO, TB, TBP, T, TZ, THICKB, THICKBO, THICKBMAX, TC, SMP,

    TLSUM, TL, TEMPO, TLOLD, UA, V, VV, VM, W, W2G, X, XC1, XC2, XCPVT,
    UAO, YSUMN, DYSUMN, YTOTAL, YSUM, BETAO, VZ, ETAP, RMEAN, ZCE, Z,
    ZO, Z1, ZC, GAMA;
   FORMAT
     FEXTRA1(X25,"EXTRAPOLATION OUTPUT"/X15,"OLD",X25,"NEW"//X3,"Z",
      X11,E14.7,X14,E14.7/X3,"P",X11,E14.7,X14,E14.7/X3,"T",X11,E14.7,
      X14,E14.7/X3,"W",X11,E14.7,X14,E14.7/X3,"X",X11,E14.7,X14,E14.7/
      X3,"DELTAT",X6,E14.7,X14,E14.7/X3,"VV",X10,E14.7,X14,E14.7/);
   LIST LEXTRA1(OLDZ, Z, OLDP, P, OLDT, T, OLDW, W, OLDX, X, OLDDELTAT,
    DELTAT, OLDVV, VV);
   FORMAT
     FTHICK("NEW THICKNESS = ",E14.7/);
   LIST LEXTRA(KETA, CETA, TSTART, VSTARV, WSTARW, ASTARA, CCRITSQ,
    GETA, A2, ZC, S);
```

```
FORMAT
   FEXTRA(X1,X8,"KETA",X8,"CETA",X8,"T*/T",X8,"V*/V",X8,"W*/W",X8,
    "A*/A",X2,"W-CRIT*2   "/X1,7E12.4//X1,X8,"GETA",X10,"A2",X10,"ZC"
    ,X11,"S"/X1,4E12.4//);
FORMAT
   FEXTRA2(X10,
"ATTEMPTED EXTRAPOLATION-MINIMUM AREA DOES NOT MATCH, RETURN TO INLET"
   //X10,"OLDZ WAS ",F15.5," OLDW WAS",F15.5/);
FORMAT
   FGEOM(X15," TURBINE GEOMETRY TABULATION"///"ROW",X3,"DIA.-IN",
    " HEIGHT-IN",X2,"DIA.-OUT",X2,"HEIGHT-O",X3,"ETAP",X3,"LENGTH",
    X1,"BETA-IN",X1,"BETAOUT",X1,"BLADESPACE",X3,"THICKBO    UB",X1,
    "THICKBMAX"/(I3,4F10.4,F7.3,F9.4,F8.2,F8.2,F11.4,F10.4,I4,F10.4/
    /));
LIST GEOM(FOR S← 1 STEP 1 UNTIL STAGES DO[S, DIAMI[S], HEIGHTI[S],
 DIAMO[S], HEIGHTO[S], ETAPI[S], LI[S], BETAIN[S], BETAOUT[S],
 BSPACE[S], THICKBOI[S], UB[S], THICKBMAXI[S]]);
FORMAT
   FSUMY(X20,"SUMMARY OF RESULTS OF CONDENSATION CALCULATIONS"///
    "ROW",X7,"T",X7,"P",X6,"VV",X7,"W",X6,"UA",X7,"YE",X7,"YS",X8,
    "Y",X7,"RMEAN",X6,"NTOTAL"//(I3,2F8.1,F8.2,2F8.1,3F9.5,2E12.4//)
    /);
LIST LSUMY(FOR S← 0 STEP 1 UNTIL STAGES DO[S, OT[S], OP[S], OVV[S],
 OW[S], OUA[S], OYE[S], OYS[S], OY[S], ORMEAN[S], ONT[S]]);
LIST LADAM(H, CALLC, HMAX, HMIN, RELB, ABSB);
LIST LMAIN1(UAO, TEMPO, PO, LENGTHB);
LIST LMAIN2(M, RO, KV, NEUV, JCRIT, JINC, J, UB[S]);
LIST LMAIN3(B1, B2, C1, C2, C3, D1, D2, E1);
LIST LMAIN4(ACPO, ACP1, ACP2, ARHO, ARHO1, ARHO2);
LIST LMAIN5(CPL, APS, APS1, APS2, AK2, AK21, AK4, AK41);
LIST LMAIN5A(AHG, AHG1, AHG2, AHG3, AHL, AHL1, AHL2, AHL3);
LIST LMAIN6(DIA1I, DIA1O, DIA2I, DIA2O, BETAI, BETAO, BLADESPACE,
 THICKBO);
LIST LMAIN6A(STAGES, FOR S← 1 STEP 1 UNTIL STAGES DO[ROTOR[S], DIAMI
 [S], HEIGHTI[S], DIAMO[S], HEIGHTO[S], ETAPI[S], LI[S], UB[S],
 BETAIN[S], BETAOUT[S], BSPACE[S], THICKBOI[S], THICKBMAXI[S]]);
LIST LMAIN7(THICKBMAX, PATM, TC, SMP, SIGMAO, ETAP, GROUPMAX);
LIST LMAIN7A(PATM, TC, SMP, SIGMAO, GROUPMAX);
LIST LMAIN8(OME, ERRORA, ERRDT, AA1, SUSPEND, NOSURF);
LIST LMAIN9(S, P, T, VV, UA, W);
LIST LMAIN11(TAMB, HAMB, RABS);
FORMAT
   FA2("A2=",E14.7);
LIST LRESTART(GROUPS, FOR I← 1 STEP 1 UNTIL GROUPS DO[RLO[I], NL[I]]
 , YSUM, TLOLD, VV);
FORMAT
   FMAIN1(X3,X26,"INPUT CONSTANTS AND PARAMETERS"//X3,X9,"UAO",X7,
    "TEMPO",X10,"PO",X6,"LENGTHB"/X3,4E12.4//),
   FMAIN2(X3,X11,"M",X10,"RO",X10,"KV",X8,"NEUV",X3,"J-CRITICAL",X2,
    "JINCREMENT",X11,"J",X10,"UB"/X3,8E12.4//),
   FMAIN3(X3,X10,"B1",X10,"B2",X10,"C1",X10,"C2",X10,"C3",X10,"D1",
    X10,"D2",X10,"E1"/X3,8E12.4//),
   FMAIN4(X3,X8,"ACPO",X8,"ACP1",X8,"ACP2",X8,"ARHO",X7,"ARHO1",X7,
    "ARHO2"/X3,6E12.4//),
   FMAIN5(X3,X9,"CPL",X9,"APS",X8,"APS1",X8,"APS2",X9,"AK2",X8,
    "AK21",X9,"AK4",X8,"AK41"/X3,8E12.4//),
   FMAIN5A(X3,X9,"AHG",X8,"AHG1",X8,"AHG2",X8,"AHG3",X9,"AHL",X8,
    "AHL1",X8,"AHL2",X8,"AHL3"/X3,8F12.4//),
   FMAIN6(X3,X7,"DIA1I",X7,"DIA1O",X7,"DIA2I",X7,"DIA2O",X7,"BETAI",
    X7,"BETAO",X2,"BLADESPACE",X5,"THICKBO"/X3,8E12.4//),
   FMAIN8(X3,X9,"OME",X6,"ERRORA",X7,"ERRDT",X9,"AA1",X5,"SUSPEND",
    X6,"NOSURF"/X3,6E12.4//),
   FMAIN10(X5,"XSTAR=",F12.6,X5,"DELTATSTAR=",F12.5,X2,"DYDZ=",F14.5
    /),
   FMAIN11(X3,X4,"TAMBIENT",X4,"HAMBIENT",X8,"RABS"/X3,3E12.4//),
   FMAIN7(X3,X3,"THICKBMAX",X8,"PATM",X10,"TC",X9,"SMP",X6,"SIGMAO",
    X8,"ETAP",X4,"GROUPMAX"/X3,7E12.4//);
```

```
   FORMAT
      FRESTART(X8,"GROUPS",X13,"I",X12,"RL",X12,"NL",X6,"MOISTURE",X7,
       "TLIQUID",X12,"VV"/2I14,5E14.5/(X15,I14,2E14.7/)//);
   FORMAT
      FADAM(X25,"ICE-ADAMS PARAMETERS"//X5,X13,"H",X9,"CALLC",X10,
       "HMAX     ",X6,"HMIN",X10,"RELB",X10,"ABSB"/X5,6F14.8//);
   FORMAT
      FAREA(/"AMIN=",E12.4,"ZMIN=",E12.4,"AEXIT=",E12.4);
   FORMAT
      FSTG(X5,X12,"PP",X12,"VV",X13,"T",X10,"CETA",X10,"GETA",X10,
       "KETA     ",X6,"PHIP"/X5,7E14.5//);
   FORMAT
      FMAIN9(X15,"STATIC PROPERTIES AT INLET OF BLADE ROW NO.",I2//X1,
       X11,"P",X11,"T",X10,"VV",X10,"UA",X11,"W"/X1,5E12.4);
$$ 8 ICEADAMS                                                                   00000000
COMMENT      BEGIN ICE-ADAMS;
   PROCEDURE BOXA(Z, Y, DY);
   VALUE Z;
   REAL Z;
   ARRAY Y, DY[*];
   BEGIN
      LABEL LABELC, LABELG, SKIPGSTART, SKIPGROUPS, VANISH, GSTART;
COMMENT      BEGIN Y TRANSLATION;
      FOR N← 1 STEP 1 UNTIL GROUPMAX DO
         BEGIN
            N2← N+GROUPMAX;
            NL[N]← Y[N];
            RLD[N]← Y[N2];
         END;
      W← Y[EQNS-3];
      P← Y[EQNS-2];
      T← Y[EQNS-1];
      VV← Y[EQNS];
COMMENT      TURBINE DESCRIPTION;
      DIA1← DIA1I+(DIA1O-DIA1I)×Z/LENGTHB;
      DIA2← DIA2I+(DIA2O-DIA2I)×Z/LENGTHB;
      THICKB← THICKBO+(THICKBMAX-THICKBO)×(1-Z/LENGTHB)×4×Z/LENGTHB;
      AREAA← PI×(DIA2*2-DIA1*2)×(1-THICKB/BLADESPACE)/4;
      DAREAA← 2×(DIA2×(DIA2O-DIA2I)-DIA1×(DIA1O-DIA1I))/(LENGTHB×(DIA2*
       2-DIA1*2))-4×(THICKBMAX-THICKBO)×(1-2×Z/LENGTHB)/(LENGTHB×(
       BLADESPACE-THICKB));
      COTB← COTBI+(COTBO-COTBI)×Z/LENGTHB;
      SINB← 1/SQRT(1+COTB*2);
      DBETADZ←(SINB*2×(COTBO-COTBI)/LENGTHB)×COTB×(-1);
COMMENT          ***** CALC AXIAL VELOCITY;
      UA← W×SINB;
      DA← DAREAA+DBETADZ;
COMMENT       V IS FT*3/LB-MOLE;
      V← VV×M;
COMMENT       CALC Z AND CPV;
      B←-EXP((B1+B2/T)/ML+LN(T));
      C← EXP((C1+(C2+C3/T)/T)/ML);
      D←-EXP((D1+D2/T)/ML);
      E← E1;
      BDOT←+(1-(B2)/(ML×T))/T;
      CDOT←-(C2+2×C3/T)/(ML×T*2);
      DDOT←-D2/(T*2×ML);
      BDDOT←((2×B2)/(ML×T)-1)/T*2;
      CDDOT←(2×C2+6×C3/T)/(ML×T*3);
      DDDOT←(2×D2)/(ML×T*3);
      BPRIME← B×BDOT;
      BPPRIME← B×(BDOT*2+BDDOT);
      CPRIME← C×CDOT;
      CPPRIME← C×(CDOT*2+CDDOT);
      DPRIME← D×DDOT;
      DPPRIME← D×(DDOT*2+DDDOT);
      ZC← 1+(((E/V+D)/V+C)/V+B)/V;
      DZDT←(((DPRIME)/V+CPRIME)/V+BPRIME)/V;
      DZDV←-(((4×E/V+3×D)/V+2×C)/V+B)/V*2;
```

```
        CPVO← ACPO+ACP1×EXP(-ACP2/T);
        XC1←(ZC+T×DZDT)*2/((((5×E/V+4×D)/V+3×C)/V+2×B)/V+1);
        XC2←((T×DPPRIME+2×DPRIME)/(3×V)+CPRIME+T×CPPRIME/2)/V+2×BPRIME+T×
         BPPRIME;
        CPV← CPVO-(RO/(M×J))×(1-XC1+T×XC2/V);
        HGO← AHG+AHG1×T+AHG2×EXP(-AHG3/T);
        DHGODT← AHG1+AHG2×AHG3×EXP(-AHG3/T)/T*2;
        DHGDV←(RO×T/M)×(DZDV+T×((DPRIME/V+CPRIME)/V+BPRIME)/V*2)/J;
        DHGDT← DHGODT+(RO×T/M)×(DZDT+(ZC-1)/T-2×((DPRIME/(3×V)+CPRIME/2)/
         V+BPRIME)/V-T×((DPPRIME/(3×V)+CPPRIME/2)/V+BPPRIME)/V)/J;
COMMENT       CALC RHOL,HFG,AND SIGMA;
        HG← HGO+(RO×T/M)×(ZC-1-T×((DPRIME/(3×V)+CPRIME/2)/V+BPRIME)/V)/J;
        HL← AHL+AHL1×T+AHL2×T*2+AHL3×T*3;
        HFG←(HG-HL);
        RHOL← ARHO+ARHO1×T+ARHO2×T*2;
        SIGMA← SIGMAO×(1-T/TC)*SMP;
COMMENT       CALC SATURATION PRESSURE AND T;
        PS← EXP((APS+APS1/T)/ML+APS2×LN(T)+LNPA);
        LAMBDAO← LN(P/PS);
        DELTAT← LAMBDAO×T/(APS2-LAMBDAO-APS1/(ML×T));
COMMENT       CALC OF ASSOCIATION AT P AND T;
        K2← EXP((AK2+AK21/T)/ML);
        K4← EXP((AK4+AK41/T)/ML);
        K2PRIME← K2+K4×(P/PATM)*2×(3-2×K2×P/PATM);
        N1PRIME←(SQRT(1+4×P×K2PRIME/PATM)-1)/(2×P×K2PRIME/PATM);
        P1← P×N1PRIME;
COMMENT      CALC OF ASSOCIATION AT PS AND T;
        K2PRIMES← K2+K4×(PS/PATM)*2×(3-2×K2×PS/PATM);
        N1PRIMES←(SQRT(1+4×PS×K2PRIMES/PATM)-1)/(2×PS×K2PRIMES/PATM);
        P1S← PS×N1PRIMES;
        LAMBDA1← LN(P1/P1S);
 COMMENT          SURFACE CONDENSATION;
         PRANDTL← NEUV×CPV/(KV×G×VV);
         TSAT← T+DELTAT;
         RECF← PRANDTL*(1/3);
         TR← T+RECF×W*2/(2×G×J×CPV)+NOSURF×TSAT;
         IF TSAT>TR THEN
            BEGIN
               TF←(BLADESPACE-THICKB)/12;
               SOA← 2/(TF×SINB);
               SOAO← 12/BLADESPACE;
               REYNOLDS← 2×TF×W/NEUV;
               HB← 0.023×KV×REYNOLDS*0.8×PRANDTL*0.4/(2×TF);
               DYB← SOA×HB×VV×(TSAT-TR)/(HFG×UA);
               DYBO←(SOAO×HB×VV/(HFG×UA))×(TSAT-TR+HAMB×(TSAT-TAMB)/HB)
            END
         ELSE
            DYB← DYBO← 0;
         IF DELTAT>0 THEN
            BEGIN
               HABS← KV/(RABS+2.38×NEUV/SQRT(G×RO×T/M));
               DYABS← 3×YABS×DELTAT×HABS/(RABS×RHOL×HFG×UA);
            END;
 COMMENT          WHEN P1/P1S < 0 VAPOR IS SUPERHEATED;
         IF LAMBDA1<0 THEN
            IF CASE[1]=0 THEN
               GO TO SKIPGROUPS
            ELSE
               BEGIN
                  RCRIT← 0;
                  GO TO LABELC;
               END;
```

```
COMMENT      CALC OF NUCLEATION RATE;
        NEFF← NO;
        PEFF← P1+2×(P-P1)×SQRT(2);
        RCRIT← 2×SIGMA×M/(RHOL×RO×T×LAMBDA1);
        Z0← NEFF×SQRT(2×G×SIGMA×NO×M/PI)/(RHOL×(RO×T)↑2);
        Z1← 16×PI×NO×(SIGMA×M/(RO×T))↑3/(3×RHOL↑2×M);
        JDOT← P×PEFF×Z0×EXP(-Z1×0.5/LAMBDA1↑2)×EXP(-Z1×0.5/LAMBDA1↑2);
        IF CASE[1]=0 THEN
          GO TO SKIPGROUPS;
        NEU← JDOT×VV×X/UA;
    LABELC:
    COMMENT      CALC OF DROP GROWTH AND NUMBER;
        IF GROUPS<2 THEN

        GO TO GSTART;
      FOR I← 1 STEP 1 UNTIL GROUPS-1 DO
        BEGIN
          RI← RL[I]← RLO[I]+RLD[I];
          IF LAMBDA1<0.1 THEN
            GO TO LABELG;
          IF RI≤0.5×RCRIT THEN
            BEGIN
              NL[I]← DRLD[I]← RLD[I]← RLO[I]← 0;
              GO TO VANISH;
            END;
LABELG:       IF RI>0 THEN
            BEGIN
              DTL[I]←(1-RCRIT/RI)×DELTAT;
              DRLD[I]← KV×DTL[I]/((1+2.38×NEUV/(RI×SQRT(G×RO×T/M)))
               ×(UA×RHOL×RI×HFG));
            END;
VANISH:       DNL[I]← 0;
          WR[I]← 4×PI×RHOL×RI↑3/3;
          MY[I]← WR[I]×NL[I];
          DMY[I]← 4×PI×RHOL×RI↑2×DRLD[I]×NL[I];
        END;
GSTART: I← GROUPS;
      IF CASE[I]=0 THEN
        DRLD[I]← DMY[I]← DNL[I]← 0
      ELSE
        BEGIN
          DRLD[I]← 0;
          DNL[I]← NEU;
          RL[I]← RLO[]+RLD[I];
          WR[I]← 4×PI×RHOL×RL[I]↑3/3;
          DMY[I]← WR[I]×DNL[I];
          MY[I]← WR[I]×NL[I];
        END;
SKIPGSTART: FOR I← GROUPS+1 STEP 1 UNTIL GROUPMAX DO
        DRLD[I]← DMY[I]← DNL[I]← 0;
      YSUM← DYSUM← TLSUM← DYSUMN← YSUMN← 0;
      FOR I← 1 STEP 1 UNTIL GROUPS DO
        BEGIN
          DYSUMN← DYSUMN+DMY[I];
          YSUMN← YSUMN+MY[I];
          TLSUM← TLSUM+MY[I]×DTL[I];
        END;
SKIPGROUPS: DYSUM← DYSUMN+DYB+DYBO+DYABS;
      YSUM← YSUMN+YB+YBO+YABS;

      TL← IF YSUM=0 THEN T ELSE T+TLSUM/YSUM;
      DTLIQ←(TL-TLOLD)/H;
      X← 1-YSUM;
```

```
COMMENT      FLOW EQUATIONS;
       TZ← 1+T×DZDT/ZC;
       VZ← 1-V×DZDV/ZC;
       PXVN← P×X×VV×ETAP;
       XCPVT← X×CPV×T;
       W2G← W*2/G;
       DELO← PXVN×(W2G×TZ/J+X×T×VZ×DHGDT+TZ×X×V×DHGDV)-W2G×X×T×DHGDT;
       DELOS← DELO/(PXVN×(X×T×VZ×DHGDT+TZ×X×V×DHGDV));
       IF DELOS<DME AND Z<ZMIN×LENGTHB THEN
           GO TO CHECKSTAR;
       DELW← PXVN×((HFG×DYSUM-YSUM×CPL×DTLIQ)×TZ+(-DA-DYSUM/X)×(X×T×VZ×
        DHGDT+X×TZ×V×DHGDV));
       DW←(DELW/DELO)×W;
       DVV← VV×(DW/W+DAREAA+DBETADZ+DYSUM/X);
       DP←-P×(W2G/PXVN)×DW/W;
       DT← T×(DP/P+VZ×DVV/VV)/TZ;
COMMENT      BEGIN INVERSE Y TRANSLATION;
       FOR N← 1 STEP 1 UNTIL GROUPMAX DO
           BEGIN
               N2← N+GROUPMAX;
               Y[N]← NL[N];
               Y[N2]← RLD[N];
               DY[N]← DNL[N];
               DY[N2]← DRLD[N];
           END;
       Y[EQNS-3]← W;
       DY[EQNS-3]← DW;
       Y[EQNS-2]← P;
       DY[EQNS-2]← DP;
       Y[EQNS-1]← T;
       DY[EQNS-1]← DT;
       Y[EQNS]← VV;
       DY[EQNS]← DVV;
COMMENT      END INVERSE TRANSLATION;
    END BOXA;
    PROCEDURE BOXB(Z, Y, DY);
    VALUE Z;
    REAL Z;
    ARRAY Y, DY[*];
    BEGIN
        LABEL ALLSAME;
        IF JDOT<JCRIT AND CASE[1]=0 THEN

        GO TO ALLSAME;
    IF WILSONO THEN
        WILSON← IF JDOT>JCRIT AND JDOT>JO2 AND JDOT>JO1 AND JDOT>JOLD
         THEN FALSE ELSE TRUE
    ELSE
        WILSON← IF JDOT<JOLD AND JDOT<JO1 AND JDOT<JO2 THEN TRUE ELSE
         FALSE;
    IF WILSONO THEN
        BEGIN
            IF WILSON THEN
                GO TO ALLSAME
            ELSE
                BEGIN
                    I← GROUPS;
                    CASE[I]← 1;
                    JS[I]← JDOT;
                    RLD[I]← RCRIT;
                    GO TO ALLSAME;
                END;
```

```
            END
         ELSE
            IF WILSON THEN
               BEGIN
                  GROUPS← GROUPS+1;
                  GO TO ALLSAME;
               END;
         I← GROUPS;
         IF JDOT>JS[I]×JINC THEN
            BEGIN
               GROUPS← GROUPS+1;
               I← GROUPS;
               CASE[I]← 1;
               JS[I]← JDOT;
               RLO[I]← RCRIT;
            END;
ALLSAME: IF GROUPS>GROUPMAX THEN
            GROUPS← GROUPMAX;
         YB← YB+H×DYB;
         YBO← YBO+H×DYBO;
         YABS← YABS+H×DYABS;
         YSURFACE← YB+YBO+YABS;
         NATOMIZE← 3×YABS/(4×PI×RHOL×RABS*3);
         JO2← JO1;
         JO1← JOLD;
         WILSONO← WILSON;
         JOLD← JDOT;
         TLOLD← TL;
         COUNT← COUNT+1;
         OLDW← W;
         OLDVV← VV;
         OLDP← P;
         OLDT← T;
         OLDZ← Z;
         OLDDELOS← DELOS;
         OLDDHGDV← DHGDV;
         OLDPXVN← PXVN;
         OLDDHGDT← DHGDT;
         OLDVZ← VZ;
         OLDTZ← TZ;
         OLDX← X;
         OLDV← V;
         OLDAREA← AREAA×SINB;
         OLDDELTAT← DELTAT;
         OLDHFG← HFG;
         OLDDYDZ← 0;
         FOR I← 1 STEP 1 UNTIL GROUPS-1 DO
            OLDDYDZ← OLDDYDZ+DMY[I];
   END BOXB;
   PROCEDURE BOXC(Z, Y, DY);
   VALUE Z;
   REAL Z;
   ARRAY Y, DY[*];
   BEGIN
      FORMAT
         FC1(X5,X13,"P",X13,"T",X3,"SP. VOL.-V",X13,"W",X7,"U-AXIAL",X3
          ,"Z-COMPRESS"/X5,6E14.5//);
      FORMAT
         FC2(X5,X12,"DP",X12,"DT",X12,"DV",X12,"DW",X4,"-(DP/DT)/P",X10
          ,"AREAA",X9,"DA/A"/X5,7E14.5//);
      FORMAT
         FC3(X5,X8,"DELTAT",X7,"TLIQUID",X7,"LAMBDAO",X7,"LAMBDA1",X10,
          "JDOT",X5,"RCRITICAL",X9,"DN/DZ"/X5,7E14.5//);
```

```
FORMAT
    FC4(X5,X12,"K2",X12,"K4",X7,"K2PRIME",X11,"HFG",X10,"CPVO",X11
      ,"CPV",X9,"SIGMA"/X5,7E14.5//);
FORMAT
    FC5(X5,"TOTAL MOISTURE",X4,"PARTIAL P1",X7,"QUALITY",X3,
      "MEAN RADIUS",X3,"TOTAL DROPS",X3,"K2PRIME SAT",X7,"SINBETA"/
      X5,7E14.5//);
FORMAT
    FC5A(X5,X5,"Y-EQUILIB",X12,"HG",X12,"HL",X11,"HFG",X10,"DELO",
    X10,"DELW",X9,"1-M+2"/X5,7E14.5//);
FORMAT
    FC0(X5,X9,"COUNT",X3,"STEP SIZE H",X13,"Z"/X5,I14,2E14.7//);
FORMAT
    FC6(X5,X9,"GROUP",X6,"MOISTURE",X8,"NUMBER",X8,"RADIUS",X5,
     "DMOISTURE",X7,"DNUMBER",X7,"DRADIUS"/(X5,I14,6E14.7));
FORMAT
    FC7(X5,X4,"YB=Y BLADE",X4,"YBO=Y CASE",X1,"YABS=YATOMIZED",X5,
     "YSURFACE",X6,"NATOMIZE"/X5,5E14.5//);
LIST LC7(YB, YBO, YABS, YSURFACE, NATOMIZE);
LIST LC6(FOR I← 1 STEP 1 UNTIL GROUPPRINT DO[I, MY[I], NL[I], RL[
 I], DMY[I], DNL[I], DRLD[I]]);
COMMENT     CALCULATE       PDOT,NTOTAL,MEANRADIUS;
GROUPPRINT← IF GROUPS<GROUPMAX THEN GROUPS+1 ELSE GROUPMAX;
YEQUILIB← YSUM+CPV×DELTAT/HFG;
PDOT←-(DP/P)×UA;
NTOTAL← YTOTAL← 0;
FOR I← 1 STEP 1 UNTIL GROUPS-1 DO
   BEGIN
      NTOTAL← NTOTAL+NL[I];
      YTOTAL← YTOTAL+MY[I];
   END;
IF NTOTAL>0 THEN
   RMEAN←(3×YTOTAL/(4×PI×RHOL×NTOTAL))*0.3333333;
WRITE(PRINT[PAGE]);
WRITE(PRINT, FC0, COUNT, H, Z);
WRITE(PRINT, FC1, P, T, VV, W, UA, ZC);
WRITE(PRINT, FC2, DP, DT, DVV, DW, PDOT, AREAA, DA);
WRITE(PRINT, FC3, DELTAT, TL, LAMBDA0, LAMBDA1, JDOT, RCRIT, NEU)
 ;
WRITE(PRINT, FC4, K2, K4, K2PRIME, HFG, CPVO, CPV, SIGMA);
WRITE(PRINT, FC5, YSUM, P1, X, RMEAN, NTOTAL, K2PRIMES, SINB);
WRITE(PRINT, FC5A, YEQUILIB, HG, HL, HFG, DELO, DELW, DELOS);
WRITE(PRINT, FC7, LC7);
WRITE(PRINT, FC6, LC6);
COUNT← 0;
CALLC← IF LENGTHB-Z<CALLC THEN(LENGTHB-Z) ELSE CALLCO;
IF Z≥LENGTHB THEN
   BEGIN
      YABS← YSURFACE;
      YB← YBO← 0;
      OT[S]← T;
      OP[S]← P;
      OVV[S]← VV;
      OW[S]← W;
      OUA[S]← UA;
      OYE[S]← YEQUILIB;
      OYS[S]← YSURFACE;
      OY[S]← YSUM;
      ORMEAN[S]← RMEAN;
      ONT[S]← NTOTAL;
```

```
            IF GROUPS>0 THEN
               FOR I← 1 STEP 1 UNTIL GROUPS DO
                  RLD[I]← RL[I];
            COSB← COS(BETAO×PI/180);
            IF ROTOR[S]=0 THEN
               PHI← ARCTAN((W×COSB-UB[S+1])/UA)×180/PI
            ELSE
               PHI← ARCTAN((W×COSB+UB[S])/UA)×180/PI;
            BETAI← 90-PHI;
            S← S+1;
            IF S>STAGES THEN
               GO TO EXIT;
            BETAIN[S]← BETAI;
            GO TO NEWSTAGE;
         END;
   END BOXC;
   PROCEDURE BOXD(Z, Y, DY);
   VALUE Z;
   REAL Z;
   ARRAY Y, DY[*];
   BEGIN
      FORMAT
         FD1(X5,"FAILED AT Z=",E15.5,X5,"H=",E15.5);
      FORMAT
         FD2(//X5,X13,"P",X13,"T",X12,"VV",X13,"W",X7,"U-AXIAL",X6,
          "MACH",X3,"Z-COMPRESS"/X5,7E14.5//);
      FORMAT
         FD3(X5,X12,"DP",X12,"DT",X11,"DVV",X12,"DW",X10,"DELO",X10,
          "DELW",X10,"YSUM"/X5,7E14.5//);
      FORMAT
         FD4(X5,"TL= ",E14.4,X5,"TLOLD= ",E14.4/);
      WRITE(PRINT, FD1, Z, H);
      WRITE(PRINT, FD2, P, T, VV, W, UA, MACH, ZC);
      WRITE(PRINT, FD3, DP, DT, DVV, DW, DELO, DELW, YSUM);
      WRITE(PRINT, FD4, TL, TLOLD);
      GO TO EXIT;
   END BOXD;
COMMENT  MAIN PROGRAM ;
      G← 32.17;
      NO← 2.732@+26;
      PI← 3.141592653;
      ML← 0.434294482;
      J← 778;
      RO← 1545;
      PATM← 2116.8;
      READ(READER,/, H, CALLC, HMAX, HMIN, RELB, ABSB, OME, ERRORA, ERRDT,
       AA1, RESTART, WILSONO, EXTRAPOLATED, SUSPEND, NOSURF, JCRIT, JINC,
       GROUPMAX, B1, B2, C1, C2, C3, D1, D2, E1, AK2, AK21, AK4, AK41,
       ACPO, ACP1, ACP2, ARHO, ARHO1, ARHO2, AHG, AHG1, AHG2, AHG3, AHL,
       AHL1, AHL2, AHL3, APS, APS1, APS2, M, TC, SIGMAO, SMP, CPL, KV,
       NEUV, TAMB, HAMB, RABS, UAO, PO, TEMPO);
      READ(READER,/, LMAIN6A);
      IF RESTART THEN
         READ(READER,/, LRESTART);
      CLOSE(READER, RELEASE);
      WRITE(PRINT[PAGE]);
      WRITE(PRINT, FGEOM, GEOM);
      WRITE(PRINT[PAGE]);
      CALLCO← CALLC;
      JS[0]← JCRIT/JINC;
      LNPA← LN(PATM);
    INITIAL: P← PO;
      T← TEMPO;
      UA← UAO;
```

```
COMMENT CALCULATE INITIAL SPECIFIC VOLUME;
   IF RESTART THEN
      GO TO SKIPV;
   ETAP← ETAPI[1];
   K2← EXP((AK2+AK21/T)/ML);
   K4← EXP((AK4+AK41/T)/ML);
   K2PRIME← K2+K4×(P/PATM)*2×(3-2×K2×P/PATM);
   N1PRIME←(SQRT(1+4×P×K2PRIME/PATM)-1)/(2×P×K2PRIME/PATM);
   ZC← 1/(2-N1PRIME);
   VV← ZC×RO×T/(P×M);
LABELV: V← VV×M;
   B←-EXP((B1+B2/T)/ML+LN(T));
   C← EXP((C1+(C2+C3/T)/T)/ML);
   D←-EXP((D1+D2/T)/ML);
   E← E1;
   ZCE← 1+(((E/V+D)/V+C)/V+B)/V;
   IF ABS(ZCE-ZC)>0.0005 THEN
      BEGIN
         ZC← ZCE;
       VV← ZC×RO×T/(P×M);
       GO TO LABELV;
    END;
  W← UAO/SIN(BETAIN[1]×PI/180);
  VV← V/M;
  X← 1-YSUM;
  BDOT←(1-B2/(ML×T))/T;
  BDDOT←((2×B2)/(ML×T)-1)/T*2;
  CDOT←-(C2+2×C3/T)/(ML×T*2);
  CDDOT←(2×C2+6×C3/T)/(ML×T*3);
  DDOT←-D2/(T*2×ML);
  DDDOT←(2×D2)/(ML×T*3);
  BPRIME← B×BDOT;
  BPPRIME← B×(BDOT*2+BDDOT);
  CPRIME← C×CDOT;
  CPPRIME← C×(CDOT*2+CDDOT);
  DPRIME← D×DDOT;
  DPPRIME← D×(DDOT*2+DDDOT);
  DZDT←(((DPRIME)/V+CPRIME)/V+BPRIME)/V;
  DZDV←-(((4×E/V+3×D)/V+2×C)/V+B)/V*2;
  DHGODT← AHG1+AHG2×AHG3×EXP(-AHG3/T)/T*2;
  DHGDV←(RO×T/M)×(DZDV+T×((DPRIME/V+CPRIME)/V+BPRIME)/V*2)/J;
  DHGDT← DHGODT+(RO×T/M)×(DZDT+(ZC-1)/T-2×((DPRIME/(3×V)+CPRIME/2)/V+
   BPRIME)/V-T×((DPPRIME/(3×V)+CPPRIME/2)/V+BPPRIME)/V)/J;
  PXVN← P×X×VV×ETAP;
  TZ← 1+T×DZDT/ZC;
  VZ← 1-V×DZDV/ZC;
  PHIV← X×V×DHGDV×J/(PXVN);
  PHIT←(T×X×DHGDT×J)/PXVN;
  PHIP←(PHIV×TZ+PHIT×VZ)/(PHIV+VZ);
  KETA← 1+(PHIV+VZ)/(PHIT-TZ);
  CETA← X×DHGDT-X×V×DHGDV/((KETA-1)×T);
  PHIG← X×(DHGDT×VZ+V×DHGDV×TZ/T);
  GETA←(PHIG×M/RO)/(T×X×DHGDT/PXVN-TZ/J);
  T← TEMPO-W*2/(2×G×J×CETA);
  VV← VV×(T/TEMPO)*(1/(1-KETA));
  V← VV×M;
  PP← PO×(T/TEMPO)*PHIP;
  B←-EXP((B1+B2/T)/ML+LN(T));
  C← EXP((C1+(C2+C3/T)/T)/ML);
  D←-EXP((D1+D2/T)/ML);
  E← E1;
  ZC← 1+(((E/V+D)/V+C)/V+B)/V;
  P← ZC×RO×T/(M×VV);
  WRITE(PRINT, FSTG, PP, VV, T, CETA, GETA, KETA, PHIP);
```

```
 SKIPVI S← 0;
    OT[S]← T;
    OP[S]← P;
    OVV[S]← VV;
    OW[S]← W;
    OUA[S]← UA;
    OYE[S]← YEQUILIB;
    OYS[S]← YSURFACE;
    OY[S]← YSUM;
    ORMEAN[S]← RMEAN;
    ONT[S]← NTOTAL;
    S← 1;
    BETAI← BETAIN[1];
    FOR I← 1 STEP 1 UNTIL GROUPMAX DO
        BEGIN
            N2← GROUPMAX+I;
            CASE[I]← 0;
            F[N2]← F[I]← 0;
        END;
    IF RESTART THEN
        FOR I← 1 STEP 1 UNTIL GROUPS DO
            CASE[I]← 1;
    IF RESTART THEN
        FOR I← 1 STEP 1 UNTIL GROUPS DO
            BEGIN
                F[I]← NL[I];
                N2← I+GROUPMAX;
                F[N2]← RLO[I];
                RLO[I]← 0;
            END;
    GROUPO← GROUPS;
 NEWSTAGE: Z← 0;
    DIA1I← DIAMI[S]-HEIGHTI[S];
    DIA1O← DIAMO[S]-HEIGHTO[S];
    DIA2I← DIAMI[S]+HEIGHTI[S];
    DIA2O← DIAMO[S]+HEIGHTO[S];
    BETAU← BETAOUT[S];
    BLADESPACE← BSPACE[S];
    THICKBO← THICKBOI[S];
    LENGTHB← LI[S];
    ETAP← ETAPI[S];
    THICKBMAX← THI  BMAXI[S];
    WRITE(PRINT[PAGE]);
    WRITE(PRINT, FADAM, LADAM);
    WRITE(PRINT, FMAIN1, LMAIN1);
   WRITE(PRINT, FMAIN2, LMAIN2);
   WRITE(PRINT, FMAIN3, LMAIN3);
   WRITE(PRINT, FMAIN4, LMAIN4);
   WRITE(PRINT, FMAIN5, LMAIN5);
   WRITE(PRINT, FMAIN5A, LMAIN5A);
   WRITE(PRINT, FMAIN6, LMAIN6);
   WRITE(PRINT, FMAIN7, LMAIN7);
   WRITE(PRINT, FMAIN8, LMAIN8);
   WRITE(PRINT, FMAIN11, LMAIN11);
COMMENT CALC OF CONSTANTS AND INITIAL CONDITIONS;
   SINB← SIN(K2← PI×BETAO/180);
   COTBO← COS(K2)/SINB;
   SINB← SIN(K2← PI×BETAI/180);
   COTBI← COS(K2)/SINB;
   W← UA/SINB;
   EQNS← 4+2×GROUPMAX;
   FOR I← 0 STEP 1 UNTIL 100 DO
```

```
      BEGIN
         ZF← I/100;
         DIA1← DIA1I+(DIA1O-DIA1I)×ZF;
         DIA2← DIA2I+(DIA2O-DIA2I)×ZF;
         THICKB← THICKBO+(THICKBMAX-THICKBO)×(1-ZF)×4×ZF;
         AREAA← PI×(DIA2*2-DIA1*2)×(1-THICKB/BLADESPACE)/4;
         COTB← COTBI+(COTBO-COTBI)×ZF;
         SINB← 1/SQRT(1+COTB*2);
         ASAVE[I]← AREAA×SINB;
         IF ZF=0 THEN
            AMIN← AREAA×SINB;
         IF AMIN>AREAA×SINB THEN
            BEGIN
               AMIN← AREAA×SINB;
               ZMIN← ZF;
            END;
      END;
   WRITE(PRINT, FAREA, AMIN, ZMIN, ASAVE[100]);
COMMENT  INITIALIZATION BEGINS;
ENTERICE: WRITE(PRINT[PAGE]);
   WRITE(PRINT, FMAIN9, LMAIN9);
   FOR I← 1 STEP 1 UNTIL GROUPMAX DO
      BEGIN
         N2← GROUPMAX+I;
         OLDCASE[I]← CASE[I];
         F[N2]← RL[I];
         RLO[I]← 0;
         F[I]← NL[I];
      END;
    F[EQNS-3]← W;
    F[EQNS-2]← P;
    F[EQNS-1]← T;
    F[EQNS]← VV;
    FOR I← 1 STEP 1 UNTIL EQNS DO
       OLDF[I]← F[I];
    OLDGROUPS← GROUPS;
  LABELICE: CALLC← IF LENGTHB-Z<CALLC THEN(LENGTHB-Z) ELSE CALLCO;
    ICEADAMS(EQNS, Z, H, CALLC, HMAX, HMIN, RELB, ABSB, F, BOXA, BOXB,
     BOXC, BOXD);
  CHECKSTAR:
  COMMENT      THIS SECTION CHECKS AND CORRECTS INLET OR EXTRAPOLATES PAST
               THE THROAT TO SUPERSONIC CONDITION;
    BEGIN
       REAL MUMMY;
       LABEL M2CHANGE, REXS, SKIPZ, ADJUSTGEOMETRY, A2CHANGE;
       PHIV← OLDX×OLDV×OLDDHGDV×J/OLDPXVN;
       PHIT← OLDT×OLDX×OLDDHGDT×J/OLDPXVN;
       PHIP←(PHIV×OLDTZ+PHIT×OLDVZ)/(PHIV+OLDVZ);
       KETA← 1+(PHIV+OLDVZ)/(PHIT-OLDTZ);
       CETA← OLDX×OLDDHGDT-OLDX×OLDV×OLDDHGDV/((KETA-1)×OLDT);
       PHIG← OLDX×(OLDDHGDT×OLDVZ+OLDV×OLDDHGDV×OLDTZ/OLDT);
       GETA←(PHIG×M/RO)/(OLDT×OLDX×OLDDHGDT/OLDPXVN-OLDTZ/J);
       CCRITSQ← G×GETA×RO×OLDT/M;
       PHIO← OLDT×OLDVZ×OLDDHGDT+OLDV×OLDTZ×OLDDHGDV;
       LETA← J×OLDHFG×OLDX/(OLDPXVN×(PHIT-OLDTZ));
       HETA← OLDHFG-LETA×OLDV×OLDDHGDV/(KETA-1);
       TD← OLDDELTAT;
 REXS: DYDZ←(OLDDYDZ×TD/OLDDELTAT)×SUSPEND;
       XSTAR← OLDX-DYDZ×(ZMIN×LENGTHB-OLDZ);
       TSTART←(1+OLDW*2/(2×G×J×CETA×OLDT)+HETA×(OLDX-XSTAR)/(CETA×OLDT))
        /(1+RO×GETA/(2×M×J×CETA));
       VSTARV←(TSTART×(XSTAR/OLDX)+LETA)*(1/(1-KETA));
       PSTARP←(TSTART)*OLDTZ×VSTARV*(-OLDVZ);
```

```
WSTARW← SQRT(CCRITSQ×TSTART)/OLDW;
ASTARA← VSTARV×XSTAR/(WSTARW×OLDX);
T← OLDT×TSTART;
PS← EXP((APS+APS1/T)/ML+APS2×LN(T)+LNPA);
LAMBDA0← LN(PSTARP×OLDP/PS);
DELTAT← LAMBDA0×T/(APS2-LAMBDA0-APS1/(ML×T));
TDS←(OLDDELTAT+DELTAT)/2;
IF ABS((TDS-TD)/OLDDELTAT)>ERRDT THEN
   BEGIN
      TD← TDS;
     GO TO REXS;
  END;
WRITE(PRINT[PAGE]);
WRITE(PRINT, FMAIN10, XSTAR, DELTAT, OLDDYDZ);
IF EXTRAPOLATED THEN
   GO TO ADJUSTGEOMETRY;
IF ABS(ASTARA-AMIN/OLDAREA)>ERRORA THEN
   BEGIN
      UA0← UA0×AMIN/(ASTARA×OLDAREA);
      WRITE(PRINT, FEXTRA2, OLDZ, OLDW);
      GROUPS← 0;
      FOR I← 1 STEP 1 UNTIL GROUPMAX DO
         RL[I]← CASE[I]← NL[I]← 0;
      WILSON0← FALSE;
      GO TO INITIAL;
   END;
EXTRAPOLATED← TRUE;
OLDAREA← AMIN/ASTARA;
IF ZMIN<0.98 AND ASAVE[100]/AMIN>1.01 THEN
   BEGIN
      A2←(1+AA1)×AMIN;
      FOR I← 100×ZMIN STEP 1 UNTIL 100 DO
         IF ASAVE[I]-A2>0 THEN
            BEGIN
               Z2←((I-(ASAVE[I]-A2)/(ASAVE[I]-ASAVE[I-1]))/100)×
                LENGTHB;
               X2← XSTAR-SUSPEND×(DYDZ×(1-ZMIN)×LENGTHB)×DELTAT/
                OLDDELTAT;
               M2← SQRT(2×(AA1)/(3-KETA))+1;
               GO TO M2CHANGE;
            END;
   END;
M2← IF ASAVE[100]>AMIN THEN 1+SQRT(2×((ASAVE[100]/AMIN-1))/(3-
 KETA)) ELSE 1;
Z2← LENGTHB;
X2←-SUSPEND×OLDDYDZ×(1-ZMIN)×LENGTHB×DELTAT/OLDDELTAT+XSTAR;
M2CHANGE: T2← OLDT×(1+OLDW*2/(2×G×J×OLDT×CETA)+HETA×(OLDX-X2)/(CETA×
 OLDT))/(1+GETA×RO×M2*2/(2×M×J×CETA));
W2← M2×SQRT(GETA×RO×G×T2/M);
VV2← OLDVV×((T2/OLDT)×(X2/OLDX)*LETA)*(1/(1-KETA));
A2← OLDAREA×OLDW×VV2×X2/(OLDVV×OLDX×W2);
WRITE(PRINT, FA2, A2);
IF ZMIN<0.98 AND ASAVE[100]/AMIN>1.01 THEN
   BEGIN
      IF(A2-AMIN×(1+AA1))/A2>ERRORA THEN

   BEGIN
      M2← 1+(M2-1)×SQRT(AMIN×AA1/(A2-AMIN))×0.99;
      GO TO M2CHANGE;
   END;
FOR I← 100×ZMIN STEP 1 UNTIL 100 DO
   BEGIN
      IF ASAVE[I]-A2>0 THEN
```

```
                    BEGIN
                       Z2←((I-(ASAVE[I]-A2)/(ASAVE[I]-ASAVE[I-1]))/100
                        )×LENGTHB;
                       GO TO SKIPZ;
                    END
                 ELSE
                    Z2← LENGTHB;
              END;
SKIPZ:        Z← Z2;
              T← T2;
              W← W2;
              VV← VV2;
              V← M×VV;
              B←-EXP((B1+B2/T)/ML+LN(T));
              C← EXP((C1+(C2+C3/T)/T)/ML);
              D←-EXP((D1+D2/T)/ML);
              E← E1;
              ZC← 1+(((E/V+D)/V+C)/V+B)/V;
              P← ZC×RO×T/V;
              PS← EXP((APS+APS1/T)/ML+APS2×LN(T)+LNPA);
              LAMBDAO← LN(P/PS);
              DELTAT← LAMBDAO×T/(APS2-LAMBDAO-APS1/(T×ML));
              X← X2;
              YSUM← 1-X2;
              IF OLDX<1 THEN
                 BEGIN
                    FOR I← 1 STEP 1 UNTIL GROUPS-1 DO
                       RL[I]← RL[I]×((1-X2)/(1-OLDX))+(1/3);
                    YBO← YBO×(1-X2)/(1-OLDX);
                    YB← YB×(1-X2)/(1-OLDX);
                    YABS← YABS×(1-X2)/(1-OLDX);
                 END;
              TLSUM← 0;
              FOR I← 1 STEP 1 UNTIL GROUPS-1 DO
                 BEGIN
                    MY[I]← NL[I]×4×PI×RHOL×RL[I]+2×(RL[I]-RCRIT)×DELTAT/3
                     ;
                    TLSUM← TLSUM+MY[I];
           END;
        TLOLD← TL← IF YSUM=0 THEN T ELSE T+TLSUM/YSUM;
        WRITE(PRINT[PAGE]);
        WRITE(PRINT, FEXTRA1, LEXTRA1);
        WRITE(PRINT, FEXTRA, LEXTRA);
        GO TO ENTERICE;
     END;
  SINB← COS(PI×BETAO/180)/COTBO;
  Z← 0;
  T← T2;
  W← W2;
  VV← VV2;
  V← M×VV;
  B←-EXP((B1+B2/T)/ML+LN(T));
  C← EXP((C1+(C2+C3/T)/T)/ML);
  D←-EXP((D1+D2/T)/ML);
  E← E1;
  ZC← 1+(((E/V+D)/V+C)/V+B)/V;
  P← ZC×RO×T/V;
  PS← EXP((APS+APS1/T)/ML+APS2×LN(T)+LNPA);
  LAMBDAO← LN(P/PS);
  DELTAT← LAMBDAO×T/(APS2-LAMBDAO-APS1/(T×ML));
  X← X2;
  YSUM← 1-X2;
  IF OLDX<1 THEN
```

```
   BEGIN
      FOR I← 1 STEP 1 UNTIL GROUPS-1 DO
         RL[I]← RL[I]×((1-X2)/(1-OLDX))*(1/3);
      YABS← YSURFACE← YSURFACE×(1-X2)/(1-OLDX);
      YB← YB0← 0;
   END;
UA← W×SINB;
OT[S]← T;
OP[S]← P;
OVV[S]← VV;
OW[S]← W;
OUA[S]← UA;
OYE[S]← YEQUILIB;
OYS[S]← YSURFACE;
OY[S]← YSUM;
ORMEAN[S]← RMEAN;
ONT[S]← NTOTAL;
COSB← COS(BETADO×PI/180);
IF ROTOR[S]=0 THEN
   PHI← ARCTAN((W×COSB-UB[S+1])/(W×SINB))×180/PI
      ELSE
         PHI← ARCTAN((W×COSB+UB[S])/(W×SINB))×180/PI;
      BETAI← 90-PHI;
      S← S+1;
      WRITE(PRINT[PAGE]);
      WRITE(PRINT, FEXTRA1, LEXTRA1);
      WRITE(PRINT, FEXTRA, LEXTRA);
      IF S>STAGES THEN
         GO TO EXIT;
      BETAIN[S]← BETAI;
      TLSUM← 0;
      FOR I← 1 STEP 1 UNTIL GROUPS-1 DO
         BEGIN
            MY[I]← NL[I]×4×PI×RHOL×RL[I]*2×(RL[I]-RCRIT)×DELTAT/3;
            TLSUM← TLSUM+MY[I];
         END;
      TLOLD← TL← IF YSUM=0 THEN T ELSE T+TLSUM/YSUM;
      GO TO NEWSTAGE;
ADJUSTGEOMETRY: IF ABS(AMIN/OLDAREA-ASTARA)>ERRORA THEN
         BEGIN
            TB←(THICKBMAX-THICKB0)×ZMIN×(1-ZMIN)×4+THICKB0;
            TBP← TB-0.7×(ASTARA×OLDAREA/AMIN-1)×(BLADESPACE-TB);
            THICKBMAX← THICKB0+((TBP-THICKB0)/(ZMIN×(1-ZMIN)))/4;
            WRITE(PRINT, FTHICK, THICKBMAX);
            IF THICKBMAX<0 THEN
               BEGIN
                  GO TO EXIT;
               END;
            FOR I← 1 STEP 1 UNTIL EQNS DO
               F[I]← OLDF[I];
            GROUPS← OLDGROUPS;
            FOR I← 1 STEP 1 UNTIL GROUPMAX DO
               CASE[I]← OLDCASE[I];
            Z← 0;
            GO TO LABELICE;
         END
      ELSE
         BEGIN
            M2← IF ASAVE[100]>AMIN THEN 1+SQRT(2×((ASAVE[100]/AMIN-1))/
             (3-KETA)) ELSE 1;
            Z2← LENGTHB;
            X2←-SUSPENDXOLDDYDZ×(1-ZMIN)×LENGTHB×DELTAT/OLDDELTAT+XSTAR
             ;
A2CHANGE:   T2← OLDT×(1+OLDW*2/(2×G×J×OLDT×CETA)+HETA×(OLDX-X2)/(CETA×
             OLDT))/(1+GETA×RO×M2*2/(2×M×J×CETA));
```

```
W2← M2×SQRT(GETA×RO×G×T2/M);
VV2← OLDVV×((T2/OLDT)×(X2/OLDX)*LETA)*(1/(1-KETA));
OLDAREA← AMIN/ASTARA;
A2← OLDAREA×OLDW×VV2×X2/(OLDVV×OLDX×W2);
WRITE(PRINT, FA2, A2);
IF(A2-ASAVE[100])/A2>ERRORA THEN
   BEGIN
      M2← 1+(M2-1)×SQRT((ASAVE[100]-AMIN)/(A2-AMIN))×0.995;
      GO TO A2CHANGE;
   END;
SINB← COS(PI×BETAO/180)/COTBO;
Z← 0;
T← T2;
W← W2;
VV← VV2;
V← M×VV;
B←-EXP((B1+B2/T)/ML+LN(T));
C← EXP((C1+(C2+C3/T)/T)/ML);
D←-EXP((D1+D2/T)/ML);
E← E1;
ZC← 1+(((E/V+D)/V+C)/V+B)/V;
P← ZC×RO×T/V;
PS← EXP((APS+APS1/T)/ML+APS2×LN(T)+LNPA);
LAMBDAO← LN(P/PS);
DELTAT← LAMBDAO×T/(APS2-LAMBDAO-APS1/(T×ML));
X← X2;
YSUM← 1-X2;
IF OLDX<1 THEN
   BEGIN
      FOR I← 1 STEP 1 UNTIL GROUPS DO
         RL[I]← RL[I]×((1-X2)/(1-OLDX))*(1/3);
      YABS← YSURFACE← YSURFACE×(1-X2)/(1-OLDX);
      YB← YBO← 0;
   END;
UA← W×SINB;
YEQUILIB← YSUM+CPV×DELTAT/HFG;
OT[S]← T;
OP[S]← P;
OVV[S]← VV;
OW[S]← W;
OUA[S]← UA;
OYE[S]← YEQUILIB;
OYS[S]← YSURFACE;
OY[S]← YSUM;
ORMEAN[S]← RMEAN;
ONT[S]← NTOTAL;
COSB← COS(BETAO×PI/180);
IF ROTOR[S]=0 THEN
   PHI← ARCTAN((W×COSB-UB[S+1])/(W×SINB))×180/PI
ELSE
   PHI← ARCTAN((W×COSB+UB[S])/(W×SINB))×180/PI;
BETAI← 90-PHI;
S← S+1;
TLSUM← 0;
FOR I← 1 STEP 1 UNTIL GROUPS-1 DO
   BEGIN
      MY[I]← NL[I]×4×PI×RHOL×RL[I]*2×(RL[I]-RCRIT)×DELTAT/3
       ;
      TLSUM← TLSUM+MY[I];
   END;
```

```
            TLOLD← TL← IF YSUM=0 THEN T ELSE T+TLSUM/YSUM;
            WRITE(PRINT, FEXTRA1, LEXTRA1);
            WRITE(PRINT, FEXTRA, LEXTRA);
            IF S>STAGES THEN
               GO TO EXIT;
            BETAIN[S]← BETAI;
            GO TO NEWSTAGE;
         END;
   END;
 EXIT: WRITE(PRINT[PAGE]);
   WRITE(PRINT, FGEOM, GEOM);
   WRITE(PRINT[PAGE]);
   WRITE(PRINT, FSUMY, LSUMY);
 END.
```

APPENDIX 2.2B

LISTING OF ICEADAMS INTEGRATION PROCEDURE

```
PROCEDURE ICEADAMS(N,T,H,CALLC,HMAX,HMIN,RELB,ABSB,XO,
    BOXA,BOXB,BOXC,BOXD);                                              1600104
COMMENT
N=NO. OF EQUATIONS,                                                    2630104
T=INDEPENDENT VARIABLE, SET IT=INITIAL T WHEN ICEADAMS IS FIRST CALLED, 2630106
H=STEP SIZE, SET IT = SUGGESTED STEP SIZE WHEN ICEADAMS FIRST CALLED,  2630108
CALLC= CHANGE IN T  BETWEEN CALLS ON BOXC,                             2630110
HMAX=MAXIMUM STEP SIZE ACCEPTABLE,                                     2630112
HMIN=MINIMUM STEP SIZE ACCEPTABLE,                                     2630114
RELB=MAXIMUM ACCEPTABLE RELATIVE ERROR,                                2630116
ABSB=MAXIMUM ACCEPTABLE ERROR,                                         2630118
XO=VECTOR OF INITIAL VALUES OF DEPENDENT VARIABLES,                    2630120
BOXA(T,X,F)=PROCEDURE GIVING THE XDOT VECTOR,IN F,WHEN CALLED WITH THE 2630122
    CURRENT VALUES OF THE VECTOR X  OF DEPENDENT VARIABLES AND THE     2630124
    INDEPENDENT VARIABLE T,                                            2630126
BOXB(T,X,F)=PROCEDURE CALLED AFTER EACH SUCCESSFUL INTEGRATION STEP,   2630201
BOXC(T,X,F)=PROCEDURE CALLED AFTER T HAS INCREASED BY "CALLC" SINCE
BEGINNING OF ICEADAMS OR SINCE BOXC WAS LAST CALLED,
BOXD(T,X,F)=PROCEDURE CALLED WHEN SUCCESSFUL INTEGRATION STEP CANNOT BE 2630205
    MADE WITHOUT REDUCING STEP SIZE BELOW HMIN;                        2630207
COMMENT ADAMS SOLVES A SYSTEM OF FIRST ORDER DIFFERENTIAL EQUATIONS BY A
    4TH ORDER ADAMS P-C METHOD.  STARTING IS BY RUNGE-KUTTA;
COMMENT
                          WEI  AND  GEIL  ;                            2630209
VALUE RELB,ABSB,HMIN,N;
INTEGER N      ;                                                       1600108
REAL T,H,CALLC,RELB,ABSB,HMAX;
REAL HMIN;
ARRAY XO[*];
PROCEDURE BOXA,BOXB,BOXC,BOXD;                                         1600112
BEGIN
INTEGER I,J,A,B;                                                       1600114
REAL ABSTEST,BOUND,D1,D2,FACTOR,LB,RELTEST,TTEMP;                      1600116
LABEL S11,S22,S33,S44,S55,S66,RETN;                                    1600118
 ARRAY X,K,F[0:5,0:N],E,XP[0:N];
COMMENT SET UP INITIAL VALUES;
FOR I←1 STEP 1 UNTIL N DO
X[1,I]←XO[I];                                                          2620105
BOUND←T+CALLC - .01×HMIN;
RELTEST←14.2×RELB;
```

```
ABSTEST←14.2×ABSB;
FACTOR←RELB/ABSE;
LB←RELTEST/200;
H←2.0×H;
COMMENT RUNGA-KUTTA STARTING METHOD;
S11:A←2;
B←2;
S22:FOR J←A STEP 1 UNTIL B DO
BEGIN
BOXA(T,X[J-1,*],F[J-1,*]);                                                        1600122
FOR I←1 STEP 1 UNTIL N DO
BEGIN
K[1,I]←H×F[J-1,I];                                                                2620109
X[J,I]←X[J-1,I]+0.5×K[1,I] END;                                                   2620111
TTEMP←T+0.5×H;
BOXA(TTEMP,X[J,*],F[J,*]);                                                        1600124
FOR I←1 STEP 1 UNTIL N DO
BEGIN
K[2,I]←H×F[J,I];                                                                  2620115
X[J,I]←X[J-1,I]+0.5×K[2,I] END;                                                   2620117
BOXA(TTEMP,X[J,*],F[J,*]);                                                        1600124
FOR I←1 STEP 1 UNTIL N DO BEGIN
K[3,I]←H×F[J,I];                                                                  2620121
X[J,I]←X[J-1,I]+K[3,I] END;                                                       2620123
T←T+H;
BOXA(T,X[J,*],F[J,*]);                                                            1600126
FOR I←1 STEP 1 UNTIL N DO BEGIN
K[4,I]←H×F[J,I];                                                                  2620201
X[J,I]←X[J-1,I]+0.16666667×(K[1,I]+2.0×(K[2,I]+K[3,I])+K[4,I]);                   2620203
END; END;
IF B = 2 THEN BEGIN
S33:
FOR I←1 STEP 1 UNTIL N DO XP[I]←X[2,I];                                           2620205
COMMENT XP[I]=DOUBLE INTERVAL RESULT TO BE USED IN ERROR ANALYSIS;
T←T-H;
H←0.5×H;
IF H<HMIN THEN BOXD(T,X[1,*],F[1,*]);                                             1600202
B←3;
GO TO S22 END;
IF B = 3 THEN BEGIN
COMMENT IS ACCURACY CRITERION MET;
J←3;
S44:FOR I←1 STEP 1 UNTIL N DO BEGIN
E[I]←ABS(XP[I]-X[J,I]);                                                           2620207
IF E[I] < ABS(X[J,I])×RELTEST THEN                                                2620209
E[I]←E[I]/ABS(X[J,I]) ELSE                                                        2620211
IF E[I] < ABSTEST THEN
E[I]←E[I]×FACTOR ELSE
BEGIN T←T-H;
IF J = 5 THEN BEGIN FOR I←1 STEP 1 UNTIL N DO X[1,I]←X[4,I];                      2620213
GO TO S11 END;
GO TO S33 END;
END;
IF J = 5 THEN GO TO S66;
A←4; B←4;
GO TO S22 END;
COMMENT SHOULD ANY OF THE STARTING VALUES BE PRINTED OUT;
T←T-3.0×H;
FOR J←2,3,4 DO BEGIN
T←T+H;                                                                          1600204
BOXB(T,X[J,*],F[J,*]);                                                          1600206
IF T>BOUND THEN BEGIN                                                           1600208
    BOXC(T,X[J,*],F[J,*]);                                                      1600210
    BOUND←BOUND+CALLC  END;                                                     1600212
```

```
END;
COMMENT BEGIN ADAMS METHOD;
S55:
BOXA(T,X[4,*],F[4,*]);                                                   1600214
FOR I←1 STEP 1 UNTIL N DO
XP[I]←X[4,I]+0.04166667×H×(55.0×F[4,I]-                                  2620217
    59.0×F[3,I]+37.0×F[2,I]-9.0×F[1,I]);                                 2620219
T←T+H;
BOXA(T,XP,F[5,*]);                                                       1600216
FOR I←1 STEP 1 UNTIL N DO
X[5,I]←X[4,I]+0.041666667×H×(9.0×F[5,I]+19×F[4,I]-5×F[3,I]+F[2,I]);      2620223
J←5; GO S44;
S66:                                                                     1600218
FOR I←1 STEP 1 UNTIL N DO BEGIN X[4,I]←X[5,I];                           2620225
FOR J←2 STEP 1 UNTIL 5 DO F[J-1,I]←F[J,I] END;                           2620301
BOXB(T,X[4,*],F[4,*]);                                                   1600220
IF T≥ BOUND THEN BEGIN                                                   1600222
BOXC(T,X[4,*],F[4,*]);                                                   1600224
BOUND←BOUND+CALLC END;
COMMENT TEST WHETHER INTERVAL CAN BE DOUBLED;
FOR I←1 STEP 1 UNTIL N DO BEGIN
IF E[I] > LB THEN GO S55 END;
IF CALLC<(DI+2×H) OR (BOUND-T)<DI OR DI>HMAX THEN GO TO S55;
FOR I←1 STEP 1 UNTIL N DO X[1,I]←X[4,I];                                 1600307
H←4.0×H;
GO S11;
RETN: END OF ICEADAMS ;
```

APPENDIX 2.2C

LIST OF INPUT DATA

LIST OF INPUT DATA

Code Symbol	Text Symbol or Description	Numerical Values * Potassium	Cesium++
H	Step size	(0.0005)	
CALLC	Interval between output	(0.010)	
HMAX	Max. step size	(0.0005)	
HMIN	Min. step size	(0.000001)	
RELB	Integration error allowed	(0.0001)	
ABSB	Integration error allowed	(0.0001)	
DME	$(1-W^2/C^2_{crit})$ to start extrapolation	(0.05)	
ERRØRA	ϵ_A	(0.002)	
ERRDT	ϵ_T	(0.01)	
AA1	$(A_2-A_{min})/A_{min}$	(0.005)	
RESTART	Control variable	(0)	
WILSØNØ	Control variable	(0)	
EXTRAPØLATED	Control variable	(0)	
SUSPEND	Control variable	(1.0)	
NØSURF	Control variable	(1.0)	
JCRIT	Control variable	(5.0×10^{15})	
JNC	Control variable	(2.5)	
GRØUPMAX	Max. number of groups allowed	(15)	
B1	B_1	-3.8787	-3.62
B2	B_2	4890.7	4000.0
C1	C_1	0.5873	3.3551
C2	C_2	6385.7	-5331.5
C3	C_3	0.0	1.0825×10^7
D1	D_1	1.4595	4.1856
D2	D_2	7863.8	880.0
E1	E_1^2 or E	0.0	6×10^5
AK2	k_{20}	-3.8611	-3.6561
AK21	k_{21}	5312.5	4570.0
AK4	k_{40}	-10.145	-9.05
AK41	k_{41}	13745.0	8420.0
ACPO	C_{po}	0.127	0.037361
ACP1	C_{p1}	2.888	1.3099
ACP2	C_{p2}	28070.0	25633.0
ARHØ	ρ_o	52.768	124.18
ARHØ1	ρ_1	-0.0074975	-0.01597
ARHØ2	ρ_2	-5.255×10^{-7}	1.6855×10^{-6}
AHG	h_{go}	998.95	252.18
AHG1	h_{g1}	0.127	0.037361
AHG2	h_{g2}	24836.0	2480.0
AHG3	h_{g3}	39375.0	31290.0
AHL	h_{Lo}	-10.29	-2.6769
AHL1	h_{L1}	0.2271	0.05683
AHL2	h_{L2}	-3.245×10^{-5}	0.
AHL3	h_{L3}	7.741×10^{-9}	0.
APS	ϵ_1	6.1276	5.873

LIST OF INPUT DATA (CONTINUED)

Code Symbol	Text Symbol or Description	Numerical Values * Potassium	Cesium++
APS1	ϵ_2	-8128.8	-7040.7
APS2	ϵ_3	-0.53299	-0.5329
M	M	39.1	132.91
TC	T_c	4310	3700
SIGMAØ	σ_o	(7.84×10^{-3})	(5.75×10^{-3})
SMP	Exponent in σ_L expression	(1.25)	(1.25)
CPL	C_{pL}	0.190	0.5683
KV	k_v	(2.22×10^{-6})	(0.9×10^{-6})
NEUV	ν_v	(2.14×10^{-4})	$(2.31 \times 10^{-})$
TAMB	T_{amb}	(560)	
HAMB	h_{amb}	(0.0)	
RABS	r_{abs}	(1.64×10^{-6})	
UAØ	U_{∞}	(333)	
PØ	p^o	(4400)	
TEMPØ	T^o	(1982.9)	
STAGES	Number of blade rows	(6)	
Following items are repeated in order for each blade row.)+			
RØTØR[ ]	Control variable	o for stator row 1 for rotor row	
DIAMI[ ]	Inlet mean diameter, (in.)		
HEIGHTI[ ]	Inlet blade height, (in.)		
DIAMØ[ ]	Outlet blade diameter, (in.)		
HEIGHTØ[ ]	Outlet blade height, (in.)		
ETAP[ ]	η_p		
LI[ ]	L, (ft)		
UB[ ]	Blade velocity, (ft/sec)		
BETAIN[ ]	β_i		
BETAØUT[ ]	β_o		
BSPACE[ ]	t_{bs}, (in.)		
THICKBØI[ ]	t_{bo}, (in.)		
THICKBMAXI[ ]	t_{bm} (in.)		
Following list is input only if RESTART is true)			
GRØUPS	Number of droplet size groups		
RLD [1]	r_{L1}		
NL [1]	N_1		
RLD [2]	r_{L2}		
NL [2]	N_2		
o	o		
o	o		
o	o		
RLD GRØUPS			
NL GRØUPS			
YSUM	y at inlet		
TLØLD	T, inlet		
VV	inlet		

*Numerical values which may be changed without changing properties as reported in References 4 and 7 are enclosed in parentheses, and are values used in the example problem. For Boolean variables, 1 denotes TRUE, 0 denotes FALSE.

** See Appendix E for a description of the control variables.

+ All turbine geometry dimensions should be in inches except axial length L, which is in ft. Other dimensional units in code agree with text.

++ Since a cesium turbine was not examined here, the entries simply serve to define the property relations which would be used.

APPENDIX 2.2D

PROGRAM FLOW CHART

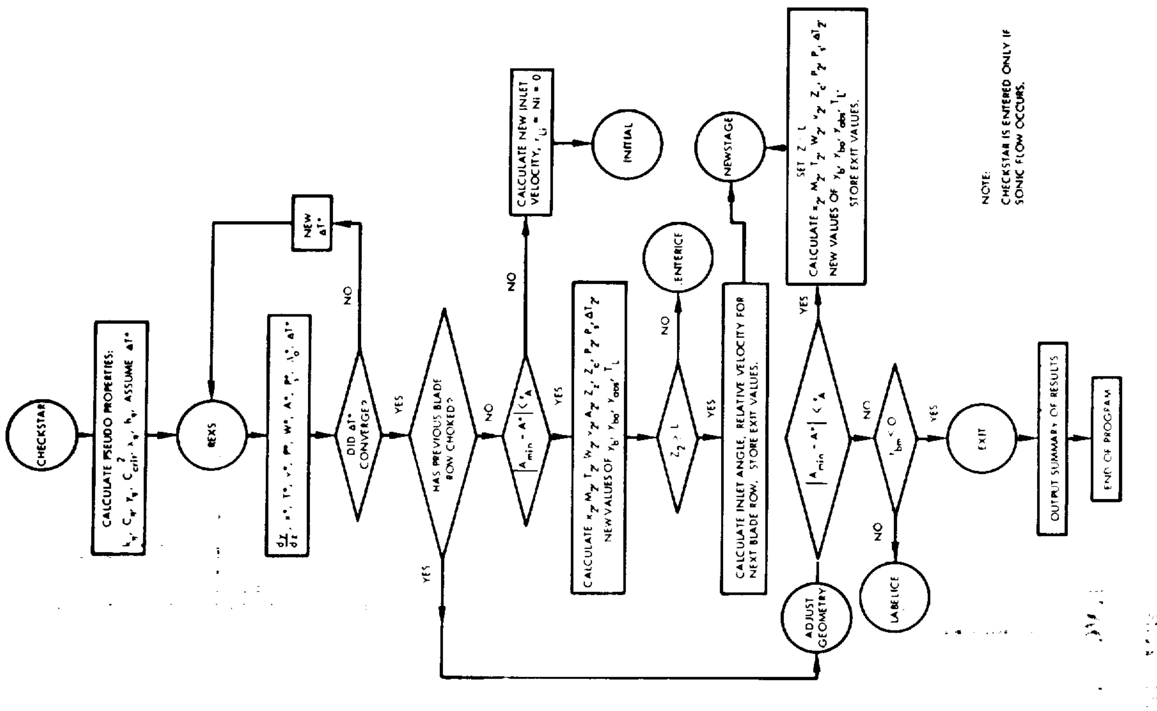

Figure 2.2D-2 Flow Diagram of the Sonic Flow Section of the Condensation Code

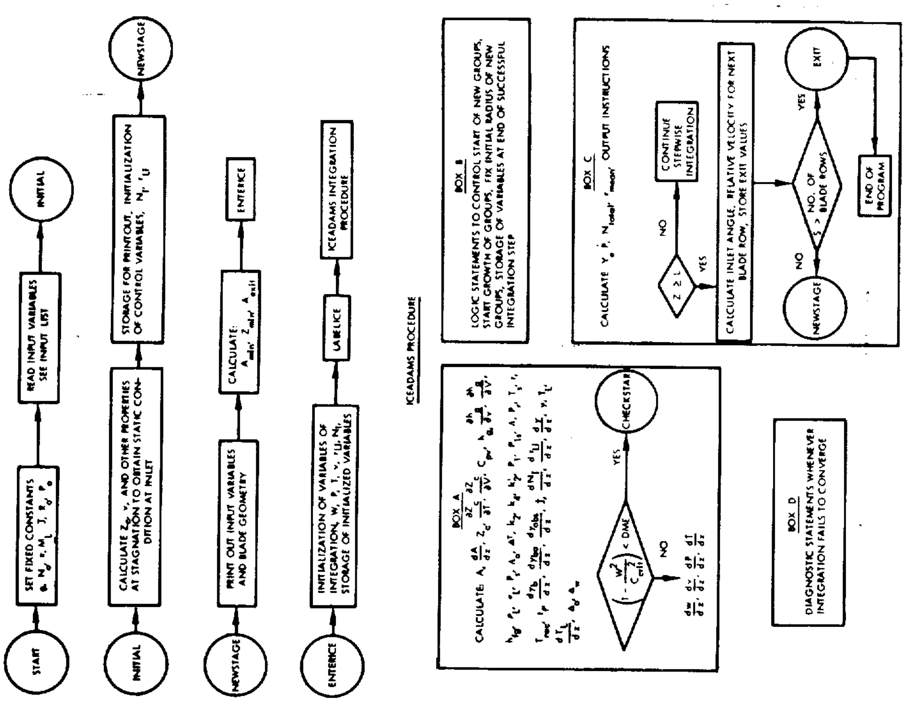

Figure 2.2D-1 Flow Diagram of the Condensation Code

APPENDIX 2.2.E

DESCRIPTION OF INPUT CONTROL VARIABLES

The use of the following control variables in the computer code is as follows:

AA1 The extrapolation from subsonic to supersonic flow in the first blade row having critical flow is from area A_1 to area A_2, where $A_2 = A_{min}$ (1 + AA1).

DME Defines the minimum value of $(1 - W^2/C_{crit}^2)$ which is allowed before extrapolation is initiated.

EERDT Maximum allowable difference between assumed and calculated ΔT.

ERRØRA Maximum allowable value of $(A^* - A_{min})/A_{min}$ which permits extrapolation to occur.

EXTRAPØLATED Input of TRUE means a previous blade row has critical flow, and requires the program to adjust blade thickness to accommodate the flow.

GRØUPMAX The maximum number of droplet groups permitted. (Code limits GRØUPMAX to maximum value of 25.)

JCRIT The value of j must exceed the value of JCRIT before the counting or growth of drops is begun, except that surface condensation may occur independently.

RESTART Input of TRUE permits input of additional data necessary to continue calculation from a prior run. For example, an error was contained in the data for blade row 4. Calculations could be continued from the results at exit of blade row 3 used as input for Blade row 4. Input of FALSE causes inlet properties to be treated as stagnation conditions.

SUSPEND Input of 0.0 freezes the amount of condensate during extrapolation. Input of 1.0 causes condensation to occur during extrapolation at a rate proportional to $\overline{\Delta T}$.

WILSØNØ Input of TRUE when restarting after the Wilson point has occurred in a previous blade row. Otherwise, input is FALSE.

JINC A new group of droplets is initiated each time j increases by the factor JINC.

NØSURF Input of 1.0 causes all surface condensation to be neglected. Input of 0.0 causes surface condensation to be included.

2.3 TWO-D AXISYMMETRIC FLOWS BEHIND BLADE ROWS IN WET VAPOR TURBINE*

2.3.1 Background

This report is designed to be used in conjunction with NASA CR-710 (Reference 1) to give the user sufficient information to allow utilization of the NASA Performance Computer Code for Axial Flow Turbines as modified at WANL. The modified code is written entirely in FORTRAN IV for the CDC 6600 computer. But the code should be capable of being used with appropriate control cards on any computer having at least 32 K of core storage.

The following sections of the report give: the applicability and modifications made from the original code, definitions of the input and output nomenclature, a method for making the code input applicable for wet vapor turbines, suggestions for further possible future modifications, three sample problems illustrating the usage of the code, a FORTRAN listing of the entire code, and control cards showing proper deck setup. No attempt is made to discuss the method of calculation of turbine performance or to give computer flow diagrams since these topics are adequately covered in Reference (1). The modifications made to the code do not significantly change the original program logic or capability. These modifications for the most part were necessary to enable the code to accurately calculate wet vapor turbine performance. Ideal gas turbines can still be analyzed as well as air breathing fossil fuel burning turbines for which the code was originally designed.

2.3.2 Intent of Code

- Applicability of Code and Limiting Assumptions

The principal purpose of the original code as written by E. E. Flagg(1) is to provide a complete performance map of axial flow turbines suitable for use in air breathing fossil fuel fired jet engines. In the process of accomplishing this end, the code calculates the two-dimensional bulk flow conditions fore and aft of the turbine rows.

*by James D. Milton, Doctoral Candidate-Nuclear Engineering, University of Cincinnati

1. Description and Scope of Modified Code

a) Axial flow turbines.

b) Up to 8 stages.

c) Up to 6 radial sectors (although only 5 are usually used for reasons of symmetry).

d) Each sector is a quasi-one-dimensional element with the properties at the radial centers of these sectors being joined, utilizing simple radial equilibrium at the stator and rotor exits.

e) Semi-perfect gas properties (gas constant and specific heat ratio) are assumed and are input at the entrance and exit of each blade row. Provision is also made to simulate changes in gas flow rates at the entrance and exit of each blade row. Energy balance effects are simulated by changing the values of the gas constant and specific heat ratio.

f) The turbine geometry may be either input as a passage distributed area (SPA and RPA)* or as effective exit vector flow angles (SDEA and RDEA). The assumption that the effective exit flow angles are approximately equal to the design blade exit angles is usually valid. Mandatory inputs are the diameters of the root (DR) and tip (DT) for the entrance and exit of each blade row and the stator and rotor design inlet angles (SDIA and RDIA) for each of the radial sectors.

g) Even though there are two subroutines (LØSS 1 and LØSS 2) which are capable of calculating losses by a total pressure loss coefficient method, the values for the coefficients of the series expansion are not generally known. (See page 11 of NASA CR-710.) The standard method is to input the values of optimum recovery coefficients for stator and rotor (SREC and RREC) together with exponents to be used in the event of both negative and positive (EXPN and EXPP) incidence. (See page 10 of NASA CR-710 for equations used.)

* Nomenclature defined in Section 2.3.3 of this report.

h) Separate cases may be run for various turbine speeds by merely changing the RPM and indicating that is a change case (STGCH = 0.0).

i) The FORTRAN IV code calculates a performance map for the case of a given turbine at a particular RPM by in effect varying the exit back pressure. The output for each "iteration" (i.e., value of back pressure) gives flow rates, velocities, flow angles, temperatures, pressures, densities, Mach numbers, efficiencies, and work done both for an overall stage output and also row-by-row output for each of the radial sectors. An exact choke point is found during the calculation of the performance map and the turbine back-pressure is effectively further reduced until the discharge annulus area is choked at the pitchline sector (assuming AACS = 1.0). A single performance point can be obtained by simply setting all pressure ratio increments (DELC, DELL, and DELA) to zero. This is the usual case when fixed operating conditions are known at design.

j) The gas flow at the entrance to the first stator is assumed to have uniform radial temperature, pressure, and velocity. The flow is further assumed to be exactly aligned with the turbine axial direction (i.e., no tangential velocity component).

- Modifications to Code

As stated previously, as originally programmed the code was principally intended for analysis of JP-4 burning, air breathing jet engines. Internal to the code is a subroutine for calculating the thermodynamic properties of reacted JP-4-air mixtures. It also had a capability to input thermodynamic properties which was extended as required by the method used in determining the performance of wet vapor turbines. It was decided that the thermodynamic properties fore and aft of each blade row would be inputted in terms of representative values for the particular working fluid and its state. The variables to be input would be the ratio of specific heats at constant pressure to that at constant volume and Boyles and Charles law gas constant. The internals of the program are then used to calculate effective specific heat and various other effective thermodynamic properties.

The following modifications were made in the code:

1) Wherever the Boyles and Charles gas law constant RG appeared in the code, it was replaced by a two-dimensional variable RV (I,K) with proper choice of axial blade position I and stage number K to correspond to the location in the turbine for which the calculation is being performed.

2) A change was made in the input NAMELIST format to allow reading in of a variable RV. Also a modification was made to read in reference values for the gas constant, temperature, pressure, and specific heat ratio all at standard sea level conditions. Formerly the code contained these values for air internally in a DATA statement. But since gases other than air will be used, it was thought useful to include a capability for inputting these values for each case rather than requiring a recompilation whenever a different working fluid was used.

3) The output was expanded to print out the values for the flow, γ (ratio of specific heats), gas constant, and RWG (the ratio of the flow at a particular station to turbine inlet flow). To insure that these variables were being properly handled within the code, decreasing values of γ, RV, and RWG were fed in. The output was found to be consistent after a slight change in the logic.

4) Since values for γ and RV are now fed in for all cases, the subroutines to calculate γ, RG, and C_p, are superfluous since they would never be called upon. If by inadvertently omitting the inputting of γ and/or RV and subsequently a subroutine for calculating its value is entered, then an error message was added which would print out the words "SUBRØUTINE ( ) HAS BEEN CALLED UPØN" followed by a string of asterisks so that attention would be immediately drawn to the error. The ( ) is filled in by the name of the subroutine being called. After the error message is printed out, the calculation is allowed to proceed using properties for air, water and JP-4 fuel.

5) On page 193 of NASA CR-170 the statement:

```
21 PTP(I, K + 1) = PTBAR (K) * ( ( TTRA (I, K)/
TTBAR (K) ) ** E 3                        ST2A  153
```

was found to be incorrect and should read:

```
21 PTP(I, K + 1) = PTBAR (K) * (TT2A(I,K)/
TTBAR (K)) ** E  3
```

6) On page 208 of NASA CR-710 the statement:

```
ASOH = SQRT (GAM (I,K) * G * RG * STTSO(L) )
INST 175
```

was found to be incorrect and should read:

```
ASOH = SQRT (GAM (1,K) * G * RG * STTSO(L) )
```

7) Any cards from the original code which had to be removed rather than modified were denoted by a comment card with the words "CARD DELETED" followed by a string of asterisks.

8) As an aid in debugging a computer run, an option was added to allow the printout of when entry or exit was made from each subroutine. This enables the user to examine the program logic as an aid in determining where discrepancies occur. This option is not recommended for other than de - bugging runs since a large amount of output results.

2.3.3 Nomenclature for Input and Output of Modified Code

- Input Definitions *

1) "TRUE" or "FALSE" card depending on whether or not a listing of when an entrance and exit is made from each subroutine is desired. This card is input only once per case.

2) Two heading cards of 60 characters each inputted only once per case.

3) Constants input once per case:

Code Name	Definition	Units
STAGE **	Stage identification number	---
STGCH	Flag indicating whether following data is for the basic case (1.0) or for a change case (0.0)	---
TTIN	Turbine inlet total temperature	°R
PTIN	Turbine inlet total pressure	psia
WAIR	Water to air ratio (not used in modified code); should be input as 0.0	---
FAIR	Fuel to air ratio (not used in modified code); should be input as 0.0	---
PTPS	Pitchline pressure ratio (total to static) across first stator for 0th calculation. This ratio is incremented by DELC, DELL, or DELA for next calculation	---
DELC	First try at increment to PTPS	---
DELL	Increment to PTPS after first stator has critical flow and also when choke iteration is complete	---
DELA	Increment to PTPS when last rotor is choked	---
STG	Number of stages in turbine (8 maximum)	---
SECT	Number of radial sectors (6 maximum)	---
EXPN	Exponent of cosine term for negative incidence used in calculating an inlet recovery factor (see page 10 of Reference 1)	---
EXPP	Exponent of cosine term for positive incidence used in calculating an inlet recovery factor (see page 10 of Reference 1)	---
PAF	Profile averaging fork (either 0.0, 1.0, or 2.0); gives the next stage inlet conditions for either: uniform (0.0) at the average value of the preceding stage, or the radial sector profiles (1.0) of pressure and temperature of the preceding stage, or a third option which keeps the exit total temperature radial profile and "smooths" (2.0) the exit total pressure profile from the preceding stage	---
SLI	Stage loss indicator (0.0 means that recovery, efficiency, and flow coefficients are inputed for each stage; 1.0 means that they are inputed only once and are assumed constant throughout the turbine)	---
AACS	Discharge annulus area choke stop which is the maximum limit for the turbine exit axial Mach number at the pitchline sector. This code will continue to decrease the back pressure until this limit is reached (assuming DELC, DELL, and DELA $\neq$ 0.0)	---
RPM	Turbine speed	RPM
VCTD	Vector diagram interstage output (either 0.0 for overall stage performance output only or 1.0 for row-by-row sector performance in addition to overall stage output printout)	---
RSL	Gas constant at sea level standard conditions	ft lb/lb °R
TSL	Standard temperature at sea level = 518.688	°R
PSL	Standard pressure at sea level = 14.696	psia
GAMSL	Specific heat ratio at sea level standard conditions	---
ENDSTG	0.0 if more stage data to follow; 1.0 if last stage data has been read in	---
ENDJØB	0.0 if more cases to follow; 1.0 if all data for all cases has been input	---
PCNH	Percent station height distribution (example: if 5 equal (in height) radial sectors were desired, then PCNH = 0.2, 0.2, 0.2, 0.2, 0.2)	---

* Refer to Standard Option Input Sheet (page 11).
** Must be input every time new stage data is read in.

4) Axial station input for each stage (stations 0, 1, 1A, 2, and 2A)

Code Name	Definition	Units
RG	Gas constant	ft lb/lb °R
GAMG	Specific heat ratio	---
DR	Diameter of root or hub of turbine	in
DT	Diameter of tip of turbine	in
RWG	Ratio of station flow to turbine inlet flow	---

5) Stator radial distributions for each stage (hub to tip sectors)

Code Name	Definition	Units
SDIA	Stator design inlet angle	(° from axis)
SDEA	Stator effective exit flow angle — should not be input if SPA is input	(° from axis)
SREC	Stator optimum recovery coefficient ($\eta_{sr_{opt}}$)	---
SETA	Stator efficiency coefficient (η_s)	---
SCF	Stator flow coefficient (C_{fs})	---
SPA	Stator passage area per unit height — should not be input if SDEA is input	in^2/in
SESTH *	Stator ratio of exit blade height to throat height	---

6) Rotor radial distributions for each stage (hub to tip sectors)

Code Name	Definition	Units
RDIA	Rotor design inlet angle	(° from axis)
RDEA	Rotor effective exit flow angle — should not be input if RPA is input	(° from axis)
RREC	Rotor optimum recovery coefficient ($\eta_{rr_{opt}}$)	---
RETA	Rotor efficiency coefficient (η_r)	---
RCF	Rotor flow coefficient (C_{fr})	---
RPA	Rotor passage area per unit height — should not be input if DREA is input	in^2/in
RTF	Rotor test factor used to represent the non-uniform work extraction due to blade end effects	---
RERTH *	Rotor ratio of exit blade height to throat height	---

* Only a single value is input.

WANL MODIFIED
TURBINE COMPUTER PROGRAM
STANDARD OPTION
INPUT SHEET

Start All Input Cards in Column 2

Subroutine Entry and Exit Listing Option (TRUE or FALSE)

Name (Comment Information)

Title (Comment Information)

```
$DATAIN   STAGE =   ,
STGCH=            ,
TTIN=             ,PTIN=          ,WAIR=          ,FAIR=          ,
PTPS=             ,DELC=          ,DELL=          ,DELA=          ,
STG=              ,SECT=          ,EXPN=          ,EXPP=          ,
PAF=              ,SLI=           ,AACS=          ,RPM=           ,
VCTD=             ,RSL=           ,TSL=           ,PSL=           ,
GAMSL=            ,ENDSTG=        ,ENDJØB=        ,
                         INLET RADIAL PROFILE
PCNH(1)=          ,         ,          ,          ,          ,
                           AXIAL STATIONS
            STA. 0     STA. 1     STA. 1A     STA. 2      STA. 2A
RG(1) =           ,         ,          ,          ,          ,
GAMG(1) =         ,         ,          ,          ,          ,
DR(1)=            ,         ,          ,          ,          ,
DT(1)=            ,         ,          ,          ,          ,
RWG(1)=           ,         ,          ,          ,          ,
                    STATOR RADIAL DISTRIBUTIONS
            ROOT                   PITCH                      TIP
SDIA(1)=          ,         ,          ,          ,          ,
SDEA(1)=          ,         ,          ,          ,          ,
SREC(1)=          ,         ,          ,          ,          ,
SETA(1)=          ,         ,          ,          ,          ,
SCF(1)=           ,         ,          ,          ,          ,
SPA(1)=           ,         ,          ,          ,          ,
SESTH=            ,
                    ROTOR RADIAL DISTRIBUTIONS
            ROOT                   PITCH                      TIP
RDIA(1)=          ,         ,          ,          ,          ,
RDEA(1)=          ,         ,          ,          ,          ,
RREC(1)=          ,         ,          ,          ,          ,
RETA(1)=          ,         ,          ,          ,          ,
RCF(1)=           ,         ,          ,          ,          ,
RPA(1)=           ,         ,          ,          ,          ,
RTF(1)=           ,         ,          ,          ,          ,
RERTH=            ,
ENDSTG=           ,     ENDSTG=1.0 IF LAST CASE
ENDJØB=           $     ENDJØB=1.0 IF LAST STAGE
```

- **Output Definitions**

1) Station Nomenclature

The axial station numbers (0, 1, 1A, 2, and 2A) following a parameter refer to the following designations:

Station Number	0	1	1A	2	2A
Definition	Stator Inlet	Stator Exit	Rotor Inlet	Rotor Exit	Next Stage Stator Inlet

Also see Figure 2.3-1 for further clarification of terminology.

In the stage and overall performance output printout several parameters are given in terms of the equivalent parameter referenced to standard sea level conditions. This provides a common basis for comparison of performance maps for different turbine cases.

2) Stage Performance Parameters

Symbol	Definition	Units
TTBAR 0	Stage average inlet total temperature	$^{\circ}$R
PTBAR 0	Stage average inlet total pressure	psia
WG 0	Stage inlet total weight flow	lb/sec
DEL H	Stage enthalpy drop (energy output)	BTU/lb
WRT/P	Stage corrected weight flow function	(lb/sec) ($^{\circ}$R/psia)$^{1/2}$
DH/TTBAR0	Stage energy function	BTU/lb $^{\circ}$R
N/RT	Stage corrected speed	RPM/($^{\circ}$R)$^{1/2}$
ETA TT	Stage total to total efficiency	---
ETA TS	Stage total to static efficiency	---
ETA AT	Stage total to axial total efficiency	---
PT0/PS1	Stator total to static pressure ratio at pitchline	---
PTBAR0/PTBAR2	Stage average total to total pressure ratio	---
I TBAR0/PS2	Stage average total to pitchline static pressure ratio	---
PTR2/PS2	Rotor exit relative total to static pressure ratio at pitchline	---
TTBAR2/TTBAR0	Stage average total to total temperature ratio	---
TTR1A/TTBAR0	Rotor inlet pitchline relative total to stage inlet average total temperature ratio	---
WG 1	Stator exit total weight flow	lb/sec
PS 1A	Rotor inlet static pressure at pitchline	psia
TTR 1A	Rotor inlet relative total temperature at pitchline	$^{\circ}$R
PTR 1A	Rotor inlet relative total pressure at pitchline	psia
WG 1A	Rotor inlet total weight flow	lb/sec
PS 2	Rotor exit static pressure at pitchline	psia
TTBAR 2	Stage exit average total temperature	$^{\circ}$R
PTBAR 2	Stage exit average total pressure	psia
WG 2	Rotor exit total weight flow	lb/sec
WG 2A	Next stage stator inlet total weight flow	lb/sec
UP/VI	Wheel speed to isentropic velocity ratio at pitchline	---
UR/VI	Root wheel speed to pitchline isentropic velocity ratio	---
PSI P	Kinetic energy loading parameter at pitchline	---
PSI R	Kinetic energy loading parameter at root	---
RX P	Reaction ratio at pitchline	---
RX R	Reaction ratio at root	---
ALPHA 0	Stator inlet gas angle at pitchline	°
I STATOR	Stator inlet incidence angle at pitchline	°
BETA 1A	Rotor inlet gas angle at pitchline	°
I RØTØR	Rotor inlet incidence angle at pitchline	°
ALPHA 2A	Next stage stator inlet gas angle at pitchline	°
DBETA R	Rotor root turning angle	°
M 1	Stator exit Mach number at pitchline	---
M1 RT	Stator exit Mach number at root	---
MR 1A	Rotor inlet relative Mach number at pitchline	---
MR1A RT	Rotor inlet relative Mach number at root	---
MR 2	Rotor exit relative Mach number at pitchline	---
MR2 TIP	Rotor exit relative Mach number at tip	---
E/TH CR	Stage equivalent energy, corrected to standard inlet critical conditions	BTU/lb
N/RTH CR	Stage equivalent speed, corrected to standard inlet critical conditions	RPM
WRTHCRE/D	Stage equivalent flow, correct to standard inlet critical conditions	lb/sec

3) Overall Turbine Performance Parameters

Symbol	Definition	Units
PSI P	Overall kinetic energy loading parameter at pitchline	---
PSI R	Overall kinetic energy loading parameter at root	---
DEL H	Overall enthalpy drop (energy output)	BTU/lb
WRT/P	Turbine inlet corrected weight flow function	(lb/sec) ($^{\circ}$R/psia)$^{1/2}$
N/RT	Turbine inlet corrected speed	RPM/($^{\circ}$R)$^{1/2}$
DELH/TTIN	Overall energy function	BTU/lb $^{\circ}$R
PT0/PTBAR2	Overall average total pressure ratio	---
PT0/PS2	Overall total to static pressure ratio at pitchline	---
PT0/PAT2A	Overall total to axial total pressure ratio at pitchline	---
ETA TT	Overall total to total efficiency	---
ETA TS	Overall total to static efficiency	---
ETA TAT	Overall total to axial total efficiency	---
WNE/60D	Turbine inlet equivalent flow-speed parameter	lb/sec^2
N/RTH CR	Turbine inlet equivalent speed, corrected to standard inlet critical conditions	RPM
E/TH CR	Overall equivalent energy, corrected to standard inlet critical conditions	BTU/lb

4) Inter-Stage Radial Sector Performance Parameters

Symbol	Definition	Units
DIAM 0	Diameter of mid-points of radial sectors at stator inlet	in
TT 0	Total temperature at stator inlet	$^{\circ}$R
PT 0	Total pressure at stator inlet	psia
ALPHA 0	Gas angle (with respect to axial direction) at stator inlet	°
I STATØR	Incidence angle at stator inlet	°
V 0	Gas velocity (composed of tangential and axial components) at stator inlet	ft/sec
VU 0	Tangential gas velocity at stator inlet	ft/sec
VZ 0	Axial gas velocity at stator inlet	ft/sec

Symbol	Definition	Units
TS 0	Static temperature at stator inlet	^oR
PS 0	Static pressure at stator inlet	psia
DENS 0	Static density at stator inlet	lb/ft^3
M 0	Mach number at stator inlet	---
CP 0	Specific heat at constant pressure at station inlet	BTU/lb ^oR
RG 0	Gas constant at stator inlet	ft lb/lb ^oR
GAMG 0	Ratio of specific heats at stator inlet	---
RWG 0	Ratio of station flow to turbine inlet flow (by definition this must be 1.0 at the first stator inlet of turbine)	---
WG 0	Weight flow at stator inlet	lb/sec
DIAM 1	Diameter of mid-points of radial sectors at stator exit	in
ALPHA 1	Gas angle (with respect to axial direction) at stator exit	o
DEL A	Gas turning angle ($\alpha_o + \alpha_1$)	o
V 1	Gas velocity (composed of tangential and axial components (at stator exit	ft/sec
VU 1	Tangential gas velocity at stator exit	ft/sec
VZ 1	Axial gas velocity at stator exit	ft/sec
TS 1	Static temperature at stator exit	^oR
PS 1	Static pressure at stator exit	psia
DENS 1	Static density at stator exit	lb/ft^3
M 1	Mach number at stator exit	---
ZWI INC	Zweifel parameter, incompressible	---
CP S	Stator pressure coefficient, incompressible	---
CP 1	Specific heat at constant pressure at stator exit	BTU/lb ^oR
RG 1	Gas constant at stator exit	ft lb/lb ^oR
GAMG 1	Ratio of specific heats at stator exit	---
RWG 1	Ratio of stator exit flow to turbine inlet flow	---
WG 1	Weight flow at stator exit	lb/sec
DIAM 1A	Diameter of mid-points of radial sectors at root inlet	in
PTR 1A	Relative total pressure at rotor inlet	psia
TTR 1A	Relative total temperature at rotor inlet	^oR
BETA 1A	Relative gas angle at rotor inlet	o
I RØTØR	Incidence angle at rotor inlet	o
R 1A	Relative gas velocity at rotor inlet	ft/sec
RU 1A	Relative gas tangential velocity at rotor inlet	ft/sec
MR 1A	Relative Mach number at rotor inlet	---
U 1A	Wheel speed at rotor inlet	ft/sec
PS 1A	Static pressure at rotor inlet	psia
TS 1A	Static temperature at rotor inlet	^oR
CP 1A	Specific heat at constant pressure at rotor inlet	BTU/lb ^oR
RG 1A	Gas constant at rotor inlet	ft lb/lb ^oR
GAMG 1A	Ratio of specific heats at rotor inlet	---
RWG 1A	Ratio of rotor inlet flow to turbine inlet flow	---
WG 1A	Weight flow at rotor inlet	lb/sec
DIAM 2	Diameters of mid-points of radial sectors at rotor exit	in
PTR 2	Relative total pressure at rotor exit	psia
TTR 2	Relative total temperature at rotor exit	^oR
BETA 2	Relative gas angle at rotor exit	o
DBETA	Gas turning angle ($\beta_{1A} + \beta_2$)	o
R 2	Relative gas velocity at rotor exit	ft/sec

Symbol	Definition	Units
RU 2	Relative tangential gas velocity at rotor exit	ft/sec
MR 2	Relative Mach number at rotor exit	---
U 2	Wheel speed at rotor exit	ft/sec
RX	Reaction	---
DELH	Entholpy drop (energy output)	BTU/lb
PSI P	Kinetic energy loading parameter	---
ETA TT	Total to total efficiency	---
ETA TS	Total to static efficiency	---
ETA AT	Total to axial total efficiency	---
ZWI INC	Zweifel parameter, incompressible	---
CP R	Rotor pressure coefficient, incompressible	---
PS 2	Static pressure at rotor exit	psia
TS 2	Static temperature at rotor exit	^oR
CP 2	Specific heat at constant pressure at rotor exit	BTU/lb ^oR
RG 2	Gas constant at rotor exit	ft lb/lb ^oR
GAMG 2	Ratio of specific heats at rotor exit	---
RWG 2	Ratio of rotor exit flow to turbine inlet flow	---
WG 2	Weight flow at rotor exit	lb/sec
PT 2A	Total pressure at inlet to next stator	psia
TT 2A	Total temperature at inlet to next stator	^oR
V 2A	Gas velocity (composed of tangential and axial components) at inlet to next stator	ft/sec
VU 2A	Tangential gas velocity at inlet to next stator	ft/sec
ALPHA 2A	Gas angle (with respect to axial direction) at inlet to next stator	o
MF 2A	Axial Mach number at inlet to next stator	---
VZ 2A	Axial gas velocity at inlet to next stator	ft/sec
TS 2A	Static temperature at inlet to next stator	^oR
PS 2A	Static pressure at inlet to next stator	psia
DENS 2A	Static density at inlet to next stator	lb/ft^3
M 2A	Mach number at inlet to next stator	---
CP 2A	Specific heat at constant pressure at inlet to next stator	BTU/lb ^oR
RG 2A	Gas constant at inlet to next stator	ft lb/lb ^oR
GAMG 2A	Ratio of specific heats at inlet to next stator	---
RWG 2A	Ratio of flow at inlet to next stator to turbine inlet flow	---
WG 2A	Weight flow at inlet to next stator	lb/sec

2.3.4 Method for Calculation of Modified Parameters for Wet Vapor Turbines

• Assumptions Used and Development of Equations for Modified Parameters

In wet vapor turbines since there exists two distinct phases (gas and liquid), the usual ideal thermodynamic relationships which are valid for gas turbines are not directly applicable. The approach used to determine the performance of wet vapor turbines involved making a minimum of changes in the code but required modifying the input data appropriately to closely simulate the thermodynamic processes of a turbine operating within the saturation dome of a T-S (temperature entropy) diagram. The following method was derived and gives good agreement with the results from the WSD 2-D code as run by Fentress (2).

In order to arrive at a consistent set of relatively simple relationships, the following assumptions were made:

1) The inlet hub and tip diameters for a given blade row are assumed equal to the exit hub and tip diameters from the preceding blade row. The same assumption holds true for the modified γ^*, η^*, and R^*. The superscript * indicates that it is a modified value for specific heat ratio, blade efficiency, and gas constant.

2) All inefficiencies are assumed to be lumped into the single blade efficiency parameter η^*. This includes such items as incidence and exit losses and flow coefficients. Consequently EXPP = EXPN = 0.0, SREC = RREC = 1.0, SCF = RCF = 1.0, RTF = 1.0, and SESTH = RERTH = 1.0. The definitions of these computer code terms may be found in Section 2.3.3.

3) The exit gas flow angle from each blade row is taken to be equal to the exit blade angle. Therefore, actual blade exit angles (SDEA and RDEA) are input rather than distributed passage areas (SPA and RPA).

4) Since all energy changes are accounted for in the calculation of the modified parameters, there is no need to take into consideration the decrease in the gas flow rate due to condensation effects. Consequently RWG = 1.0.

5) Radial variations in γ^*, η^*, and R^* are assumed to be negligible.

In applying the following formulae to determine the modified values of R^*, γ^*, and η^*, care must be exercised to obtain the proper relative velocity either entering or leaving a blade row. See Figure 2.3-1 for clarification of the station terminology used in the example potassium turbine.

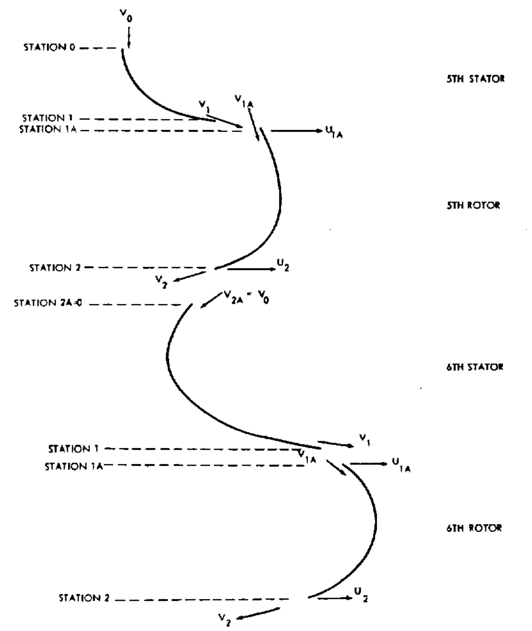

Figure 2.3-1 Axial Station Velocity Nomenclature

The initial values for static temperatures, pressures, specific volumes, and velocities are obtained from previous 1-D calculations. Definitions of the nomenclature used are given in Section 2.3.4.2

FIFTH STAGE

$$R_0^* = \frac{144\, P_{S0}\, v_{S0}}{T_{S0}} \tag{1}$$

$$\gamma_0^* = \frac{1}{1 - \dfrac{2\, g\, R_0^* \left(T_{T0} - T_{S0}\right)}{V_0^2}} \tag{2}$$

$$P_{T0}^* = P_{S0} \left(\frac{T_{T0}}{T_{S0}}\right)^{\frac{\gamma_0^*}{\gamma_0^* - 1}} \tag{3}$$

$$PTPS = \frac{P_{T0}^*}{P_{S1}} \tag{4}$$

$$R_1^* = \frac{144\, P_{S1}\, v_{S1}}{T_{S1}} \tag{5}$$

$$\gamma_1^* = \frac{1}{1 - \frac{2\,g\,R_1^*\,(T_{T0} - T_{S1})}{V_1^2}} \quad (6)$$

$$\eta_1^* = \frac{T_{T0} - T_{S1}}{T_{T0}\left[1 - \left(\frac{P_{S1}}{P_{T0}^*}\right)^{\frac{\gamma_1^* - 1}{\gamma_1^*}}\right]} \quad (7)$$

$$D_{R1A}^* = D_{R1} \quad (8)$$

$$D_{T1A}^* = D_{T1} \quad (9)$$

$$R_{1A}^* = R_1^* \quad (10)$$

$$\gamma_{1A}^* = \gamma_1^* \quad (11)$$

$$R_2^* = \frac{144\,P_{S2}\,v_{S2}}{T_{S2}} \quad (12)$$

$$T_{T2g} = T_{S1A} + \frac{\left(\gamma_{1A}^* - 1\right)\left(V_{1A}^2 + U_2^2 - U_{1A}^2\right)}{2g\,\gamma_{1A}^*\,R_{1A}^*} \quad (13)$$

$$P_{T2g} = P_{S1A}\left[1 + \frac{\left(\gamma_{1A}^* - 1\right)\left(V_{1A}^2 + U_2^2 - U_{1A}^2\right)}{2g\,\gamma_{1A}^*\,R_{1A}^*\,T_{S1A}}\right]^{\frac{\gamma_{1A}^*}{\gamma_{1A}^* - 1}} \quad (14)$$

$$\gamma_2^* = \frac{1}{1 - \frac{2g\,R_2^*\,(T_{T2g} - T_{S2})}{V_2^2}} \quad (15)$$

$$\eta_2^* = \frac{T_{T2g} - T_{S2}}{T_{T2g}\left[\left(1 - \frac{P_{S2}}{P_{T2g}}\right)^{\frac{\gamma_2^* - 1}{\gamma_2^*}}\right]} \quad (16)$$

$$D_{R2A}^* = D_{R2} \quad (17)$$

$$D_{T2A}^* = D_{T2} \quad (18)$$

$$R_{2A}^* = R_2^* \quad (19)$$

$$\gamma_{2A}^* = \gamma_2^* \quad (20)$$

$$D_{R0}^* = D_{R2A}^* \quad (21)$$

$$D_{T0}^* = D_{T2A}^* \quad (22)$$

$$R_0^* = R_{2A}^* \quad (23)$$

$$\gamma_0^* = \gamma_{2A}^* \quad (24)$$

$$R_1^* = \frac{144\,P_{S1}\,v_{S1}}{T_{S1}} \quad (25)$$

$$T_{T0g} = T_{S2A} + \frac{V_{2A}^2}{\frac{2g\,\gamma_{2A}^*\,R_{2A}^*}{\gamma_{2A}^* - 1}} \quad (26)$$

$$P_{T0g} = P_{S2A}\left(\frac{T_{T0g}}{T_{S2A}}\right)^{\frac{\gamma_{2A}^*}{\gamma_{2A}^* - 1}} \quad (27)$$

$$\gamma_1^* = \frac{1}{1 - \frac{2g\,R_1^*\,(T_{T0g} - T_{S1})}{V_1^2}} \quad (28)$$

$$\eta_1^* = \frac{T_{T0g} - T_{S1}}{T_{T0g}\left[1 - \left(\frac{P_{S1}}{P_{T0g}}\right)^{\frac{\gamma_1^* - 1}{\gamma_1^*}}\right]} \quad (29)$$

The remainder of the expressions for the modified parameters for the rest of the sixth stage are the same as those in Equations (8) through (20). For turbines with more than two stages, the same relationships are repeated for each succeeding stage. Since there is a significant amount of hand calculations involved in obtaining the modified parameters, a small computer program could be written to punch out these values in a format compatible with the input to the modified NASA turbine code.

• Nomenclature Used in Calculation of Modified Parameters

Symbol	Definition	Units
D_R	Root diameter	in
D_T	Tip diameter	in
g	Gravitational acceleration (32.2)	ft/sec^2
P_S	Static pressure	psia
P_T	Total pressure	psia
PTPS	Total-to-static pressure ratio across first stator	---
R	Gas constant	$ft/^{o}R$
T_S	Static temperature	^{o}R
T_T	Total temperature	^{o}R
U	Wheel speed	ft/sec
V	Gas velocity	ft/sec
v_S	Specific volume	ft^3/lb
γ	Ratio of specific heats	---
η	Overall effective blade efficiency	---

2.3.5 POSSIBLE FUTURE MODIFICATIONS TO CODE

1) With the advent of the CDC 6600 computer and its 65 K core (as compared to the IBM 7094 and its core of 32 K), it is possible to expand the maximum number of radial sectors to greater than 6 and the maximum number of stages to exceed 8. Of course computer run times would be longer and a different method of printing out data would have to be used.

2) The code could be changed so as to iterate to a desired exit pressure condition automatically by comparing the average turbine exit total pressure with that desired. If the difference between the exit total pressures were not within some given tolerance, the first stator pressure ratio PTPS would be adjusted accordingly.

3) Non-uniform turbine inlet radial distributions in pressure, temperature, and velocity could be achieved by inputting such quantities. The assumption in the code as presently programmed is that the inlet radial distributions are uniform.

2.3.6 REFERENCES

1. E. E. Flagg, "Analytical Procedure and Computer Program for Determining the Off-Design Performance of Axial Flow Turbines," NASA CR-710, February 1967.

2. Westinghouse Electric Corporation, Astronuclear Laboratory, Report WANL-PR (DD)-017, January 1967, Contract NAS 7-390.

APPENDICES TO SECTION 2.3

APPENDIX 2.3 A

SAMPLE PROBLEMS ILLUSTRATING USE OF CODE

2.3 A-1 NASA Reference Two-Stage Gas Turbine (5 Radial Sectors)

1. Comparison of Results

The sample problem given in NASA CR-710 was run both on the IBM 7094 (II) and CDC 6600 computer. The data output from both machines was in exact agreement to at least the sixth significant figure. The minor discrepancies noted were thought to be due to the difference in the number of significant places carried in the respective machines. It was found that the sample problem data output given in NASA CR-710 did not exactly correspond to that report's data input. When the data input was appropriately changed, the subsequent output was in substantial agreement (at least to the fourth significant place) with that given in NASA CR-710. No explanation can be given at this time as to why there was not agreement to at least the sixth place. But it is felt that the agreement is more than adequate to satisfy engineering criteria.

2. Data Input

```
                          TURBINE COMPUTER PROGRAM
    NASA TWO STAGE REFERENCE TURBINE
    1.00  5041  -8  DEG.  LOSS  PROFILE  .98  .946.  .977  .90.
$DATAIN
 STGCH=      1.000
  TTIN=    700.000   PTIN=     17.140    WAIR=      0.000  FAIR=      0.000
  PTPS=      1.600   DELC=      0.000    DELL=      0.000  DELA=      0.000
   STG=      2.000   SECT=      5.000    EXPN=      3.000  EXPP=      3.000
   PAF=      0.000    SLI=      0.000    AACS=      1.000   RPM=   5041.000
  VCTD=      1.000    RSL=     53.350     TSL=    518.688   PSL=     14.696
 GAMSL=      1.400 ENDSTG=      0.000  ENDJOB=      0.000

                          INLET RADIAL PROFILES
  PCNH=     .200       .200       .200       .200       .200       0.000



                          STANDARD OPTION
STAGE=  1                 AXIAL STATIONS
        STA. 0     STA. 1     STA.1A     STA. 2     STA.2A
   RG=  53.350     53.350     53.350     53.350     53.350     0.000
 GAMG=   1.400      1.400      1.400      1.400      1.400     0.000
   DR=  19.110     19.110     18.969     18.406     18.265     0.000
   DT=  28.000     28.000     28.141     28.704     28.845     0.000
  RWG=   1.000      1.000      1.000      1.000      1.000     0.000

                    STATOR RADIAL DISTRIBUTIONS
           ROOT               PITCH                 TIP
 SDIA=   0.000      0.000      0.000      0.000      0.000     0.000
 SDEA=   0.000      0.000      0.000      0.000      0.000     0.000
 SREC=   1.000      1.000      1.000      1.000      1.000     0.000
 SETA=    .970       .980       .980       .980       .970     0.000
  SCF=    .977       .977       .977       .977       .977     0.000
  SPA=  22.140     26.035     30.135     34.194     38.499     0.000
SESTH=   1.000

                    ROTOR RADIAL DISTRIBUTIONS
 RDIA=  50.600     44.900     38.100     30.200     20.900     0.000
 RDEA=   0.000      0.000      0.000      0.000      0.000     0.000
 RREC=   1.000      1.000      1.000      1.000      1.000     0.000
 RETA=    .919       .946       .946       .946       .919     0.000
  RCF=    .950       .950       .950       .950       .950     0.000
  RPA=  33.408     36.352     38.976     41.280     43.008     0.000
  RTF=   1.000      1.000      1.000      1.000      1.000     0.000
RERTH=   1.010

                          STANDARD OPTION
STAGE=  2                 AXIAL STATIONS
        STA. 0     STA. 1     STA.1A     STA. 2     STA.2A
   RG=  53.350     53.350     53.350     53.350     53.350     0.000
 GAMG=   1.400      1.400      1.400      1.400      1.400     0.000
   DR=  18.265     17.814     17.673     17.110     17.110     0.000
   DT=  28.845     29.296     29.437     30.000     30.000     0.000
  RWG=   1.000      1.000      1.000      1.000      1.000     0.000
```

STATOR RADIAL DISTRIBUTIONS

	ROOT		PITCH		TIP	
SDIA=	25.000	22.400	20.200	18.300	16.600	0.000
SDEA=	0.000	0.000	0.000	0.000	0.000	0.000
SREC=	1.000	1.000	1.000	1.000	1.000	0.000
SETA=	.970	.980	.980	.980	.970	0.000
SCF=	.925	.925	.925	.925	.925	0.000
SPA=	30.420	36.855	43.485	50.765	58.240	0.000
SESTH=	1.010					

ROTOR RADIAL DISTRIBUTIONS

RDIA=	36.600	26.900	16.100	4.600	-6.700	0.000
RDEA=	0.000	0.000	0.000	0.000	0.000	0.000
RREC=	1.000	1.000	1.000	1.000	1.000	0.000
RETA=	.919	.946	.946	.946	.919	0.000
RCF=	.900	.900	.900	.900	.900	0.000
RPA=	43.350	48.150	52.350	55.750	58.550	0.000
RTF=	1.000	1.000	1.000	1.000	1.000	0.000
RFRTH=	1.010					

3. Listing of Data Output

NASA TURBINE COMPUTER PROGRAM
NASA TWO STAGE REFERENCE TURBINE
1.00 5041 -8 DEG. LOSS PROFILE .98 .946, .977 .90,
CASE 1. 0
STAGE PERFORMANCE

	STAGE 1	STAGE 2	STAGE 3	STAGE 4
TTBAR 0	700.0	608.5		
PTBAR 0	17.140	10.120		
WG 0	43.612	43.612		
DEL H	21.960	11.370		
WRT/P	67.320	106.303		
DH/TTBAR0	.03137	.01869		
N/RT	190.532	204.358		
ETA TT	.93545	.93026		
ETA TS	.82312	.74101		
ETA AT	.92064	.92376		
PT0/PS1	1.600	1.327		
PTBAR0/PTBAR2	1.694	1.358		
PTBAR0/PS2	1.840	1.475		
PTR2/PS2	1.340	1.216		
TTBAR2/TTBAR0	.86926	.92212		
TTR1A/TTBAR0	.91710	.94793		
WG 1	43.612	43.612		
PS 1A	10.770	7.659		
TTR 1A	642.0	576.8		
PTR 1A	12.470	8.343		
WG 1A	43.612	43.612		
PS 2	9.314	6.860		
TTBAR 2	608.5	561.1		
PTBAR 2	10.120	7.452		
WG 2	43.612	43.612		
WG 2A	43.612	43.612		
UP/VI	.44821	.59095		
UR/VI	.35559	.43632		
PSI P	1.02409	.53026		
PSI R	1.62705	.97270		
RX P	.21420	.26054		
RX R	-.08793	-.07253		
ALPHA 0	0.000	20.327		
I STATOR	0.000	.127		
BETA 1A	46.336	15.343		
I ROTOR	8.236	-.757		

3. Output Data (continued)

ALPHA 2A	20.327	-9.259
DRETA R	116.216	86.338
M 1	.83798	.64215
M1 RT	1.01118	.78439
MR 1A	.47064	.35156
MR1A RT	.69181	.50438
MR 2	.64048	.52077
MR2 TIP	.69787	.61846
E/TH CR	16.272	9.692
N/RTH CR	4339.3	4654.2
WRTHCRE/C	43.440	68.554

OVERALL PERFORMANCE

PSI P	.77717	PSI R	1.32335	DEL H	33.33004
WRT/P	67.31951	N/RT	190.53189	DELH/TTIN	.04761
PT0/PTBAR2	2.29991	PT0/PS2	2.49847	PT0/PAT2A	2.30903
ETA TT	.93700	ETA TS	.86213	ETA TAT	.93477
WNE/60C	3141.641	N/RTH CR	4339.329	E/TH CR	26.69720

NASA TURBINE COMPUTER PROGRAM
NASA TWO STAGE REFERENCE TURBINE
1.00 5041 -8 DEG. LOSS PROFILE .98 .946. .977 .90.
CASE 1. 0
INTER-STAGE PERFORMANCE

STA 0	STATOR INLET		STAGE 1.				
DIAM 0	19.999	21.777	23.555	25.333	27.111		
TT 0	700.0	700.0	700.0	700.0	700.0		
PT 0	17.140	17.140	17.140	17.140	17.140		
ALPHA 0	0.000	0.000	0.000	0.000	0.000		
I STATOR	0.000	0.000	0.000	0.000	0.000		
V 0	299.463	299.463	299.463	299.463	299.463		
VU 0	0.000	0.000	0.000	0.000	0.000		
VZ 0	299.463	299.463	299.463	299.463	299.463		
TS 0	692.5	692.5	692.5	692.5	692.5		
PS 0	16.509	16.509	16.509	16.509	16.509		
DENS 0	.06434	.06434	.06434	.06434	.06434		
M 0	.23213	.23213	.23213	.23213	.23213		
CP 0	.23996	.23996	.23996	.23996	.23996		
RG 0	53.350	53.350	53.350	53.350	53.350		
GAMG 0	1.40000	1.40000	1.40000	1.40000	1.40000		
RWG 0	1.00000	1.00000	1.00000	1.00000	1.00000		
WG 0	6.58435	7.70666	8.60273	9.78081	10.73712	43.61168	TOTAL FLOW
STA 1	STATOR EXIT						
DIAM 1	19.999	21.777	23.555	25.333	27.111		
ALPHA 1	69.539	67.940	66.303	64.911	63.359		
DEL A	69.539	67.940	66.303	64.911	63.359		
V 1	1147.972	1080.202	1017.726	954.148	895.217		
VU 1	1075.549	1001.125	931.914	864.123	800.175		
VZ 1	401.291	405.692	409.026	404.586	401.413		
TS 1	590.3	602.9	613.8	624.2	633.3		
PS 1	9.252	10.046	10.712	11.379	11.936		
DENS 1	.04230	.04498	.04711	.04920	.05087		
M 1	.96384	.89763	.83798	.77904	.72567		
ZWI INC	-.65502	-.69615	-.73603	-.76804	-.80159		
CP S	.93195	.92314	.91342	.90150	.88810		
CP 1	.23996	.23996	.23996	.23996	.23996		
RG 1	53.350	53.350	53.350	53.350	53.350		
GAMG 1	1.40000	1.40000	1.40000	1.40000	1.40000		
RWG 1	1.00000	1.00000	1.00000	1.00000	1.00000		
WG 1	6.58435	7.70666	8.60273	9.78081	10.73712	43.61168	TOTAL FLOW

3. Output Data (continued)

```
                 NASA TURBINE COMPUTER PROGRAM
   NASA TWO STAGE REFERENCE TURBINE
   1.00  5041  -8  DEG.  LOSS  PROFILE  .98  .946,  .977  .90,
                          CASE   1.  0
                    INTER-STAGE PERFORMANCE
```

STA 1A	ROTOR INLET		STAGE 1.				
DIAM 1A	19.886	21.721	23.555	25.389	27.224		
PTR 1A	11.994	12.251	12.478	12.778	13.083		
TTR 1A	637.2	639.2	642.0	645.8	650.4		
BETA 1A	58.685	53.188	46.336	37.964	27.212		
I ROTOR	8.085	8.288	8.236	7.764	6.312		
R 1A	754.102	656.963	572.034	493.769	433.126		
RU 1A	644.243	525.969	413.810	303.751	198.059		
MR 1A	.63340	.54564	.47064	.40274	.35068		
U 1A	437.407	477.755	516.104	558.452	598.801		
PS 1A	9.225	10.067	10.770	11.461	12.035		
TS 1A	589.8	603.3	614.7	625.5	634.8		
CP 1A	.23996	.23996	.23996	.23996	.23996		
RG 1A	53.350	53.350	53.350	53.350	53.350		
GAMG 1A	1.40000	1.40000	1.40000	1.40000	1.40000		
RWG 1A	1.00000	1.00000	1.00000	1.00000	1.00000		
WG 1A	6.58435	7.70666	8.60273	9.78081	10.73712	43.61168	TOTAL FLOW

STA 2	ROTOR EXIT						
DIAM 2	19.436	21.495	23.555	25.615	27.674		
PTR 2	11.947	12.225	12.478	12.810	13.154		
TTR 2	636.5	638.8	642.0	646.3	651.4		
BETA 2	57.531	58.629	59.379	60.258	60.964		
UBETA	116.216	111.817	105.715	98.223	88.175		
R 2	700.060	738.940	764.765	797.556	818.486		
RU 2	590.630	630.922	658.123	692.496	715.611		
MR 2	.58512	.61884	.64048	.66793	.68411		
U 2	427.500	472.802	516.104	563.406	608.708		
RX	-.00402	.11699	.21420	.30756	.38295		
DELH	21.683	22.139	22.182	22.137	21.658		
PST P	2.90236	2.45376	2.06895	1.76143	1.48743		
ETA TT	.91418	.94184	.94518	.94752	.92554		
ETA TS	.80596	.82681	.83127	.83236	.81639		
ETA AT	.89419	.92233	.92980	.93438	.91677		
ZWI INC	-1.85326	-1.61317	-1.42033	-1.24554	-1.09099		
CP R	-.16035	.20959	.44051	.61671	.71997		
PS 2	9.277	9.295	9.314	9.330	9.342		
TS 2	595.7	593.3	593.3	593.3	595.7		
CP 2	.23996	.23996	.23996	.23996	.23996		
RG 2	53.350	53.350	53.350	53.350	53.350		
GAMG 2	1.40000	1.40000	1.40000	1.40000	1.40000		
RWG 2	1.00000	1.00000	1.00000	1.00000	1.00000		
WG 2	6.89815	7.85826	8.73519	9.66391	10.45615	43.61166	TOTAL FLOW
PT 2A	10.061	10.112	10.122	10.149	10.138		
TT 2A	609.6	607.7	607.6	607.7	609.7		
V 2A	402.148	406.590	403.078	404.007	398.169		
VU 2A	164.083	158.536	140.019	128.806	106.469		
ALPHA 2A	24.080	22.949	20.327	18.592	15.509		
MF 2A	.30674	.31338	.31636	.32046	.32044		
VZ 2A	367.151	374.409	377.978	382.924	383.670		
TS 2A	596.2	594.0	594.0	594.2	596.5		
PS 2A	9.304	9.334	9.355	9.376	9.391		
DENS 2A	.04213	.04241	.04251	.04259	.04249		
M 2A	.33598	.34032	.33736	.33811	.33255		
CP 2A	.23996	.23996	.23996	.23996	.23996		
RG 2A	53.350	53.350	53.350	53.350	53.350		
GAMG 2A	1.40000	1.40000	1.40000	1.40000	1.40000		
RWG 2A	1.00000	1.00000	1.00000	1.00000	1.00000		
WG 2A	6.89815	7.85826	8.73519	9.66391	10.45615	43.61166	TOTAL FLOW

3. Output Data (continued)

```
                    NASA TURBINE COMPUTER PROGRAM
 NASA TWO STAGE REFERENCE TURBINE
 1.00  5041  -8  DEG.  LOSS  PROFILE  .98  .946,  .977  .90,
                          CASE   1,  0
                     INTER-STAGE PERFORMANCE
```

STA 0	STATOR INLET		STAGE 2.				
DIAM 0	19.323	21.439	23.555	25.671	27.767		
TT 0	608.5	608.5	608.5	608.5	608.5		
PT 0	10.120	10.120	10.120	10.120	10.120		
ALPHA 0	24.080	22.949	20.327	18.592	15.509		
I STATOR	-.920	.549	.127	.292	-1.090		
V 0	402.148	406.590	403.078	404.007	398.169		
VU 0	164.083	158.536	140.019	128.806	106.469		
VZ 0	367.151	374.409	377.978	382.924	383.670		
TS 0	596.2	594.0	594.0	594.2	596.5		
PS 0	9.304	9.334	9.355	9.376	9.391		
DENS 0	.04213	.04241	.04251	.04259	.04249		
M 0	.33598	.34032	.33736	.33811	.33255		
CP 0	.23996	.23996	.23996	.23996	.23996		
RG 0	53.350	53.350	53.350	53.350	53.350		
GAMG 0	1.40000	1.40000	1.40000	1.40000	1.40000		
RWG 0	1.00000	1.00000	1.00000	1.00000	1.00000		
WG 0	6.89815	7.85826	8.73519	9.66391	10.45615	43.61166	TOTAL FLOW

STA 1	STATOR EXIT						
DIAM 1	18.962	21.259	23.555	25.851	28.148		
ALPHA 1	61.651	59.301	57.068	54.670	52.236		
DEL A	85.731	82.250	77.395	73.262	67.744		
V 1	852.196	795.576	746.339	695.126	650.709		
VU 1	749.990	684.085	626.415	567.111	514.398		
VZ 1	404.665	406.169	405.742	401.978	398.519		
TS 1	548.0	555.8	562.1	568.3	573.2		
PS 1	6.934	7.321	7.624	7.926	8.158		
DENS 1	.03415	.03556	.03661	.03765	.03841		
M 1	.74259	.68839	.64215	.59484	.55441		
ZWI INC	-1.03734	-1.09869	-1.13154	-1.16854	-1.17646		
CP S	.77731	.73881	.70832	.66221	.62558		
CP 1	.23996	.23996	.23996	.23996	.23996		
RG 1	53.350	53.350	53.350	53.350	53.350		
GAMG 1	1.40000	1.40000	1.40000	1.40000	1.40000		
RWG 1	1.00000	1.00000	1.00000	1.00000	1.00000		
WG 1	6.56380	7.69027	8.76394	9.79979	10.79323	43.61164	TOTAL FLOW

STA 1A	ROTOR INLET		STAGE 2.				
DIAM 1A	18.849	21.202	23.555	25.908	28.261		
PTR 1A	7.983	8.161	8.343	8.600	8.871		
TTR 1A	570.7	573.3	576.8	581.8	587.6		
BETA 1A	40.535	28.960	15.343	-.585	-15.815		
I ROTOR	3.935	2.060	-.757	-5.185	-9.115		
W 1A	522.762	457.435	409.333	389.963	400.905		
WU 1A	339.876	219.552	108.311	-3.979	-109.261		
MR 1A	.45573	.39220	.35196	.33344	.34128		
U 1A	414.602	466.353	518.104	569.855	621.606		
PS 1A	6.930	7.341	7.659	7.970	8.209		
TS 1A	548.0	556.2	562.9	569.2	574.3		
CP 1A	.23996	.23996	.23996	.23996	.23996		
RG 1A	53.350	53.350	53.350	53.350	53.350		
GAMG 1A	1.40000	1.40000	1.40000	1.40000	1.40000		
RWG 1A	1.00000	1.00000	1.00000	1.00000	1.00000		
WG 1A	6.56380	7.69027	8.76394	9.79979	10.79383	43.61164	TOTAL FLOW

```
                 NASA TURBINE COMPUTER PROGRAM
 NASA TWO STAGE REFERENCE TURBINE
 1.00  5041  -8  DEG.  LOSS  PROFILE  .98  .946,  .977  .90,
                          CASE   1.  0
                   INTER-STAGE PERFORMANCE
 STA 2   ROTOR EXIT
 DIAM 2      18.399      20.977      23.555      26.133      28.711
  PTR 2       7.950       8.142       8.343       8.625       8.926
  TTR 2       570.0       573.0       576.8       582.3       588.7
 BETA 2      45.803      47.980      49.600      51.528      52.888
  DBETA      86.338      76.940      64.943      50.944      37.072
    W 2     510.818     558.390     597.132     646.661     635.002
   WU 2     366.232     414.834     454.736     506.279     546.256
   MR 2      .44500      .48703      .52077      .56377      .59605
    U 2     404.695     461.399     518.104     574.808     631.513
     RX      .02767      .16069      .26054      .35780      .43067
   DELH      11.872      11.918      11.652      11.307      10.570
  PSI P     1.77162     1.38665     1.08674      .86417      .67406
 ETA TT      .92495      .94980      .94776      .94026      .89652
 ETA TS      .77200      .77551      .75903      .73739      .69018
 ETA AT      .92288      .94655      .94164      .93302      .88571
 ZWI INC   -1.83075    -1.49053    -1.21766     -.96625     -.75608
   CP R     -.04811      .34059      .53009      .63634      .65747
   PS 2       6.855       6.857       6.860       6.863       6.867
   TS 2       548.3       547.0       547.1       547.5       549.6
   CP 2      .23996      .23996      .23996      .23996      .23996
   RG 2      53.350      53.350      53.350      53.350      53.350
 GAMG 2     1.40000     1.40000     1.40000     1.40000     1.40000
  RWG 2     1.00000     1.00000     1.00000     1.00000     1.00000
   WG 2     6.21734     7.46048     8.67619    10.00385    11.25376   43.61162   TOTAL FLOW
  PT 2A       7.334       7.399       7.439       7.491       7.537
  TT 2A       559.0       558.8       559.9       561.4       564.4
   V 2A     358.174     376.670     392.171     408.102     422.019
  VU 2A     -38.463     -46.565     -63.368     -68.529     -85.256
ALPHA 2A     -6.165      -7.101      -9.299      -9.667     -11.655
  MF 2A      .31022      .32601      .33752      .35074      .35964
  VZ 2A     356.162     373.780     387.017     402.308     413.318
  TS 2A       546.3       547.0       547.1       547.5       549.6
  PS 2A       6.855       6.857       6.860       6.863       6.867
DENS 2A      .03374      .03384      .03384      .03384      .03372
   M 2A      .31202      .32853      .34202      .35579      .36721
  CP 2A      .23996      .23996      .23996      .23996      .23995
  RG 2A      53.350      53.350      53.350      53.350      53.350
GAMG 2A     1.40000     1.40000     1.40000     1.40000     1.40000
 RWG 2A     1.00000     1.00000     1.00000     1.00000     1.00000
  WG 2A     6.21734     7.46048     8.67619    10.00385    11.25376   43.61162   TOTAL FLOW
```

2.3 A-2 Wet-Vapor Potassium Turbine*(5 Radial Sectors)

1. Calculation of Modified Parameters

Using the equations given in Section 2.3.4, the values for the modified parameters (given in Table 2.3 A-1) were calculated by hand and used as data input to the modified NASA turbine code. Only the 5th and 6th stages are analyzed and correspond to stages 1 and 2 in the output listing.

2. Comparison of Results from Modified NASA Code and WSD Code

Table 2.3A-2 shows a comparison of the results between the 1-D and 2-D codes from WSD and the NASA code using the modified parameters. The total-to-static pressure ratio (PTPS) across the first stator was adjusted until the turbine exit conditions were identical to those obtained in the Steam Division codes. The modified parameters were assumed to remain constant during the small changes in PTPS. Unfortunately, a completely consistent set of input data was impossible to be obtained from either Table I or Table II of Reference (2) or

TABLE 2.3A-1

MODIFIED PARAMETERS FOR POTASSIUM TURBINE

Station	D_R^*	D_T^*	R^*	γ^*	η^*	
0	5.29	7.51	31.158	1.1825	---	P_{TO}^* = 38.828; PTPS = 1.3619
1	5.15	7.83	30.842	1.1437	0.92577	
1A	5.15	7.83	30.842	1.1437	---	
2	5.04	8.28	30.689	1.16607	0.81662	
2A	5.04	8.28	30.689	1.16607	---	
0	5.04	8.28	30.689	1.16607	---	
1	4.88	8.62	30.828	1.1447	0.94752	
1A	4.88	8.62	30.828	1.1447	---	
2	4.60	9.10	30.763	1.1637	0.8155	
2A	4.60	9.10	30.763	1.1637	---	

*Described in Reference (2).

TABLE 2.3A-2

COMPARISON OF POTASSIUM TURBINE DATA AT MEAN DIAMETER

BLADE ROW EXIT CONDITIONS	Fourth Rotor 1-D Code (1)	Fourth Rotor NASA Code (2)	Fourth Rotor % Difference	Fifth Stator 1-D Code (1)	Fifth Stator NASA Code (2)	Fifth Stator % Difference	Fifth Rotor 1-D Code (1)	Fifth Rotor NASA Code (2)	Fifth Rotor % Difference	Sixth Stator 1-D Code (1)	Sixth Stator NASA Code (2)	Sixth Stator % Difference	Sixth Rotor 1-D Code (1)	Sixth Rotor NASA Code (2)	Sixth Rotor % Difference
BLADE HEIGHT (inch)	1.11	1.11 *	0.0	1.34	1.34 *	0.0	1.62	1.62 *	0.0	1.87	1.87 *	0.0	2.25	2.25 *	0.0
MEAN DIAMETER (inch)	6.40	6.40 *	0.0	6.49	6.49*	0.0	6.66	6.66 *	0.0	6.75	6.75 *	0.0	6.85	6.85 *	0.0
FLOW ANGLE (degree)	64.37	--	--	64.37(65.03)	65.03*	+1.03(0.0)	64.37(63.65)	63.65*	-1.12(0.0)	57.32(57.57)	57.57 *	+0.436(0.0)	60.30(58.98)	58.98*	-2.19(0.0)
STATIC PRESSURE (psia)	37.00	--	--	28.51	28.198	-1.09	22.04	21.963	-0.349	19.69	19.495	-0.950	16.90	16.892	-0.047
STATIC TEMPERATURE °R	2052	--	--	1994	1991.9	-0.105	1937	1936.7	-0.015	1914	1911.9	-0.110	1882	1882.0	0.0
FLOW RATE (lb/sec)	5.76	--	--	5.76	5.75951	0.0	5.76	5.75951	0.0	5.76	5.75951	0.0	5.76	5.75951	0.0
JET VELOCITY (ft/sec)	1034	--	--	1049(1076.5)	1091.3	+4.03(+1.37)	1075(1033.5)	1028.4	-4.33(-0.496)	815 (811.7)	823.0	+0.982(1.39)	822(790.6)	779.9	-4.77(-1.35)
GAMMA	1.211	1.1825*	--	1.203	1.1437*	--	1.196	1.6607*	-	1.195	1.1447*	--	1.194	1.1637	--
GAS CONSTANT (ft/°R)	31.51	31.158*	--	31.23	30.842*	--	30.93	30.689*	--	30.80	30.828*	--	30.65	30.763 *	--
EFFICIENCY COEFFICIENT FOR BLADE ROW	--	--	--	--	0.92577	--	--	0.81662*	--	--	0.94752*	--	--	0.8155	--

(1) From Reference (2)

(2) Using modified NASA Code (5 radial sectors)

Terms in parentheses are from 2-D code. See Reference (2)

Flow angles are with respect to axial direction

* Indicates NASA code input data.

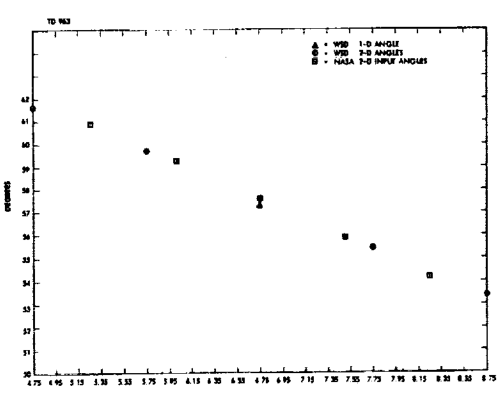

Figure 2.3A-1 6th Stator Blade Exit Angles

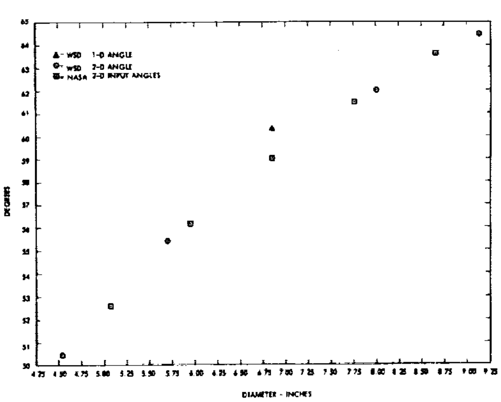

Figure 2.3A-2 6th Rotor Blade Exit Angles

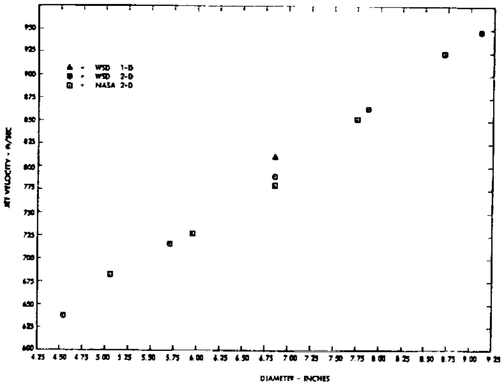

Figure 2. 3A-3 6th Rotor Exit Jet Velocity

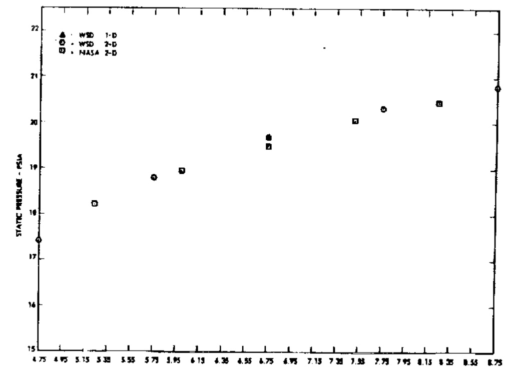

Figure 2. 3A-4 5th Stator Exit Static Pressure

a combination of the two. The difference in the 2-D blade angle distribution from that used in the 1-D calculation is most likely the primary reason that the jet velocities at the mean diameters are not in better agreement.

Figures 2. 3A-1 and 2. 3A-2 show the slight differences in the angles used in WSD 2-D calculations and those used as input to the NASA code 2-D analysis. Figure 2.3A-3 shows the good agreement between the turbine exit jet velocities as calculated by both codes. In Figure 2.3A-4 there is also good agreement with the static pressure distributions from the 5th stator exit.

It is therefore concluded that if one performs a hand solution (or uses an appropriate computer code) for a 1-D turbine analysis, then this method of using modified γ, R, and η parameters with the NASA code will give a valid and thermodynamically consistent two-dimensional analysis of a turbine operating in the wet vapor region.

3. Data Input

```
                          TURBINE COMPUTER PROGRAM
    TWO STAGE POTASSIUM TURBINE
    FIVE RADIAL SECTORS
 $DATAIN
  STGCH=     1.000
   TTIN=  2067.300    PTIN=     38.828    WAIR=     0.000  FAIR=      0.000
   PTPS=     1.377    DELC=      0.000    DELL=     0.000  DELA=      0.000
    STG=     2.000    SECT=      5.000    EXPN=     0.000  EXPP=      0.000
    PAF=     1.000     SLI=      0.000    AACS=     1.000   RPM=  24000.000
   VCTO=     1.000     HSL=     37.600     TSL=  1800.000   PSL=     11.200
  GAMSL=     1.618 ENDSTG=      0.000  ENDJOB=     0.000

                          INLET RADIAL PROFILES
   PCNH=     .200       .200       .200       .200       .200       0.000

                             STANDARD OPTION
  STAGE=   1                 AXIAL STATIONS
           STA. 0     STA. 1     STA.1A     STA. 2     STA.2A
     RG=   31.158     30.842     30.842     30.689     30.689      0.000
   GAMG=    1.182      1.144      1.144      1.166      1.166      0.000
     DR=    5.290      5.150      5.150      5.040      5.040      0.000
     DT=    7.510      7.830      7.830      8.280      8.280      0.000
    RWG=    1.000      1.000      1.000      1.000      1.000      0.000

                        STATOR RADIAL DISTRIBUTIONS
            ROOT                  PITCH                  TIP
   SDIA=    0.000      0.000      0.000      0.000      0.000      0.000
   SDEA=   66.100     65.600     65.030     64.350     63.650      0.000
   SREC=    1.000      1.000      1.000      1.000      1.000      0.000
   SETA=     .926       .926       .926       .926       .926      0.000
    SCF=    1.000      1.000      1.000      1.000      1.000      0.000
    SPA=    0.000      0.000      0.000      0.000      0.000      0.000
  SESTH=    1.000
```

ROTOR RADIAL DISTRIBUTIONS

RDIA=	40.850	41.500	33.060	22.000	8.500	0.000
RDEA=	61.600	62.650	63.650	64.550	65.350	0.000
RREC=	1.000	1.000	1.000	1.000	1.000	0.000
RETA=	.817	.817	.817	.817	.817	0.000
RCF=	1.000	1.000	1.000	1.000	1.000	0.000
RPA=	0.000	0.000	0.000	0.000	0.000	0.000
RTF=	1.000	1.000	1.000	1.000	1.000	0.000
RERTH=	1.000					

STANDARD OPTION
AXIAL STATIONS

STAGE= 2	STA. 0	STA. 1	STA. 1A	STA. 2	STA. 2A	
RG=	30.689	30.828	30.828	30.763	30.763	0.000
GAMG=	1.166	1.145	1.145	1.164	1.164	0.000
DR=	5.040	4.880	4.880	4.600	4.600	0.000
DT=	8.280	8.620	8.620	9.100	9.100	0.000
RWG=	1.000	1.000	1.000	1.000	1.000	0.000

STATOR RADIAL DISTRIBUTIONS

	ROOT		PITCH		TIP	
SDIA=	37.300	29.700	26.540	23.400	20.000	0.000
SDEA=	60.900	59.250	57.570	55.850	54.150	0.000
SREC=	1.000	1.000	1.000	1.000	1.000	0.000
SETA=	.948	.948	.948	.948	.948	0.000
SCF=	1.000	1.000	1.000	1.000	1.000	0.000
SPA=	0.000	0.000	0.000	0.000	0.000	0.000
SESTH=	1.000					

ROTOR RADIAL DISTRIBUTIONS

RDIA=	32.800	16.000	-2.860	-20.500	-35.000	0.000
RDEA=	52.600	56.100	58.980	61.450	63.600	0.000
RREC=	1.000	1.000	1.000	1.000	1.000	0.000
RETA=	.816	.816	.816	.816	.816	0.000
RCF=	1.000	1.000	1.000	1.000	1.000	0.000
RPA=	0.000	0.000	0.000	0.000	0.000	0.000
RTF=	1.000	1.000	1.000	1.000	1.000	0.000
RERTH=	1.000					

4. Output Data

NASA TURBINE COMPUTER PROGRAM
TWO STAGE POTASSIUM TURBINE
FIVE RADIAL SECTORS
CASE 2. 0
STAGE PERFORMANCE

	STAGE 1	STAGE 2	STAGE 3	STAGE 4
TTBAR 0	2067.3	1955.8		
PTBAR 0	38.823	23.524		
WG 0	5.759	5.758		
DEL H	32.871	17.954		
WRT/P	6.743	10.825		
DH/TTBAR0	.01590	.00918		
N/RT	527.549	542.687		
ETA TT	.82986	.82761		
ETA TS	.73329	.71650		
ETA AT	.80877	.82531		
PT0/PS1	1.377	1.205		
PTBAR0/PTBAR2	1.651	1.331		
PTBAR0/PS2	1.768	1.393		
PTR2/PS2	1.396	1.219		
TTBAR2/TTBAR0	.94606	.96900		
TTR1A/TTBAR0	.97296	.98389		
WG 1	5.758	5.758		
PS 1A	26.190	19.495		
TTR 1A	2011.4	1924.3		
PTR 1A	30.472	20.520		
WG 1A	5.758	5.758		
PS 2	21.963	16.892		
TTBAR 2	1955.8	1895.2		
PTBAR 2	23.524	17.676		
WG 2	5.758	5.758		
WG 2A	5.759	5.758		
UP/VI	.45953	.63693		
UR/VI	.35610	.44398		
PSI P	.96799	.44324		
PSI R	1.44550	.91223		
RX P	.42914	.42908		

4. Output Data (continued)

RX R	.20904	.12560
ALPHA 0	0.000	26.147
I STATOR	0.000	-.393
BETA 1A	33.910	-1.584
I ROTOR	.850	1.276
ALPHA 2A	26.147	-6.951
DBETA R	109.973	84.948
M 1	.72584	.55860
M1 RT	.86583	.70312
MR 1A	.36920	.29968
MR1A RT	.55090	.42459
MR 2	.68866	.52969

NASA TURBINE COMPUTER PROGRAM
TWO STAGE POTASSIUM TURBINE
FIVE RADIAL SECTORS

CASE 2. 0
STAGE PERFORMANCE

	STAGE 1	STAGE 2	STAGE 3	STAGE 4
MR2 TIP	.75376	.65843		
E/TH CR	39.397	23.242		
N/RTH CR	26274.6	27306.5		
WRTHCRE/D	1.806	2.893		

OVERALL PERFORMANCE

PSI P	.64847	PSI R	1.19809	DEL H	50.82569
WRT/P	6.74307	N/RT	527.84874	DELH/TTIN	.02459
PTO/PTRAB2	2.19659	PTO/PS2	2.29857	PTO/PAT2A	2.20133
ETA TT	.83219	ETA TS	.78926	ETA TAT	.83138
WNE/60C	791.002	N/RTH CR	26274.585	E/TH CR	60.91617

NASA TURBINE COMPUTER PROGRAM
TWO STAGE POTASSIUM TURBINE
FIVE RADIAL SECTORS

CASE 2. 0
INTER-STAGE PERFORMANCE

STA 1A	ROTOR INLET		STAGE 1.			
DIAM 1A	5.418	5.954	6.490	7.026	7.562	
PTR 1A	29.654	30.037	30.472	31.095	31.763	
TTR 1A	2006.4	2008.6	2011.4	2015.7	2020.5	
BETA 1A	48.373	42.053	33.910	22.748	9.389	
I ROTOR	-.477	.553	.850	.748	.889	
R 1A	754.950	644.729	555.112	479.687	433.031	
RU 1A	564.315	431.849	309.689	185.482	70.646	
MR 1A	.50486	.42985	.36920	.31830	.28681	
U 1A	567.371	623.501	679.631	735.760	791.890	
PS 1A	25.666	27.044	28.198	29.351	30.308	
TS 1A	1970.3	1982.3	1991.9	2001.2	2008.6	
CP 1A	.31545	.31545	.31545	.31545	.31545	
RG 1A	30.842	30.842	30.842	30.842	30.842	
GAMG 1A	1.14370	1.14370	1.14370	1.14370	1.14370	
RMG 1A	1.00000	1.00000	1.00000	1.00000	1.00000	
WG 1A	.96621	1.06158	1.15544	1.24444	1.33073	5.75839 TOTAL FLOW
STA 2	ROTOR EXIT					
DIAM 2	5.364	6.012	6.660	7.308	7.956	
PTR 2	29.607	30.095	30.660	31.441	32.298	
TTR 2	2006.0	2009.1	2013.0	2018.6	2024.8	
BETA 2	61.600	62.650	63.650	64.550	65.350	
DBETA	109.973	104.703	97.560	87.298	74.739	
R 2	982.663	1002.932	1028.350	1063.272	1100.654	
RU 2	864.397	890.820	921.504	960.092	1000.536	
MR 2	.65812	.67166	.68866	.71198	.73709	
U 2	561.716	629.575	697.433	765.291	833.150	
RX	.27374	.35918	.42914	.49716	.55252	
DELH	32.437	32.851	33.097	33.027	32.852	
PSI P	2.54805	2.09519	1.74763	1.44741	1.24504	

4. Output Data (continued)

ETA TT	.82775	.83218	.83334	.83074	.82585
ETA TS	.71574	.72958	.73822	.73985	.73811
ETA AT	.79117	.80466	.81300	.81534	.81449
ZWI INC	-1.34588	-1.19694	-1.06034	-.93090	-.81566
CP R	.40976	.58675	.70861	.79647	.84527
PS 2	21.823	21.907	21.963	22.019	22.058
TS 2	1936.3	1936.5	1936.7	1937.0	1937.4
CP 2	.27692	.27692	.27692	.27692	.27692
RG 2	30.689	30.689	30.689	30.689	30.689

NASA TURBINE COMPUTER PROGRAM
TWO STAGE POTASSIUM TURBINE
FIVE RADIAL SECTORS
CASE 2. 0
INTER-STAGE PERFORMANCE

STA 0	STATOR INLET		STAGE 1.			
DIAM 0	5.512	5.956	6.400	6.844	7.288	
TT 0	2067.3	2067.3	2067.3	2067.3	2067.3	
PT 0	38.828	38.828	38.828	38.828	38.828	
ALPHA 0	0.000	0.000	0.000	0.000	0.000	
I STATOR	0.000	0.000	0.000	0.000	0.000	
V 0	447.396	447.396	447.396	447.396	447.396	
VU 0	0.000	0.000	0.000	0.000	0.000	
VZ 0	447.396	447.396	447.396	447.396	447.396	
TS 0	2051.9	2051.9	2051.9	2051.9	2051.9	
PS 0	36.991	36.991	36.991	36.991	36.991	
DENS 0	.08332	.08332	.08332	.08332	.08332	
M 0	.28686	.28686	.28686	.28686	.28686	
CP 0	.25944	.25944	.25944	.25944	.25944	
RG 0	31.158	31.158	31.158	31.158	31.158	
GAMG 0	1.18250	1.18250	1.18250	1.18250	1.18250	
RWG 0	1.00000	1.00000	1.00000	1.00000	1.00000	
WG 0	.96621	1.06158	1.15544	1.24444	1.33073	5.75839 TOTAL FLOW

STA 1	STATOR EXIT					
DIAM 1	5.418	5.954	6.490	7.026	7.562	
ALPHA 1	66.100	65.600	65.030	64.350	63.650	
DEL A	66.100	65.600	65.030	64.350	63.650	
V 1	1237.625	1158.855	1091.327	1021.951	962.546	
VU 1	1131.686	1055.350	989.319	921.243	862.536	
VZ 1	501.495	476.729	460.698	442.375	427.230	
TS 1	1970.3	1982.3	1991.9	2001.2	2008.6	
PS 1	25.666	27.044	28.198	29.351	30.308	
DENS 1	.06082	.06370	.06609	.06848	.07045	
M 1	.82778	.77262	.72584	.67812	.63751	
ZWI INC	-.74081	-.75242	-.76537	-.78043	-.79547	
CP S	.86926	.85095	.83194	.80834	.78396	
CP 1	.31545	.31545	.31545	.31545	.31545	
RG 1	30.842	30.842	30.842	30.842	30.842	
GAMG 1	1.14370	1.14370	1.14370	1.14370	1.14370	
RWG 1	1.00000	1.00000	1.00000	1.00000	1.00000	
WG 1	.96621	1.06158	1.15544	1.24444	1.33073	5.75839 TOTAL FLOW
GAMG 2	1.16607	1.16607	1.16607	1.16607	1.16607	
RWG 2	1.00000	1.00000	1.00000	1.00000	1.00000	
WG 2	.93714	1.03939	1.14342	1.25898	1.37946	5.75839 TOTAL FLOW
PT 2A	23.655	23.560	23.492	23.480	23.473	
TT 2A	1957.3	1955.9	1955.0	1955.3	1955.9	
V 2A	556.829	529.680	505.471	496.706	488.699	
VU 2A	302.681	261.246	224.071	194.801	167.385	
ALPHA 2A	32.928	29.552	26.147	23.091	20.030	
MF 2A	.31302	.30858	.30566	.30596	.30742	
VZ 2A	467.379	460.772	456.437	456.913	459.139	
TS 2A	1936.3	1936.5	1936.7	1937.0	1937.4	
PS 2A	21.823	21.907	21.963	22.019	22.058	
DENS 2A	.05288	.05306	.05321	.05334	.05342	
M 2A	.37293	.35473	.34051	.33260	.32721	
CP 2A	.27692	.27692	.27692	.27692	.27692	
RG 2A	30.689	30.689	30.689	30.689	30.689	
GAMG 2A	1.16607	1.16607	1.16607	1.16607	1.16607	
RWG 2A	1.00000	1.00000	1.00000	1.00000	1.00000	
WG 2A	.93714	1.03939	1.14342	1.25898	1.37946	5.75839 TOTAL FLOW

4. Output Data (continued)

```
                   NASA TURBINE COMPUTER PROGRAM
TWO STAGE POTASSIUM TURBINE
FIVE RADIAL SECTORS
                          CASE   2.   0
                      INTER-STAGE PERFORMANCE
```

STA 0	STATOR INLET		STAGE 2.				
DIAM 0	5.364	6.012	6.660	7.308	7.956		
TT 0	1957.3	1955.9	1955.0	1955.3	1955.9		
PT 0	23.655	23.566	23.492	23.480	23.473		
ALPHA 0	32.928	29.552	26.147	23.091	20.030		
I STATOR	.628	-.168	-.393	-.309	.030		
V 0	556.829	529.680	508.471	496.706	488.699		
VU 0	302.681	261.246	224.071	194.801	167.386		
VZ 0	467.379	460.772	456.437	456.913	459.139		
TS 0	1936.3	1936.5	1936.7	1937.0	1937.4		
PS 0	21.823	21.907	21.963	22.019	22.058		
DENS 0	.05288	.05308	.05321	.05334	.05342		
M 0	.37293	.35473	.34051	.33260	.32721		
CP 0	.27692	.27692	.27692	.27692	.27692		
RG 0	30.689	30.689	30.689	30.689	30.689		
GAMG 0	1.16607	1.16607	1.16607	1.16607	1.16607		
RWG 0	1.00000	1.00000	1.00000	1.00000	1.00000		
WG 0	.93714	1.03939	1.14342	1.25898	1.37946	5.75839	TOTAL FLOW
STA 1	STATOR EXIT						
DIAM 1	5.254	6.002	6.750	7.498	8.246		
ALPHA 1	60.900	59.250	57.570	55.850	54.150		
DEL A	93.828	88.802	83.717	78.941	74.180		
V 1	972.507	889.612	823.007	758.647	707.705		
VU 1	849.749	764.538	694.656	627.834	573.632		
VZ 1	472.965	454.853	441.353	425.875	414.479		
TS 1	1897.0	1905.4	1911.9	1918.6	1923.9		
PS 1	18.215	18.945	19.495	20.045	20.459		
DENS 1	.04485	.04644	.04763	.04880	.04967		
M 1	.66265	.60483	.55860	.51402	.47883		
ZWI INC	-1.15624	-1.17526	-1.18763	-1.19784	-1.19952		
CP S	.67216	.64549	.61830	.57133	.52315		
CP 1	.31340	.31340	.31340	.31340	.31340		
RG 1	30.828	30.828	30.828	30.828	30.828		
GAMG 1	1.14470	1.14470	1.14470	1.14470	1.14470		
RWG 1	1.00000	1.00000	1.00000	1.00000	1.00000		
WG 1	.90940	1.03454	1.15778	1.27150	1.38518	5.75840	TOTAL FLOW

NASA TURBINE COMPUTER PROGRAM
TWO STAGE POTASSIUM TURBINE
MEAN DIAMETER CALCULATION
CASE 3. 0
INTER-STAGE PERFORMANCE

STA 0	STATOR INLET		STAGE 1.
DIAM 0	5.290	6.400	7.510
TT 0	2067.3	2067.3	2067.3
PT 0	38.828	38.828	38.828
ALPHA 0	0.000	0.000	0.000
I STATOR	0.000	0.000	0.000
V 0	447.396	447.396	447.396
VU 0	0.000	0.000	0.000
VZ 0	447.396	447.396	447.396
TS 0	2051.9	2051.9	2051.9
PS 0	36.991	36.991	36.991
DENS 0	.08332	.08332	.08332
M 0	.28686	.28686	.28686
CP 0	.25944	.25944	.25944
RG 0	31.158	31.158	31.158
GAMG 0	1.18250	1.18250	1.18250
RWG 0	1.00000	1.00000	1.00000
STA 1	STATOR EXIT		
DIAM 1	5.150	6.490	7.830
ALPHA 1	69.720	65.030	60.672
DEL A	69.720	65.030	60.672
V 1	1329.131	1091.327	940.563
VU 1	1246.734	989.319	820.011
VZ 1	460.698	460.698	460.698
TS 1	1955.5	1991.9	2011.3
PS 1	24.344	28.198	30.458
DENS 1	.05812	.06609	.07070
M 1	.89220	.72584	.62254
ZWI INC	-.65026	-.76537	-.85406
CP S	.88670	.83194	.77374
CP 1	.31545	.31545	.31545
RG 1	30.842	30.842	30.842
GAMG 1	1.14370	1.14370	1.14370
RWG 1	1.00000	1.00000	1.00000

2.3A-3 Wet-Vapor Potassium Turbine * (Mean Diameter Calculation)

1. Comparison of Results

The same modified parameters given in Table 2.3A-1 are used in the one radial sector (mean diameter) calculation. The results are in good agreement with the 5 radial sector calculation as can be seen by comparing the calculated parameters at the mean diameter. In the single sector case the hub and tip values are calculated assuming a free vortex distribution.** There is a slight inconsistency in the results in that P_S, T_S, ρ, and M for station 0 of the second stage are not identical to those at station 2A of the first stage. The discrepancies are small and thought not to be significant. At this time there is no explanation for this anomaly. The output format for the mean diameter case is slightly different from that using 5 radial sectors.

2. Data Input

```
                         TURBINE COMPUTER PROGRAM
     TWO STAGE POTASSIUM TURBINE
     MEAN DIAMETER CALCULATION
 $DATAIN
  STGCH=      1.000
   TTIN=   2067.300     PTIN=     38.828     WAIR=       0.000   FAIR=       0.000
   PTPS=      1.377     DELC=      0.000     DELL=       0.000   DELA=       0.000
    STG=      2.000     SECT=      1.000     EXPN=       0.000   EXPP=       0.000
    PAF=      1.000      SLI=      0.000     AACS=       1.000    RPM=   24000.000
   VCTD=      1.000      HSL=     37.600      TSL=    1800.000    PSL=      11.200
  GAMSL=      1.618 ENDSTG=      0.000  ENDJOB=       0.000

                         INLET RADIAL PROFILES
   PCNH=    1.000        0.000        0.000        0.000        0.000        0.000
```

*Described in Westinghouse Electric Corporation, Astronuclear Laboratory Report WANL-PR(DD)-017, January 1967, Contract NAS 7-390.

** Assumes a constant axial velocity component

2. Data Input (continued)

STANDARD OPTION
AXIAL STATIONS

STAGE= 1						
	STA. 0	STA. 1	STA.1A	STA. 2	STA.2A	
RG=	31.158	30.842	30.842	30.689	30.689	0.000
GAMG=	1.182	1.144	1.144	1.166	1.166	0.000
DR=	5.290	5.150	5.150	5.040	5.040	0.000
DT=	7.510	7.830	7.830	8.280	8.280	0.000
RWG=	1.000	1.000	1.000	1.000	1.000	0.000

STATOR RADIAL DISTRIBUTIONS

	ROOT		PITCH		TIP	
SDIA=	0.000	0.000	0.000	0.000	0.000	0.000
SDEA=	65.030	0.000	0.000	0.000	0.000	0.000
SREC=	1.000	0.000	0.000	0.000	0.000	0.000
SETA=	.926	0.000	0.000	0.000	0.000	0.000
SCF=	1.000	0.000	0.000	0.000	0.000	0.000
SPA=	0.000	0.000	0.000	0.000	0.000	0.000
SESTH=	1.000					

ROTOR RADIAL DISTRIBUTIONS

RDIA=	33.060	0.000	0.000	0.000	0.000	0.000
RDEA=	63.650	0.000	0.000	0.000	0.000	0.000
RREC=	1.000	0.000	0.000	0.000	0.000	0.000
RETA=	.817	0.000	0.000	0.000	0.000	0.000
RCF=	1.000	0.000	0.000	0.000	0.000	0.000
RPA=	0.000	0.000	0.000	0.000	0.000	0.000
RTF=	1.000	0.000	0.000	0.000	0.000	0.000
RERTH=	1.000					

STANDARD OPTION
AXIAL STATIONS

STAGE= 2						
	STA. 0	STA. 1	STA.1A	STA. 2	STA.2A	
RG=	30.689	30.828	30.828	30.763	30.763	0.000
GAMG=	1.166	1.145	1.145	1.164	1.164	0.000
DR=	5.040	4.880	4.880	4.600	4.600	0.000
DT=	8.280	8.620	8.620	9.100	9.100	0.000
RWG=	1.000	1.000	1.000	1.000	1.000	0.000

STATOR RADIAL DISTRIBUTIONS

	ROOT		PITCH		TIP	
SDIA=	26.540	0.000	0.000	0.000	0.000	0.000
SDEA=	57.570	0.000	0.000	0.000	0.000	0.000
SREC=	1.000	0.000	0.000	0.000	0.000	0.000
SETA=	.948	0.000	0.000	0.000	0.000	0.000
SCF=	1.000	0.000	0.000	0.000	0.000	0.000
SPA=	0.000	0.000	0.000	0.000	0.000	0.000
SESTH=	1.000					

ROTOR RADIAL DISTRIBUTIONS

RDIA=	-2.860	0.000	0.000	0.000	0.000	0.000
RDEA=	58.980	0.000	0.000	0.000	0.000	0.000
RREC=	1.000	0.000	0.000	0.000	0.000	0.000
RETA=	.816	0.000	0.000	0.000	0.000	0.000
RCF=	1.000	0.000	0.000	0.000	0.000	0.000
RPA=	0.000	0.000	0.000	0.000	0.000	0.000
RTF=	1.000	0.000	0.000	0.000	0.000	0.000
RERTH=	1.000					

3. Listing of Data Output

NASA TURBINE COMPUTER PROGRAM
TWO STAGE POTASSIUM TURBINE
MEAN DIAMETER CALCULATION
CASE 3. 0
STAGE PERFORMANCE

	STAGE 1	STAGE 2	STAGE 3	STAGE 4
TTBAR 0	2067.3	1952.6		
PTBAR 0	38.828	23.187		
WG 0	5.777	5.777		
DEL H	33.818	19.562		
WRT/P	6.765	11.910		
DH/TTBAR0	.01636	.01002		
N/RT	527.849	543.133		
ETA TT	.83062	.83613		
ETA TS	.73030	.72533		
ETA AT	.80615	.83602		
PT0/PS1	1.377	1.212		
PTBAR0/PTBAR2	1.675	1.362		
PTBAR0/PS2	1.803	1.430		
PTR2/PS2	1.423	1.248		
TTBAR2/TTBAR0	.94451	.96618		
TTR1A/TTBAR0	.97296	.98377		
WG 1	5.777	5.777		
PS 1A	28.199	19.126		
TTR 1A	2011.4	1920.9		
PTR 1A	30.472	20.164		
WG 1A	5.777	5.777		
PS 2	21.540	16.219		
TTBAR 2	1952.6	1886.5		
PTBAR 2	23.187	17.022		
WG 2	5.777	5.777		
WG 2A	5.777	5.777		
UP/VI	.45217	.61276		
UR/VI	.35039	.42713		
PSI P	.89299	.48294		
PSI R	1.48713	.99392		
RX P	.44730	.45539		
RX R	.18072	.10147		
ALPHA 0	0.000	28.042		
I STATOR	0.000	1.502		
BETA 1A	33.910	-.209		
I ROTOR	.850	2.651		
ALPHA 2A	28.042	-1.642		
DBETA R	97.560	58.771		
M 1	.72584	.56766		
M1 RT	.89220	.73450		
MR 1A	.36920	.30442		
MR1A RT	.56669	.44181		
MR 2	.70879	.56012		
MR2 TIP	.78183	.70431		
E/TH CR	40.532	25.366		
N/RTH CR	26274.6	27329.0		
WRTHCRE/D	1.812	2.942		

OVERALL PERFORMANCE

PSI P	.68107	PSI R	1.25831	DEL H	53.38050
WRT/P	6.76508	N/RT	527.84874	DELH/TTIN	.02582
PT0/PTBAR2	2.28102	PT0/PS2	2.39404	PT0/PAT2A	2.20112
ETA TT	.83611	ETA TS	.79231	ETA TAT	.83607
WNE/60D	793.584	N/RTH CR	26274.585	E/TH CR	63.97818

3. Output Data (continued)

NASA TURBINE COMPUTER PROGRAM
TWO STAGE POTASSIUM TURBINE
FIVE RADIAL SECTORS
CASE 2. 0
INTER-STAGE PERFORMANCE

STA 1A	ROTOR INLET		STAGE 2.			
DIAM 1A	5.254	6.002	6.750	7.498	8.246	
PTR 1A	19.788	20.105	20.520	21.156	21.871	
TTR 1A	1917.0	1919.8	1924.3	1931.7	1940.2	
BETA 1A	32.348	16.648	-1.584	-20.279	-34.969	
I ROTOR	-.452	.648	1.276	.221	.031	
R 1A	559.846	474.753	441.522	454.016	505.793	
RU 1A	299.552	136.010	-12.202	-157.354	-289.886	
MR 1A	.38147	.32277	.29968	.30762	.34222	
U 1A	550.197	628.527	706.858	785.168	863.518	
PS 1A	18.215	18.945	19.495	20.045	20.459	
TS 1A	1897.0	1905.4	1911.9	1918.6	1923.9	
CP 1A	.31340	.31340	.31340	.31340	.31340	
RG 1A	30.828	30.828	30.828	30.828	30.828	
GAMG 1A	1.14470	1.14470	1.14470	1.14470	1.14470	
RWG 1A	1.00000	1.00000	1.00000	1.00000	1.00000	
WG 1A	.90940	1.03454	1.15778	1.27150	1.38518	5.75840 TOTAL FLOW
STA 2	ROTOR EXIT					
DIAM 2	5.050	5.950	6.850	7.750	8.650	
PTR 2	19.669	20.069	20.600	21.390	22.300	
TTR 2	1915.5	1919.4	1925.2	1934.4	1945.0	
BETA 2	52.600	56.100	58.980	61.450	63.600	
DBETA	84.948	72.748	57.396	41.171	28.631	
R 2	682.758	726.616	779.865	851.208	924.085	
RU 2	542.393	603.100	668.334	747.701	827.713	
MR 2	.46369	.49354	.52969	.57800	.62726	
U 2	528.834	623.082	717.330	811.577	905.825	
RX	.22043	.33978	.42908	.51389	.57638	
DELH	18.960	18.696	18.208	17.619	16.959	
PSI P	1.63020	1.19519	.89898	.69187	.54219	
ETA TT	.85797	.85186	.83888	.81776	.79218	
ETA TS	.74297	.74135	.72943	.70720	.68159	
ETA AT	.85783	.85155	.83705	.81470	.78772	
ZWI INC	-1.43231	-1.11191	-.86859	-.67083	-.51999	
CP R	.32764	.57310	.67947	.71551	.70041	
PS 2	16.889	16.889	16.892	16.895	16.899	
TS 2	1882.4	1881.8	1882.0	1882.9	1884.3	
CP 2	.28103	.28103	.28103	.28103	.28103	
RG 2	30.763	30.763	30.763	30.763	30.763	
GAMG 2	1.16370	1.16370	1.16370	1.16370	1.16370	
RWG 2	1.00000	1.00000	1.00000	1.00000	1.00000	
WG 2	.86346	.99454	1.13553	1.30005	1.46480	5.75839 TOTAL FLOW
PT 2A	17.685	17.650	17.650	17.679	17.708	
TT 2A	1893.3	1892.7	1893.6	1895.8	1898.6	
V 2A	414.913	405.759	404.869	411.799	418.240	
VU 2A	13.559	-19.982	-48.996	-63.877	-78.112	
ALPHA 2A	1.873	-2.823	-6.951	-8.924	-10.764	
MF 2A	.28163	.27527	.27297	.27624	.27890	
VZ 2A	414.691	405.267	401.894	406.814	410.881	
TS 2A	1882.4	1881.8	1882.0	1882.9	1884.3	
PS 2A	16.889	16.889	16.892	16.895	16.899	
DENS 2A	.04200	.04201	.04201	.04200	.04198	
M 2A	.28178	.27561	.27499	.27963	.28390	
CP 2A	.28103	.28103	.28103	.28103	.28103	
RG 2A	30.763	30.763	30.763	30.763	30.763	
GAMG 2A	1.16370	1.16370	1.16370	1.16370	1.16370	
RWG 2A	1.00000	1.00000	1.00000	1.00000	1.00000	
WG 2A	.86346	.99454	1.13553	1.30005	1.46480	5.75839 TOTAL FLOW

3. Output Data (continued)

```
                              NASA TURBINE COMPUTER PROGRAM
       TWO STAGE POTASSIUM TURBINE
       MEAN DIAMETER CALCULATION
                                        CASE   3.   0
                                    INTER-STAGE PERFORMANCE
```

STA 1A	ROTOR INLET		STAGE 1.
DIAM 1A	5.150	6.490	7.830
PTR 1A	29.190	30.472	32.116
TTR 1A	2000.0	2011.4	2024.7
BETA 1A	56.927	33.910	.007
I ROTOR	.291	.850	1.473
R 1A	844.214	555.112	460.698
RU 1A	707.428	309.689	.056
MR 1A	.56669	.36920	.30493
U 1A	539.306	679.631	819.955
PS 1A	24.344	28.198	30.458
TS 1A	1955.5	1991.9	2011.3
CP 1A	.31545	.31545	.31545
RG 1A	30.842	30.842	30.842
GAMG 1A	1.14370	1.14370	1.14370
RWG 1A	1.00000	1.00000	1.00000
STA 2	ROTOR EXIT		
DIAM 2	5.040	6.660	8.280
BETA 2	61.327	63.650	66.283
DBETA	118.254	97.560	66.290
R 2	977.999	1057.223	1166.653
RU 2	858.070	947.377	1068.121
MR 2	.65625	.70879	.78183
U 2	527.787	697.433	867.079
RX	.21685	.44730	.57436
DELH	33.818	33.818	33.818
PSI P	2.97392	1.78568	1.18905
ETA TT	.83062	.83062	.83062
ETA TS	.73030	.73030	.73030
ETA AT	.80615	.80615	.80615
ZWI INC	-1.54897	-1.06034	-.73654
CP R	.25488	.72431	.84406
PS 2	21.278	21.540	21.664
TS 2	1929.0	1932.4	1933.9
CP 2	.27692	.27692	.27692
RG 2	30.689	30.689	30.689
GAMG 2	1.16607	1.16607	1.16607
RWG 2	1.00000	1.00000	1.00000
PT 2A	23.187	23.187	23.187
TT 2A	1952.6	1952.6	1952.6
V 2A	573.834	531.667	510.506
VU 2A	330.283	249.944	201.042
ALPHA 2A	35.140	28.042	23.192
MF 2A	.31487	.31460	.31447
VZ 2A	469.253	469.253	469.253
TS 2A	1929.0	1932.4	1933.9
PS 2A	21.278	21.540	21.664
DENS 2A	.05176	.05230	.05256
M 2A	.38505	.35644	.34212
CP 2A	.27692	.27692	.27692
RG 2A	30.689	30.689	30.689
GAMG 2A	1.16607	1.16607	1.16607
RWG 2A	1.00000	1.00000	1.00000

3. Output Data (continued)

```
                     NASA TURBINE COMPUTER PROGRAM
TWO STAGE POTASSIUM TURBINE
MEAN DIAMETER CALCULATION
                                CASE    3.   0
                           INTER-STAGE PERFORMANCE
```

STA 0	STATOR INLET		STAGE 2.
DIAM 0	5.040	6.660	6.280
TT 0	1952.6	1952.6	1952.6
PT 0	23.187	23.187	23.187
ALPHA 0	35.140	28.042	23.192
I STATOR	1.715	1.502	1.305
V 0	573.834	531.667	510.506
VU 0	330.283	249.944	201.042
VZ 0	469.253	469.253	469.253
TS 0	1928.8	1932.4	1933.8
PS 0	21.266	21.540	21.652
DENS 0	.05173	.05230	.05254
M 0	.38506	.35644	.34213
CP 0	.27692	.27692	.27692
RG 0	30.689	30.689	30.689
GAMG 0	1.16607	1.16607	1.16607
RWG 0	1.00000	1.00000	1.00000
STA 1	STATOR EXIT		
DIAM 1	4.880	6.750	6.620
ALPHA 1	65.329	57.570	50.945
DEL A	100.469	85.612	74.137
V 1	1073.451	835.528	711.146
VU 1	975.465	705.225	552.235
VZ 1	448.068	448.068	448.068
TS 1	1879.2	1908.1	1920.4
PS 1	16.948	19.126	20.120
DENS 1	.04213	.04682	.04894
M 1	.73490	.56766	.48161
ZWI INC	-1.00388	-1.21163	-1.31870
CP S	.71424	.59509	.48467
CP 1	.31340	.31340	.31340
RG 1	30.828	30.828	30.828
GAMG 1	1.14470	1.14470	1.14470
RWG 1	1.00000	1.00000	1.00000

NASA TURBINE COMPUTER PROGRAM
TWO STAGE POTASSIUM TURBINE
MEAN DIAMETER CALCULATION
CASE 3. 0
INTER-STAGE PERFORMANCE

STA 1A	ROTOR INLET		STAGE 2.
DIAM 1A	4.880	6.750	8.620
PTR 1A	18.936	20.164	21.894
TTR 1A	1905.7	1920.9	1941.0
BETA 1A	46.027	-.209	-38.030
I ROTOR	.940	2.651	2.043
R 1A	645.339	448.071	568.840
RU 1A	464.433	-1.633	-350.448
MR 1A	.44181	.30442	.38524
U 1A	511.032	706.858	902.504
PS 1A	16.948	19.126	20.120
TS 1A	1879.2	1908.1	1920.4
CP 1A	.31340	.31340	.31340
RG 1A	30.828	30.828	30.828
GAMG 1A	1.14470	1.14470	1.14470
RWG 1A	1.00000	1.00000	1.00000
STA 2	ROTOR EXIT		
DIAM 2	4.600	6.850	9.100
BETA 2	47.552	58.980	65.806
DBETA	93.579	58.771	27.776
R 2	628.292	822.853	1034.685
RU 2	463.610	705.175	943.799
MR 2	.42768	.56012	.70431
U 2	481.710	717.330	952.949
RX	.12058	.45539	.59732
DELH	19.562	19.562	19.562
PSI P	1.98611	.96582	.56053
ETA TT	.83613	.83613	.83613
ETA TS	.72533	.72533	.72533
ETA AT	.83602	.83602	.83602
ZWI INC	-1.94035	-.88134	-.48493
CP R	-.05500	.70348	.69775
PS 2	16.218	16.219	16.219
TS 2	1873.7	1873.7	1873.7
CP 2	.28103	.28103	.28103
RG 2	30.763	30.763	30.763
GAMG 2	1.16370	1.16370	1.16370
RWG 2	1.00000	1.00000	1.00000
PT 2A	17.022	17.022	17.022
TT 2A	1886.5	1886.5	1886.5
V 2A	424.434	424.222	424.146
VU 2A	-18.101	-12.155	-9.150
ALPHA 2A	-2.444	-1.642	-1.236
MF 2A	.28865	.28865	.28865
VZ 2A	424.047	424.047	424.047
TS 2A	1873.7	1873.7	1873.7
PS 2A	16.218	16.219	16.219
DENS 2A	.04052	.04052	.04052
M 2A	.28892	.28877	.28872
CP 2A	.28103	.28103	.28103
RG 2A	30.763	30.763	30.763
GAMG 2A	1.16370	1.16370	1.16370
RWG 2A	1.00000	1.00000	1.00000

APPENDIX 2.3B
LISTING OF CODE

The asterisks in the identification columns (73-80) indicate that the card has been changed from the orginal listing given in NASA CR-710. Most of the changes are in format statements so as to make the output nomenclature agree with the names of program variables used in the computer code.

```
      PROGRAM JIM(INPUT,OUTPUT,TAPE5=INPUT,TAPE6=OUTPUT)                NTCP 001
CNTCP                                                                   NTCP 002
C     NASA TURBINE PROGRAM                                              NTCP 003
C                                                                       NTCP 004
      REAL MFSTOP                                                       ********
      LOGICAL PREVER,SRFLAG                                             ********
      COMMON  SRFLAG                                                    NTCP 006
      COMMON /SNTCP/G,AJ,PRPC,ICASE,PREVER,MFSTOP,JUMP,LOPIN,ISCASE,    NTCP 007
     1KN,GANF,IP,SCHIT,PTRN,ISECT,KSTG,WTOL,RHOTOL,PRTOL,TRLOOP,LSTG,   NTCP 008
     2LBRC,IBRC,ICHOKE,ISORR,CHOKE,PTOPS1(6,8),PTRS2(6,8),TRDIAG,SC,RC, NTCP 009
     3DELPR,PASS,IPC,LOPC,ISS                                           NTCP 010
C                                                                       ********
      COMMON /SINPUT/ RSL,TSL,PSL,GAMSL,                                NTCP 012
     1PTPS,PTIN,TTIN,WAIR,FAIR,DELC,DELL,DELA,AACS,VCTD,STG,SECT,EXPN,  ********
     2EXPP,EXPRE,   RPM,PAF,SLI,STGCH,ENDJOB,NAME(10),TITLE(10),PCNH(6),********
     3RV(6,8),GAM(6,8),DR(6,8),DT(6,8),RWG(6,8),ALPHAS(6,8),ALPHA1(6,8),NTCP 015
     4ETARS(6,8),ETAS(6,8),CFS(6,8),ANDO(6,8),BETA1(6,8),BETA2(6,8),ETARNTCP 016
     5R(6,8),ETAR(6,8),CFR(6,8),TFR(6,8),ANDOR(6,8),OMEGAS(6,8),AS0(6,8)NTCP 017
     6,ASMP0(6,8),ACMN0(6,8),A1(6,8),A2(6,8),A3(6,8),A4(6,8),A5(6,8),A6(NTCP 018
     76,8),OMEGAR(6,8),BSIA(6,8),BSMPIA(6,8),BCMNIA(6,8),B1(6,8),B2(6,8)NTCP 019
     8,B3(6,8),B4(6,8),B5(6,8),B6(6,8),SESTHI(8),RERTHI(8)              NTCP 020
C                                                                       NTCP 021
      REAL MR2,M2     ,MF2                                              NTCP 022
      COMMON /SFLOW2/TS2(6,8),CP2(8),R2(6,8),RHOS2(6,8),BET2E(6,8),RU2(6NTCP 023
     1,8),VU2(6,8),DPDR2(6,8),VZ2(6,8),MR2(6,8),MF2(6,8),M2(6,8)        NTCP 024
C                                                                       NTCP 025
      DIMENSION CS(8),CR(8)                                             NTCP 026
C                                                                       NTCP 027
C                                                                       NTCP 028
      CALL SLITE(0)                                                     NTCP 029
      WAIR=0.0                                                          NTCP 030
      FAIR=0.0                                                          NTCP 031
      PTPS=1.02                                                         NTCP 032
      DELC=0.0                                                          NTCP 033
      DELL=0.0                                                          NTCP 034
      DELA=0.0                                                          NTCP 035
      EXPN=2.0                                                          NTCP 036
      EXPP=2.0                                                          NTCP 037
      EXPRE=0.0                                                         ********
      RV(1,1)=0.0                                                       NTCP 039
      PAF=0.0                                                           NTCP 040
      SLI=0.0                                                           NTCP 041
      AACS=1.0                                                          NTCP 042
      SECT=1.0                                                          NTCP 043
      VCTD=0.0                                                          NTCP 044
      WTOL=1.E-04                                                       NTCP 045
      RHOTOL=1.E-04                                                     NTCP 046
      PRTOL=1.E-06                                                      NTCP 047
      PCNH(1)=1.0                                                       NTCP 048
      GAM(1,1)=0.0                                                      NTCP 049
      RWG(1,1)=1.0                                                      NTCP 050
      ETAS(1,1)=0.0                                                     NTCP 051
      ALPHA1(1,1)=0.0                                                   NTCP 052
      ETAR(1,1)=0.0                                                     NTCP 053
      BETA2(1,1)=0.0
      TRLOOP=0.
```

Listing of Code (continued)

```
      TRDIAG=0.0
      G=32.17405
      AJ=778.161
      ICASE=0
    1 PREVER=.FALSE.
      READ(5,100) SRFLAG
  100 FORMAT(1X,L1)
      IF(SRFLAG) WRITE(6,10000)
10000 FORMAT(1H1,39H AN ENTRY HAS BEEN MADE IN MAIN PROGRAM)
      CALL INIT
      ISCASE=0
      IF (PREVER) GO TO 1
      DO 25 I=1,8
      CS(I)=0.0
   25 CR(I)=0.0
      PASS=0
    2 PRPC=CS(KN)
      CALL STA01
      IF (PREVER) GO TO 40
      IF(ICHOKE.NE.0)  GO TO 3
      IF(SCRIT.EQ.1.) SC=SC+1.
    3 CALL STA1A
      IF (PREVER) GO TO 40
      LOPIN=0
    4 JUMP=0
      PRPC=CR(KN)
      CALL STA2
      CR(KN)=PRPC
      IF (PREVER) GO TO 40
      IF (1.-MF2(1,KN))24,5,5
    5 IF (JUMP)6,6,20
    6 CALL STA2A
      IF (PREVER) GO TO 40
      IF (KN-KSTG)7,9,9
    7 KN=KN+1
      LOPIN=0
    8 JUMP=0
      PRPC=CS(KN)
      CALL STA1
      CS(KN)=PRPC
      IF (PREVER) GO TO 40
      IF (JUMP)3,3,20
    9 CALL OVRALL
      IF (VCTD)11,11,10
   10 CALL INSTG
   11 PASS=1.
      IF (TRDIAG)13,13,12
   12 CALL DIAGT(0)
   13 IF (1.-MFSTOP)24,24,14
   14 IF (DELC)24,24,15
   15 IF (DELL)17,17,16
   16 IF(DELPR)24,24,18
   17 IF (CHOKE)24,18,24
   18 ISCASE=ISCASE+1
   19 JL=(ISORR-1)*8+LSTG
      IF(SC.EQ.1.) DELPR=DELL
      PTOPS1(IP,JL)=PTOPS1(IP,JL)+DELPR
   20 LOPIN=1
      KN=LSTG
      IBRC=LBRC
      IPC=0
      IF (KN-1)21,21,22
```

```
                                                                        NTCP 112
                                                                        NTCP 113
   21 IF (ISORR-1)2,2,4                                                 NTCP 114
   22 IF (ISORR-1)8,8,4                                                 NTCP 115
   40 WRITE(6,106)                                                      NTCP 116
   24 IF (ENDJOB-1.)1,23,23                                             ********
   23 IF(SRFLAG) WRITE(6,20000)                                         ********
20000 FORMAT(1H1,40H AN EXIT HAS BEEN MADE FROM MAIN PROGRAM)           ********
      CALL EXIT
  106 FORMAT(//3X65HTHE PREVIOUS CASE HAS BEEN TERMINATED DUE TO ERRORS NTCP 118
     1- CHECK DUMP.)                                                    NTCP 119
      STOP                                                              NTCP 120
      END                                                               NTCP 121
      SUBROUTINE INIT                                                   INIT 001
CINIT                                                                   INIT 002
C     SUBROUTINE FOR INITIALIZATION OF INPUT DATA                       INIT 003
C                                                                       INIT 004
C                                                                       INIT 005
      REAL MFSTOP                                                       ********
      LOGICAL PREVER,SRFLAG                                             ********
      COMMON  SRFLAG
      COMMON /SNTCP/G,AJ,PRFC,ICASE,PREVER,MFSTOP,JUMP,LOPIN,ISCASE,    INIT 007
     1KN,GAMF,IP,SCRIT,PTRN,ISECT,KSTG,WTOL,RHOTOL,PRTOL,TRLOOP,LSTG,   INIT 008
     2LBRC,IBRC,ICHOKE,ISORR,CHOKE,PTOPS1(6,8),PTRS2(6,8),TRDIAG,SC,RC, INIT 009
     3DELPR,PASS,IPC,LOPC,ISS                                           INIT 010
C                                                                       INIT 011
      COMMON /SINIT/H1(6,8),H2(6,8),DP0(6,8),DP1(6,8),DP1A(6,8),DP2(6,8)INIT 012
     1,DP2A(6,8),CSALF1(6,8),ALF1(6,8),CSBET2(6,8),BET2(6,8),RADSD(6,8),INIT 013
     2RADRD(6,8),ANN1(6,8),ANN2(6,8),ANN2A(6,8),ANN1A(6,8),U1A(6,8),    INIT 014
     3U2(6,8),ANN0(6,8),PT0(6,8),TT0(6,8),ALPHA0(6,8),PTP(6,8)          INIT 015
C                                                                       INIT 016
      COMMON /SINPUT/ RSL,TSL,PSL,GAMSL,                                ********
     1PTPS,PTIN,TTIN,WAIR,FAIR,DELC,DELL,DELA,AACS,VCTD,STG,SECT,EXPN,  INIT 018
     2EXPP,EXPRE,    RPM,PAF,SLI,STGCH,ENDJOB,NAME(10),TITLE(10),PCNM(6),********
     3RV(6,8),GAM(6,8),DR(6,8),DT(6,8),RWG(6,8),ALPHAS(6,8),ALPHA1(6,8),********
     4ETARS(6,8),ETAS(6,8),CFS(6,8),ANDO(6,8),BETA1(6,8),BETA2(6,8),ETARINIT 021
     5R(6,8),ETAR(6,8),CFR(6,8),TFR(6,8),ANDCR(6,8),OMEGAS(6,8),AS0(6,8)INIT 022
     6,ASMP0(6,8),ACMN0(6,8),A1(6,8),A2(6,8),A3(6,8),A4(6,8),A5(6,8),A6(INIT 023
     76,8),OMEGAR(6,8),BSIA(6,8),BSMPIA(6,8),BCMNIA(6,8),B1(6,8),B2(6,8)INIT 024
     8,B3(6,8),B4(6,8),B5(6,8),B6(6,8),SESTHI(8),RERTHI(8)              INIT 025
C                                                                       INIT 026
      DIMENSION                                 H1A(6,8),H0(6,8),H2A(6,8) INIT 027
C                                                                       INIT 028
C     READ INPUT DATA, CHECK FOR ERRORS,                                INIT 029
C         SKIP CHANGE CASES IF BASIC CASE HAS AN ERROR                  INIT 030
      IF(SRFLAG) WRITE(6,10000)                                         ********
10000 FORMAT(44H AN ENTRY HAS BEEN MADE IN SUBROUTINE INIT  )           ********
    3 CALL INPUT                                                        INIT 031
      ICASE=ICASE+1                                                     INIT 032
      IF(STGCH)5,5,4                                                    INIT 033
    4 IK=1                                                              INIT 034
    5 CALL CHECK(L)                                                     INIT 035
      GO TO(6,8),L                                                      INIT 036
    6 WRITE(6,100)ICASE                                                 INIT 037
      IF(STGCH)3,3,7                                                    INIT 038
    7 IK=2                                                              INIT 039
      GO TO 3                                                           INIT 040
    8 IF (IK-2)9,3,3                                                    INIT 041
C         INITIALIZE INDEX REGISTERS AND FORKS                          INIT 042
    9 ISECT=SECT+.0001                                                  INIT 043
```

Listing of Code (continued)

```
      KSTG= STG+.0001
      LOPC=0
      CHOKE=0.
      ICHOKE=0
      ISORR=1
      KN=1
      LSTG=1
      IHRC=1
      LHRC=1
      DELPR=DELC
      SC=0.0
      RC=0.0
      PRPC=0.0
      IPC=0
      ISS=0
      PTRN=0.0
C        TEST STAGE LOSS INDICATOR
      IF(SLI)13,13,11
   11 DO 12 I=1,ISECT
      DO 12 J=1,KSTG
      ETARS(I,J)=ETARS(I,1)
      ETAS(I,J)=ETAS(I,1)
      CFS(I,J)=CFS(I,1)
      ETARR(I,J)=ETARR(I,1)
      ETAR(I,J)=ETAR(I,1)
      CFR(I,J)=CFR(I,1)
      TFR(I,J)=TFR(I,1)
   12 CONTINUE
C        TEST FOR EQUAL SECTORS
   13 IF(PCNH(1)-1.)16,14,14
   14 DO 15 I=1,ISECT
   15 PCNH(I)=      1./SECT
C        SET UP SECTOR HEIGHT, PITCH DIAMETER, ANNULUS AREA,
C              PITCHLINE WHEEL SPEED
   16 DO 19 K=1,KSTG
         SH0=DT(1,K)-DR(1,K)
         SH1=DT(2,K)-DR(2,K)
         SH1A=DT(3,K)-DR(3,K)
         SH2=DT(4,K)-DR(4,K)
         SH2A=DT(5,K)-DR(5,K)
      DO 18 I=1,ISECT
      H0(I,K)=.5*PCNH(I)*SH0
      H1(I,K)=.5*PCNH(I)*SH1
      H1A(I,K)=.5*PCNH(I)*SH1A
      H2(I,K)=.5*PCNH(I)*SH2
      H2A(I,K)=.5*PCNH(I)*SH2A
      IF(I-1)20,20,17
```

Listing of Code (continued)

```
                                                                           INIT 091
   20 DP0(I,K)=DR(1,K)+    H0(I,K)                                         INIT 092
      DP1(I,K)=DR(2,K)+    H1(I,K)                                         INIT 093
      DP1A(I,K)=DR(3,K)+    H1A(I,K)                                       INIT 094
      DP2(I,K)=DR(4,K)+    H2(I,K)                                         INIT 095
      DP2A(I,K)=DR(5,K)+    H2A(I,K)                                       INIT 096
      GO TO 21                                                             INIT 097
   17 DP0(I,K)=           H0(I-1,K)+    H0(I,K)+DP0(I-1,K)                 INIT 098
      DP1(I,K)=           H1(I-1,K)+    H1(I,K)+DP1(I-1,K)                 INIT 099
      DP1A(I,K)=           H1A(I-1,K)+    H1A(I,K)+DP1A(I-1,K)             INIT 100
      DP2(I,K)=           H2(I-1,K)+    H2(I,K)+DP2(I-1,K)                 INIT 101
      DP2A(I,K)=           H2A(I-1,K)+    H2A(I,K)  +DP2A(I-1,K)           ********
   21 ANN0(I,K)=.0218166*DP0(I,K)*H0(I,K)                                  ********
      ANN1(I,K)=.0218166*DP1(I,K)*H1(I,K)                                  ********
      ANN1A(I,K)=DP1A(I,K)*H1A(I,K)*.0218166                               ********
      ANN2(I,K)=.0218166*DP2(I,K)*H2(I,K)                                  ********
      ANN2A(I,K)=.0218166*DP2A(I,K)*H2A(I,K)                               INIT 107
      U1A(I,K)= 3.14159*DP1A(I,K)*RPM/720.                                 INIT 108
      U2(I,K)= 3.14159*DP2(I,K)*RPM/720.                                   INIT 109
   18 CONTINUE                                                             INIT 110
   19 CONTINUE                                                             INIT 111
C        DEFINE PITCHLINE INDEX                                            INIT 112
      IT=ISECT-2*(ISECT/2)                                                 INIT 113
      IF(IT)22,22,23                                                       INIT 114
   22 IP=ISECT/2                                                           INIT 115
      GO TO 24                                                             INIT 116
   23 IP=(ISECT+1)/2                                                       INIT 117
C        CALCULATE INLET AND EXIT ANGLES IN RADIANS                        INIT 118
   24 IF (ALPHA1(1,1))25,25,27                                             INIT 119
   25 SDEAF=0.                                                             INIT 120
      DO 26 K=1,KSTG                                                       INIT 121
      DO 26 I=1,ISECT                                                      INIT 122
      CSALF1(I,K)=ANDO(I,K)*CFS(I,K)/(SESTHI(K)*3.14159*DP1(I,K)*          INIT 123
     1SQRT(ETAS(I,K)))                                                     INIT 124
   26 ALF1(I,K)=ATAN2(SQRT(1.-CSALF1(I,K)*CSALF1(I,K)),CSALF1(I,K))        INIT 125
      GO TO 31                                                             INIT 126
   27 DO 28 K=1,KSTG                                                       INIT 127
      DO 28 I=1,ISECT                                                      ********
        ALF1(I,K)=    ALPHA1(I,K)*.01745328                                INIT 129
   28 CSALF1(I,K)=COS(ALF1(I,K))                                           INIT 130
   31 IF (BETA2(1,1))29,29,32                                              INIT 131
   29 RDEAF=0.                                                             INIT 132
      DO 30 K=1,KSTG                                                       INIT 133
      DO 30 I=1,ISECT                                                      INIT 134
      CSBET2(I,K)=ANDOR(I,K)*CFR(I,K)/(RERTHI(K)*3.14159*DP2(I,K)*         INIT 135
     1SQRT(ETAR(I,K)))                                                     INIT 136
   30 BET2(I,K)=ATAN2( SQRT(1.-CSBET2(I,K)*CSBET2(I,K)),CSBET2(I,K))       INIT 137
      GO TO 34
```

Listing of Code (continued)

```
   32 DO 33 K=1,KSTG
      DO 33 I=1,ISECT
        BET2(I,K)=    BETA2(I,K)*.01745328
   33 CSBET2(I,K)=COS(BET2(I,K))
   34 DO 35 K=1,KSTG
      DO 35 I=1,ISECT
      PTP(I,K)=PTIN
      PTO(I,K)=PTIN
      TTO(I,K)=TTIN
      ALPHAO(I,K)=0.0
      PTOPS1(I,K)=PTPS
      RADSO(I,K)=ALPHAS(I,K)*.01745328
   35 RADHO(I,K)=BETA1(I,K)*.01745328
      IF(RV(1,1))36,36,37
   36 CALL R(PTIN,TTIN,FAIR,WAIR,RV(1,1))
      GAMF=0.0
      GO TO 38
   37 GAMF=1.0
   38 CALL CHECK(J)
      GO TO (39,40),J
   39 GO TO 3
   40 IF(SRFLAG) WRITE(6,20000)
20000 FORMAT(45H AN EXIT HAS BEEN MADE FROM SUBROUTINE INIT    )
      RETURN
  100 FORMAT(28X,6HCASE   I5,13H HAS AN ERROR)
      END
```

```
      SUBROUTINE INPUT
CINPUT
C*****************************************************************************
C
      REAL MFSTOP
      LOGICAL PREVER,SRFLAG
      COMMON  SRFLAG
      COMMON /SNTCP/G,AJ,PRFC,ICASE,PREVER,MFSTOP,JUMP,LOPIN,ISCASE,
     1KN,GAMF,IP,SCRIT,PTRN,ISECT,KSTG,WTOL,RHOTOL,PRTOL,TRLOOP,LSTG,
     2LBRC,IBRC,ICHOKE,ISORR,CHOKE,PTOPS1(6,8),PTRS2(6,8),TRDIAG,SC,RC,
     3DELPR,PASS,IPC,LOPC,ISS
C
      COMMON /SINPUT/ RSL,TSL,PSL,GAMSL,
     1PTPS,PTIN,TTIN,WAIR,FAIR,DELC,DELL,DELA,AACS,VCTD,STG,SECT,EXPN,
     2EXPP,EXPRE,    RPM,PAF,SLI,STGCH,ENDJOB,NAME(10),TITLE(10),PCNH(6),
     3RV(6,8),GAM(6,8),SR(6,8),ST(6,8),SWG(6,8),ALPHAS(6,8),ALPHA1(6,8),
     4ETARS(6,8),ETAS(6,8),CFS(6,8),ANDO(6,8),BETA1(6,8),BETA2(6,8),ETAR
     5R(6,8),ETAR(6,8),CFR(6,8),TFR(6,8),ANDOR(6,8),OMEGAS(6,8),AS0(6,8)
     6,ASMP0(6,8),ACMN0(6,8),A1(6,8),A2(6,8),A3(6,8),A4(6,8),A5(6,8),A6(
     76,8),OMEGAR(6,8),BSIA(6,8),BSMPIA(6,8),BCMNIA(6,8),B1(6,8),B2(6,8)
     8,B3(6,8),B4(6,8),B5(6,8),B6(6,8),SESTHI(8),RERTHI(8)
C
      DIMENSION X(6,8,38),Y(6,38)
C
      EQUIVALENCE (X(1,1,1), RV(1,1)),(Y(1,1),  RG(1))
C
      COMMON RG(6),
     1        GAMG(6),DR(6),DT(6),RWG(6),SDIA(6),SDEA(6),SREC(6),SETA(6),
     1SCF(6),SPA(6),RDIA(6),RDEA(6),RREC(6),RETA(6),RCF(6),RTF(6),RPA(6)
     2,STPLC(6),SINR(6),SINMP(6),SINMN(6),SCPS(6),SCPC(6),SCPQ(6),SCNS(6
     3),SCNC(6),SCNQ(6),RTPLC(6),RINR(6),RINMP(6),RINMN(6),RCPS(6),RCPC(
     46),RCPQ(6),RCNS(6),RCNC(6),RCNQ(6)
C
      NAMELIST/DATAIN/ RSL,TSL,PSL,GAMSL,
     1                 PTPS,PTIN,TTIN,WAIR,FAIR,DELC,DELL,DELA,AACS,VCTD
     1,STG,SECT,STAGE,EXPN,EXPP,EXPRE,RPM,PAF,SLI,ENDSTG,ENDJOB,PCNH,RG,
     2GAMG,DR,DT,RWG,SDIA,SDEA,SREC,SETA,SCF,SPA,RDIA,RDEA,RREC,RETA,RCF
     3,RTF,RPA,STPLC,SINR,SINMP,SIMMN,SCPS,SCPC,SCPQ,SCNS,SCNC,SCNQ,RTPL
     4C,RINR,RINMP,RINMN,RCPS,RCPC,RCPQ,RCNS,RCNC,RCNQ,SESTH,RERTH,
     5WTOL,RHOTOL,PRTOL,TRLOOP,TRDIAG,STGCH
C
      DATA BLANKS/66666666/
C
C
C     READ THE HEADING CARDS EVERY TIME ENTRY IS MADE
      IF(SRFLAG) WRITE(6,10000)
```

```
10000 FORMAT(44H AN ENTRY HAS BEEN MADE IN SUBROUTINE INPUT )          ********
   10 READ(5,6669) (NAME(I),I=1,10)                                    INPT 043
   20 READ(5,6669) (TITLE(I),I=1,10)                                   INPT 044
      J=0                                                              INPT 045
   30 DO 25 L=1,38                                                     ********
      DO 25 I=1,6                                                      INPT 047
   25 Y(I,L)=BLANKS                                                    INPT 048
      SESTH=BLANKS                                                     INPT 049
      RERTH=BLANKS                                                     INPT 050
      READ(5,DATAIN)                                                   INPT 051
   40 K=STAGE+.0001                                                    INPT 052
   50 ISECT=SECT+.0001                                                 INPT 053
   60 DO 80 L=1,38                                                     ********
   70 DO 80 I=1,6                                                      INPT 055
      IF (Y(I,L).NE.BLANKS)  GO TO 71                                  INPT 056
      Y(I,L)=0.0                                                       INPT 057
      GO TO 80                                                         INPT 058
   71 X(I,K,L)=Y(I,L)                                                  INPT 059
   80 CONTINUE                                                         INPT 060
      IF(SESTH.EQ.BLANKS) GO TO 95                                     INPT 061
   90 SESTHI(K)=SESTH                                                  INPT 062
      GO TO 96                                                         INPT 063
   95 SESTH=0.                                                         INPT 064
   96 IF(RERTH.EQ.BLANKS) GO TO 105                                    INPT 065
  100 RERTHI(K)=RERTH                                                  INPT 066
      GO TO 110                                                        INPT 067
  105 RERTH=0.                                                         INPT 068
  110 IF (K-1)120,120,130                                              INPT 069
  120 WRITE(6,6670)NAME,TITLE,STGCH,TTIN,PTIN,WAIR,FAIR,PTPS,DELC,DELL, ********
     1DELA,STG,SECT,EXPN,EXPP,   PAF,SLI,AACS,RPM,VCTD,RSL,TSL,PSL,GAMSL********
     2,ENDSTG,ENDJOB,PCNH                                              ********
      J=J+1                                                            INPT 073
  130 WRITE(6,6671) K,RG,GAMG,DR,DT,RWG,SDIA,SDEA,SREC,SETA,SCF,SPA,   ********
     1SESTH,                                                           INPT 075
     1RDIA,RDEA,RREC,RETA,RCF,RPA,RTF,RERTH                            ********
  140 IF (OMEGAS(1,K))160,160,150                                      INPT 077
  150 WRITE(6,6672)STPLC,SINR,SINMP,SINMN,SCPS,SCPC,SCPQ,SCNS,SCNC,SCNQ,INPT 078
     1RTPLC,RINR,RINMP,RINMN,RCPS,RCPC,RCPQ,RCNS,RCNC,RCNQ             INPT 079
  160 J=J+1                                                            INPT 080
  180 AM= J-2*(J/2)                                                    INPT 081
  190 IF(AM)200,210,200                                                INPT 082
  200 WRITE(6,6673)                                                    INPT 083
  210 IF (ENDSTG-1.)30,170,170                                         INPT 084
  170 IF(SRFLAG) WRITE(6,20000)                                        ********
20000 FORMAT(1H1,45H AN EXIT HAS BEEN MADE FROM SUBROUTINE INPUT )     ********
      RETURN                                                           ********
 6669 FORMAT(10A6)                                                     INPT 086
```

Listing of Code (continued)

```
6670 FORMAT (1H1,24X,24HTURBINE COMPUTER PROGRAM/6X,10A6/6X,10A6/2X,   INPT 087
    17HSCATAIN/2X,7H STGCH=F10.3/2X7H  TTIN=F10.3,1X,7H  PTIN=F10.3,2X,********
    16H WAIR=F10.3,2X,                                                 ********
    25HFAIR=F10.3/2X,7H  PTPS=F10.3,1X,7H  CELC=F10.3,2X,6H DELL=F10.3,********
    32X,5HDELA=F10.3/2X,7H   STG=F10.3,1X,7H  SECT=F10.3,2X,6H EXPN=F10********
    4.3,2X,5HEXPP=F10.3/2X,                       7H   PAF=F10.3,2X,6H  SLI=********
    5F10.3,3X,5HAACS=F10.3,  2X,5H RPM=F10.3/2X,7H  VCTD=F10.3,4X,4HRSL********
    6=F10.3,4X,4HTSL=F10.3,3X,4HPSL=F10.3/2X,7H GAMSL=F10.3,1X,7HENDSTG********
    7=F10.3,1X,7HENDJOB=F10.3//25X,21HINLET RADIAL PROFILES             ********
    8          /4X,5HPCNH=6(F8.3,2X)/1H1)                              ********
6671 FORMAT(28X,15HSTANDARD OPTION/3X,6HSTAGE=I3,16X,14HAXIAL STATIONS/********
    111X,6HSTA. 04X,6HSTA. 14X,6HSTA.1A4X,6HSTA. 23X,7H STA.2A/         ********
    23X,6H   RG=6(F8.3,2X)/                                            ********
    33X,6H GAMG=6(F8.3,2X)/3X,6H   DR=6(F8.3,2X)/3X,6H   DT=6(F8.3,2X)/INPT 097
    33X,6H  RWG=6(F8.3,2X)//22X,27HSTATOR RADIAL DISTRIBUTIONS/        INPT 098
    413X,4HROOT,15X,5HPITCH,16X,3HTIP/                                 ********
    53X,6H SDIA=6(F8.3,2X)/3X,6H SDEA=6(F8.3,2X)/3X,6H SREC=6(F8.3,2X)/INPT 100
    63X,6H SETA=6(F8.3,2X)/3X,6H  SCF=6(F8.3,2X)/3X,6H  SPA=6(F8.3,2X)/INPT 101
    73X,6HSESTH=F8.3//22X,26HROTOR RADIAL DISTRIBUTIONS/               ********
    83X,6H RDIA=6(F8.3,2X)/3X,6H RDEA=6(F8.3,2X)/3X,6H RREC=6(F8.3,2X)/INPT 103
    93X,6H RETA=6(F8.3,2X)/3X,6H  RCF=6(F8.3,2X)/3X,6H  RPA=6(F8.3,2X)/********
    13X,6H  RTF=6(F8.3,2X)/3X,6HRERTH=1F8.3/)                          ********
6672 FORMAT(/25X,23HLOSS COEFFICIENT OPTION/22X,27HSTATOR RADIAL DISTRIINPT 106
    1BUTIONS/                                                          INPT 107
    23X,6HSTPLC=6(F8.3,2X)/3X,6H SINR=6(F8.3,2X)/3X,6HSINMP=6(F8.3,2X)/INPT 108
    33X,6HSINMN=6(F8.3,2X)/3X,6H SCPS=6(F8.3,2X)/3X,6H SCPC=6(F8.3,2X)/INPT 109
    43X,6H SCPQ=6(F8.3,2X)/3X,6H SCNS=6(F8.3,2X)/3X,6H SCNC=6(F8.3,2X)/INPT 110
    53X,6H SCNQ=6(F8.3,2X)/023X,26HROTOR RADIAL DISTRIBUTIONS/         INPT 111
    63X,6HRTPLC=6(F8.3,2X)/3X,6H RINR=6(F8.3,2X)/3X,6HRINMP=6(F8.3,2X)/INPT 112
    73X,6HRINMN=6(F8.3,2X)/3X,6H RCPS=6(F8.3,2X)/3X,6H RCPC=6(F8.3,2X)/INPT 113
    83X,6H RCPQ=6(F8.3,2X)/3X,6H RCNS=6(F8.3,2X)/3X,6H RCNC=6(F8.3,2X)/INPT 114
    93X,6H RCNQ=6(F8.3,2X))                                            INPT 115
6673 FORMAT (1H1)                                                      INPT 116
     END                                                               INPT 117
```

```
      SUBROUTINE STA01
CSTA01
C     ESTABLISH FIRST STATOR EXIT FLOW, ADJUST FLOWS FOR COOLING
C        AIR INJECTION BETWEEN STATIONS 0 AND 1. FIND INLET
C        MACH NUMBER AND INCIDENCE ANGLE LOSS AT STATION 0,
C        ADJUST PT, GET NEW FLOW AT STATION 1 FOR FINAL RESULT.
C
      REAL MFSTOP
      LOGICAL PREVER,SRFLAG
      COMMON  SRFLAG
      COMMON /SNTCP/G,AJ,PRPC,ICASE,PREVER,MFSTOP,JUMP,LOPIN,ISCASE,
     1KN,GAMF,IP,SCRIT,PTRN,ISECT,KSTG,WTOL,RHOTOL,PRTOL,TRLOOP,LSTG,
     2LBRC,IBRC,ICHOKE,ISORR,CHOKE,PTOPS1(6,8),PTRS2(6,8),TRDIAG,SC,RC,
     3DELPR,PASS,IPC,LOPC,ISS
C
      COMMON /SINIT/H1(6,8),H2(6,8),DP0(6,8),DP1(6,8),DP1A(6,8),DP2(6,8)
     1,DP2A(6,8),CSALF1(6,8),ALF1(6,8),CSBET2(6,8),BET2(6,8),RADSD(6,8),
     2RADRD(6,8),ANN1(6,8),ANN2(6,8),ANN2A(6,8),ANN1A(6,8),U1A(6,8),
     3U2(6,8),ANN0(6,8),PT0(6,8),TT0(6,8),ALPHA0(6,8),PTP(6,8)
C
      COMMON /SINPUT/ RSL,TSL,PSL,GAMSL,
     1PTPS,PTIN,TTIN,WAIR,FAIR,DELC,DELL,DELA,AACS,VCTD,STG,SECT,EXPN,
     2EXPP,EXPRE,    RPM,PAF,SLI,STGCH,ENDJOB,NAME(10),TITLE(10),PCNH(6),
     3RV(6,8),GAM(6,8),DR(6,8),UT(6,8),RWG(6,8),ALPHAS(6,8),ALPHA1(6,8),
     4ETARS(6,8),ETAS(6,8),CFS(6,8),ANDO(6,8),BETA1(6,8),BETA2(6,8),ETAR
     5R(6,8),ETAR(6,8),CFR(6,8),TFR(6,8),ANDOH(6,8),OMEGAS(6,8),AS0(6,8)
     6,ASMP0(6,8),ACMN0(6,8),A1(6,8),A2(6,8),A3(6,8),A4(6,8),A5(6,8),A6(
     76,8),OMEGAR(6,8),BSIA(6,8),BSMPIA(6,8),BCMNIA(6,8),B1(6,8),B2(6,8)
     8,B3(6,8),B4(6,8),B5(6,8),B6(6,8),SESTHI(8),RERTHI(8)
C
      REAL M0
      COMMON /SSTA01/CP0(8),                    PS0(6,8),V0(6,8),TS0(6,
     18),VU0(6,8),VZ0(6,8),RHOS0(6,8),PS1(6,8),WGT1(8),TA1(8),WG1(6,8),
     2              CPDR1(6,8),SI(6,8),   CP1(8),PHI1(6,8),TS1(6,8),V1(6,8)
     3,RHOS1(6,8),ALF1E(6,8),VU1(6,8),VZ1(6,8),M0(6,8),WGT0(8),WG0(6,8)
C
      DIMENSION         TA0(8),          TTOTS0(6,8),PTOPS0(6,8),FFA0(6,8
     1),AAS0(6,8)
C
C
      IF(SRFLAG) WRITE(6,10000)
10000 FORMAT(44H AN ENTRY HAS BEEN MADE IN SUBROUTINE STA01 )
      K=KN
      SCRIT=0.0
      I=IP
      ID=-1
```

Listing of Code (continued)

```
      WGT1(K)=0.0
      JW=1
      IF(GAMF)2,2,3
    2 TA1(K)=.95*TT0(IP,K)
      CALL GAMMA(PTIN,TA1(K),FAIR,WAIR,GAM(2,K))
    3 CALL FLOW1(I)
      IF (PREVER) GO TO 26
      WGT1(K)=WGT1(K)+WG1(I,K)
C        TEST FOR TIP SECTOR
      IF(ISECT-I)5,5,4
    4 I=I+ID
      IF(I)6,6,22
   22 L=I-ID
      PS1(I,K)=PS1(   L,K)+FLOAT(ID)*DPDR1(   L,K)*(
     1H1(I,K)+H1(   L,K))/2.
      PTOPS1(I,K)=PT0(I,K)/PS1(I,K)
      IF (PTOPS1(I,K)-1.)27,3,3
   27 PTRN=-1.
      PTOPS1(I,K)= 1.0
      GO TO 3
    6 ID=1
      I=IP+ID
      GO TO 22
C        CALCULATE STA 0 FOR INCIDENCE CORRECTION
    5 IF (JW-1)16,16,18
   16 IF(GAMF)7,7,17
    7 GAM(1,K)=GAM(2,K)
   17 EX=(GAM(1,K)-1.)/GAM(1,K)
      EXI=1./EX
      WGT0(K)=WGT1(K)/RWG(2,K)
      I= IP
      WG0(I,K)=WG1(I,K)/RWG(2,K)
      FFA0(I,K)=WG0(I,K)*SQRT(   TT0(I,K))/(144.*PT0(I,K)*
     1ANN0(I,K))
   19 J=1
    8 CALL PRATIO(FFA0(I,K),GAM(1,K),RV(1,K) ,PTOPS0(I,K),PRTOL)
      PS0(I,K)=PTP(I,K)/PTOPS0(I,K)
      TTOTS0(I,K)=PTOPS0(I,K)**EX
      TS0(I,K)=TT0(I,K)/TTOTS0(I,K)
    9 IF(GAMF) 10,10,12
   10 TA0(K)=.5*(TT0(I,K)+TS0(I,K))
      CALL GAMMA(PTIN,TA0(K),FAIR,WAIR,GAM(1,K))
      EX=(GAM(1,K)-1.)/GAM(1,K)
      EXI=1./EX
      IF(J-1)11,11,12
   11 J=J+1
      GO TO 8
```

Listing of Code (continued)

```
   12 CP0(K)=RV(1,K)*EXI/AJ
      DO 14 I=1,ISECT
      WG0(I,K)=WG1(I,K)/RWG(2,K)
      PTOMO= PT0(I,K)
      FFA0(I,K)=WG0(I,K)*SQRT(    TT0(I,K))/(144.*PT0(I,K)*
     1ANNO(I,K))
      IF(I.EQ.IP) GO TO 28
      PS0(I,K) =  PS0(IP,K)
      PTOPS0(I,K) = PTP(I,K)/ PS0(I,K)
   28 TTOTS0(I,K)=PTOPS0(I,K)**EX
      TS0(I,K)=TT0(I,K)/TTOTS0(I,K)
   13 V0(I,K)=SQRT(2.*G*AJ*CP0(K)*(TT0(I,K)-TS0(I,K)))
      AAS0(I,K)=SQRT(GAM(1,K)*G*RV(1,K)*TS0(I,K))
      M0(I,K)=V0(I,K)/AAS0(I,K)
      SI(I,K)=ALPHA0(I,K)- RADSD(I,K)
      IF(SI(I,K))24,24,20
   24 EXPS=EXPN
      GO TO 21
   20 EXPS=EXPP
   21 PTOPS0(I,K)=(1.+EX*M0(I,K)*ETARS(I,K)*GAM(1,K)*M0(I,K)/2.
     1*(COS(SI(I,K))**EXPS))**EXI
      PT0(I,K)=PS0(I,K)*PTOPS0(I,K)
      WG0(I,K)=WG0(I,K)*PT0(I,K)/PTOMO
      WG1(I,K)=WG1(I,K)*PT0(I,K)/PTOMO
      RHOS0(I,K)=144.*PS0(I,K)/(RV(1,K)*TS0(I,K))
      VU0(I,K)=V0(I,K)*SIN(ALPHA0(I,K))
      VZ0(I,K)=V0(I,K)*COS(ALPHA0(I,K))
   14 CONTINUE
C        END OF INCIDENCE LOSS CORRECTION LOOP
      WGT1(K)=0.
      I=IP
      ID=-1
      JW=2
   15 GO TO 3
   18 CONTINUE
      WGT0(K)=WGT1(K)/RWG(2,K)
      IF(TRLOOP.EQ.0.) GO TO 23
      WRITE(6,1000) WGT0(K),WGT1(K),(WG0(L,K),L=1,ISECT)
      WRITE(6,1001)                (PTOPS0(L,K),L=1,ISECT)
      WRITE(6,1002)                   (WG1(L,K),L=1,ISECT)
      WRITE(6,1003)                (PTOPS1(L,K),L=1,ISECT)
 1000 FORMAT(2X,6H WGT0=F8.3,2X,6H WGT1=F8.3/2X,6H  WG0=6F8.3)
 1001 FORMAT(1X,7HPTOPS0=6F8.5)
 1002 FORMAT(2X,6H  WG1=6F8.3)
 1003 FORMAT(1X,7HPTOPS1=6F8.5)
   23 CALL CHECK         (J)
      GO TO (25,26),J
```

Listing of Code (continued)

```
                                                                  ST01 137
   25 CALL DIAGT(1)                                               ********
   26 IF(SRFLAG) WRITE(6,20000)                                   ********
20000 FORMAT(45H AN EXIT HAS BEEN MADE FROM SUBROUTINE STA01 )    ********
      RETURN                                                      ST01 139
      END
```

Listing of Code (continued)

```
      SUBROUTINE FLOW1(I)                                               FLW1 001
CFLOW1                                                                  FLW1 002
C     ESTABLISH VALUES FOR STATOR EXIT FLOW                             FLW1 003
C                                                                       FLW1 004
      REAL MFSTOP                                                       FLW1 005
      LOGICAL PREVER,SRFLAG                                             ********
      COMMON  SRFLAG                                                    ********
      COMMON /SNTCP/G,AJ,PREC,ICASE,PREVER,MFSTOP,JUMP,LOPIN,ISCASE,    FLW1 007
     1KN,GAMF,IP,SCRIT,PTRN,ISECT,KSTG,WTOL,RHOTOL,PRTOL,TRLOOP,LSTG,   ********
     2LBRC,IBRC,ICHOKE,ISORR,CHOKE,PTOPS1(6,8),PTRS2(6,8),TRDIAG,SC,RC, FLW1 009
     3DELPR,PASS,IPC,LOPC,ISS                                           FLW1 010
C                                                                       FLW1 011
      COMMON /SINIT/H1(6,8),H2(6,8),DP0(6,8),DP1(6,8),DP1A(6,8),DP2(6,8)FLW1 012
     1,DP2A(6,8),CSALF1(6,8),ALF1(6,8),CSBET2(6,8),BET2(6,8),RADSD(6,8),FLW1 013
     2RADRD(6,8),ANN1(6,8),ANN2(6,8),ANN2A(6,8),ANN1A(6,8),U1A(6,8),    FLW1 014
     3U2(6,8),ANN0(6,8),PT0(6,8),TT0(6,8),ALPHA0(6,8),PTP(6,8)          FLW1 015
C                                                                       FLW1 016
      COMMON /SINPUT/ RSL,TSL,PSL,GAMSL,                                ********
     1PTPS,PTIN,TTIN,WAIR,FAIR,DELC,DELL,DELA,AACS,VCTD,STG,SECT,EXPN,  FLW1 018
     2EXPP,EXPHE,   RPM,PAF,SLI,STGCH,ENDJOB,NAME(10),TITLE(10),PCNH(6),********
     3RV(6,8),GAM(6,8),DR(6,8),DT(6,8),RWG(6,8),ALPHAS(6,8),ALPHA1(6,8),********
     4ETARS(6,8),ETAS(6,8),CFS(6,8),ANDO(6,8),BETA1(6,8),BETA2(6,8),ETARFLW1 021
     5R(6,8),ETAR(6,8),CFR(6,8),TFR(6,8),ANDOR(6,8),OMEGAS(6,8),AS0(6,8)FLW1 022
     6,ASMP0(6,8),ACMN0(6,8),A1(6,8),A2(6,8),A3(6,8),A4(6,8),A5(6,8),A6(FLW1 023
     76,8),OMEGAR(6,8),BSIA(6,8),BSMPIA(6,8),BCMNIA(6,8),B1(6,8),B2(6,8)FLW1 024
     8,B3(6,8),B4(6,8),B5(6,8),B6(6,8),SESTHI(8),RERTHI(8)              FLW1 025
C                                                                       FLW1 026
      REAL M0                                                           FLW1 027
      COMMON /SSTA01/CP0(8),                        PS0(6,8),V0(6,8),TS0(6,FLW1 028
     18),VU0(6,8),VZ0(6,8),RHOS0(6,8),PS1(6,8),WGT1(8),TA1(8),WG1(6,8), FLW1 029
     2             DPDR1(6,8),SI(6,8),  CP1(8),PHI1(6,8),TS1(6,8),V1(6,8)FLW1 030
     3,RHOS1(6,8),ALF1E(6,8),VU1(6,8),VZ1(6,8),M0(6,8),WGT0(8),WG0(6,8) ********
C                                                                       FLW1 032
      DIMENSION PHI1C(8),PTPS1C(8),V1C(6,8),TS1C(6,8),RHOS1C(6,8),WG1C(6FLW1 033
     1,8),CSAL1E(6,8),SFF(6,8)                                          FLW1 034
C                                                                       FLW1 035
C                                                                       FLW1 036
      IF(SRFLAG) WRITE(6,10000)                                         ********
10000 FORMAT(44H AN ENTRY HAS BEEN MADE IN SUBROUTINE FLOW1 )           ********
      K=KN                                                              ********
      EX=(GAM(2,K)-1.)/GAM(2,K)                                         FLW1 037
C        COMPUTE ISENTROPIC STATOR TEMPERATURE RATIO                    FLW1 038
    7 PHI1(I,K)=PTOPS1(I,K)**EX                                         FLW1 039
C        TEST FOR LOSS COEFFICIENT INPUT                                FLW1 040
      IF (OMEGAS(1,1))2,2,1                                             FLW1 041
    1 CALL LOSS1(I,K,EX)                                                FLW1 042
```

Listing of Code (continued)

```
    2 TS1(I,K)=TTO(I,K)*(1.-ETAS(I,K)*(1.-1./PHI1(I,K)))                FLW1 043
      IF(I-IP)6,3,6                                                     FLW1 044
    3 IF(GAMF)4,4,5                                                     FLW1 045
    4 TA1(K)=.5*(TTO(I,K)+TS1(I,K))                                     FLW1 046
      CALL GAMMA(PTO(IP,K),TA1(K),FAIR,WAIR,GAM(2,K))                   FLW1 047
    5 EX=(GAM(2,K)-1.0)/GAM(2,K)                                        FLW1 048
      EXI=1./EX                                                         FLW1 049
C     CRITICAL PRESSURE RATIO                                           FLW1 050
      CALL PHIM(EXI,ETAS(I,K),PHI1C(K),PTPS1C(K))                       FLW1 051
      CP1(K)=RV(2,K)*EXI/AJ                                             ********
C        EXIT VELOCITY                                                  FLW1 053
    6 V1(I,K)=SQRT(2.*G*AJ*CP1(K)*(TTO(I,K)-TS1(I,K)))                  FLW1 054
C        EXIT PRESSURE                                                  FLW1 055
      PS1(I,K)=PTO(I,K)/PTOPS1(I,K)                                     FLW1 056
C        EXIT DENSITY                                                   FLW1 057
      RHOS1(I,K)=144.*PS1(I,K)/(RV(2,K)*TS1(I,K))                       ********
C        TEST CRITICAL PRESSURE RATIO                                   FLW1 059
      IF(PTOPS1(I,K)-PTPS1C(K))15, 8,8                                  FLW1 060
C        GREATER THAN CRITICAL                                          FLW1 061
    8 IF (IP-1) 21,9,21                                                 FLW1 062
    9 IF (PRPC)10,10,22                                                 FLW1 063
C        PREVIOUS PITCH NONCRITICAL                                     FLW1 064
   10 PRPC=1.                                                           FLW1 065
      PTOPS1(I,K)=PTPS1C(K)*(1.+PRTOL)                                  FLW1 066
      GO TO 7                                                           FLW1 067
   21 IF (PTOPS1(I,K).LE.PTOPS1(IP,K))  GO TO 22                        FLW1 068
      GO TO 12                                                          FLW1 069
   22 IF ((I.EQ.1).OR.(I.EQ.ISECT))  SCRIT=1.                           FLW1 070
      GO TO 11                                                          FLW1 071
C        PITCH OR OUTBOARD SECTOR                                       FLW1 072
   11 CONTINUE                                                          FLW1 073
      V1C(I,K)=SQRT(2.*G*AJ*CP1(K)*TTO(I,K)*ETAS(I,K)*(PHI1C(K)         FLW1 074
     1-1.)/PHI1C(K))                                                    FLW1 075
      TS1C(I,K)=TTO(I,K)*(1.-ETAS(I,K)*(1.-1./PHI1C(K)))                FLW1 076
      RHOS1C(I,K)=144.*PTO(I,K)/(  PTPS1C(K)*TS1C(I,K)*RV(2,K))         ********
      WG1C(I,K)=RHOS1C(I,K)*V1C(I,K)*ANN1(I,K)*CSALF1(I,K)              FLW1 078
      WG1(I,K)=WG1C(I,K)                                                FLW1 079
   13 CSAL1E(I,K)=WG1(I,K)/(RHOS1(I,K)*V1(I,K)*ANN1(I,K))               FLW1 080
C     EFFECTIVE STATOR EXIT ANGLE                                       FLW1 081
   14 ALF1E(I,K)=ATAN2(SQRT(1.-CSAL1E(I,K)*CSAL1E(I,K)),                FLW1 082
     1CSAL1E(I,K))                                                      FLW1 083
      GO TO 16                                                          FLW1 084
   12 IF(   PRPC-1.)15,15,24                                            FLW1 085
   24 WG1(I,K)=SFF(I,K)*PTO(I,K)/SQRT(TTO(I,K))                         FLW1 086
      GO TO 13                                                          FLW1 087
C        PRESSURE RATIO LESS THAN CRITICAL OR SUPERSONIC FLOW DECREASE  FLW1 088
   15 WG1(I,K)=RHOS1(I,K)*V1(I,K)*ANN1(I,K)*CSALF1(I,K)                 FLW1 089
```

Listing of Code (continued)

```
      CSAL1E(I,K)=CSALF1(I,K)                                           FLW1 090
      ALF1E(I,K)=ALF1(I,K)                                              FLW1 091
      SFF(I,K)=WG1(I,K)*SQRT(TTO(I,K))/PTO(I,K)                         FLW1 092
   16 VU1(I,K)=V1(I,K)*SIN(ALF1E(I,K))                                  FLW1 093
      DPDR1(I,K)=.01388889*RHOS1(I,K)*VU1(I,K)*VU1(I,K)/                ********
     1(G*DP1(I,K))                                                      FLW1 095
      VZ1(I,K)=V1(I,K)*CSAL1E(I,K)                                      FLW1 096
      IF(I.LT.ISECT) GO TO 17                                           FLW1 097
      IF(PRPC.EQ.1.) PRPC=2.                                            FLW1 098
   17 CALL CHECK(J)                                                     FLW1 099
      GO TO (19,20),J                                                   FLW1 100
   19 CALL DIAGT(2)                                                     FLW1 101
   20 IF(SRFLAG) WRITE(6,20000)                                         ********
20000 FORMAT(45H AN EXIT HAS BEEN MADE FROM SUBROUTINE FLOW1 )          ********
      RETURN                                                            ********
      END                                                               FLW1 103
```

Listing of Code (continued)

```
      SUBROUTINE LOSS1(I,K,EX)
CLOSS1
C
C     CALCULATE EFFICIENCY
C
      REAL MFSTOP
      LOGICAL PREVER,SRFLAG
      COMMON  SRFLAG
      COMMON /SNTCP/G,AJ,PRPC,ICASE,PREVER,MFSTOP,JUMP,LOPIN,ISCASE,
     1KN,GAMF,IP,SCRIT,PTRN,ISECT,KSTG,WTOL,RHOTOL,PRTOL,TRLOOP,LSTG,
     2LBRC,IBRC,ICHOKE,ISORR,CHOKE,PTOPS1(6,8),PTRS2(6,8),TRDIAG,SC,RC,
     3DELPR,PASS,IPC,LOPC,ISS
C
      COMMON /SINIT/H1(6,8),H2(6,8),DP0(6,8),DP1(6,8),DP1A(6,8),DP2(6,8)
     1,DP2A(6,8),CSALF1(6,8),ALF1(6,8),CSBET2(6,8),BET2(6,8),RADSD(6,8),
     2RADRD(6,8),ANN1(6,8),ANN2(6,8),ANN2A(6,8),ANN1A(6,8),U1A(6,8),
     3U2(6,8),ANN0(6,8),PT0(6,8),TT0(6,8),ALPHA0(6,8),PTP(6,8)
C
      COMMON /SINPUT/ RSL,TSL,PSL,GAMSL,
     1PTPS,PTIN,TTIN,WAIR,FAIR,DELC,DELL,DELA,AACS,VCTD,STG,SECT,EXPN,
     2EXPP,EXPRE,    RPM,PAF,SLI,STGCH,FNDJOB,NAME(10),TITLE(10),PCNH(6),
     3RV(6,8),GAM(6,8),DR(6,8),DT(6,8),RWG(6,8),ALPHAS(6,8),ALPHA1(6,8),
     4ETARS(6,8),ETAS(6,8),CFS(6,8),ANDO(6,8),BETA1(6,8),BETA2(6,8),ETAR
     5R(6,8),ETAR(6,8),CFR(6,8),TFR(6,8),ANDOR(6,8),OMEGAS(6,8),ASO(6,8)
     6,ASMPO(6,8),ACMNO(6,8),A1(6,8),A2(6,8),A3(6,8),A4(6,8),A5(6,8),A6(
     76,8),OMEGAR(6,8),BSIA(6,8),BSMPIA(6,8),BCMNIA(6,8),B1(6,8),B2(6,8)
     8,B3(6,8),B4(6,8),B5(6,8),B6(6,8),SESTHI(8),RERTHI(8)
C
      REAL M0
      COMMON /SSTA01/CP0(8),                     PS0(6,8),V0(6,8),TS0(6,
     18),VU0(6,8),VZ0(6,8),RHOS0(6,8),PS1(6,8),WGT1(8),TA1(8),WG1(6,8),
     2               DPDR1(6,8),SI(6,8),   CP1(8),PHI1(6,8),TS1(6,8),V1(6,8)
     3,RHOS1(6,8),ALF1E(6,8),VU1(6,8),VZ1(6,8),M0(6,8),WGT0(8),WG0(6,8)
C
C
      IF(SRFLAG) WRITE(6,10000)
10000 FORMAT(44H AN ENTRY HAS BEEN MADE IN SUBROUTINE LOSS1 )
      EXPN=0.0
      EXPP=0.0
      ETARS(I,K)=1.0
      SI(I,K)=ALPHA0(I,K)- RADSD(I,K)
      IF(SI(I,K))5,1,2
    1 W01=OMEGAS(I,K)
      GO TO 9
    2 AS=A1(I,K)
      AC=A2(I,K)
```

Listing of Code (continued)

```
      AQ=A3(I,K)
      IF(ASMPO(I,K)-SI(I,K))3,4,4
    3 WMWS=SI(I,K)/ASMPO(I,K)
      AR=ASMPO(I,K)/ASO(I,K)
      GO TO 8
    4 WMWS=1.0
      AR=SI(I,K)/ASO(I,K)
      GO TO 8
    5 AS=A4(I,K)
      AC=A5(I,K)
      AQ=A6(I,K)
      IF(SI(I,K)-ACMNO(I,K))6,4,4
    6 WMWS=SI(I,K)/ACMNO(I,K)
      AR=ACMNO(I,K)/ASO(I,K)
    8 W01=(1.+AR*AR*(AS+AR*(AC+AR*AQ)))*WMWS*OMEGAS(I,K)
    9 ETAS(I,K)=(1.-(1./(PTOPS1(I,K)*(1.-W01)+W01))**EX)*PHI1(I,K)/
     1(PHI1(I,K)-1.)
      CALL CHECK(J)
      IF(SRFLAG) WRITE(6,20000)
20000 FORMAT(45H AN EXIT HAS BEEN MADE FROM SUBROUTINE LOSS1 )
      RETURN
      END
```

Listing of Code (continued)

```
      SUBROUTINE R(P,T,F,W,RX)
CR
C     CALCULATE GAS CONSTANT
      WRITE (6,100)
  100 FORMAT (//120H SUBROUTINE  R  HAS BEEN CALLED UPON ********************
     1************************************************************************
     2**,//)
      RX=53.35045+(.658*F+32.433*W)/(1.+F+W)
      RETURN
      END
```

Listing of Code (continued)

```
      SUBROUTINE GAMMA(P,T,F,W,GAMX)                                    GAMA 001
CGAMMA                                                                  GAMA 002
C                                                                       GAMA 003
C     CALCULATE SPECIFIC HEAT RATIO FOR MIXTURE                         GAMA 004
      WRITE (6,100)                                                     ********
  100 FORMAT (//120H SUBROUTINE GAMMA HAS BEEN CALLED UPON  ********************
     1**************************************************************************
     2**,//)                                                            ********
      CALL CPA(P,T,F,W,CPAX)                                            GAMA 005
      IF(F)2,2,1                                                        GAMA 006
    1 CALL CPF(P,T,F,W,CPFX)                                            GAMA 007
    2 IF(W)4,4,3                                                        GAMA 008
    3 CALL CPW(P,T,F,W,CPWX)                                            GAMA 009
    4 CPGX=(CPAX+F*CPFX+W*CPWX)/(1.+F+W)                                GAMA 010
      CALL R(P,T,F,W,RX)                                                GAMA 011
      GAMX=CPGX/(CPGX-RX/778.161)                                       GAMA 012
      RETURN                                                            GAMA 013
      END                                                               GAMA 014
```

Listing of Code (continued)

```
      SUBROUTINE CPA(P,T,F,*,CPAX)
CCPA
C     CALCULATE SPECIFIC HEAT RATIO FOR AIR
      DIMENSION
     1XT(7),A(7)                                                        ********
      WRITE (6,100)
  100 FORMAT (//120H SUBROUTINE CPA HAS BEEN CALLED UPON ********************
     1**************************************************************************
     2**,//)
      IF(T-100.)1,2,2
    1 TX=100.
      GO TO 5
    2 IF(6400.-T)3,4,4
    3 TX=6400.
      GO TO 5
    4 TX=T
    5 XT(1)=TX/1000.
      DO 6 I=2,7
    6 XT(I)=XT(I-1)*XT(1)
      CPAX=2.4264907E-01-2.6657395E-02*XT(1)+4.6617756E-02*XT(2)
     1-1.3546542E-02*XT(3)-8.4500931E-04*XT(4)+1.0303393E-03*
     2XT(5)-1.7159795E-04*XT(6)+9.1627911E-06*XT(7)
      RETURN
      END
```

```
      SUBROUTINE CPF(P,T,F,*,CPFX)
CCPF
C     CALCULATE SPECIFIC HEAT RATIO FOR FUEL
      DIMENSION
     1XT(7),A(7)
      WRITE (6,100)
  100 FORMAT (//120H SUBROUTINE CPF HAS BEEN CALLED UPON *****************************
     1***********************************************************************
     2**,//)
      IF(T-400.)1,2,2
    1 TX=400.
      GO TO 5
    2 IF(3000.-T)3,4,4
    3 TX=3000.
      GO TO 5
    4 TX=T
    5 XT(1)=TX/1000.
      DO 6 I=2,7
    6 XT(I)=XT(I-1)*XT(1)
      CPFX=1.0625243E-01+9.5291284E-01*XT(1)-7.2605169E-01*XT(2)
     1+2.4481406E-01*XT(3)+5.3332162E-02*XT(4)-6.4699814E-02*XT(5)
     2+1.7495567E-02*XT(6)-1.6029820E-03*XT(7)
      RETURN
      END
```

Listing of Code (continued)

```
      SUBROUTINE CPW(P,T,F,*,CPWX)
CCPW
C     CALCULATE SPECIFIC HEAT FOR WATER VAPOR
      DIMENSION
     1XT(7),A(7)
      WRITE (6,100)                                                     ********
  100 FORMAT (//120H SUBROUTINE CPW HAS BEEN CALLED UPON  ************************
     1*****************************************************************************
     2**,//)                                                            ********
      IF(T-400.)1,2,2
    1 TX=400.
      GO TO 5
    2 IF(3000.-T)3,4,4
    3 TX=3000.
      GO TO 5
    4 TX=T
    5 XT(1)=TX/1000.
      DO 6 I=2,7
    6 XT(I)=XT(I-1)*XT(1)
      CPWX=4.5728850E-01+9.7007556E-02*XT(1)+1.6536409E-01
     1*XT(2)-4.1138066E-02*XT(3)-2.6979575E-02*XT(4)+2.2619243E-02
     2*XT(5)-6.2706207E-03*XT(6)+6.2246710E-04*XT(7)
      RETURN
      END
```

Listing of Code (continued)

```
      SUBROUTINE PRATIO(TFF,GAMX,RX,PTPS,PRTOL)                         PRIO 001
CPRATIO                                                                 PRIO 002
C     CALCULATE PRESSURE RATIO                                          PRIO 003
      LOGICAL PREVER,SRFLAG                                             ********
      COMMON  SRFLAG                                                    ********
      IF(SRFLAG) WRITE(6,10000)                                         ********
10000 FORMAT(44H AN ENTRY HAS BEEN MADE IN SUBROUTINE PRATIO)           ********
      A=GAMX/(GAMX-1.)                                                  PRIO 004
      B=2./GAMX                                                         PRIO 005
      C=(GAMX+1.)/GAMX                                                  PRIO 006
      D=TFF*SQRT(RX/(64.3481*A))                                        PRIO 007
      PCRIT=((GAMX+1.)/2.)**A                                           PRIO 008
      PUP=PCRIT                                                         PRIO 009
      PLOW=1.0                                                          PRIO 010
      PTRMO=0.0                                                         PRIO 011
    1 PTR=(PUP+PLOW)/2.                                                 PRIO 012
      DELFM=SQRT(1./(PTR**B)-1./(PTR**C))-D                             PRIO 013
      IF(DELFM)2,3,3                                                    PRIO 014
    2 PLOW=PTR                                                          PRIO 015
      GO TO 4                                                           PRIO 016
    3 PUP=PTR                                                           PRIO 017
    4 PRE=(PTR-PTRMO)/PTR                                               PRIO 018
      IF (ABS(PRE)-PRTOL)6,6,5                                          PRIO 019
    5 PTRMO=PTR                                                         PRIO 020
      GO TO 1                                                           PRIO 021
    6 IF(PCRIT-PTR)7,8,8                                                PRIO 022
    7 PTPS=PCRIT                                                        PRIO 023
      GO TO 9                                                           PRIO 024
    8 PTPS=PTR                                                          PRIO 025
    9 CONTINUE                                                          PRIO 026
      IF(SRFLAG) WRITE(6,20000)                                         ********
20000 FORMAT(45H AN EXIT HAS BEEN MADE FROM SUBROUTINE PRATIO)          ********
      RETURN                                                            PRIO 027
      END                                                               PRIO 028
```

Listing of Code (continued)

```
      SUBROUTINE CHECK(J)                                               CHCK 001
CCHECK                                                                  CHCK 002
C       SUBROUTINE TO CHECK SENSE LIGHTS                                CHCK 003
C                                                                       CHCK 004
      REAL MFSTOP                                                       CHCK 005
      LOGICAL PREVER,SRFLAG                                             ********
      COMMON  SRFLAG                                                    ********
      COMMON /SNTCP/G,AJ,PRPC,ICASE,PREVER,MFSTOP,JUMP,LOPIN,ISCASE,    CHCK 007
     1KN,GAMF,IP,SCRIT,PTRN,ISECT,KSTG,WTOL,RHOTOL,PRTOL,TRLOOP,LSTG,   CHCK 008
     2LBRC,IBRC,ICHOKE,ISORR,CHOKE,PTOPS1(6,8),PTRS2(6,8),TRDIAG,SC,RC, CHCK 009
     3DELPR,PASS,IPC,LOPC,ISS                                           CHCK 010
C                                                                       CHCK 011
      IF(SRFLAG) WRITE(6,10000)                                         ********
10000 FORMAT(44H AN ENTRY HAS BEEN MADE IN SUBROUTINE CHECK )           ********
      DO 1 I=1,4                                                        CHCK 012
      CALL SLITET(I,J)                                                  CHCK 013
      GO TO (2,1),J                                                     CHCK 014
    1 CONTINUE                                                          CHCK 015
      J=2                                                               CHCK 016
      IF(SRFLAG) WRITE(6,20000)                                         ********
      RETURN                                                            CHCK 017
    2 J=1                                                               CHCK 018
      PREVER=.TRUE.                                                     CHCK 019
      IF(SRFLAG) WRITE(6,20000)                                         ********
20000 FORMAT(45H AN EXIT HAS BEEN MADE FROM SUBROUTINE CHECK )          ********
      RETURN                                                            CHCK 020
      END                                                               CHCK 021
```

```
      SUBROUTINE STA1A
CSTA1A
C
      REAL MFSTOP
      LOGICAL PREVER,SRFLAG
      COMMON  SRFLAG
      COMMON /SNTCP/G,AJ,PRFC,ICASE,PREVER,MFSTOP,JUMP,LOPIN,ISCASE,
     1KN,GAMF,IP,SCRIT,PTRN,ISECT,KSTG,WTOL,RHOTOL,PRTOL,TRLOOP,LSTG,
     2LBRC,IBRC,ICHOKE,ISORR,CHOKE,PTOPS1(6,8),PTRS2(6,8),TRDIAG,SC,RC,
     3DELPR,PASS,IPC,LOPC,ISS
C
      COMMON /SINIT/H1(6,8),H2(6,8),DP0(6,8),DP1(6,8),DP1A(6,8),DP2(6,8)
     1,DP2A(6,8),CSALF1(6,8),ALF1(6,8),CSBET2(6,8),BET2(6,8),RADSD(6,8),
     2RADRD(6,8),ANN1(6,8),ANN2(6,8),ANN2A(6,8),ANN1A(6,8),U1A(6,8),
     3U2(6,8),ANN0(6,8),PT0(6,8),TT0(6,8),ALPHA0(6,8),PTP(6,8)
C
      COMMON /SINPUT/ RSL,TSL,PSL,GAMSL,
     1PTPS,PTIN,TTIN,WAIR,FAIR,DELC,DELL,DELA,AACS,VCTD,STG,SECT,EXPN,
     2EXPP,EXPRE,    RPM,PAF,SLI,STGCH,ENDJOB,NAME(10),TITLE(10),PCNH(6),
     3RV(6,8),GAM(6,8),DR(6,8),DT(6,8),RWG(6,8),ALPHAS(6,8),ALPHA1(6,8),
     4ETARS(6,8),ETAS(6,8),CFS(6,8),ANDO(6,8),BETA1(6,8),BETA2(6,8),ETAR
     5R(6,8),ETAR(6,8),CFR(6,8),TFR(6,8),ANDOR(6,8),OMEGAS(6,8),AS0(6,8)
     6,ASMP0(6,8),ACMN0(6,8),A1(6,8),A2(6,8),A3(6,8),A4(6,8),A5(6,8),A6(
     76,8),OMEGAR(6,8),BSIA(6,8),BSMPIA(6,8),BCMNIA(6,8),B1(6,8),B2(6,8)
     8,B3(6,8),B4(6,8),B5(6,8),B6(6,8),SESTHI(8),RERTHI(8)
C
      REAL M0
      COMMON /SSTA01/CP0(8),                      PS0(6,8),V0(6,8),TS0(6,
     18),VU0(6,8),VZ0(6,8),RHOS0(6,8),PS1(6,8),WGT1(8),TA1(8),WG1(6,8),
     2               CPDR1(6,8),SI(6,8),  CP1(8),PHI1(6,8),TS1(6,8),V1(6,8)
     3,RHOS1(6,8),ALF1E(6,8),VU1(6,8),VZ1(6,8),M0(6,8),WGT0(8),WG0(6,8)
      REAL MR1A
      COMMON /SSTA1A/VU1A(6,8),WG1A(6,8),WGT1A(8),VZ1A(6,8),  CP1A(8),
     1PS1A(6,8),RU1A(6,8),R1A(6,8),BET1A(6,8),RI(6,8),TTR1A(6,8),PTR1A(6
     2,8),MR1A(6,8),TS1A(6,8)
C        DETERMINE FLOW CONDITIONS RELATIVE TO ROTOR.  FIND INCIDENCE
C         ANGLE RECOVERY ROTOR INLET STATIONS.  OBTAIN GAS PROPERTIES,
C         ABSOLUTE TANGENTIAL COMPONENT VELOCITY ADJUSTED FOR DIAMETER
C         CHANGE TO CONSERVE ANGULAR MOMENTUM.  AXIAL COMPONENT
C         VELOCITY ADJUSTED FOR WEIGHT FLOW, AREA,, AND DENSITY CHANGE
C         FROM STA  1.
C
C
      IF(SRFLAG) WRITE(6,10000)
10000 FORMAT(44H AN ENTRY HAS BEEN MADE IN SUBROUTINE STA1A )
      K=KN
```

Listing of Code (continued)

```
      I=IP                                                              ST1A 043
      ID=-1                                                             ST1A 044
      TS1A(I,K)=TS1(I,K)                                                ********
C        RATIO OF FLOW CHANGE                                           ST1A 046
      WR=RWG(3,K)/RWG(2,K)                                              ST1A 047
C        TOTAL STATION FLOW                                             ST1A 048
      WGT1A(K)=WR*WGT1(K)                                               ST1A 049
C        ADJUST TANGENTIAL VELOCITY                                     ST1A 050
   13 VU1A(I,K)=VU1(I,K)*DP1(I,K)/DP1A(I,K)                             ST1A 051
C        ADJUST FLOW                                                    ST1A 052
      WG1A(I,K)=WR*WG1(I,K)                                             ST1A 053
      RHOSTR=RHOS1(I,K)                                                 ST1A 054
C        ADJUST AXIAL VELOCITY                                          ST1A 055
    1 VZ1A(I,K)=WR*VZ1(I,K)*ANN1(I,K)*RHOS1(I,K)/(ANN1A(I,K)            ST1A 056
     1*RHOSTR)                                                          ST1A 057
      V1A     =SQRT(VU1A(I,K)*VU1A(I,K)+VZ1A(I,K)*VZ1A(I,K))            ST1A 058
      IF(I-IP)2,3,2                                                     ST1A 059
    2 EX=(GAM(3,K)-1.)/GAM(3,K)                                         ST1A 060
      EXI=1./EX                                                         ST1A 061
      GO TO 4                                                           ST1A 062
    3 IF(GAMF)12,12,2                                                   ST1A 063
   12 TA1A    =.5*(TT0(I,K)+TS1A(I,K))                                  ********
      CALL GAMMA(PT0(I,K),TA1A    ,FAIR,WAIR,GAM(3,K))                  ST1A 065
      EX=(GAM(3,K)-1.)/GAM(3,K)                                         ST1A 066
      EXI=1./EX                                                         ST1A 067
    4 CP1A(K)=RV(3,K)*EXI/AJ                                            ********
      DELTS=(V1(I,K)*V1(I,K)-V1A     *V1A     )/(2.*G*AJ*CP1A(K))       ST1A 069
      TS1A(I,K)=TS1(I,K)+DELTS                                          ********
      PS1A(I,K)=PS1(I,K)*(1.+DELTS/TS1(I,K))**EXI                       ST1A 071
      RHOS1A     =144.*PS1A(I,K)/(RV(3,K)*TS1A(I,K))                    ********
C        DENSITY ERROR                                                  ST1A 073
      RHOE=(RHOS1A     -RHOSTR)/RHOS1A                                  ST1A 074
      IF (ABS(RHOE)-RHOTOL)6,6,5                                        ST1A 075
    5 RHOSTR=RHOS1A                                                     ST1A 076
      GO TO 1                                                           ST1A 077
    6 RU1A(I,K)=VU1A(I,K)-U1A(I,K)                                      ST1A 078
      R1A(I,K)=SQRT(RU1A(I,K)*RU1A(I,K)+VZ1A(I,K)*VZ1A(I,K))            ST1A 079
      SBET1A     =RU1A(I,K)/R1A(I,K)                                    ST1A 080
      BET1A(I,K)=ATAN2(SBET1A     ,SQRT(1.-SBET1A     *SBET1A     ))    ST1A 081
      IF(OMEGAR(I,K))8,8,7                                              ST1A 082
    7 ETARR(I,K)=1.                                                     ST1A 083
      EXPRE=0.0                                                         ST1A 084
    8 MR1A(I,K)=R1A(I,K)/SQRT(GAM(3,K)*G*RV(3,K)*TS1A(I,K))             ********
      TRTS1A     =1.+(GAM(3,K)-1.)*MR1A(I,K)*MR1A(I,K)/2.               ST1A 086
      IF(TRTS1A.GT.1.) GO TO 32                                         ST1A 087
      PREVER = .TRUE.                                                   ST1A 088
      GO TO 17                                                          ST1A 089
```

Listing of Code (continued)

```
   32 TTR1A(I,K)=TS1A(I,K)*TRTS1A                                    ********
      RI(I,K)=BET1A(I,K)-RACRD(I,K)                                  ST1A 091
      IF(RI(I,K).GT.1.570796) RI(I,K)=1.570796                       ********
      IF(RI(I,K).LT.-1.570796) RI(I,K)= -1.570796                    ********
      IF(RI(I,K))9,9,10                                              ST1A 094
    9 EXPR=EXPN                                                      ST1A 095
      GO TO 11                                                       ST1A 096
   10 EXPR=EXPP                                                      ST1A 097
   11 PRPS1A      =(1.+(TRTS1A      -1.)*ETARR(I,K)*(COS(RI(I,K))**  ST1A 098
     1EXPR))**EXI                                                    ST1A 099
      PTR1A(I,K)=PS1A(I,K)*PRPS1A                                    ST1A 100
      IF  (ISECT-I)14,16,14                                          ST1A 101
   14 I=I+ID                                                         ST1A 102
      IF  (I)15,15,13                                                ST1A 103
   15 ID=1                                                           ST1A 104
      I=IP+ID                                                        ST1A 105
      GO TO 13                                                       ST1A 106
   16 CONTINUE                                                       ST1A 107
      CALL CHECK(J)                                                  ST1A 108
      GO TO (17,18),J                                                ST1A 109
   17 CALL DIAGT(3)                                                  ST1A 110
   18 IF(SRFLAG) WRITE(6,20000)                                      ********
20000 FORMAT(45H AN EXIT HAS BEEN MADE FROM SUBROUTINE STA1A )       ********
      RETURN                                                         ********
      END                                                            ST1A 112
```

Listing of Code (continued)

```
      SUBROUTINE STA2
CSTA2
C     SATISFY CONTINUITY OF FLOW AT ROTOR EXIT
C
      REAL MFSTOP
      LOGICAL PREVER,SRFLAG
      COMMON  SRFLAG
      COMMON /SNTCP/G,AJ,PRPC,ICASE,PREVER,MFSTOP,JUMP,LOPIN,ISCASE,
     1KN,GAMF,IP,SCRIT,PTRN,ISECT,KSTG,WTOL,RHOTOL,PRTOL,TRLOOP,LSTG,
     2LBRC,IBRC,ICHOKE,ISORR,CHOKE,PTOPS1(6,8),PTRS2(6,8),TRDIAG,SC,RC,
     3DELPR,PASS,IPC,LOPC,ISS
C
      COMMON /SINIT/H1(6,8),H2(6,8),DP0(6,8),DP1(6,8),DP1A(6,8),DP2(6,8)
     1,DP2A(6,8),CSALF1(6,8),ALF1(6,8),CSBET2(6,8),BET2(6,8),RADSD(6,8),
     2RADRD(6,8),ANN1(6,8),ANN2(6,8),ANN2A(6,8),ANN1A(6,8),U1A(6,8),
     3U2(6,8),ANN0(6,8),PT0(6,8),TT0(6,8),ALPHA0(6,8),PTP(6,8)
C
      COMMON /SINPUT/ RSL,TSL,PSL,GAMSL,
     1PTPS,PTIN,TTIN,WAIR,FAIR,DELC,DELL,DELA,AACS,VCTD,STG,SECT,EXPN,
     2EXPP,EXPRE,    RPM,PAF,SLI,STGCH,ENDJOB,NAME(10),TITLE(10),PCNH(6),
     3RV(6,8),GAM(6,8),DR(6,8),DT(6,8),RWG(6,8),ALPHAS(6,8),ALPHA1(6,8),
     4ETARS(6,8),ETAS(6,8),CFS(6,8),ANDO(6,8),BETA1(6,8),BETA2(6,8),ETAR
     5R(6,8),ETAR(6,8),CFR(6,8),TFR(6,8),ANDOR(6,8),OMEGAS(6,8),AS0(6,8)
     6,ASMP0(6,8),ACMN0(6,8),A1(6,8),A2(6,8),A3(6,8),A4(6,8),A5(6,8),A6(
     76,8),OMEGAR(6,8),BSIA(6,8),BSMPIA(6,8),BCMNIA(6,8),B1(6,8),B2(6,8)
     8,B3(6,8),B4(6,8),B5(6,8),B6(6,8),SESTHI(8),RERTHI(8)
C
      REAL MR1A
      COMMON /SSTA1A/VU1A(6,8),WG1A(6,8),WGT1A(8),VZ1A(6,8),   CP1A(8),
     1PS1A(6,8),RU1A(6,8),R1A(6,8),BET1A(6,8),RI(6,8),TTR1A(6,8),PTR1A(6
     2,8),MR1A(6,8),TS1A(6,8)
C
      COMMON /SSTA2/V2(6,8),TTR2(6,8),PTR2(6,8),WG2(6,8),WGT2(8),TA2(8),
     1              PS2(6,8),PHI2(6,8)
C
      REAL MR2,M2     ,MF2
      COMMON /SFLOW2/TS2(6,8),CP2(8),R2(6,8),RHOS2(6,8),BET2E(6,8),RU2(6
     1,8),VU2(6,8),DPDR2(6,8),VZ2(6,8),MR2(6,8),MF2(6,8),M2(6,8)
C
      DIMENSION WGT2C(8),FFA2(6,8),IS2(8)
C
C
      IF(SRFLAG) WRITE(6,10000)
10000 FORMAT(44H AN ENTRY HAS BEEN MADE IN SUBROUTINE STA2   )
      K=KN
      J=1
```

Listing of Code (continued)

```
      SCRIT=0.0
      PTRMO=1.
      IS2(K)=0
      EXI=GAM(3,K)/(GAM(3,K)-1.)
      WR=RWG(4,K)/RWG(3,K)
      DO 1 I=1,ISECT
      TTR2(I,K)=TTR1A(I,K)+(U2(I,K)**2 - U1A(I,K)**2)/(2.*G*AJ*CP1A(K))
      PTR2(I,K)=PTR1A(I,K)*(TTR2(I,K)/TTR1A(I,K))**EXI
    1 WG2(I,K)=WR*WG1A(I,K)
      WGT2(K)=WR*WGT1A(K)
      I=IP
      ID=-1
      WGT2C(K)=0.
      IF(ICHOKE)26,26,3
   26 IF(LOPIN)27,27,3
   27 IF(GAMF)2,2,16
    2 TA2(K)=.95*TTR2(IP,K)
      CALL GAMMA(PTR2(I,K),TA2(K),FAIR,WAIR,GAM(4,K))
   16 FFA2(I,K)=WG2(I,K)*SQRT(TTR2(I,K))/(144.*PTR2(I,K)*CSBET2(I,K)*
     1ANN2(I,K))
      CALL PRATIO(FFA2(I,K),GAM(4,K),RV(4,K),PTRS2(I,K),PRTOL)
    3 CALL FLOW2(I)
      IF (PREVER) GO TO 22
      WGT2C(K)=WGT2C(K)+WG2(I,K)
      L=1
      IF (PTRS2(I,K).LE.PTRS2(IP,K))   L=I
      IF(ISECT-I)7,7,4
    4 I=I+ID
      IF(I)5,5,6
    5 ID=1
      I=IP+ID
    6 L=I-ID
      PS2(I,K)=PS2(L,K)+FLOAT(ID)*DPDR2(L,K)*(H2(I,K)+H2(L,K)
     1)/2.
      PTRS2(I,K)=PTR2(I,K)/PS2(I,K)
      IF (PTRS2(I,K)-1.)19,19,3
   19 PTRS2(I,K) = 1.0  + PHTOL
      GO TO 3
    7 IF(IS2(K))8,8,9
    8 EXI=GAM(4,K)/(GAM(4,K)-1.)
      CALL PHIM(EXI,ETAR(L,K),PHIX,PRCRIT)
      PRUP=PTR2(IP,K)*PRCRIT*PS2(L,K)/(PTR2(L,K)*PS2(IP,K))
     1*(1.+PRTOL)
      PRLOW=1.
      GO TO 10
    9 IS2(K)=IS2(K)+1
   10 L = IHRC + 1
```

Listing of Code (continued)

```
      IF(ICHOKE.EQ.L) PTRS2(IP,K) = PRUP
      IF(WGT2(K)-WGT2C(K))12,15,11
   11 PRLOW= PTRS2(IP,K)
      GO TO 13
   12 PRUP= PTRS2(IP,K)
      IS2(K)=1
   13 WE=1.-WGT2(K)/WGT2C(K)
      J=J+1
      IF(J-32)29,18,18
   29 IF(ICHOKE-L) 30,31,30
   31 SCRIT= -WE
      GO TO 15
   30 IF(LOPIN)14,14,15
   14 PRE=(PTRS2(IP,K)-PTRMO)/PTRS2(IP,K)
      IF (ABS(PRE)-PRTOL)17,17,24
   17 CONTINUE
      IF (ABS(WE)-WTOL)15,15,23
   24 PTRMO=PTRS2(IP,K)
      WGT2C(K)=0.0
      I=IP
      ID=-1
      IF (SCRIT)28,28,15
   28 PTRS2(IP,K)=.5*(PRLOW+PRUP)
      IF (PTRS2(IP,K).LE.PRCRIT)   PRPC=0.0
      GO TO 3
   23 SCRIT= 1.
   15 IF(TRLOOP.EQ.0.) GO TO 25
   18 WRITE(6,1000)K,PRUP,PRLOW,WE,PRCRIT,J,WGT2(K),WGT2C(K),(WG2(L,K),
     1 L=1,ISECT)
      WRITE(6,1001)(PTRS2(L,K),L=1,ISECT)
 1000 FORMAT(2X,2HK=I4,    2X,6H PRUP=F8.5,2X,6HPRLOW=F8.5,2X,6H    WE=
     1F8.5,1X,7HPRCRIT=F8.5,2X,2HJ=I4/
     22X,6H WGT2=F8.3,2X,6HWGT2C=F8.3/
     32X,6H  WG2=6F8.3)
 1001 FORMAT(2X,6HPTPS2=6F8.5)
   25 CALL CHECK(J)
      GO TO (20,21),J
   20 CALL DIAGT(4)
      GO TO 22
   21 CALL LOOP
   22 IF(SRFLAG) WRITE(6,20000)
20000 FORMAT(45H AN EXIT HAS BEEN MADE FROM SUBROUTINE STA2  )
      RETURN
      END
```

```
      SUBROUTINE FLOW2(I)
CFLOW2
C     CALCULATE ROTOR EXIT SECTOR FLOW
C
      REAL MFSTOP
      LOGICAL PREVER,SRFLAG
      COMMON  SRFLAG
      COMMON /SNTCP/G,AJ,PRPC,ICASE,PREVER,MFSTOP,JUMP,LOPIN,ISCASE,
     1KN,GAMF,IP,SCRIT,PTRN,ISECT,KSTG,WTOL,RHOTOL,PRTOL,TRLOOP,LSTG,
     2LBRC,IBRC,ICHOKE,ISORR,CHOKE,PT0PS1(6,8),PTRS2(6,8),TRDIAG,SC,RC,
     3DELPR,PASS,IPC,LOPC,ISS
C
      COMMON /SINIT/H1(6,8),H2(6,8),DP0(6,8),DP1(6,8),DP1A(6,8),DP2(6,8)
     1,DP2A(6,8),CSALF1(6,8),ALF1(6,8),CSBET2(6,8),BET2(6,8),RADSD(6,8),
     2RADRD(6,8),ANN1(6,8),ANN2(6,8),ANN2A(6,8),ANN1A(6,8),U1A(6,8),
     3U2(6,8),ANN0(6,8),PT0(6,8),TT0(6,8),ALPHA0(6,8),PTP(6,8)
C
      COMMON /SINPUT/ RSL,TSL,PSL,GAMSL,
     1PTPS,PTIN,TTIN,WAIR,FAIR,DELC,DELL,DELA,AACS,VCTD,STG,SECT,EXPN,
     2EXPP,EXPRE,    RPM,PAF,SLI,STGCH,ENDJOB,NAME(10),TITLE(10),PCNH(6),
     3RV(6,8),GAM(6,8),DR(6,8),DT(6,8),RWG(6,8),ALPHAS(6,8),ALPHA1(6,8),
     4ETARS(6,8),ETAS(6,8),CFS(6,8),ANDO(6,8),BETA1(6,8),BETA2(6,8),ETAR
     5R(6,8),ETAR(6,8),CFR(6,8),TFR(6,8),ANDOR(6,8),OMEGAS(6,8),AS0(6,8)
     6,ASMP0(6,8),ACMN0(6,8),A1(6,8),A2(6,8),A3(6,8),A4(6,8),A5(6,8),A6(
     76,8),OMEGAR(6,8),BSIA(6,8),BSMPIA(6,8),BCMNIA(6,8),B1(6,8),B2(6,8)
     8,B3(6,8),B4(6,8),B5(6,8),B6(6,8),SESTHI(8),RERTHI(8)
C
      COMMON /SSTA2/V2(6,8),TTR2(6,8),PTR2(6,8),WG2(6,8),WGT2(8),TA2(8),
     1             PS2(6,8),PHI2(6,8)
C
      REAL MR2,M2      ,MF2
      COMMON /SFLOW2/TS2(6,8),CP2(8),R2(6,8),RHOS2(6,8),BET2E(6,8),RU2(6
     1,8),VU2(6,8),DPDR2(6,8),VZ2(6,8),MR2(6,8),MF2(6,8),M2(6,8)
C
      DIMENSION P1AS2C(8),PHI2C(8),R2C(6,8),TS2C(6,8),RHOS2C(6,8),WG2C(6
     1,8),CBET2E(6,8),AS2(6,8),RFF(6,8)
C
C
      IF(SRFLAG) WRITE(6,10000)
10000 FORMAT(44H AN ENTRY HAS BEEN MADE IN SUBROUTINE FLOW2 )
      K=KN
      EX=(GAM(4,K)-1.)/GAM(4,K)
C        ISENTROPIC ROTOR RELATIVE TEMPERATURE RATIO
   10 PHI2(I,K)= PTRS2(I,K)**EX
      IF(OMEGAR(I,K))2,2,1
    1 CALL LOSS2(I,K)
```

Listing of Code (continued)

```
C        EXIT TEMPERATURES
    2 TS2(I,K)=TTR2(I,K)*(1.-ETAR(I,K)*(1.-1./PHI2(I,K)))
      IF(I-IP)6,3,6
    3 IF(    GAMF)4,4,5
    4 TA2(K)=.5*(TTR2(I,K)+TS2(I,K))
      CALL GAMMA(PTR2(I,K),TA2(K),FAIR,WAIR,GAM(4,K))
    5 EXI=GAM(4,K)/(GAM(4,K)-1.)
      EX=1./EXI
C        CRITICAL PRESSURE RATIO
      CALL PHIM(EXI,ETAR(I,K),PHI2C(K),P1AS2C(K))
C        SPECIFIC HEAT AT CONSTANT PRESSURE
    6 CP2(K)= RV(4,K)*EXI/AJ
C        RELATIVE EXIT VELOCITY
      R2(I,K)=SQRT(2.*G*AJ*CP2(K)*(TTR2(I,K)-TS2(I,K)))
C        EXIT PRESSURE
      PS2(I,K)= PTR2(I,K)/ PTRS2(I,K)
C        EXIT DENSITY
      RHOS2(I,K)=144.*PS2(I,K)/(RV(4,K)*TS2(I,K))
C        TEST CRITICAL PRESSURE RATIO
      IF( PTRS2(I,K)-P1AS2C(K))15, 7,7
    7 IF (IP-1) 22,8,22
    8 IF (PHPC)9,9,18
    9      PHPC=1.
       PTRS2(I,K)=P1AS2C(K)*(1.+PRTOL)
      GO TO 10
   22 IF (PTRS2(I,K).LE.PTRS2(IP,K))    GO TO 18
      GO TO 13
   18 IF ((I.EQ.1).OR.(I.EQ.ISECT))  SCRIT=1.
      GO TO 11
   11 CONTINUE
      R2C(I,K)=SQRT(2.*G*AJ*CP2(K)*TTR2(I,K)*ETAR(I,K)*(
     1PHI2C(K)-1.)/PHI2C(K))
      TS2C(I,K)=TTR2(I,K)*(1.-ETAR(I,K)*(1.-1./PHI2C(K)))
      RHOS2C(I,K)=144.*PTR2(I,K)/(RV(4,K)*P1AS2C(K)*TS2C(I,K))
      WG2C(I,K)=RHOS2C(I,K)*R2C(I,K)*ANN2(I,K)*CSBET2(I,K)
   12 WG2(I,K)=WG2C(I,K)
      GO TO 14
   13 IF(    PHPC-1.)15,15,24
   24 WG2(I,K)=RFF(I,K)*PTR2(I,K)/SQRT(TTR2(I,K))
      GO TO 14
C        OVEREXPANSION AFTER SUPERSONIC FLOW DECREASE
   14 CBET2E(I,K)=WG2(I,K)/(RHOS2(I,K)*R2(I,K)*ANN2(I,K))
      BET2E(I,K)=ATAN2(SQRT(1.-CBET2E(I,K)*CBET2E(I,K)),CBET2E(I,K))
      GO TO 16
   15 WG2(I,K)=RHOS2(I,K)*R2(I,K)*ANN2(I,K)*CSBET2(I,K)
      CBET2E(I,K)=CSBET2(I,K)
      BET2E(I,K)= BET2(I,K)
```

Listing of Code (continued)

```
      RFF(I,K)=WG2(I,K)*SQRT(TTR2(I,K))/PTR2(I,K)                       FLW2 090
   16 RU2(I,K)=R2(I,K)*SIN(BET2E(I,K))                                  FLW2 091
      VU2(I,K)=RU2(I,K)-U2(I,K)                                         FLW2 092
      DPDR2(I,K)=  (RHOS2(I,K)*VU2(I,K)*VU2(I,K)/(G*DP2(I,K)))*.01388889********
      VZ2(I,K)=R2(I,K)*CBET2E(I,K)                                      FLW2 094
      AS2(I,K)=SQRT(GAM(4,K)*G*RV(4,K)*TS2(I,K))                        ********
      V2(I,K)=SQRT(VZ2(I,K)*VZ2(I,K)+VU2(I,K)*VU2(I,K))                 FLW2 096
      M2(I,K)=V2(I,K)/AS2(I,K)                                          FLW2 097
      MR2(I,K)=R2(I,K)/AS2(I,K)                                         FLW2 098
      MF2(I,K)=MR2(I,K)*CBET2E(I,K)                                     FLW2 099
      IF(I.LT.ISECT) GO TO 17                                           FLW2 100
      IF(PRPC.EQ.1.) PRPC=2.                                            FLW2 101
   17 CALL CHECK(J)                                                     FLW2 102
      GO TO (19,21),J                                                   FLW2 103
   19 CALL DIAGT(4)                                                     FLW2 104
   21 IF(SRFLAG) WRITE(6,20000)                                         ********
20000 FORMAT(45H AN EXIT HAS BEEN MADE FROM SUBROUTINE FLOW2 )          ********
      RETURN                                                            ********
      END                                                               FLW2 106
```

```
      SUBROUTINE LOSS2(I,K)
CLOSS2
C     CALCULATE ETA R FROM QUADRATIC POLYNMONIAL
C
      REAL MFSTOP
      LOGICAL PREVER,SRFLAG
      COMMON  SRFLAG
      COMMON /SNTCP/G,AJ,PRPC,ICASE,PREVER,MFSTOP,JUMP,LOPIN,ISCASE,
     1KN,GAMF,IP,SCRIT,PTRN,ISECT,KSTG,WTOL,RHOTOL,PRTOL,TRLOOP,LSTG,
     2LBRC,IBRC,ICHOKE,ISORR,CHOKE,PTOPS1(6,8),PTRS2(6,8),TRDIAG,SC,RC,
     3DELPR,PASS,IPC,LOPC,ISS
C
      COMMON /SINPUT/ RSL,TSL,PSL,GAMSL,
     1PTPS,PTIN,TTIN,WAIR,FAIR,DELC,DELL,DELA,AACS,VCTD,STG,SECT,EXPN,
     2EXPP,EXPHE,   RPM,PAF,SLI,STGCH,ENDJOB,NAME(10),TITLE(10),PCNH(6),
     3RV(6,8),GAM(6,8),DR(6,8),DT(6,8),RWG(6,8),ALPHAS(6,8),ALPHA1(6,8),
     4ETARS(6,8),ETAS(6,8),CFS(6,8),ANDO(6,8),BETA1(6,8),BETA2(6,8),ETAR
     5R(6,8),ETAR(6,8),CFR(6,8),TFR(6,8),ANDOR(6,8),OMEGAS(6,8),AS0(6,8)
     6,ASMP0(6,8),ACMN0(6,8),A1(6,8),A2(6,8),A3(6,8),A4(6,8),A5(6,8),A6(
     76,8),OMEGAR(6,8),BSIA(6,8),BSMPIA(6,8),BCMNIA(6,8),B1(6,8),B2(6,8)
     8,B3(6,8),B4(6,8),B5(6,8),B6(6,8),SESTHI(8),RERTHI(8)
C
      REAL MR1A
      COMMON /SSTA1A/VU1A(6,8),WG1A(6,8),WGT1A(8),VZ1A(6,8),  CP1A(8),
     1PS1A(6,8),RU1A(6,8),R1A(6,8),RET1A(6,8),RI(6,8),TTR1A(6,8),PTR1A(6
     2,8),MR1A(6,8),TS1A(6,8)
C
      COMMON /SSTA2/V2(6,8),TTR2(6,8),PTR2(6,8),WG2(6,8),WGT2(8),TA2(8),
     1             PS2(6,8),PHI2(6,8)
C
C
      IF(SRFLAG) WRITE(6,10000)
10000 FORMAT(44H AN ENTRY HAS BEEN MADE IN SUBROUTINE LOSS2 )
      ETARR(I,K)=1.0
      IF(RI(I,K))4,1,2
    1 W1A2=OMEGAR(I,K)
      GO TO 8
    2 AS=B1(I,K)
      AC=B2(I,K)
      AQ=B3(I,K)
      IF(BSMPIA(I,K)-RI(I,K))3,6,6
    3 WMWR=RI(I,K)/BSMPIA(I,K)
      AR=BSMPIA(I,K)/BSIA(I,K)
      GO TO 7
    4 AS=B4(I,K)
      AC=B5(I,K)
```

```
      AQ=H6(I,K)                                                       LOS2 n44
      IF(RI(I,K)-HCMNIA(I,K))5,6,6                                     LOS2 n45
    5 WMWR=RI(I,K)/BCMNIA(I,K)                                         LOS2 n46
      AR=HCMNIA(I,K)/BSIA(I,K)                                         LOS2 n47
      GO TO 7                                                          LOS2 n48
    6 WMWR=1.0                                                         LOS2 n49
      AR=RI(I,K)/HSIA(I,K)                                             LOS2 n50
    7 W1A2=OMEGAR(I,K)*(1.+AR*AR*(AS+AR*(AC+AR*AQ)))*WMWR              LOS2 n51
    8 EX=(GAM(3,K)-1.)/GAM(3,K)                                        LOS2 n52
      ETAR(I,K)=(1.-(1./(PTRS2(I,K)*(1.-W1A2)+W1A2))**EX)*PHI2(I,K)/   LOS2 n53
     1(PHI2(I,K)-1.)                                                   LOS2 n54
      CALL CHECK(J)                                                    LOS2 n55
      IF(SRFLAG) WRITE(6,20000)                                        ********
20000 FORMAT(45H AN EXIT HAS BEEN MADE FROM SUBROUTINE LOSS2 )         ********
      RETURN                                                           LOS2 n56
      END                                                              LOS2 n57
```

Listing of Code (continued)

```
      SUBROUTINE LOOP
CLOOP
C         HANDLES ALL LOGIC FOR ITERATING TO OBTAIN EXACT CHOKE POINT-
C                    UNDERFLOW, NO CHOKE INITIAL CHOKE, CHOKE ITERATION
C                    SUBCRITICAL, CHOKE ITERATION SUPERCRITICAL,MULTIPLE
C                    CHOKE, CHOKE ITERATION COMPLETE
C
      REAL MFSTOP
      LOGICAL PREVER,SRFLAG
      COMMON  SRFLAG
      COMMON /SNTCP/G,AJ,PRPC,ICASE,PREVER,MFSTOP,JUMP,LOPIN,ISCASE,
     1KN,GAMF,IP,SCRIT,PTRN,ISECT,KSTG,WTOL,RHOTOL,PRTOL,TRLOOP,LSTG,
     2LBRC,IBRC,ICHOKE,ISORR,CHOKE,PTOPS1(6,8),PTRS2(6,8),TRDIAG,SC,RC,
     3DELPR,PASS,IPC,LOPC,ISS
C
      COMMON /SINPUT/ RSL,TSL,PSL,GAMSL,
     1PTPS,PTIN,TTIN,WAIR,FAIR,DELC,DELL,DELA,AACS,BLLD,STG,SECT,EXPN,
     2EXPP,EXPRE,    RPM,PAF,SLI,STGCH,ENDJOB,NAME(10),TITLE(10),PCNH(6),
     3RV(6,8),GAM(6,8),DR(6,8),DT(6,8),RWG(6,8),ALPHAS(6,8),ALPHA1(6,8),
     4ETARS(6,8),ETAS(6,8),CFS(6,8),ANDO(6,8),BETA1(6,8),BETA2(6,8),ETAR
     5R(6,8),ETAR(6,8),CFR(6,8),TFR(6,8),ANDOR(6,8),OMEGAS(6,8),AS0(6,8)
     6,ASMP0(6,8),ACMN0(6,8),A1(6,8),A2(6,8),A3(6,8),A4(6,8),A5(6,8),A6(
     76,8),OMEGAR(6,8),BSIA(6,8),BSMPIA(6,8),BCMNIA(6,8),B1(6,8),B2(6,8)
     8,B3(6,8),B4(6,8),B5(6,8),B6(6,8),SESTHI(8),RERTHI(8)
C
      IF(SRFLAG) WRITE(6,10000)
10000 FORMAT(44H AN ENTRY HAS BEEN MADE IN SUBROUTINE LOOP   )
      IJ=8+KSTG
C     INCREASE BLADE ROW COUNTER
      IBRC=IBRC+1
C     TEST NEGATIVE SECTOR PRESSURE RATIO
      IF (PTRN)18,1,1
C     TEST CHOKE ITERATION ON BLADE ROW
    1 IF (ICHOKE-IBRC)3,2,3
C     TEST INCREMENT TOLERANCE
    2 IF (PRTOL-DELPR)3,3,4
C     TEST STATION FLOW CRITICAL
    3 IF (SCRIT)5,5,6
C     CHOKE ITERATION COMPLETE
    4 ICHOKE=0
      IPC=IBRC
      ISS=IBRC
      ISORR=2+(IBRC/2)*2-IBRC
      JL=(ISORR-1)*8+KN
      IF (JL-IJ)22,23,23
   22 DELPR=DELL
```

Listing of Code (continued)

```
   24 LOPC=0
      CHOKE=1.
      LSTG=KN
      LBRC=IBRC-1
      GO TO 18
   23 DELPR=DELA
      GO TO 24
    5 IF (ICHOKE-IBRC)18,7,18
C     TEST CHOKE ITERATION LOOP
    6 IF(ISS-IBRC)8,18,18
C     CHOKE ITERATION
C     ISORR = 1 FOR STATOR
C           = 2 FOR ROTOR
    7 DELPR=DELPR/2.
      JL=(ISORR-1)*8+LSTG
      PTOPS1(IP,JL)=PTOPS1(IP,JL)+DELPR
       GO TO 16
C     CHOKE HAS OCURRED
    8 IF(ICHOKE)80,80,13
   80 J=(IBRC-2*(KN-1)-1)*8+KN
      WRITE(6,801)IBRC,PTOPS1(IP,J)
  801 FORMAT(16X10HBLADE RO= I3,8H CHOKED,4X5HPTPS=F10.5)
C     TEST SINGLE CALCULATICN POINT
    9 IF (DELC)18,18,10
C     TEST PREVIOUS CHOKE
   10 IF (IPC)11,11,12
C     SAVE COMBINATIONS PRICR FIRST CHOKE
   11 LBRCS=LBRC
      ISORRS=ISORR
      JL=(ISORR-1)*8+LSTG
      SPTPS=PTOPS1(IP,JL)-DELPR
      LSTGS=LSTG
      SDELPR=DELPR
      GO TO 13
   12 JL=LSTGS+(ISORRS-1)*8
      DELNU = (PTOPS1(IP,JL)-SPTPS)/4.
      IF (DELNU.LE.0.0001) DELNU = SDELPR/4.
      DELPR = DELNU
      SDELPR = DELNU
      WRITE(6,1201)IPC,IBRC,DELPR
 1201 FORMAT(6X11HBLADE ROWS I5,5H AND I5,25H, CHOKED - INCREMENT NOW
     1F10.5)
      LBRC=LBRCS
      LSTG=LSTGS
      ISORR=ISORRS
      PTOPS1(IP,JL) = SPTPS + SDELPR
      LOPC=10
```

```
      ICHOKE=0
      IPC=0
      ISS=0
      CHOKE=0.0
      GO TO 17
C     TEST PREVIOUS COMPLETE CALCULATION
   13 IF (PASS)15,15,14
   14 ICHOKE=IBRC
      DELPR=.5*DELPR
   15 JL=(ISORR-1)*8+LSTG
      PTOPS1(IP,JL)=PTOPS1(IP,JL)-DELPR
C     SET INDEX REGISTERS
   16 CONTINUE
      LOPC=LOPC+1
C SET JUMP FOR CHOKE ITERATION
   17 JUMP=1
      GO TO 19
C     JUMP SET FOR NO CHOKE OR CHOKE COMPLETE
   18 JUMP=0
C     TEST LOOP-TRACE
   19 IF (TRLOOP)21,21,20
   20 WRITE(6,2001)IBRC,LBRC,ISORR,KN,LSTG,IPC,ISS,ICHOKE,JUMP,LBRCS,
     1ISORRS,LSTGS,SPTPS,PTOPS1(IP,JL),DELPR,DELL,SCRIT,LOPC
 2001 FORMAT(3X12I5/3X4F10.5,F10.0,I10)
   21 IF(SRFLAG) WRITE(6,20000)
20000 FORMAT(45H AN EXIT HAS BEEN MADE FROM SUBROUTINE LOOP   )
      RETURN
      END
```

Listing of Code (continued)

```
      SUBROUTINE STA2A
CSTA2A
C     DETERMINE INLET FLOW CONDITIONS TO ALL STATORS
C                     AFTER THE FIRST STATOR
C
      REAL MFSTOP
      LOGICAL PREVER,SRFLAG
      COMMON  SRFLAG
      COMMON /SNTCP/G,AJ,PRPC,ICASE,PREVER,MFSTOP,JUMP,LOPIN,ISCASE,
     1KN,GAMF,IP,SCRIT,PTRN,ISECT,KSTG,WTOL,RHOTOL,PRTOL,TRLOOP,LSTG,
     2LBRC,IBRC,ICHOKE,ISORR,CHOKE,PTOPS1(6,8),PTRS2(6,8),TRDIAG,SC,RC,
     3DELPR,PASS,IPC,LOPC,ISS
C
      COMMON /SINIT/H1(6,8),H2(6,8),DP0(6,8),DP1(6,8),DP1A(6,8),DP2(6,8)
     1,DP2A(6,8),CSALF1(6,8),ALF1(6,8),CSBET2(6,8),BET2(6,8),RADSD(6,8),
     2RADRD(6,8),ANN1(6,8),ANN2(6,8),ANN2A(6,8),ANN1A(6,8),U1A(6,8),
     3U2(6,8),ANN0(6,8),PT0(6,8),TT0(6,8),ALPHA0(6,8),PTP(6,8)
C
C
      COMMON /SINPUT/ RSL,TSL,PSL,GAMSL,
     1PTPS,PTIN,TTIN,WAIR,FAIR,DELC,DELL,DELA,AACS,VCTD,STG,SECT,EXPN,
     2EXPP,EXPRE,    RPM,PAF,SLI,STGCH,FNDJOB,NAME(10),TITLE(10),PCNH(6),
     3RV(6,8),GAM(6,8),DR(6,8),DT(6,8),RWG(6,8),ALPHAS(6,8),ALPHA1(6,8),
     4ETARS(6,8),ETAS(6,8),CFS(6,8),ANDO(6,8),BETA1(6,8),BETA2(6,8),ETAR
     5R(6,8),ETAR(6,8),CFR(6,8),TFR(6,8),ANDOR(6,8),OMEGAS(6,8),AS0(6,8)
     6,ASMP0(6,8),ACMN0(6,8),A1(6,8),A2(6,8),A3(6,8),A4(6,8),A5(6,8),A6(
     76,8),OMEGAR(6,8),BSIA(6,8),BSMPIA(6,8),BCMNIA(6,8),B1(6,8),B2(6,8)
     8,B3(6,8),B4(6,8),B5(6,8),B6(6,8),SESTHI(8),RERTHI(8)
C
      REAL M0
      COMMON /SSTA01/CP0(8),                       PS0(6,8),V0(6,8),TS0(6,
     18),VU0(6,8),VZ0(6,8),RHOS0(6,8),PS1(6,8),WGT1(8),TA1(8),WG1(6,8),
     2              DPDR1(6,8),SI(6,8),   CP1(8),PHI1(6,8),TS1(6,8),V1(6,8)
     3,RHOS1(6,8),ALF1E(6,8),VU1(6,8),VZ1(6,8),M0(6,8),WGT0(8),WG0(6,8)
C
      REAL MR1A
      COMMON /SSTA1A/VU1A(6,8),WG1A(6,8),WGT1A(8),VZ1A(6,8),  CP1A(8),
     1PS1A(6,8),RU1A(6,8),R1A(6,8),BET1A(6,8),RI(6,8),TTR1A(6,8),PTR1A(6
     2,8),MR1A(6,8),TS1A(6,8)
C
      COMMON /SSTA2/V2(6,8),TTR2(6,8),PTR2(6,8),WG2(6,8),WGT2(8),TA2(8),
     1             PS2(6,8),PHI2(6,8)
C
      REAL MR2,M2      ,MF2
      COMMON /SFLOW2/TS2(6,8),CP2(8),R2(6,8),RHOS2(6,8),BET2E(6,8),RU2(6
     1,8),VU2(6,8),DPDR2(6,8),VZ2(6,8),MR2(6,8),MF2(6,8),M2(6,8)
```

Listing of Code (continued)

```
                                                                       ST2A 046
      REAL M2A,MF2A                                                    ST2A 047
      COMMON /SSTA2A/WG2A(6,8),WGT2A(8),VU2A(6,8),VZ2A(6,8),PS2A(6,8),  ST2A 048
     1ALF2A(6,8),TT2A(6,8),FT2A(6,8),TTBAR(8),PTBAR(8),STT0(8),SPT0(8), ST2A 049
     2M2A(6,8),MF2A(6,8),CP2A(8),V2A(6,8),TS2A(6,8),TAS(8),PAS(8),GAMS(8ST2A 050
     3),CPS(8),DELHVD(6,8),HVBAR(8)                                    ********
C                                                                      ST2A 052
      DIMENSION            TTTS2A(6,8)                                 ST2A 053
C                                                                      ST2A 054
C                                                                      ST2A 055
      IF(SRFLAG) WRITE(6,10000)                                        ********
10000 FORMAT(44H AN ENTRY HAS BEEN MADE IN SUBROUTINE STA2A )          ********
      K=KN                                                             ********
      ID=-1                                                            ST2A 056
      I=IP                                                             ST2A 057
      TS2A(I,K)=TS2(I,K)                                               ST2A 058
      WR=RWG(5,K)/RWG(4,K)                                             ST2A 059
      SUMT=0.0                                                         ST2A 060
      SUMLT=0.0                                                        ST2A 061
      SUMLP=0.0                                                        ST2A 062
      WGT2A(K)=WR*WGT2(K)                                              ST2A 063
   12 VU2A(I,K)=VU2(I,K)*DP2(I,K)/DP2A(I,K)                            ST2A 064
      WG2A(I,K)=WR*WG2(I,K)                                            ST2A 065
      RHOSTR=RHOS2(I,K)                                                ST2A 066
    1 VZ2A(I,K)=WR*VZ2(I,K)*ANN2(I,K)*RHOS2(I,K)/(ANN2A(I,K)*RHOSTR)   ST2A 067
      V2A(I,K)=SQRT(VU2A(I,K)*VU2A(I,K)+VZ2A(I,K)*VZ2A(I,K))           ST2A 068
      IF(I-IP)4,2,4                                                    ST2A 069
    2 IF(     GAMF)3,3,4                                               ST2A 070
    3 TA2A    =.5*(TTR2(I,K)+TS2A(I,K))                                ST2A 071
      CALL GAMMA(PTR2(IP,K),TA2A    ,FATR,WAIR,GAM(5,K))               ST2A 072
    4 EX=(GAM(5,K)-1.)/GAM(5,K)                                        ST2A 073
      EXI=1./EX                                                        ST2A 074
      CP2A(K)=RV(5,K)*EXI/AJ                                           ********
      DELTS=(V2(I,K)*V2(I,K)-V2A(I,K)*V2A(I,K))/(2.*G*AJ*CP2A(K))      ST2A 076
      TS2A(I,K)=TS2(I,K)+DELTS                                         ST2A 077
      IF(TS2A(I,K).GT.0.) GO TO 32                                     ST2A 078
      PREVER = .TRUE.                                                  ST2A 079
      MFSTOP = 2.                                                      ST2A 080
      GO TO 30                                                         ST2A 081
   32 PS2A(I,K)=PS2(I,K)*(1.+DELTS/TS2(I,K))**EXI                      ST2A 082
      RHOS2A    =144.*PS2A(I,K)/(RV(5,K)*TS2A(I,K))                    ********
      IF(ABS(RHOSTR-RHOS2A      )-1.E-07)6,6,5                         ST2A 084
    5 RHOSTR=RHOS2A                                                    ST2A 085
      GO TO 1                                                          ST2A 086
    6 SALF2A      =VU2A(I,K)/V2A(I,K)                                  ST2A 087
      ALF2A(I,K)=ATAN2(SALF2A      ,SQRT(1.-SALF2A      *SALF2A      ))  ST2A 088
   11 IF (I-IP)28,24,28                                                ST2A 089
```

Listing of Code (continued)

```
24 IF (GAMF)25,25,26                                              ST2A 090
25 TAS(K)=.5*(TA1(K)+TA2(K))                                      ST2A 091
   PAS(K)=.5*(PT0(IP,K)+PT2A(IP,K))                               ST2A 092
   CALL GAMMA(PAS(K),TAS(K),FAIR,WATR,GAMS(K))                    ST2A 093
   GO TO 27                                                       ST2A 094
26 GAMS(K)=.5*(GAM(2,K)+GAM(4,K))                                 ST2A 095
27 E4=GAMS(K)/(GAMS(K)-1.)                                        ST2A 096
   RVBAR(K)=.5*(RV(2,K)+RV(4,K))                                  ********
   CPS(K)=RVBAR(K)*E4/AJ                                          ********
28 DELHVD(I,K)=(U1A(I,K)*VU1A(I,K)+U2(I,K)*VU2(I,K))/AJ/G         ST2A 098
   M2A(I,K)=V2A(I,K)/SQRT(GAM(5,K)*G*RV(5,K)*TS2A(I,K))           ********
   DELTT=TFR(I,K)*DELHVD(I,K)/CPS(K)                              ST2A 100
   TT2A(I,K)=TT0(I,K)-DELTT                                       ST2A 101
   TTTS2A(I,K)=1.+(M2A(I,K)*M2A(I,K)*(GAM(5,K)-1.)/2.)            ST2A 102
   PTPS2A      = (TTTS2A(I,K))**EXI                               ST2A 103
   PT2A(I,K)=PS2A(I,K)*PTPS2A                                     ST2A 104
   MF2A(I,K)=M2A(I,K)*COS(ALF2A(I,K))                             ST2A 105
   IF (ISECT-I)13,15,13                                           ST2A 106
13 I=I+ID                                                         ST2A 107
   IF (I)14,14,12                                                 ST2A 108
14 ID=1                                                           ST2A 109
   I=IP+ID                                                        ST2A 110
   GO TO 12                                                       ST2A 111
15 CONTINUE                                                       ST2A 112
   DO 16 I=1,ISECT                                                ST2A 113
   RW=WG2A(I,K)/WGT2A(K)                                          ST2A 114
   TR=TT2A(I,K)/TT2A(IP,K)                                        ST2A 115
   PR=PT2A(I,K)/PT2A(IP,K)                                        ST2A 116
   SUMT=SUMT+RW*TR                                                ST2A 117
   SUMLT=SUMLT+RW*ALOG(TR)                                        ST2A 118
16 SUMLP=SUMLP+RW*ALOG(PR)                                        ST2A 119
   E3=GAM(5,K)/(GAM(5,K)-1.)                                      ST2A 120
   TTBAR(K)=TT2A(IP,K)*SUMT                                       ST2A 121
   PTBAR(K)=PT2A(IP,K)*EXP(SUMLP+E3*(ALOG(SUMT)-SUMLT))           ST2A 122
   IF (K-KSTG)17,18,18                                            ST2A 123
17 STT0(K+1)=TTBAR(K)                                             ST2A 124
   SPT0(K+1)=PTBAR(K)                                             ST2A 125
   DO 23 I=1,ISECT                                                ST2A 126
29 SI(I,K+1)=ALF2A(I,K)- RADSD(I,K+1)                             ST2A 127
   IF(SI(I,K+1).GT. 1.570796) SI(I,K+1)= 1.570796                 ********
   IF(SI(I,K+1).LT.-1.570796) SI(I,K+1)=-1.570796                 ********
   IF(OMEGAS(I,K))8,8,7                                           ST2A 130
 7 ETARS(I,K+1)=1.0                                               ST2A 131
   EXPSI=0.                                                       ST2A 132
   GO TO 117                                                      ST2A 133
 8 IF(SI(I,K+1))9,9,10                                            ST2A 134
 9 EXPSI=EXPN                                                     ST2A 135
```

```
      GO TO 117
   10 EXPSI=EXPP
  117 IF (PAF-1.)19,20,21
C     UNIFORM PROFILES
   19 PTP(I,K+1)=PTBAR(K)
      PTO(I,K+1)= PTP(I,K+1)
     1*(1.+(TTTS2A(I,K)-1.)*ETARS(I,K+1)*(COS(SI(I,K+1))**EXPSI))**EXI
     2/(TTTS2A(I,K))**EXI
      TTO(I,K+1)=TTBAR(K)
      GO TO 23
C     SAVE PROFILES
   20 PTP(I,K+1)=PT2A(I,K)
      PTO(I,K+1)= PTP(I,K+1)
     1*(1.+(TTTS2A(I,K)-1.)*ETARS(I,K+1)*(COS(SI(I,K+1))**EXPSI))**EXI
     2/(TTTS2A(I,K))**EXI
      GO TO 22
C     SMOOTH PRESSURE PROFILES
   21 PTP(I,K+1)=PTBAR(K)*(TT2A(I,K)/TTBAR(K))**E3
      PTO(I,K+1)= PTP(I,K+1)
     1*(1.+(TTTS2A(I,K)-1.)*ETARS(I,K+1)*(COS(SI(I,K+1))**EXPSI))**EXI
     2/(TTTS2A(I,K))**EXI
   22 TTO(I,K+1)=TT2A(I,K)
   23 CONTINUE
   18 MFSTOP=MF2A(IP,K)/AACS
      CALL CHECK(J)
      GO TO (30,31),J
   30 CALL DIAGT(5)
   31 IF(SRFLAG) WRITE(6,20000)
20000 FORMAT(45H AN EXIT HAS BEEN MADE FROM SUBROUTINE STA2A )
      RETURN
      END
```

```
      SUBROUTINE STA1
CSTA1
C     SATISFY CONTINUITY OF FLOW AT EXIT OF ALL STATORS
C                          AFTER THE FIRST STATOR
C
      REAL MFSTOP
      LOGICAL PREVER,SRFLAG
      COMMON  SRFLAG
      COMMON /SNTCP/G,AJ,PRPC,ICASE,PREVER,MFSTOP,JUMP,LOPIN,ISCASE,
     1KN,GAMF,IP,SCRIT,PTRN,ISECT,KSTG,WTOL,RHOTOL,PRTOL,TRLOOP,LSTG,
     2LBRC,IBRC,ICHOKE,ISORR,CHOKE,PTOPS1(6,8),PTRS2(6,8),TRDIAG,SC,RC,
     3DELPR,PASS,IPC,LOPC,ISS
C
      COMMON /SINIT/H1(6,8),H2(6,8),DP0(6,8),DP1(6,8),DP1A(6,8),DP2(6,8)
     1,DP2A(6,8),CSALF1(6,8),ALF1(6,8),CSBET2(6,8),BET2(6,8),RADSD(6,8),
     2RADRD(6,8),ANN1(6,8),ANN2(6,8),ANN2A(6,8),ANN1A(6,8),U1A(6,8),
     3U2(6,8),ANN0(6,8),PT0(6,8),TT0(6,8),ALPHA0(6,8),PTP(6,8)
C
      COMMON /SINPUT/ RSL,TSL,PSL,GAMSL,
     1PTPS,PTIN,TTIN,WAIR,FAIR,DELC,DELL,DELA,AACS,VCTD,STG,SECT,EXPN,
     2EXPP,EXPRE,    RPM,PAF,SLI,STGCH,ENDJOB,NAME(10),TITLE(10),PCNH(6),
     3RV(6,8),GAM(6,8),DR(6,8),DT(6,8),RWG(6,8),ALPHAS(6,8),ALPHA1(6,8),
     4ETARS(6,8),ETAS(6,8),CFS(6,8),ANDO(6,8),BETA1(6,8),BETA2(6,8),ETAR
     5R(6,8),ETAR(6,8),CFR(6,8),TFR(6,8),ANDOR(6,8),OMEGAS(6,8),AS0(6,8)
     6,ASMP0(6,8),ACMN0(6,8),A1(6,8),A2(6,8),A3(6,8),A4(6,8),A5(6,8),A6(
     76,8),OMEGAR(6,8),BSIA(6,8),BSMPIA(6,8),BCMNIA(6,8),B1(6,8),B2(6,8)
     8,B3(6,8),B4(6,8),B5(6,8),B6(6,8),SESTHI(8),RERTHI(8)
C
      REAL M0
      COMMON /SSTA01/CP0(8),                          PS0(6,8),V0(6,8),TS0(6,
     18),VU0(6,8),VZ0(6,8),RHOS0(6,8),PS1(6,8),WGT1(8),TA1(8),WG1(6,8),
     2               CPDR1(6,8),SI(6,8),   CP1(8),PHI1(6,8),TS1(6,8),V1(6,8)
     3,RHOS1(6,8),ALF1E(6,8),VU1(6,8),VZ1(6,8),M0(6,8),WGT0(8),WG0(6,8)
C
      REAL M2A,MF2A
      COMMON /SSTA2A/WG2A(6,8),WGT2A(8),VU2A(6,8),VZ2A(6,8),PS2A(6,8),
     1ALF2A(6,8),TT2A(6,8),PT2A(6,8),TTBAR(8),PTBAR(8),STT0(8),SPT0(8),
     2M2A(6,8),MF2A(6,8),CP2A(8),V2A(6,8),TS2A(6,8),TAS(8),PAS(8),GAMS(8
     3),CPS(8),DELHVD(6,8),HVBAR(8)
C
      DIMENSION WGT1C(8),LC1(8),FFA1(6,8)
C
C
      IF(SRFLAG) WRITE(6,10000)
10000 FORMAT(44H AN ENTRY HAS BEEN MADE IN SUBROUTINE STA1    )
      K=KN
```

Listing of Code (continued)

```
      J=1
      SCRIT=0.0
      PTRMO=1.
      WR1=RWG(1,K)/RWG(5,K-1)
      WR=RWG(2,K)/RWG(5,K-1)
      DO 1 I=1,ISECT
      WG0(I,K)=WR1*WG2A(I,K-1)
      WG1(I,K)=WR*WG2A(I,K-1)
      ALPHA0(I,K)  =ALF2A(I,K-1)
        PS0(I,K)  =   PS2A(I,K-1)
         V0(I,K)  =    V2A(I,K-1)
        TS0(I,K)  =   TS2A(I,K-1)
        VU0(I,K)  =   VU2A(I,K-1)
        VZ0(I,K)  =   VZ2A(I,K-1)
         M0(I,K)  =    M2A(I,K-1)
    1 CONTINUE
      CP0(K)=CP2A(K-1)
      WGT0(K)=WR1*WGT2A(K-1)
      WGT1(K)=WR*WGT2A(K-1)
      I=IP
      ID=-1
      WGT1C(K)=0.0
      LC1(K)=0
      IF(ICHOKE)17,17,16
   17 IF(LOPIN)18,18,16
   18 IF(GAMF)2,2,3
    2 TA1(K)=.95*TT0(IP,K)
      CALL GAMMA(PT0(IP,K),TA1(K),FAIR,WAIR,GAM(2,K))
    3 FFA1(I,K)=WG1(I,K)*SQRT(TT0(I,K))/(144.*PT0(I,K)*ANN1(I,K)
     1*CSALF1(I,K))
      CALL PRATIO(FFA1(I,K),GAM(2,K),RV(2,K),PTOPS1(I,K),PRTOL)
   16 CALL FLOW1(T)
      IF (PREVER) GO TO 25
      WGT1C(K)=WGT1C(K)+WG1(I,K)
      L=1
      IF (PTOPS1(I,K).LE.PTOPS1(IP,K)) L=I
      IF(ISECT-I)7,7,4
    4 I=I+ID
      IF(I)5,5,6
    5 ID=1
      I=IP+ID
    6 L=I-ID
      PS1(I,K)=PS1(L,K)+FLOAT(ID)*DPDR1(L,K)*(H1(I,K)+H1(L,K))/2.
      PTOPS1(I,K)=PT0(I,K)/PS1(I,K)
      GO TO 16
    7 IF(LC1(K))8,8,9
    8 LC1(K)=1
```

```
      EX=GAM(2,K)/(GAM(2,K)-1.)
      CALL PHIM(EX,ETAS(L,K),PHIX,PRCRIT)
      PRUP= PTOPS1(IP,K)*PRCRIT/PTOPS1(L,K)
     1*(1.+PRTOL)
      PRLOW=1.0
      GO TO 10
    9 LC1(K)=LC1(K)+1
   10 L = IBRC + 1
      IF(ICHOKE.EQ.L) PTOPS1(IP,K) = PRUP
      IF(WGT1(K)-WGT1C(K))12,15,11
   11 PRLOW=PTOPS1(IP,K)
      GO TO 13
   12 PRUP=PTOPS1(IP,K)
   13 WE=1.-WGT1(K)/WGT1C(K)
      J=J+1
      IF(J-32)29,22,22
   29 IF(ICHOKE-L) 30,31,30
   31 SCRIT= -WE
      GO TO 15
   30 IF(LOPIN)14,14,15
   14 PRE=(PTOPS1(IP,K)-PTRMO)/PTOPS1(IP,K)
      IF (ABS(PRE)-PRTOL)21,21,27
   21 CONTINUE
      IF (ABS(WE)-WTOL)15,15,20
   27 PTRMO=PTOPS1(IP,K)
      WGT1C(K)=0.0
      I=IP
      ID=-1
      IF (SCRIT)19,19,15
   19 PTOPS1(IP,K)=.5*(PRLOW+PRUP)
      IF (PTOPS1(IP,K).LE.PRCRIT)    PRPC=0.
      GO TO 16
   20 SCRIT= 1.
   15 IF(THLOOP.EQ.0.) GO TO 28
   22 WRITE(6,1000)K,PRUP,PRLOW,WE,PRCRIT,J,WGT1(K),WGT1C(K),(WG1(L,K),
     1 L=1,ISECT)
      WRITE(6,1001)(PTOPS1(L,K),L=1,ISECT)
 1000 FORMAT(2X,2HK=I4,     2X,6H PRUP=F8.5,2X,6HPRLOW=F8.5,2X,6H    WE=
     1F8.5,1X,7HPRCRIT=F8.5,2X,2HJ=I4/
     22X,6H WGT1=F8.3,2X,6HWGT1C=F8.3/
     32X,6H  WG1=6F8.3)
 1001 FORMAT(1X,7HPTOPS1=6F8.5)
   28 CALL CHECK(J)
      GO TO (23,24),J
   23 CALL DIAGT(2)
      GO TO 25
   24 CALL LOOP
```

Listing of Code (continued)

```
   25 IF(SHFLAG) WRITE(6,20000)                                    ********
20000 FORMAT(45H AN EXIT HAS BEEN MADE FROM SUBROUTINE STA1   )    ********
      RETURN                                                       ********
      END                                                          ST1  133
```

Listing of Code (continued)

```
      SUBROUTINE OVRALL
COVRALL
C     PURPOSE IS TO CALCULATE STAGE PERFORMANCE VALUES
C     AFTER FLOW ITERATION IS COMPLETED THROUGH THE LAST STAGE
C
      REAL MFSTOP
      LOGICAL PREVER,SRFLAG
      COMMON  SRFLAG
      COMMON /SNTCP/G,AJ,PRPC,ICASE,PREVER,MFSTOP,JUMP,LOPIN,ISCASE,
     1KN,GAMF,IP,SCRIT,PTRN,ISECT,KSTG,WTOL,RHOTOL,PRTOL,TRLOOP,LSTG,
     2LBRC,IBRC,ICHOKE,ISORR,CHOKE,PTOPS1(6,8),PTRS2(6,8),TRDIAG,SC,RC,
     3DELPR,PASS,IPC,LOPC,ISS
C
      COMMON /SINIT/H1(6,8),H2(6,8),DP0(6,8),DP1(6,8),DP1A(6,8),DP2(6,8)
     1,DP2A(6,8),CSALF1(6,8),ALF1(6,8),CSBET2(6,8),BET2(6,8),RADSD(6,8),
     2RADRD(6,8),ANN1(6,8),ANN2(6,8),ANN2A(6,8),ANN1A(6,8),U1A(6,8),
     3U2(6,8),ANN0(6,8),PT0(6,8),TT0(6,8),ALPHA0(6,8),PTP(6,8)
C
      COMMON /SINPUT/ RSL,TSL,PSL,GAMSL,
     1PTPS,PTIN,TTIN,WAIR,FAIR,DELC,DELL,DELA,AACS,VCTD,STG,SECT,EXPN,
     2EXPP,EXPRE,   RPM,PAF,SLI,STGCH,FNDJOB,NAME(10),TITLE(10),PCNH(6),
     3RV(6,8),GAM(6,8),DR(6,8),DT(6,8),RWG(6,8),ALPHAS(6,8),ALPHA1(6,8),
     4ETARS(6,8),ETAS(6,8),CFS(6,8),ANDO(6,8),BETA1(6,8),BETA2(6,8),ETAR
     5R(6,8),ETAR(6,8),CFR(6,8),TFR(6,8),ANDOR(6,8),OMEGAS(6,8),AS0(6,8)
     6,ASMP0(6,8),ACMN0(6,8),A1(6,8),A2(6,8),A3(6,8),A4(6,8),A5(6,8),A6(
     76,8),OMEGAR(6,8),BSIA(6,8),BSMPIA(6,8),BCMNIA(6,8),B1(6,8),B2(6,8)
     8,B3(6,8),B4(6,8),B5(6,8),B6(6,8),SESTHI(8),RERTHI(8)
C
      REAL M0
      COMMON /SSTA01/CP0(8),                      PS0(6,8),V0(6,8),TS0(6,
     18),VU0(6,8),VZ0(6,8),RHOS0(6,8),PS1(6,8),WGT1(8),TA1(8),WG1(6,8),
     2             DPDR1(6,8),SI(6,8),  CP1(8),PHI1(6,8),TS1(6,8),V1(6,8)
     3,RHOS1(6,8),ALF1E(6,8),VU1(6,8),VZ1(6,8),M0(6,8),WGT0(8),WG0(6,8)
C
      REAL MR1A
      COMMON /SSTA1A/VU1A(6,8),WG1A(6,8),WGT1A(8),VZ1A(6,8),  CP1A(8),
     1PS1A(6,8),RU1A(6,8),R1A(6,8),BET1A(6,8),RI(6,8),TTR1A(6,8),PTR1A(6
     2,8),MR1A(6,8),TS1A(6,8)
      COMMON /SSTA2/V2(6,8),TTR2(6,8),PTR2(6,8),WG2(6,8),WGT2(8),TA2(8),
     1             PS2(6,8),PHI2(6,8)
C
      REAL MR2,M2     ,MF2
      COMMON /SFLOW2/TS2(6,8),CP2(8),R2(6,8),RHOS2(6,8),BET2E(6,8),RU2(6
     1,8),VU2(6,8),DPDR2(6,8),VZ2(6,8),MR2(6,8),MF2(6,8),M2(6,8)
C
      REAL M2A,MF2A
```

Listing of Code (continued)

```
      COMMON /SSTA2A/WG2A(6,8),WGT2A(8),VU2A(6,8),VZ2A(6,8),PS2A(6,8),  OVLL 046
     1ALF2A(6,8),TT2A(6,8),PT2A(6,8),TTBAR(8),PTBAR(8),STT0(8),SPT0(8), OVLL 047
     2M2A(6,8),MF2A(6,8),CP2A(8),V2A(6,8),TS2A(6,8),TAS(8),PAS(8),GAMS(8OVLL 048
     3),CPS(8),DELHVD(6,8),HVBAR(8)                                     ********
C                                                                       OVLL 050
      COMMON /SOVRAL/DELHT(6,8),DELHTI(6,8),DELHSI(6,8),DEHATI(6,8),    OVLL 051
     1ETATT(6,8),ETATS(6,8),ETATAT(6,8)                                 OVLL 052
C                                                                       OVLL 053
      REAL MIS(8),MIRS(8),MH1AR(8),MR2T(8)                              OVLL 054
      DIMENSION SA0(8),SIS(8),SB1A(8),SIR(8),SA2(8),THCR(8),EPSI(8),DELTOVLL 055
     1(8),SETATT(8),SETATS(8),SETAAT(8),SWRTP(8),SNRT(8),SDHT(8),SETHC(8OVLL 056
     2),SNRTHC(8),SWRTED(8),SPTPT2(8),SPTPS2(8),ST2TT0(8),STRTT0(8),UPS(OVLL 057
     38),UPUPS(8),URS(8),URURS(8),VIS(8),UPVIS(8),URVIS(8),PSIPS(8),PSIROVLL 058
     4S(8),RXP(8),RXR(8),DBETAR(8),DELHTS(8),DEHTIS(8),DEHSIS(8),DHATIS(OVLL 059
     58),PAT2A(6,8)                                                     ********
C                                                                       OVLL 061
C ************** CARD DELETED ******************                        ********
C                                                                       OVLL 063
C                                                                       OVLL 064
      IF(SRFLAG) WRITE(6,10000)                                         ********
10000 FORMAT(44H AN ENTRY HAS BEEN MADE IN SUBROUTINE OVRALL)           ********
      STT0(1)=TTIN                                                      OVLL 065
      SPT0(1)=PTIN                                                      OVLL 066
      RGO=0.0                                                           ********
      TAO=0.0                                                           OVLL 067
      PAO=0.0                                                           OVLL 068
      GAMC=0.0                                                          OVLL 069
      OUPUP=0.0                                                         OVLL 070
      OURUR=0.0                                                         OVLL 071
      ODELHT=0.0                                                        OVLL 072
    5 E1=GAMSL/(GAMSL-1.)                                               OVLL 073
      DO 17 K=1,KSTG                                                    OVLL 074
      RGO=RGO+RVBAR(K)                                                  ********
      IF (GAMF)1,1,2                                                    OVLL 075
    1 TAO=TAO+TAS(K)                                                    OVLL 076
      PAO=PAO+PAS(K)                                                    OVLL 077
      GO TO 3                                                           OVLL 078
    2 GAMO=GAMO+GAMS(K)                                                 OVLL 079
    3 E2=GAM(1,K)/(GAM(1,K)-1.)                                         OVLL 080
      E3=GAM(5,K)/(GAM(5,K)-1.)                                         OVLL 081
      E4=GAMS(K)/(GAMS(K)-1.)                                           OVLL 082
      E5=1./E4                                                          OVLL 083
      DELHTS(K)=0.0                                                     OVLL 084
      DEHTIS(K)=0.0                                                     OVLL 085
      DEHSIS(K)=0.0                                                     OVLL 086
      DHATIS(K)=0.0                                                     OVLL 087
      DO 6 I=1,ISECT                                                    OVLL 088
```

```
      RW=WG2A(I,K)/WGT2A(K)                                            OVLL 089
      DELHT(I,K)=DELHVD(I,K)*TFR(I,K)                                  OVLL 090
      DELHTI(I,K)=CPS(K)*TT0(I,K)*(1.-(PT2A(I,K)/PTP(I,K))**E5)        OVLL 091
      ETATT(I,K)=DELHT(I,K)/DELHTI(I,K)                                OVLL 092
      DELHSI(I,K)=CPS(K)*TT0(I,K)*(1.-(PS2A(I,K)/PTP(I,K))**E5)        OVLL 093
      ETATS(I,K)=DELHT(I,K)/DELHSI(I,K)                                OVLL 094
      PAT2A(I,K)=PS2A(I,K)*(1.+(GAM(5,K)-1.)*MF2A(I,K)*MF2A(I,K)       OVLL 095
     1/2.)**E3                                                         OVLL 096
      DEHATI(I,K)=CPS(K)*TT0(I,K)*(1.-(PAT2A(I,K)/PTP(I,K))**E5)       OVLL 097
      ETATAT(I,K)=DELHT(I,K)/DEHATI(I,K)                               OVLL 098
      DELHTS(K)=DELHTS(K)+RW*DELHT(I,K)                                OVLL 099
      DEHTIS(K)=DEHTIS(K)+RW*DELHTI(I,K)                               OVLL 100
      DEHSIS(K)=DEHSIS(K)+RW*DELHSI(I,K)                               OVLL 101
      DHATIS(K)=DHATIS(K)+RW*DEHATI(I,K)                               OVLL 102
    6 CONTINUE                                                         OVLL 103
   13 SA0(K)=ALPHA0(IP,K)*57.2958                                      OVLL 104
      SIS(K)=SI(IP,K)*57.2958                                          OVLL 105
      SB1A(K)=BET1A(IP,K)*57.2958                                      OVLL 106
      SIR(K)=RI(IP,K)*57.2958                                          OVLL 107
      SA2(K)=ALF2A(IP,K)*57.2958                                       OVLL 108
      THCR(K)= GAM(1,K)*(GAMSL+1.)*RV(1,K)*STT0(K)/                    ********
     1(GAMSL*(GAM(1,K)+1.)*RSL*TSL)                                    OVLLA109
      EPSI(K)=GAMSL*((GAM(1,K)+1.)/2.)**E2/(GAM(1,K)*((GAMSL           OVLL 110
     1+1.)/2.)**E1)                                                    OVLL 111
      DELT(K)=SPT0(K)/PSL                                              OVLL 112
      SETATT(K)=DELHTS(K)/DEHTIS(K)                                    OVLL 113
      SETATS(K)=DELHTS(K)/DEHSIS(K)                                    OVLL 114
      SETAAT(K)=DELHTS(K)/DHATIS(K)                                    OVLL 115
C ******* CARD DELETED*********                                        ********
      SWRTP(K)= WGT0(K)*SQRT(STT0(K))/SPT0(K)                          OVLL 117
      SNRT(K)=RPM/SQRT(STT0(K))                                        OVLL 118
      SDHT(K)=DELHTS(K)/STT0(K)                                        OVLL 119
      SETHC(K)=DELHTS(K)/THCR(K)                                       OVLL 120
      RTHCR=SQRT(THCR(K))                                              OVLL 121
      SNRTHC(K)=RPM/RTHCR                                              OVLL 122
      SWRTED(K)=WGT0(K)*RTHCR*EPSI(K)/DELT(K)                          OVLL 123
      SPTPT2(K)=SPT0(K)/PTBAR(K)                                       OVLL 124
      SPTPS2(K)=SPT0(K)/PS2(IP,K)                                      OVLL 125
      ST2TT0(K)=TTBAR(K)/STT0(K)                                       OVLL 126
      STRTT0(K)=TTR1A(IP,K)/STT0(K)                                    OVLL 127
      UPS(K)=.5*(U1A(IP,K)+U2(IP,K))                                   OVLL 128
      UPUPS(K)=UPS(K)*UPS(K)                                           OVLL 129
      OUPUP=OUPUP+UPUPS(K)                                             OVLL 130
      URS(K)=.5*(U1A(1,K)*DR(3,K)/DP1A(1,K)+U2(1,K)*DR(4,K)/DP2(1,K))  OVLL 131
      URURS(K)=URS(K)*URS(K)                                           OVLL 132
      OURUR=OURUR+URURS(K)                                             OVLL 133
      ODELHT=ODELHT+DELHTS(K)                                          OVLL 134
```

Listing of Code (continued)

```
      IF (DELHSI(IP,K))14,14,15
14    VIS(K)=1.
      GO TO 16
15    VIS(K)=SQRT(2.*G*AJ*DELHSI(IP,K))
16    UPVIS(K)=UPS(K)/VIS(K)
      URVIS(K)=URS(K)/VIS(K)
      PSIPS(K)=G*AJ*DELHTS(K)/(2.*UPUPS(K))
      PSIRS(K)=G*AJ*DELHTS(K)/(2.*URURS(K))
      RXP(K)=1.-(1.-(PS1(IP,K)/PTP(IP,K))**E5)/(1.-(PS2(IP,K)/
     1PTP(IP,K))**E5)
      VU1R=VU1(1,K)*DP1(1,K)/DR(2,K)
      V1R=SQRT(VU1R**2+VZ1(1,K)**2)
      PH1R=1./(1.-V1R**2/(2.*G*AJ*CP1(K)*TT0(1,K)*ETAS(1,K)))
      PTPS1R=PH1R**(GAM(2,K)/(GAM(2,K)-1.))*PTP(1,K)/PT0(1,K)
      RXR(K)=1.-(1.-(1./PTPS1R)**E5)/(1.-(PS2(1,K)/PTP(1,K))**E5)
      DBETAR(K)=(BET1A(1,K)+BET2E(1,K))*57.2958
      MIS(K)=V1(IP,K)/SQRT(GAM(2,K)*G*RV(2,K)*TS1(IP,K))
      TS1R=TT0(1,K)-V1R**2/(2.*G*AJ*CP1(K))
      MIRS(K)=V1R/SQRT(GAM(2,K)*G*RV(2,K)*TS1R)
      VU1AR=VU1A(1,K)*DP1A(1,K)/DR(3,K)
      V1AR=SQRT(VU1AR**2+VZ1A(1,K)**2)
      TS1AR=TT0(1,K)-V1AR**2/(2.*G*AJ*CP1A(K))
      RU1AR=VU1AR-U1A(1,K)*DR(3,K)/DP1A(1,K)
      R1AR=SQRT(RU1AR**2+VZ1A(1,K)**2)
      MR1AR(K)=R1AR/SQRT(GAM(3,K)*G*RV(3,K)*TS1AR)
      VU2T=VU2(ISECT,K)*DP2(ISECT,K)/DT(4,K)
      V2T=SQRT(VU2T**2+VZ2(ISECT,K)**2)
      TS2T=TS2(ISECT,K)+(V2(ISECT,K)**2-V2T**2)/(2.*G*AJ*CP2(K))
      RU2T=VU2T+U2(ISECT,K)*DT(4,K)/DP2(ISECT,K)
      R2T=SQRT(RU2T**2+VZ2(ISECT,K)**2)
      MR2T(K)=R2T/SQRT(GAM(4,K)*G*RV(4,K)*TS2T)
17    CONTINUE
      IF (GAMF)4,4,7
4     TAO=TAO/STG
      PAO=PAO/STG
      CALL GAMMA(PAO,TAO,FAIR,WAIR,GAMO)
      GO TO 8
7     GAMO=GAMO/STG
8     EO=(GAMO-1.)/GAMO
      RGO=RGO/STG
      CPO=RGO/EO/AJ
      K=KSTG
      ODEHTI = 0.
      ODEHSI = 0.
      ODHATI = 0.
      DO 9 I=1,ISECT
      RW=WG2A(I,K)/WGT2A(K)
```

```
      ODEHTI = CPO*TTO(I,1)*(1.-(PT2A(I,K)/PTP(I,1))**EO)*RW+ODEHTI
      ODEHSI = CPO*TTO(I,1)*(1.-(PS2A(I,K)/PTP(I,1))**EO)*RW+ODEHSI
    9 ODHATI = CPO*TTO(I,1)*(1.-(PAT2A(I,K)/PTP(I,1))**EO)*RW+ODHATI
      OPSIP=G*AJ*ODELHT/(2.*OUPUP)
      OPSIR=G*AJ*ODELHT/(2.*OURUR)
      OWRTP=SWRTP(1)
      OWNED=SWRTED(1)*SNRTHC(1)/60.
      ONRTHC=SNRTHC(1)
      ONRT=SNRT(1)
      ODHT=ODELHT/TTIN
      OPTOT2=PTIN/PTBAR(KSTG)
      OPTOS2=PTIN/PS2(IP,KSTG)
      OPTAT2=PTIN/PAT2A(IP,KSTG)
      OETATT=ODELHT/ODEHTI
      OETATS=ODELHT/ODEHSI
      OETAAT=ODELHT/ODHATI
      OETHC=ODELHT/THCR(1)
C
C                         PRINT OUT FOR STAGE PERFORMANCE
      I=1
      WRITE(6,1000)NAME,TITLE,ICASE,ISCASE
 1000 FORMAT(1H1,21X,29HNASA TURBINE COMPUTER PROGRAM /6X,10A6/
     1  6X,10A6/ 30X,6HCASE  I3,1H.,I3/28X,17HSTAGE PERFORMANCE /19X
     27HSTAGE 1,6X,7HSTAGE 2,6X,7HSTAGE 3,6X,7HSTAGE 4/ )
      IF (KSTG-4)19,19,18
   18 KS=4
      GO TO 20
   19 KS=KSTG
   20 WRITE(6,1001)(STTO(K),K=I,KS)
 1001 FORMAT(2X,12H     TTBAR 02X,F10.1,3X,F10.1,3X,F10.1,3X,F10.1)
      WRITE(6,1002)(SPTO(K),K=I,KS)
 1002 FORMAT(2X,12H     PTBAR 02X,F10.3,3X,F10.3,3X,F10.3,3X,F10.3)
      WRITE(6,1003)(WGTO(K),K=I,KS)
 1003 FORMAT(2X,12H        WG 02X,F10.3,3X,F10.3,3X,F10.3,3X,F10.3)
      WRITE(6,1004)(DELHTS(K),K=I,KS)
 1004 FORMAT(2X,12H       DEL H2X,F10.3,3X,F10.3,3X,F10.3,3X,F10.3)
      WRITE(6,1005)(SWRTP(K),K=I,KS)
 1005 FORMAT(2X,12H       WHT/P2X,F10.3,3X,F10.3,3X,F10.3,3X,F10.3)
      WRITE(6,1006)(SDHT(K),K=I,KS)
 1006 FORMAT(2X,12H   DH/TTBAR02X,F10.5,3X,F10.5,3X,F10.5,3X,F10.5)
      WRITE(6,1007)(SNRT(K),K=I,KS)
 1007 FORMAT(2X,12H       N/RT2X,F10.3,3X,F10.3,3X,F10.3,3X,F10.3)
      WRITE(6,1008)(SETATT(K),K=I,KS)
 1008 FORMAT(2X,12H     ETA TT2X,F10.5,3X,F10.5,3X,F10.5,3X,F10.5)
      WRITE(6,1009)(SETATS(K),K=I,KS)
 1009 FORMAT(2X,12H     ETA TS2X,F10.5,3X,F10.5,3X,F10.5,3X,F10.5)
      WRITE(6,1010)(SETAAT(K),K=I,KS)
```

```
1010 FORMAT(2X,12H       ETA AT2X,F10.5,3X,F10.5,3X,F10.5,3X,F10.5)      ********
     WRITE(6,1011)(PTOPS1(IP,K),K=I,KS)                                 OVLL 229
1011 FORMAT(2X,12H       PT0/PS12X,F10.3,3X,F10.3,3X,F10.3,3X,F10.3)     ********
     WRITE(6,1012)(SPTPT2(K),K=I,KS)                                    OVLL 231
1012 FORMAT(1X,13HPTBAR0/PTBAR2,2X,F10.3,3X,F10.3,3X,F10.3,3X,F10.3)     ********
     WRITE(6,1013)(SPTPS2(K),K=I,KS)                                    OVLL 233
1013 FORMAT(2X,12H  PTBAR0/PS22X,F10.3,3X,F10.3,3X,F10.3,3X,F10.3)       ********
     WRITE(6,1014)(PTRS2(IP,K),K=I,KS)                                  OVLL 235
1014 FORMAT(2X,12H     PTR2/PS22X,F10.3,3X,F10.3,3X,F10.3,3X,F10.3)      ********
     WRITE(6,1015)(ST2TT0(K),K=I,KS)                                    OVLL 237
1015 FORMAT(1X,13HTTBAR2/TTBAR02X,F10.5,3X,F10.5,3X,F10.5,3X,F10.5)      ********
     WRITE(6,1016)(STRTT0(K),K=I,KS)                                    OVLL 239
1016 FORMAT(2X,12HTTR1A/TTBAR02X,F10.5,3X,F10.5,3X,F10.5,3X,F10.5)       ********
     WRITE(6,2003)(WGT1(K),K=I,KS)                                      ********
2003 FORMAT(2X,12H         WG 12X,F10.3,3X,F10.3,3X,F10.3,3X,F10.3)      ********
     WRITE(6,1017)(PS1A(IP,K),K=I,KS)                                   ********
1017 FORMAT(2X,12H        PS 1A2X,F10.3,3X,F10.3,3X,F10.3,3X,F10.3)      ********
     WRITE(6,1018)(TTR1A(IP,K),K=I,KS)                                  OVLL 243
1018 FORMAT(2X,12H       TTR 1A2X,F10.1,3X,F10.1,3X,F10.1,3X,F10.1)      ********
     WRITE(6,1019)(PTR1A(IP,K),K=I,KS)                                  OVLL 245
1019 FORMAT(2X,12H       PTR 1A2X,F10.3,3X,F10.3,3X,F10.3,3X,F10.3)      ********
     WRITE(6,3003)(WGT1A(K),K=I,KS)                                     ********
3003 FORMAT(2X,12H        WG 1A2X,F10.3,3X,F10.3,3X,F10.3,3X,F10.3)      ********
     WRITE(6,1020)(PS2(IP,K),K=I,KS)                                    OVLL 247
1020 FORMAT(2X,12H        PS 22X,F10.3,3X,F10.3,3X,F10.3,3X,F10.3)       ********
     WRITE(6,1021)(TTBAR(K),K=I,KS)                                     OVLL 249
1021 FORMAT(2X,12H     TTBAR 22X,F10.1,3X,F10.1,3X,F10.1,3X,F10.1)       ********
     WRITE(6,1022)(PTBAR(K),K=I,KS)                                     OVLL 251
1022 FORMAT(2X,12H     PTBAR 22X,F10.3,3X,F10.3,3X,F10.3,3X,F10.3)       ********
     WRITE(6,4003)(WGT2(K),K=I,KS)                                      ********
4003 FORMAT(2X,12H         WG 22X,F10.3,3X,F10.3,3X,F10.3,3X,F10.3)      ********
     WRITE(6,5003)(WGT2A(K),K=I,KS)                                     ********
5003 FORMAT(2X,12H        WG 2A2X,F10.3,3X,F10.3,3X,F10.3,3X,F10.3)      ********
     WRITE(6,1023)(UPVIS(K),K=I,KS)                                     OVLL 253
1023 FORMAT(2X,12H        UP/VI2X,F10.5,3X,F10.5,3X,F10.5,3X,F10.5)      ********
     WRITE(6,1024)(URVIS(K),K=I,KS)                                     OVLL 255
1024 FORMAT(2X,12H        UR/VI2X,F10.5,3X,F10.5,3X,F10.5,3X,F10.5)      ********
     WRITE(6,1025)(PSIPS(K),K=I,KS)                                     OVLL 257
1025 FORMAT(2X,12H        PSI P2X,F10.5,3X,F10.5,3X,F10.5,3X,F10.5)      ********
     WRITE(6,1026)(PSIRS(K),K=I,KS)                                     OVLL 259
1026 FORMAT(2X,12H        PSI R2X,F10.5,3X,F10.5,3X,F10.5,3X,F10.5)      ********
     WRITE(6,1027)(RXP(K),K=I,KS)                                       OVLL 261
1027 FORMAT(2X,12H         RX P2X,F10.5,3X,F10.5,3X,F10.5,3X,F10.5)      ********
     WRITE(6,1028)(RXR(K),K=I,KS)                                       OVLL 263
1028 FORMAT(2X,12H         RX R2X,F10.5,3X,F10.5,3X,F10.5,3X,F10.5)      ********
     WRITE(6,1029)(SA0(K),K=I,KS)                                       OVLL 265
1029 FORMAT(2X,12H     ALPHA 02X,F10.3,3X,F10.3,3X,F10.3,3X,F10.3)       ********
```

Listing of Code (continued)

```
      WRITE(6,1030)(SIS(K),K=I,KS)
 1030 FORMAT(2X,12H     I STATOR2X,F10.3,3X,F10.3,3X,F10.3,3X,F10.3)
      WRITE(6,1031)(SB1A(K),K=I,KS)
 1031 FORMAT(2X,12H       BETA 1A2X,F10.3,3X,F10.3,3X,F10.3,3X,F10.3)
      WRITE(6,1032)(SIR(K),K=I,KS)
 1032 FORMAT(2X,12H      I RCTOR2X,F10.3,3X,F10.3,3X,F10.3,3X,F10.3)
      WRITE(6,1033)(SA2(K),K=I,KS)
 1033 FORMAT(2X,12H    ALPHA 2A2X,F10.3,3X,F10.3,3X,F10.3,3X,F10.3)
      WRITE(6,1034)(DBETAR(K),K=I,KS)
 1034 FORMAT(2X,12H      DBETA R2X,F10.3,3X,F10.3,3X,F10.3,3X,F10.3)
      WRITE(6,1035)(MIS(K),K=I,KS)
 1035 FORMAT(2X,12H           M 12X,F10.5,3X,F10.5,3X,F10.5,3X,F10.5)
      WRITE(6,1036)(MIRS(K),K=I,KS)
 1036 FORMAT(2X,12H         M1 RT2X,F10.5,3X,F10.5,3X,F10.5,3X,F10.5)
      WRITE(6,1037)(MR1A(IP,K),K=I,KS)
 1037 FORMAT(2X,12H         MR 1A2X,F10.5,3X,F10.5,3X,F10.5,3X,F10.5)
      WRITE(6,1038)(MR1AR(K), K=I,KS)
 1038 FORMAT(2X,12H       MR1A RT2X,F10.5,3X,F10.5,3X,F10.5,3X,F10.5)
      WRITE(6,1039)(MR2(IP,K),K=I,KS)
 1039 FORMAT(2X,12H         MR 22X,F10.5,3X,F10.5,3X,F10.5,3X,F10.5)
      WRITE(6,1040)(MR2T(K),      K=I,KS)
 1040 FORMAT(2X,12H       MR2 TIP2X,F10.5,3X,F10.5,3X,F10.5,3X,F10.5)
      WRITE(6,1041)(SETHC(K),K=I,KS)
 1041 FORMAT(2X,12H       E/TH CR2X,F10.3,3X,F10.3,3X,F10.3,3X,F10.3)
      WRITE(6,1042)(SNRTHC(K),K=I,KS)
 1042 FORMAT(2X,12H     N/RTH CR2X,F10.1,3X,F10.1,3X,F10.1,3X,F10.1)
      WRITE(6,1043)(SWRTED(K),K=I,KS)
 1043 FORMAT(2X,12H    WRTHCRE/D2X,F10.3,3X,F10.3,3X,F10.3,3X,F10.3)
      IF (KSTG-KS)22,22,21
   21 WRITE(6,1045)NAME,TITLE,ICASE,ISCASE
 1045 FORMAT(1H1,21X,29HNASA TURBINE COMPUTER PROGRAM /6X,10A6/
     1  6X,10A6/ 30X,6HCASE  I3,1H.,I3/28X,17HSTAGE PERFORMANCE /19X
     27HSTAGE 5,6X,7HSTAGE 6,6X,7HSTAGE 7,6X,7HSTAGE 8/ )
      I=5
      KS=KSTG
      GO TO 20
   22 WRITE(6,1044)OPSIP,OPSIR,ODELHT,OWRTP,CNRT,ODHT,OPTOT2,
     1OPTOS2,OPTAT2,OETATT,OETATS,OETAAT,OWNED,ONRTHC,OETHC
 1044 FORMAT(//31X,19HOVERALL PERFORMANCE/7X,9HPSI P
     1F10.5, 5X,10HPSI R      F10.5, 5X9HDEL H     F10.5/7X,9HWRT/P
     2F10.5, 5X,10HN/RT       F10.5, 5X9HDELH/TTINF10.5/7X,10HPTO/PTBAR2
     3F9.5,  5X,10HPTO/PS2    F10.5, 5X9HPTO/PAT2AF10.5/7X,9HETA TT
     4F10.5, 5X,10HETA TS     F10.5, 5X9HETA TAT  F10.5/7X,9HWNE/60D
     5F10.3, 5X,10HN/RTH CR  F10.3, 5X,9HE/TH CR  F10.5/)
      IF(SRFLAG) WRITE(6,20000)
20000 FORMAT(1H1,45H AN EXIT HAS BEEN MADE FROM SUBROUTINE OVRALL)
      RETURN
```

Listing of Code (continued)

```
 END                                                                    OVLL 312
```

```
      SUBROUTINE DIAGT(M)                                               DIGT 001
CDIAGT                                                                  DIGT 002
C                                                                       DIGT 003
      REAL MFSTOP                                                       DIGT 004
      LOGICAL PREVER,SRFLAG                                             ********
      COMMON  SRFLAG                                                    ********
      COMMON /SNTCP/G,AJ,PRPC,ICASE,PREVER,MFSTOP,JUMP,LOPIN,ISCASE,    DIGT 006
     1KN,GAMF,IP,SCRIT,PTRN,ISECT,KSTG,WTOL,RHOTOL,PRTOL,TRLOOP,LSTG,   DIGT 007
     2LBRC,IBRC,ICHOKE,ISORR,CHOKE,PTOPS1(6,8),PTRS2(6,8),TRDIAG,SC,RC, DIGT 008
     3DELPR,PASS,IPC,LOPC,ISS                                           DIGT 009
C                                                                       DIGT 010
      COMMON /SINIT/H1(6,8),H2(6,8),DP0(6,8),DP1(6,8),DP1A(6,8),DP2(6,8)DIGT 011
     1,DP2A(6,8),CSALF1(6,8),ALF1(6,8),CSBET2(6,8),BET2(6,8),RADSD(6,8),DIGT 012
     2RADRD(6,8),ANN1(6,8),ANN2(6,8),ANN2A(6,8),ANN1A(6,8),U1A(6,8),    DIGT 013
     3U2(6,8),ANN0(6,8),PT0(6,8),TT0(6,8),ALPHA0(6,8),PTP(6,8)          DIGT 014
C                                                                       DIGT 015
      COMMON /SINPUT/ RSL,TSL,PSL,GAMSL,                                ********
     1PTPS,PTIN,TTIN,WAIR,FAIR,DELC,DELL,DELA,AACS,VCTD,STG,SECT,EXPN,  DIGT 017
     2EXPP,EXPRE,    RPM,PAF,SLT,STGCH,ENDJOB,NAME(10),TITLE(10),PCNH(6),********
     3RV(6,8),GAM(6,8),DR(6,8),DT(6,8),RWG(6,8),ALPHAS(6,8),ALPHA1(6,8),********
     4ETARS(6,8),ETAS(6,8),CFS(6,8),ANDO(6,8),BETA1(6,8),BETA2(6,8),ETARDIGT 020
     5R(6,8),ETAR(6,8),CFR(6,8),TFR(6,8),ANDOR(6,8),OMEGAS(6,8),AS0(6,8)DIGT 021
     6,ASMP0(6,8),ACMN0(6,8),A1(6,8),A2(6,8),A3(6,8),A4(6,8),A5(6,8),A6(DIGT 022
     76,8),OMEGAR(6,8),BSIA(6,8),BSMPIA(6,8),BCMNIA(6,8),B1(6,8),B2(6,8)DIGT 023
     8,B3(6,8),B4(6,8),B5(6,8),B6(6,8),SESTHI(8),RERTHI(8)              DIGT 024
C                                                                       DIGT 025
      REAL M0                                                           DIGT 026
      COMMON /SSTA01/CP0(8),                      PS0(6,8),V0(6,8),TS0(6DIGT 027
     18),VU0(6,8),VZ0(6,8),RHOS0(6,8),PS1(6,8),WGT1(8),TA1(8),WG1(6,8), DIGT 028
     2              DPDR1(6,8),S1(6,8),  CP1(8),PHI1(6,8),TS1(6,8),V1(6,8)DIGT 029
     3,RHOS1(6,8),ALF1E(6,8),VU1(6,8),VZ1(6,8),M0(6,8),WGT0(8),WG0(6,8) ********
C                                                                       DIGT 031
      REAL MR1A                                                         DIGT 032
      COMMON /SSTA1A/VU1A(6,8),WG1A(6,8),WGT1A(8),VZ1A(6,8),  CP1A(8),  DIGT 033
     1PS1A(6,8),RU1A(6,8),R1A(6,8),BET1A(6,8),RI(6,8),TTR1A(6,8),PTR1A(6DIGT 034
     2,8),MR1A(6,8),TS1A(6,8)                                           ********
C                                                                       DIGT 036
      COMMON /SSTA2/V2(6,8),TTR2(6,8),PTR2(6,8),WG2(6,8),WGT2(8),TA2(8),DIGT 037
     1              PS2(6,8),PHI2(6,8)                                  DIGT 038
C                                                                       DIGT 039
      REAL MR2,M2      ,MF2                                             DIGT 040
      COMMON /SFLOW2/TS2(6,8),CP2(8),R2(6,8),RHOS2(6,8),BET2E(6,8),RU2(6DIGT 041
     1,8),VU2(6,8),DPDR2(6,8),VZ2(6,8),MR2(6,8),MF2(6,8),M2(6,8)        DIGT 042
C                                                                       DIGT 043
      REAL M2A,MF2A                                                     DIGT 044
      COMMON /SSTA2A/WG2A(6,8),WGT2A(8),VU2A(6,8),VZ2A(6,8),PS2A(6,8),  DIGT 045
```

```
     1ALF2A(6,8),TT2A(6,8),PT2A(6,8),TTBAR(8),PTBAR(8),STT0(8),SPT0(8), DIGT 046
     2M2A(6,8),MF2A(6,8),CP2A(8),V2A(6,8),TS2A(6,8),TAS(8),PAS(8),GAMS(8DIGT 047
     3),CPS(8),DELHVD(6,8),HVBAR(8)                                     ********
C                                                                       DIGT 049
      IF(SRFLAG) WRITE(6,10000)                                         ********
10000 FORMAT(44H AN ENTRY HAS BEEN MADE IN SUBROUTINE DIAGT )           ********
      WRITE(6,1000)NAME,TITLE                                           DIGT 050
 1000 FORMAT(1H1,5X,10A6/6X,10A6/20X,29HNASA TURBINE COMPUTER PROGRAM/  DIGT 051
     131X,10HDIAGNOSTIC)                                                DIGT 052
      IF (M.EQ.0)  GO TO 10                                             DIGT 053
      GO TO (10,19,11,12,13),M                                          DIGT 054
   10 DO 14 K=1,KN                                                      DIGT 055
      WRITE(6,1001)K,CP0(K),GAM(1,K)                                    DIGT 056
 1001 FORMAT(9X,1HK,I5,9X,3HCP0,F10.3,9X,5HGAMMA,F10.5)                 DIGT 057
      WRITE(6,1002) (PTP(I,K),I=1,ISECT)                                DIGT 058
 1002 FORMAT(3X,6H   PTP,6F10.3)                                        DIGT 059
      WRITE(6,1003) (PT0(I,K),I=1,ISECT)                                DIGT 060
 1003 FORMAT(3X,6H   PT0,6F10.3)                                        DIGT 061
      WRITE(6,1004) (PS0(I,K),I=1,ISECT)                                DIGT 062
 1004 FORMAT(3X,6H   PS0,6F10.3)                                        DIGT 063
      WRITE(6,1005) (TT0(I,K),I=1,ISECT)                                DIGT 064
 1005 FORMAT(3X,6H   TT0,6F10.1)                                        DIGT 065
      WRITE(6,1006) (TS0(I,K),I=1,ISECT)                                DIGT 066
 1006 FORMAT(3X,6H   TS0,6F10.1)                                        DIGT 067
      WRITE(6,1007) (V0(I,K),I=1,ISECT)                                 DIGT 068
 1007 FORMAT(3X,6H    V0,6F10.3)                                        DIGT 069
      WRITE(6,1008) (ALPHA0(I,K),I=1,ISECT)                             DIGT 070
 1008 FORMAT(3X,6HALPHA0,6F10.3)                                        DIGT 071
   14 WRITE(6,1009) (SI(I,K),I=1,ISECT)                                 DIGT 072
      IF (M.EQ.0)  GO TO 19                                             DIGT 073
      GO TO 18                                                          DIGT 074
   19 DO 20 K=1,KN                                                      DIGT 075
 1009 FORMAT(3X,6H    SI,6F10.3)                                        DIGT 076
      WRITE(6,1010) K,CP1(K),GAM(2,K)                                   DIGT 077
 1010 FORMAT(9X,1HK,I5,9X,3HCP1,F10.3,9X,5HGAMMA,F10.5)                 DIGT 078
      WRITE(6,1011) (PS1(I,K),I=1,ISECT)                                DIGT 079
 1011 FORMAT(3X,6H   PS1,6F10.3)                                        DIGT 080
      WRITE(6,1012) (DPDR1(I,K),I=1,ISECT)                              DIGT 081
 1012 FORMAT(3X,6H DPDR1,6F10.5)                                        DIGT 082
      WRITE(6,1013) (TS1(I,K),I=1,ISECT)                                DIGT 083
 1013 FORMAT (3X,6H   TS1,6F10.1)                                       DIGT 084
      WRITE(6,1014) (WG1(I,K),I=1,ISECT)                                DIGT 085
 1014 FORMAT(3X,6H   WG1,6F10.3)                                        DIGT 086
      WRITE(6,1015) (V1(I,K),I=1,ISECT)                                 DIGT 087
 1015 FORMAT(3X,6H    V1,6F10.3)                                        DIGT 088
      WRITE(6,1016) (ALF1E(I,K),I=1,ISECT)                              DIGT 089
 1016 FORMAT (3X,6H ALF1E,6F10.3)                                       DIGT 090
```

Listing of Code (continued)

```
   20 WRITE(6,1017) (ALF1(I,K),I=1,ISECT)
 1017 FORMAT(3X,6H  ALF1,6F10.3)
      IF (M.EQ.0)  GO TO 11
      GO TO 18
   11 DO 15 K=1,KN
      WRITE(6,1018) K,CP1A(K),GAM(3,K)
 1018 FORMAT(9X,1HK,I5,9X,4HCP1A,F10.3,8X,5HGAMMA,F10.5)
      WRITE(6,1019) (PTR1A(I,K),I=1,ISECT)
 1019 FORMAT(3X,6H PTR1A,6F10.3)
      WRITE(6,1020) (PS1A(I,K),I=1,ISECT)
 1020 FORMAT(3X,6H  PS1A,6F10.3)
      WRITE(6,1021) (TTR1A(I,K),I=1,ISECT)
 1021 FORMAT(3X,6H TTR1A,6F10.1)
      WRITE(6,1022) (WG1A(I,K),I=1,ISECT)
 1022 FORMAT (3X,6H  WG1A,6F10.3)
      WRITE(6,1023) (R1A(I,K),I=1,ISECT)
 1023 FORMAT (3X,6H   R1A,6F10.3)
      WRITE(6,1024) (BET1A(I,K),I=1,ISECT)
 1024 FORMAT (3X,6H BET1A,6F10.3)
   15 WRITE(6,1025) (RI(I,K),I=1,ISECT)
 1025 FORMAT (3X,6H    RI,6F10.3)
      IF (M.EQ.0)  GO TO 12
      GO TO 18
   12 DO 16 K=1,KN
      WRITE(6,1026)K,CP2(K),GAM(3,K)
 1026 FORMAT(9X,1HK,I5,9X,3HCP2,F10.3,9X,5HGAMMA,F10.5)
      WRITE(6,1027) (PTR2(I,K),I=1,ISECT)
 1027 FORMAT (3X,6H  PTR2,6F10.3)
      WRITE(6,1028) (PS2(I,K),I=1,ISECT)
 1028 FORMAT (3X,6H   PS2,6F10.3)
      WRITE(6,1029) (DPDR2(I,K),I=1,ISECT)
 1029 FORMAT (3X,6H DPDR2,6F10.5)
      WRITE(6,1030) (TTR2(I,K),I=1,ISECT)
 1030 FORMAT (3X,6H  TTR2,6F10.1)
      WRITE(6,1031) (TS2(I,K),I=1,ISECT)
 1031 FORMAT (3X,6H   TS2,6F10.1)
      WRITE(6,1032) (WG2(I,K),I=1,ISECT)
 1032 FORMAT (3X,6H   WG2,6F10.3)
      WRITE(6,1033) (R2(I,K),I=1,ISECT)
 1033 FORMAT (3X,6H    R2,6F10.3)
      WRITE(6,1034) (BET2E(I,K),I=1,ISECT)
 1034 FORMAT (3X,6H BET2E,6F10.3)
   16 WRITE(6,1035) (BET2(I,K),I=1,ISECT)
 1035 FORMAT (3X,6H  BET2,6F10.3)
      IF (M.EQ.0)  GO TO 13
      GO TO 18
   13 DO 17 K=1,KN
```

Listing of Code (continued)

```
      L=K +1                                                            DIGT 138
      WRITE(6,1036)K,CP2A(K),GAM(5,K)                                   DIGT 139
 1036 FORMAT(9X,1HK,I5,9X,4HCP2A,F10.3,8X,5HGAMMA,F10.5)                DIGT 140
      WRITE(6,1037) (PT2A(I,K),I=1,ISECT)                               DIGT 141
 1037 FORMAT (3X,6H  PT2A,6F10.3)                                       DIGT 142
      WRITE(6,1038) (PS2A(I,K),I=1,ISECT)                               DIGT 143
 1038 FORMAT (3X,6H  PS2A,6F10.3)                                       DIGT 144
      WRITE(6,1039) (TT2A(I,K),I=1,ISECT)                               DIGT 145
 1039 FORMAT (3X,6H  TT2A,6F10.1)                                       DIGT 146
      WRITE(6,1040) (TS2A(I,K),I=1,ISECT)                               DIGT 147
 1040 FORMAT (3X,6H  TS2A,6F10.1)                                       DIGT 148
      WRITE(6,1041) (WG2A(I,K),I=1,ISECT)                               DIGT 149
 1041 FORMAT (3X,6H  WG2A,6F10.3)                                       DIGT 150
      WRITE(6,1042) (V2A(I,K),I=1,ISECT)                                DIGT 151
 1042 FORMAT (3X,6H   V2A,6F10.3)                                       DIGT 152
      WRITE(6,1043) (ALF2A(I,K),I=1,ISECT)                              DIGT 153
 1043 FORMAT (3X,6H ALF2A,6F10.3)                                       DIGT 154
      WRITE(6,1044) (SI(I,K),I=1,ISECT)                                 DIGT 155
 1044 FORMAT (3X,6H    SI,6F10.3)                                       DIGT 156
      WRITE(6,1045) L,CPS(K),GAMS(K)                                    DIGT 157
 1045 FORMAT(9X,1HL,I5,9X,3HCPS,F10.3,9X,5HGAMMA,F10.5)                 DIGT 158
      WRITE(6,1046) (PTP(I,L),I=1,ISECT)                                DIGT 159
 1046 FORMAT (3X,6H   PTP,6F10.3)                                       DIGT 160
      WRITE(6,1047) (PT0(I,L),I=1,ISECT)                                DIGT 161
 1047 FORMAT (3X,6H   PT0,6F10.3)                                       DIGT 162
   17 WRITE(6,1048) (TT0(I,L),I=1,ISECT)                                DIGT 163
 1048 FORMAT (3X,6H   TT0,6F10.1)                                       DIGT 164
   18 CONTINUE                                                          DIGT 165
      IF(SHFLAG) WRITE(6,20000)                                         ********
20000 FORMAT(1H1,45H AN EXIT HAS BEEN MADE FROM SUBROUTINE DIAGT )      ********
      RETURN                                                            DIGT 166
      END                                                               DIGT 167
```

Listing of Code (continued)

```
      SUBROUTINE INSTG
CINSTG
C     INTERSTAGE OUTPUT
C      NUMBER OF SECTORS IS THREE OR LESS,HUB AND CASING VALUES ARE
C         CALCULATED AND PRINTED
C     NUMBER OF SECTORS IS MORE THAN THREE,ONLY SECTOR PITCHLINE
C         VALUES ARE PRINTED
C
      REAL MFSTOP
      LOGICAL PREVER,SRFLAG
      COMMON  SRFLAG
      COMMON /SNTCP/G,AJ,PRPC,ICASE,PREVER,MFSTOP,JUMP,LOPIN,ISCASE,
     1KN,GAMF,IP,SCRIT,PTRN,ISECT,KSTG,WTOL,RHOTOL,PRTOL,TRLOOP,LSTG,
     2LBRC,IBRC,ICHOKE,ISORR,CHOKE,PTOPS1(6,8),PTRS2(6,8),TRDIAG,SC,RC,
     3DELPR,PASS,IPC,LOPC,ISS
C
      COMMON /SINIT/H1(6,8),H2(6,8),DP0(6,8),DP1(6,8),DP1A(6,8),DP2(6,8)
     1,DP2A(6,8),CSALF1(6,8),ALF1(6,8),CSBET2(6,8),BET2(6,8),RADSD(6,8),
     2RADRD(6,8),ANN1(6,8),ANN2(6,8),ANN2A(6,8),ANN1A(6,8),U1A(6,8),
     3U2(6,8),ANN0(6,8),PT0(6,8),TT0(6,8),ALPHA0(6,8),PTP(6,8)
C
      COMMON /SINPUT/ RSL,TSL,PSL,GAMSL,
     1PTPS,PTIN,TTIN,WAIR,FAIR,DELC,DELL,DELA,AACS,VCTD,STG,SECT,EXPN,
     2EXPP,EXPRE,   RPM,PAF,SLI,STGCH,ENDJOB,NAME(10),TITLE(10),PCNH(6),
     3RV(6,8),GAM(6,8),DR(6,8),DT(6,8),RWG(6,8),ALPHAS(6,8),ALPHA1(6,8),
     4ETARS(6,8),ETAS(6,8),CFS(6,8),ANDO(6,8),BETA1(6,8),BETA2(6,8),ETAR
     5R(6,8),ETAR(6,8),CFR(6,8),TFR(6,8),ANDOR(6,8),OMEGAS(6,8),AS0(6,8)
     6,ASMP0(6,8),ACMN0(6,8),A1(6,8),A2(6,8),A3(6,8),A4(6,8),A5(6,8),A6(
     76,8),OMEGAR(6,8),BSIA(6,8),BSMPIA(6,8),BCMNIA(6,8),B1(6,8),B2(6,8)
     8,B3(6,8),B4(6,8),B5(6,8),B6(6,8),SESTHI(8),RERTHI(8)
C
      REAL M0
      COMMON /SSTA01/CP0(8),                         PS0(6,8),V0(6,8),TS0(6,
     18),VU0(6,8),VZ0(6,8),RHOS0(6,8),PS1(6,8),WGT1(8),TA1(8),WG1(6,8),
     2            DPDH1(6,8),SI(6,8),   CP1(8),PHI1(6,8),TS1(6,8),V1(6,8)
     3,RHOS1(6,8),ALF1E(6,8),VU1(6,8),VZ1(6,8),M0(6,8),WGT0(8),WG0(6,8)
C
      REAL MR1A
      COMMON /SSTA1A/VU1A(6,8),WG1A(6,8),WGT1A(8),VZ1A(6,8),  CP1A(8),
     1PS1A(6,8),RU1A(6,8),R1A(6,8),BET1A(6,8),RI(6,8),TTR1A(6,8),PTR1A(6
     2,8),MR1A(6,8),TS1A(6,8)
C
      COMMON /SSTA2/V2(6,8),TTR2(6,8),PTR2(6,8),WG2(6,8),WGT2(8),TA2(8),
     1           PS2(6,8),PHI2(6,8)
C
      REAL MR2,M2      ,MF2
```

```
      COMMON /SFLOW2/TS2(6,8),CP2(8),R2(6,8),RHOS2(6,8),BET2E(6,8),RU2(6INST 046
     1,8),VU2(6,8),DPDR2(6,8),VZ2(6,8),MR2(6,8),MF2(6,8),M2(6,8)        INST 047
                                                                        INST 048
C                                                                       INST 049
      REAL M2A,MF2A                                                     INST 050
      COMMON /SSTA2A/WG2A(6,8),WGT2A(8),VU2A(6,8),VZ2A(6,8),PS2A(6,8),  INST 051
     1ALF2A(6,8),TT2A(6,8),PT2A(6,8),TTBAR(8),PTBAR(8),STT0(8),SPT0(8), INST 052
     2M2A(6,8),MF2A(6,8),CP2A(8),V2A(6,8),TS2A(6,8),TAS(8),PAS(8),GAMS(8********
     3),CP0(8),DELHVD(6,8),HVBAR(8)                                     INST 054
C                                                                       INST 055
      COMMON /SOVRAL/DELHT(6,8),DELHTI(6,8),DELHSI(6,8),DEHATI(6,8),    INST 056
     1ETATT(6,8),ETATS(6,8),ETATAT(6,8)                                 INST 057
C                                                                       INST 058
      COMMON     STDP0(7),STFT0(7),STALF(7),STSI(7),STV0(7),STVU0(7),   INST 059
     1STVZ0(7),STTS0(7),STPS0(7),STDEN0(7),STM0(7),STDP1(7),STALFE(7),  INST 060
     2STDELA(7),STV1(7),STVU1(7),STVZ1(7),STTS1(7),STPS1(7),STDEN1(7),  INST 061
     3STM1(7),ZWIINC(7),                           CPS(7),STDP1A(7),    INST 062
     4STPTR1(7),STBET1(7),STR1(7),STR1A(7),STRU1A(7),STMR1A(7),STU1A(7),INST 063
     5STDP2(7),STBET2(7),SDBETA(7),SR2(7),SRU2(7),SMR2(7),SU2(7),RX(7), INST 064
     6STDELH(7),STPSI(7),SETATT(7),SETATS(7),SETAAT(7),RZWINC(7),       ********
     7                        CFR(7),STPT2A(7),STTT2A(7),STV2A(7),STVU2A(7),********
     8STALF2(7),STMF2A(7),STTTR1(7),STVZ2A(7),STTS2A(7),STPS2A(7),STDEN2********
     9(7),STM2A(7),STTT0(7),LJ,JJ,K,STWG0(7),STWG1(7),STWG1A(7),STWG2(7)********
     9,STWG2A(7),SFLO0,SFLO1,SFLO1A,SFLO2,SFLO2A,STPS1A(7),STTS1A(7),   ********
     9STPTR2(7),STTTR2(7),STPS2(7),STTS2(7)                             INST 068
C                                                                       INST 069
C                                                                       ********
      IF(SHFLAG) WRITE(6,10000)                                         ********
10000 FORMAT(44H AN ENTRY HAS BEEN MADE IN SUBROUTINE INSTG )           INST 070
    1 DO 9 K=1,KSTG                                                     ********
      SFLO0 =0.0                                                        ********
      SFLO1 =0.0                                                        ********
      SFLO1A=0.0                                                        ********
      SFLO2 =0.0                                                        ********
      SFLO2A=0.0                                                        INST 071
      E1=(GAMS(K)-1.)/GAMS(K)                                           INST 072
      E2=GAM(1,K)/(GAM(1,K)-1.)                                         INST 073
      E3=GAM(2,K)/(GAM(2,K)-1.)                                         INST 074
      E4=GAM(3,K)/(GAM(3,K)-1.)                                         INST 075
      E5=GAM(4,K)/(GAM(4,K)-1.)                                         INST 076
      E6=GAM(5,K)/(GAM(5,K)-1.)                                         INST 077
C     RELOCATE PITCHLINE VALUES                                         INST 078
      J=ISECT+1                                                         INST 079
    4 DO 5 I=1,ISECT                                                    INST 080
      KS=J-I+1                                                          ********
      STWG0(KS)=WG0(KS-1,K)                                             ********
      SFLO0 =SFLO0 +STWG0(KS)                                           INST 081
      STTT0(KS)=TT0(KS-1,K)
```

Listing of Code (continued)

```
      STDP0(KS)=DP0(KS-1,K)                                             INST 082
      STPT0(KS)=PTP(KS-1,K)                                             INST 083
      STALF(KS)=ALPHA0(KS-1,K)*57.2958                                  INST 084
      STSI(KS)=SI(KS-1,K)*57.2958                                       INST 085
      STV0(KS)=V0(KS-1,K)                                               INST 086
      STVU0(KS)=VU0(KS-1,K)                                             INST 087
      STVZ0(KS)=VZ0(KS-1,K)                                             INST 088
      STTS0(KS)=TS0(KS-1,K)                                             INST 089
      STPS0(KS)=PS0(KS-1,K)                                             INST 090
      STDEN0(KS)=144.*STPS0(KS)/(STTS0(KS)*RV(1,K))                     ********
      STM0(KS)=M0(KS-1,K)                                               INST 092
      STWG1(KS)=WG1(KS-1,K)                                             ********
      SFL01 =SFL01 +STWG1(KS)                                           ********
      STDP1(KS)=DP1(KS-1,K)                                             INST 093
      STALFE(KS)=ALF1E(KS-1,K)*57.2958                                  INST 094
      STDELA(KS)=(ALPHA0(KS-1,K)+ALF1E(KS-1,K))*57.2958                 INST 095
      STV1(KS)=V1(KS-1,K)                                               INST 096
      STVU1(KS)=VU1(KS-1,K)                                             INST 097
      STVZ1(KS)=VZ1(KS-1,K)                                             INST 098
      STTS1(KS)=TS1(KS-1,K)                                             INST 099
      STPS1(KS)=PS1(KS-1,K)                                             INST 100
      STDEN1(KS)=RHOS1(KS-1,K)                                          INST 101
      STM1(KS)=V1(KS-1,K)/(SQRT(GAM(2,K)*G*RV(2,K)*TS1(KS-1,K)))        ********
       ZS =-2.*ALF1E(KS-1,K) -1.570796                                  INST 103
      ZWIINC(KS)=COS(           ZS   )*(SIN(ALPHA0(KS-1,K))*COS(ALF1E(KSINST 104
     1-1,K))/(COS(ALPHA0(KS-1,K))*SIN(ALF1E(KS-1,K)))+1.)               INST 105
      CPS(KS)=1.-(STV0(KS)/STV1(KS))**2                                 INST 106
      STWG1A(KS)=WG1A(KS-1,K)                                           ********
      SFL01A=SFL01A+STWG1A(KS)                                          ********
      STDP1A(KS)=DP1A(KS-1,K)                                           INST 107
      STPTR1(KS)=PTR1A(KS-1,K)                                          INST 108
      STTTR1(KS)=TTR1A(KS-1,K)                                          INST 109
      STBET1(KS)=BET1A(KS-1,K)*57.2958                                  INST 110
      STRI(KS)=RI(KS-1,K)*57.2958                                       INST 111
      STR1A(KS)=R1A(KS-1,K)                                             INST 112
      STRU1A(KS)=RU1A(KS-1,K)                                           INST 113
      STMR1A(KS)=MR1A(KS-1,K)                                           INST 114
      STU1A(KS)=U1A(KS-1,K)                                             INST 115
      STPS1A(KS)=PS1A(KS-1,K)                                           ********
      STTS1A(KS)=TS1A(KS-1,K)                                           ********
      STWG2(KS)=WG2(KS-1,K)                                             ********
      SFL02 =SFL02 +STWG2(KS)                                           ********
      STDP2(KS)=DP2(KS-1,K)                                             INST 116
      STBET2(KS)=BET2E(KS-1,K)*57.2958                                  INST 117
      SDBETA(KS)=(BET1A(KS-1,K)+BET2E(KS-1,K))*57.2958                  INST 118
      SR2(KS)=R2(KS-1,K)                                                INST 119
      SRU2(KS)=RU2(KS-1,K)                                              INST 120
```

Listing of Code (continued)

```
                                                                          INST 121
      SU2(KS)=U2(KS-1,K)                                                  INST 122
      STPTR2(KS)=PTR2(KS-1,K)                                             ********
      STTTR2(KS)=TTR2(KS-1,K)                                             ********
      RX(KS)=1.-(1.-(PS1(KS-1,K)/PTP(KS-1,K))**E1)/(1.-(PS2(KS-1,K)/      INST 123
     1PTP(KS-1,K))**E1)                                                   INST 124
      STDELH(KS)=DELHT(KS-1,K)                                            INST 125
      STPSI(KS)=2.*G*AJ*DELHT(KS-1,K)/(U1A(KS-1,K)*U1A(KS-1,K)            INST 126
     1+U2(KS-1,K)*U2(KS-1,K))                                             INST 127
      SETATT(KS)=ETATT(KS-1,K)                                            INST 128
      SETATS(KS)=ETATS(KS-1,K)                                            INST 129
      SETAAT(KS)=ETATAT(KS-1,K)                                           INST 130
      ZR = -2.*BET2E(KS-1,K) -1.570796                                    INST 131
      R2WINC(KS)=COS(             ZR )*(SIN(BET1A(KS-1,K))*COS(BET2E(KS-INST 132
     11,K))/(COS(BET1A(KS-1,K))*SIN(BET2E(KS-1,K)))+1.)                   INST 133
      CPR(KS)=1.-(STR1A(KS)/SR2(KS))**2                                   INST 134
      STPS2(KS)=PS2(KS-1,K)                                               ********
      STTS2(KS)=TS2(KS-1,K)                                               ********
      STWG2A(KS)=WG2A(KS-1,K)                                             ********
      SFLO2A=SFLO2A+STWG2A(KS)                                            ********
      STPT2A(KS)=PT2A(KS-1,K)                                             ********
      STTT2A(KS)=TT2A(KS-1,K)                                             ********
      STV2A(KS)=V2A(KS-1,K)                                               ********
      STVU2A(KS)=VU2A(KS-1,K)                                             ********
      STALF2(KS)=ALF2A(KS-1,K)*57.2958                                    INST 139
      STMF2A(KS)=MF2A(KS-1,K)                                             ********
      STVZ2A(KS)=VZ2A(KS-1,K)                                             ********
      STPS2A(KS)=PS2A(KS-1,K)                                             ********
      STTS2A(KS)=TS2A(KS-1,K)                                             ********
      STM2A(KS)=M2A(KS-1,K)                                               ********
      STDEN2(KS)=144.*STPS2A(KS)/(STTS2A(KS)*RV(5,K))                     ********
    5 CONTINUE                                                            INST 146
      IF (ISECT-3)3,3,6                                                   INST 147
C          CALCULATE HUB VALUES                                           INST 148
    3 LJ=1                                                                INST 149
      JJ=ISECT+2                                                          INST 150
      I=1                                                                 INST 151
      L=1                                                                 INST 152
      STDPO(L)=DR(1,K)                                                    ********
      R1=CPO(I,K)/DR(1,K)                                                 ********
      STDP1(L)=DR(2,K)                                                    ********
      R2=CP1(I,K)/DR(2,K)                                                 INST 156
      STDP1A(L)=DR(3,K)                                                   ********
      R3=CP1A(I,K)/DR(3,K)                                                INST 158
      STDP2(L)=DR(4,K)                                                    INST 159
      R4=CP2(I,K)/DR(4,K)                                                 ********
      TALF=SIN(ALF1(I,K))*R3/COS(ALF1(I,K))                               INST 161
```

Listing of Code (continued)

```
      R5=CP2A(I,K)/DR(5,K)                                              INST 162
C         STATION     0          STATOR   INLET                         INST 163
   10 STTT0(L)=TT0(I,K)                                                 INST 164
      STPT0(L)=PTP(I,K)                                                 INST 165
      STVZ0(L)=VZ0(I,K)                                                 INST 166
      STVU0(L)=VU0(I,K)*R1                                              INST 167
      STV0(L)=SQRT(VZ0(I,K)*VZ0(I,K)+STVU0(L)*STVU0(L))                 INST 168
      STTS0(L)=TT0(I,K)-STV0(L)*STV0(L)/(2.*G*AJ*CP0(K))                INST 169
      STPS0(L)=PS0(I,K)*(STTS0(L)/TS0(I,K))**E2                         INST 170
      STDEN0(L)=144.*STPS0(L)/(RV(1,K)*STTS0(L))                        ********
       STALF(L)=ATAN2(STVU0(L),STVZ0(L))*57.2958                        INST 172
      STSI(L)=STALF(L)-ATAN2(SIN( RADSD(I,K))*R1,COS( RADSD(I,K)))      INST 173
     1*57.2958                                                          INST 174
      AS0H=SQRT(GAM(1,K)*G*RV(1,K)*STTS0(L))                            ********
      STM0(L)=STV0(L)/AS0H                                              INST 176
C         STATION     1          STATOR   EXIT                          INST 177
      STVZ1(L)=VZ1(I,K)                                                 INST 178
      STVU1(L)=VU1(I,K)*R2                                              INST 179
      STV1(L)=SQRT(VZ1(I,K)*VZ1(I,K)+STVU1(L)*STVU1(L))                 INST 180
      STTS1(L)=TT0(I,K)-STV1(L)*STV1(L)/(2.*G*AJ*CP1(K))                INST 181
      STPS1(L)=PS1(I,K)*(STTS1(L)/TS1(I,K))**E3                         INST 182
      STDEN1(L)=144.*STPS1(L)/STTS1(L)/RV(2,K)                          ********
      STALFE(L)=ATAN2(STVU1(L),STVZ1(L))*57.2958                        INST 184
      STDELA(L)=STALF(L)+STALFE(L)                                      INST 185
      AS1H=SQRT(GAM(2,K)*G*RV(2,K)*STTS1(L))                            ********
      STM1(L)=STV1(L)/AS1H                                              INST 187
      ZS =-2.*STALFE(L)/ 57.2958 -1.570796                              INST 188
      ZWIINC(L)= COS(    ZS)*(STVU0(L)*STVZ1(L) /(STVZ0(L)*STVU1(L))+1.) INST 189
      CPS(L)=1.-(STV0(L)/STV1(L))**2                                    INST 190
C         STATION    1A          ROTOR    INLET                         INST 191
      VU1AH=VU1A(I,K)*R3                                                INST 192
      STRU1A(L)=VU1AH-U1A(I,K)/R3                                       INST 193
      STBET1(L)=ATAN2(STRU1A(L),VZ1A(I,K))*57.2958                      INST 194
      T=TALF-(TALF/R3 - SIN(RADRD(I,K))/COS(RADRD(I,K)))/R3             INST 195
      STRI(L)=STBET1(L)-ATAN2(     T,1.        )*57.2958                INST 196
      STR1A(L)=SQRT(STRU1A(L)*STRU1A(L)+VZ1A(I,K)*VZ1A(I,K))            INST 197
      V1A1AH=VZ1A(I,K)*VZ1A(I,K)+VU1AH*VU1AH                            INST 198
      DELTSH=(V1(I,K)*V1(I,K)-V1A1AH)/(2.*G*AJ*CP1A(K))                 INST 199
      TS1AH=TS1(I,K)+DELTSH                                             INST 200
      STTS1A(L)=TS1AH                                                   ********
      STMR1A(L)=STR1A(L)/SQRT(GAM(3,K)*G*RV(3,K)*TS1AH)                 ********
      TTRSH=1.+STMR1A(L)*STMR1A(L)*(GAM(3,K)-1.)/2.                     INST 202
      STTTR1(L)=TS1AH*TTRSH                                             INST 203
      IF (RI(I,K))2,2,7                                                 INST 204
    2 EXPRI=EXPN                                                        INST 205
      GO TO 11                                                          INST 206
    7 EXPRI=EXPP                                                        INST 207
```

Listing of Code (continued)

```
11 PTRSH=(1.+(TTRSH-1.)*ETARR(I,K)*COS(RI(I,K))**EXPRI)**E4
   PS1AH=PS1(I,K)*(1.+DELTSH/TS1(I,K))**E4
   STPS1A(L)=PS1AH
   STPTR1(L)=PS1AH*PTRSH
   STU1A(L)=U1A(I,K)/R3
C        STATION    2          ROTOR     EXIT
   VU2H=VU2(I,K)*R4
   SHU2(L)=VU2H+U2(I,K)/R4
   STBET2(L)=ATAN2(SHU2(L),VZ2(I,K))*57.2958
   SDBETA(L)=STHET1(L)+STBET2(L)
   SR2(L)=SQRT(SHU2(L)*SHU2(L)+VZ2(I,K)*VZ2(I,K))
   V2V2H=VZ2(I,K)*VZ2(I,K)+VU2H*VU2H
   DELTSH=(V2(I,K)*V2(I,K)-V2V2H)/(2.*G*AJ*CP2(K))
   TS2H=TS2(I,K)+DELTSH
   STTS2(L)=TS2H
   SMR2(L)=SR2(L)/SQRT(GAM(4,K)*G*RV(4,K)*TS2H)
   SU2(L)=U2(I,K)/R4
   PS2H=PS2(I,K)*(TS2H/TS2(I,K))**E5
   STPS2(L)=PS2H
   RX(L)=1.-(1.-(STPS1(L)/PTP(I,K))**E1)/(1.-(PS2H/PTP(I,K))**E1)
   STDELH(L)=(STU1A(L)*VU1AH+SU2(L)*VU2H)*TFR(I,K)/(    G*AJ)
   STPSI(L)=2.*G*AJ*STDELH(L)/(STU1A(L)**2+SU2(L)**2)
   SETATT(L)=STDELH(L)/DELHT1(I,K)
   SETATS(L)=STDELH(L)/DELHS1(I,K)
   SETAAT(L)=STDELH(L)/DEHAT1(I,K)
   ZR =-2.*STBET2(L)/57.2958 -1.570796
   RZ#INC(L)=COS(    ZR)*(STRU1A(L)*VZ2(I,K)  /(VZ1A(I,K)*SRU2(L))+1.)
   CPR(L)=1.-(STR1A(L)/SR2(L))**2
   STPT2A(L)=PT2A(I,K)
   STTT2A(L)=TT2A(I,K)
   STVZ2A(L)=VZ2A(I,K)
   STVU2A(L)=VU2A(I,K)*R5
   V2A2AH=STVU2A(L)**2+VZ2A(I,K)**2
   STV2A(L)=SQRT(V2A2AH)
   STALF2(L)=ATAN2(STVU2A(L),VZ2A(I,K))*57.2958
   DELTS2=(V2A(I,K)**2-V2A2AH)/(2.*G*AJ*CP2A(K))
   STTS2A(L)=TS2A(I,K)+DELTS2
   STPS2A(L)=PS2A(I,K)*(1.+DELTS2/TS2A(I,K))**E6
   STDEN2(L)=144.*STPS2A(L)/(RV(5,K)*STTS2A(L))
   STM2A(L)=STV2A(L)/SQRT(GAM(5,K)*G*RV(5,K)*STTS2A(L))
   STMF2A(L)=STM2A(L)*COS(STALF2(L)/57.2958)
   IF (L.GT.1) GO TO 8
C        CALCULATE   TIP    VALUES
   I=ISECT
   L=ISECT+2
   STDPO(L)=DT(1,K)
   R1=DPO(I,K)/DT(1,K)
```

Listing of Code (continued)

```
      STDP1(L)=DT(2,K)                                                   INST 252
      R2=CP1(I,K)/DT(2,K)                                                INST 253
      STDP1A(L)=DT(3,K)                                                  INST 254
      R3=CP1A(I,K)/DT(3,K)                                               INST 255
      STDP2(L)=DT(4,K)  .                                                INST 256
      R4=CP2(I,K)/DT(4,K)                                                INST 257
      TALF=SIN(ALF1(I,K))*R3/COS(ALF1(I,K))                              INST 258
      R5=CP2A(I,K)/DT(5,K)                                               INST 259
      GO TO 10                                                           INST 260
    6 LJ=2                                                               INST 261
      JJ=ISECT+1                                                         INST 262
    8 CALL WOUT                                                          INST 263
    9 CONTINUE                                                           INST 264
      IF(SWFLAG) WRITE(6,20000)                                          ********
20000 FORMAT(45H AN EXIT HAS BEEN MADE FROM SUBROUTINE INSTG )          ********
      RETURN                                                             INST 265
      END                                                                INST 266
```

```
      SUBROUTINE WOUT
CWOUT
C
      REAL MFSTOP
      LOGICAL PREVER,SRFLAG
      COMMON  SRFLAG
      COMMON /SNTCP/G,AJ,PRFC,ICASE,PRFVER,MFSTOP,JUMP,LOPIN,ISCASE,
     1KN,GAMF,IP,SCRIT,PTRN,ISECT,KSTG,WTOL,RHOTOL,PRTOL,TRLOOP,LSTG,
     2LBRC,IBRC,ICHOKE,ISORR,CHOKE,PTOPS1(6,8),PTRS2(6,8),TRDIAG,SC,RC,
     3DELPR,PASS,IPC,LOPC,ISS
C
      COMMON /SINIT/H1(6,8),H2(6,8),DP0(6,8),DP1(6,8),DP1A(6,8),DP2(6,8)
     1,DP2A(6,8),CSALF1(6,8),ALF1(6,8),CSBET2(6,8),BET2(6,8),RADSD(6,8),
     2RADRD(6,8),ANN1(6,8),ANN2(6,8),ANN2A(6,8),ANN1A(6,8),U1A(6,8),
     3U2(6,8),ANN0(6,8),PT0(6,8),TT0(6,8),ALPHA0(6,8),PTP(6,8)
C
      COMMON /SINPUT/ RSL,TSL,PSL,GAMSL,
     1PTPS,PTIN,TTIN,WAIR,FAIR,DELC,DELL,DELA,AACS,VCTD,STG,SECT,EXPN,
     2EXPP,EXPRE,   RPM,PAF,SLI,STGCH,FNDJOH,NAME(10),TITLE(10),PCNH(6),
     3RV(6,8),GAM(6,8),DR(6,8),DT(6,8),RWG(6,8),ALPHAS(6,8),ALPHA1(6,8),
     4ETARS(6,8),ETAS(6,8),CFS(6,8),ANDO(6,8),BETA1(6,8),BETA2(6,8),ETAR
     5R(6,8),ETAR(6,8),CFR(6,8),TFR(6,8),ANDOR(6,8),OMEGAS(6,8),AS0(6,8)
     6,ASMP0(6,8),ACMN0(6,8),A1(6,8),A2(6,8),A3(6,8),A4(6,8),A5(6,8),A6(
     76,8),OMEGAR(6,8),BSIA(6,8),BSMPIA(6,8),BCMNIA(6,8),B1(6,8),B2(6,8)
     8,B3(6,8),B4(6,8),B5(6,8),B6(6,8),SESTHI(8),RERTHI(8)
C
      REAL M0
      COMMON /SSTA01/CP0(8),                       PS0(6,8),V0(6,8),TS0(6,
     18),VU0(6,8),VZ0(6,8),RHOS0(6,8),PS1(6,8),WGT1(8),TA1(8),WG1(6,8),
     2              DPDR1(6,8),SI(6,8),  CP1(8),PHI1(6,8),TS1(6,8),V1(6,8)
     3,RHOS1(6,8),ALF1E(6,8),VU1(6,8),VZ1(6,8),M0(6,8),WGT0(8),WG0(6,8)
C
      REAL MR1A
      COMMON /SSTA1A/VU1A(6,8),WG1A(6,8),WGT1A(8),VZ1A(6,8),  CP1A(8),
     1PS1A(6,8),RU1A(6,8),R1A(6,8),BET1A(6,8),RI(6,8),TTR1A(6,8),PTR1A(6
     2,8),MR1A(6,8),TS1A(6,8)
C
      COMMON /SSTA2/V2(6,8),TTR2(6,8),PTR2(6,8),WG2(6,8),WGT2(8),TA2(8),
     1              PS2(6,8),PHI2(6,8)
C
      REAL MR2,M2,MF
      COMMON /SFLOW2/TS2(6,8),CP2(8),R2(6,8),RHOS2(6,8),BET2E(6,8),RU2(6
     1,8),VU2(6,8),DPDR2(6,8),VZ2(6,8),MR2(6,8),MF2(6,8),M2(6,8)
C
      REAL M2A,MF2A
      COMMON /SSTA2A/WG2A(6,8),WGT2A(8),VU2A(6,8),VZ2A(6,8),PS2A(6,8),
```

```
     1ALF2A(6,8),TT2A(6,8),PT2A(6,8),TTBAR(8),PTBAR(8),STT0(8),SPT0(8), ********
     2M2A(6,8),MF2A(6,8),CP2A(8),V2A(6,8),TS2A(6,8),TAS(8),PAS(8),GAMS(8********
     3),CP0(8),DELHVD(6,8),HVBAR(8)                                     ********
C                                                                       ********
      COMMON /SOVRAL/DELHT(6,8),DELHTI(6,8),DELHSI(6,8),DEHATI(6,8),    ********
     1ETATT(6,8),ETATS(6,8),ETATAT(6,8)                                 ********
C                                                                       WOUT 025
      COMMON     STDP0(7),STPT0(7),STALF(7),STSI(7),STV0(7),STVU0(7),   WOUT 026
     1STVZ0(7),STTS0(7),STPS0(7),STDEN0(7),STM0(7),STDP1(7),STALFE(7),  WOUT 027
     2STDELA(7),STV1(7),STVU1(7),STVZ1(7),STTS1(7),STPS1(7),STDEN1(7),  WOUT 028
     3STM1(7),ZWIINC(7),                             CPS(7),STDP1A(7),  WOUT 029
     4STPTR1(7),STBET1(7),STR1(7),STR1A(7),STRU1A(7),STMR1A(7),STU1A(7),WOUT 030
     5STDP2(7),STHET2(7),SDBETA(7),SR2(7),SRU2(7),SMR2(7),SU2(7),RX(7), WOUT 031
     6STDELH(7),STPSI(7),SETATT(7),SETATS(7),SETAAT(7),RZWINC(7),       WOUT 032
     7                    CPR(7),STPT2A(7),STTT2A(7),STV2A(7),STVU2A(7),********
     8STALF2(7),STMF2A(7),STTTR1(7),STVZ2A(7),STTS2A(7),STPS2A(7),STDEN2********
     9(7),STM2A(7),STTT0(7),LJ,JJ,K,STWG0(7),STWG1(7),STWG1A(7),STWG2(7)********
     9,STWG2A(7),SFLO0,SFLO1,SFLO1A,SFLO2,SFLO2A,STPS1A(7),STTS1A(7),   ********
     9STPTR2(7),STTTR2(7),STPS2(7),STTS2(7)                             ********
C                                                                       WOUT 036
C          PRINT  OUT  FOR  INTERSTAGE  DATA                            WOUT 037
      IF(SRFLAG) WRITE(6,10000)                                         ********
10000 FORMAT(44H AN ENTRY HAS BEEN MADE IN SUBROUTINE WOUT   )          ********
    8 WRITE(6,1000)NAME,TITLE,ICASE,ISCASE                              WOUT 038
 1000 FORMAT(1H1,20X29HNASA TURBINE COMPUTER PROGRAM/6X10A6/6X10A6/30X  WOUT 039
     15HCASE I3,1H.I3/24X23HINTER-STAGE PERFORMANCE//)                  WOUT 040
      WRITE(6,1001)K,(STDP0(I),I=LJ,JJ)                                 WOUT 041
 1001 FORMAT(5X5HSTA 02X12HSTATOR INLET10X5HSTAGEI3,1H./4X6HDIAM 02X,   WOUT 042
     16F10.3)                                                           WOUT 043
      WRITE(6,1002)(STTT0(I),I=LJ,JJ)                                   WOUT 044
 1002 FORMAT (10H       TT 0,2X,6F10.1)                                 WOUT 045
      WRITE(6,1003)( STPT0(I),I=LJ,JJ)                                  WOUT 046
 1003 FORMAT (10H       PT 0,2X,6F10.3)                                 WOUT 047
      WRITE(6,1004)( STALF(I),I=LJ,JJ)                                  WOUT 048
 1004 FORMAT (10H    ALPHA 0,2X,6F10.3)                                 WOUT 049
      WRITE(6,1005)(   STSI(I),I=LJ,JJ)                                 WOUT 050
 1005 FORMAT (10H  I STATOR,2X,6F10.3)                                  WOUT 051
      WRITE(6,1006)(   STV0(I),I=LJ,JJ)                                 WOUT 052
 1006 FORMAT (10H        V 0,2X,6F10.3)                                 WOUT 053
      WRITE(6,1007)( STVU0(I),I=LJ,JJ)                                  WOUT 054
 1007 FORMAT (10H       VU 0,2X,6F10.3)                                 WOUT 055
      WRITE(6,1008)( STVZ0(I),I=LJ,JJ)                                  WOUT 056
 1008 FORMAT (10H       VZ 0,2X,6F10.3)                                 WOUT 057
      WRITE(6,1009)( STTS0(I),I=LJ,JJ)                                  WOUT 058
 1009 FORMAT (10H       TS 0,2X,6F10.1)                                 WOUT 059
      WRITE(6,1010)( STPS0(I),I=LJ,JJ)                                  WOUT 060
 1010 FORMAT (10H       PS 0,2X,6F10.3)                                 WOUT 061
```

Listing of Code (continued)

```
      WRITE(6,1011)(STDENO(I),I=LJ,JJ)                                  WOUT 062
 1011 FORMAT (10H     DENS 0,2X,6F10.5)                                 WOUT 063
      WRITE(6,1012)(  STMO(I),I=LJ,JJ)                                  WOUT 064
 1012 FORMAT (10H        M 0,2X,6F10.5)                                 ********
      WRITE(6,1999)( CP0(K),I=LJ,JJ)                                    ********
 1999 FORMAT(10H       CP 0,2X,6F10.5)                                  ********
      WRITE(6,2000)(RV(1,K),I=LJ,JJ)                                    ********
 2000 FORMAT (10H       RG 0,2X,6F10.3)                                 ********
      WRITE(6,2001)(GAM(1,K),I=LJ,JJ)                                   ********
 2001 FORMAT (10H     GAMG 0,2X,6F10.5)                                 ********
      WRITE  (6,2002)(RWG(1,K),I=LJ,JJ)                                 ********
 2002 FORMAT (10H      RWG 0,2X,6F10.5)                                 ********
      IF(ISECT.LE.3)GO TO 11013                                         ********
      WRITE(6,2003)( STWG0(I),I=LJ,JJ),SFL00                            ********
 2003 FORMAT (10H       WG 0,2X,6F10.5,2X,11HTOTAL FLOW ,F10.5)         ********
11013 WRITE(6,1013)(STOP1(I),I=LJ,JJ)                                   ********
 1013 FORMAT(/5X5HSTA 12X11HSTATOR EXIT/4X6HDIAM 12X,6F10.3)            WOUT 067
      WRITE(6,1014)(STALFE(I),I=LJ,JJ)                                  WOUT 068
 1014 FORMAT (10H    ALPHA 1,2X,6F10.3)                                 WOUT 069
      WRITE(6,1015)(STDELA(I),I=LJ,JJ)                                  WOUT 070
 1015 FORMAT (10H      DEL A,2X,6F10.3)                                 WOUT 071
      WRITE(6,1016)(   STV1(I),I=LJ,JJ)                                 WOUT 072
 1016 FORMAT (10H        V 1,2X,6F10.3)                                 WOUT 073
      WRITE(6,1017)( STVU1(I),I=LJ,JJ)                                  WOUT 074
 1017 FORMAT (10H       VU 1,2X,6F10.3)                                 WOUT 075
      WRITE(6,1018)( STVZ1(I),I=LJ,JJ)                                  WOUT 076
 1018 FORMAT (10H       VZ 1,2X,6F10.3)                                 WOUT 077
      WRITE(6,1019)( STTS1(I),I=LJ,JJ)                                  WOUT 078
 1019 FORMAT (10H       TS 1,2X,6F10.1)                                 WOUT 079
      WRITE(6,1064)( STPS1(I),I=LJ,JJ)                                  WOUT 080
 1064 FORMAT (10H       PS 1,2X,6F10.3)                                 WOUT 081
      WRITE(6,1020)(STDEN1(I),I=LJ,JJ)                                  WOUT 082
 1020 FORMAT (10H     DENS 1,2X,6F10.5)                                 WOUT 083
      WRITE(6,1021)(   STM1(I),I=LJ,JJ)                                 WOUT 084
 1021 FORMAT (10H        M 1,2X,6F10.5)                                 WOUT 085
      WRITE(6,1022)(ZWIINC(I),I=LJ,JJ)                                  WOUT 086
 1022 FORMAT (10H   ZWI INC,2X,6F10.5)                                  ********
      WRITE(6,1026)(    CPS(I),I=LJ,JJ)                                 WOUT 088
 1026 FORMAT (10H       CP S,2X,6F10.5)                                 ********
      WRITE(6,2999)( CP1(K),I=LJ,JJ)                                    ********
 2999 FORMAT(10H       CP 1,2X,6F10.5)                                  ********
      WRITE(6,3000)(RV(2,K),I=LJ,JJ)                                    ********
 3000 FORMAT (10H       RG 1,2X,6F10.3)                                 ********
      WRITE(6,3001)(GAM(2,K),I=LJ,JJ)                                   ********
 3001 FORMAT (10H     GAMG 1,2X,6F10.5)                                 ********
      WRITE  (6,3002)(RWG(2,K),I=LJ,JJ)                                 ********
 3002 FORMAT (10H      RWG 1,2X,6F10.5)                                 ********
```

```
      IF(ISECT.LE.3)GO TO 11000                                          ********
      WRITE(6,3003)( STWG1(I),I=LJ,JJ),SFLO1                             ********
 3003 FORMAT (10H       WG 1,2X,6F10.5,2X,11HTOTAL FLOW ,F10.5)         ********
11000 WRITE(6,1000)NAME,TITLE,ICASE,ISCASE                               ********
      WRITE(6,1028)K,(STDP1A(I),I=LJ,JJ)                                 WOUT 091
 1028 FORMAT(4X6HSTA 1A2X11HROTOR INLET10X5HSTAGEI3,1H./3X7HDIAM 1A2X,  WOUT 092
     16F10.3)                                                            WOUT 093
      WRITE(6,1027)(STPTR1(I),I=LJ,JJ)                                   WOUT 094
 1027 FORMAT (10H      PTR 1A,2X,6F10.3)                                 WOUT 095
      WRITE(6,1029)(STTTR1(I),I=LJ,JJ)                                   WOUT 096
 1029 FORMAT (10H      TTR 1A,2X,6F10.1)                                 WOUT 097
      WRITE(6,1030)(STHET1(I),I=LJ,JJ)                                   WOUT 098
 1030 FORMAT (10H     BETA 1A,2X,6F10.3)                                 WOUT 099
      WRITE(6,1031)(  STRI(I),I=LJ,JJ)                                   WOUT 100
 1031 FORMAT (10H    I ROTOR,2X,6F10.3)                                  WOUT 101
      WRITE(6,1032)( STR1A(I),I=LJ,JJ)                                   WOUT 102
 1032 FORMAT (10H        R 1A,2X,6F10.3)                                 WOUT 103
      WRITE(6,1033)(STRU1A(I),I=LJ,JJ)                                   WOUT 104
 1033 FORMAT (10H       RU 1A,2X,6F10.3)                                 WOUT 105
      WRITE(6,1034)(STMR1A(I),I=LJ,JJ)                                   WOUT 106
 1034 FORMAT (10H       MR 1A,2X,6F10.5)                                 WOUT 107
      WRITE(6,1035)( STU1A(I),I=LJ,JJ)                                   WOUT 108
 1035 FORMAT (10H        U 1A,2X,6F10.3)                                 WOUT 109
      WRITE (6,2035)(STPS1A(I),I=LJ,JJ)                                  ********
 2035 FORMAT (10H       PS 1A,2X,6F10.3)                                 ********
      WRITE (6,2036)(STTS1A(I),I=LJ,JJ)                                  ********
 2036 FORMAT (10H       TS 1A,2X,6F10.1)                                 ********
      WRITE(6,3999)(CP1A(K),I=LJ,JJ)                                     ********
 3999 FORMAT(10H       CP 1A,2X,6F10.5)                                  ********
      WRITE(6,4000)(RV(3,K),I=LJ,JJ)                                     ********
 4000 FORMAT (10H       RG 1A,2X,6F10.3)                                 ********
      WRITE(6,4001)(GAM(3,K),I=LJ,JJ)                                    ********
 4001 FORMAT (10H     GAMG 1A,2X,6F10.5)                                 ********
      WRITE (6,4002)(RWG(3,K),I=LJ,JJ)                                   ********
 4002 FORMAT (10H      RWG 1A,2X,6F10.5)                                 ********
      IF(ISECT.LE.3)GO TO 11037                                          ********
      WRITE(6,4003)(STWG1A(I),I=LJ,JJ),SFLO1A                            ********
 4003 FORMAT (10H       WG 1A,2X,6F10.5,2X,11HTOTAL FLOW ,F10.5)        ********
11037 WRITE(6,1037)(STDP2(I),I=LJ,JJ)                                    ********
 1037 FORMAT(/5X5HSTA 22X10HROTOR EXIT/4X6HDIAM 22X,6F10.3)             WOUT 111
      IF(ISECT.LE.3)GO TO 11036                                          ********
      WRITE (6,2037)(STPTR2(I),I=LJ,JJ)                                  ********
 2037 FORMAT (10H      PTR 2,2X,6F10.3)                                  ********
      WRITE (6,2038)(STTTR2(I),I=LJ,JJ)                                  ********
 2038 FORMAT (10H      TTR 2,2X,6F10.1)                                  ********
11036 WRITE(6,1036)(STHET2(I),I=LJ,JJ)                                   ********
 1036 FORMAT (10H     BETA 2,2X,6F10.3)                                  WOUT 113
```

Listing of Code (continued)

```
      WRITE(6,1038)(SDBETA(I),I=LJ,JJ)                                  WOUT 114
1038  FORMAT (10H      DBETA,2X,6F10.3)                                 WOUT 115
      WRITE(6,1039)(   SR2(I),I=LJ,JJ)                                  WOUT 116
1039  FORMAT (10H      R 2,2X,6F10.3)                                   WOUT 117
      WRITE(6,1040)(  SRU2(I),I=LJ,JJ)                                  WOUT 118
1040  FORMAT (10H      RU 2,2X,6F10.3)                                  WOUT 119
      WRITE(6,1041)(  SMR2(I),I=LJ,JJ)                                  WOUT 120
1041  FORMAT (10H      MR 2,2X,6F10.5)                                  WOUT 121
      WRITE(6,1042)(   SU2(I),I=LJ,JJ)                                  WOUT 122
1042  FORMAT (10H       U 2,2X,6F10.3)                                  WOUT 123
      WRITE(6,1043)(    RX(I),I=LJ,JJ)                                  WOUT 124
1043  FORMAT (10H        RX,2X,6F10.5)                                  WOUT 125
      WRITE(6,1044)(STDELH(I),I=LJ,JJ)                                  WOUT 126
1044  FORMAT (10H      DELH,2X,6F10.3)                                  WOUT 127
      WRITE(6,1045)( STPSI(I),I=LJ,JJ)                                  WOUT 128
1045  FORMAT (10H     PSI P,2X,6F10.5)                                  WOUT 129
      WRITE(6,1046)(SETATT(I),I=LJ,JJ)                                  WOUT 130
1046  FORMAT (10H    ETA TT,2X,6F10.5)                                  WOUT 131
      WRITE(6,1047)(SETATS(I),I=LJ,JJ)                                  WOUT 132
1047  FORMAT (10H    ETA TS,2X,6F10.5)                                  WOUT 133
      WRITE(6,1048)(SETAAT(I),I=LJ,JJ)                                  WOUT 134
1048  FORMAT (10H    ETA AT,2X,6F10.5)                                  WOUT 135
      WRITE(6,1049)(RZWINC(I),I=LJ,JJ)                                  WOUT 136
1049  FORMAT (10H    ZWI INC,2X,6F10.5)                                 ********
      WRITE(6,1065)(   CPR(I),I=LJ,JJ)                                  WOUT 138
1065  FORMAT (10H      CP R,2X,6F10.5)                                  ********
      WRITE (6,2065)( STPS2(I),I=LJ,JJ)                                 ********
2065  FORMAT (10H      PS 2,2X,6F10.3)                                  ********
      WRITE (6,2066)( STTS2(I),I=LJ,JJ)                                 ********
2066  FORMAT (10H      TS 2,2X,6F10.1)                                  ********
      WRITE(6,4999)( CP2(K),I=LJ,JJ)                                    ********
4999  FORMAT(10H      CP 2,2X,6F10.5)                                   ********
      WRITE(6,5000)(RV(4,K),I=LJ,JJ)                                    ********
5000  FORMAT (10H      RG 2,2X,6F10.3)                                  ********
      WRITE(6,5001)(GAM(4,K),I=LJ,JJ)                                   ********
5001  FORMAT (10H    GAMG 2,2X,6F10.5)                                  ********
      WRITE (6,5002)(RWG(4,K),I=LJ,JJ)                                  ********
5002  FORMAT (10H     RWG 2,2X,6F10.5)                                  ********
      IF(ISECT.LE.3)GO TO 11053                                         ********
      WRITE(6,5003)( STWG2(I),I=LJ,JJ),SFLO2                            ********
5003  FORMAT (10H      WG 2,2X,6F10.5,2X,11HTOTAL FLOW ,F10.5)          ********
11053 WRITE(6,1053)( STPT2A(I),I=LJ,JJ)                                 WOUT 141
1053  FORMAT (10H     PT 2A,2X,6F10.3)                                  ********
      WRITE(6,1054)( STTT2A(I),I=LJ,JJ)                                 WOUT 143
1054  FORMAT (10H     TT 2A,2X,6F10.1)                                  ********
      WRITE(6,1055)( STV2A(I),I=LJ,JJ)                                  WOUT 145
1055  FORMAT (10H      V 2A,2X,6F10.3)
```

Listing of Code (continued)

```
      WRITE(6,1056)( STVU2A(I),I=LJ,JJ)                                         ********
 1056 FORMAT (10H      VU 2A,2X,6F10.3)                                         WOUT 147
      WRITE(6,1057)(STALF2(I),I=LJ,JJ)                                          WOUT 148
 1057 FORMAT (10H   ALPHA 2A,2X,6F10.3)                                         WOUT 149
      WRITE(6,1058)( STMF2A(I),I=LJ,JJ)                                         ********
 1058 FORMAT (10H      MF 2A,2X,6F10.5)                                         WOUT 151
      WRITE(6,1059)( STVZ2A(I),I=LJ,JJ)                                         ********
 1059 FORMAT (10H      VZ 2A,2X,6F10.3)                                         WOUT 153
      WRITE(6,1060)( STTS2A(I),I=LJ,JJ)                                         ********
 1060 FORMAT (10H      TS 2A,2X,6F10.1)                                         WOUT 155
      WRITE(6,1061)( STPS2A(I),I=LJ,JJ)                                         ********
 1061 FORMAT (10H      PS 2A,2X,6F10.3)                                         WOUT 157
      WRITE(6,1062)(STDEN2(I),I=LJ,JJ)                                          WOUT 158
 1062 FORMAT (10H    DENS 2A,2X,6F10.5)                                         WOUT 159
      WRITE(6,1063)(  STM2A(I),I=LJ,JJ)                                         ********
 1063 FORMAT (10H       M 2A,2X,6F10.5)                                         WOUT 161
      WRITE(6,5999)(CP2A(K),I=LJ,JJ)                                            ********
 5999 FORMAT(10H      CP 2A,2X,6F10.5)                                          ********
      WRITE(6,6000)(RV(5,K),I=LJ,JJ)                                            ********
 6000 FORMAT (10H      RG 2A,2X,6F10.3)                                         ********
      WRITE(6,6001)(GAM(5,K),I=LJ,JJ)                                           ********
 6001 FORMAT (10H    GAMG 2A,2X,6F10.5)                                         ********
      WRITE  (6,6002)(RWG(5,K),I=LJ,JJ)                                         ********
 6002 FORMAT (10H     RWG 2A,2X,6F10.5)                                         ********
      IF(ISECT.LE.3)GO TO 21000                                                 ********
      WRITE(6,6003)(STWG2A(I),I=LJ,JJ),SFLO2A                                   ********
 6003 FORMAT (10H      WG 2A,2X,6F10.5,2X,11HTOTAL FLOW ,F10.5)                 ********
21000 IF(SRFLAG) WRITE(6,20000)                                                 ********
20000 FORMAT(1H1,45H AN EXIT HAS BEEN MADE FROM SUBROUTINE WOUT    )            ********
      RETURN                                                                    WOUT 162
      END                                                                       WOUT 163
```

Listing of Code (continued)

```
      SUBROUTINE PHIM(EXI,ETA,TR,PR)                                    PHIM 001
CPHIM                                                                   PHIM 002
      LOGICAL PHEVER,SRFLAG                                             ********
      COMMON  SRFLAG                                                    ********
      IF(SRFLAG) WRITE(6,10000)                                         ********
10000 FORMAT(44H AN ENTRY HAS BEEN MADE IN SUBROUTINE PHIM  )           ********
      A = EXI-.5                                                        PHIM 003
      B = -(EXI+(1.-ETA)/2.)                                            PHIM 004
      C = ETA/2.                                                        PHIM 005
      X = (-B -SQRT(B**2 -4.*A*C))/(2.*A)                               PHIM 006
      TR = ETA/(ETA-X)                                                  PHIM 007
      PH = TR**EXI                                                      PHIM 008
      IF(SRFLAG) WRITE(6,20000)                                         ********
20000 FORMAT(45H AN EXIT HAS BEEN MADE FROM SUBROUTINE PHIM   )         ********
      RETURN                                                            PHIM 009
      END                                                               PHIM 010
```

APPENDIX 2.3C
CONTROL CARDS FOR WANL CDC-6600 COMPUTER

A. Control Cards for FORTRAN Deck Setup

	Example
JØB Card	JØB , 10.
Account Number Card	AS77987.
ID Card	ASD1097, TURBIN, 120, 75000, 01.
RUN Card	RUN (P,,,,,, 14000)
LØC Card*	LØC, 75000.
LGØ Card	LGØ .
End-of-Record Card	7/8/9
FORTRAN Deck	PRØGRAM JIM ....
, ,	, ,
, ,	, ,
, ,	, ,
, ,	, ,
, ,	, ,
, ,	, ,
, ,	END
End-of-Record Card	7/8/9
End-of-Record Card	7/8/9
Data Deck	FALSE
,	,
,	,
,	,
,	,
,	,
,	,
,	,
	ENDJØB = 1.0 $
End-of-File Card	6/7/8/9

B. Control Cards for Binary Deck Setup

	Example
JØB Card	JØB, 10.
Account Number Card	AS77987.
ID Card	ASD1097, TURBIN, 120, 7500, 01.
LØC Card	LØC, 75000.
LØAD Card	LØAD (INPUT)
EXECUTE Card	EXECUTE.
End-of-Record Card	7/8/9
End-of-Record Card	7/8/9
Binary Deck	Binary Cards
,	,
,	,
,	,
,	,
,	,
End-of-Record Card	7/8/9
End-of-Record Card	7/8/9
Data Deck	Data Cards
,	,
,	,
,	,
,	,
,	,
	ENDJØB = 1.0 $
End-of-File Card	6/7/8/9

* The LØC card is required to initialize the core to zero before compilation and execution.

2.4 BLADE SURFACE VELOCITY CALCULATIONS*

2.4.1 Background

As a part of the Westinghouse Astronuclear Laboratory analytical investigation of turbine erosion phenomena, calculations are made in the various areas of turbine flow. These procedures include the present calculation to determine the velocity distribution along the suction and pressure side of the turbine blades. Surface velocities from this calculation are then used as input to the AD-ROP code discussed in Section 2.6.

The purpose of this report is to show how the computer program was used in performing the calculation for the G.E. blade and to compare the results of this calculation with those by other methods. Comments on the use of this program extend the detailed account to include: the modifications for the CDC 6400 machine, the input and output for the G.E. blade calculation, and additional comment on the features of the program.

2.4.2 Calculation of G. E. Blade

Calculations were made on the 3rd stage stator blade, mean diameter section, for the G.E., 3 stage potassium turbine. This blade section, shown in Figure 2.4.2-1 is reproduced from Figure 11 of Reference 2.

Input

The input to the calculation is given by Table 2.4.2-1. Its format is identical to that in Reference 1. The input data are identified by the Figure 2.4.2-2 sketch and by the Description of Input in Reference 1. Note that all linear dimensions given by Table 2.4.2-1 and Figure 2.4.2-2 are ten times the actual blade size.

*W. K. Fentress, Fellow Engineer, Development Engineering Department, Westinghouse Steam Divisions, Westinghouse Electric Corp., Lester, Pa.

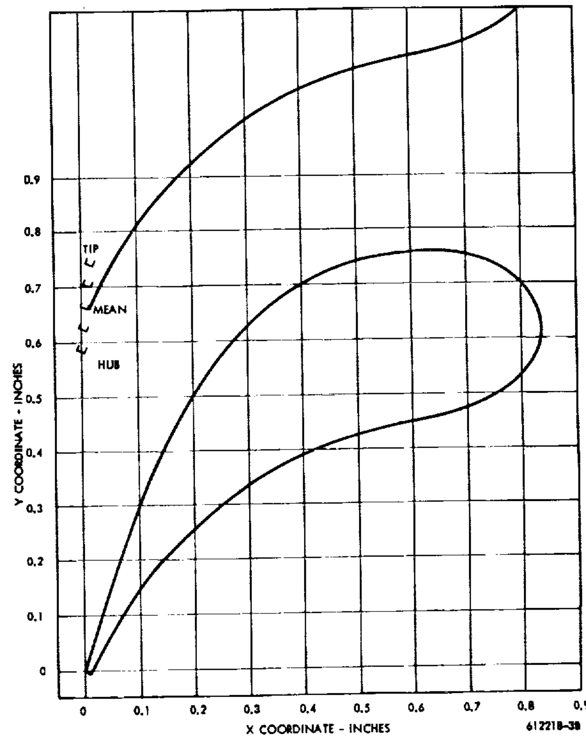

Figure 2.4.2-1 Third Stage Nozzle Mean Section

TABLE 2.4.2-1

INPUT

```
1          11         21         31         41         51         61         71
  PITCH      CHORD      STGR      THETAI     THETAO     DTLR

  6.67       8.37      -6.19      28.2      -68.9      .0005
   RI        ALUI       ALLI       RO        ALUO       ALLO
 1.09       46.0      -37.3       .03
  .6         .16        .26        .36      -72.9      -61.4
MXBI  MXBO   MX   NBBI  NUSP  NLSP  NINT

 30   60     90   25    19    10    6
ZU ARRAY

           1.43       2.61       3.81       5.07       6.10       7.09       7.72


XSPU ARRAY

           1.36       1.405      1.12       .39       -.78       -2.6       -4.17


ZL ARRAY

           1.35       2.01       2.83       3.80       4.99       5.98       6.99

 7.78
XSPL ARRAY

           5.33       5.11       4.95       4.69       4.10       3.43       2.49

 1.39
BLDATANULAKIERPRT STRFN SLCRD SLPLT ARPRT INTVELSURVEL

 1     0     1     1     1     0     1     1     1
 W           WR          TOLER       BDA         BDD

 1.6         .01         .0001       .63         3.2
```

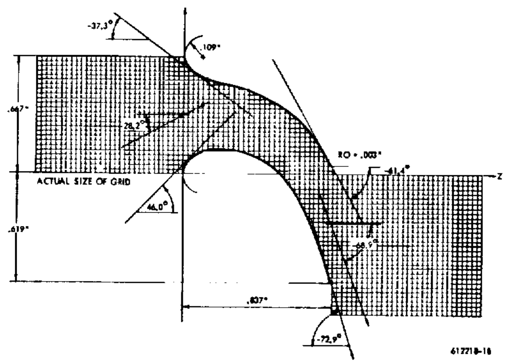

Figure 2.4.2-2 Geometric Data for the G. E. Blade

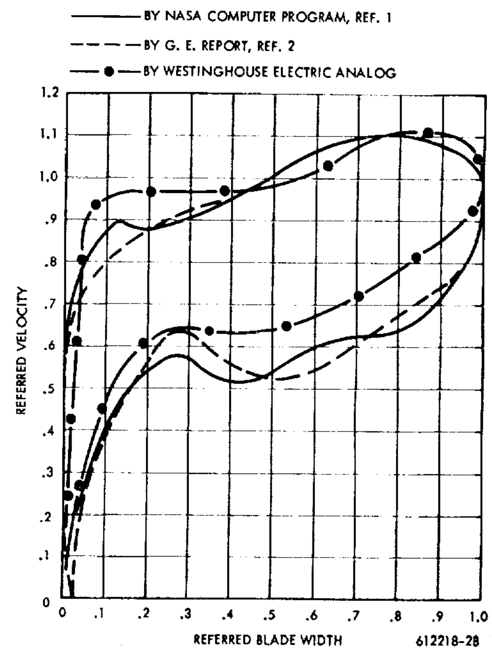

Figure 2.4.2-3 Surface Velocities Computed for the G. E. Blade

Listing

The program is the same as listed in Reference 1 save for minor mechanical changes to allow for the use of the program on the CDC 6400 machine. For the most part, these changes are in the format statements and in the indexing for the arrays listed in the Equivalence Statements; e.g., variables such as A(2500,4) were changed to equivalent statements involving single indices. The original program used a computer system-dependent plotting package which has been eliminated by deleting reference to subroutine PLOTMY.

Output

A considerable amount of printout is generated by the program; for the present calculation only a small portion is pertinent. In Reference 1 the items of output are identified by item numbers 1 to 12. Items 4 and 5 are all that is necessary to construct the blade surface velocity curve, Figure 2.4.2-3. Output Item 4 gives the computed velocities at interior mesh points.

A sample of the latter is given in Table 2.4.2-2. The quantity IA refers to the axial coordinate index; thus at IA = 90 the free stream velocities across the exit plane of the blade section are given and at IA = 1 the inlet plane velocities are given. In the given problem the approximate average exit velocity is 0.4165 and the average inlet velocity is 0.170.

Item 5 gives the calculated surface velocities based on axial and tangential components. Thus, the referred velocity, with respect to the exit velocity is the ratio of the Item 5.surface velocity to 0.4165. Note that the value of velocity at the inlet and exit of the blade, corresponding to $Z \approx 0$ and $Z = 8.37$, are taken as 0.170 and 0.4165 in constructing the velocity curve (Figure 2.4.2-3). The referred length, with respect to the axial length of the blade, is the ratio of Z to 8.37. A sample of Item 5 output is given in Table 2.4.2-3.

2.4.3 Discussion

The following discusses the use of the program and compares the calculation results with those by other methods.

TABLE 2.4.2-2

SAMPLE OF ITEM 4 OUTPUT

```
IA=88   VELOCITY    ANGLE(DEG)   VELOCITY    ANGLE(DEG)   VELOCITY    ANGLE(DEG)   VELOCITY    ANGLE(DEG)   VELOCITY    ANGLE(DEG)
        4.1646-001  -68.89       4.1646-001  -68.90       4.1644-001  -68.90       4.1645-001  -68.90       4.1645-001  -68.90
        4.1645-001  -68.90       4.1645-001  -68.90       4.1646-001  -68.90       4.1646-001  -68.90       4.1646-001  -68.90
        4.1646-001  -68.90       4.1646-001  -68.90       4.1646-001  -68.90       4.1646-001  -68.90       4.1646-001  -68.90
        4.1646-001  -68.90       4.1646-001  -68.90       4.1645-001  -68.90       4.1645-001  -68.90       4.1645-001  -68.90
        4.1644-001  -68.90       4.1644-001  -68.90       4.1644-001  -68.90       4.1644-001  -68.90       4.1644-001  -68.90
        4.1643-001  -68.90
IA=89   VELOCITY    ANGLE(DEG)   VELOCITY    ANGLE(DEG)   VELOCITY    ANGLE(DEG)   VELOCITY    ANGLE(DEG)   VELOCITY    ANGLE(DEG)
        4.1648-001  -68.89       4.1647-001  -68.90       4.1646-001  -68.90       4.1646-001  -68.90       4.1646-001  -68.90
        4.1646-001  -68.90       4.1646-001  -68.90       4.1647-001  -68.90       4.1647-001  -68.90       4.1647-001  -68.90
        4.1647-001  -68.90       4.1647-001  -68.90       4.1647-001  -68.90       4.1647-001  -68.90       4.1647-001  -68.90
        4.1647-001  -68.90       4.1647-001  -68.90       4.1647-001  -68.90       4.1647-001  -68.90       4.1647-001  -68.90
        4.1646-001  -68.90       4.1646-001  -68.90       4.1646-001  -68.90       4.1646-001  -68.90       4.1646-001  -68.90
        4.1645-001  -68.91
IA=90   VELOCITY    ANGLE(DEG)   VELOCITY    ANGLE(DEG)   VELOCITY    ANGLE(DEG)   VELOCITY    ANGLE(DEG)   VELOCITY    ANGLE(DEG)
        4.1649-001  -68.90       4.1649-001  -68.90       4.1647-001  -68.90       4.1647-001  -68.90       4.1647-001  -68.90
        4.1647-001  -68.90       4.1647-001  -68.90       4.1647-001  -68.90       4.1647-001  -68.90       4.1648-001  -68.90
        4.1648-001  -68.90       4.1648-001  -68.90       4.1648-001  -68.90       4.1648-001  -68.90       4.1648-001  -68.90
        4.1648-001  -68.90       4.1648-001  -68.90       4.1648-001  -68.90       4.1648-001  -68.90       4.1648-001  -68.90
        4.1648-001  -68.90       4.1648-001  -68.90       4.1647-001  -68.90       4.1647-001  -68.90       4.1647-001  -68.90
        4.1646-001  -68.91
```

Program

Machine time for the blade calculation was approximately 2 minutes with the CDC 6400 machine. This is in line with a tolerance of 10^{-4}(TOLER), an assumed overrelaxation factor (ω) of 1.6, and 2006 mesh points. The tolerance is with respect to the maximum change in stream function in successive iterations, specified by the Item 8 printout as ERROR.

From the printout of ERROR it is evident that the number of iterations increases with decrease in tolerance (ERROR); e.g., 6, 30, 43 and 380 iterations for $1. \times 10^{-2}$, $1. \times 10^{-3}$, $6. \times 10^{-4}$, and $1. \times 10^{-4}$ tolerance. Here there is a very large increase in the number of iterations between 6. and $1. \times 10^{-4}$ tolerance, but this is consistent with the use of a factor (ω) of 1.6 in the calculation. It is shown by the following comparison, with other calculations for the same data, that the choice of the factor has a noticeable effect on the number of iterations, particularly in the region of close tolerance.

Factor	Number of Iterations					
	$1. \times 10^{-2}$ Tolerance	$1. \times 10^{-3}$ Tolerance	$6. \times 10^{-4}$ Tolerance	$1. \times 10^{-4}$ Tolerance	$2. \times 10^{-5}$ Tolerance	$1. \times 10^{-5}$ Tolerance
1.949	45	105	106	157	199	213
1.90	24	75	88	---	---	---
1.80	12	40	86	---	---	---
1.70	7	30	46	---	---	---
1.60	6	30	43	380	718	---
1.50	6	30	43	---	---	---
1.40	5	31	44	---	---	---

Note that (ω) = 1.949, the optimum factor computed by subroutine SOR, requires less iterations at close tolerance, but generally requires a greater number of iterations at coarse tolerance. Thus the "optimum" factor is only optimum for a large number of iterations, i.e., for close tolerance.

It is probable that a tolerance of 5. to $1. \times 10^{-4}$ is sufficiently close for most calculations based on the following check. Here calculations were made with 10^{-2}, 10^{-3}, 10^{-4}, and 10^{-5} tolerance and, while the velocity plot for 10^{-2} tolerance was noticeably different in the region of the leading edge, there was very little change with respect to 10^{-3} and 10^{-5} and no visible change with respect to 10^{-4} and 10^{-5} tolerance.

Actually, several features of the program are not clearly explained by Reference 1.

a) Solution of the Laplace Equation

Referring to Figures 4 and 5 of Reference 1: To solve the Laplace equation it is evident that the boundary conditions must be fully defined. Hence, as the boundary conditions are only defined, explicitly, along the upper and lower blade surface, it is probable that the stream function is specified along the other boundary surfaces by a process of interpolation based on: the stream function at points B, G, C and F, Q_{in} and Q_{out}, and the assumption (certainly in the first approximation) that the inlet and outlet stagnation streamline is straight.

TABLE 2.4.2-3

SAMPLE OF ITEM 5 OUTPUT

SURFACE VELOCITIES BASED ON AXIAL COMPONENTS

	UPPER SURFACE			LOWER SURFACE		
Z	VELOCITY	ANGLE (DEG)	WZ	VELOCITY	ANGLE (DEG)	WZ
-2.6921-010	0.0000+000	90.00	1.7583-003	0.0000+000	-90.00	-1.2521-002
2.7900-001	3.2218-001	48.08	2.1526-001	6.9851-002	-49.75	4.6670-002
5.5800-001	3.4315-001	37.34	2.7281-001	1.3167-001	-34.91	1.0950-001
8.3700-001	3.6507-001	27.42	3.2405-001	1.6791-001	-27.91	1.4965-001
1.1160+000	3.7321-001	18.52	3.5387-001	1.8830-001	-23.16	1.7412-001
1.3950+000	3.6616-001	11.95	3.5622-001	2.0514-001	-21.29	1.9206-001
1.6740+000	3.6858-001	7.29	3.6559-001	2.2354-001	-19.50	2.1156-001
1.9530+000	3.7183-001	2.92	3.7135-001	2.3912-001	-16.06	2.3040-001
2.2320+000	3.7490-001	-1.13	3.7483-001	2.3903-001	-12.08	2.3408-001
2.5110+000	3.7798-001	-4.81	3.7665-001	2.3421-001	-10.25	2.3072-001
2.7900+000	3.8206-001	-8.18	3.7617-001	2.2646-001	-10.73	2.2277-001
3.0690+000	3.8717-001	-11.57	3.7930-001	2.2082-001	-12.88	2.1562-001
3.3480+000	3.9607-001	-14.97	3.8263-001	2.1754-001	-15.59	2.1006-001
3.6270+000	4.0210-001	-18.35	3.8165-001	2.1758-001	-18.78	2.0676-001
3.9060+000	4.0934-001	-21.73	3.8025-001	2.1974-001	-22.32	2.0436-001
4.1850+000	4.2240-001	-25.57	3.8103-001	2.2646-001	-25.50	2.0583-001
4.4640+000	4.3070-001	-29.88	3.7345-001	2.3206-001	-28.18	2.0714-001
4.7430+000	4.4052-001	-34.48	3.6314-001	2.4144-001	-30.41	2.1039-001
5.0220+000	4.4678-001	-39.18	3.4631-001	2.4773-001	-32.22	2.1206-001
5.3010+000	4.5055-001	-43.84	3.2499-001	2.5375-001	-33.96	2.1326-001
5.5800+000	4.5271-001	-48.31	3.0109-001	2.5862-001	-35.83	2.1283-001
5.8590+000	4.5407-001	-52.50	2.7643-001	2.6161-001	-37.80	2.1023-001
6.1380+000	4.5300-001	-56.33	2.5118-001	2.6363-001	-40.01	2.0588-001
6.4170+000	4.5380-001	-59.62	2.2947-001	2.6534-001	-43.05	1.9844-001
6.6960+000	4.5361-001	-62.40	2.1018-001	2.6955-001	-46.76	1.8999-001
6.9750+000	4.5399-001	-64.75	1.9365-001	2.7787-001	-50.86	1.8177-001
7.2540+000	4.5320-001	-66.86	1.7613-001	2.9144-001	-54.70	1.7598-001
7.5330+000	4.5234-001	-69.05	1.6173-001	3.0919-001	-57.85	1.7333-001
7.8120+000	4.4295-001	-71.17	1.4298-001	3.1740-001	-60.47	1.6639-001
8.0910+000	4.2696-001	-72.44	1.2283-001	3.4152-001	-62.43	1.6907-001
8.3700+000	0.0000+000	-90.00	1.1023-001	0.0000+000	90.00	6.4765-002

SURFACE VELOCITIES BASED ON TANGENTIAL COMPONENTS

UPPER SURFACE				LOWER SURFACE			
Z	VELOCITY	ANGLE (DEG)	WX	Z	VELOCITY	ANGLE (DEG)	WX
-2.6921-010	1.5396-001	90.00	1.5396-001	3.3200-002	8.2697-002	-75.82	8.0178-002
3.3200-002	2.3652-001	75.82	2.2932-001	1.3965-001	4.8237-003	-60.68	4.2057-003
1.3965-001	2.8998-001	60.68	2.5283-001	3.5022-001	8.5141-002	-42.74	-5.7785-002
3.4871-001	3.2046-001	44.59	2.2498-001	7.3531-001	1.5217-001	-29.23	-7.4307-002
6.7758-001	3.5449-001	33.06	1.9339-001	1.3342+000	1.9768-001	-20.75	-7.0033-002
1.3123+000	3.8710-001	13.60	9.1020-002	2.1824+000	2.5271-001	-12.22	-5.3483-002
3.0690+000	4.0588-001	-11.57	-8.1419-002	3.4578+000	2.1587-001	-16.22	-6.0314-002
3.9447+000	4.2174-001	-22.23	-1.5954-001	4.1731+000	2.2115-001	-24.52	-9.1784-002
4.4880+000	4.4052-001	-30.27	-2.2203-001	4.6981+000	2.3675-001	-29.06	-1.1500-001
4.8891+000	4.4555-001	-36.94	-2.6778-001	5.1504+000	2.4942-001	-31.89	-1.3176-001
5.2107+000	4.4937-001	-42.34	-3.0268-001	5.5587+000	2.5649-001	-34.48	-1.4519-001
5.4813+000	4.5124-001	-46.76	-3.2870-001	5.9294+000	2.6221-001	-37.02	-1.5787-001
5.7163+000	4.5181-001	-50.40	-3.4611-001	6.2663+000	2.6407-001	-39.91	-1.6942-001
5.9251+000	4.5178-001	-53.44	-3.6288-001	6.5664+000	2.6684-001	-43.45	-1.8352-001
6.1138+000	4.5254-001	-56.01	-3.7522-001	6.8308+000	2.7265-001	-47.07	-1.9962-001
6.2862+000	4.5146-001	-58.15	-3.8348-001	7.0646+000	2.8178-001	-50.42	-2.1717-001
6.4461+000	4.5099-001	-59.94	-3.9032-001	7.2746+000	2.9323-001	-53.10	-2.3450-001
6.5958+000	4.5165-001	-61.45	-3.9675-001	7.4671+000	3.0367-001	-55.23	-2.4946-001
6.7369+000	4.5149-001	-62.77	-4.0139-001	7.6461+000	3.1523-001	-56.98	-2.6432-001
6.8708+000	4.5208-001	-63.92	-4.0603-001	7.8145+000	3.3101-001	-58.45	-2.8207-001
6.9984+000	4.5188-001	-64.93	-4.0931-001	7.9745+000	3.3509-001	-59.62	-2.8907-001
7.1206+000	4.5231-001	-65.84	-4.1270-001	8.1280+000	3.4303-001	-60.53	-2.9664-001
7.2378+000	4.5286-001	-66.73	-4.1603-001	8.2764+000	3.4797-001	-61.24	-3.0505-001
7.3502+000	4.5209-001	-67.60	-4.1799-001				
7.4577+000	4.5124-001	-68.45	-4.1971-001				
7.5608+000	4.4892-001	-69.27	-4.1986-001				
7.6598+000	4.4687-001	-70.05	-4.2006-001				
7.7547+000	4.4358-001	-70.78	-4.1665-001				
7.8460+000	4.3844-001	-71.38	-4.1549-001				
7.9347+000	4.3403-001	-71.84	-4.1242-001				
8.0213+000	4.2943-001	-72.21	-4.0689-001				
8.1061+000	4.2376-001	-72.48	-4.0411-001				
8.1898+000	4.1867-001	-72.68	-3.9970-001				
8.2726+000	4.1344-001	-72.82	-3.9499-001				
8.3549+000	4.1539-001	-72.89	-3.9702-001				
8.3700+000	3.8802-001	-90.00	-3.8602-001				

b) Inlet Stagnation Point

Points B and G (Figure 2 of Reference 1) are at the inlet extremity with respect to the axial direction and, by the numerical treatment, the velocity is zero at both of these points. This does not consider that the location of the stagnation point depends on the angle of incidence and, with large incidence can deviate from point B by a notable amount. It appears that the effect of this approximation is to displace the upper and lower velocity curves in the region of the blade inlet, but without affecting the velocity curve downstream of the leading edge region.

The surface velocity plot, Figure 2.4.2-3, compares the calculation results for the G.E. blade with those by the G. E. report (Reference 2) and with those by the Westinghouse Electric analog. From the general agreement, it appears that the calculation is sufficiently accurate for its intended use in the boundary layer calculation.

2.4.4 Conclusions

The NASA computer program (Reference 1) specifies the blade surface velocity with sufficient accuracy for its intended use in the boundary layer calculation. This is shown by comparing the calculation results with those by two other methods of calculation (Figure 2.4.2.3).

2.4.5 References

1. A Computer Program for Calculating Velocities and Streamlines for Two-Dimensional, Incompressible Flow in Axial Blade Rows - Theodore Katsanis - NASA TN D-3762 January 1967.

2. Three Stage Potassium Test Turbine, Final Design, Vol. 1, Third Design - R. J. Rossbach, et al - NASA CR 72249.

2.5 COLLECTION OF CONDENSATE AND MOVEMENT OF CONDENSATE ON TURBINE SURFACES *

2.5.1 Nomenclature for Section 2.5

A	Shear profile empirical constant
A_1, A_3	Blade geometric constants
a	Condensate fog particle deposition constant for blade concave surface
B	Shear profile empirical constant
b	Condensate fog particle deposition constant for blade nose
C_D	Fog particle drag coefficient
C_f	Wall friction drag coefficient, stator blade surface drag coefficient
d	Drop diameter, feet or microns
D	Turbine housing inside diameter, inches
E	Condensate particle collection efficiency
F	Indicates relationship between variables
F	Centrifugal force on liquid film on rotor blades - lb
g_n	A function of K_{cn}
G	Mass velocity of vapor, lb/hr-ft^2

* W. K. Fentress, Fellow Engineer, Development Engineering Dept., Steam Divisions, Westinghouse Electric Corp., Lester, Pa.; J. W. H. Chi, Fellow Engineer, Systems & Technology Dept., Astronuclear Laboratory, Westinghouse Electric Corp., Pittsburgh, Pa. 15236; W. D. Pouchot, Advisory Engineer, Systems & Technology Dept., Astronuclear Laboratory, Westinghouse Electric Corp., Pittsburgh, Pa. 15236.

h Blade height, ft.

K_{cc} Condensate fog particle inertial impaction parameter for collection on concave surface of blades

K_{cn} Condensate fog particle inertial impaction parameter for collection on nose of blades

K_n Knudsen No. based on condensate fog particle radius

L Blade nose radius, ft

L Mass velocity of collected condensate, $lb/hr\text{-}ft^2$

ℓ_b Length of blade in radial direction, hub to tip

$\dot{m}_L$ Mass flow rate per unit of casing periphery or per blade, slugs/sec-ft, or mass flow rate - slugs/sec

m Total turbine mass flow rate, lb/sec

N_b Number of blades

$N_{re,v}$ Vapor Reynolds No.

P_{cc} Portion of condensate fog particles collected on concave surface of blades in a given row

P_{cn} Portion of condensate fog particles collected on nose of blade in a given row

q_b Liquid from condensate fog particles collected by a representative blade in a blade row per unit of blade height, lb/sec/ft.

Q_ℓ, Q_L Total liquid collected by a given blade row in the form of bulk flow condensate fog particles, lb/sec.

$Q_L{}^+$ Dimensionless liquid film flow rate :

$$\frac{\delta\, U_L}{\nu}$$

r Average condensate fog particle radius, microns or ft

R Gas Constant, $ft/lb\text{-}^{o}R$

Re Condensate particle Reynolds Number

R_o Pipe or channel equivalent radius, ft or inches

S Pitch (spacing of blades around turbine periphery) of blades in a row, ft

T Absolute temperature, ^{o}R

Va Bulk flow axial flow velocity - ft/sec

U_L Mean longitudinal velocity of collected film, ft/sec

$U_v{}'$ Bulk flow velocity relative to casing, ft/sec

U_t Bulk flow tangential velocity - ft/sec

U^* Friction velocity, ft/sec = $\sqrt{\tau_s/\rho}$

U Liquid film velocity on stator or rotor blades

V_a Condensate particle axial flow velocity, ft/sec

V_r Bulk flow velocity relative to blades at inlet of blade row, ft/sec

V_t Condensate particle tangential velocity - ft/sec

W Width of blade row in axial direction from inlet to exit, ft

W_L Liquid flow rate, lb/sec, slugs/sec

ζ_v Average quality of vapor in a blade row

X Circumference of turbine casing or axial distance, or geometric coordinate - ft/in.

Y Geometric coordinate - ft

Y_ℓ Average fraction of mixture flow as condensate fog particles

Z Axial width of blade measured along blade surface - ft, in.

$\not{g}$ Blade geometry parameter, ft

α_i Angle between normal to turbine axis and stator inlet velocity vector, degrees

δ Condensate film thickness, inches, mils, or feet

$\delta+$ Film parameter = U*/U

ζ Inlet width of concave surface capture curve - ft

λ A density parameter, dimensionless

μ_v Viscosity of vapor, lb/ft-sec or (lb-sec)/ft^2

μ_L, μ Viscosity of liquid,lb/ft-sec or lb-sec/ft^2

ν Kinematic viscosity, μ/ρ , ft^2/sec

ρ Mixture bulk flow density, lb/ft^3 or slugs/ft^3

ρ_ℓ ρ_L Working fluid density as a liquid, lb/ft^3 or slugs/ft^3

ρ_v ρ_G Working fluid density as a vapor, lb/ft^3 or slugs/ft^3

τ_s Wall friction drag per unit area, lb/ft^2

σ Surface tension, lb/ft

$\varphi, \varphi_1, \varphi_2$ Indicates relationship

ψ Surface tension parameter

ω Rotor rotative speed - radius/sec

2.5.2 Deposition of Moisture on the Surface of Blades

• Single Row Collection

When the moisture in the bulk flow is in the form of small spontaneously formed condensate particles (as in steam or alkali metal vapor turbines), the mechanism of deposition of moisture on blade surfaces is considered to be that of inertial impaction based on the macroscopic application of the laws of motion. In this we have followed Gyarmathy[1]. While deposition by diffusion of particles (Brownian motion and/or eddy diffusion) is recognized as a possible factor, inertial impaction is thought to warrant first consideration. Even between inertial impaction calculations, as between Gyarmathy and Brun et al[2], there is substantial difference in numerical values which we have been unable to resolve.

The inertial deposition of moisture is considered to be principally on the inlet edge (nose) of the blades and on the concave face of the blades. Therefore by definition the inertial deposition on a single row of blades may be written as:

$$Q_\ell = m\, Y_\ell \left(P_{cn} + P_{cc}\right)$$

• Deposition on the Inlet Edge of the Blades

The analysis considers the nose of the blade as a circular cylinder. Thus the impingement of moisture particles is specified by the path of the particles when acted upon by the potential flow about a circular cylinder.

The path and impingement of particles with respect to circular cylinders, based on two-dimensional trajectory calculations and suitable drag coefficients, is given in a number of reports. In addition to Gyarmathy[1] NACA Report 1215 by Brun, et al[2], for example. In the Brun report the data are shown by a non-dimensional plot in terms of the conventional inertia parameter (K), a Reynolds Number parameter, and the collection efficiency. (Collection efficiency is the ratio of the width of the free stream capture stream tube, within which all particles strike the cylinder, to the diameter of the cylinder).

In symbolic terms the efficiency of collection may be written:

$$E = \frac{2\,L}{2\,L'} = \varphi(K_{cn}) = \varphi(K, Re) = \varphi\left(\left(\frac{2\,\rho_L\, r^2 V_r}{9\,\mu_v\, 2\,L}\right), Re\right) \quad (1)$$

or in the Stokes Law region applicable to these miniature moisture drops:

$$E = \varphi\left(\left(\frac{24}{C_D\,Re}\right)\left(\frac{2\rho_L\, r^2 V_r}{9\,\mu_v\, 2\,L}\right)\right) \quad (2)$$

As the flow about the miniature moisture drops is often in the slip flow regime, it is necessary to correct this formulation for the reduction in drag due to slip flow. Correction is made by multiplying the continuum value of the inertia parameter by the ratio ($C_{D,\text{slip flow}}/C_D$) where C_D is the conventional drag coefficient for continuum flow. This correction is specified by an empirical expression in terms of Knudsen Number. As shown in Figure 2.5.2-1,

Gyarmathy's expression, $\dfrac{C_{D,\text{ slip flow}}}{C_D} = \dfrac{1}{1 + 2.53\,K_n}$,

is a simple approximation to the more complicated Emmons[3] expression. As shown also by this curve, the drag on 0.4 micron radius drops under Yankee turbine conditions is only 45% of the continuum drag. In fact, the drag on particles will only approach continuum values at approximately 15 microns or greater radius.

Making the slip flow correction to equation 2 and observing that in the Stokes flow regime that $\dfrac{24}{C_D\;Re} = 1$. yields:

$$E = \varphi\;(1 + 2.53\,K_n)\left(\frac{2\,\rho_L\, r^2 V_r}{9\,\mu_r\, 2\,L}\right) \quad (3)$$

By use of the relationship of equation 3, as established in numerical terms by Gyarmathy or Brun et al, the collection efficiency for the nose sections of a turbine row can be calculated. Collection efficiencies have been calculated for the noses of the ninth stator blade row, 3/4 blade height position of the Yankee steam turbine, and are shown in Figure 2.5.2-2. As can be seen the data of Gyarmathy predicts higher collection efficiencies than that of Brun et al.

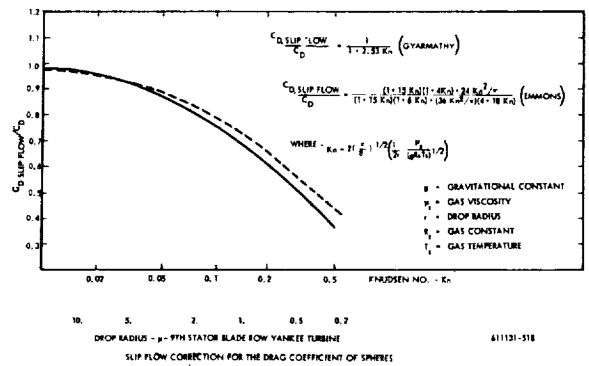

Figure 2.5.2-1 Knudsen Number Corrections

This difference cannot be explained by the fact that the Brun, et al, data account for the increase in Stokes law drag with Reynolds Number, as in this instance the fluid properties are nearly coincident with the Brun curve for zero Reynolds Number. Possibly, the difference could be explained by differences in trajectory calculation, but this calculation is not qualified in Gyarmathy's report.

The portion of the total number of condensate particles in the total flow which are collected by the noses of the blades of a given turbine row is given from simple geometric considerations, as indicated in Figure 2.5.2-3 as:

$$P_{cn} = \frac{2\,L'}{S\,\sin\alpha_i} = \frac{2\,L\,E}{S\,\sin\alpha_i} \quad (4)$$

Figure 2.5.2-3 also gives the calculated portion collected by the ninth stator noses of the Yankee turbine. It will be noted that the portion of the total drops collected by the noses of the blades of a row cannot exceed $2L/S \sin\alpha_i$.

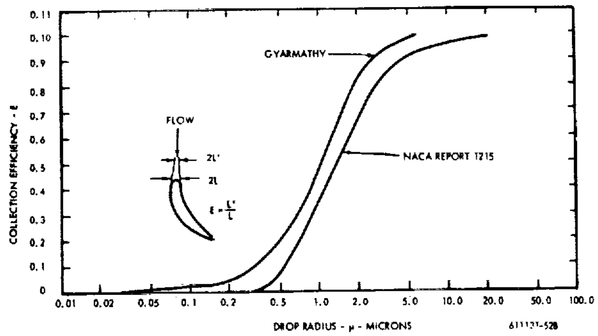

Figure 2.5.2-2 Collection Efficiency Ninth Stage Stator Nose Yankee Turbine

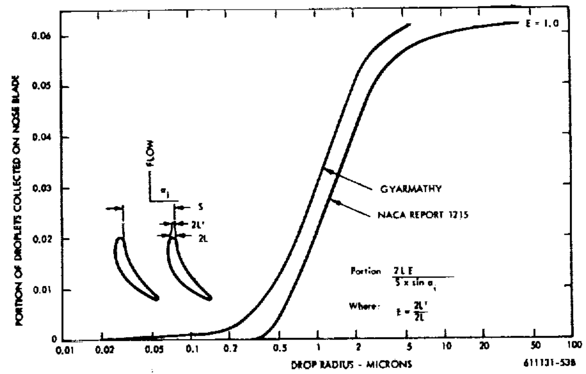

Figure 2.5.2-3 Portion Collected Ninth Stage Stator Nose Yankee Turbine

• <u>Deposition of Moisture on the Concave Face of the Blade</u>

Generally, the analysis is performed along the lines of Gyarmathy's [1] approach. The contour of the blade surface is approximated by a polynomial expression. The path of the vapor corresponds to the blade contour and the path of the particles, acted upon by the drag of the vapor, is calculated by trajectory equations. The drag on the particles is by Stokes law with correction for slip flow. By simplifying assumptions of constant vapor velocity with respect to the distance between blades and equal and constant moisture-particle axial velocity, the particle acceleration is described by a linear differential equation. By further assumptions as to boundary conditions, the integrated equation gives the width of the band at the blade inlet, within which all moisture particles impinged on the blade surface. Finally, the ratio of band width to the space between blades gives the amount of the collection with respect to the total moisture approaching the blades.

Thus, by the above assumptions, the collection of moisture is specified by closed form calculation. The detail derivation follows:

The concave surface of the blade is approximated by the third degree polynomial (see Figure 2.5.2-4)

$$F\ (x) = A_1 X + A_3\ X^3 \qquad (1)$$

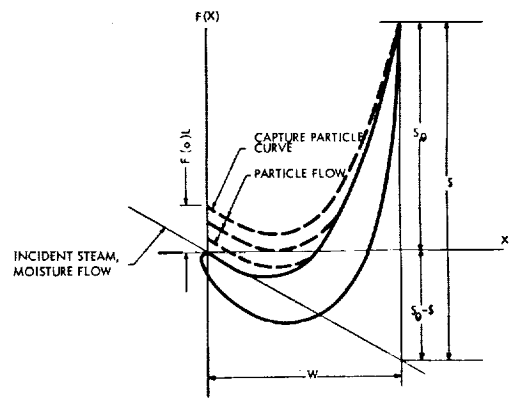

Figure 2.5.2-4 Collection of Moisture on the Concave Side of the Blade

The coefficients are specified by the inlet angle and the exit point as:

$$F'\ (o) = A_1 = (S_\theta - \not{S})\ /W \qquad (2)$$

$$F\ (W) = S_\theta - \not{S} + A_3\ W^3 = S_\theta\ ;\ A_3 = \not{S}/W^3 \qquad (3)$$

Assume that the path of the steam is the same as the blade surface shape; then, the path and direction of the steam flow is:

$$F\ (X)_s = A_1\ X + A_3\ X^3 \qquad (4)$$

$$F'\ (X)_s = A_1 + 3\ A_3\ X^2 \qquad (5)$$

where constants A_1 and A_3 are as defined by equations 2 and 3, and the subscript s is for the vapor.

The path of the moisture particles is related to that of the vapor by the conventional trajectory equations:

$$\dot{V}_t = \frac{C_D R_e}{24} \frac{C_{D,\ \text{slip flow}}}{C_D} \frac{9 \mu_s}{2 \rho_L r^2} (U_t - V_t) - \text{tangential} \quad (6)$$

$$\dot{V}_a = \frac{C_D R_e}{24} \frac{C_{D,\ \text{slip flow}}}{C_D} \frac{9 \mu_s}{2 \rho_L r^2} (U_a - V_a) - \text{axial}$$

where U and V are the absolute vapor and particle velocity.

Assume that the vapor and particle axial velocity are equal and constant:

$$U_a = V_a = \text{const}$$

By this assumption the particle acceleration is described in equation 6, and noting that:

$$U_t = V_a \ F' \ (X)_s \quad (7)$$

$$V_t = V_a \ F' \ (X)_L \quad (8)$$

$$\dot{V}_t = V_a^{\ 2} \ F'' \ (X)_L \quad (9)$$

where subscripts v and L are for vapor and moisture particles. By substituting in equation 6:

$$W \ F'' \ (X)_L = (1/K_c) \ (F' \ (X)_s - F' \ (X)_L) \quad (10)$$

where K_{cc}, the inertia parameter, is as follows:

$$K_c = \frac{24}{C_D R_e} \frac{C_D}{C_{D,\ \text{slip flow}}} \frac{2 \rho_L r^2 V_a}{9 \mu_s W} \quad (11)$$

Substituting in equation 5 yields:

$$W \ F' \ (X)_L + (1/K_c) \ F' \ (X)_L = (1/K_c) \ (A_1 + 3 A_3 X^2) \quad (12)$$

This is the final differential equation of motion for the moisture particles.

Integrating equation 12 gives the following general solution:

$$F(x)_L = C_1 + C_2 e^{-X(W K_c)} + A_3 X^3 - 3 A_3 W K_c X^2$$

$$- (A_1 + 6 A_3 W^2 K_c^{\ 2}) X - W K_c (A_1 + 6 A_3 W^2 K_c^{\ 2}) \quad (13)$$

Constants C_1 and C_2 are determined by the following boundary conditions:

1) the direction of flow of the vapor and moisture particles is the same at the blade inlet position; thus, by equation 5, $F'(o)_L = F'(o) = A_1$.

2) the end point position of the capture particle curve is coincident with the blade surface point at the trailing edge; thus by equation 3, $F(W)_L = F(W) = S_\theta$.

Solving for C_1 and C_2 and substituting in equation 13 gives the following equation for the capture particle curve:

$$F(x)_L = 6 A_3 W^3 K_c^{\ 3} (1 - e^{-1/K_c}) + A_3 (X^3 - W^3) - 3 A_3 K_c W (X^2 - W^2)$$

$$+ (A_1 + 6 A_3 K_c^{\ 2} W^2) (X - W) + S_\theta \quad (14)$$

The inlet width of the capture band is specified by the value of equation 14 for the inlet of blade as:

$$F(o)_L = 6 A_3 K_c^{\ 3} W^3 (1 - e^{-1/K_c}) - A_3 W^3 + 3 A_3 K_c W^3$$

$$- (A_1 + 6 A_3 K_c^{\ 2} W^2) W + S_\theta \quad (15)$$

Substituting for A_1 and A_3 (equations 2 and 3) in equations 14 and 15 gives the final equations for the capture particle curve and for the referred inlet width of the band.

$$F(x)_L / \$ = 6 K_c^{\ 3} (e^{(-1/K_c)} \ (X/W) - e^{-1/K_c}) + (X/W)^3 - 3 K_c (X/W)^2$$

$$+ ((S_\theta/\$) + 6 K_c^{\ 2} - 1) \ (X/W) + 3 K_c - 6 K_c^{\ 2} \quad (14a)$$

$$F(o)_L/\$ = 6 K_c^{\ 3} (1 - e^{-1/K_c}) - 6 K_c^{\ 2} + 3 K_c \quad (15a)$$

$$F(o)_L/\$ \approx 3 K_c : K_c < .03 \approx 3 K_c - 6 K_c^{\ 2} : K_c < .10 \quad (15b)$$

where the inertia parameter K_{cc} is:

$$K_c = \frac{24}{C_D R_e} \frac{C_D}{C_{D}, \text{ slip flow}} \frac{2 \rho_L r^2 V_a}{9 \mu_s W}$$

Note that the referred inlet width of the band is, in effect, the referred collection efficiency.

The above equations consider the blade surface shape as by a third degree polynomial. A similar development assuming the surface as by a second degree polynomial gives the following equation for the inlet referred width of the capture band:

$$F(o)_L/\not{S} = 2 K_c^2 (e^{-1/K_c} - 1) + 2 K_c \qquad (16)$$

$$F(o)_L/\not{S} \approx 2 K_c : K_c < .05 \qquad (16a)$$

where K_{cc} is as before.

Equations 15a and 16 are plotted and shown in figure 2.4.2-5.

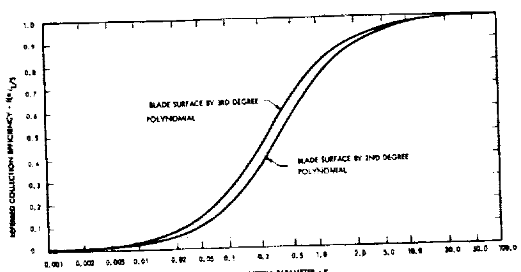

Figure 2.5.2-5 Referred Collection Efficiency on the Concave Side of the Blade

The calculation of collection drops on the concave side of the Yankee turbine ninth stator blade is illustrated by the following point calculation:

Moisture drop size: 0.4 micron radius = 1.311×10^{-6} ft radius

Fluid Properties: $\rho_L = 1.935$ slugs/ft^3, $\mu_v = 2.4 \times 10^{-7}$ lb-sec/ft^2, $V_a = 456$ ft/sec

Blade geometry: $W = 0.715$ ft, $\not{S} = 0.566$ ft, $S = 0.485$ ft

Inertia parameter:

$$K_c = \frac{24}{C_D R_e} \frac{C_D}{C_{D}, \text{ slip flow}} \frac{2 \rho_L r^2 V_a}{9 \mu_s W} = .00445$$

where:

$$\frac{24}{C_D R_e} = 1, \text{ assuming Stokes' law drag}$$

$$\frac{C_D}{C_{D}, \text{ slip flow}} = 1/.44 = 2.275 \quad \text{(Figure 2.5.2-1)}$$

The blade surface shape in this instance is closely approximated by the average between a 2 and 3 degree polynomial. Hence, the referred efficiency is specified by the average curve value, or by the average of equations 15b and 16a:

$$F(o)_L/\not{S} \quad 2.5 K_c = .0111$$

The inlet width of the capture curve

$$\zeta = (F(o)_L/\not{S}) \; \not{S} = .00629 \text{ f}$$

The portion of drops collected with respect to the total number approaching the blade is the ratio of the band width to the blade pitch.

$$\text{Portion} = \zeta/S = .013$$

Calculation results for the Yankee steam turbine are shown in figure 2.5.2-6. This figure gives the portion of moisture collected as a function of drop size. As shown by the curve sketch, the portion collected is specified by the inlet width of the band (ζ), within which all particles impinge on the blade with respect to the blade pitch. The band width cannot exceed the space between blades (pitch minus inlet edge blockage) which accounts for the break in the curve at 93.5 percent. Collection by Gyarmathy's data is 20 percent less in the range $\lesssim$ 0.4 micron drop radius. The difference is due to the fact that Gyarmathy specifies the blade shape by a quadratic expression compared to a higher order curve fit which, in this instance, better matches the blade.

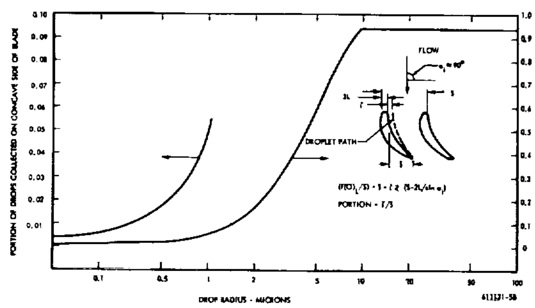

Figure 2.5.2-6 Portion Collected; Concave Side, Ninth Stator Yankee Turbine

- Simplified Model of Single Row Collection

The general collection analysis does not give a completely closed form result.

The foregoing analysis has been recast by approximations to give a closed form result which may be more useful in making observations about turbine moisture collection.

Following Section 2.5.2.1 the expression for inertial deposition on a single row of turbine blades is:

$$Q_\ell = m Y_\ell \; (P_{cn} + P_{cc}) \qquad (1)$$

where

$$P_{cn} = \frac{2L}{S \sin \alpha_i} \; \varphi_1 (K_{cn}) = \frac{2L}{S \sin \alpha_i} \; \varphi_1 (1 + 2.53\,Kn) \left(\frac{2\varrho_\ell \, r^2 V_r}{9 \mu_v \, 2L} \right) \qquad (2)$$

$$P_{cc} = \frac{g}{S} \, \varphi_2 (K_{cc}) = \frac{g}{S} \, \varphi_2 \; (1 + 2.53\,Kn) \left(\frac{2\varrho_\ell \, r^2 V_a}{9 \mu_v W_r} \right) \qquad (3)$$

Equation 1 may be written, using continuity of flow, for collection of condensate fog particles on a single blade as

$$q_b = \frac{Q_\ell}{N_b \ell_b} = \varrho S V_a Y_\ell (P_{cn} + P_{cc}) \quad (4)$$

and since

$$\varrho Y_\ell = \varrho_v \left(\frac{1 - x_v}{x_v} \right) \qquad (5)$$

then

$$q_b = \varrho_v S V_a \left(\frac{1 - x_v}{x_v} \right) (P_{cn} + P_{cc}) \qquad (6)$$

From numerical examinations of concave surface collection it can be observed that for the range of condensate particle sizes likely to be encountered in turbines (for concave surface collection),

$$\varphi_2 (K_{cc}) \sim a \, K_{cc} \qquad (7)$$

where a is the order of the polynomial expression needed to adequately describe the boundary of a tangential cross section of the concave surface of a particular blade in rectangular coordinates.

It can also be observed from numerical examination of the blade nose collection that, if the particle radius is between 0.4 and 2 microns in large steam turbines, a good approximation for nose collection is

$$\varphi_1 \; (K_{cn}) \sim b \, K_{cn} \qquad (8)$$

where b is a constant.

Substitution of Eq. 8 in Eq. 2 and Eq. 7 in Eq. 3 with further substitution of these results in Eq. 6 and simplifying and rearranging gives

$$q_b \approx \frac{\varrho_\ell \bar{r} \; V_r (1 + 2.53\, k_n)}{9} \left(\frac{2\varrho_v \bar{r} V_r}{\mu_v} \right) \left(\frac{1 - x_v}{x_v} \right) \left[b + a \frac{g}{W_r} \sin^2 \alpha_i \right] \qquad (9)$$

One of the more interesting observations which can be made from Eq. 9 is that the amount of moisture collected (q_b) per unit of blade height is independent of blade size for geometrically similar blade tangential cross sections.* This says that between two turbine blade rows of equal height and geometrically similar tangential cross sections, the row with the smallest blade chords will collect the most total moisture when operating under the same working fluid conditions. If the smaller row has a chord one-half that of the larger, the moisture collected by the larger will be one-half that collected by the smaller, i.e., the same collection per blade but half as many blades in the larger row for geometrically similar tangential cross sections.

*The cross section in a plane with one direction generally in the turbine axial direction and the other direction normal to corresponding diameters at the blade row inlet and exit stations.

The foregoing conclusion offers a definitive experimental way to check the basic premise that the dominant mechanism of collection is by inertial impaction rather than by eddy or molecular diffusion. Deposition by diffusion is proportional to the surface area, and the surface areas of the two hypothetical blade rows are equal.

A corollary to the Eq. 9 observations is that, other things being equal, big turbines could collect proportionately less moisture than small turbines and the amount of damaging impact liquid per unit of exposed rotor blade surface will reduce with an increase in turbine size.

The Knudsen number K_n in Eq. 9 is defined by

$$K_n = \frac{0.6275\mu_v}{\bar{r}\varrho_v\sqrt{g_c RT}} \qquad (10)$$

With μ_v in lb/ft-sec, r in microns, ρ_v in lb/ft^3, and T in °R, Eq. 2 becomes

$$K_n = \frac{5.35 \times 10^3 \mu_v}{\varrho_v \bar{r} \sqrt{T}} \qquad (11)$$

Substituting Eq. 11 into Eq. 9, using the same set of units as for Eq. 11, yields

$$q_b = 2.36 \times 10^{-12} \varrho_L \bar{r} V_r \left(1 + \frac{1.354 \times 10^4 \mu_v}{\varrho_r \bar{r}\sqrt{T}}\right)\left(\frac{\varrho_v \bar{r} V_r}{\mu_v}\right)$$

$$\left(\frac{1 - x_v}{x_v}\right)\left(b + a\frac{\$}{W_r}\sin^2 a_i\right) \qquad (12)$$

where q_b is in lb/ft-sec and V_r is in ft/sec.

Let N_b = number of blades per row, and h = blade height in feet; then, the total amount collected per row is given by

$$Q_L = 2.36 \times 10^{-12} \varrho_L \bar{r} V_r h N_b \left(1 + \frac{1.35 \times 10^4 \mu_v}{\varrho_v \bar{r} \sqrt{T}}\right)$$

$$\left(\frac{\varrho_v \bar{r} V_r}{\mu_v}\right)\left(\frac{1 - x_v}{x_v}\right)\left[b + a\left(\frac{\$}{W_r}\right)\sin^2 a_i\right] \qquad (13)$$

The constant a in Eq. 13 was taken to be 2.5. The constant b was evaluated from Gyarmathy's calculations[1], from which it was determined that

$$g_n = \emptyset(K_{cn}) = \frac{b}{2K_{cn}} \qquad (14)$$

where b is approximately equal to unity.* For some Westinghouse-type turbine geometries, $\$/W_r = 1.0$ for stators, and $\$/W_r = 1.25$ for rotors.

Substituting these values into Eq. 13 for stators:

$$Q_L = 2.36 \times 10^{-12} \bar{r} V_r h N_b \varrho_L \left(1 + \frac{1.354 \times 10^4 \mu_v}{\varrho_v \bar{r} \sqrt{T}}\right) \qquad (15)$$

$$\left(\frac{\bar{r} V_r \rho_v}{\mu_v}\right)\left(\frac{1 - x_v}{x_v}\right)\left(1 + 2.5\sin^2 a_i\right)$$

and for rotors:

$$Q_L = 2.36 \times 10^{-12} \bar{r} V_r h N_b \varrho_L \left(1 + \frac{1.354 \times 10^4 \mu_v}{\varrho_v \bar{r} \sqrt{T}}\right) \qquad (16)$$

$$\left(\frac{\bar{r} V_r \rho_v}{\mu_v}\right)\left(\frac{1 - x_v}{x_v}\right)\left(1 + 3.125\sin^2 a_i\right)$$

- Comparison of Experimental and Calculated Moisture Collection

A. Smith of Parsons Company has published the results of water extraction tests on a scale model of a Parsons steam turbine.[4] These tests were run on a four-stage machine with the water extraction between the third and fourth stages. The theoretical amount of moisture present at the exit of the third stage was varied by changing the amount of superheat in the vapor at the turbine inlet. Smith's data are shown as X's in Figure 2.5.2-7. This is a plot of theoretical moisture against the portion of the theoretical moisture collected. Superimposed on this figure is a curve representing theoretical calculations of the portion of moisture which would be collected by the Yankee steam turbine ninth stage stator if the turbine were operated to provide the varying amounts of theoretical moisture. In addition, the conditions and geometry are also adjusted to make the Wilson Point (at some location ahead of the ninth stator) occur at a value of $\{1/P\}$ dp/dt of pressure and dP/dt is the rate of change of this pressure with time at the Wilson Point.

---

* The numerical value of b will be different from that for other turbines and operating conditions.

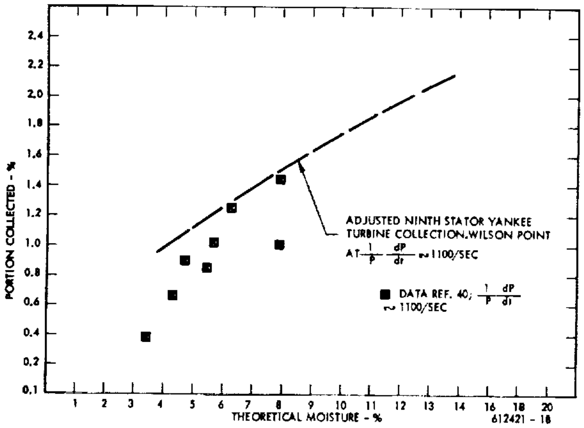

Figure 2.5.2-7 Calculated and Experimental Turbine Moisture Collection

The only "real" point on the calculated curves is that marked at 13.5% theoretical moisture,(1) considering the actual operation conditions and geometry of the Yankee turbine. If a line is drawn from this point through Smith's data, there is apparently excellent agreement. However, the calculations are for collection on a single turbine row, whereas Smith's data represent collection on a varying number of turbine rows and fractions thereof. That is, the Wilson Point in Smith's turbine is moving toward the front end of the turbine as the amount of theoretical moisture available at the third stage exit rises. Therefore, the collecting surface area subject to the condensing region is increasing. The moisture collected at the drain port between third and fourth stages probably represents that collected on less than one row for 3% theoretical moisture and on up to two or more rows for 8% theoretical moisture. This explains why the slope of the data points is substantially greater than the slope of the calculated lines. If the drain ports in Smith's experimental turbine are catching nearly all of the moisture collected on the blades and if the blade sections, spacing, and amount of turning of the experimental turbine rows are quite similar to that of the ninth stator of the Yankee turbine, then the theories of condensate spontaneous nucleation and deposition (taken together) somewhat over-estimate the actual amounts of moisture being collected in steam turbines. However, in the absence of definite knowledge on these points, no change in the present steam models of spontaneous nucleation and collection is indicated.

2.5.3 Movement of Moisture on Blade Surfaces

- Movement on Rotor and Stator Blades

The movement of collected moisture over the blade surfaces is not a critical part of the overall erosion model with respect to numerical precision. The main value of the analysis is in pointing out certain variables which may be neglected and in the added qualitative understanding of one of the sequences of events leading to turbine blade erosion. A most important conclusion which can be drawn from the analysis is that the carryover of collected moisture from stage to stage will be negligible in a well-drained turbine because the flow of liquid on the rotor blades is essentially radial. The liquid is therefore slung from the tip against the outer casing and can be efficiently collected by suitable drain slots. Another conclusion is that the liquid flow on the stators is essentially along the vapor streamlines.

In this analysis, it is assumed that the collected moisture forms a continuous film controlled by the laws of viscous flow. Generally, the thickness and velocity of the moisture film are based on the force balance between the viscous shear of the film, vapor stream friction, and centrifugal force. The force on such a film from the radial pressure gradients in the turbines examined is small compared to the other forces mentioned. It is also assumed that the moisture collects only on the concave side of the blades for purposes of numerical calculation. (Collection on the convex sides through the action of secondary flows is neglected.) This is a conservative assumption since it places a higher liquid load per unit of surface on the blade than is probably actually present. Since different procedures are involved for the stator and rotor blade calculations, the discussion is by separate topics.

- Rotor Blade Moisture Transport Model & Results

The main equation, based on the Navier-Stokes equations, relates the centrifugal force to the viscous shear of the film. This assumes that the flow is in the radial direction and is only acted upon by the centrifugal force. The error in this assumption is shown by calculating the axial force on the film (due to steam friction) and the axial film velocity for the ninth stator of the Yankee turbine.

Assuming 2 percent moisture collection, the axial velocity is 0.88 fps compared to 6.5 fps velocity in the radial direction, corresponding to a 7.8 degree angle of flow with respect to the radial direction. Assuming the flow is in the radial direction only and disregarding the low order terms, the Navier-Stokes equations reduce to:

$$F = -\mu \frac{\partial^2 u}{\partial y^2}$$

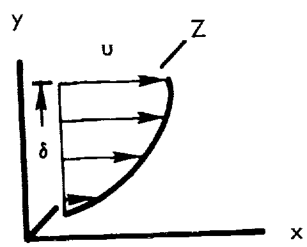

611131-56B

where the body force F is the centrifugal force.

Integration with boundary conditions as specified by a parabolic velocity distribution gives:

$$\frac{F y^2}{2} - F \delta y = -\mu u \tag{1}$$

The mass flow and velocity are specified by continuity as:

$$d\dot{m}_L = \rho_L Z u dy$$

$$u = \frac{1}{\rho_L Z} \frac{d\dot{m}_L}{dy} \tag{2}$$

Combining (1) and (2) and integrating force gives:

$$\frac{F \delta^3}{3} = \frac{\mu}{\rho_L Z} \dot{m}_L$$

Substituting for the centrifugal force: $P_L \omega^2 r$ gives the final expression for δ at the tip of the blade:

$$\delta = \left(\frac{3 \mu_L \dot{m}_L}{Z \rho_L^2 r w^2} \right)^{1/3} \tag{3}$$

$$\bar{u} = \frac{\dot{m}_L}{\rho_L Z \delta} = \left(\frac{\dot{m}_L^2 r w^2}{3 \rho_L Z^2 \mu_L} \right)^{1/3} \tag{4}$$

This assumes that the flow is uniformly distributed over the surface of the blade.

The calculation also assumes a parabolic velocity distribution with film thickness. The latter assumption is for calculation purposes and could be improved upon by detailed investigation of the amount and distribution of moisture. As to the width of the film, the film thickness and mass average velocity at the tip of the blade are inversely proportional to the 1/3 power and 2/3 power of the film width respectively; thus, the film thickness and mass average velocity would be 1.26 and 1.59 times the calculated values, for full width, if the film extended over half the width of the blade. In the case of radial distributions, with a triangular distribution of film thickness along the height of the blade, the centrifugal force F would be roughly 0.58, the film thickness 1.2, and the velocity 0.83 times the calculated values for constant radial thickness. As to the moisture flow ($\dot{m}_L$), the film thickness and velocity are directly proportional to the 1/3 power and 2/3 power of the flow.

TABLE 2.5.3-1

YANKEE TURBINE, EIGHTH ROTOR LIQUID FLOW

ϵ	$\dot{m}_L \times 10^4$ p-s/f	$\delta \times 10^5$ f	$\bar{u}$ fps	Re_L
0.005	0.215	1.59	2.58	7.65
0.010	0.43	2.02	4.11	15.3
0.020	0.86	2.52	6.49	30.6
0.050	2.15	3.44	12.0	76.5
0.100	4.30	4.31	18.9	153.0

Using the expressions just developed, parametric calculations for the eighth rotor of the Yankee steam turbine were carried out. The results are shown in Table 2.5.3-1. The parameter varied is the fraction (ϵ) of equilibrium moisture collected since this quantity depends upon inputs from the rest of the model. Note that the film velocity ($\bar{u}$) is the mass average at the tip of the blade.

- <u>Stator Blade Moisture Transport Model & Results</u>

The main equation, based on the viscosity expression, relates the viscous shear to the axial force due to the steam friction drag and the impingement of the moisture particles. It is assumed that there is a linear velocity distribution with film thickness and that the flow per unit blade height (at the 3/4 section) is the average unit flow along the height of the blade. This assumption could be improved upon by detailed investigation of the radial distribution. The viscous shear in the liquid film is given by:

$$\tau = \mu_L \frac{\partial u}{\partial y}$$

assuming a linear velocity distribution:

$$\tau = \mu_L \frac{u_{max}}{\delta} = \frac{2\mu_L \bar{u}}{\delta} \qquad (5)$$

where δ and $\bar{u}$ are the film thickness and mass average velocity. The flow of liquid is by continuity:

$$\dot{m}_L = \rho_L Z \delta \bar{u}$$

and

$$\bar{u} = \frac{\dot{m}_L}{\rho_L Z \delta} \qquad (6)$$

at the blade exit position assuming that the flow is evenly distributed over the distance Z (see sketch that follows).

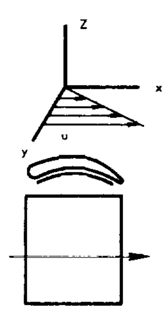

Combining (5) and (6) gives

$$\delta = \left(\frac{2\,\dot{m}_L\,\mu_L}{\rho_L\,Z\tau}\right)^{1/2} \qquad (7)$$

The viscous shear on the film is due to the drag of the vapor and the force of the impinging drops, i.e.,

$$\tau = C_f\,\rho_S\,\frac{V_S^{\,2}}{2} + \frac{\dot{m}_L}{ZX}\,V_S \qquad (8)$$

where the boundary layer friction coefficient (C_f). in the region of the trailing edge is specified as:

$$C_f = 2 \times 0.123 \times 10^{-0.678\,H}\left(\frac{V\theta\rho}{\mu}\right)^{-0.268} \qquad \text{(Schlichting)} \qquad (9)$$

where θ and H are boundary layer parameters.

Equations (7) and (8) may be combined to give:

$$\delta = \left(\frac{2\,\dot{m}_L\,\mu_L}{\rho_L\,Z}\;\frac{1}{\tau + \frac{\dot{m}_L V_S}{XZ}}\right)^{1/2} \qquad (10)$$

The film Reynolds Number is by definition:

$$Re_L = \bar{u}\;\delta\rho_L/\mu_L \qquad (11)$$

Note that the axial force by the drag of the vapor is specified by the wall shearing stress of the boundary layer. The axial force due to the momentum of the impinging drops depends on the amount of the collection: for 1/2, 2, and 10 percent collection, the momentum force is roughly 5, 20, and 100 percent of the vapor drag force (τ).

As the amount of moisture collected depends on inputs from the other parts of the program, calculated film properties are,with respect to the amount of equilibrium moisture collected, designated as ϵ. Results for the Yankee steam turbine ninth stator are given in Table 2.4.3-2, following. As shown, the film thickness and velocity are roughly proportional to the square root of ϵ, when ϵ is less than 0.05. The velocity ($\bar{u}$) is the mass average value at the trailing edge of the blade.

TABLE 2.5.3-2

YANKEE STEAM TURBINE, NINTH STATOR LIQUID FLOW

ϵ	$\dot{m}_L \times 10^4$ p-s/f	$\delta \times 10^5$ f	$\bar{u}$ fps	Re_L
0.005	0.63	2.58	0.404	1.55
0.010	1.26	3.56	0.585	3.1
0.020	2.53	4.81	0.869	6.23
0.050	6.30	6.75	1.54	15.5
0.100	12.6	8.22	2.54	31.0

From limited data (Gardner[5], Baker[6]) it appears that there are ripples on the surface of the film when the film Reynolds Number (Re_L) is greater than 4, corresponding to ϵ greater than roughly 1 percent. These ripples probably affect the size of the drops from the blades as discussed in Section 2.7 under atomization.

2.5.4 Collection on Turbine Casing*

- **Background**

In conventional (steam) wet vapor turbine designs, the moisture leaving the turbine vanes and collecting on the turbine casing is removed by slots in the casing. The design of alkali metal vapor turbines might be considerably simplified if slots were unnecessary. However, if an appreciable amount of condensate collects on the turbine casing and is not removed, casing and rotor blade seal strip erosion may result. A rudimentary examination of casing flows for the cesium and potassium turbines design of NAS 5-250* is reported in the following paragraphs.

- **Condensate Collection on the Turbine Casing**

It is expected that essentially all of the liquid collected on the turbine blades ends up on the turbine casing because of the centrifugal action of the turbine rotors. The drops formed departing the rotor blade tips impinge on the turbine casing. Along the turbine stages, a liquid film builds up on the turbine casing. The impingement of liquid drops on the condensate film probably causes splashing and some removal of the liquid from the film. However, the net amount of condensate collected on the casing cannot be easily estimated; therefore, it is assumed that all of the condensate impinging on the turbine casing is collected. The amount of fog particles collected per turbine blade per unit blade height can be estimated by use of equations 15 and 16 of Section 2.5.2, and it is assumed that this same amount impinges and collects on the turbine housing.

The calculation of the amount of moisture collected per stage required an iteration procedure. The total condensed moisture was used to initiate the calculations. From these values, the average moisture content was calculated, from which the term $(1 - x_v)/x_v$ was calculated. The condensate collected was then calculated from equation 15 or 16. The amount collected was then subtracted from the total condensate to yield the moisture content of the vapor. The calculations converged rapidly, however. The results of the calculations for the six-stage potassium turbine and the two-stage cesium turbine are presented in Tables 2.5.4-1 and 2.5.4-2 respectively.

TABLE 2.5.4-1

MOISTURE COLLECTION ON TURBINE HOUSING SIX-STAGE POTASSIUM TURBINE

Row Number	Net Collection Efficiency (%)	Effective Moisture	Q_L, Net (lb/sec)	Cumulative Condensate Collected (lb/sec)
3R	0.12	0.0005	3.6×10^{-6}	3.6×10^{-6}
4S	0.83	0.040	0.0019	0.0019
4R	1.55	0.088	0.0078	0.0097
5S	1.60	0.107	0.0098	0.0195
5R	1.76	0.119	0.0121	0.0316
6S	1.90	0.127	0.0139	0.0555
6R	0.78	0.136	0.0061	0.0616

Final percentage of total moisture collected is 7.8%

TABLE 2.5.4-2

MOISTURE COLLECTION ON TURBINE HOUSING TWO-STAGE CESIUM TURBINE

Row Number	Net Collection Efficiency (%)	Effective Moisture	Q_L, Net (lb/sec)	Cumulative Condensate Collected (lb/sec)
1S	0.04	0.011	9.1×10^{-5}	9.1×10^{-5}
1R	0.55	0.059	3.3×10^{-4}	4.2×10^{-4}
2S	0.62	0.122	0.0011	0.0015
2R	0.34	0.153	0.0016	0.0031

Final percentage of total moisture collected is 0.106%

*See Section 1.2.3 for additional detail on the turbines.

The last two columns of the tables give, respectively, the total condensate collected on each row and the cumulative condensate collected on the turbine housing. It is seen that, for the six-stage potassium turbine, 7.8 percent of the total moisture content eventually collected on the turbine housing. In comparison, the percentage of the total moisture collected on the cesium turbine housing is 0.106 percent. The significantly smaller amount of moisture collected on the cesium turbine housing is due to the fact that fewer stages are required for the cesium turbine.

The estimated moisture collection may be conservative since it was assumed that impingement of liquid droplets on the condensate film and the resulting splashing does not cause a net removal of the condensate; consequently, the actual collection may be less than that indicated by the calculated results.

- Stability of Condensate Collected on the Turbine Casing

In addition to the possibility of condensate removal by splashing, there is also the possibility that under the given hydrodynamic conditions the liquid film may be unstable and the condensate may be removed by shear forces at the vapor-liquid interface. In an attempt to resolve this question, the mode(s) of two-phase flow expected under the given conditions are related to the two-phase flow map of Baker.[38] Baker presents a map showing regions of various modes of two-phase flow as functions of two-phase flow parameters. Baker's map is reproduced in Figure 2.5.4-1. The map consists of a plot of the logarithm of G/λ versus the logarithm of $L\lambda\psi/G$, where G and L are the vapor and liquid mass velocities, respectively. Here, λ is a density parameter defined as

$$\lambda = \left[\left(\frac{\rho_G}{0.075}\right)\left(\frac{\rho_L}{62.3}\right)\right]$$

and ψ is a surface tension parameter defined by

$$\psi = \frac{73}{\sigma_L}\left[\mu_L\left(\frac{62.3}{\rho_L}\right)^2\right]^{1/3}$$

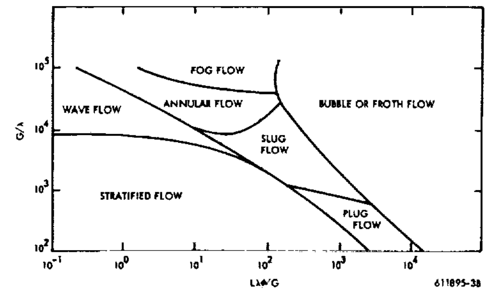

Figure 2.5.4-1 Bakers Map of Two-Phase Flow

Calculations for the various stages of the two turbines give values of G/λ on the order of 10^5 and values of $L\lambda\psi/G$ less than 10^{-2}. As can be seen, these values are out of the range from Baker's map. An "eyeball" extrapolation of the map would place the flow in the wave flow regime. Such an extrapolation is, of course, not trustworthy. In wave flow, it is expected that some of the wave crests would be carried away into the vapor. If annular flow prevails, substantial removal of liquid from the casing film is expected. If fog flow is present, then all of the liquid film would be entrained in the vapor as fog. About the best that can be concluded at this time is that some dispersion of the casing liquid is indicated.

- Condensate Film Thicknesses on the Turbine Housings

The condensate film thicknesses on the turbine housings were estimated by the theory of Wrobel and McManus.[7] These investigators analyzed the film depth and wave height in annular two-phase flow and derived an equation relating the film depth to the film flow rate and the gas Reynold's number. The results checked reasonably well with the limited available data. The complete equation of Wrobel and McManus is

$$\frac{\delta}{R_o}\left(1 + \frac{2_\delta}{R_o} - \frac{3\nu_L}{\nu_v}\frac{Q_L^+}{N_{re,v}}\right)\left[\ln\left(2.95\,\frac{(R_o/\delta) - 1}{1 - 10/\delta^+}\right)\right]^{-1} N_{re,v}$$

$$= \frac{\nu_L}{\nu_v}\left(\frac{\rho_L}{\rho_v}\right)^{1/2}\frac{B}{A}\,(24)^{1/2}\left(Q_L^{+2} + 2AQ_L^+\right)^{1/2} \qquad (12)$$

where Q_L^+ is the dimensionless liquid flow rate given by

$$Q_L^+ = \frac{\delta U_L}{\nu} \quad \text{and} \quad \delta^+ = \frac{U^*}{\nu}$$

where Q_L^+ is the dimensionless liquid flow rate given by with U* the friction velocity $\sqrt{\tau_s/\varrho}$.

The constants A and B in Eq. (12) depend on the shear profile assumed. For a constant shear profile, A = 265 and B = 17.9.

From continuity,

$$W_L = \pi D \varrho_L \delta U_L \qquad (13)$$

where U_L is the mean film velocity, and D is the local turbine casing inside diameter. From Eq. (13)

$$\delta U_L = \frac{W_L}{\pi D \varrho_L} \qquad (14)$$

whence

$$Q_L^+ = \frac{\delta U_L}{\nu} = \frac{W_L}{\pi D \mu_L} \qquad (15)$$

with

$$\delta^+ = 10 + 28 \left(\frac{\varrho_v}{\varrho_L}\right)^{1/2} \left(\frac{\nu_v}{\nu_L}\right)$$

The condensate flow rates are based on the turbine casing inside diameter. Parametric curves for the film height are presented in Figures 2.5.4-2 and 3. Estimates on the depth of liquid film on the potassium and cesium turbines of NAS 5-250 are given in Tables 2.5.4-3 and 4.

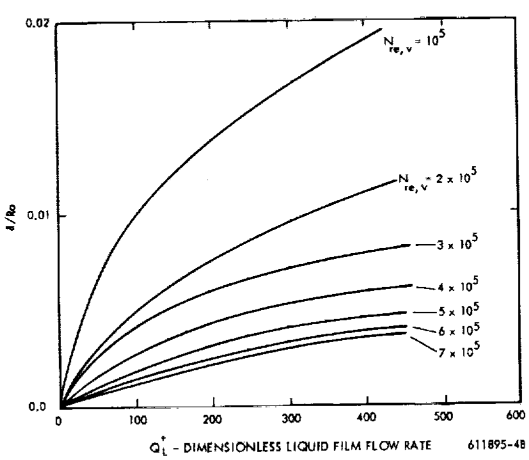

Figure 2.5.4-2 Effect of Condensate Film Reynold's Number on Film Thickness

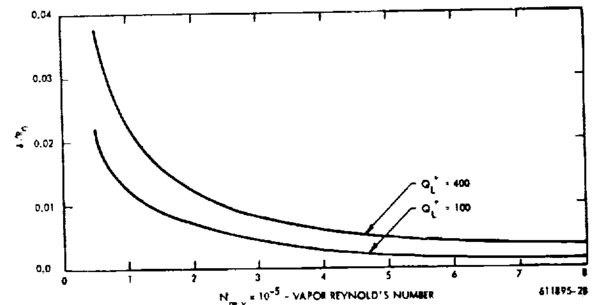

Figure 2.5.4-3 Effect of Vapor Reynold's Number on Film Thickness

TABLE 2.5.4-3

ESTIMATED CONDENSATE FILM DEPTH ON TURBINE HOUSING SIX-STAGE POTASSIUM TURBINE

Blade Row Exit	Cumulative Condensate Flow Rate (pps)	Q^+	$N_{re,v} \times 10^{-5}$	$\delta/R_o \times 10^4$	δ (mils)
3R	3.6×10^{-6}	0.028	5.12	0.071	0.006
4S	1.89×10^{-3}	14.3	5.04	1.28	0.122
4R	9.71×10^{-3}	71.5	4.94	2.84	0.317
5S	0.0195	133.	4.95	3.69	0.496
5R	0.0316	197.	4.89	4.38	0.712
6S	0.0555	326.	4.86	5.70	1.07
6R	0.0616	338.	4.83	5.66	1.28

TABLE 2.5.4-4

ESTIMATED CONDENSATE FILM DEPTH ON TURBINE HOUSING TWO-STAGE CESIUM TURBINE

Blade Row Exit	Cumulative Condensate Flow Rate (pps)	Q^+	$N_{re,v} \times 10^{-6}$	$\delta/R_o \times 10^5$	δ (mils)
1S	9.1×10^{-5}	0.981	1.17	3.22	0.0126
1R	4.2×10^{-4}	3.77	1.26	4.19	0.0259
2S	0.0015	11.6	1.31	5.77	0.0649
2R	0.0031	20.2	1.35	6.48	0.129

- Average Drop Size Sheared From Casing Liquid

It is anticipated that the condensate film flowing over the casing will at least in part be atomized. Since this is presumably a random process, some of the drops will have relatively short time-of-flight available before impinging on the rotor blades. These drops can be relatively large and the resulting erosion on the rotor blades might be severe.

The average droplet size was estimated on the basis of the sheet atomization mechanism as given in Section 2.7. The equation derived for the average droplet size is

$$\bar{d} = 17.0 \left[\frac{\dot{m}_L \mu_L}{\varrho_L \left(\tau_s + \frac{\dot{m}_L U_v}{X}\right)}\right]^{1/4} \left(\frac{\mu_L}{\tau_s} \sqrt{\frac{\sigma_L}{\varrho_L}}\right)^{1/3}$$

For the turbine casing, the momentum term is negligible compared to the wall friction term, and the equation reduces to

$$\bar{d} = 17 \left(\frac{\dot{m}_L \mu_L}{\varrho_L \tau_s}\right)^{1/4} \left(\frac{\mu_L}{\tau_s} \sqrt{\frac{\sigma_L}{\varrho_L}}\right)^{1/3}$$

where $\bar{d}$ is in microns. The wall friction drag per unit area, τ_s, was calculated from the Wrobel and McManus equation for the wall friction drag coefficient C_f, or

$$C_f \approx 0.33 \left[\ln\left(\frac{3 R_0}{\delta(1 - 10/\delta^+)}\right)\right]^{-2}$$

To calculate the average droplet size, the condensate flow rates $\dot{m}_l$ were based on the housing inside diameters. The results are presented in Table 2.5.4-5.

These average droplet sizes are significantly larger than the average droplet size entering the rotor blades from the stators of either turbine. In the case of the potassium turbine, the drops are certainly large enough to cause physical impact erosion damage. Therefore, periodic moisture removal similar to that in steam turbines is indicated for the potassium turbine if erosion is to be minimized.

TABLE 2.5.4-5

MEAN DROPLET SIZES FROM SHEET ATOMIZATION OF CONDENSATE ON THE POTASSIUM AND CESIUM TURBINE HOUSINGS

Turbine Housing at Blade Row Exit	$\bar{d}$ (microns)
6K - 3R	4.48
6K - 4S	75.3
6K - 4R	149.
6K - 5S	235.
6K - 5R	331.
6K - 6S	455.
6K - 6R	667.
2Cs - 1S	5.38
2Cs - 1R	5.06
2Cs - 2S	17.4
2Cs - 2R	40.7

2.5.5 References

1. Gyarmathy, G., "The Bases for a Theory of the Wet Steam Turbine," Juris-Verlag, Zurich, 1962.

2. Brun, R. J., W. Lewis, P. J. Perkins, and J. S. Serafini, NACA Report 1215, 1955.

3. Emmons, H. W., Fundamentals of Gas Dynamics, Vol. III, Sect. H., Princeton University Press, Princeton, N. J., 1958.

4. Smith, A., "The Influence of Moisture on the Efficiency of a One-Third Scale Model Low Pressure Steam Turbine," Institution of Mechanical Engineers, Thermodynamics and Fluid Mechanics Convention, Paper 10, Liverpool (Gr. Brit.), April 13-15, 1966.

5. Gardner, G. C., "Events Leading to Erosion in the Steam Turbine," Proc. Inst. Mech. Engrg., 178, Pt I, No. 23, pp. 593 to 623, 1963-1964.

6. Baker, O., "Simultaneous Flow of Oil and Gas," The Oil Gas Jour., July 26, 1954.

7. Wrobel, J. R., and H. N. McManus Jr., "An Analytic Study of Film Depth, Wave Height, and Pressure Drop in Annular Two-Phase Flow," Development in Mechanics, Vol. I, Proceedings of the 7th Midwest Mechanics Conference, Sept. 6-8, 1961, Plenum Press, Inc., New York, 1961.

8. Baker, O., "Simultaneous Flow of Oil and Gas," The Oil Gas Jour., July 26, 1954.

2.6 TRANSPORT OF ATOMIZED DROPS BETWEEN STATORS AND ROTORS (ADROP CODE)*

2.6.1 Background

This section describes the detailed aspects of the tubular blade erosion model which deals with the transport of potentially damaging liquid in the axial space between stator exit planes and rotor inlet planes.

The source of most of the potentially damaging moisture in steam and alkali metal turbines is the process of condensation in the bulk vapor by spontaneous nucleation. The condensate particles are generally less than a micron in diameter, so that if the turbine is well designed and orderly flow prevails, most of the moisture will follow the vapor streamlines and will exit from the turbine without interacting with the blades. A small fraction of the condensate fog will, however, tend to collect on blade surfaces because of the curvature of the flow passages and the rotation of the moving blades.

These impacts by themselves cause negligible damage because of the small size of the particles involved. The moisture collected in this fashion on stator passage walls is carried along axially by the drag forces of the vapor stream toward the downstream end of the stator. The liquid is then torn away from the stator trailing edge in a primary atomization process. A wide spectrum of drop sizes is produced, with some diameters approaching the stator trailing-edge thickness. Most of the observed impact erosion damage is caused by drops formed in this manner.

Condensation directly on blade surfaces and boiler carry-over are other sources of moisture which may be considered. These would tend to dominate in mercury vapor machines, for instance, where condensation in the bulk vapor is theoretically negligible.

The work presented here is concerned with the motion of the moisture, regardless of its origin, after the conclusion of primary atomization. The analytical basis of the transport model will be discussed and a digital computer code package called ADROP will be described. This code is written in FORTRAN IV and was developed to unify the various numerical procedures involved in this phase of the overall turbine blade erosion model.

2.6.2 Analytical Model of Atomized Drop Transport

The central problem is the solution of the equation of motion of a drop of liquid in the space between the stator from which it was discharged and the rotor inlet plane. Mechanical erosion rates tend to be drop-size and velocity dependent. The upper limit of drop sizes which will impact the rotor blades is largely determined by the vapor wake characteristics immediately downstream of the stators.

The primary drops are caught up in the decaying wake. Some of these will simply be accelerated to some fraction of the local vapor velocity and will ultimately impact upon the rotors. Drops at the upper end of the size spectrum produced by primary

* T. C. Varljen, Supervisor, Systems & Technology, Astronuclear Laboratory, Westinghouse Electric Corporation, Pittsburgh, Pa. 15236

atomization will be unstable with respect to the applied aerodynamic forces and will fragment prior to impact. The latter process will be termed "secondary atomization." Drops traveling along streamlines near the edge of the stator wakes are subject to the greatest aerodynamic forces, while drops moving along the wake axis, essentially in the trough of the velocity defect, will experience the least amount of disruption. The largest, and hence potentially the most damaging, drops which reach the rotors will be those which move on streamlines near the wake centerline.

The study of the motion of atomized condensate has been undertaken on several levels. First, relatively simple closed form solutions of the equation of motion were obtained for certain special cases. A completely general dimensionless formulation of the equation of motion was also obtained and solved numerically. Finally, a detailed calculational procedure was developed to provide special solutions.

- The Bulk Flow Impact Velocity

A closed form solution to the drop motion problem has been derived for the special case of a drop moving along the wake-edge under bulk flow conditions. The aerodynamic force on a detached drop is given by:

$$F_d = 1/2\, C_D\, \rho_v V_r^2 A_d \qquad (1)$$

where A_d is the drop cross-sectional area and V_r is the relative velocity of the drop with respect to the local vapor stream velocity. That is $V_r = U - Vd$. If the drop remains intact, its equation of motion will be:

$$F_d = \frac{\pi}{6} D_d^3 \rho_v \frac{dV_d}{dt}$$

or:

$$\frac{dV_d}{dt} = \frac{3}{4} \frac{C_D}{D_d} \frac{\rho_v}{\rho_L} (U-V_d)^2 \qquad (2)$$

Two assumptions were made to get a closed-form solution to the above. First, the local vapor velocity was assumed to be constant and equal to the bulk flow velocity at the stator exit plane ($U = U_o$), and second, the following form of the drag coefficient was assumed:

$$C_D = a\mathrm{Re}^b = a\left[\frac{(U_o - V_d)\,\rho_v D_d}{\mu_v}\right]^b \qquad (3)$$

Unfortunately the drag coefficient cannot (as far as we know) be represented by a single general relationship $a\mathrm{Re}^b$ over the Reynolds Number range of interest. According to Lambiris and Combs[1], for the distorted drops:

$$C_D = 27\,\mathrm{Re}^{-84} \qquad 0 \le \mathrm{Re} \le 80 \qquad (4a)$$

$$C_D = .271\,\mathrm{Re}^{.217} \qquad 80 < \mathrm{Re} \le 10^4 \qquad (4b)$$

$$C_D = 2 \qquad 10^4 < \mathrm{Re} \qquad (4c)$$

The data which the above relations fit is shown graphically in Figure 2.6-1. Experimental data from References (1) and (2) are shown. The solution to the equation of motion, relating distance traveled and drop terminal velocity, covering cases (4a) and (4b), was found to be

$$X = \frac{4}{3}\left(\frac{D_d}{C_{Do}}\right)\left(\frac{\rho_L}{\rho_v}\right)\frac{1}{b\,(b+1)}\left\{1 + \left[\frac{V_d}{U_o}(b+1) - 1\right]\left(1 - \frac{V_d}{U_o}\right)^{-(b+1)}\right\} \qquad (5)$$

For the case of a constant drag coefficient (case 4c for instance) the following solution was obtained:

$$X = \frac{4}{3}\left(\frac{D_d}{C_{Do}}\right)\left(\frac{\rho_L}{\rho_v}\right)\left\{\frac{V_d/U_o}{1 - V_d/U_o} + \ln\left(1 - \frac{V_d}{U_o}\right)\right\} \qquad (6)$$

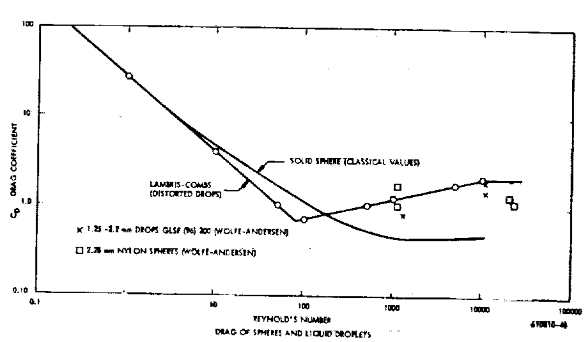

Figure 2.6-1 Drag of Spheres and Liquid Drops

Note that C_{Do} is associated with Re_o, the bulk flow Reynolds Number. Three distinct closed form solutions have therefore been obtained corresponding to the three Reynolds Number ranges used to represent the drag coefficient. A convenient dimensionless representation of these solutions is shown in Figure 2.6-2. The drop terminal-to-free-stream velocity ratio is plotted as a function of the parameter group $\left(\frac{X}{D_d}\right)\left(\frac{\rho_v}{\rho_L}\right)C_{Do}$. If the local Reynolds Number of a drop stays completely within one of the Reynolds Number ranges throughout its trajectory, the appropriate general trajectory curve will be followed. Otherwise, the curves form an envelope covering the behavior of cases where the Reynolds Number drops from one range to the next.

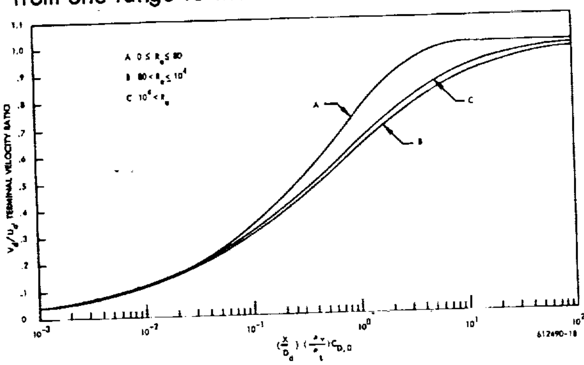

Figure 2.6-2 Analytic Solutions for the Bulk Flow Drop Impact Velocity

- General Dimensionless Formulation

For the general case of motion with a variable field (i.e., within a stator wake for instance) a closed form solution does not seem possible because of the complexity of the resulting equation of motion. It has been noted that from the point of view of the erosion model the most important path of drop motion is near the axis of the stator wake.

Leiblein and Roudebush[3] have correlated the variation of wake trough velocity with downstream distance with the following expression:

$$U_{min} = U_o \left(1 - .13/\sqrt{\frac{x}{c} + .025}\right) \quad (7)$$

The above is based on a limited amount of data for blade cascades with essentially zero trailing-edge thicknesses.

The basic equation of motion, now written for the wake axis streamline is then:

$$\frac{dV_d}{dt} = V_d \frac{dV_d}{dx} = \frac{3}{4}\left(\frac{\rho_v}{\rho_L}\right)\frac{1}{D_d} f\left[\left(U_{min} - V_d\right)\frac{\rho_v D_d}{\mu_v}\right]\left(U_{min} - V_d\right)^2 \quad (8)$$

when the drag coefficient is represented functionally by:

$$C_d = f\left[\left(U_{min} - V_d\right)\frac{\rho_v D_d}{\mu_v}\right]$$

Now abbreviating eq (8) so that $U_{min} = U_o g(\epsilon)$, where $\epsilon = x/c$, leads to

$$\left(\frac{V_d}{U_o}\right)\frac{d V_d/U_o}{d\epsilon} = K_d f\left\{\left[g(\epsilon) - V_d/U_o\right] Re_o\right\}\left[g(\epsilon) - V_d/U_o\right]^2 \quad (9)$$

with K_d as the inertial parameter:

$$K_d = \frac{3}{4}\left(\frac{\rho_v}{\rho_L}\right)\left(\frac{c}{D_d}\right)$$

The above has been solved numerically for the velocity ratio as a function of referred distance along the wake axis (x/c) with K_d and Re_o as parameters. Figure 2.6-3 shows a few of the solutions which have been obtained.

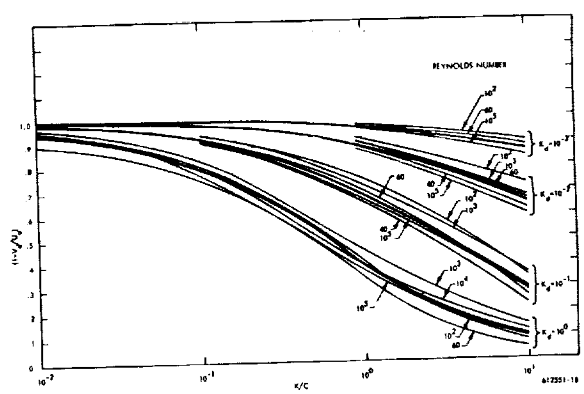

Figure 2.6-3 General Solutions for the Terminal Velocity of Drops Traveling along Stator Wake Axis Streamlines

These solutions by themselves are instructive guides to the overall relations between the parameters. It is conceivable that a least squares analysis of the various relations could be used to produce a "universal solution" curve of the form:

$$\frac{V_d}{U_o} = \left(\frac{x}{c}\right)^{n_1} K_d^{\;n_2} \; Re_o^{\;n_3} \qquad (10)$$

From the point of view of turbine erosion, however, knowledge of the ultimate impact velocity is not sufficient and must be complemented by a secondary atomization study. It is for this reason that the detailed computer model was developed.

2.6.3 Computer Model of Atomized Drop Transport

The scope of the ADROP code package is as follows:

a) Estimation of stator blade boundary-layer characteristics

b) Generation of the local velocity field within the vapor wake downstream of stator blades

c) Numerical integration of the equation of motion of drops traveling along various wake streamlines and the estimation of secondary atomization effects.

d) Solution of drop impact velocity triangles to provide information on the magnitude of the normal component of impact velocity and the physical location of erosion.

- Stator Blade Boundary Layer Characteristics

The vapor wake downstream of stator blades is assumed to be controlled primarily by the viscous dissipation of the boundary layer at the trailing-edge of the blades. The boundary layer properties required include the momentum thickness, displacement thickness, full thickness, and the form factor. The local momentum thickness of the boundary layer is found by integrating a form of Truckenbrodt's[4] equation:

$$\frac{\theta}{S_o} = \left(\frac{U}{U_o}\right)^{-3} \left(\frac{C_f}{2}\right)^{\frac{n+1}{n}} \int_0^{S/S_o} \left(\frac{U}{U_o}\right)^{3+2/n} d\left(\frac{S}{S_o}\right)^{n/(n+1)} \qquad (11)$$

where the exponent n is taken to be six, corresponding to large Reynolds numbers, and the friction factor is specified by the empirical expression for flat plate, turbulent flow:

$$C_f = .074/Re^{0.2} \qquad (12)$$

In this statement of the Truckenbrodt equation it was assumed that the boundary layer is turbulent along the entire blade length. This is a useful approximation and does not have an appreciable effect on the results at the trailing edge. The shape factor may be obtained as shown in

$$L = -.23 + .0076\left(\frac{n}{n+1}\right) + .0304\,\ln Re + \ln\left(\frac{U}{U_o}\right) + .0076\left(\frac{n}{n+1}\right)\ln\xi - \frac{1.0608}{\xi}\int_0^{\xi} \ln\left(\frac{U}{U_o}\right) d\xi \qquad (13)$$

where:

$$\xi = \left[\left(\frac{C_f}{2}\right)^{\frac{n+1}{n}} \int_0^{S/S_o} \left(\frac{U}{U_o}\right)^{3+2/n} d(S/S_o)\right]^4$$

As before laminar terms do not appear in the equations and the integrations are performed to the inlet edge of the blade, rather than to the laminar-turbulent transition point. The form factor H is related to the shape factor by:

$$L = \int_{E_o}^{E} \frac{1}{H-1} \frac{dE}{E} \qquad (14)$$

where E and H are related empirically by:

$$E = \frac{1.269\,H}{H - .379} \qquad (15)$$

The lower limit of integration, E_o, is taken as 1.74 to make L = zero correspond to the case of the flat plate with zero pressur. gradient, i.e., H = 1.4. The empirical form (eq. 15) is in good agreement with experimental data below H = 1.7 (Ref. 6). For larger values of H the correlation breaks down so that the equation is supplemented by a table of experimental data for use when $1.6 < H < 2.6$.

The remaining local boundary layer characteristics may be found after Schlichting[6] by applying the general power-law velocity-distribution where:

$$\frac{u}{U} = \frac{y}{\delta}^{1/n} \qquad (16)$$

so that:

$$n = \frac{2}{H-1} \qquad (17)$$

and

$$\frac{\delta^*}{\delta} = \frac{1}{1+n} \qquad (18)$$

$$\delta^* = \theta H \tag{19}$$

- The Generation of Stator Wake Velocity Profiles

The objective is to obtain a two-dimensional representation of the vapor velocity field between a stator exit plane and the inlet plane of the following rotor. Most of the work which has been done in this area has been oriented toward evaluating overall loss coefficients. There has apparently been very little interest in the fine structure of wakes per se. The work of Lieblein and Roudebush[3] comes closest to satisfying the requirements of the transport model in this respect. The analysis just cited deals with the low-speed wake characteristics of two-dimensional cascade and isolated airfoil sections. Strictly speaking, the conditions present in axial flow turbines are not quite the same as those assumed in the analysis.

The approach taken by Lieblein and Roudebush is to assume that the wake is formed by the merging of the boundary layers on the upper and lower blade surfaces at the trailing edge. The wake is eventually re-energized by a mixing process between the wake and the free-stream flow. The variation of certain wake properties with downstream distance is then predicted from both empirical and theoretical considerations.

A qualitative picture of the velocity profiles normal to the wake trough is shown in Figure 2.6-4. Note that the inclination of the wake centerline to the turbine axis is a slowly varying function of axial distance. Similarly, the wake minimum velocity increases and the wake-edge velocity or free-stream velocity decreases slightly with distance as a result of momentum transfer as the wake re-energizes.

The wake model appears to be particularly good where the ratio of blade trailing-edge thickness to chord length approaches zero and at a nominal distance downstream of the trailing edge. It is clear that very complex flow patterns will exist immediately downstream of blades of finite trailing-edge thickness. In fact, separate vortex flow may exist in many cases. The characteristics of the wake near the trailing edge are very important from the erosion point of view and directly affect the question of the upper size limit of drops reaching the rotor plane.

The atomized drops from the stator are shed into this region of complex flow. There is probably a sheltered region immediately downstream of the blade with components of flow both transverse and axial. Steam turbine observations indicate that the drops will migrate rather slowly deep in the wake, and at some point downstream are suddenly caught up and accelerated. Because of the uncertainty in this process a "dead-space" correction of about four trailing edge thicknesses has been arbitrarily introduced. The integration of the drop equation of motion is therefore begun at the edge of the dead space rather than at the blade trailing-edge.

The variation of wake trough velocity has previously been given (eq. 7 above). No consistent quantitative model for the actual shape of the transverse profile has been advanced. Provided the minimum and wake-edge velocities are reasonably correct, a half-sine curve fit to the two known points should yield consistent results for the transverse velocity profile. This method does not, however, account for the observed asymmetry in the wake. At the trailing edge the effective total boundary layer thickness is the sum:

$$\delta_{te} = \delta_{p,te} + \delta_{s,te} \tag{20}$$

The remaining trailing edge properties may be obtained from:

$$\delta^*_{te} = \delta_{p,te} + \delta_{s,te} \tag{21}$$

$$\theta_{te} = \theta_{p,te} + \theta_{s,te} \tag{22}$$

$$H_{te} = \delta^*_{te} / \theta_{te} \tag{23}$$

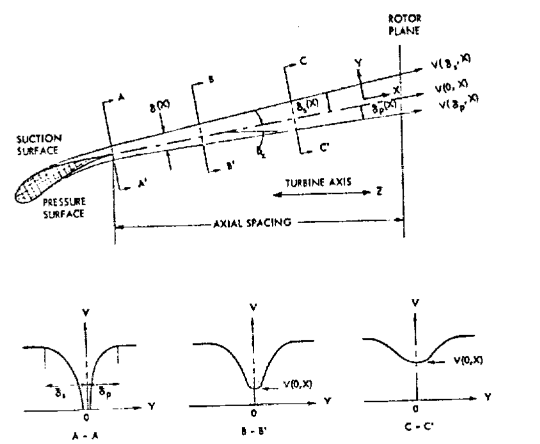

Figure 2.6-4 Qualitative Representation of Vapor Wake Development Downstream of a Stator Blade Section

The variation of the wake form factor was fitted in (6) by:

$$H_x = \frac{\sqrt{1 - 40 \times c}}{\sqrt{1 - 40 \times c} - \left(\frac{H_{te} - 1}{H_{te}}\right)} \quad (24)$$

The wake momentum thickness parameters, $\hat{\theta}$, and the flow angle simultaneously satisfy:

$$\frac{1 - \hat{\theta}_x (1 + H_x) - \frac{1}{2 \cos^2 \beta_x}}{(1 - \hat{\theta}_x H_x)^2} = \text{constant} = k_1 \quad (25)$$

$$\frac{1 - \hat{\theta}_x (1 - H_x)}{(1 - \hat{\theta}_x H_x)^2} \tan \beta_x = \text{constant} = \sqrt{K_2} \quad (26)$$

where:

$$\hat{\theta}_x = \left(\frac{\theta}{c}\right)_x \frac{\sigma}{\cos \beta_x} \quad (27)$$

Equations (25) and (26) may be solved by simultaneous iteration for $\hat{\theta}_x$ and β_x. The constants are evaluated in terms of the trailing edge condition, H_{te}, θ_{te} and β_{te}. The wake-edge velocity may then be found from:

$$V(\delta/2, x) \cos \beta_x (1 - \hat{\theta}_x H_x) = \text{constant} = k_3 \quad (28)$$

The ratio $V_{min}, x/V(\delta, x)$ is specified by the trough velocity equation(7) so that by applying (28) the trough velocity is obtained. Using a half-sine fit the transverse velocity profile is then:

$$\frac{V(y,x)}{V(\delta/2,x)} = \frac{1}{2}\left[\left(1 + \frac{V_{min,x}}{V(\delta/2,x)}\right) - \left(1 - \frac{V_{min,x}}{V(\delta/2,x)}\right) \cos \frac{\pi y}{\delta/2}\right] \quad (29)$$

Transverse wake position is specified by the ratio $y/(\delta/2)$, which is unity at the wake edge and zero at the centerline.

The latter positions are generally the most interesting. It is assumed that if a drop starts out on a particular streamline $y/(\delta/2)$, it continues in this relative position until it impacts.

- Drop Acceleration and Secondary Atomization*

The drop size spectrum from primary atomization may be estimated using the method given in Section 2.7. The empirical Nukiyama-Tanasawa distribution function is applied and from these results a suitable group of drop sizes may be chosen for the drop transport analysis. The general drop equation of motion (eq. 2) may be solved for the drop terminal velocity as a function of drop size and wake position, with the local vapor velocity within the wake obtained following the procedure outlined above.

The conditions for subsequent drop fragmentation or secondary atomization may be correlated in terms of a critical Weber Number. This subject has been given much attention in the atomization literature in recent years; however, a consistent guide to its formulation remains to be found.** Much of the empirical work has been done with steam or air streams and correlations suitable for use with liquid metal systems remain to be substantiated. Gardner(7), for instance, recognized two regimes for the critical Weber Number in steam systems. For cases where drops were introduced into a relatively slow-moving stream, which was gradually accelerated, he recommends a "steady-flow" critical Weber Number of 22. For the case of abrupt acceleration he recommends a "shock" critical Weber Number of 13. Other authors (Nicholson(8) for instance) have reported an even wider range of critical Weber numbers. In lieu of more definitive data we have tentatively adopted Gardners' results with the following rationale. The Weber Number is defined by:

$$We = \frac{\rho_v V_r^2 D_d}{\sigma_L} \quad (30)$$

and is essentially the ratio of the local dynamic force to the surface tension. In the low pressure end of steam turbines the drop relative velocity, hence drop Weber Number, increases gradually to a maximum and then decreases with downstream travel. The conditions fit the "steady-flow" Weber Number

* A comparison of calculated values of drop velocity for the Yankee turbine and experimental values from a CERL steam cascade is given in Appendix 2.6 to this section.

** A more detailed discussion of this subject is undertaken in Section 2.7.

criterion of 22. In small alkali metal turbines the onset of acceleration is quite abrupt, with the peak Weber Number occurring initially. This situation suggests use of the "shock" critical Weber Number for these systems.

As far as the trajectory model is concerned, therefore, secondary atomization is assumed to begin when a certain fixed Weber Number is exceeded anywhere along the trajectory of a drop. The disruption process takes a finite amount of time and it is usually important to know whether the distance between blade rows is sufficient to insure complete atomization of all unstable drops. From basic considerations it can be shown (9) that the disruption time shows the following dependence:

$$t \propto \frac{D_d}{V_r} \sqrt{\frac{\rho_L}{\rho_v}} \qquad (31)$$

From the data of Wolfe and Anderson[2] the time to the start of disruption was estimated to be:

$$t' = 1.1 \frac{D_d}{V_r} \sqrt{\frac{\rho_L}{\rho_v}} \qquad (32)$$

and the elapsed time to complete breakup was:

$$t'' = 2.8 \frac{D_d}{V_r} \sqrt{\frac{\rho_L}{\rho_v}} \qquad (33)$$

In the trajectory model reported here, when the local drop Weber Number exceeds the critical value at some time t, the disruption time t'' is computed. Disruption is assumed to be completed at that point on the trajectory where time t + t'' has elapsed. Presumably for drops with maximum Weber Numbers close to critical the drop may revert to a more stable condition prior to time t + t''. However, the uncertainty in the magnitude of the critical Weber Number precludes the use of such a refinement at this time.

When a primary drop disintegrates, a spectrum of secondary drop sizes may be expected, just as in the case of primary atomization. The mass mean diameter D'_d of the secondary drops is evaluated from the Wolfe-Anderson expression:

$$D_d = \left(\frac{136 \mu_L \sigma^{3/2} D_d^{1/2}}{\rho_v^2 V_r^4 \sqrt{\rho_L C_D}} \right)^{1/3} \qquad (34)$$

where all the quantities are evaluated for conditions at time t, that is, at the point where the critical Weber Number is first exceeded.

When the above analysis is concluded for a given turbine stage, an upper limit for the size of impacting drops will be obtained. The original primary drop distribution will be modified such that the "tail" extending beyond the maximum stable drop size will be removed. The fraction of the total spray volume represented by the tail represents the new secondary drop distribution which is now added to the original distribution. The mechanics of these calculations are discussed in Section 2.7. Comparison of calculated secondary drop distributions obtained using equation 34 with actual measurements in a large steam turbine are in poor agreement.

- Impact Velocity and the Geometry of Impact

The geometry conventions employed in this discussion are shown in Figure 2.6-5. Consider the inlet region of a rotor section at some fixed blade height. The pitch, S, tangential blade speed U_1, and the rotor inlet blade angle are thus fixed. The velocity V_d is the terminal drop velocity which is obtained from the solution of the equation of motion discussed previously. The direction of V_d is essentially that of the stator jet velocity; however, its magnitude depends on drop size. The drop velocity relative to the rotor is given by:

$$W_d = \sqrt{U_1^{\,2} + V_d^{\,2} - 2U_1 V_d \sin\alpha} \qquad (35)$$

The "shadow angle" α_d satisfies:

$$\cos\alpha_d = \frac{U_1 - V_d \sin\alpha}{W_d} \qquad (36)$$

Depending on the angle of the blades and the angle of incidence of the drops, there will be generally a blade region which will be shadowed and free of damaging impacts. To estimate the extent of unshadowed blade surface, a first approximation is to consider the "impaction length" ΔL defined along the tangent to the blade centerline at its nose. The actual impaction zone is the convex surface cut by the tangent line. A relation for ΔL in terms of the blade spacing S and angles α_i and α_d is:

$$\Delta L \approx S \frac{\sin\alpha_d}{\sin(\alpha_i + \alpha_d)} \qquad (37)$$

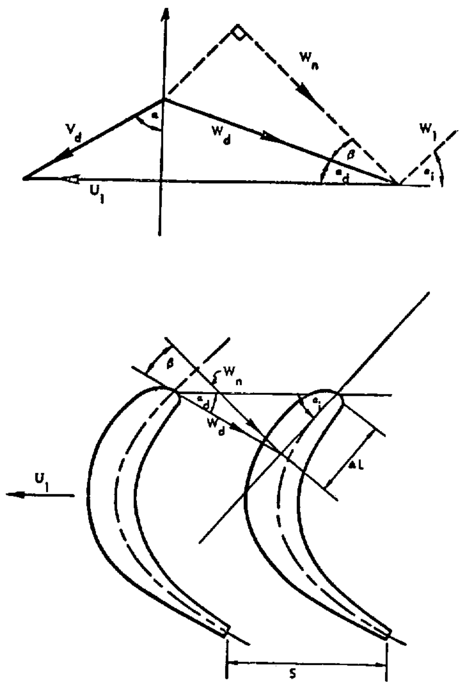

Figure 2.6-5 Drop Impingement Geometry

If the angles α_d and α_i are acute, the approximation is relatively good. Otherwise, scale drawings of the blades must be used.

The treatment employed by the overall erosion model to estimate material removal holds that it is the normal component of the component of the impacting drop velocity which is most directly related to the extent of damage. This component is obtained by noting that the angle β included between W_d and W_n is $\pi/2 - \alpha_d - \alpha_i$. Therefore:

$$W_n = W_d \cos\beta = W_d \sin(\alpha_d + \alpha_i) \qquad (38)$$

Drops at the upper end of the size spectrum will have the smallest arrival velocity. In the limit, for very small V_d, $|W_d| \rightarrow |U_1|$ and the impact region is essentially confined to the blade nose. Such a situation is very unlikely since the unbroken drops below the secondary atomization limit are accelerated to an appreciable fraction of the free stream velocity.

At the other extreme some of the smallest drops will arrive at essentially free stream velocity so that $|W_d| \rightarrow o$. The normal velocity W_n will be largest when $V_d = o$ and will decrease linearly to zero when V_d reaches the free stream value. For some value of drop terminal velocity the vectors W_n and W_d will coincide. Beyond this point, in the direction of higher terminal velocities and smaller drop diameters, the impact length concept breaks down. The significant impact area is the nose since W_d is normal to the nose at some point. The cross-over point is represented analytically by the condition $\beta = o$. It follows then that:

$$\alpha_{do} = \frac{\pi}{2} - \alpha_i \qquad (39)$$

$$V_{do} = \frac{U_1}{\sin\ (\cot\alpha_{do} - 1)} \qquad (40)$$

$$W_{do} = V_{do} \frac{\sin\alpha}{\sin\alpha_{do}} \qquad (41)$$

Therefore, when $V_d > V_{do}$ the relative velocity W_d will exceed W_n and should be considered as far as potential damage is concerned. Note that increasing the blade speed has the effect of increasing V_{do}, thus decreasing the tendency of the damage to be confined to the nose area.

2.6.4 Description of the ADROP Code Package

The ADROP code is designed to examine in detail the transport of atomized condensate from the stator exit plane to the rotor inlet plane in wet vapor axial flow turbines. The code facilitates parameter surveys and can be used to systematically test the implications of various assumptions made in the model. The computational model as outlined in the previous section is far from definitive, in fact it represents a first cut at a comprehensive explanation of observed phenomena.

A single stage and blade height position is examined at one time, however, as many problems as necessary may be run consecutively. Temperature-dependent working fluid properties are computed by an auxiliary subroutine, with a present capacity of eight materials: lithium, sodium, potassium, rubidium, cesium, mercury, NaK-78, and water. For a given stage, geometry, and bulk flow condition, a range of drop sizes are introduced into the vapor stream at various wake positions. Terminal velocities are obtained for all drops. If the flow conditions are such that a drop satisfies the condition of aerodynamic instability, the approximate location of disruption is noted and the mass mean diameter of secondary drops is estimated.

The program source language is FORTRAN IV. The code is oriented toward the CDC machines 3600, 6400, and 6600; however, compatibility with equivalent IBM equipment can be achieved with a minimum of effort. On the CDC 6600 system operated by the Westinghouse Tele-Computer Center the field length required by the code, associated system routines, and storage areas is 18,000 words decimal. Calculations and output are in cgs units, with inputs in common engineering units. Options are available to control the quantity of printed output and the sequence of calculations. A source language listing of each item in the code package may be found in Appendix B to this section.

- The Main Program

Input functions, initialization, and option selection are handled by the main program. Data is input using the format-free NAMELIST feature. For each individual problem the input consists of a title card, and a sequence of cards defining quantities in the NAMELIST DRP. The 80-column card image of the title card is used to identify the output listing. Variables in the DRP list are /DRP/KOP, TR, VFREE, GDAT, XS, VS, XP, VP, PD, SD, PDS, SDS, PTH, STH, XQ, DIAM.

It should be emphasized that only those numbers required to do a particular problem configuration need to be input. Data is transferred from one problem to the next. Thus, the first problem in a series might have a complete input set, while subsequent problems might only require one or two input numbers. The input list variables involved are defined in Table 2.6-1. Blade surface velocity plots may be obtained in several ways. Our usual practice has been to employ the code of Reference 14 to generate this data.

Material properties required for the working fluid in question are the density of vapor and liquid, the viscosity of vapor and liquid and the surface tension of the liquid. These are obtained by calling subroutine PROPM. The data is then stored in common block/PRP/ for later use. Table 2.6-2 lists the important common blocks used for intersubroutine communication. A specific sample problem will be discussed in Section 2.6 to illustrate the input and output formats.

- Subroutine TRUCK

The calculation of the boundary layer properties along blade surface is handled in a code devised by W. K. Fentress. The code has been recast into subroutine form and incorporated into the ADROP system. The input surface velocity tables, which may contain as few as four points each is expanded into a 40-point table using parabolic spline interpolation (subroutine SPLINT). The Truckenbrodt boundary layer equation and the shape factor equation are then integrated by the trapezoidal method.

TABLE 2.6-1

ADROP INPUT NAMELIST DEFINITIONS

Name	Definition
KOP(1)	Working fluid sentinel (see definition of JFLUID on page 42)
KOP(2)	Number of stator blades
KOP(3)	Number of rotor blades
KOP(4)	Shaft RPM
KOP(5)	Boundary-layer calculation option (subroutine TRUCK) ≤ 3 calculation is deleted. Otherwise KOP(5) specifies the number of referred position-velocity pairs to be input.
KOP(6)	TRUCK IO sentinel. If KOP(6) > 0 detailed boundary layer results will be printed.
KOP(7)	TRAX option sentinel. If KOP(7) $\leq$ 0 trajectory calculations will be deleted. A value greater than zero sets the trajectory print interval.
KOP(8)	IMPAX option. If KOP(8) $\geq$ 0 the drop impact geometry will be examined.
KOP(9)	Wake option. If KOP(9) $\geq$ 0 full wake treatment will be used. Otherwise the approximate treatment is specified.
KOP(10)	Debug option = 0 option ignored >0 data will be printed out during each wake iteration = 2 trajectory data will be printed for each trial integration step.
TR	Bulk vapor temperature at stator exit (°R)
V FREE	Stator exit jet velocity (feet/sec.)
XQ	Bulk vapor quality at stator exit.
GDAT(1)	Stator exit flow angle (angle α in Figure 5)
GDAT(2)	Inlet rotor blade angle (angle α_i in Figure 5)
GDAT(3)	Trailing-edge multiplier used to define the dead-space.
GDAT(4)	Critical Weber Number
GDAT(5)	Stator exit section diameter (inches)
GDAT(6)	Rotor inlet section diameter (inches)
GDAT(7)	Axial space between stator exit and rotor inlet planes (inches)
GDAT(8)	Stator trailing-edge thickness (inches)
GDAT(9)	Stator chord length (inches)
GDAT(10)	Pressure surface length (inches)
GDAT(11)	Suction surface length (inches)
DIAM	Array of nine drop diameters (microns)
XS, XP	Arrays of referred positions in suction and pressure sides
VS, VP	Arrays of referred surface velocities on suction and pressure sides.
PD, SD	Pressure and suction side boundary layer thicknesses (cm)
PDS, SDS	Pressure and suction side displacement thicknesses (cm)
PTH, STH	Pressure and suction side momentum thicknesses (cm)

TABLE 2.6-2

COMMON BLOCK LAYOUT IN PROGRAM
ADROP

BLOCK DEFINITIONS

/PRP/MAT,TEMP, RHOV, RHOL, SIGL, VISL, VISV

/TBG/CHORD, PITCH, BTE, PD , SD, PDS, SDS, PTH, STH, VZERO

/GEO/NSTAT, NROTR, RPM, ALPHA, ALPHI, F DEAD, WDC, DSTAT, DROTR, AXSP, STE,
SCHD, SPARC, SSARC

/CST/JOB(10), JMAT(10), PI, RD, NYD, DIAM(10)

/BUG/IBUG

/ICON/H, HMAX, HMIN, RELB, ABS B

/TRX/ . . .

BLOCK REFERENCES

	MAIN	TRUCK	TRAX	DERIV	IMPAX	WAKE	ICEAD
PRP	X	X	X	X			
TBG	X	X	X	X		X	
GEO	X		X	X			
CST	X	X	X	X	X		
BUG	X			X		X	
ICON			X	X			X
TRX			X	X			

Calling Sequence

Call TRUCK (M, SS, SP, XXS, XVS, XXP, XVP, IØ) where:

M is the number of surface velocity points to be input for each surface.

SS is the length of the suction surface.

SP is the length of the pressure surface.

XXS is the array of M suction surface referred position points.

XVS is the array of referred surface velocities corresponding to each value of XXS.

XXP,XVP are the position and velocity arrays for the pressure side

IØ is the output listing control sentinel. If IØ> 0 a listing of boundary layer properties along the blade will be obtained.

Output quantities required for subsequent calculations in other subroutines are placed in common block/TBG/. These are PD, SD, PDS, SDS, PTH, STH, which are the pressure and suction side trailing edge values of boundary layer, displacement and momentum thicknesses. No assumptions are made internally concerning units. The unit of length used for the surface lengths SS and SP, however, should be the same as that used in the thermophysical properties. In the context of the ADROP code the units are cgs.

Probable flow separation is indicated if the shape factor (Eq. 13 above) $L(\xi) < -0.18$ at any point. This condition is identified by a diagnostic message. If this situation occurs, the integer IØ is set to -10 before control returns to the main program. This is used to prevent the subsequent trajectory calculations from starting. Data for the next problem is then read in so that the failure of one problem will not interrupt the entire sequence.

Output listings which may be obtained are:

a) The input surface velocity tables

b) Boundary layer properties at each surface position (optional)

c) Summary of the trailing-edge boundary layer values.

A listing of the subroutine is given in Appendix B to this section. Note that common blocks PRP/, TBG/ and EST/ are required by the subroutine.

- Subroutine WAKE

The function of this subroutine is to provide the local vapor velocity at a specified position within a stator blade wake. Common block/TBG/is used to transmit the numerical values of the stator chord, exit pitch, jet velocity, and the boundary layer displacement and momentum thicknesses at the stator trailing-edge. The calling sequence for the subroutine is:

CALL WAKE (NS, XX, YD, VXY, BX)

where:

XX is the distance from the trailing edge along the wake centerline where the vapor velocity is required

YD is the transverse position $y/(\delta/2)$ within the wake. It is necessary that $0 \leq YD \leq 1$

VXY is the output local vapor velocity

BX is the local wake angle in radians, i.e., the inclination of the wake centerline to the turbine axis.

NS is used as a control sentinel which is set prior to the first WAKE CALL. If NS = 0 when WAKE is called, the constants defined by Equations 25, 26 and 28 are evaluated using trailing edge boundary layer data. WAKE changes NS to unity so that on subsequent calls the initialization section of the subroutine is skipped. If boundary layer data is not available, useful approximate solutions may be obtained assuming a constant free stream velocity and flow angle downstream of the stator. In this case the user must preset NS = 1. Only two values of YD may be used; YD = 0 or YD = 1 in this situation.

The simultaneous iterative solution of equations 25, 26 and 28 is accomplished with the assistance of the auxiliary subroutine VERGE. If convergence of the iterative process has not been accomplished after 20 attempts, there is usually something wrong with the input data. The process is suspended and a diagnostic printed out. The sentinel NS is set to 10 and control returned to the calling routine. It is recommended that NS be tested after each return so that appropriate action may be taken in the event of an iteration failure.

It is required that the unit of length used in the data in common block/TBG/be consistent with those employed in the input arguments XX and VXY.

- Subroutine TRAX

TRAX is the control subroutine for the integration of the drop equation of motion. A fourth-order Adams predictor-corrector method is used in auxiliary subroutine ICEAD to perform the actual numerical integration. TRAX initializes ICEAD for each trajectory and stores final results. These results are eventually listed in a problem summary. Normally thirty trajectories are computed for each problem, i.e, one for each combination of the three wake positions ($Y/(\delta/2) = 0, 0.35$, and 1) and the ten input drop diameters. If the approximate wake treatment is used, the two limiting wake positions ($Y/(\delta/2) = 0., 1$) are used so that twenty trajectories are computed.

The summary printout lists, for each drop diameter and wake positions, the time-of-flight, terminal drop velocity, initial and final relative velocities, the maximum Weber Number, and the final flow angle. A secondary atomization summary is also given. For each drop that satisfies the disruption criteria the summary lists the time-to-complete disruption, mass-mean diameter of secondary drops produced, drop velocity when the critical Weber Number is reached, and the referred distances to disruption. The absolute disruption distance is the total path length from the stator trailing edge to the estimated point of complete disruption. The first referred quantity gives the distance in drop diameters. The second gives the ratio of the absolute disruption distance to the total path length available between the stator and rotor planes. The distances are used to indicate whether there is sufficient space for the unstable primary drops to completely disintegrate before impact.

The input argument IØ controls the print interval for the printout of values along the trajectory. If IØ ≤ 0 the printout is deleted. The print interval is computed by:

$$ZP = (AXSP-XDEAD)/(IØ-1)$$

The effective total axial distance is the axial blade space minus the dead space. An input value of 11, for instance, will yield 11 sets of values spaced at intervals of one-tenth the total distance. The actual printing is done by subroutine DERIV.

- Subroutine DERIV

This subroutine is used in conjunction with the integration scheme ICEAD to provide derivatives, intermediate printouts, and secondary atomization calculations. Three entry points DERIV, STEP and FAIL are employed. These satisfy the requirements of ICEAD. For each trail integration step ICEAD will call DERIV to obtain the derivatives associated with the simultaneous differential equations at that point. Certain error criteria are checked and if a given time step produces satisfactory results ENTRY STEP is called (the logic employed by ICEAD will be discussed below). When a trial integration fails, the step size (in the time variable) is halved. The process continues until an integration step yields satisfactory results or a fixed lower step size limit is reached. In the latter event ICEAD calls FAIL which takes appropriate action.

Common blocks used in the subroutine are listed in Table 2.6-2. The calling sequence is as follows:

CALL DERIV (T, Y, DY, IRET)

where:

T	is the present value of the time variable
Y	is a two-word array containing the present values of drop velocity, Y (1), and distance along the wake axis, Y (2).
DY	is a two word array containing the derivatives of Y (1) and Y (2).
IRET	is a return sentinel. During the integration process IRET remains zero. When the integration is completed IRET is set to unity.

A debug option (see main program for definition of KOP (10) is provided so that present values of distance, time and velocity are listed for each trial time step. After each successful integration STEP is entered and if a print interval has elapsed, the present values of time, distance along the wake axis, distance along the turbine axis, absolute and relative drop velocity, local Weber and Reynolds Numbers, and the time step used are printed.

Subroutine WAKE is called after each time step to get the local vapor velocity. If the wake iteration fails, diagnostics are printed and IRET is set to unity. This eventually returns control to subroutine TRAX so that the next trajectory may be started. The terminal flow angle is set to -1 if the wake calculation fails. Failure of the integration is indicated by inserting a value of -1 in the final velocity array.

- Subroutine IMPAX

The geometry of drop impingement is evaluated with subroutine IMPAX. The range of possible absolute drop impact velocities is bounded by zero and the stator exit jet velocity. Actually, the secondary atomization limit prevents the larger and slower moving drops from reaching the rotor. In any case the subroutine runs through all possible impact velocities and computes the drop velocity relative to the rotor, the normal component of impact velocity, and the impact length (these are defined as Wd, Wn, and ΔL in Figure 2.6-5).

Calling Sequence

Call IMPAX (NB, BDIA, RPM, AL, AI, VZERO)

where:

NB	is the number of rotor blades
BDIA	is the inlet diameter at the blade height in question
RPM	is the rotor RPM
AL	is the stator exit flow angle with respect to the turbine axis.
AI	is the actual rotor inlet blade angle (see α_i in Figure 2.6-5) with respect to the rotor inlet plane.
VZERO	is the stator jet velocity.

It was pointed out previously that the impact length approximation is only useful when impacts on the convex blade surface occur. When the conditions expressed by equations (39), (40) and (41) occur, nose impacts are important and the listed values of ΔL will be set to:

$$\Delta L_{max} = S \cos \alpha_i$$

- Auxiliary Subroutines

Four general purpose subroutines are included in the code package. These were developed in the context of the overall turbine erosion model; however, they represent valuable tools which can be used in many other circumstances. Each is described fully in a separate report so that an abbreviated discussion is presented here.

- Subroutine SPLINT

This subroutine is designed to perform interpolation and differentiation using the parabolic spline. The spline is generated by a closed form expression, and an important characteristic of the method is that the first derivatives of the array of interpolated results are continuous. Unequal tabular intervals may be employed and a special search scheme has been devised to permit the independent variable to be either monotonically increasing or decreasing. A useful by-product of this method of interpolation is that an estimate of the local derivative (of the interpolated curve) may be readily obtained. The closed-form solutions used are due to Mintz and Jordan.

The subroutine has two entry points called SPLINT and DYDX, the former for interpolation and the latter for differentiation. The calling sequences are:

CALL SPLINT (XT, YT, NT, XI, YI, NI, JX, JY)

CALL DYDX (XT, YT, HT, XI, DY, NI, JX, JY)

where:

XT	is the name of the independent variable array
YT	is the name of the dependent variable array
NT	is the number of input (XT, YT) pairs. It is required that NT $\geq$ 4.
XI	is the name of the array of input interpolation arguments
YI	is the name of the output array of interpolated values
DY	is the name of the output array of first derivatives
JX,JY	are integers representing the storage increments in arrays XT and YT (standard values: JX = JY = 1).

The set (XT, YT) is the table in which the interpolation is to be done. Dummy dimensions are used for all arrays so that the storage space required is set by the calling program. XI, YI and DY are listed as arrays; however, they may represent single values.

- Subroutine VERGE

VERGE is designed to accelerate the convergence of iterative processes. Many equations encountered in the numerical solution of engineering problems do not permit explicit solution for certain variables; these must be solved by iterative techniques. A good example is the simultaneous set of equations (25), (26), and (28) employed in the stator wake treatment discussed above. The scheme utilized by VERGE accelerates the rate of convergence if the iteration converges and induces convergence if the basic iteration process tends to diverge. The subroutine is based on the convergence algorithm of Wegstein[12]. The general class of problems which is of interest is that which may be written in the form: $x = f(x)$. The right-hand side is typically a complicated transcendental relation or perhaps the result of a lengthy numerical operation.

- Calling Sequence

Call VERGE (XI, FØX, IK)

where:

XI	is the present value of the interated variable. User must supply an initial guess, and at each pass through VERGE XI will be modified to induce convergence.
FØX	is the value of the function F(XI) for the present XI
IK	is an iteration counter. User must preset IK for the first iteration. It is updated by VERGE and set negative when the convergence test is met. Normally IK is preset to zero. The user should test present values of IK as they are returned from VERGE to detect convergence.

• Convergence Criteria

It is necessary to insure that machine underflows will not result. If one is searching for a root near the origin, very small numbers (in absolute value) will be encountered during the iteration. Convergence is assumed if either of the following conditions is satisfied.

$$|f(x_n) - x_n| < EPS$$

$$|x_n| < ETA$$

where EPS and ETA are quantities defined in a DATA statement and may be modified by the user to fit special situations. In the subroutine version described here they have been given the values 1×10^{-10} and 1×10^{-30}, respectively. Non-convergence is not detected explicitly. The user should check the present value of the iteration counter IK against some upper limit appropriate for the particular problem at hand. For the wake parameter iteration in subroutine WAKE it has been found that if convergence is not reached after 20 iterations, the input data is usually at fault.

• Subroutine ICEAD

This subroutine is a general purpose scheme for solving systems of ordinary differential equations. A fourth-order Adams predictor-corrector method is used with automatic error control. It is based on ICEADAMS, an ALGOL-5000 procedure by Geil and Wei(13) which was translated into FORTRAN by the author and modified for this application.

• Calling Sequence and Required Common Block

CALL ICEAD (N, T, XI, IRET)

COMMON/ICON/H, HMAX, HMIN, RELB, ASBS

where:

N is the number of dependent variables. (simultaneous differential equations)

T is input as the initial value of the independent variable

XI input as the vector (one-dimensional array) of initial values of each of the N dependent variables.

IRET output integer return sentinel which must be zero initially: When the subroutine detects a non-zero value of IRET, control is returned to the calling program. May be used to indicate that the integration is completed-either successfully or otherwise.

H is input as the suggested initial step-size. Will thereafter contain the present step size selected by ICEAD.

HMAX is the maximum acceptable step size.

HMIN is the minimum acceptable step size.

RELB is the maximum acceptable relative error (the ratio of the absolute difference between the predictor and corrector for each independent variable).

ABSB is the maximum acceptable absolute error. (If RELB is exceeded but the absolute difference between the predictor and corrector values is smaller than ABSB, ICEAD will accept the integration step as successful. ABSB is used to guard against exceeding the machine accuracy limits.

• General Use of the Subroutine

The analytical basis of the subroutine is given in Reference 13 which describes the ALGOL version. Certain mechanical aspects have been changed due to language incompatibilities; however, the basic numerical steps are identical in the two versions.

The common block ICON was incorporated to permit optional user control of the error bounds in the auxiliary subroutines. The FORTRAN version described here has been dimensioned to permit the solution of up to ten simultaneous differential equations. The user is required to provide three auxiliary subroutines with the names DERIV, STEP, and FAIL. It is usually convenient to use one subroutine with three entry points to perform the appropriate functions.

- Subroutine DERIV (T, X, DX, IRET)

The argument list consists of:

T the present value of the independent variable (input)

X vector of values of the dependent variables (input)

DX vector of derivatives of array x (output)

IRET return sentinel

The calling program provides ICEAD with a set of initial values for the independent and dependent variables. ICEAD will then determine trial step sizes and will call DERIV to calculate required derivatives based on present values of each dependent variable and associated derivatives. Note the initial values for the derivatives can be defined if necessary in DERIV. IRET is normally not used in DERIV. It may be set non-zero if an anomalous condition is encountered. If ICEAD detects a non-zero value at any time, control is returned to the calling program.

- Subroutine STEP (T, X, DX, IRET)

STEP is called by ICEAD after each successful integration step. The argument list is the same as for DERIV so that STEP may be defined alternately as an entry point in DERIV. A printout section may be provided here to list results at predetermined increments of any of the variables. A test for the termination of integration must be included in STEP. The user may simply call EXIT or STEP, or set IRET> 0. Control will then pass to the routine which originally called ICEAD. Normally, the last integration step will over-run the integration limit. This can be avoided by adjusting the step size limit HMAX just before the integration limit is reached to force termination at the desired point.

- Subroutine FAIL (T, X, DX, IRET)

FAIL is called by ICEAD when the integration step size has been reduced below HMIN. ICEAD will strive to select the largest step size available. Trial steps are taken at one-half and twice the present step size and the error criteria checked. If the criteria cannot be satisfied for any H such that HMAX > H $\geq$ HMIN,FAIL is called. In FAIL the user may wish to print some diagnostic comments. It is necessary then to call EXIT, STOP, or set IRET> 0 and RETURN.

- Subroutine PROPM

This subroutine was designed to generate comprehensive thermophysical properties of various power system working fluids. It provides a central data source, with a consistent set of units, to support computerized design and analysis efforts. The basic system of units is metric; however, a conversion subroutine is supplied to communicate in engineering units. The user supplies a temperature and specifies a material and a property, and gets the required property value back.

All properties are taken along a saturation line and are assumed to be functions of temperature only. Most of the properties are described by equations obtained from least square fits. In a few cases this was not feasible and spline interpolation (subroutine SPLINT) is used on tabular data. In general the empirical fits are more desirable. They offer a speed advantage and require far less storage space than tabular data.

Eight working fluids are represented in the data compilation. Four of these, potassium, cesium, water,and mercury, have received the most attention since they have been required in various phases of turbine erosion analysis under the subject contract. The remaining fluids, lithium, sodium, rubidium,and NaK-78, have been given a cursory treatment and were included for the sake of completeness. No attempt at evaluation was made at this time The primary source of the potassium and cesium data is the work of Ewing, et. al. (14, 15) and Achener (16). Water data was obtained from the recently completed ASME steam tables (17). The mercury data was required for an erosion-oriented analysis of the Sunflower turbine series so that for the sake of compatibility at TRW data compilation (18) was used.

Calling Sequence

Call PROPM (XM, TK, JPROP, JFLUID)

Call PROPE (XE, TR, JPROP, JFLUID)

where

XM is the output property value in metric units.

XE is the output property value in engineering units.

TK is the input temperature in degrees Kelvin.

TR is the input temperature in degrees Rankine.

JPROP specifies a particular property according to the following table:

JPROP	Property	PROPM Units	PROPE Units
1	Liquid density	g/cm^3	lbm/ft^3
2	Vapor density	g/cm^3	lbm/ft^3
3	Liquid viscosity	g/sec-cm (poise)	lbm/ft-sec
4	Vapor viscosity	g/sec-cm	lbm/ft-sec
5	Liquid thermal conductivity	W/cm-°K	Btu/sec-ft°R
6	Vapor thermal conductivity	W/cm-°K	Btu/sec-ft°R
7	Liquid specific heat	joule/g-°K	Btu/lbm-°R
8	Vapor specific heat	joule/g-°K	Btu/lbm-°R
9	Surface tension	dyn/cm	lb/ft
10	Not Used	---	---
11	Liquid sonic velocity	cm/sec	ft/sec
12	Vapor sonic velocity	cm/sec	ft/sec
13	Vapor pressure	bars	psia
14	Latent heat of vaporization	joule/g	Btu/lbm
15	Liquid electrical resistivity	ohm-cm	ohm-in.

The rationale of the metric system chosen is that it almost completely eliminates the use of conversion factors. The unnecessary distinction between heat and energy units has not been made. JFLUID specifies a particular working fluid according to the following convention:

JFLUID	MATERIAL
1	Lithium
2	Sodium
3	Potassium
4	Rubidium
5	Cesium
6	Mercury
7	NaK-78
8	Water

2.6.5 The Solution of an Illustrative Problem

The sample problem chosen is an analysis of drop transport in a steam test rig used by Rocketdyne in a NASA-sponsored experimental program under Contract NAS 7-391. This program involves the examination of drop formation in a system using six stator blade shapes and a variety of flow conditions. Blade shape 1-A and the conditions designated as test 114A were chosen for the illustrative problem.

The series of input cards required for this problem are shown in Table 2.6-3. Input for a subsequent problem test 114B, is also given to show how the code makes use of data carried from one problem to the next. Only those values which are different from the previous case need to be specified.

The code-produced summary of input data is given in Table 2.6-4. Working fluid properties evaluated at the input temperature and quality are also tabulated. If a boundary layer calculation is required the listing shown in Table 2.6-5 will appear. This is a tabulation of the input blade surface velocity arrays and the blade Reynolds numbers, based on exit conditions and the surface lengths, for both pressure and suction sides. A sample of the detailed boundary layer result listing is given in Table 2.6-6. Since this output is optional, a summary of the boundary layer results evaluated at the blade trailing edge will always appear and is shown in Table 2.6-7.

A sample of the detailed results obtained from the drop trajectory calculations is shown in Table 2.6-8. Such a listing will appear for each possible combination of drop size and wake position.

TABLE 2.6-3

ADROP INPUT DATA CARDS FOR THE SAMPLE PROBLEM

```
ROCKETDYNE BLADE 1-A   TIP SECTION        TEST 114A

$DRP KOP(1)=8,29,29,0,11,1,12,-8,0,0, TR=601.5,VFREE=1170.,XQ=.986,

 GDAT(1)= 68.8,0.,4.,22.,5.9318,0.,1.,.0075,1.2,1.412,1.142,

 XS(1) = 0.,.1,.2,.3,.4,.5,.6,.7,.8,.9,1.,

 VS(1) = .408,.84,.898,.964,1.06,1.092,1.1,1.099,1.09,1.076,1.,

 XP(1) = 0.,.1,.2,.3,.4,.5,.6,.7,.8,.9,1.,

 VP(1) = .180,.42,.55,.567,.565,.61,.63,.662,.728,.814,1.    $ TEST 114A


 ROCKETDYNE BLADE 1-A   TIP SECTION        TEST 114B

 $DRP              TR=636.85,VFREE=540.,XQ=.963,   $  TEST 114B
```

TABLE 2.6-4

ADROP INPUT DATA SUMMARY

```
INPUT DATA       ROCKETDYNE BLADE 1-A   TIP SECTION      TEST 114A
OPTIONS    KOP =       8      29      29      0      11      1      12      -8      0      0

     BULK FLUID TEMPERATURE (DEG R) =    601.50     FREE-STREAM VELOCITY (FPS)    =   1170.00
     BULK FLUID QUALITY             =     .9860     EXIT FLOW ANGLE (DEG)         =     68.80
     INLET ROTOR BLADE ANGLE (DEG)  =      0.00     DEAD-SPACE MULTIPLIER         =      4.00
     CRITICAL WEBER NUMBER          =     22.00     EXIT STATOR DIAMETER (IN)     =    5.9318
     INLET ROTOR DIAMETER (IN)      =    0.0000     AXIAL INTER-ROW SPACE (IN)    =    1.0000
     STATOR TE THICKNESS (IN)       =     .0075     STATOR CHORD (IN)             =    1.2000
     PRESSURE SURF. LENGTH (IN)     =    1.4120     SUCTION SURF. LENGTH (IN)     =    1.1420

WATER   WORKING FLUID AT T(K) =  334.2
          RHOV (G/CC) =    1.3702E-04
          RHOL (G/CC) =    9.8271E-01
          VISV (P)    =    1.0523E-04
          VISL (P)    =    4.5600E-03
          SIGL DYN/CM =    6.2320E+01
```

TABLE 2.6-5

BOUNDARY LAYER INPUT DATA SUMMARY

TWO-D BOUNDARY LAYER CALCULATION   ROCKETDYNE BLADE 1-A   TIP SECTION   TEST 1144

FLUID = WATER   RES = 1.354E+05   REP = 1.676E+05

INPUT POSITION AND SURFACE VELOCITY ARRAYS

SUCTION X	SUCTION V	PRESSURE X	PRESSURE V
0.0000	.4080	0.0000	.1800
.1000	.8400	.1000	.4200
.2000	.8980	.2000	.5500
.3000	.9640	.3000	.5470
.4000	1.0600	.4000	.5650
.5000	1.0920	.5000	.6100
.6000	1.1000	.6000	.6300
.7000	1.0990	.7000	.6620
.8000	1.0900	.8000	.7280
.9000	1.0760	.9000	.8140
1.0000	1.0000	1.0000	1.0000

TABLE 2.6-6

DETAILED BOUNDARY LAYER RESULT PRINTOUT

TWO-D BOUNDARY LAYER CALCULATION   ROCKETDYNE BLADE 1-A   TIP SECTION   TEST 1144

SUCTION SURFACE

REFERRED DISTANCE	REFERRED VELOCITY	REFERRED MOM THIC	SHAPE FACTOR	FORM FACTOR	EXPONENT N	MOMENTUM THICKNESS	DISPL. THICKNESS	FULL THICKNESS
.025000	.551062	.000089	0.000000	1.400000	5.000000	.000256	.000362	.002171
.050000	.670750	.000159	-.049584	1.488689	4.092583	.000463	.000689	.003507
.075000	.767062	.000214	-.064016	1.520442	3.842889	.000621	.000945	.004576
.100000	.840000	.000270	-.072000	1.540074	3.703193	.000783	.001206	.005471
.125000	.880409	.000342	-.083056	1.578128	3.459439	.000992	.001565	.006979
.150000	.891875	.000437	-.096479	1.624942	3.200298	.001268	.002061	.008656
.175000	.891703	.000543	-.102353	1.647349	3.089522	.001576	.002597	.010519
.200000	.898000	.000634	-.095873	1.621864	3.216136	.001838	.002981	.012549
.225000	.913234	.000700	-.083212	1.575511	3.475170	.002032	.003201	.014324
.250000	.928625	.000762	-.074713	1.547736	3.651405	.002211	.003422	.015917
.275000	.945203	.000817	-.067381	1.528290	3.785735	.002371	.003623	.017360
.300000	.966000	.000863	-.059912	1.511317	3.911465	.002504	.003785	.018689
.325000	.987391	.000895	-.050444	1.490957	4.073680	.002596	.003870	.019634
.350000	1.014125	.000916	-.041444	1.472337	4.234264	.002657	.003912	.020677
.375000	1.039797	.000939	-.036387	1.462039	4.328439	.002725	.003984	.021230
.400000	1.060000	.000976	-.036426	1.462305	4.326146	.002832	.004141	.022056
.425000	1.073062	.001031	-.040895	1.470846	4.247472	.002989	.004397	.023074
.450000	1.081500	.001096	-.045058	1.481089	4.157237	.003176	.004708	.024278
.475000	1.087187	.001167	-.050257	1.490127	4.080579	.003385	.005044	.025429
.500000	1.092000	.001239	-.052879	1.495811	4.033797	.003595	.005377	.027066
.525000	1.095898	.001313	-.054602	1.499624	4.003010	.003808	.005711	.028470
.550000	1.098062	.001391	-.056494	1.503628	3.969607	.004035	.006068	.030157
.575000	1.099195	.001472	-.058104	1.507363	3.941951	.004270	.006437	.031812
.600000	1.100000	.001554	-.059076	1.509485	3.925532	.004506	.006802	.033505
.625000	1.100570	.001635	-.059585	1.510590	3.916067	.004743	.007166	.035227
.650000	1.100562	.001718	-.060090	1.511706	3.908496	.004984	.007535	.036985
.675000	1.100023	.001803	-.060615	1.512861	3.899696	.005231	.007914	.038778
.700000	1.099000	.001891	-.061174	1.514090	3.890367	.005484	.008303	.040606
.725000	1.097430	.001980	-.061859	1.515606	3.878930	.005744	.008705	.042473
.750000	1.095312	.002073	-.062694	1.517465	3.864997	.006012	.009123	.044396
.775000	1.092789	.002167	-.063579	1.519452	3.850210	.006287	.009553	.046433
.800000	1.090000	.002264	-.064427	1.521377	3.835995	.006567	.009991	.048317
.825000	1.088305	.002354	-.064122	1.520682	3.841116	.006828	.010383	.050266
.850000	1.087187	.002440	-.063286	1.518791	3.855114	.007077	.010749	.052186
.875000	1.083977	.002540	-.064288	1.521062	3.838318	.007366	.011207	.054222
.900000	1.076000	.002675	-.069234	1.532860	3.753334	.007760	.011896	.056444
.925000	1.062812	.002855	-.078189	1.558500	3.581019	.008280	.012905	.059118
.950000	1.045750	.003075	-.089814	1.599321	3.337108	.008919	.014264	.061866
.975000	1.024812	.003345	-.104234	1.655031	3.053292	.009703	.016058	.065990
1.000000	1.000000	.003678	-.121706	1.741637	2.696737	.010668	.018580	.068696

In the given sample problem 30 such sets will be generated. At each time point listed the drop position on the wake axis, along the turbine axis, the drop velocity, drop relative velocity, local drop Reynolds number, local drop Weber Number, and the present integration time step are tabulated. Table 2.6-9 shows the summary of trajectory results which appears at the conclusion of each problem. For each diameter and wake position the following items are given:

TFLIGHT This is the time-of-flight (seconds) of the drop along the trajectory.

VDFINAL This is the terminal velocity of the drop (cm/sec)at the rotor inlet plane.

VRELI This is the initial relative velocity of the drop (cm/sec) when it leaves the trailing edge dead band.

VRELF This is the final relative velocity of the drop (cm/sec).

WEDM This is the maximum local drop Weber Number which occurred along the trajectory.

ALPHA This is the terminal inclination of the velocity vector VDFINAL, with respect to the turbine axis, at the rotor inlet plane.

A secondary atomization data summary then appears as shown in Table 2.6-10. For each drop diameter-wake position combination where the critical Weber Number has been exceeded the following quantities are listed:

TDIS is the time (Equation 33) required to complete disruption.

DSTC is the mass mean diameter (cm) of secondary drops formed.

/DIS is the relative drop velocity at the point at which the critical Weber Number was exceeded.

XDC is the distance along the path from the trailing edge to the point of complete disruption divided by the drop diameter.

XDIS is the path length to the point of complete disruption, divided by the total possible path. A value greater than or equal to unity implies there is insufficient time for the drop to shatter prior to impact.

The sample problem used did not involve an examination of the impact geometry since the test rig did not incorporate a stator section downstream of the nozzle examined. The results of another problem are included here (Table 2.6-11) to illustrate the output form of the impact geometry summary. These data are taken from an analysis of drop transport in the last stage of the Sunflower mercury turbine. The nomenclature used on the printout corresponds with that used in Figure 2.6-5 and in the defining Equations 35 through 41.

2.6.6 Summary

A model describing the transport of atomized condensate in wet vapor turbines has been assembled. The basic problem which is considered is the trajectories of drops of liquid in the space between the rotor, where it is discharged, and the rotor inlet plane. Relatively simple closed-form solutions for the drop equation of motion have been obtained for certain special cases. A detailed calculational procedure was developed to provide specific solutions to the problem in a more general context.

The drop transport code package (ADROP) has been described in detail. The scope of the numerical treatment is as follows:

a) Estimation of stator blade boundary-layer characteristics.

b) Generation of the local velocity field within the vapor wake downstream of stator blades.

c) Numerical integration of the equation of motion of drops traveling along various wake streamlines and the estimation of secondary atomization effects.

d) Solution of drop impact velocity triangles to provide information on the magnitude of the normal component of impact velocity and the physical location of erosion.

TABLE 2.6-7

TRAILING EDGE BOUNDARY LAYER DATA
SUMMARY

TRAILING EDGE BOUNDARY LAYER DATA   ROCKETDYNE BLADE 1-A   TIP SECTION   TEST 1144

	PRESSURE SIDE	SUCTION SIDE
MOMENTUM THICKNESS (CM)	.00359	.01067
DISPLACEMENT THICKNESS (CM)	.00474	.01856
FULL THICKNESS (CM)	.03448	.06868

TABLE 2.6-8

PRINTOUT OF DETAILED TRAJECTORY RESULTS

DROP TRAJECTORY STUDY   ROCKETDYNE BLADE 1-A   TIP SECTION   TEST 1144

DROP DIAMETER = 170.00 MICRONS   WAKE Y/D = 0.00

TIME	X-WAKE	Z-WAKE	VDROP	VREL	WED	RED	H
6.20117E-06	7.62315E-02	2.74186E-02	9.15723E+00	1.49087E+04	8.36201E+00	3.42159E+02	6.2012E-06
7.99951E-04	7.02592E-01	2.51401E-01	1.96436E+03	2.44865E+04	2.25572E+01	5.45550E+02	6.2012E-06
1.05420E-03	1.33584E+00	4.77621E-01	3.03727E+03	2.57673E+04	2.49787E+01	5.74085E+02	6.2012E-06
1.24023E-03	1.97833E+00	7.07063E-01	3.87378E+03	2.60919E+04	2.56126E+01	5.81317E+02	6.2012E-06
1.39526E-03	2.63392E+00	9.41040E-01	4.58013E+03	2.61132E+04	2.56539E+01	5.81792E+02	6.2012E-06
1.52549E-03	3.26859E+00	1.16774E+00	5.17109E+03	2.60120E+04	2.54554E+01	5.79537E+02	6.2012E-06
1.64331E-03	3.90908E+00	1.39440E+00	5.69972E+03	2.58534E+04	2.51459E+01	5.76004E+02	6.2012E-06
1.75493E-03	4.57289E+00	1.63337E+00	6.19297E+03	2.56598E+04	2.47707E+01	5.71690E+02	6.2012E-06
1.85415E-03	5.20879E+00	1.86037E+00	6.62401E+03	2.54611E+04	2.43886E+01	5.67264E+02	6.2012E-06
1.94717E-03	5.84347E+00	2.08692E+00	7.02104E+03	2.52575E+04	2.40002E+01	5.62728E+02	6.2012E-06
2.04019E-03	6.51473E+00	2.32653E+00	7.41086E+03	2.50411E+04	2.35907E+01	5.57907E+02	6.2012E-06
2.11915E-03	7.11284E+00	2.54002E+00	7.73586E+03	2.48497E+04	2.32314E+01	5.53642E+02	1.0000E-08

TABLE 2.6-9

SUMMARY OF TRAJECTORY RESULTS

DROP TRAJECTORY STUDY   ROCKETDYNE BLADE 1-A   TIP SECTION   TEST 1144

SUMMARY OF RESULTS

DIAM	YD	TFLIGHT	VDFINAL	VRELI	VRELF	WEDM	ALPHA
170.00	0.00	2.1192E-03	7.7358E+03	1.4917E+04	2.4850E+04	2.5679E+01	6.9078E+01
150.00	0.00	2.0269E-03	8.0471E+03	1.4917E+04	2.4538E+04	2.2333E+01	6.9078E+01
140.00	0.00	1.9779E-03	8.2226E+03	1.4917E+04	2.4363E+04	2.0676E+01	6.9078E+01
130.00	0.00	1.9268E-03	8.4141E+03	1.4917E+04	2.4171E+04	1.9031E+01	6.9078E+01
120.00	0.00	1.8732E-03	8.6246E+03	1.4917E+04	2.3961E+04	1.7394E+01	6.9078E+01
100.00	0.00	1.7573E-03	9.1179E+03	1.4917E+04	2.3468E+04	1.4176E+01	6.9078E+01
90.00	0.00	1.6940E-03	9.4117E+03	1.4917E+04	2.3174E+04	1.2590E+01	6.9078E+01
70.00	0.00	1.5531E-03	1.0138E+04	1.4917E+04	2.2448E+04	9.4765E+00	6.9078E+01
50.00	0.00	1.3851E-03	1.1164E+04	1.4917E+04	2.1422E+04	6.4460E+00	6.9078E+01
190.50	0.00	2.2071E-03	7.4607E+03	1.4917E+04	2.5125E+04	2.9149E+01	6.9078E+01
170.00	.35	1.8375E-03	8.0958E+03	2.0573E+04	2.5312E+04	2.8066E+01	6.9078E+01
150.00	.35	1.7581E-03	8.4206E+03	2.0573E+04	2.4988E+04	2.4460E+01	6.9078E+01
140.00	.35	1.7160E-03	8.6036E+03	2.0573E+04	2.4805E+04	2.2672E+01	6.9078E+01
130.00	.35	1.6720E-03	8.8034E+03	2.0573E+04	2.4505E+04	2.0894E+01	6.9078E+01
120.00	.35	1.6259E-03	9.0228E+03	2.0573E+04	2.4385E+04	1.9129E+01	6.9078E+01
100.00	.35	1.5261E-03	9.5371E+03	2.0573E+04	2.3871E+04	1.5637E+01	6.9078E+01
90.00	.35	1.4717E-03	9.8432E+03	2.0573E+04	2.3565E+04	1.3915E+01	6.9078E+01
70.00	.35	1.3505E-03	1.0599E+04	2.0573E+04	2.2809E+04	1.0524E+01	6.9078E+01
50.00	.35	1.2060E-03	1.1667E+04	2.0573E+04	2.1741E+04	7.2292E+00	6.9078E+01
190.50	.35	1.9132E-03	7.8087E+03	2.0573E+04	2.5600E+04	3.1799E+01	6.9078E+01
170.00	1.00	1.3950E-03	9.0961E+03	3.5635E+04	2.6503E+04	4.6876E+01	6.9078E+01
150.00	1.00	1.3356E-03	9.4582E+03	3.5635E+04	2.6141E+04	4.1281E+01	6.9078E+01
140.00	1.00	1.3040E-03	9.6622E+03	3.5635E+04	2.5937E+04	3.8484E+01	6.9078E+01
130.00	1.00	1.2711E-03	9.8849E+03	3.5635E+04	2.5714E+04	3.5689E+01	6.9078E+01
120.00	1.00	1.2366E-03	1.0129E+04	3.5635E+04	2.5470E+04	3.2894E+01	6.9078E+01
100.00	1.00	1.1619E-03	1.0701E+04	3.5635E+04	2.4897E+04	2.7300E+01	6.9078E+01
90.00	1.00	1.1211E-03	1.1042E+04	3.5635E+04	2.4557E+04	2.4518E+01	6.9078E+01
70.00	1.00	1.0305E-03	1.1882E+04	3.5635E+04	2.3717E+04	1.4963E+01	6.9078E+01
50.00	1.00	9.2230E-04	1.3065E+04	3.5635E+04	2.2534E+04	1.3703E+01	6.9078E+01
190.50	1.00	1.4517E-03	8.7757E+03	3.5635E+04	2.6823E+04	5.2612E+01	6.9078E+01

TABLE 2.6-10

SECONDARY ATOMIZATION SUMMARY

DROP TRAJECTORY STUDY   ROCKETDYNE BLADE 1-A   TIP SECTION   TEST 114A

SECONDARY ATOMIZATION SUMMARY

DIAM	YD	TDIS	DSEC	VDIS	XDC	XDIS
170.00	0.00	1.6612E-06	1.8155E-03	2.4188E+04	5.8397E+01	1.3957E-01
150.00	0.00	1.3770E-04	1.6396E-03	2.5747E+04	1.3544E+02	2.8563E-01
190.50	0.00	1.9674E-04	1.9878E-03	2.2885E+04	3.8937E+01	1.0429E-01
170.00	.35	1.6610E-04	1.8152E-03	2.4191E+04	2.8254E+01	6.7524E-02
150.00	.35	1.3755E-04	1.6373E-03	2.5774E+04	5.0742E+01	1.0701E-01
140.00	.35	1.2414E-04	1.5496E-03	2.6655E+04	8.3975E+01	1.6529E-01
190.50	.35	1.9649E-04	1.9843E-03	2.2915E+04	1.9361E+01	5.1853E-02
170.00	1.00	1.1383E-04	1.0819E-03	3.5298E+04	9.3325E+00	2.2305E-02
150.00	1.00	1.0054E-04	1.0658E-03	3.5264E+04	1.0090E+01	2.1279E-02
140.00	1.00	9.3887E-05	1.0570E-03	3.5244E+04	1.0039E+01	1.9759E-02
130.00	1.00	8.7238E-05	1.0478E-03	3.5221E+04	1.1099E+01	2.0285E-02
120.00	1.00	8.0587E-05	1.0380E-03	3.5195E+04	1.1130E+01	1.8777E-02
100.00	1.00	6.7283E-05	1.0162E-03	3.5129E+04	1.2684E+01	1.7633E-02
90.00	1.00	6.0628E-05	1.0040E-03	3.5086E+04	1.2964E+01	1.6404E-02
190.50	1.00	1.2745E-04	1.0969E-03	3.5327E+04	8.7118E+00	2.3332E-02

TABLE 2.6-11

IMPACT GEOMETRY DATA SUMMARY

SUNFLOWER TURBINE   STAGE 3   MEAN SECTION   SEC = 13

SECTION DIAMETER (CM) = 4.5720		WHEEL RPM	= 40000.0
WHEEL SPEED (CM/SEC) = 9575.57		ALPHA	= 73.50
BLADE PITCH (CM) = .1818		ALPHAI	= 28.70
MAX DELTA L (CM) = .1595		ALPHADO (DEG)	= 61.30
VDROPO (CM/SEC) = 6453.60		WD =WN (CM/SEC)	= 7054.51
VZERO (CM/SEC) = 21781.01			

VD	WD	WN	ALPHAD	BETA	IMPACT LENGTH
0.00	9575.57	4598.42	0.00	61.30	0.00000
1090.00	8536.08	4368.07	2.08	59.22	.01289
2180.00	7510.91	4137.73	4.73	56.57	.02721
3270.00	6506.85	3907.38	8.21	53.09	.04321
4360.00	5535.41	3677.04	12.93	48.37	.06123
5450.00	4617.19	3446.69	19.59	41.71	.08165
6540.00	3791.10	3216.35	29.34	31.96	.10500
7630.00	3130.92	2986.00	43.80	17.50	.13195
8720.00	2758.44	2755.66	63.87	-2.57	.15948
9810.00	2791.34	2525.31	86.52	-25.22	.15948
10900.00	3217.20	2294.97	105.79	-44.49	.15948
11990.00	3909.64	2064.62	119.42	-58.12	.15948
13080.00	4753.58	1834.28	128.60	-67.30	.15948
14170.00	5681.89	1603.93	134.90	-73.60	.15948
15260.00	6659.39	1373.59	139.40	-78.10	.15948
16350.00	7667.28	1143.24	142.72	-81.42	.15948
17440.00	8695.01	912.90	145.27	-83.97	.15948
18530.00	9736.29	682.56	147.28	-85.98	.15948
19620.00	10787.20	452.21	148.90	-87.60	.15948
20710.00	11845.18	221.87	150.23	-88.93	.15948
21781.01	12889.92	0.00	151.32	-90.02	.15948

The model represents a first cut at a comprehensive explanation of observed phenomena. Unfortunately, the kinds of experimental data required to verify and improve the model simply do not exist. Key areas of uncertainty are the critical Weber Number estimates and wake behavior immediately downstream of stator trailing edges. The criterion for disruption should reflect the abruptness of the onset of accelerating forces and should be sufficiently general to permit its use with dissimilar working fluids. These deficiencies in the model, however, do not negate its usefulness in most circumstances. When a series of similar turbine designs is being considered, the model will give an excellent estimate of the relative erosion potential of the competing designs. The key effect of axial stator-rotor spacing can certainly be examined and with the use of a conservative critical Weber Number estimate these results can be expressed directly as a design limit. Another important factor which can be examined on a parametric basis is the effect of shaft rpm (hence, tip speed) on the erosion potential.

2.6.7 Nomenclature

a, b, n_1, n_2, n_3	Empirical constants
A_d	Drop cross-sectional area
C	Stator blade chord length
C_d	Drop drag coefficient
C_f	Friction factor
D_d, D'_d	Primary and secondary drop diameters
E	Defined by Equation 15
F_d	Aerodynamic force on a drop
f, g	Functional relationship
H	Form factor
K_d	Inertial parameter group
L	Shape factor
Re	Reynolds Number
S	Blade pitch
t, t', t''	Time, time-to-disruption, time-to-complete disruption
U, U_o, U_{min}	Local vapor velocity, wake-edge, and wake axis vapor velocities
U_1	Tangential blade speed
V_d	Absolute drop velocity
V_r	Relative velocity between drop and vapor stream
W_e	Drop Weber Number
W_d	Drop terminal velocity relative to the rotor blade.
W_n	Drop terminal velocity normal to the stator blade.
X	Distance along the wake axis
Y	Distance normal to the wake axis
Z	Distance along the turbine axis
α	Stator exit flow angles
α_i, α_d	Velocity triangle angles defined in Figure 2.6-5.
β	Local wake angle
ΔL	Impact length
ξ	Defined in Equation 13
ϵ	Normalized distance (x/6) along the wake axis
δ, δ^*	Wake full thickness, displacement thickness
ρ_v, ρ_L	Vapor and liquid density
σ_L	Surface tension
θ, $\hat{\theta}$	Wake momentum thickness and thickness parameter
μ_v	Vapor viscosity

2.6.8 References

1. Lambiris, S. and L. P. Combs, "Steady-State Combustion Measurements in a LOX/RP-1 Rocket Chamber and Related Spray Burning Analysis," Detonation and Two-Phase Flow, Academic Press, p. 283, 1962.

2. Wolfe, H. E. and W. H. Anderson, "Kinetics, Mechanism and Resultant Drop Sizes of the Aerodynamic Breakup of Liquids, "Report 6395-04-185P, Aerojet-General Corp., April 1964.

3. Lieblein, S. and W. H. Roudebush, "Low-Speed Wake Characteristics of Two-Dimensional Cascade and Isolated Airfoil Sections," NACA-TN-3771, October 1956.

4. Truckenbrodt, E., "A Method of Quadrature for Calculation of the Laminar and Turbulent Boundary Layer in Plane and Rotationally Symmetrical Flow," NACA-TM-1379, 1955.

5. Speidel, L., "Untersuchungen uber die Stromungsverluste in Ebenen Schaufelgittern," VDI-Forschungsheft 464, 1957.

6. Schlichting, H., Boundary Layer Theory, Chapter XXII, McGraw-Hill, New York, 1960.

7. Gardner, G. C., "Events Leading to Erosion in the Steam Turbine," Proc. Inst. Mech. Engrs. Vol. 78, No. 23, pp 593-623, 1963-64.

8. Nicholson, J. E., "Drop Breakup by Airstream Impact," Paper presented at the 2nd Rain Erosion Conference, Meersburg, Germany, August 1967.

9. Clark, B. J. "Breakup of a Liquid Jet in a Transverse Flow of Gas," NASA-TN-D-2424, August 1964.

10. Katsanis, T., "A Computer Program for Calculating Velocities and Streamlines for Two-Dimensional, Incompressible Flow in Axial Blade Rows," NASA-TN-D-3762, January 1967.

11. Mintz, M. D. and Jordan, D. P., "A Progressive Interpolation Scheme for Hand and Digital Computer Analysis of Tabulated Data," UCRL-7681, February 1964.

12. Wegstein, J. H., "Accelerating Convergence of Iterative Processes," Comm. of the ACM, Volume I, No. 6, June 1958.

13. Geil, E. and Wei, D. P., "ICEADAMS-A Computer Package for Solving Systems of Ordinary Differential Equations," Report 65-IC4-COMP-R2, Westinghouse Research Laboratories, February 1965.

14. Ewing, C. E., et al., "High Temperature Properties of Potassium," NRL 6233, September 1965.

15. Ewing, C. E., et al., "High Temperature Properties of Cesium," NRL 6246, September 1965.

16. Achener, P. Y., et al., "Thermophysical and Heat Transfer Properties of Alkali Metals," AGN-8195, Volume 1, April 1968.

17. Thermodynamic and Transport Properties of Steam, American Society of Mechanical Engineers, New York, 1967.

18. Ross, D. P., "Thermodynamic Properties of Mercury," TRW Technical Memorandum (TM-777), June 1957.

APPENDIX 2.6A

CALCULATED AND EXPERIMENTAL ATOMIZED DROP VELOCITIES IN LAST STAGE OF CENTRAL STATION STEAM TURBINES

There are several aspects to the acceleration of the drops discharged from wet turbine stators. The first is the acceleration of the primary drops immediately after formation and up to the time of disruption. The second is the continued acceleration of the liquid as secondary drops. A third is where will the drops hit on the rotor blades?

Limited experimental information on primary and secondary drop accelerations under turbine-like conditions is available from steam cascade tests reported by the Central Electricity Research Laboratories (CERL) of the United Kingdom.* These experiments were conducted on a stator cascade simulating the last row of stators in large central station steam turbines and using system conditions appropriate to such last stator rows.

The CERL results are compared to calculated values for the Yankee Atomic Plant steam turbine last stage at the mean diameter. Complete geometric data on the CERL cascade blades is not given in the referenced material.** However, such dimensions as are supplied are within 20 percent of the mean diameter section values for the Yankee last stage, and the nozzle exit angles are nearly identical. Figure 2.6A-1 compares the CERL observed velocities for various sizes of primary drops at a location 0.74 in. downstream of the stators to those calculated for the Yankee steam turbine. Figure 2.6A-2 compares the CERL observed velocities of 150 micron diameter secondary drops at various downstream distances with calculated curves for 100 micron and 200 micron diameter secondary drops for the Yankee turbine. In both cases, the observed velocities are on the average higher than the calculated velocities.

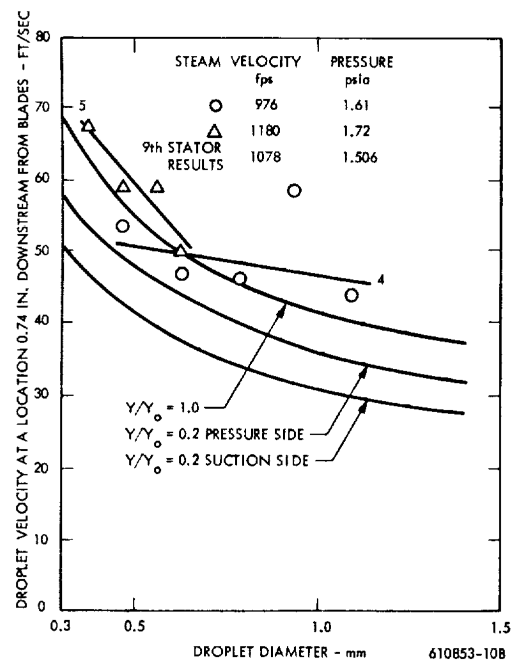

Figure 2.6A-1 Drop Velocity

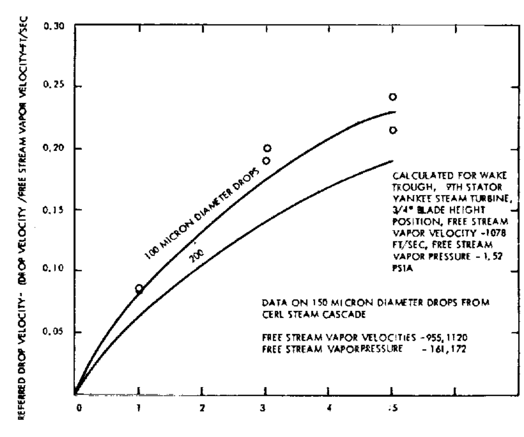

Figure 2.6A-2 Secondary Drop Velocity

* Hays, L.G., Turbine Erosion Research in Great Britain, NASA Jet Propulsion Laboratory, C.I.T. Tech Memo, No. 33-271.

** Christie, D.G., Experimental Investigation of Internal Flow in Turbines, Jet Propulsion Laboratory, C.I.T. Tech. Memo 33-354, Sect. 12, June 15, 1967.

Figure 2.6A-3 compares two sets of predicted values for drop impingement locations on last stage rotor blades aft of the nose of the rotor blade for various-size secondary drops. The solid line is that predicted by CERL on the basis of their stator experiments as applied to a hypothetical turbine at full load. The points are predicted values for impact on the last rotor blades of the Yankee Turbine at the mean diameter, using the Yankee calculated values.

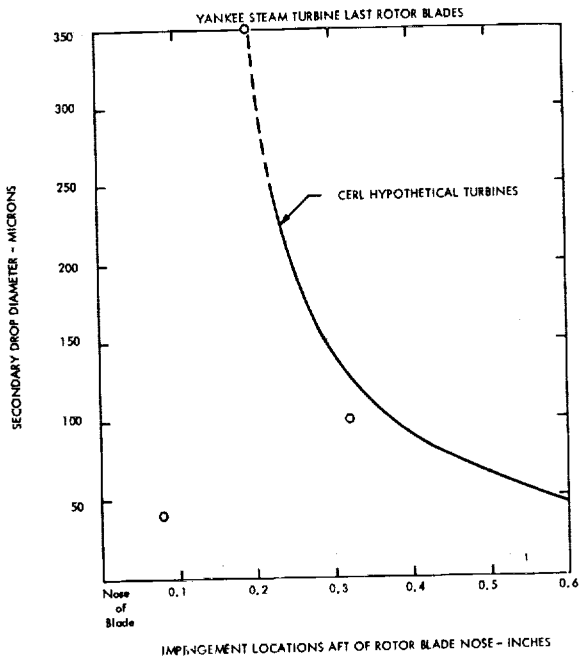

Figure 2.6A-3 Rotor Blade Impingement Locations

APPENDIX 2.6B

ADROP CODE SOURCE PROGRAM LISTING

B.1 ADROP Main Program Listing

```
JOB,10.
ASB0440.
ASD1197,VARLJEN,60,20000,01.
C
      PROGRAM ADROP(INPUT,OUTPUT,TAPE5=INPUT,TAPE6=OUTPUT)
C
C     TRANSPORT OF ATOMIZED CONDENSATE IN WET VAPOR TURBINES
C
      COMMON /PRP/MAT,TEMP,RHOV,RHOL,SIGL,VISL,VISV
     1       /TBG/CHORD,PITCH,BTE,PD,SD,PDS,SDS,PTH,STH,VZERO
     2       /GEO/NSTAT,NROTR,RPM,ALPHA,ALPHI,FDEAD,WDC,DSTAT,DROTR,
     3            AXSP,STE,SCHD,SPARC,SSARC
     4       /CST/JOB(10),JMAT(10),PI,RD,NYD,DIAM(10)
     5       /BUG/IBUG
     C
     C
      DIMENSION GDAT(14),TDAT(14),XS(50),VS(50),XP(50),VP(50),KOP(10)
      EQUIVALENCE (ALPHA,TDAT)
      DATA PI,RD,KOP,GDAT/ 3.14159265,.0174533,10*0,14*0. /
      DATA JMAT / 7HLITHIUM,6HSODIUM,7HPOTASS.,8HRUBIDIUM,6HCESIUM,
     1 7HMERCURY,6HNAK-78,5HWATER /
      DATA XS,VS,XP,VP,PD,SD,PDS,SDS,PTH,STH /206*0./, XO/1./
      NAMELIST/DRP/KOP,TR,VFREE,GDAT,XS,VS,XP,VP,PD,SD,PDS,SDS,PTH,STH
     1, XO,DIAM
 100  READ(5,10) JOB
      READ(5,DRP)
      IF (KOP(1).EQ.0) STOP
      MAT = KOP(1)  $  NSTAT = KOP(2)  $  NROTR = KOP(3) $  MS = KOP(5)
      RPM = KOP(4)  $  IOK = KOP(6)    $  NYD = KOP(9)   $  IBUG=KOP(10)
      WRITE(6,14) JOB,KOP
C
C     CONVERSION OF INPUT UNITS TO CGS
C
      TEMP = TR/1.8
      VZERO = VFREE*30.48
      ALPHA = GDAT(1)  $  ALPHI = GDAT(2)
      FDEAD = GDAT(3)  $  WDC = GDAT(4)
      DO 110 I=5,11
 110  TDAT(I) = GDAT(I)*2.54
      CHORD = SCHD  $  PITCH = PI*DSTAT/NSTAT  $  BTE = ALPHA
      IF (MS.LE.0.AND.KOP(7).LT.0) GO TO 200
      WRITE(6,16) TR,VFREE,XO, (GDAT(L),L=1,7)
      WRITE(6,19) (GDAT(L),L=8,11)
C
C     GENERATE FLUID PROPERTIES AT STATOR EXIT CONDITIONS
C
      CALL PROPM(RHOV,TEMP,2,MAT)
      CALL PROPM(RHOL,TEMP,1,MAT)
      CALL PROPM(VISV,TEMP,4,MAT)
      CALL PROPM(VISL,TEMP,3,MAT)
      VL = 1./RHOL
      CALL PROPM(SIGL,TEMP,9,MAT)
      VV = 1./RHOV
      VM = XO*VV+(1.-XO)*VL
      RHOV = 1./VM
```

```
C
C     CHECK FOR PROPERTY ERROR SIGNAL
C
      WRITE(6,12) JMAT(MAT),TEMP,RHOV,RHOL,VISV,VISL,SIGL
      IF (RHOV*RHOL*VISV*VISL*SIGL.LE.0.) GO TO 400
C
C     CALCULATE TRAILING EDGE BOUNDARY LAYER DATA
C
      IF (MS.LE.0) GO TO 150
      CALL TRUCK(MS,SSARC,SPARC,XS,VS,XP,VP,IOK)
      IF (IOK.EQ.10) GO TO 200
C
C     EXAMINE BALLISTICS OF ATOMIZED DROPS
C
  150 IF (KOP(7).LT.0) GO TO 200
      CALL TRAX(KOP(7))
C
C     EXAMINE DROP IMPACT GEOMETRY
C
  200 IF (KOP(8).LT.0) GO TO 400
      CALL IMPAX(NROTR,DROTR,RPM,ALPHA,ALPHI,VZERO)
  400 CONTINUE
      GO TO 100
      CALL EXIT
   10 FORMAT(10A8)
   12 FORMAT(1X, A8,23HWORKING FLUID AT T(K) = F7.1 / 10X,13HRHOV (G/CC)
     1 = E14.4 /10X,13HRHOL (G/CC) = E14.4 /10X,13HVISV (P)     = E14.4 /
     2 10X,13HVISL (P)     = E14.4 /10X,13HSIGL DYN/CM = E14.4 )
   14 FORMAT(1H1,11H INPUT DATA,6X,10A8//17H OPTIONS    KOP = 10I8 //)
   16 FORMAT(6X,32HBULK FLUID TEMPERATURE (DEG R) = F10.2,
     1        8X,32HFREE-STREAM VELOCITY (FPS)      = F10.2/
     2        6X,32HBULK FLUID QUALITY              = F10.4,
     3        8X,32HEXIT FLOW ANGLE (DEG)           = F10.2/
     4        6X,32HINLET ROTOR BLADE ANGLE (DEG)   = F10.2,
     5        8X,32HDEAD-SPACE MULTIPLIER           = F10.2/
     6        6X,32HCRITICAL WEBER NUMBER           = F10.2,
     7        8X,32HEXIT STATOR DIAMETER (IN)       = F10.4/
     8        6X,32HINLET ROTOR DIAMETER (IN)       = F10.4,
     9        8X,32HAXIAL INTER-ROW SPACE (IN)      = F10.4  )
   18 FORMAT(6X,32HSTATOR TE THICKNESS (IN)        = F10.4,
     1        8X,32HSTATOR CHORD (IN)               = F10.4/
     2        6X,32HPRESSURE SURF. LENGTH (IN)      = F10.4,
     3        8X,32HSUCTION SURF. LENGTH (IN)       = F10.4  //)
      END
```

Appendix B.2 Subroutine TRUCK Listing

```
C
      SUBROUTINE TRUCK(M,SS,SP,XXS,XVS,XXP,XVP,IO)
C
C     TWO DIMENSIONAL BOUNDARY-LAYER CALCULATION       MARCH 1968
C        REVISED VERSION OF CODE OF WANL-TME-1689
C
      COMMON /PRP/MAT,TEMP,RHOV,RHOL,SIGL,VISL,VISV
     1       /TBG/CHORD,PITCH,BTE,PD,SD,PDS,SDS,PTH,STH,VZERO
     4       /CST/JOB(10),JMAT(10),PI,RD,NYD,DIAM(10)
      DIMENSION XXS(2),XVS(2),XXP(2),XVP(2),XS(51),VS(51),TS(51),ZS(51),
     1 FS(51),D(31),E(31),HS(51),EXN(51),TSIN(51),DSIN(51),DFSIN(51)
      DATA(D=-.1803, -.1902, -.18, -.177, -.172, -.165,
     1-.1555, -.145, -.130, -.123, -.1145, -.103, -.090,
     2   -.075473, -.054770, -.030020,  .0, .037065, .083859, .144673,
     3.226930, .345038, .425548, .530005, .639995, .789418,  1.013354,
     41.176106, 1.414472, 1.854390, 2.303073),
     5(E= 2.6, 2.5, 2.4, 2.3, 2.2, 2.1, 2.0, 1.9, 1.8, 1.75, 1.70, 1.65,
     61.60, 1.55, 1.50, 1.45, 1.40, 1.35, 1.30, 1.25, 1.20, 1.15, 1.125,
     71.10, 1.08, 1.06, 1.04, 1.03, 1.02, 1.01, 1.005)
```

```
C
C       COMPUTE BLADE REYNOLDS NUMBER AND LIST INPUT
C
        RES = RHOV*VZERO*SS/VISV        $  REP = RES*SP/SS
        RE = RES                        $  S = SS
        XS(1) = XXS(1) = XXP(1) = VS(1) = 0.
        WRITE(6,102) JOB
        WRITE(6,103) JMAT(MAT),RES,REP
        WRITE(6,104) (XXS(I),XVS(I),XXP(I),XVP(I),I=1,M)
        ISUR = 1    $  IDELT = 40       $  DELTA = 1./IDELT
        I1 = IDELT+1                    $  MI = I1-2
        DO 5 J=2,I1
    5   XS(J)=XS(J-1)+DELTA
        XS(I1) = VS(I1) = 1.
        CALL SPLINT(XXS,XVS,M,XS(2),VS(2),MI,1,1)
   10   SUMS1 = FS(2) = 0.
        DO 16 I=2,I1
        SUMS1=SUMS1+(XS(I)-XS(I-1))*(VS(I)**3.33+VS(I-1)**3.33)/2.0
        AS=((0.074/(RE**0.2))/2.0)**1.166
        BS=0.0304*(ALOG(RE))-0.23651
        TS(I)=(AS*SUMS1)**0.8571/VS(I)**3
        ZS(I)=(AS*SUMS1)**4
        IF(I-2)14,14,15
   14   SUMS2=(BS+ALOG(VS(I))+0.00651*ALOG(ZS(I))-FS(2))*ZS(I)/1.0608
        GO TO 25
   15   SUMS2=SUMS2+(ZS(I)-ZS(I-1))*(ALOG(VS(I))+ALOG(VS(I-1)))/2.0
        FS(I)=BS+ALOG(VS(I))+0.00651*ALOG(ZS(I))-1.0608*SUMS2/ZS(I)
        IF (FS(I).GT.(-.18)) GO TO 25
        XI=I      $  IO = 10
        POSITN = S*(.02*XI-.02)
        WRITE(6,111)I,POSITN,FS(I),TSIN(I-1),DSIN(I-1),DFSIN(I-1)
        GO TO 17
   25   CALL SPLINT(D,E,31,FS(I),HS(I),1,1,1)
        EXN(I) = 2./(HS(I)-1.)
        TSIN(I) = TS(I)*S
        DSIN(I)=TSIN(I)*HS(I)
   16   DFSIN(I) = DSIN(I)*(EXN(I)+1.)
   17   IF (ISUR.GT.1) GO TO 50
        ISUR = 2      $  RE = REP       $  S = SP
        IF (IO.LE.0) GO TO 40
        WRITE(6,102) JOB
        WRITE(6,105)
        WRITE(6,106)
        WRITE(6,107) (XS(I),VS(I),TS(I),FS(I),HS(I),EXN(I),TSIN(I),
       1 DSIN(I),DFSIN(I),I=2,I1)
   40   CALL SPLINT(XXP,XVP,M,XS(2),VS(2),MI,1,1)
        SO = DFSIN(I1)
        STH = TSIN(I1)
        SDS = DSIN(I1)
        GO TO 10
   50   IF (IO.LE.0) GO TO 70
        WRITE(6,102) JOB
        WRITE(6,109)
        WRITE(6,106)
        WRITE(6,107) (XS(I),VS(I),TS(I),FS(I),HS(I),EXN(I),TSIN(I),
       1 DSIN(I),DFSIN(I),I=2,I1)
        PD = DFSIN(I1)
        PDS = DSIN(I1)
        PTH = TSIN(I1)
   70   RETURN
C
C
  102   FORMAT(1H1,2X,32HTWO-D BOUNDARY LAYER CALCULATION,6X,10A8 / )
  103   FORMAT(9H FLUID =  A8, 6X, 5HRES = E12.3, 5X, 5HREP =
       1 E12.3///43H INPUT POSITION AND SURFACE VELOCITY ARRAYS//8H SUCTIO
       2N,11X,1HX,9X,1HV,10X,8HPRESSURE,11X,1HX,9X,1HV//)
  104   FORMAT(F20.4,F10.4,F30.4,F10.4)
  105   FORMAT(10X,15HSUCTION SURFACE )
```

```
106 FORMAT(/2X8HREFFERRED, 4X8HREFERRED, 4X8HREFERRED, 6X5HSHAPE,7X4HFO
   1RM,6X8HEXPONENT, 4X8HMOMENTUM, 5X6HDISPL.,7X4HFULL,/2X8HDISTANCE,4
   2X9HVELOCITY,4X8HMOM THIC,5X6HFACTOR, 6X6HFACTOR,8X1HN,8X9HTHICKNES
   3S,3X9HTHICKNESS, 3X9HTHICKNESS )
107 FORMAT (2XF8.6,4XF8.6, 4XF8.6, 3XF9.6, 4XF8.6, 4XF8.6, 4XF8.6, 4XF
   18.6, 4XF8.6)
109 FORMAT(10X,16HPRESSURE SURFACE )
111 FORMAT(1H0, 1X, 60H****FLOW SEPARATION***SHAPE FACTOR .LT.-0.18
   1                       //1X, 2HI= E12.5, 2X, 10HSURF.POSN=E12.5, 5H(
   2IN.), 2X, 11HSHAPE FAC=  E12.5,2X,16HACT.MOM.TK(I-1)= E12.5,4H(IN)
   3 /1X, 17HACT.DISP.TK(I-1)= E12.5, 4H(IN),2X,14HBNDRY.TK(I-1)= E12.
   45, 4H(IN), 36H******CONTINUING CALCULATION*******              )
    END
```

Appendix B.3 Subroutine WAKE Listing

```
      SUBROUTINE WAKE(NS,XX,YD,VXY,BX)
      COMMON/TBG/CHORD,PITCH,BTE,PD,SD,PDS,SDS,PTH,STH,VZ
      COMMON /BUG/IBUG
C
C     GENERATION OF STATOR WAKE VELOCITY
C
      DATA (RD = .0174533), (PI = 3.1415926)
      IF (NS) 200,90,100
 90   SOLID = CHORD/PITCH
      COBX = COS(RD*BTE)              $   TABX = TAN(RD*BTE)
      DSTE= (PDS+SDS)/CHORD           $   DTE = ( PD+SD)/CHORD
      THTE = (PTH+STH)/CHORD          $   HTE = DSTE/THTE
      CHTE = THTE*SOLID/COBX          $   OLDT = CHTE
      BA = 1.- CHTE*(1.+HTE)
      BB = (1.- CHTE*HTE)**2
      CK1 = (BA-1./(2.*COBX*COBX)   )/BB
      CK2 = (TABX*BA/BB)**2
      CK3=(COBX-SOLID*THTE*HTE)
      NS = 1
 100  X = XX/CHORD
      AA = SQRT(1.+40.*X)
      HX = AA/(AA-(HTE-1.)/HTE)
      DO 115 LL=1,5
      KNT = 2-LL
 110  AA = ((1.-OLDT*(1.+HX))**2
      AB = 1.-OLDT*HX
      FOX = (1.-CK1*AB*AB-(CK2*AB**4+AA)/(2.*AA))/(1.+HX)
      IF (IBUG.EQ.2) WRITE(6,6) LL,KNT,XX,OLDT,FOX
      CALL VERGE(OLDT,FOX,KNT)
      IF (KNT.GE.20) GO TO 160
      IF (KNT.GE.1) 110,120
 160  IF (ABS((OLDT-FOX)/OLDT).LE..001) GO TO 120
 115  CONTINUE
      WRITE(6,5) KNT,XX,CHTE,OLDT
      NS= 10
      GO TO 150
 120  CTHTX = OLDT
      BX = ATAN (TABX*AB*AB/BB*BA/(1.-OLDT*(1.+HX)))
      THX = CTHTX*COS(BX)/SOLID
      VX= CK3/(COS(BX)-SOLID*THX*HX)
      VMIN = 1.-.13/SQRT(X+.025)
      YD = ABS(YD)
      VXY = VX*VZ*.5*((1.+VMIN)-(1.-VMIN)*COS(PI*YD))
```

```
150   RETURN
200   BX = BTE*RD
      VXY = VZ
      IF (YD.NE.0.) GO TO 150
      VXY = VZ*(1.-.13/SQRT(XX/CHORD+.025))
      GO TO 150
    5 FORMAT(1H0,39H *** NON-CONVERGENCE IN WAKE, ITERATION, I6, 6H  XX
     1=  F6.4,7H CHTE =  E12.5, 7H OLDT = E12.5 )
    6 FORMAT(2I10,3E20.5)
      END
```

Appendix B.4 Subroutine TRAX Listing

```
      SUBROUTINE TRAX(IO)
C
C     CALCULATION OF THE TRAJECTORIES OF ATOMIZED DROPS
C
      COMMON /PRP/MAT,TEMP,RHOV,RHOL,SIGL,VISL,VISV
     1       /TBG/CHORD,PITCH,BTE,PD,SD,POS,SDS,PTH,STH,VZERO
     2       /GEO/NSTAT,NROTR,RPM,ALPHA,ALPHI,FDEAD,WDC,DSTAT,DROTR,
     3            AXSP,STE,SCHD,SPARC,SSARC
     4       /CST/JOB(10),JMAT(10),PI,RD,NYD,DIAM(10)
      COMMON/ICON/H,HMAX,HMIN,RELB,ABSB
      COMMON/TRX/ ZP,ZPR,DPD,WDP,DPP,TRIG,YY,DD,KCRIT,I,J, TOF(10,3),
     1VRELI(10,3),VRELF(10,3),WEDM(10,3),TP2(10,3),VCX(10,3),XDC(10,3),
     2 BEX(10,3),VDF(10,3),DP2(10,3),XDIS(10,3),NS
      DIMENSION YD(3),Y(50)
      DATA HMIN,RELB,ABSB /3*1.E-8/
      DATA (YD = 0.,.35,1.),
     1     (DIAM = 1.,2.,5.,10.,20.,50.,100.,200.,500.)
      DIAM(10) = AMIN1(STE*1.E4,1000.)
      DO 80 I=1,300
   80 TOF(I) = 0.
      HI = AXSP/50.
      XDEAD = FDEAD*STE
      NE = 0
      IF (NYD) 85,90,92
   85 NYD = 2      $  NF = -1
      YD(1) = 0.
      YD(2) = 1.
      GO TO 95
   90 NYD = 3
   92 WRITE(6,35) JOB,PTH,STH,POS,SOS,PD,SD
   95 ZP = 10.
      IF (IO.GT.1) ZP = (AXSP-XDEAD)/(IO-1.)
      NS = NF
      DO 500 J=1,NYD
      DO 500 I=1,10
      ZPR = T = 0.
      Y(1) = 1.
      Y(2) = XDEAD          $   YY = YD(J)
      TRET = KCRIT = 0       $ H = HMAX = HI
      DD = DIAM(I)*1.E-4     $  TRIG = 0.
      DPD = RHOV*DD/VISV
      WDP = RHOV*DD/SIGL
      DPP = .75*RHOV/(RHOL*DD)
      XDIS(I,J) = 100.
      CALL WAKE(NS,Y(2),YD(J),VXY,BX)
      IF (NS.NE.10) GO TO 100
      BEX(I,J) = -1.
      GO TO 500
```

```
510   VRELI(I,J) = VXY
      WEDM(I,J) = 0.
      CALL ICEAD(2,T,Y,IRET)
500   CONTINUE
      WRITE(6,5) JOB
      WRITE(6,20)
      WRITE(6,25) ((DIAM(I),YD(J),TOF(I,J),VDF(I,J),VRELI(I,J),
     1 VRELF(I,J),WEDM(I,J),REX(I,J),I=1,10),J=1,NYD)
      WRITE(6,5) JOB
      WRITE(6,30)
      DO 520 J=1,NYD
      DO 520 I=1,10
      IF (TP2(I,J).EQ.0) GO TO 520
      WRITE(6,26) DIAM(I),YD(J),TP2(I,J),DP2(I,J),VCX(I,J),XDC(I,J),
     1 XDIS(I,J)
520   CONTINUE
      RETURN
  5   FORMAT(23H1 DROP TRAJECTORY STUDY,6X,10A8 //)
 20   FORMAT( 19H SUMMARY OF RESULTS //6X,4HDIAM,6X,2HYD,7X,7HTFLIGHT,
     1 7X,7HVDFINAL,9X,5HVRELI,9X,5HVRELF,10X,4HWEDM,9X,5HALPHA // )
 25   FORMAT(2X,2F8.2,6E14.4)
 26   FORMAT(2X,2F8.2,6E14.4,F14.2)
 30   FORMAT( 30H SECONDARY ATOMIZATION SUMMARY // 6X,4HDIAM,6X,2HYD,
     1 10X,4HTDIS,10X,4HDSEC,10X,4HVDIS,11X,3HXDC,10X,4HXDIS //)
 35   FORMAT(1H1,35HTRAILING EDGE BOUNDARY LAYER DATA   ,10A8 // 40X,13HP
     1RESSURE SIDE,17X,12HSUCTION SIDE // 30H MOMENTUM THICKNESS (CM)
     2     F23.5,F29.5 / 30H DISPLACEMENT THICKNESS (CM)    F23.5,F29.5 /
     3 30H FULL THICKNESS (CM)             F23.5,F29.5   )
      END
```

Appendix B.5 Subroutine DERIV Listing

```
C
      SUBROUTINE DERIV(T,Y,DY,IRET)
C
C        DERIVATIVE CALCULATION
C
      COMMON /PRP/MAT,TEMP,RHOV,RHOL,SIGL,VISL,VISV
     1        /TBG/CHORD,PITCH,BTE,PD,SD,PDS,SDS,PTH,STH,VZERO
     2        /GEO/NSTAT,NROTR,RPM,ALPHA,ALPHI,FDEAD,WDC,DSTAT,DROTR,
     3             AXSP,STF,SCHD,SPARC,SSARC
     4        /CST/JOB(10),JMAT(10),PI,RD,NYD,DIAM(10)
     5        /BUG/IBUG
      COMMON/ICON/H,HMAX,HMIN,RELB,ABSB
      COMMON/TRX/ ZP,ZPR,DPD,WDP,DPP,TRIG,YY,DD,KCRIT,I,J, TOF(10,3),
     1VRELI(10,3),VRELF(10,3),WEDM(10,3),TP2(10,3),VCX(10,3),XDC(10,3),
     2 REX(10,3),VDF(10,3),DP2(10,3),XDIS(10,3),NS
      DIMENSION Y(50),DY(50)
      DATA KA,KB,LINES,TLAST,WED,Z /0,0,70,1.E10,0.,0./
      KA = KA+1
      CALL WAKE(NS,Y(2),YY,VXY,BX)
      IF (NS.EQ.10) GO TO 480
      Y(1) = AMAX1(1.E-6,AMIN1(Y(1),VXY))
      VREL = VXY-Y(1)
      RED = VREL*DPD
      CD = 2.
```

```
      IF (RED.GT.0. .AND. RED.LT.80.)      CD = 27./RED**.84
      IF (RED.GE.80..AND. RED.LE.1.E4)     CD = .271*RED**.217
      DY(1) = DPP*VREL*VREL*CD
      DY(2) = Y(1)
      IF (IBUG) WRITE(6,20) KA,KB,T,Y(1),Y(2),DY(1),DY(2),VXY,H,RED,
     1 WED,Z,ZP,ZPR,TRIG
      IF (KA.GT.500.AND.KB.LT.2)  GO TO 380
      RETURN
C
C       SUCESSFUL INTEGRATION STEP
C
      ENTRY STEP
C
      KB = KB+1
      Z = Y(2)*COS(BX)   $   X = Y(2)   $   VD = Y(1)
      WED = VREL*VREL*WDP
      IF (WED.GT.WEDM(I,J))   WEDM(I,J) = WED
 342  IF (WED.GE.WDC     .OR.KCRIT.NE.0) GO TO 400
 344  IF (Z.GE.AXSP) GO TO 450
      IF (VD.NE.0.)          TLAST = (AXSP-Z)/VD
      IF (TLAST.LT.H)        H=HMAX=AMAX1(HMIN,1.001*TLAST)
      IF (Z.LT.ZPR.OR.ZP.EQ.10.) RETURN
C
C       DETAILED PRINT SECTION
C
      ZPR = Z+ZP
      IF (LINES.LT.40) GO TO 364
      WRITE(6,5) JOB
      DQ = DD*1.E4
      WRITE(6,6) DQ,YY
      WRITE(6,15)
      LINES = 4
 364  WRITE(6,10) T,X,Z,VD,VREL,WED,RED,H
      LINES = LINES+1
      RETURN
C
C     DROP DISRUPTION DETECTED
C
 400  IF (TRIG.EQ.0..AND.KCRIT.EQ.0) GO TO 410
      IF (T.LT.TRIG) GO TO 344
      XDIS(I,J) = X
      XDC(I,J) = X/DD
      TRIG = 10.  $     KCRIT = 0
      GO TO 344
 410  VCX(I,J) = VREL
      TPP = TP2(I,J) = 2.8*DD/VREL*SQRT(RHOL/RHOV)
      TRIG = T+TPP
      DP2(I,J) = (136.*VISL*SIGL**1.5*DD**.5/(CD**.5*RHOV*RHOV*RHOL**.5
     1 *VREL**4.))**(1./3.)
      KCRIT = 1
      GO TO 344
C
C     END-OF-TRAJECTORY
C
 450  IF (ZP.NE.10.)     WRITE(6,10) T,X,Z,VD,VREL,WED,RED,H
      KA = KB = 0          $  IPET = 1
      LINES = 70
      TLAST = 1.E10
      TOF(I,J) = T
      VRELF(I,J) = VREL
      VDF(I,J) = VD
      BEX(I,J) = BX/RD
      XDIS(I,J) = XDIS(I,J)/X
      RETURN
```

```
C
C     WAKE CALCULATION ERROR
 480  BEX(I,J) = -1.
      KA = KB = 0            $  IRET = 1
      TLAST = 1.E10
      RETURN
C
      ENTRY FAIL
C
C        NON-CONVERGENCE IN INTEGRATION
C
 380  KD = KD+1
      VDF(I,J) = VRELF(I,J) = -1.
      KA = KB = 0            $  IRET = 1
      TLAST = 1.E10
      RETURN
    5 FORMAT(23H1 DROP TRAJECTORY STUDY,6X,10A8 //)
    6 FORMAT( 17H  DROP DIAMETER = F8.2, 8H MICRONS,12X,10HWAKE Y/D =,
     1F6.2 //)
   10 FORMAT(7E14.5,E12.4)
   15 FORMAT(10X,4HTIME,8X,6HX-WAKE,8X,6HZ-WAKE,9X,5HVDROP,10X,4HVREL ,
     1 11X,3HWED,11X,3HRED,11X,1HH //)
   20 FORMAT(2I9/(8E15.5))
      END
```

Appendix B.6 Subroutine IMPAX Listing

```
C
      SUBROUTINE IMPAX(NB,BDIA,RPM,AL,AI,VZERO)
C
C     CALCULATION OF DROPLET IMPINGEMENT GEOMETRY
C
      COMMON/CST/JOB(10),JMAT(10),PI,RD,NYD
      DIMENSION VD(40),WD(40),WN(40),DLS(40),ASD(40),BETA(40)
      JV = 21
      KX = VZERO/100.          $  KX = KX+1
      VD(1) = 0.               $  AV = 5.*KX
      DO 19 K=2,21
   19 VD(K) = VD(K-1)+AV
      VD(21) = VZERO
C
C     I/O ANGLES IN DEGREES, USE RADIANS INTERNALLY
C
      SAL = SINF(AL*RD)
      SAI = SINF(AI*RD)
      PB = PI*BDIA
      UB = PB*RPM/60.
      S = PB/FLOATF(NB)
      ADO = 90.-AI
      VDO = UB/(SAL*(1.+1./TAN(RD*ADO)))
      WDO = VDO*SAL/SIN(RD*ADO)
      DLO = S*COS(AI*RD)
      DO 60 J=1,JV
      WD(J) = UB*UB+VD(J)*VD(J)-2.*UB*VD(J)*SAL
      WD(J) = SQRTF(WD(J))
      AD = ACOSF  ((UB-VD(J)*SAL)/WD(J))
      WN(J) = WD(J)*SINF(AD+AI*RD)
      WN(J) = AMAX1(WN(J),0.)
      ASD(J) = AD/RD
      BETA(J) = 90.-AI-ASD(J)
      DOM = SINF(AD+AI*RD)
      IF (ABS(DOM).LT.1.E-10) GO TO 58
      DLS(J) = ABS(S*SIN(AD)/DOM)
      IF (DLS(J).GT.DLO)  DLS(J) = DLO
      GO TO 60
   58 DLS(J) = DLO
```

```
60   CONTINUE
     WRITE(6,12) (JOB(K),K=1,10),BDIA,RPM,UB,AL,S,AI
     WRITE(6,16) DLO,ADO,VDC,WDO,VZERO
     WRITE(6,14)
     WRITE(6,10) (VD(K),WD(K),WN(K),ASD(K),BETA(K),DLS(K),K=1,JV)
     RETURN
10   FORMAT(5F12.2,F15.5)
12   FORMAT(1H1, 10X,10A8 // 6X,23HSECTION DIAMETER (CM) = F10.4,10X,
    1 23HWHEEL RPM              = F10.1 / 6X,23HWHEEL SPEED (CM/SEC)  =
    2 F10.2,10X,23HALPHA                   = F10.2 /6X,23HBLADE PITCH (CM
    3)        = F10.4,10X,23HALPHAI            = F10.2 )
14   FORMAT(10X,2HVD,10X,2HWD,10X,2HWN,8X,6HALPHAD,8X,4HBETA,5X,
    1 14HIMPACT LENGTH /)
16   FORMAT(    6X,23HMAX DELTA L (CM)       = F10.4,10X,23HALPHADO (DEG
    1)          = F10.2/6X,23HVDROPO (CM/SEC)         = F10.2, 10X,23HWD =
    2WN (CM/SEC)        = F10.2/6X,23HVZERO (CM/SEC)          = F10.2//)
     END
C
```

Appendix B.7 Subroutine SPLINT Listing

```
C
        SUBROUTINE SPLINT(XT,YT,NT,XI,YI,NI,JX,JY)
C
C    XT IS THE FWA OF TABULATED INDEPENDENT VARIABLE ARRAY
C    YT IS THE FWA OF TABULATED DEPENDENT VARIABLE ARRAY
C    NT IS THE NUMBER OF (XT,YT) PAIRS
C    XI IS THE FWA OF INTERPOLATION ARGUMENTS
C    YI IS THE FWA OF INTERPOLATED VALUES
C    NI IS THE NUMBER OF INTERPOLATION ARGUMENTS (XI-YI PAIRS)
C    JX AND JY SPECIFY THE STORAGE INCREMENTS IN ARRAYS XT AND YT
C
     DIMENSION XT(2),YT(2),XI(2),YI(2)
     DATA (KX=1),(KY=1),(NN=1)
C
     IT = 1
 8   KX = JX
     KY = JY
     NN = NI
     ICF = 1
     ICB = 0
     NA = (NT-1)*KX+1
     IF (XT(NA).GT.XT(1)) GO TO 10
     ICF = 0
     ICB = 1
10   NTT = NT - 1
     DO 90 I=1,NN
     X = XI(I)
     CA = CB = 1.
     DCA = DCB = 0.
     DO 20 J=2,NTT
     L = J*ICF+(NT+1-J)*ICB
     NA = (L-1)*KX+1
     IF (XT(NA).GE.X) GO TO 30
20   CONTINUE
     L = (NT-3)*ICF+ICB
     CA = ICB
     CB = ICF
     GO TO 60
30   IF (J.GT.2) GO TO 50
     L = 3*ICF+(NT-2)*ICB
     CA = ICF
     CB = ICB
50   L = (L-2)*ICF+(L-1)*ICB
```

```
 60   NA = (L-1)*KX+1
      X1 = XT(NA)
      NA = (L-1)*KY+1
      Y1 = YT(NA)
      NA = L*KX+1
      X2 = XT(NA)
      NA = L*KY+1
      Y2 = YT(NA)
      NA = (L+1)*KX+1
      X3 = XT(NA)
      NA = (L+1)*KY+1
      Y3 = YT(NA)
      NA = (L+2)*KX+1
      X4 = XT(NA)
      NA = (L+2)*KY+1
      Y4 = YT(NA)
      D1  = (X1-X2)*(X1-X3)
      D2  =-(X1-X2)*(X2-X3)
      D3  = (X1-X3)*(X2-X3)
      D4  = (X2-X3)*(X2-X4)


      A1  = (X-X2)*(X-X3)/D1
      A2  = (X-X1)*(X-X3)/D2
      A3  = (X-X1)*(X-X2)/D3
      A4  = (X-X3)*(X-X4)/D4
      A5  = (X-X2)*(X-X4)/D5
      A6  = (X-X2)*(X-X3)/D6
      IF ((CA.EQ.0.).OR.(CB.EQ.0.)) GO TO 64
      DCA = X2-X3
      DCB = -DCA
      CA  = (X-X3)/DCA
      CB  = (X-X2)/DCB
 64   PA  = Y1*A1+Y2*A2+Y3*A3
      PB  = Y2*A4+Y3*A5+Y4*A6
      IF (IT.EQ.2) GO TO 70
      YI(I)  = CA*PA+CB*PB
      GO TO 90
 70   A1  = Y1*((X-X2)+(X-X3))/D1
      A2  = Y2*((X-X1)+(X-X3))/D2
      A3  = Y3*((X-X1)+(X-X2))/D3
      A4  = Y2*((X-X3)+(X-X4))/D4
      A5  = Y3*((X-X2)+(X-X4))/D5
      A6  = Y4*((X-X2)+(X-X3))/D6
      YI(I)  = CA*(A1+A2+A3)+PA*DCA+CB*(A4+A5+A6)+PB*DCB
 90   CONTINUE
      RETURN
C
      ENTRY DYDX
C     YI IS THE DERIVATIVE OF THE TABULATED DATA AT XI
C
      IT = 2
      GO TO 8
      END
```

Appendix B.8 Subroutine VERGE Listing

```
      SUBROUTINE VERGE(XI,FOX,IK)
C
C        ACCELERATED CONVERGENCE OF ITERATIVE PROCESSES
C                    T.C.VARLJEN   WANL  4/15/68
C
      DIMENSION QO(5)
      DATA EPS,ETA,QO / 1.E-10,1.E-30,0.,.3,.55,-1.,5. /
      IK = IK+1
      IF (IK.GT.1) GO TO 20
      K = IABS(IK-2)
      IK = 1
      ZB = XI
      XI = QO(K)*ZB+(1.-QO(K))*FOX
      GO TO 50
   20 IF (ABS(FOX-XI).LT.EPS) GO TO 30
      ZC = (FOX*ZB-XA*XI)/(FOX+ZB-XA-XI)
      ZB = XI
      XI = ZC
      IF (ABS(ZB).GT.ETA) GO TO 50
   30 IK = -IK
   50 XA = FOX
      RETURN
      END
```

Appendix B.9 Subroutine ICEAD Listing

```
C
      SUBROUTINE ICEAD(N,T,XI,IRET)
      COMMON/ICON/H,HMAX,HMIN,RELB,ABSB
      DIMENSION XI(2),F(10),X(10,5),DY(10,5),XP(10),C(10,4)
C
C     N = NO. OF EQUATIONS
C     T = INDEPENDENT VARIABLE---SET IT=INITIAL T
C     H = STEP SIZE---SET IT=INITIAL H
C     HMAX = MAXIMUM STEP SIZE ACCEPTABLE
C     HMIN = MINIMUM STEP SIZE ACCEPTABLE
C     RELB = MAXIMUM ACCEPTABLE RELATIVE ERROR
C     ABSB = MAXIMUM ACCEPTABLE ABSOLUTE ERROR
C
C     INITIALIZATION
C
      RELT = 14.2*RELB   $  ABST = 14.2*ABSB
      FACT = RELB/ABSB   $  RB = RELT/200.
      CA = 1./6.         $  CB = 1./24.
      IRET = 0           $  H = 2.*H
      DO 100 I=1,N
  100 X(I,1) = XI(I)
C
C     RUNGE-KUTTA STARTING METHOD
C
  110 IA = IB = 2
  120 DO 160 J=IA,IB
      CALL DERIV(T,X(1,J-1),DY(1,J-1),IRET)
      IF (IRET) RETURN
      DO 130 I=1,N
      C(I,1) = H*DY(I,J-1)
  130 X(I,J) = X(I,J-1)+.5*C(I,1)
      TEMP = T+.5*H
      CALL DERIV(TEMP,X(1,J),DY(1,J),IRET)
      IF (IRET) RETURN
      DO 140 I=1,N
      C(I,2) = H*DY(I,J)
```

```
140   X(I,J) = X(I,J-1)+.5*C(I,2)
      CALL DERIV(TEMP,X(1,J),DY(1,J),IRET)
      IF (IRET) RETURN
      DO 150 I=1,N
      C(I,3) = H*DY(I,J)
150   X(I,J) = X(I,J-1)+C(I,3)
      T = T+H
      CALL DERIV(T,X(1,J),DY(1,J),IRET)
      IF (IRET) RETURN
      DO 160 I=1,N
      C(I,4) = H*DY(I,J)
160   X(I,J) = X(I,J-1)+C6*(C(I,1)+2.*(C(I,2)+C(I,3))+C(I,4))
      IF (IB.NE.2) 190,170
170   DO 180 I=1,N
180   XP(I) = X(I,2)
      T = T-H  $  H = .5*H
      IF (H.LT.HMIN) CALL FAIL(T,X,DY,IRET)
      IF (IRET) RETURN
      IB = 3
      GO TO 120
190   IF (IB.NE.3) GO TO 255
      J = 3
200   DO 250 I=1,N
      E(I) = ABS(XP(I)-X(I,J))
      IF (E(I).GE.ABS(X(I,J))*RELT) GO TO 220
      E(I) = E(I)/ABS(X(I,J))
      GO TO 250
220   IF (E(I).GE.ABST) GO TO 230
      E(I) = E(I)*FACT
      GO TO 250
230   T = T-H
      IF (J.NE.5) GO TO 170
      DO 240 K=1,N
240   X(K,1) = X(K,4)
      GO TO 110
250   CONTINUE
      IF (J.EQ.5) GO TO 310
      IA = IB = 4
      GO TO 120
C
C     SEND STARTING VALUES TO STEP
C
255   T = T-3.*H
      DO 260 J=2,4
      T = T+H
260   CALL STEP(T,X(1,J),DY(1,J),IRET)
      IF (IRET) RETURN
C
C     BEGIN ICF-ADAMS METHOD
C
280   CALL DERIV(T,X(1,4),DY(1,4),IRET)
      IF (IRET) RETURN
      DO 290 I=1,N
290   XP(I)    = X(I,4)+CB*H*(55.*DY(I,4)-59.*DY(I,3)+37.*DY(I,2)-9.*
     1DY(I,1))
      T = T+H
      CALL DERIV(T,XP,DY(1,5),IRET)
      IF (IRET) RETURN
      DO 300 I=1,N
300   X(I,5) = X(I,4)+CB*H*(9.*DY(I,5)+19.*DY(I,4)-5.*DY(I,3)+DY(I,2))
      J = 5
      GO TO 250
310   DO 320 I=1,N
      X(I,4) = X(I,5)
      DO 320 J=2,5
320   DY(I,J-1) = DY(I,J)
      CALL STEP(T,X(1,4),DY(1,4),IRET)
      IF (IRET) RETURN
      DO 330 I=1,N
      IF (E(I).GT.RB) GO TO 280
330   CONTINUE
      IF (2.*H.GT.HMAX) GO TO 280
      DO 340 I=1,N
340   X(I,1) = X(I,4)
      H = 4.*H
      GO TO 110
      RETURN
      END
```

Appendix B.10 Subroutine PROPM Listing

```
C
      SUBROUTINE PROPM(XX,TK,JPROP,JFLUID)
C
C       COMPUTATION OF SAT LIQUID AND VAPOR PROPERTIES OF WORKING FLUIDS
C
C      JFLUID  MATERIAL             JFLUID  MATERIAL
C         1      LITHIUM               5      CESIUM
C         2      SODIUM                6      MERCURY
C         3      POTASSIUM             7      NAK-78
C         4      RUBIDIUM              8      WATER
C
C       THIS VERSION ASSUMES INPUT TEMP IN DEGREES KELVIN
C
C
C      STEAM DATA TABULATIONS
C
      DIMENSION TH2(12),PSH2(12),VLH2(12),VGH2(12),CLH2(12),CVH2(12),
     1 HLH2(12)
      DATA TH2/.01,10.,30.,50.,80.,120.,150.,200.,250.,300.,350.,374./,
     1  PSH2/ .006112,.012271,.04242,.12335,.47358,1.9854,4.7597,15.55,
     2        39.776,85.917,165.37,220.9 /,
     3  VLH2/ 1.00021,1.0004,1.0044,1.0121,1.029,1.0603,1.0906,1.1565,
     4        1.2512,1.4036,1.741,2.8 /,
     5  VGH2/ 206146.,106422.,32929.,12045.,3408.,891.71,392.57,127.19,
     6        50.056,21.643,8.805,3.47/,
     7  CLH2/ 4.2174,4.1928,4.1787,4.1812,4.1965,4.2446,4.31,4.4966,
     8        4.8667,5.7619,10.1047,1400.5 /
      DATA CVH2 / 1.8542,1.8595,1.8745,1.8986,1.9616,2.1196,2.3144,
     1        2.8429,3.7722,5.8631,17.1505,3513.7 /,
     2     HLH2 /2500.9994,2477.01,2430.34,2382.7,2308.1,2202.3,2114.8,
     3        1942.6,1715.2,1404.,893.,114./,ITEM/0/
      TKTOF(R)= 1.8*R-459.67
      IF (ITEM.EQ.1) GO TO 10
      DO 20 I=1,12
      PSH2(I) = ALOG(PSH2(I))
      VGH2(I) = ALOG(VGH2(I))
   20 HLH2(I) = ALOG(HLH2(I))
      ITEM=1
   10 T = TK
      JF = JFLUID
      JP = JPROP
      IF(T.LT.250..OR.T.GT.3000.) GO TO 410
C
C      GO TO APPROPRIATE PROPERTY SECTION
C
      IF (JF.LT.1.OR.JF.GT.8.OR.JP.LT.1.OR.JP.GT.15)  GO TO 400
      GO TO (1001,1002,1003,1004,1005,1006,1007,1008,1009,400,1011
     1 1012,1013,1014,1015), JP
C
C         SAT LIQUID DENSITY (G/CM3)
C
 1001 GO TO (111,112,113,114,115,116,117,118), JF
  111 T = 3173.15-T
      X = .124+5.306E-3*SQRT(T)+4.135E-5*T
      GO TO 500
  112 T = T-273.18
      X = .9501-2.2976E-4*T-1.46E-8*T*T+5.638E-12*T*T*T          RL    NA
      GO TO 500
  113 X=9.083578E-1-2.244534E-4*T-1.274617E-8*T*T                R3L
      GO TO 500
  114 X=1.575802-3.074245E-4*T+3.837297E-8*T*T                   R4L
      GO TO 500
  115 X=1.985607-4.549765E-4*T-8.955005E-8*T*T                   R5L
      GO TO 500
  116 X=1.438176E1-2.861766E-3*T+3.763475E-7*T*T                 R6L
      GO TO 500
```

```
 117  X=9.3800519589E-1-2.3937338810E-4*T+3.5881034579E-9*T*T           R7L
      GO TO 500
 118  T = T-273.15
      CALL SPLINT(TH2,VLH2,12,T,X,1,1,1)
      X = 1./X
      GO TO 500
C
C          SAT VAPOR  DENSITY (G/CM3)
C
1002  GO TO (121,122,123,124,125,126,400,128), JF
 121  X=EXPF(4.324234E-1-1.560572E4/T-1.124864E6/T**2)                 R1G
      GO TO 500
 122  X=EXPF(1.000785-1.012916E4/T-5.75469E5/T**2)                     R2G
      GO TO 500
 123  X=EXPF(8.135742E-1-8.24115E3/T-4.269861E5/T**2)                  R3G
      GO TO 500
 124  X=EXPF(4.677273E-1-6.10964E3/T-9.252185E5/T**2)                  R4G
      GO TO 500
 125  X=EXPF(1.757963-7.371427E3/T-1.931032E5/T**2)                    R5G
      GO TO 500
 126  X=EXPF(3.243496-4.55902E3/T-6.07443E5/T**2)                      R6G
      GO TO 500
 128  T = T-273.18
      CALL SPLINT(TH2,VGH2,12,T,X,1,1,1)
      X = 1./EXP(X)
      GO TO 500
C
C          SAT LIQUID VISCOSITY (G/SEC-CM)
C
1003  GOTO  (131,132,133,134,135,136,137,138), JF
 131  X = 1.E-3*10.**(5.41921-155.991/T-1.61506*ALOG10(T))
      GO TO 500                                                        VL    NA
 132  X = .01*10.**(.5108+220.65/T-.4925*ALOG10(T))
      GO TO 500                                                        V3L
 133  X=-4.390586E-4+2.028652/T-5.410948E2/T**2+1.646804E5/T**3
      GO TO 500                                                        VL    RB
 134  X = 1.E-3*10.**(62.2374/T-.78639*ALOG10(T)+2.4459)
      GO TO 500                                                        VL    CS
 135  X = 1.E-3*10.**(104.013/T-.59011*ALOG10(T)+1.8781)
      GO TO 500                                                        V6L
 136  X=8.0365587E-3-3.198539/T+2.791399E3/T**2-3.544087E5/T**3
      GO TO 500                                                        V7L
 137  X=3.187261E-4*8.019051E-1/T+2.142332E2/T**2+2.596542E4/T**3
      GO TO 500                                                        VL H2O
 138  X = 241.4E-6*10.**(247.8/(T-140.))
      GO TO 500
C
C          SAT VAPOR  VISCOSITY (G/SEC-CM)
C
1004  GO TO (141,142,143,144,145,146,400,148), JF
 141  X=3.673815E-5+1.167182E-7*T-1.135025E-11*T*T                     V1G
      GO TO 500                                                        VG    NA
 142  X = .004134*(.03427+9.176E-6*TKTOF(T))
      GO TO 500                                                        V3G
 143  X=3.870094E-5+1.982508E-7*T-4.528330E-11*T*T
      GO TO 500                                                        V4G
 144  X=8.619203E-5+2.027719E-7*T-3.327784E-11*T*T
      GO TO 500                                                        V5G
 145  X=9.520804E-5+2.222279E-7*T-4.270371E-11*T*T
      GO TO 500                                                        V6G
 146  X=7.143205E-5+6.300290E-7*T+3.373475E-10*T*T
      GO TO 500
 148  X = 1.E-6*(80.4+.407*(T-273.15))
      GO TO 500
```

```
C
C         SAT LIQUID THERMAL CONDUCTIVITY (W /CM-K)
C
 1005 GO TO (151,152,153,154,155,156,157,158),  JF
 151   T = TKTOF(T)
       X=.49998+2.7992E-4*T+2.2565E-8*T*T-2.4606E-11*T*T*T               T1L
       GO TO 300
 152   T = TKTOF(T)
       X = .01731*(54.306-.01878*T+2.0914E-6*T*T)                        TL    NA
       GO TO 500
 153   T = TKTOF(T)
       X=.96689-4.7904E-4*T+1.3778E-7*T*T-2.4884E-11*T*T*T               T3L
       GO TO 300
 154   T = TKTOF(T)
       X=.49609-8.5289E-5*T-2.8444E-8*T*T+3.4248E-12*T*T*T               T4L
       GO TO 300
 155   X = 1.65E-6*SQRT(T)
       GO TO 500
 156   X=.14648003+59.8368/T-8.20005E4/T**2 +3.26295E7/T**3              T6L
      1  -4.43661E9/T**4
       GO TO 500
 157   X=1.384235E-1+2.05547E2/T-1.062331E5/T**2+1.60138E7/T**3          T7L
       GO TO 500
 158   T = T/273.15
       X = .01*(-922.47+2839.5*T-1800.7*T*T+525.77*T*T*T-73.44*T**4)     TCL H2O
       GO TO 500
 300   X = X*.7087
       GO TO 500
C
C         SAT VAPOR  THERMAL CONDUCTIVITY(W/CM-K)
C
 1006 GO TO (161,162,163,164,165,166,400,168),  JF
 161   X=1.211242E-4+5.135221E-7*T-5.902087E-11*T*T                      T1G
       GO TO 500
 162   T = TKTOF(T)
       X = .0173*(1.639E-3+.3977E-4*T-.9697E-8*T*T)                      TG    NA
       GO TO 500
 163   X=3.033089E-5 +1.400357E-7*T -3.133830E-11*T**2                   T3G
       GO TO 500
 164   X=3.979684E-5+6.325412E-8*T  -9.535292E-12*T**2                   T4G
       GO TO 500
 165   X=2.245009E-5+4.234143E-8*T-6.469024E-12*T*T                      T5G
       GO TO 500
 166   X=2.749046E-6+1.175486E-7*T-2.454670E-11*T**2                     T6G
       GO TO 500
 168   T = T-273.15
       X = 1.E-5*(17.6+.0587*T+1.04E-4*T*T-4.51E-8*T*T*T)                TCG H2O
       GO TO 500
C
C         SAT LIQUID SPECIFIC HEAT (W-SEC/G-K)
C
 1007 GO TO (171,172,173,174,175,176,177,178),  JF
 171   T = T-273.15
       X = 4.184*(1.0577-1.2152E-4*T+5.3477E-8*T*T)
       GO TO 500
 172   T = T-273.18
       X = 4.187*(0.34324-1.3868E-4*T+1.1044E-7*T*T)                     CL    NA
       GO TO 500
 173   X=9.512349E-1-4.860081E-4*T+3.122763E-7*T*T                       C3L
       GO TO 500
 174   T = TKTOF(T)
       X=4.187*(.09915-3.106E-5*T+1.299E-8*T*T)                          C4L
       GO TO 500
 175   T = TKTOF(T)
       X=4.187*(.08543-9.605E-5*T+5.985E-8*T*T)                          C5L
       GO TO 500
 176   X=1.519435E-1-5.070309E-5*T+5.301029E-8*T*T                       C6L
       GO TO 500
 177   T = T-273.18
       X = 4.187*(.232-8.82E-5*T+8.2E-8*T*T)                             CL    NAK
```

```
      GO TO 500
 178  T = T-273.15
      CALL SPLINT(TH2,CLH2,12,T,X,1,1,1)
      GO TO 500
C
C         SAT VAPOR  SPECIFIC HEAT (W-SEC/G-K)
C
 1008 GO TO (181,182,183,184,185,186,400,188),  JF
 181  X=3.96472-1.321868E4/T+7.253337E7/T**2-5.82616E10/T**3          C1G
      GO TO 500
 182  X = 4.197*(.21508+6.054*EXP(-20708./T))                         CG    NA
      GO TO 500
 183  X=-6.011841E-1+4.044715E3/T-3.393891E6/T**2+8.493131E8/T**3     C3G
      GO TO 500
 184  X=-1.730578E-2+8.663483E2/T-4.075597E5/T**2                     C4G
      GO TO 500
 185  X=-1.354922E-2+5.228561E2/T-2.32491E5/T**2                      C5G
      GO TO 500
 186  X=1.076087E-1+1.637431E-5*T+1.697121E-8*T*T                     C6G
      GO TO 500
 188  T = T-273.15
      CALL SPLINT(TH2,CLH2,12,T,X,1,1,1)
      GO TO 500
C
C         SAT LIQUID SURFACE TENSION (DYN/CM)
C
 1009 GO TO (191,192,193,194,195,196,197,198),  JF
 191  X=4.544948E2-1.356226E-1*T+1.615487E-6*T*T                      ST1
      GO TO 500
 192  X = 206.7-.1*(T-273.18)                                         ST    NA
      GO TO 500
 193  X = 115.51-.0653*(T-273.18)                                     ST    K
      GO TO 500
 194  X=1.347296E2-5.606006E-2*T-1.513351E-5*T*T                      ST4
      GO TO 500
 195  T = TKTOF(T)
      X=76.4-.03*(T-83.)                                              ST5
      GO TO 500
 196  X = 608.-.352*T                                                 ST    HG
      GO TO 500
 197  X=1.201687E2-3.890232E-2*T                                      ST7
      GO TO 500
 198  X = 53.9-.216*(T-373.15)                                        ST   H2O
      GO TO 500
C
C         LIQUID SONIC VELOCITY (CM/SEC)
C
 1011 GO TO (400,212,213,214,215,216,217,218),  JF
 212  X = 2.526E5-52.4*(T-370.78)                                     SVL   NA
      GO TO 500
 213  X = 1.969E5-53.*(T-373.18)                                      SVL   K
      GO TO 500
 214  X = 1.26E5-40.*(T-273.18)                                       SVL   RB
      GO TO 500
 215  X = 9.67E4-30.*(T-273.18)                                       SVL   CS
      GO TO 500
 216  X = 1.4608E5-45.75*(T-273.18)                                   SVL   HG
      GO TO 500
 217  X = 207000.-54.3*(T-273.18)                                     SVL   NAK
      GO TO 500
 218  X = 1.437E5+640.*(T-288.18)                                     SVL  H2O
      GO TO 500
C
C         SAT VAPOR  SONIC VELOCITY (CM/SEC)
C
 1012 GO TO (221,222,223,224,225,400,400,400),  JF
 221  X=7.650211E4+35.0503*T-2.883303E-3*T*T                          SV1
      GO TO 500
 222  X=4.710855E4+1.3694E1*T-5.391655E6/T                            SV2
      GO TO 500
 223  X=2.134288E4+2.836652E1*T-5.800705E-3*T*T                       SV3
      GO TO 500
 224  X=1.554827E4+1.626642E1*T-2.611827E-3*T*T                       SV4
      GO TO 500
 225  X=1.277488E4+1.217007E1*T-1.763269E-3*T*T                       SV5
      GO TO 500
```

```
C
C        VAPOR PRESSURE (BARS)
C
 1013 GO TO (231,232,233,234,235,236,237,238), JF
 231  X = 1.01325*10.**(-2.1974-6499.1/T+1.939*ALOG10(T))
      GO TO 500
 232  X = 1.013*EXP(6.6808-5544.41/T-.61344*ALOG(T))                    VP   NA
      GO TO 500
 233  X=EXPF(9.191863-9.030992E3/T-4.33038E5/T**2)                      VP3
      GO TO 500
 234  T = T*1.8
      X=0.06895*10.**(5.20071-6994.68/T)                                VP4
      GO TO 500
 235  X=EXPF(8.636035-7.715273E3/T-3.846408E5/T**2)                     VP5
      GO TO 500
 236  T = T*1.8
      X = .0013332*10.**(10.57757-5954.55/T-.8*ALOG10(T))              VP  HG
      GO TO 500
 237  X = 1.013*(EXP(4.114-4367./T))                                    VP   NAK
      GO TO 500
 238  T = T-273.15
      CALL SPLINT(TH2,PSH2,12,T,X,1,1,1)
      X = EXP(X)
      GO TO 500
C
C        LATENT HEAT OF VAPORIZATION (J/GM)
C
 1014 GO TO (241,242,243,400,245,400,400,248), JF
 241  T = T/3173.
      X = 4.184*6061.2*(1.-T)**.3725
      GO TO 500
 242  X=4.178649E3+2.829841E-1*T-4.765964E-4*T*T                              LV2
      GO TO 500
 243  X=2.269079E3-1.318445E-1*T-2.003039E-4*T*T                              LV3
      GO TO 500
 245  X=6.050302E2-6.543721E-2*T-5.902942E-5*T*T                              LV5
      GO TO 500
 248  T = T-273.15
      CALL SPLINT(TH2,HLH2,12,T,X,1,1,1)
      X = EXP(X)
      GO TO 500
C
C        SAT LIQUID ELECTRICAL RESISTIVITY (OHM-CM)
C
 1015 GOTO  (251,252,253,254,255,400,257,400), JF
 251  T = TKTOF(T)
      X=2.54E-6  *(10.186+2.9187E-3*T+6.8168E-7*T*T+1.1545E-10*T*T*T)     RS1
      GO TO 500
 252  T = TKTOF(T)
      X=2.54E-6  * (2.1729+7.6248E-3*T+5.8313E-7*T*T+1.1260E-9*T*T*T)     RS2
      GO TO 500
 253  T = TKTOF(T)
      X=2.54E-6  *(2.6978+1.4055E-2*T-2.0398E-6*T*T+3.5792E-9*T*T*T)      RS3
      GO TO 500
 254  T = TKTOF(T)
      X=2.54E-6  *(6.3519+2.0871E-2*T+5.1071E-6*T*T+6.2079E-9*T*T*T)      RS4
      GO TO 500
 255  T = TKTOF(T)
      X=2.54E-6  *(10.9086+3.3902E-2*T-1.6701E-5*T*T+1.0964E-8*T*T*T)     RS5
      GO TO 500
 257  T = TKTOF(T)
      X=2.54E-6  *(12.8180+1.2679E-2*T-3.6501E-7*T*T+2.852E-9*T*T*T)      RS7
      GO TO 500
C
C
 400  WRITE (6,5) JP,JF
      X = -1.
 500  XX = X
 501  RETURN
 410  WRITE (6,4) T
      X = -1.
      GO TO 501
C
C
    5 FORMAT(//72H *** ERROR IN SUBROUTINE PROP -- ILLEGAL FLUID OR PROP
     1ERTY CODE USED ***  // 5X, 7HJPROP = I6,6X,8HJFLUID = I6 //)
    4 FORMAT(//63H *** ERROR IN SUBROUTINE PROP -- OUT OF BOUNDS TEMPERA
     1TURE *** // 6X,11HT(KELVIN) = E20.5 //)
      END
```

2.7 ATOMIZATION OF COLLECTED CONDENSATE*

2.7.1 Background

As has been frequently stated, it is that fraction of the condensate which has been collected by the various turbine surfaces and then discharged in the form of macroscopic diameter drops which is capable of causing erosion damage. In wet vapor turbines two locations of particular interest are: (1) atomization of liquid torn from that flowing along the turbine housing, and (2) atomization of liquid from the vicinity of the trailing edges of stator vanes. In both instances the liquid can be carried into the path of rotor blades moving with high velocities relative to the liquid . Impact of liquid at high velocities on surfaces can cause erosion damage providing the liquid drops are of sufficient girth to drive the threshold velocity to cause damage below the impact velocity.

In considering casing liquid atomization the Westinghouse erosion model assumes that drops are produced by the same general mechanism as that of the primary stage of atomization of the liquid torn from stators. This assumption allows the same equations to be used for predicting casing liquid atomized drop diameters for rotor impingement investigation as are used in predicting the primary atomization drop diameters from stator discharged liquid. Such a casing liquid calculation has been previously reported. To our knowledge there is no experimental data by which to check this assumption. A substantial discussion of the general nature of the casing liquid flows is provided in Spies, Baughman, and Blake.(1)

Visual observations in steam turbines(1,2) reveal that the liquid collected on the stators is torn from the vicinity of the trailing edges of the stator vanes. Initially this liquid is in the form of a distribution of sizes of fairly large drops. This stage of the atomization process is called primary atomization. These large primary drops are caught up in the decaying wakes downstream of the stators and accelerated by the vapor stream. Most of the primary drops are unstable under the aerodynamic conditions prevailing during this acceleration. Providing there is sufficient distance (time of flight) between stator and rotor, these unstable drops are broken down into smaller stable drops. This stage of the atomization process is called secondary atomization. Completion of the secondary atomization process gives a relatively stable population of drops composed of a residual of primary drops which were small enough to be stable plus the secondary drops formed from shattered primary drops. In well designed turbines, it is this stabilized population of drops which impinge upon the rotor blades and can cause erosion damage. The discussion which follows is concerned with the various stages of atomization of stator discharged liquid.

2.7.2 Stator Atomization Model

a) General Description

To calculate the erosion by liquid of damaging form, it is necessary to know the size, relative velocity and number and location of impacts on the rotor blades as a relation of time. There are at least four different mechanisms of primary atomization and two for secondary atomization which have been observed under conditions related to those in turbine stators. To trace the history of all these possible processes would be a formidable, if not impossible task. Because of this, the approach taken in the Westinghouse model involves substantial simplification through gross description of droplet classes based in large part on empirical correlating relations commonly used in describing gas-atomized liquid sprays.

Furthermore, almost all the empirical observations used in preparing the numerical detail of the atomization model were taken from reference material where the tests reported were made using steam vapor or air atomization of water drops. Nonetheless, it is felt that observations on steam or air atomization of water drops, particularly observations in actual turbines or turbine-like cascades, are applicable to a broader spectrum of turbine

---

* W. D. Pouchot, Advisory Engineer, Systems & Technology Section, Westinghouse Astronuclear Laboratory, Large, Pa.

working fluids (such as the liquid metals) of low liquid-viscosity and substantial surface tension.*

- Nomenclature

In dimensional equations the units used are:

Mass-slugs, Force-pounds, Length-feet, Time-seconds

a	Constant in Nukiyama-Tanasawa distribution functions
a	Stator blade trailing edge thickness
b	Constant in Nukiyama-Tanasawa distribution function
D	Drop diameter
D_m	Most common drop diameter in terms of spray volume
D_{3-0}	Mass mean drop diameter
$D_{3\sigma}$	The drop approximately three standard deviations larger than the mean drop
D_{max}	Maximum drop diameter
K	A constant
L	Length along surface of stator blade from nose to trailing edge
M_a	Mach No. based on free stream conditions
$\dot{m}_\ell$	Collected liquid mass flow rate per unit casing periphery or blade height
N	Number of drops
n	Exponent in Nukiyama-Tanasawa distribution function
p	Gamma function argument
Re_D	Reynolds Number based on drop diameter
S_b	Tanasawa's stability number (Heinze's viscosity number) - $\mu_\ell / \sqrt{\rho_\ell \sigma a}$
U_r	Relative velocity between vapor and drop
u	Gamma function argument
U_s	Bulk stream (free stream) velocity
V	Spray Volume
V_x	Volume of spray between gamma function parameter (o) and parameter (x)
V_{tot}	Total volume of spray
W_e	Weber number - $\rho_v U_r^2 D / \sigma$ or $\rho_v U_s^2 D / \sigma$
X	Stator blade chord length
x	Gamma function parameter
ρ_v	Vapor density
ρ_ℓ	Liquid density
σ	Liquid surface tension
τ_s	Wall friction force per unit area on bulk flow
μ_v	Vapor viscosity
μ	Liquid viscosity

* Wetability of the liquid with respect to surface does not seem to be an important factor. Experiments reported in reference (4) seem to indicate that under the impress of aerodynamic forces liquids tend to become non-wetting. This is reasonable since the ground state of a liquid mass in the absence of external forces such as gravity, is a sphere and perturbations from aerodynamic sources would tend to allow films and rivulets to "ball up".

- Definition of Model

The model of atomization is defined in terms of the empirical Nukiyama-Tanasawa distribution function plus several characteristic drop diameters.

The distribution function is used in both a number of drops form and in volumetric form. These functions are:

$$\frac{dN}{dD} = a D^2 e^{-bD^n} \tag{1a}$$

$$\frac{dV}{dD} = \frac{\pi a}{6} D^5 e^{-bD^n} \tag{1b}$$

The characteristic diameters used are:

1) Dm = most common diameter drop

D = Dm when the second derivative of Eq. 1b equals zero or $\frac{d^2V}{d D^2} = 0$. This corresponds to the peak of the familiar distribution curve as:

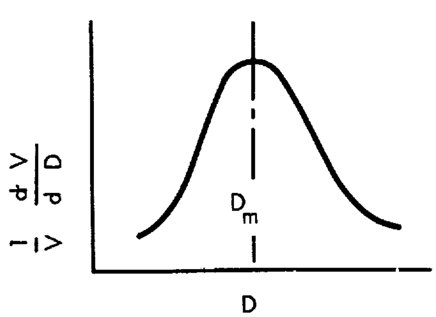

2) D_{3-0} - Mass mean diameter drop

$$D_{3-0} = \left[\frac{6}{\pi} \frac{\sum_o^\infty \Delta V}{\sum_o^\infty \Delta N}\right]^{1/3}$$

3) $D_{3\sigma}$ - The drop approximately three standard deviations larger than the mean drop

$D_{3\sigma}$ is the drop for which

$$\frac{\sum_o^{\infty \sim x} \Delta V}{\sum_o \Delta V} = 0.997$$

$$\text{where } x = \frac{5}{n}\left(\frac{D}{D_m}\right)^n$$

4) D_{max} - Defined maximum drop diameter

D_{max} is the drop for which

$$\frac{\sum_o^{x} \Delta V}{\sum_o^\infty \Delta V} = K$$

The Nukiyama-Tanasawa distribution function is often used by experimentalists in reporting data on gas atomized liquid sprays. It is a monomodal function and the constants, "a, b and n" of the expression can be determined from a knowledge of the number of volume fractions of the spray of any two drop diameters. Conversely the spray can be characterized by a value of "n" and a characteristic drop diameter such as the mass mean or surface mean drop diameter.

From the point of view of the analyst, these various relationships between characteristic drop diameters and the constants of the Nukiyama-Tanasawa expressions may be found by such means as writing an appropriate computer program or by use of Pearson's tables of the incomplete gamma function[3].

In connection with use of the reference (3) material, it may be shown that:

$$b = \frac{5}{n} \left(\frac{1}{D_m} \right)^n$$

Hence the exponential coefficient

$$(b\, d^n) = \frac{5}{n} \left(\frac{D}{D_m} \right)^n$$

If $\frac{5}{n} \left(\frac{D}{D_m} \right)^n = x$, equation (1b) may then be put in the form:

$$\frac{dV}{dx} = \frac{\pi a}{30} \left(\frac{n}{5}\right) \left(\frac{6-n}{n}\right) D_m^{\ 6} \left(x^{\frac{6-n}{n}}\right) e^{-x} \quad (2)$$

If the additional substitution $\frac{6-n}{n} = p$ is made,

$$\frac{dV}{dx} = \frac{\pi a}{30} \left(\frac{n}{5}\right)^p D_m^{\ 6} \left(x^p e^{-x}\right) \quad (3)$$

In integral form equation (3) may be written,

$$V_x = \frac{\pi a}{30} \left(\frac{n}{5}\right) D_m^{\ 6} \int_0^x x^p e^{-x} dx \quad (4)$$

When $x = \infty$, $V_x = V_{tot}$ (the total volume of the spray)

and therefore by definition:

$$\frac{V_x}{V_{tot}} = \frac{\int_0^x x^p e^{-x} dx}{\int_0^\infty x^p e^{-x} dx} \quad (5)$$

This is the ratio of the spray volume contained in all drops smaller than

$$D = \left(\frac{nx}{5} \right)^{\frac{1}{n}} (D_m)$$

to the total volume of the spray.

There is nothing fundamental in these previous substitutions and rearrangement of the Nukiyama-Tanasawa equation. They are for the purpose of putting the equation on a form for easy use with the tables of Reference (3).

The complete gamma function for the argument p is written $\Gamma(p + 1)$. It can be defined by:

$$\Gamma(p + 1) = \int_0^\infty e^{-x} x^p dx$$

The incomplete gamma function is defined after Pearson[3] to be:

$$\Gamma_x (p + 1) = \int_0^x e^{-x} x^p dx$$

Hence equation (5) may be given as:

$$\frac{V_x}{V_{tot}} = \frac{\Gamma_x (p + 1)}{\Gamma(p + 1)} = I\,(x\text{-}p) \quad (6)$$

Pearson[3] has constructed tables of this ratio in the form:

$$\frac{V_x}{V_{tot}} = I\,(u,\ p)$$

where

$$u = \frac{x}{\sqrt{p + 1}}$$

In terms of the spray parameters of interest, p and u are:

$$p = \frac{6-n}{n}$$

$$u = \left(\frac{D}{D_m}\right)^n \frac{5}{\sqrt{6n}}$$

Some numerical values for the ratios $D_{3\sigma}/D_{3-0}$, and $D_{3\sigma}/D_m$ calculated in this way are given as a function of n in Table 2.7-1.

TABLE 2.7-1

RELATIONSHIPS OF $D_{3\sigma}$, D_{3-0}, D_m, AND n

n	$D_{3\sigma}/D_{3-0}$	$D_{3\sigma}/D_m$
0.25	28.70	15.5
0.50	8.14	5.61
1.0	3.84	2.99
2.0	2.40	1.99
3.0	2.01	1.69

b) Primary Atomization

Mechanisms of primary atomization as observed in an actual turbine[5] and in turbine-like stationary cascades[4,5] are: (1) stripping of liquid or sheets from liquid puddles, (2) stripping or tip bursting of oscillating pendant drops attached to the stator trailing edge, (3) eye-dropper tearing of individual drops from the stator trailing edge, and (4) direct formation of individual drops on the convex surface of a stator by some mechanism giving results similar to a drop of water on a hot stove.

The observations reported are qualitative. Quantitative information on the relative volumes of liquid involved in each of the processes is not available. It seems reasonable that the tearing of masses or sheets of liquid from stators involves a more important part of the total liquid available than the other observed mechanisms of detachment. On this basis, a sheet atomization model is the logical tool for estimation of primary drop sizes.

The model chosen is the classical one of a sheet of liquid ruffled under the impress of aerodynamic forces, the ripples developing into ligaments, and the ligaments in turn collapsing into drops. Using this model an expression for the most common drop diameter, D_m, has been developed. It is

$$D_m = 17 \left[\frac{\dot{m}_\ell \, \mu_\ell}{\rho_\ell \left(\tau_s + \frac{\dot{m}_\ell U_s}{X}\right)}\right]^{1/4} \left[\frac{\mu_\ell}{\tau_s} \sqrt{\frac{\sigma}{\rho_\ell}}\right]^{1/3} \qquad (7)$$

The complete primary distribution is then obtained by applying the Nukiyama-Tanasawa distribution function assuming that n = 1. Given n and D_m, the ratio V_x/V_{tot}, at any value of D, can be obtained through the use of Pearson's[3] tables by calculation of Pearson's arguments p and u as a function of D.

Typical values calculated for the ninth stator of the Yankee steam turbine are given in Appendix A to this Section 2.7, along with the derivation of the expression for D_m (equation 6).

A comparison between calculated values for the Yankee steam turbine and a small amount of experimental data on stator primary atomization obtained by Hays[5] from the British CEGB is also given in Appendix A to the Section 2.7. This data comparison cannot be said to confirm the model of primary atomization proposed here, because of the small number of drops sampled experimentally, but the comparison is encouraging.

c) Secondary Atomization

To distinguish between those primary drops which are stable from origin to rotor impact and primary drops which undergo secondary atomization, a parametric time history analysis of the drops in the stator wake is carried out as previously discussed in Section 2.6. It is assumed that the primary drops become entrained by a given wake streamline and the liquid represented remains with that streamline until rotor impact. The criteria for disruption of a primary drop is taken as the exceeding of a critical drop Weber Number at some point along the path between detachment from the stator to impact with the rotor. This assumes that there is time for the drop to disrupt, after the critical Weber Number has been exceeded, before it impacts the turbine rotor. This time period for disruption is covered in Section 2.6. All primary drops which experience a Weber Number greater than the critical are presumed to disrupt to smaller stable secondary drops.

Primary drops which experience local Weber Numbers in the wake which are less than the critical Weber Number are assumed stable and retain their primary configuration. The maximum size drop which will impact the rotor is the primary drop which just experiences but does not exceed the critical Weber Number anywhere between origin and impact with the rotor.

This model uses Weber Number criteria because under local conditions at the time of breakup of the primary drops it is believed that the ratio of the dynamic pressure force to surface tension force is the single most important criteria as to whether a drop is stable or not. Unfortunately, Weber Number alone is not completely sufficient to allow a prediction of maximum drop diameters in sprays even when the local conditions at disruption are known with reasonable accuracy. For this reason, Westinghouse has varied the numerical value of the Weber Number which has been used in analysis of turbines from turbine to turbine.

For small turbines of the space type, 1" chord, 1"-2" high blades, the critical Weber Number used has been 13. For the large low pressure ends of central station steam turbines the value used has been Weber Number = 22. The rationale is due to Gardner[6] who apparently drew on the work of Heinze. According to Spies et al[1], Heinze shows that for a "non-viscous" fluid (the turbine working fluids are considered "non-viscous") that the critical value of Weber Number is 13 for shock exposure of a drop to aerodynamic forces and this critical Weber Number increases to 22 for a steadily falling drop. This latter case is that of graduated application of aerodynamic forces to the drop. From trajectory calculations on both large and small turbines, it appears that the application of aerodynamic forces to the primary drops is quite abrupt or shock-like in the small space type turbine and quite gradual in the large central station steam turbine low pressure end. The selection of Weber Number = 13 for the small turbines and Weber Number = 22 are commensurate with the trajectory observations.

Since these values were selected, a considerable amount of actual observation in large steam turbines[2] and in a small steam turbine[1] built to simulate a space potassium turbine have become available. These data clearly show that from a conceptual point of view the simplified two valued scheme of this model is inadequate. However, in a numerical sense the selection of Weber Number = 13 for the small space turbines examined is a good average value based on an analysis of the results of Spies et al[1] as given in Appendix "B" of this section 2.7. For a typical design such as the NASA-GE 3 stage potassium test turbine the procedure of Weber Number = 13 may err in estimating the maximum size drop impinging on the rotor blades of that turbine by 30 microns. The maximum size drop is about 100 microns in diameter.

Spies et al[1] give three empirical expressions which affect a good correlation of their data. These are*

$$We = 65\,(M_a)^{1.16} \qquad \text{(i)}$$

$$We = \frac{K}{S_b^{2/3}} \left(\frac{\mu}{\mu_v}\right) \left(\frac{\mu_v U_s}{\sigma}\right)^{7/6} \left(\frac{L}{a}\right)^{1/6} \qquad \text{(ii)}$$

where K = 0.31 for the data of Smith[7]

$$Re_D = 18 \qquad \text{(iii)}$$

The first of these (i) is due to Smith[7]. It also correlates his data as does the second expression (ii). Both the first and second expressions badly overestimate the maximum size drops in large central station turbines low pressure ends as reported by Christie and Hayward[2]. The writer has not evaluated the third expression (iii). As a general comment, all three expressions lack a model as a basis for understanding the phenomena the expressions purport to correlate. They, therefore, pose a high risk when applied to situations other than those exact ones from which they were obtained.

The selection of critical Weber Number = 22 for the low pressure ends of large central station steam turbines seems to be overly conservative in terms of steam stationary cascade tests as reported by Christie and Hayward[2] but not necessarily for actual turbines as reported by the same reference[2].

d) Final Drop Size Distribution

- <u>Conceptual Approach</u>

Conceptually the drop size distribution resulting from the completion of the secondary atomization process is the sum of the primary drops which escaped disruption plus the families of secondary drops formed from the disrupted primary drops.

The residual primary drops are those from the primary distribution which did not experience a greater than critical Weber Number.

The mass mean drop diameter (D_{3-0}) of the sum of the families of the secondary drops is assumed to be given by a semi-empirical expression developed by Wolfe and Anderson[8]. This is:

$$D_{3-0} = \left[\frac{136\ \mu_\ell\ \sigma^{3/2} D_m^{\ 1/2}}{\rho_v^{\ 2}\ \rho_\ell^{\ 1/2}\ \overline{U}_r^{\ 4}}\right]^{1/3}$$

where D_m is the most common drop of the initial primary distribution.

The distribution function for the sum of the families of secondary drops is then taken as that of the Nukiyama-Tanasawa function for n = 1 and the appropriate Wolfe and Anderson D_{3-0}.

Addition of this secondary distribution to the residual of the primary distribution gives the final drop size distribution impacting the turbine rotor blades.

This is the way in which the final drop size distribution used in calculating the erosion values for the Yankee steam turbine was obtained. A comparison of this distribution in dimensionless form with various test observations from the literature which have become available since the Yankee analysis was performed, reveals a rather striking lack of similarity between calculation and observation as shown in Figure 2.7-1. This may explain why the calculated erosion of the Yankee ninth rotor blades was lower than that actually observed in service.

*All values are calculated using bulk flow (free stream) conditions not local wake conditions.

- <u>An Empirical Approach</u>

Since the conceptual approach just outlined yielded a drop distribution much askew compared to actual experimental observations, a more fully empirical approach was tried in connection with the Bayshore No. 2 turbine evaluation. This approach was to apply an average of the observed distributions shown in Figure 2.7-1 to the calculated maximum drop diameter.

Reservations about this approach must also be expressed. For example, the observational curves shown in Figure 2.7-1 correspond to Nukiyama-Tanasawa "n" values in the range of 2 to 3*. This is far higher than characteristic values reported in the literature of gas atomized liquid sprays. Here a value of "n" much different from one is uncommon[9] and when values differ from one they are likely to be less than one.

A part of the difficulty may be in the interpretation of what experimentalists mean whey they report a value of n = 1 in the Nukiyama-Tanasawa expression effects a good correlation of their data. For example, turn to Figure 2.7-2. This is a plot of some data presented by Spies, Baughman, and Blake[1]. The open circles are the data. The solid line and dashed line are the Nukiyama-Tanasawa expression plotted with n = 1 and n = 3 respectively. It will be noted that the shape of distribution curves as given by the circles is very similar to the shape of other experimental results curves as shown in Figure 2.7-1.

Spies et al conclude in their report that a Nukiyama-Tanasawa distribution with n = 1 affects a satisfactory correlation of their data. As can be seen in Figure 2.7-2 it does on the average affect a better correlation than n = 3. However, Spies et al report the maximum drop diameter observed for this particular set of test conditions to be 180 microns. An n = 1 correlation implies at least 2 percent by number of drops with a diameter greater than 180 microns. This 2 percent number fraction represents a considerably larger volume fraction than number fraction because of the D-cubed effect. It seems

*This is on the writer's terms; not necessarily on the terms of the experimentalist as is discussed shortly.

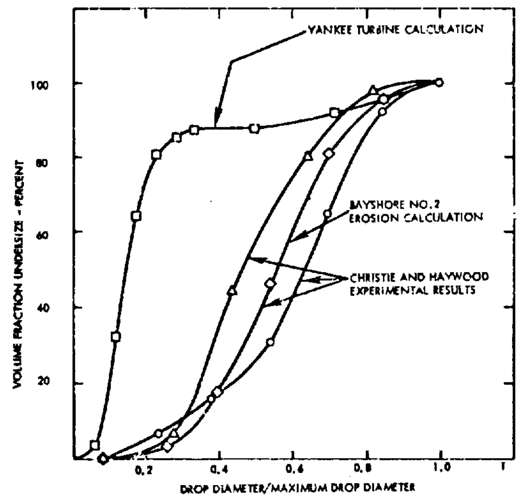

Figure 2.7-1 Drop Distribution Functions

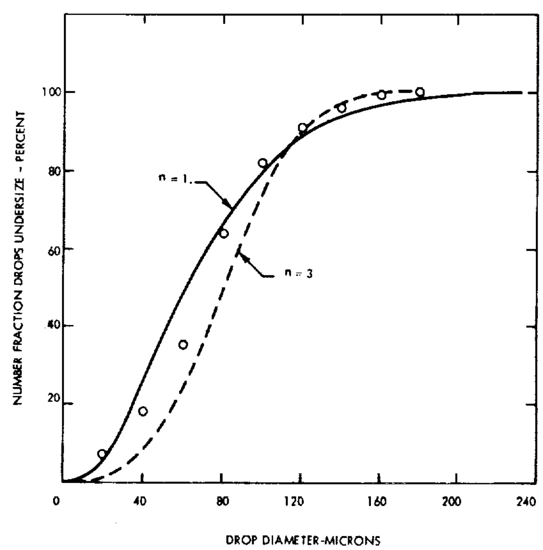

Figure 2.7-2 Distribution of Drop Sizes in a Small Steam Turbine after Spies, Baughman, and Blake

quite possible that the n = 1 selection of Spies et al is in fact more nearly correct than the actual data points. It seems quite possible that they might have observed some (say) 240 micron diameter drops if their observations had covered 10,000 drops and not hundreds of drops.

This possible inaccuracy in distribution information is compounded in the empirical approach used in the Bayshore No. 2 turbine erosion examination by a "tail wagging the dog phenomena". A tabulation from reference (2) is reproduced as Table 2.7-2 following:

TABLE 2.7-2

TABULATION FROM REFERENCE 2

Size Range of Drop Diameters (microns)	Total No. of Droplets per Second in Each Size Range at Given Load (Load 100%)	(Load 60%)	Load 40%)
50 to 150	384	1160	1283
150 to 250	322	414	744
250 to 350	16	54	125
350 to 450	0	4	10

The most drops are reported in the 40 percent load column. The number is 2162. A plot of this 40 percent load tabulation is given as "Original Data" in Figure 2.7-3. If one 500 micron drop is added to this original 2162 drops, the distribution function shifts markedly (in the direction n = 1) as shown by the curve "Original Data Plus One" of Figure 2.7-3.

The significance of the shift with respect to predicting erosion in turbines is marked in numerical evaluation using the empirical atomization model as applied to Bayshore No. 2. The model assumes that some particular characteristic diameter drop of the distribution of drops can be predicted either empirically or theoretically as a function of turbine flow and geometry for particular sets of turbine flow and geometry variables. Then the model assumes this particular characteristic diameter can be generalized to a complete particular distribution of drops by applying an empirical distribution function to the particular characteristic diameter drop.

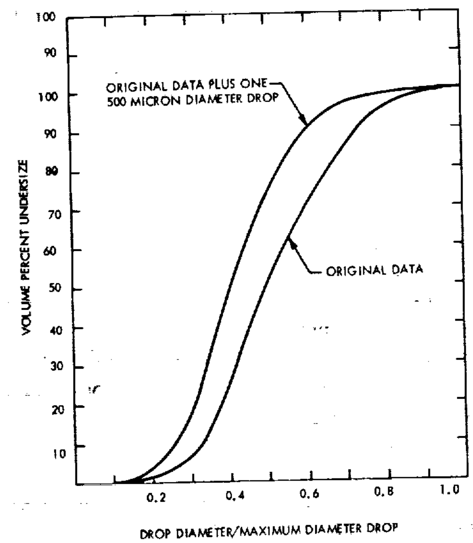

Figure 2.7-3 Manipulation of Experimental Drop Size Distribution

The foregoing are all reasonable assumptions. Unfortunately at this time the characteristic diameter drop on which there is substantial experimental data in turbines is the maximum diameter drop of the spray. While the general approach to the model is not limited to the use of the maximum diameter drop as the characteristic diameter drop, the weight of experimental evidence on maximum diameter drops has made them a logical if unfortunate choice.

Referring back to Figure 2.7-3, the actual change in total volume of the spray caused by adding one 500 micron drop is only 1.2 percent. However, if in reconstructing a distribution of drops based on a particular independently calculated maximum diameter drop, the distribution function marked "Original Data" is used, 30 percent of the volume of the spray will be predicted to be in drops greater than 0.6 the diameter at the maximum diameter drop; whereas if the distribution function marked "Original Data Plus One" is applied, only 10 percent of the volume of the spray will be predicted to be in drops greater than 0.6 the diameter of the maximum diameter drop. That is as little as 1 percent change in the experimental measurement with respect to volume (or one part in two thousand with respect to number of drops) can shift the prediction of amount of moisture contained in damaged drop diameters* by as much as 300 percent using this empirical procedure.

2.7.3 Conclusions

Means of assessing the drop sizes and distribution of liquid discharged from turbine stators have been presented. The numerical procedures suggested for predicting primary atomization drop sizes and the maximum diameter drop in the final distribution of drops impinging on turbine rotor blades have an apparent accuracy of $\pm$ 30 percent as compared to limited experimental information.

Two means of assessing the distribution of drops below the maximum drop diameter in the final distribution of drops impinging on the turbine rotor blades have been investigated.

The first of these methods which was of a semi-theoretical nature, when applied to the Yankee steam turbine low pressure end, yielded a calculated drop size distribution very different from those observed in an English steam turbine.

The second of the methods for assessing the distribution of drops in an empirical approach using an average of the observed distributions in the English steam turbine applied to a calculated maximum drop diameter. (Maximum Drop diameter Weber No. Criterion 13 for small turbines, 22 for large turbines as applied to stator wake trough conditions.) The second method is preferred although it can yield quite large inaccuracies in results with very small errors in determination of maximum drop diameter.

*The 0.6 of maximum diameter was picked by example and does not imply that only drops greater than this can cause erosion damage.

APPENDIX 2.7A

PRIMARY ATOMIZATION EXPRESSIONS

Mechanisms of primary atomization reported are: (1) stripping of masses of liquid or sheets from liquid puddles, (2) stripping or tip bursting of oscillating pendant drops attached to the stator trailing edge, and (3) eye-dropper-like tearing of individual drops on the convex surface of the stator by some mechanism, giving results similar to a drop of water on a hot stove.

Unfortunately, none of the referenced work gives quantitative information on the relative volumes of liquid involved in the observed processes. It seems reasonable that the tearing of masses or sheets of liquid from the stators involves a more important part of the total liquid available than the other observed mechanisms of detachment. The sheet atomization model is on this basis the logical tool for estimation of average primary drop sizes. As available information is insufficient for definitive conclusions, the pendant modes may be more important than assumed.

NOMENCLATURE PRIMARY ATOMIZATION

Symbol	Definition
a	Spray distribution constant
b	Spray distribution constant
B	Ligament diameter
C_f	Stator wall friction drag coefficient
d	Drop size
$\bar{d}$	An average drop size
g	Gravitational constant
H	Stator boundary layer form factor
$\dot{m}_L$	Mass flow rate per unit of stator edge length (lb/sec/ft)/g
n	Spray distribution constant
N	Number of drops
u	Gamma function parameter
U_s	Bulk steam velocity
V	Volume rate of spray formation
V_{tot}	Total volume rate of spray formation
X	Stator chord length
x	Gamma function parameter
z	Drop size
β	Drag coefficient
δ	Stator liquid film thickness
θ	Stator boundary layer form factor
λ	Wave length of ripples in liquid film
λ_B	Wave length of varicosities in ligaments
$\langle\bar{\lambda}\rangle$	Most probable wave length
ρ_L	Density of liquid
ρ_s	Density of vapor (bulk)
σ_L	Liquid surface tension
τ_s	Stator wall friction drag per unit area
μ_L	Liquid viscosity
μ_s	Vapor viscosity

SHEET ATOMIZATION

Based on actual turbine observations such as those reported by Hays [5], the flow of collected moisture over stator vane surfaces is far from uniform. The flow gathers in rivulets or puddles which feed separated atomization sites.

In an actual turbine, the location of the atomization points is probably influenced by surface and vapor flow irregularities. However, even with a perfectly uniform surface, a distribution of attachment points can be expected. Under such uniform surface conditions it is to be expected that the fluid would initially start to collect in the wake of the stator trailing edge as a roll of liquid with a cross-sectional diameter of approximately the width (W) of the trailing edge. As is well known, such a slender cylinder of liquid is unstable in the presence of surface tension forces and develops varicosities along its length. The pitch of these varicosities would then determine the atomization sites. The pitch (or length) of the varicosities would not be uniform but would have a distribution of pitches. Numerically as given by Green[10] after Rayleigh, the minimum pitch of a cylindrical instability is πW and the most probable pitch is 4.5 W. Other pitches than those, of course, have a statistical probability of existence[11].

If the distance between the atomization sites becomes fairly large, the local liquid flow rates at the site will be many times that of a uniformly distributed flow. This high local flow rate results in a thickening of the local liquid boundary layer and an opportunity for the development of sufficient liquid boundary layer momentum with ripples to give sheet type atomization rather than pendant atomization. This sheet type atomization is analogous to the stage 3-type of whirling cup atomization which takes place at high rates of liquid feed to cup or disc atomizers[10]. In this example of the whirling disc atomizer, the flow rate on a uniform basis is high enough to produce sheet atomization. Such sheet atomization could obviously also take place from wet turbine stators on a uniform or nearly uniform film basis if the liquid flow rate is high enough. In the case of the Yankee Atomic turbine low pressure end, sufficient collection of moisture on the ninth (and wettest) stator to produce uniform film sheet atomization does not seem likely. Sheet type atomization is probably a result of local flow rates greater than average.

Average Droplet Size from Sheet Atomization

Schematically, the process of sheet atomization is assumed to be as follows:

1) The liquid film of average depth (δ) flowing towards the stator trailing edge (as a result of air drag forces) develops ripples of wave length (λ).

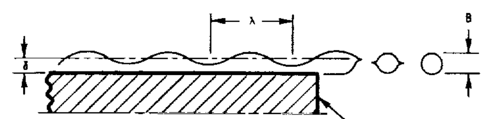

611131-60B

2) This rippled film is then blown from the trailing edge of the stator and collapses into ligaments of cross-sectional diameter B strung out parallel to the trailing edge. The cross-sectional area of the ligament is approximately equal to the product of the average film thickness times the ripple wave length or

$$B = \sqrt{\frac{4}{\pi} \delta \lambda} \qquad (1)$$

3) The ligament so formed in turn develops instabilities of wave length (λ_B) along its length and collapses into drops of diameter (d).

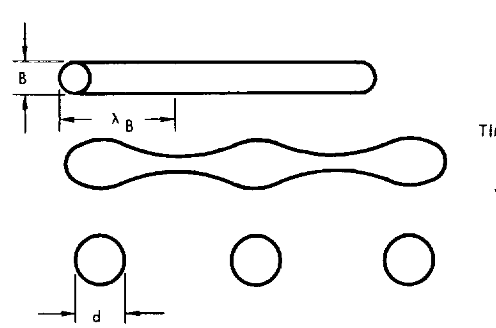

611131-61B

The volume of the drop being approximately equal to a cylindrical section of diameter B of length λ_B or:

$$\frac{\pi}{6} d^3 = \frac{\pi}{4} B^2 \lambda_B$$

$$d = (3/2 B^2 \lambda_B)^{1/3} \qquad (2)$$

As previously quoted from Green[10], the most probable value of λ_B is:

$$\lambda_B = 4.5\, B$$

$$d = \frac{3\, B}{\sqrt[3]{4}} \qquad (3)$$

Substituting for B from equation 1 into equation 3 gives:

$$d = 2.14 \sqrt{\delta \lambda} \qquad (4)$$

The average liquid boundary layer thickness at the trailing edge of turbine stators is given by*:

$$\delta = \left[\frac{2\, \dot{m}_L\, \mu_L}{\rho_L \left(\tau_s + \frac{\dot{m}_L}{X} U_s \right)} \right]^{1/2} \qquad (5)$$

$$\tau_s = \frac{C_f\, \rho_s}{2} U_s^2$$

$$C_f = (2)\ (.123)\ (10^{-.678\, H}) \left(\frac{U_s\, \theta\, \rho_s}{\mu_s} \right)^{-0.268}$$

*See Section 2.5

An analysis by Jefferys of wind-generated gravity waves has been developed by Mayer[12] to predict the most probable capillary wave length in a windblown sheet. Mayer's expression gives:

$$\bar{\lambda} = 9\pi \sqrt[3]{16} \left(\frac{\mu_L \sqrt{\sigma_L / \rho_L}}{\beta\, \rho_s\, U_s^2} \right) \qquad (6)$$

Considering the expression $\beta/2\ \rho_s\, U_s^2$ as the effective drag force per unit area of film, it may be written in terms of the boundary layer calculations (neglecting fog particle impact momentum) as:

$$\beta \rho_s U_s^2 = C_f\, \rho_s\, U_s^2 = 2\, \tau_s$$

or

$$\bar{\lambda} = 9\pi \sqrt[3]{16} \left(\frac{\mu_L \sqrt{\sigma_L / \rho_L}}{2\, \tau_s} \right)^{2/3} \qquad (7)$$

Substituting in equation 4 from equations 6 and 7 results in an expression for an "average" drop size:

$$\bar{d} = 17.0 \left(\frac{\dot{m}_L\, \mu_L}{\rho_L \left(\tau_s + \frac{\dot{m}_L U_s}{X} \right)} \right)^{1/4} \left(\frac{\mu_L}{\tau_s} \sqrt{\frac{\sigma_L}{\rho_L}} \right)^{1/3} \qquad (8)$$

In Figure 2.7A-1 "average" drop sizes from equation 8 are presented. It may be noted that the drop size predicted by equation 8 appears to become independent of flow rate at the higher values of flow rate examined. This suggests that a simplified expression such as equation 9 will be adequate for predicting the "average" drop size in many instances.

$$\bar{d} = 17.0 \left(\frac{\mu_L X}{\rho_L U_s} \right)^{1/4} \left(\frac{\mu_L}{\tau_s} \sqrt{\frac{\sigma_L}{\rho_L}} \right)^{1/3} \qquad (9)$$

Numerical evaluation of equation 9, inserting the same values for the independent variables, as used in evaluating equation 8 gives:

$\bar{d}$ = 630 microns.

Examining equation 9, it will be seen that the average drop size predicted varies slowly with most of the variables except U_s. Setting $\tau_s : : U_s^2$ gives the variation with respect to U_s as:

$$d : : U_s^{-.92}$$

Sheet Atomization Drop Size Distribution

There is a distribution of drop sizes resulting from sheet atomization (in fact from almost any atomization process). There is the distribution of sites (inflow rates) along the trailing edge, the distribution of atomization wave lengths (λ) in the direction of flow, and the distribution of cylindrical wave lengths (λB) producing the final primary drops. A distribution function could be developed from the Rayleigh[11] cylindrical instability function and the Jefferys-Mayer[12] capillary wave length function. However, an overall empirical distribution function due to Nukiyama-Tanasawa is easier to use:

$$\frac{dN}{dz} = a z^2 e^{-b z^n} \tag{10}$$

Quoting from Putnam[9], "Two Japanese investigators, S. Nukiyama and Y. Tanasawa, obtained extensive data on drop sizes in sprays by air atomization, and sought to correlate these data ---". Their investigations indicated that a value of 2 for the exponent of (z) effected a good correlation of the experimental data in every case, and that exponent (n) varied but little from unity.

While other investigators, including the writer, have found that the value of the exponent (n) may fall as low as 1/4, a numerical case can be made for the Yankee turbine to consider this exponent as having a value of unity. An exponent of the

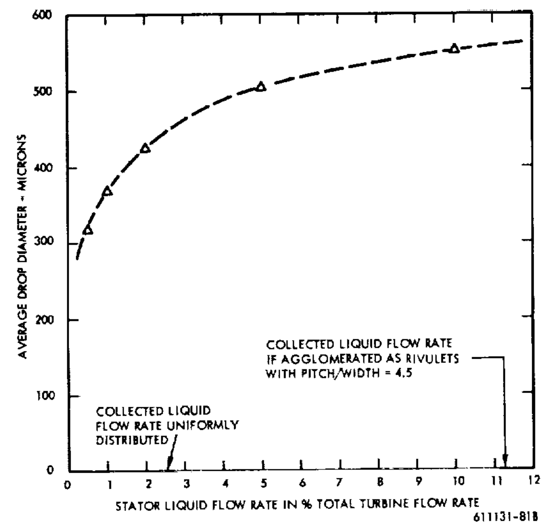

Figure 2.7A-1 Average Drop Size, Primary Atomization

order of unity is required to get a reasonable fit between an upper size limit on drops (order of 1500 to 2000 microns) resulting from the size of the trailing edge thickness and an unspecified kind of average drop size of the order of 500-600 microns.

Using n = 1 and writing equation 10 in terms of volume rather than number of drops gives:

$$\frac{dV}{dz} = \frac{\pi a}{6} z^5 e^{-bz} \tag{11}$$

This equation contains two undetermined constants, (a) and (b). Constant (a) may be determined from the total volume of the spray using the continuity relationship once constant (b) has been found. In connection with constant (b), it may be observed that if a value of the "average" drop size corresponding to the most probable flow rate of figure 2.7A-1 is selected, the rate of change of volume of spray produced is a maximum with respect to this average drop size (z_{av}) or,

$$\frac{dV}{dz} = \left(\frac{dV}{dz}\right)_{max.}$$

and

$$\frac{d^2V}{dz^2} = 0 = \frac{\pi a}{6} \left(e^{-bz}\right) z^4 (5 - zb)$$

or

$$b = 5/z_m$$

where

$$z_m \text{ is } z_{av} \text{ at } \left(\frac{dV}{dz}\right)_{max.} \qquad (12)$$

Substituting from equation 12 in equation 11 gives:

$$\frac{dV}{dz} = \frac{\pi a}{6} \quad z^5 e^{-5} \quad \frac{z}{z_m} \qquad (12a)$$

If the substitution, $x = 5\, z/z_m$ is made in equation 12a, it becomes:

$$dV = \frac{\pi a}{6} \left(\frac{z_m}{5}\right)^6 x^5 e^{-x} dx \qquad (13)$$

$$V_x = \frac{\pi a}{6} \left(\frac{z_m}{5}\right)^6 \int_0^x x^5 e^{-x} dx = \frac{\pi a}{6} \left(\frac{z_m}{5}\right)^6 \Gamma_x$$

$$\frac{V_x}{V_{tot}} = I(u, 5)$$

$$u = x/\sqrt{6} = \frac{5\, z}{z_m \sqrt{6}} \qquad (13a)$$

and I (u,5) is a form of the incomplete gamma function, as tabulated in Reference 3. The ratio of cumulative liquid volume to total liquid volume of spray is given as a function of drop size in table 2.7A-1 for the ninth stator of the Yankee turbine.

A small amount of data on stator primary atomization, obtained from the British CEGB, has been reported by Hays[5]. This information is reproduced in table 2.7A-2 for conditions which more or less bracket the conditions at the ninth stator of the Yankee Turbine. This data cannot be said to confirm the model of primary atomization used here because of the low number of drops sampled. A comparison between tables 2.7A-1 and 2.7A-2 is encouraging, however.

TABLE 2.7A-1

SPRAY LIQUID VOLUME DISTRIBUTION VERSUS DROP SIZE

Drop Size (z) (microns)	V_z/V_{tot}
100	0.0004
175	0.007
250	0.0356
350	0.12
525 = z_m	0.38
750	0.72
1050	0.93
1575	0.997

TABLE 2.7A-2

DATA ON STATOR PRIMARY ATOMIZATION

Static Pressure (psia)	Bulk Steam Velocity (ft/sec)	No. of Drops	Max. Size (microns)	Min. Size (microns)
1.61	976	5	1080	460
1.72	1180	4	620	360

APPENDIX 2.7B

ANALYSIS OF CONTRACT NAS 7-391 RESULTS *

A series of erosion-related experiments have been performed by the Rocketdyne Division of North American Rockwell, sponsored by NAS 7-391. These experiments employ a series of stator blade shapes and test conditions designed to simulate space turbine environments. The working fluid used is steam. A particular objective of the program is to observe the detachment of collected liquid from trailing edge surfaces and to estimate the ultimate limiting size of atomized drops as a function of the various test conditions.

A drop transport analysis has been completed on a series of eleven tests performed by Rocketdyne. The analysis was performed with the ADROP computer code (Section 2.6). Blade shape I-A ** was chosen for these studies. This blade is similar to that used in the last stage of the General Electric three-stage potassium test turbine, differing only in the pitch. Rocketdyne is using a stator block containing six different blade shapes and apparently could not exactly reproduce the pitch of the G. E. blades in this configuration. The mean line pitch of the Rocketdyne blade I-A is a 0.616 inch while the pitch of the G. E. blade is 0.641 inch.

The test conditions employed in this study are presented in Table 2.7B-1[1]. The tip section of the blade shape used is shown in Figure 2.7B-1. The blade surface velocities in the stator flow passage were evaluated using the two-dimensional flow analysis code of Reference(13). Figure 2.7B-2 summarizes the surface velocity results. The velocities are normalized by the exit free stream velocity. These velocities are plotted against normalized surface position, which is the ratio of the distance from the blade leading edge taken along the surface to the total surface length.

*T. C. Varljen, Supervisor, Systems and Technology, Astronuclear Laboratory, Westinghouse Electric Corporation, Pittsburgh, Pa., 15236

**Rocketdyne Dwg. N-01828-A

The surface velocities obtained for the tip section were then used to evaluate the boundary layer properties at the blade trailing edge. The properties of interest are the momentum thicknesses (Θs and Θp), the displacement thicknesses (δ_s^* and δ_p^*), and the full thicknesses (δ_s and δ_p) on both the suction and pressure sides of the blade. These are summarized in Table 2.7B-2.

Trajectory calculations were performed for a series of drop sizes ranging downward from the thickness of the stator trailing edge (190 microns). An axial distance of one inch was arbitrarily chosen between the stator exit plane and the inlet plane of a hypothetical rotor row. This distance is sufficient to observe secondary atomization effects. Figure 2.7B-3 shows the variation of the maximum Weber Number observed with drop diameter for the eleven test conditions chosen. These were obtained from trajectories along the streamline coinciding with the stator wake axis. Note that these maxima occur at different locations downstream of the trailing edge; in no case did the maximum Weber Number occur at the start of the trajectory.

The WANL turbine blade erosion model has tentatively employed fixed Weber Number criteria to predict the onset of secondary atomization. These are obtained from Gardner's work (6) which indicates that, in steam systems, the critical Weber Number is about 22 when drops are slowly accelerated and is about 13 when the acceleration is abrupt. Results obtained by Rocketdyne[1] in the tests examined are shown in Figure 2.7B-3. In each case the limiting drop size observed has been plotted. It is evident that a disruption criteria based on Weber Number alone, is inappropriate. The use of a fixed critical Weber Number may perhaps be justified for very rough estimates or for qualitative descriptions, but it lacks the precision required in detailed erosion studies.

TABLE 2.7B-1

ROCKETDYNE TEST CONDITIONS USED IN THE STUDY

Blade Shape	Test Series No.	Test Conditions: Inlet Pressure, psia 10	15	20	23	Outlet Pressure, psia 3	7	10	Inlet Quality, Percent	Steam Flow, lb/sec	Pressure at 2nd Stage Inlet, psia	2nd Stage Spouting Velocity, ft/sec
	114A	X				X			99.5	.119	4.5	1170
	B	X					X		99.5		7.8	540
	C		X					X	99.6	.175	10.8	525
	D		X				X		99.6		8.5	780
	F		X			X			99.4		6.0	1450
1	113G			X		X			98.6	.233	7.4	1680
	H			X			X		99.3		9.4	960
	I			X				X	99.4		11.5	660
	J				X			X	99.3	.270	11.8	800
	K				X		X		99.4		9.8	1150
	L				X	X			99.4		8.2	1875

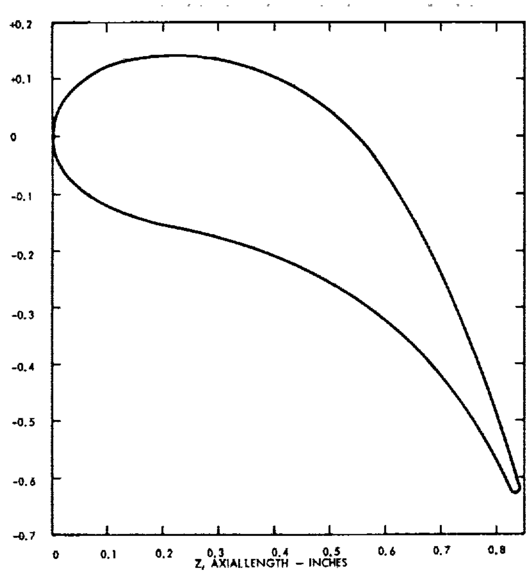

Figure 2.7B-1 Profile of Stator Blade 1-A

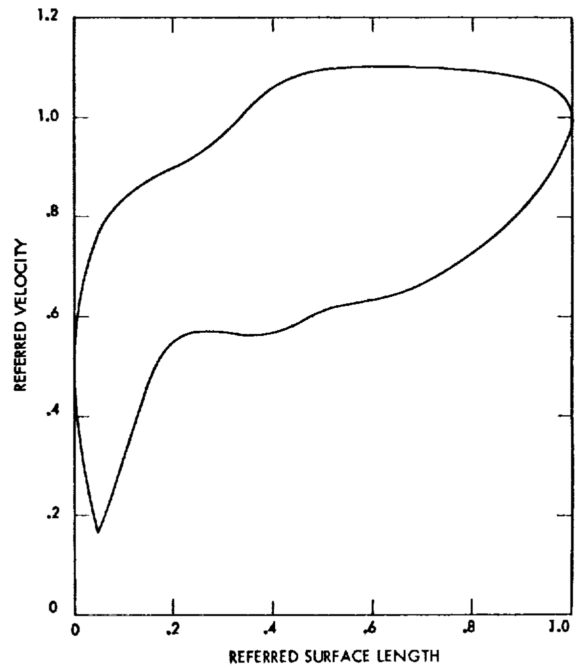

Figure 2.7B-2 Surface Velocities Computed for the Top Section of Rocketdyne Blade Shape 1-A

TABLE 2.7B-2

TRAILING EDGE BOUNDARY LAYER DATA OBTAINED FOR THE ROCKETDYNE TEST SERIES

Test	U_o (ft/sec)	P_{exit} (psia)	T (°R)	X (%)	θ_s (cm)	θ_p (cm)	δ_s^* (cm)	δ_p^* (cm)	δ_s (cm)	δ_p (cm)	D_{LIM} (Microns) $We_c=13$	$We_c=22$
114A	1170	3	601.50	98.6	.01067	.00359	.01858	.00474	.06868	.03448	92	147
114B	540	7	636.85	96.3	.01073	.00362	.01874	.00477	.06896	.03463	187	295
114C	525	10	653.21	98.8	.01021	.00344	.01746	.00452	.06664	.03335	155	245
114D	780	7	636.85	97.7	.01000	.00337	.01697	.00442	.06568	.03283	102	161
114F	1450	3	601.50	94.8	.01014	.00342	.01729	.00448	.06632	.03318	62	99
113G	1680	3	601.50	93.3	.00981	.00331	.01654	.00433	.06480	.03237	48	76
113H	960	7	636.85	96.7	.00957	.00323	.01601	.00421	.06363	.03177	71	112
113I	660	10	653.21	97.9	.00973	.00328	.01636	.00429	.06441	.03217	105	166
113J	800	10	653.21	97.6	.00936	.00315	.01556	.00411	.06259	.03124	76	120
113K	1150	7	636.85	95.1	.00920	.00310	.01521	.00403	.06181	.03084	52	82
113L	1875	3	601.50	93.2	.00960	.00323	.01607	.00422	.06376	.03184	39.5	63

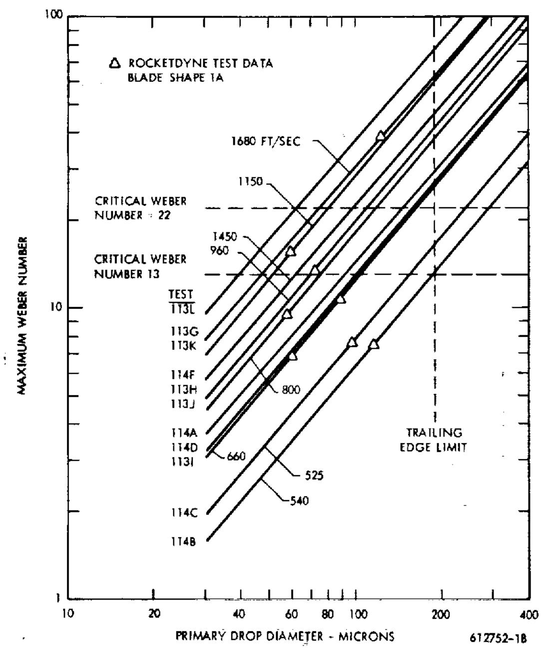

Figure 2.7B-3 Predicted Variation of Maximum Primary Drop Weber Numbers for the Rocketdyne Test Series with Blade Shape 1-A

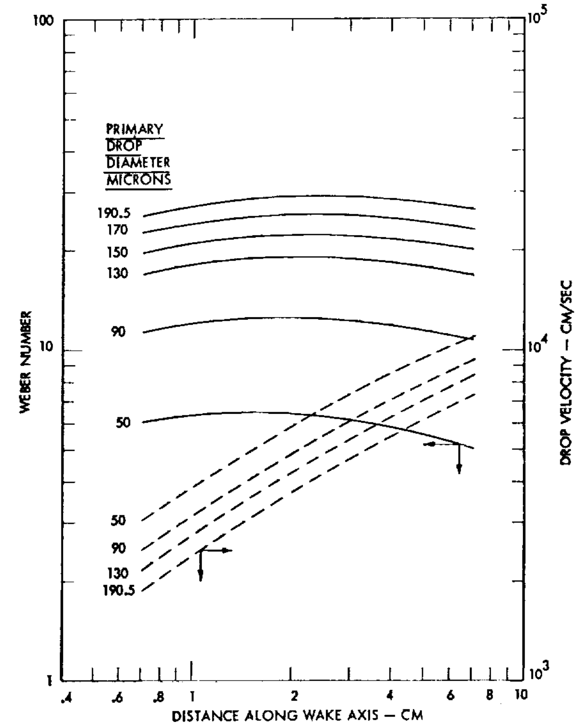

Figure 2.7B-4 Variation of Drop Weber Number and Velocity with Distance along the Wake Axis Predicted for Rocketdyne Test 114A

Trajectory results are presented in more detail in Figures 2.7B-4 (Test 114A), 2.7B-5 (Test 114 B), 2.7B-6 (Test 114 F) and 2.7B-7 (Test 113L). These show the variation of drop velocity and Weber Number with total distance downstream of the stator trailing edge and along the wake axis streamline. In all cases a "dead-band" of four trailing edge thicknesses has been used to cover uncertainties in the local wake velocity in this region.

A brief examination was also made of trajectories associated with the hub section of blade 1-A. The small difference in pitch between the two sections made very little difference in the Weber Number and velocity result.

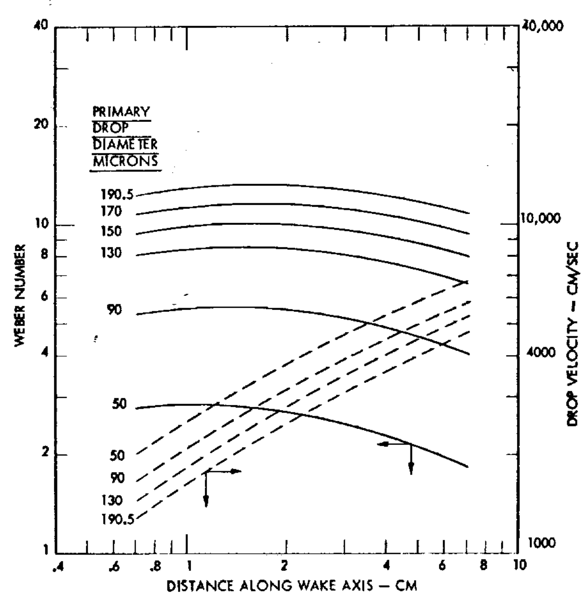

Figure 2.7B-5 Variation of Drop Weber Number and Velocity with Distance along the Wake Axis Predicted for Rocketdyne Test 114B

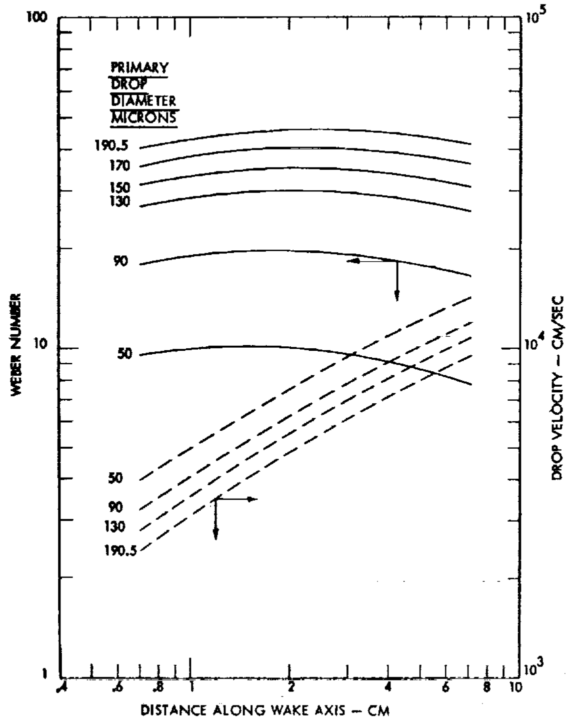

Figure 2.7B-6 Variation of Drop Weber Number and Velocity with Distance along the Wake Axis Predicted for Rocketdyne Test 114F

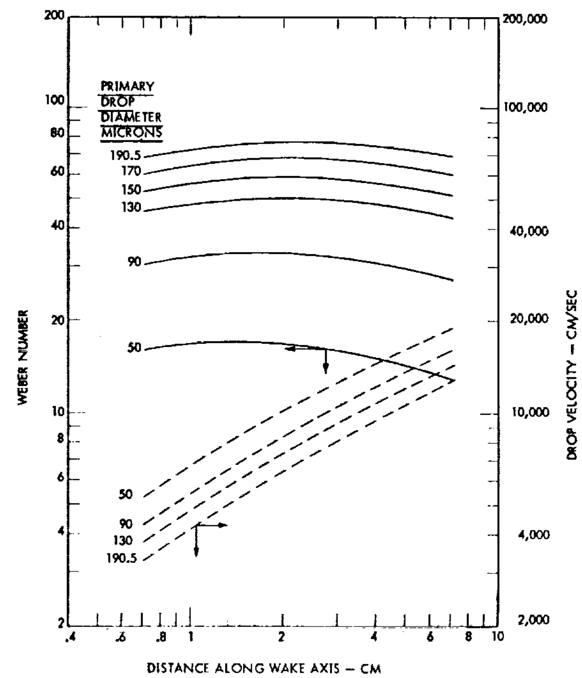

Figure 2.7B-7 Variation of Drop Weber Number and Velocity with Distance along the Wake Axis Predicted for Rocketdyne Test 113L

APPENDIX 2.7C

REFERENCES

1. Spies, R., J. R. Baughman, and J.E.T. Blake, "Investigation of Variables in Turbine Erosion, Influence of Aerodynamic and Geometric Parameters," Rocketdyne Division of North American Rockwell Corporation Report R-7650, December 1968, NASA Contract NAS7-391.

2. Christie, D. G., and G. W. Hayward, "Observation of Events Leading to the Formation of Water Drops which Cause Turbine Blade Erosion," Phil. Trans. Roy. Soc. London, Series A, No. 1110, Vol. 260, pg 183-192, 28 July 1966.

3. Pearson, Karl, ed., "Tables of the Incomplete -Function," Cambridge University Press, 1957.

4. Degner, V. R., Quarterly Status Letter No. 3, Contract NAS 7-391, "Investigation of Variables in Turbine Erosion," North American Aviation Inc., Rocketdyne Division Report 66RC5335.

5. Hays, L. G., "Turbine Erosion Research in Great Britain," NASA, Jet Propulsion Laboratory, Cal. Inst. Tech., Tech. Memo No. 33-271.

6. Gardner, G. C., "Events Leading to Erosion in Steam Turbines," Proc. Inst. Mech. Engrs. Vol. 178, Part 1: No. 23, pg. 593 to 623, 1963-1964.

7. Smith, A., R. P. Kent, and R.L. Armstrong, "Erosion of Steam Turbine Blade Shield Materials," ASTM Special Technical Publication No. 408, March 1967.

8. Wolfe, H. E. and W. H. Anderson, "Kinetics, Mechanism and Resultant Droplet Sizes of the Aerodynamic Breakup of Liquids," Aerojet-General Corp. Report 0395-04-185P, April, 1964.

9. Putnam, A. A. et al, "Injection and Combustion of Liquid Fuels," Battelle Memorial Institute, WADC Technical Report 56-344, May 1957.

10. Green, H. L., "Atomization of Liquids," In Hermans - Chapter VII, Interscience Publishers, Inc., New York, 1953.

11. Strutt, J. W. (Baron Rayleigh), "The Theory of Sound," p. 361, Dover Publ., New York, N. Y., 1945.

12. Mayer, E., "Theory of Liquid Atomization in High Velocity Gas Streams," ARS Jour. p. 1783 to 1785, December 1961.

13. Katsanis, T., "A Computer Program for Calculating Velocities and Streamlines for Two-Dimensional, Incompressible Flow in Axial Blade Rows," NASA TND-3762, January 1967.

Section-3

FOREWORD TO SECTION 3

Thanks are due to Messrs. E. A. Eaton and D. Pearson of the British Central Electricity Generating Board (CEGB) for not only personal discussions but also the reference use of a number of CEGB Marchwood Engineering Laboratories reports which have been of paramount value to this study. Acknowledgements are also due to R. I. Shrager and L. B. Godio, who collaborated on the mathematical formulations and computer programs involved in section 3.2 of this report.

ABSTRACT

This report volume is concerned with those processes of the WANL turbine blade erosion model shown on this page that can directly cause the loss of metal from turbine blqdes: mechanical removal by drop impingement and dissolution into impinged liquid.

The literature on impingement erosion is examined with a view to deducing empiric, or analytic, relationships between erosion rate and the various external variables such as impact velocity, angle of impingement, size of impacting drops, impacting fluid properties, strength of materials, and rate-time variation.

In Section 3.1 the difficulties inherent in the interpretation of erosion test data are discussed and a rationalized approach is described.

One of the major difficulties in the correlation of test data is the variation of erosion rate during a test. In Section 3.2 an analytic model is proposed to explain the variation.

Sections 3.1 and 3.2 are mainly concerned with the mechanical aspects of erosion of metals by the impingement of liquid drops as influenced by external conditions such as impact velocity, etc. Sections 3.1 and 3.2 are not directly concerned with the erosion resistance of specific materials - except in passing - with the relationship between erosion resistance and other material properties.

Sections 3.3 and 3.4, on the other hand, attempt to use the observations of Sections 3.1 and 3.2, plus added information relevant to metal dissolution by liquid metals, to establish specific numerical relationships of erosion resistance of metals in terms of external variables and properties of materials. Section 3.3 deals with the mechanical aspects of metal loss through drop impingement, assuming no chemical interaction. Section 3.4 deals with the chemical aspect of metal loss by dissolution of the metal into the liquid of impinged drops, assuming that there is no mechanical interaction.

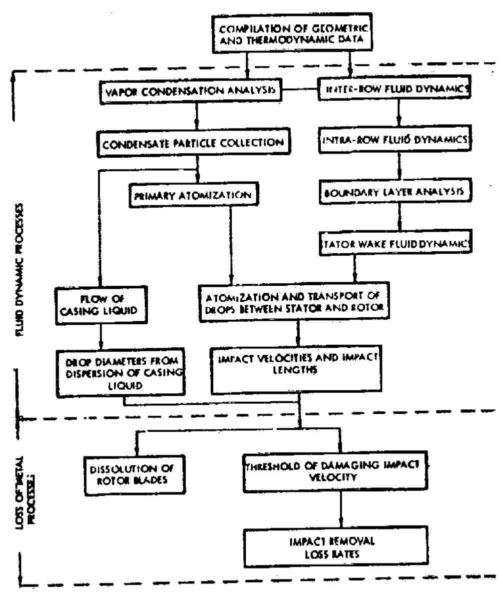

WANL Turbine Blade Erosion Model

SECTION 3

TURBINE BLADE EROSION MODEL

3.1 SURVEY OF CLUES TO THE RELATIONSHIPS BETWEEN EROSION RATE AND IMPINGEMENT CONDITIONS*

3.1.1 General Considerations Relating to the Interpretation and Correlation of Test Data

3.1.1.1 Independent Variables

The purpose of this section is to determine whether the impingement erosion test data in the literature can be made to yield generalized relationships, by which erosion can be predicted under arbitrary operating conditions. If the erosion could be expressed in terms of an empirical or semi-empirical equation, it would be a function of the operating variables and would contain constants which are properties of the materials of the target and of the impinging liquid.

The independent variables, or operating conditions, are as follows:

a) Area of target subjected to impingement
b) Shape of target
c) Size of impinging liquid drops or slugs
d) Shape of impinging liquid drops or slugs
e) Rate of impingement of liquid on target
f) Impact velocity between liquid and target
g) Angle of impact between liquid and target surface
h) Physical properties of liquid such as:
   1) density,
   2) viscosity,
   3) compressibility, or acoustic velocity.
i) Physical properties of target. While the significant properties are still unknown, the following may be listed as possibilities:
   1) hardness or other strength property
   2) strain energy to rupture or other energy property
   3) elongation or other ductility property
   4) endurance limit and fatigue S-N relationship
   5) elasticity or acoustic velocity.
j) Surface conditions of target, such as:
   1) roughness
   2) work hardening or other surface effects due to previous preparation or erosion
   3) presence of surface films of liquid.
k) Microstructure and orientation of surface layers.

In this section of the report, primary emphasis is given to the velocity and the angle of impact, and the size and shape of impacting drops. Section 3.2 includes some discussions of the fatigue properties and surface conditions of the target.

3.1.1.2 Dependent Variables

One of the greatest difficulties in the interpretation and correlation of erosion test data lies not in the multiplicity of the independent variables but in the identification of the dependent variable or variables, referred to as "the erosion". An approach must be found to characterize the erosion. Figure 3.1 (A) represents a typical weight loss versus time curve. (The axes are deliberately labeled erosion and duration since these quantities will be discussed more fully later.) This curve is characteristic of much of the data found in the literature; the various stages of the curve and possible explanations for them are discussed in Section 3.2 of this report.

* F. J. Heymann, Senior Engineer, Development Engineering Department, Westinghouse Steam Divisions, Westinghouse Electric Corp., Lester, Pa.

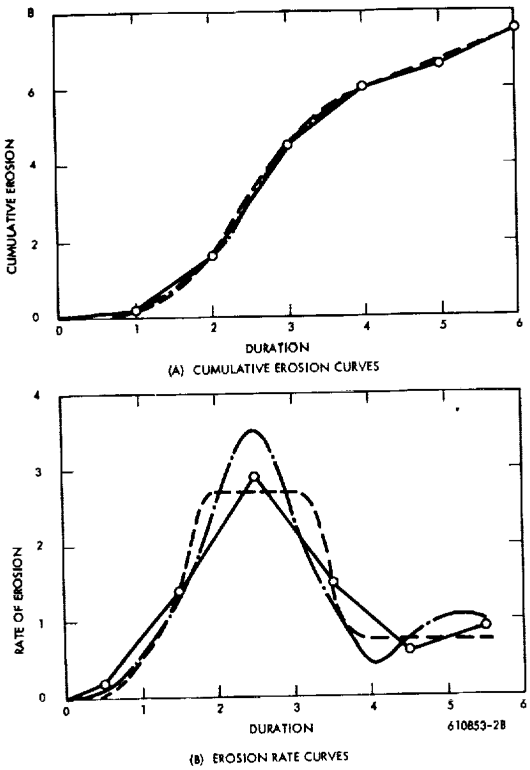

Figure 3.1-1 Various Interpretations of Same Hypothetical Erosion Data Points

A relatively well defined experimental plot is subject to a variety of interpretations. The circles in Figure 3.1 (A) represent hypothetical row data points. A conservative method of drawing the curve is to joint the experimental points by straight lines, as shown. Reference 1,* for instance, shows curves in this form. An erosion rate curve can then be constructed by plotting the slopes of these line segments versus the time corresponding to their mid-points. This is shown by the circles and solid lines in Figure 3.1-1 (B). Reference 2 presents its data in this form. This approach requires no decisions, but is not accurate unless the data points are close together.

* References cited are listed in a later section.

To draw in a smoothed curve, a decision must be made as to how smooth this curve should be. If the erosion rate rises from zero during an incubation period to a constant maximum value, and subsequently declines to a secondary constant value, a curve will be drawn such as the dashed one in Figure 3.1-1 (A), whose counterpart in Figure 3.1-1 (B) is also shown dashed. If the erosion rate reaches a rather steep peak value and then goes into a series of fluctuations, then the dash-dotted lines in Figures 3.1-1 (A) and (B) may result. This does not exhaust the possible variations, but serves to show how this decision can have a considerable effect on the shape of the erosion curve presented, particularly if data are presented in the form of erosion rate curves. (Graphical differentiation of empirical data with all its uncertainties is notoriously unreliable.)

The decision concerning what the erosion curves should be is closely related to the question of just how these curves should be quantitatively characterized, i.e., just what are the dependent variables that should correlate with the operating conditions. The objective of this empirical approach is to predict the amount of erosion expected after a given time, or at least the time required to reach some critical degree of erosion.

The parallel study reported in Section 3.2 concerns the possibility of predicting the form of the erosion versus time curve analytically, on the basis of assumed material removal mechanisms. This has not yet advanced to the stage where it can be of help in the present study. Therefore, the view adopted is the most widely held and is practical enough for present purposes. Namely, the first stage in erosion shows little or no weight loss and represents plastic deformation of the surface and initiation of fatigue cracks. This stage merges into the second stage wherein the rate of weight loss is at a maximum and approximately uniform over a period of time. This, in turn, merges into a later stage or stages wherein the erosion rate diminishes and may or may not tend toward another uniform value. Whatever the precise cause or causes of this decrease in erosion rate may be, it is usually associated with rather general and severe damage to the surface, which through geometrical effects alone may result in an effective alteration of the impingement conditions. Thus, the best parameters to describe the progress of erosion in a relatively simple and yet significant manner are:

a) A quantity representative of the duration of the initial (incubation) stage, denoted by T_o in Figure 3.1-2.

b) A quantity representative of the rate of erosion during the second stage, denoted by R in Figure 3.1-2. This is the most significant quantity, and most of the following sections deal with it.

c) Of additional interest would be some quantity representative of the degree of damage at the end of the second stage. This would help to establish whether this transition is really a geometric effect, and whether the first two stages do really cover the permissible degree of erosion in a practical application. However, very little information on this is available.

There are test data to which the foregoing generalizations and conclusions do not seem to apply, but for most of the usable data they do seem valid, and our correlation attempts are based on this type of curve. Eventually, however, the deviations from this type of curve must also be understood and accounted for. It is important to remember that more than one mechanism of material removal may be active. The above-described behavior applies to those conditions under which a fatigue mechanism predominates. This is valid for most of the material and impact velocity combinations for which test data are available and probably to most turbine operating conditions. If, however, impact velocities are increased, then material removal due to individual impacts will also occur. At sufficiently high speeds the rate of material removal by this process may be sufficiently high so that there is not enough time for fatigue failures to occur. The shape of the erosion-time curve, the significant dependent quantities, and their functional relationships to such independent variables as drop size and impact velocity can all be expected to change during this transition from one predominant mechanism to another. Test data at relatively high velocities (around 2000 ft/sec) are being generated but are not yet available. Steam turbine blades will soon be operating in this velocity range also.

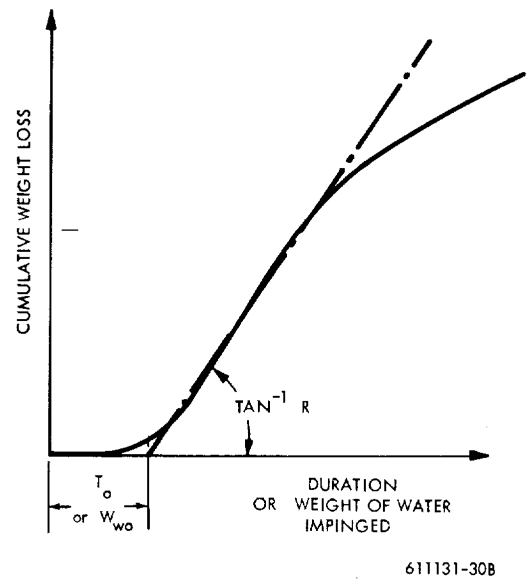

Figure 3.1-2 Definition of Incubation Period, T_o, and "Steady-State" Erosion Rate, R

3.1.1.3 Correlation Problems

Returning now to an assumed characteristic curve, another difficulty will be demonstrated. Figure 3.1-3 shows three hypothetical but typical erosion-time curves from a given test series. Curves A, B, and C might have been obtained for three different materials under the same operating conditions, or for the same material at three different impact velocities or with three different drop or jet sizes. One may then try to compare these curves, or to determine from each, a number that represents the erosion to be correlated with material properties or with operating parameters. With insufficient thought given to the problem, the temptation might be to select a convenient point in time (say T = 3 on Figure 3.1-3) and compare either the cumulative erosion, or with more sophistication, the slope of the erosion-time curve at that point. This has been done by many authors. It should be evident from the earlier discussions, however, that

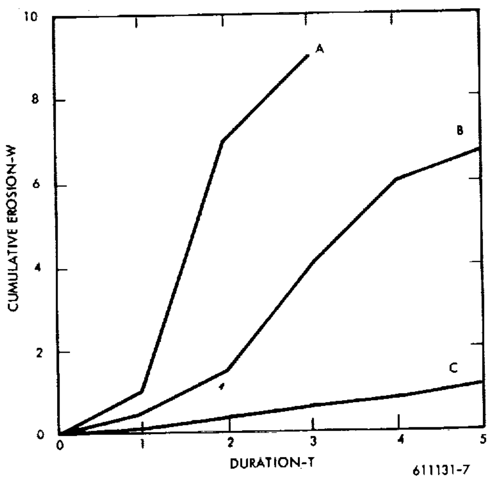

Figure 3.1-3 Hypothetical Erosion Curves

this procedure is entirely invalid. It can result in spurious comparisons between erosion rates corresponding to completely different stages of the erosion process. Thus, in Figure 3.1-3 at time T = 3, Curve B is in the probably significant second stage; Curve A has already broken and is into the third stage; Curve C may well still be in the incubation period.

For a valid comparison there are two desiderata. At least one, preferably both should be fulfilled. They are:

a) The measured slopes, or erosion rates, should be, as nearly as possible, average or effective values representative of the second stages of the erosion-time curves.

b) The measured slopes should be, as nearly as possible, the averages or effective values over the same range of cumulative erosion, i.e., associated with the same degree of damage done to the surface.

The first desideratum can be fulfilled only if the end of the second stage is clearly seen; if the test duration is not long enough for this to occur, then the second rule must suffice, and one must endeavor to choose the erosion interval over which the slope is measured in such a way that the first stage, or incubation period is excluded. In Figure 3.1-3, this is simply not possible for Curve C; when one examines the available test data, the choice is often reduced to one between doubtful comparisons or no comparisons at all.

3.1.1.4 Rationalized Parameters

It was pointed out earlier that the axes in Figure 3.1-1 have been labeled vaguely as erosion and duration. Direct comparison between different test data is often complicated by the fact that the erosion may be given in terms of weight loss, or volume loss, and the duration in terms of time, or number of impacts (for wheel-and-jet apparatus), or in other ways. The target areas involved and the quantity of water impinging on it will differ not merely between different test series, but may also vary within a given test series as a consequence of varying one of the other independent parameters. Thus, for instance, if in a wheel-and-jet apparatus the jet diameter is changed, this will effectively alter the area of the target subjected to impact and the quantity of water involved in each impact, and if the impact velocity is changed by changing the speed of rotation this also alters the weight of water impacting per unit time.

To permit valid comparisons and correlations, it is essential to express the erosion and the duration in a rationalized form which will compensate for these test variations.

Since the undesirable aspect of erosion is the loss of volume and the change of geometry - and this change of geometry in turn affects the rate of erosion - volume loss rather than weight loss should be considered. The rationalized erosion parameter is volume loss per unit area, sometimes referred to in the literature as mean depth of penetration (MDP).

The appropriate rationalized duration parameter is not quite so obvious. One could make a case for selecting the number of impacts per unit area. At present, however, preference is given to the volume of liquid impinged per unit area. This is attractive because results expressed in this way will show directly the effect of subdividing a given quantity of impinging liquid into particles of different sizes or shapes, and because it makes the rationalized erosion rate (E) a non-dimensional quantity, as follows:

$$E = \frac{\text{Volume of material lost per unit area per time}}{\text{Volume of liquid impinged per unit area per unit time}}$$

The rationalized incubation time parameter corresponding to the above is the cumulative volume of liquid impinged per unit area at time T_o as defined by Figure 3.1-2.

For some correlations, where neither the target material nor the impinging liquid is changed, the rationalized erosion rate can be satisfactorily represented in terms of weight of material lost and weight of water impinged.

3.1.2 Dependence on Impingement Angle

Only recently have investigators shown serious concern with the impingement angle. The consensus appears to be that the normal component of the impingement velocity is primarily responsible for the damage, with the tangential component playing a secondary role.

Thus, according to Fyall and King[3,4] for initially smooth surfaces the normal impact velocity can be used successfully for correlations valid during the initiation and earlier stages of erosion, but that when the surface has been roughened by erosion, the tangential component also becomes significant because the true local impact angles can become more normal to the absolute velocity. No quantitative estimate is made for the latter effect.

Langbein and Hoff[5,6] state that the normal component governs the erosion; they show loci of equal average erosion rates plotted on a field of absolute velocity versus inclination angle and state that these correspond to loci of constant normal velocity component ($V_n = V \cos \theta$).

Pearson[7,8] has proposed the following correlation equation to represent the erosion rate E in terms of the impingement velocity V, and inclination angle θ measured from the normal direction (expressed in our terminology):

$$E = K \; (V \cos \theta - V_c)^n / \cos \theta \qquad (1)$$

in which K, V_c, and n are to be regarded as constants of the target material. (Actually, at least some of these constants must also be functions of the impinging liquid properties, drop sizes, etc.)

Pearson justifies introducing the 1/cos θ term by presenting the data reproduced here as Figures 3.1-4 and 3.1-5. (These are direct copies of Pearson's figures except that our terminology has been submitted and his curves, drawn through the points, have been omitted.) It appears that E cos θ (Figure 3.1-4) correlates somewhat better with V cos θ than does simply E with V cos θ. This improvement is hardly dramatic, however, and the 1/cos θ correction should be regarded as tentative and subject to analytical or further experimental verification.

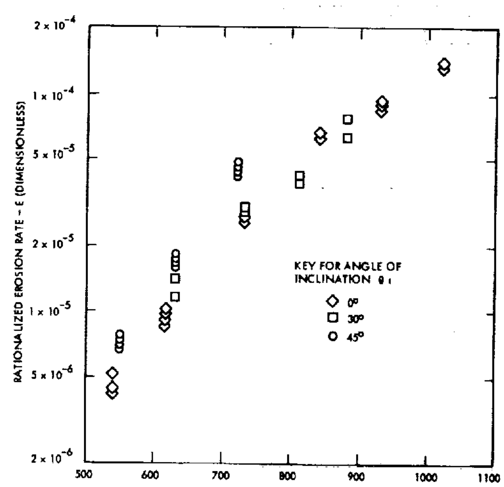

Figure 3.1-4 Rationalized Erosion Rate Versus Normal Impact Velocity

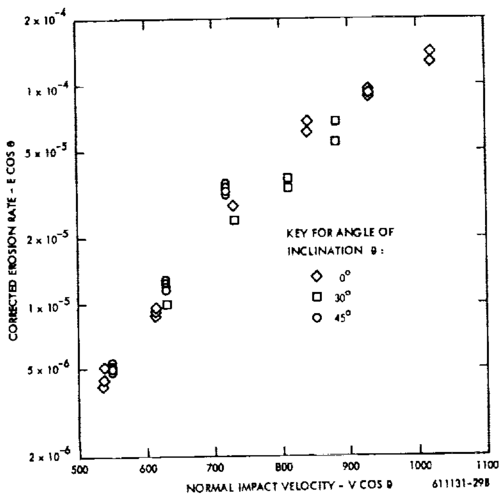

Figure 3.1-5 Corrected Erosion Rate (E cos θ) versus Normal Impact Velocity (From Figure 5 of Reference 11)

For 12 percent chromium stainless steel, Pearson obtains values of approximately 400 ft/sec for V_c, and n = 2.6 for use in Equation 1. Ratios of erosion rate at angle θ to that at normal incidence (E_θ/E_o), based on this relationship, have been plotted in Figure 3.1-6 for three different velocities. Some independent support for this formulation may be provided by data points also shown in Figure 3.1-6, which were deduced from erosion-time curves given by Busch and Hoff[9]; these were obtained in a supersonic rain erosion facility, with target cones of different angles, but of the same base diameter. The material was pure aluminum; the absolute impact velocity was Mach 1.2, or approximately 1320 ft/sec.

In this situation the area exposed to erosion changes with the angle, but the total amount of impinging water remains the same. Thus, no area correction is necessary if the slopes of the erosion-time curves are compared; on the other hand, it is necessary for a rational comparison of incubation times.

Note that the erosion rate at θ = 10 degrees is actually somewhat higher than that at θ = 0 degrees; if this is actually so, it would support an observation by Brunton[10] that the damage in single-impact tests could be greater at slight angles of inclination than with normal impact. (Note that at 1300 ft/sec on aluminum, single-impact damage occurs.) On the other hand, this may be an apparent effect only, and due to scatter or some other experimental variable. The curves in Reference 9 do not show actual data points.

The critical velocity V_c for aluminum would certainly be far lower than that for 13 percent chrome steel - perhaps on the order of 100 ft/sec. If one computes E_θ/E_o from Pearson's equation with V = 1300 ft/sec and V_c = 100 ft/sec, n remaining 2.6, one obtains Curve E, which fits the data points reasonably well. Is this a confirmation of Pearson's equation, or is it merely fortuitous? The former can be true only if the assumptions of V_c = 100 ft/sec and n = 2.6 are indeed correct. (Differences in the values of K cancel out.)

In a previous progress report,[11] it was suggested that the data of Reference 9 could also be represented by the simple relationship $E_\theta/E_o = \cos^2\theta$, which is shown as Curve A in Figure 3.1-6. This simple angle-dependence does not fit any of Pearson's results presented in Figures 3.1-4 and 3.1-5, and should be rejected.

The physical meaning of Pearson's equation is: erosion is, in the first instance, a function of the normal component of the impact velocity, and additional erosion due to a tangential component is accounted for by the 1/cos θ multiplier. Such a relation could not have been deduced from the data of Reference 9 alone, since the absolute velocity was held constant and the normal velocity component varied. Thus, there was no way of knowing whether the change in erosion with the angle was to be

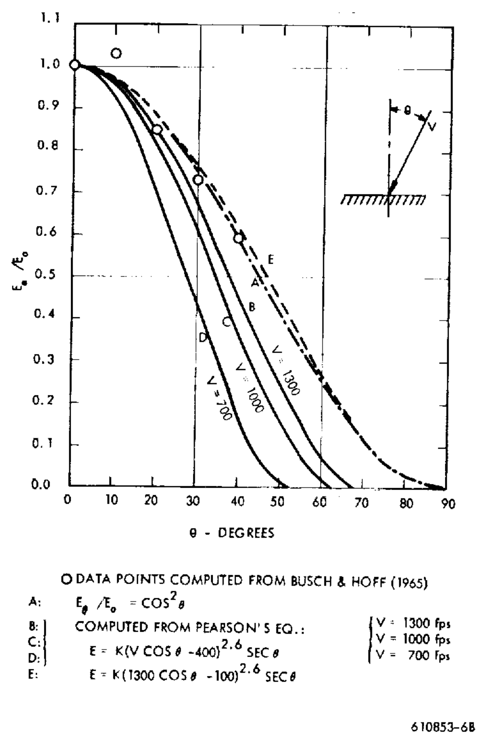

Figure 3.1-6 Comparison of Erosion versus Angle Curves

attributed to a function of the angle alone or to a combination of the changes in the angle and the normal velocity. A reliable formulation for the angle effect can be obtained only if a reliable formulation for the velocity effect is simultaneously determined, i.e., from test programs in which velocities and angles are varied independently. This is what Pearson has tried. Pending further testing of the generality of his equation, it is the best information available.

One set of data somewhat at variance with the foregoing was reported by Bradenberger and DeHaller[1]. They tested one material in a relatively low-speed, wheel-and-jet apparatus at various combinations of specimen velocity (u) and jet velocity (v). The jet velocity in a wheel-and-jet apparatus is in a direction perpendicular to the specimen velocity and the absolute impact velocity is given by $w = \sqrt{u^2 + v^2}$. If the specimen were round as in a number of similar investigations, then w would also be the effective normal impact velocity. In this case, however, the specimens were rectangular and thus the velocity w is inclined at an angle, $\theta = \tan^{-1}(v/u)$, from the normal to the specimen surface. For a given value of u, a wide variance of results was obtained for different values of v. The authors claimed that these differences were far too great to be accounted for by the resulting differences in the absolute velocity w.

They speculated that cavitation may have been induced by the flow geometry but rejected this as a likely explanation because the location of the maximum damage was not consistent with this. They finally concluded that the tangential velocity, v, had some pronounced independent effect, not presently explainable, on the erosion measured. This conclusion has been introduced at some length because it has been quoted by subsequent authors, and because examination of the actual data simply does not bear it out, as will be shown below.

Table 3.1-1 lists best estimates of the mean erosion rates, for the weight loss interval of 0.05 to 0.5 gm, from Figures 4 and 6 of Reference 1. The normal, tangential, and absolute velocities are also listed, as well as the angles and the corrected erosion rates based on Pearson's hypothesis for angle effect discussed above. Figure 3.1-7 (a) shows the data points plotted versus the normal impact velocity u, with the $1/\cos\theta$ angle correction. Figure 3.1-7 (b) shows the same data (without angle correction) plotted versus the absolute velocity w.

TABLE 3.1-1

EROSION RATE E FOR DIFFERENT SPECIMEN VELOCITIES u AND JET VELOCITIES v

(From Reference 1)

v m/sec	u m/sec	w m/sec	θ deg	E gm/10⁶ impacts	E' E cosθ - gm/10⁶ impacts
52	20	55.7	21	1.05	0.98
52	15	54.2	16	0.86	0.83
52	10	53.0	11	0.67	0.66
52	5	52.3	6	0.64	0.64
42	20	46.5	25	0.32	0.29
42	15	44.5	20	0.26	0.245
31	20	36.9	33	0.122	0.102
31	15	34.4	26	0.075	0.067

NOTE: The jet diameter was 6 mm and the target material low carbon steel.

The following observations can be made:

a) When plotted against u, there is a different curve for each value of v. A correction based on Pearson's assumption ($E_{v,\theta} = E_{v,o}/\cos\theta$) did not suffice to bring them into line.

b) When the data are plotted against the absolute velocity w, they fall quite well into one curve.

These observations not only contradict the conclusion reached by the authors of Reference 1, but also seem to provide evidence contradicting the angle effect theory proposed by Pearson (Equation 1). A possible conclusion drawn from all of the observations is that in this case there is no angle effect, or none of the commonly expected nature, as a result of the jet velocity. This is conceivable when it is considered that the direction of the tangential component of the impact velocity is also the direction in which the impacting mass of liquid is of infinite length.

3.1.3 Dependence on Drop Size and Shape

3.1.3.1 Review of Available Data

Despite the fact that the maximum impact stress is generally a function of the material properties and impact velocity and should be independent of the size of the impacting drops, there is ample evidence that both the size and the shape of the impacting liquid masses do affect the erosion measured. Here again, the quantitative data in the literature from which generalized relationships could be deduced is meager.

A frequently cited test is that of Honegger[2] in which he compared the erosion produced in a wheel-and-jet type apparatus by impact with one 1.5 mm water jet, with that produced by nine 0.5 mm jets, arranged as shown in Figure 3.1-8. The results are described as follows: "The splitting up of the jet is accompanied by a considerable reduction of the erosion, the numerical value of the reduction largely depends upon the speed, and for tests under consideration it varies from 1 to 5 for high speeds and 1 to 10 for low speeds." The test was

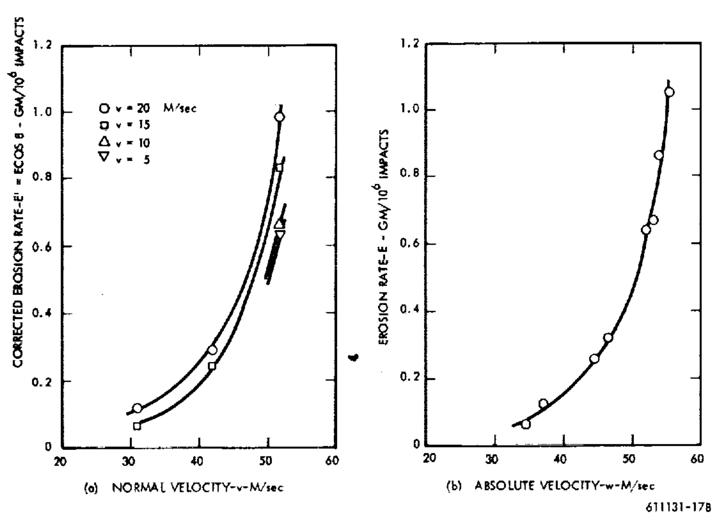

Figure 3.1-7 Erosion versus Velocities

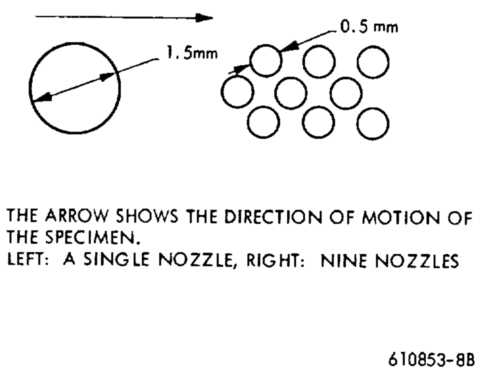

Figure 3.1-8 Arrangement of Nozzles for Water-Jet Tests

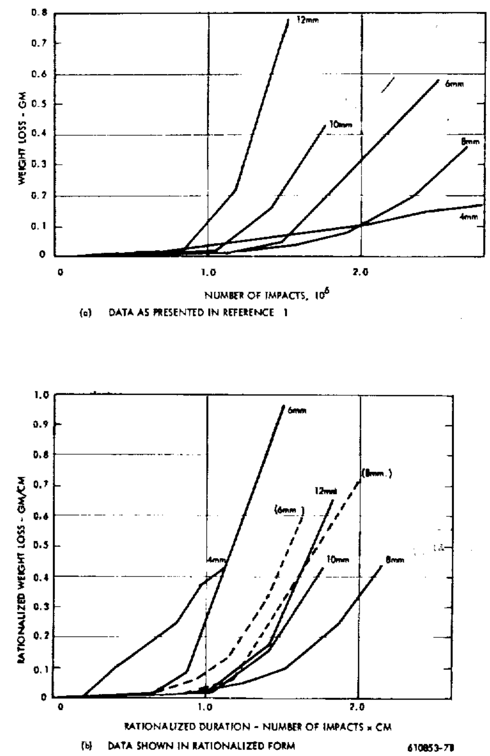

Figure 3.1-9 Erosion versus Jet Size (Adapted from Reference 1)

contrived to fulfill the requirements of a rationalized erosion measurement. Both the target area subjected to erosion and the volume of impinged water were the same for both configurations. Yet, upon reflection, one must conclude that this was not a valid test of the drop size effect, at least not if Figure 3.1-8 accurately portrays the nine-jet arrangement. This is because only the first three jets would impact on a dry surface; a liquid layer from these would almost certainly still be present to cushion the effect of the next three impacts, and similarly so for the last three. Thus, no quantitative conclusions should be drawn from these results, but the qualitative findings are of interest.

Some systematic tests with differing jet diameters were reported by Brandenberger and DeHaller.(1) The weight-loss versus number of impact time curves are reported in Figure 3.1-9a. The jet diameters varied from 4 mm to 12 mm, and attention should be given to the apparent anomaly presented by the 6 mm and 8 mm curves; this gives rise to the suspicion that these curves may have been accidentally mislabeled. This possibility will be discussed below.

The first step in evaluating these data must be to express them in rationalized form (as discussed in Paragraph 3.1.1 of this report). Figure 3.1-9b is a replot of the data in terms of rationalized coordinates. The solid lines represent the original curves as labeled, and again there seems to be an apparent anomaly between the 6 mm and 8 mm curves. If the original curves were mislabeled, then the true rationalized 6 mm and 8 mm curves would appear as shown by the dotted lines in Figure 3.1-9b. In that case, the 6 mm through 12 mm curves would all come very nearly on top of one another, with the 4 mm curve the only discrepancy.

Relative values of the slopes of these erosion-time curves have been measured for the damage interval of 0.15 to 0.4 in Figure 3.1-9b, and these have been plotted in Figure 3.1-10. Figure 3.1-10a represents the data with the original curves of Figure 9 as labeled, and Figure 3.1-10b with the 6 mm and 8 mm curves of Figure 9 reversed. In neither case can any curve be established through these points with any degree of confidence. In Figure 3.1-10a, as shown, a proportionality between erosion rate and diameter could be supported, provided the 6 mm data point is rejected. In Figure 3.1-10b a straight-line relationship, not passing through the origin, has been shown, but the most that can be said, on the basis of the data points alone, is that they would support some relatively weak function of jet diameter.

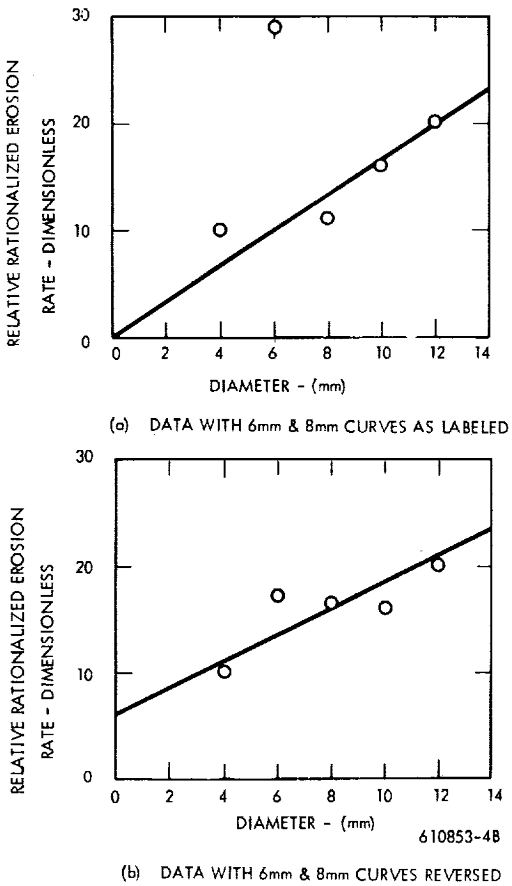

Figure 3.1-10 Erosion Rate versus Jet Diameter

Recently Pearson[(8)] has conducted systematic tests with different drop sizes in his wheel-and-spray type of apparatus. Figure 3.1-11 is a reproduction of Figure 1 of Reference 12, with our terminology. As in all of Pearson's results, the erosion rate given is an angle-corrected rationalized value of the maximum slope measured on the weight-loss versus time curve. It represents mass loss per unit area divided by mass of water impacting per unit area. This impingement angle correction used by Pearson was described in Paragraph 3.1.2. While Figure 3.1-11 shows an anomaly in the crossing of the 920 microns and 1050 microus lines, it seems to confirm that the relative effect of drop size diminishes at high drop sizes and high velocities, i.e., as one gets away from what may be considered the threshold conditions.

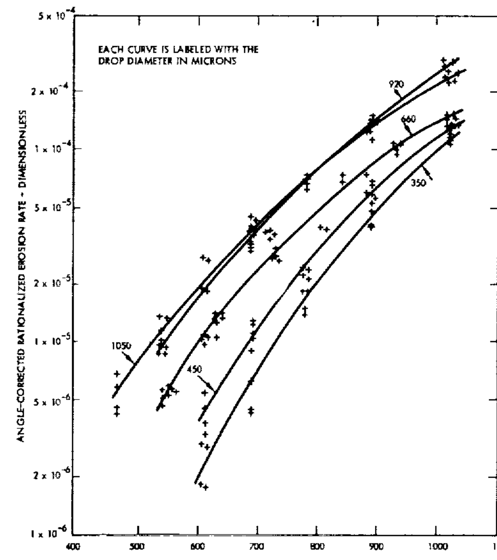

Figure 3.1-11 Effect of Drop Size on Erosion Rate

A cross-plot of the data on Figure 3.1-11 is shown in Figure 3.1-12; here as in Figure 3.1-10 it is difficult to justify a purely empirical curve other than a straight line to represent the erosion rate

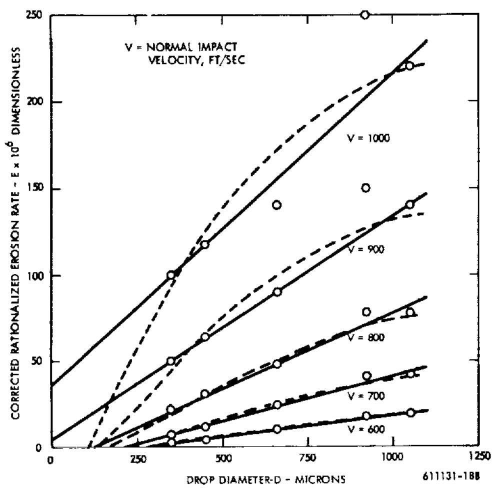

Figure 3.1-12 Effect of Drop Size on Erosion Rate Data Cross-Plotted from Figure 3.1-11 (Dotted Lines are Based on Correlation of Figure 3.1-13.)

versus drop diameter relationship in the absence of any rational basis for some other type of curve. The extrapolation of the solid straight lines to their intercepts on the coordinate axes is, however, questionable. The dotted lines are based on a correlation to be developed below. (Reference 12 does not attempt to present any analytical or empirical equation for the drop size effect.)

It is assumed that the drop size effect can be represented by a factor of the form

$$\left(1 = G/V^2 D\right)$$

where G represents a critical or threshold combination of velocity and drop diameter, such that, for $V^2D \leq G$ no significant erosion occurs. Even if the hypothesis is not completely accepted, the attempt to use the above factor to correlate data on drop-size effect may be justifiable. The data of Reference 2 is for the same material as that of Reference 1, in which a critical velocity V_c of 390 ft/sec was found when testing with a drop size D of 660 microns. Thus, $G = 390^2 \times 660 \approx 1.0 \times 10^8$, and the above-mentioned factor, which shall be denoted as the critical factor, or K_c, takes on the value

$$K_c = \left(1 - 10^8/V^2 D\right) \qquad (2)$$

for this set of data.

Table 3.1-2 lists K_c for a number of combinations of V and D, and also the values of the erosion rate E taken from the curves (not the original data points) drawn in Figure 3.1-11. These values are the same ones plotted in Figure 3.1-12.

If K_c were a simple correction factor to be added to an equation such as Equation 1, then one would expect that E/K_c would become a function of velocity only. This is not the case, as can be seen in the fifth column of Table 3.1-2.

TABLE 3.1-2

DROP SIZE CORRELATION ATTEMPTS FOR DATA OF FIGURE 3.1-11

V (ft/sec)	D (μ)	$K_c = 1 - \frac{10^8}{V^2 D}$	$E \times 10^6$ (From Figure 11)	$\frac{E \times 10^6}{K_c}$	$K_c V$
	350	0.205	2.0	9.75	123
	450	0.383	3.8	9.90	230
600	660	0.578	10.0	17.3	347
	920	0.694	17.0	24.5	416
	1050	0.735	19.0	25.9	441
	350	0.419	7.0	16.7	293
	450	0.547	10.7	19.6	383
700	660	0.690	24.0	34.8	483
	920	0.778	38.0	48.9	545
	1050	0.801	41.0	51.1	561
	350	0.554	20.5	37.0	443
	450	0.642	30	46.7	513
800	660	0.763	47	61.6	610
	920	0.830	78	94.0	664
	1050	0.851	78	91.6	680
	350	0.646	49	75.8	581
	450	0.725	64	88.3	652
900	660	0.813	88	108.0	732
	920	0.886	148	171.0	780
	1050	0.882	138	157.0	793
	350	0.714	100	140.0	714
	450	0.778	116	149.0	778
1000	660	0.848	140	155.0	848
	920	0.891	250	280.0	891
	1050	0.905	220	243.0	905

Another and really more rational way of regarding K_c, since it is a criterion of the deviation both of drop size and velocity from a threshold or critical value, is to argue that the erosion rate E should be a function of K_cV, rather than of $(V - V_c)$ as proposed by Equation 1. Here, V is understood to mean the normal component of impact velocity. The values of K_cV are listed in the last column of Table 3.1-2, and Figure 3.1-13 shows that when E is plotted versus K_cV, good correlation results.

Another valid approach would be to retain the form of Equation 1, and accept from the factor $(1 - G/V^2D)$ merely the consequence that for a given drop diameter D the critical velocity is given by $V_{cd} = \sqrt{G/D}$. That, in fact, was the reasoning which led to taking the value of $G = 10^8$. This suggests plotting E versus $(V - V_{cd})$ with V_{cd} in this instance being given by $V_c = \sqrt{10^8/D}$. The values of V_{cd} are listed in Table 3.1-3, and the points corresponding to those of Table 3.1-2 are plotted in Figure 3.1-14. Again the correlation seems good, though careful examination of the points suggests that the scatter is more systematic with drop size than that in Figure 3.1-13. No formal attempt at curve-fitting has been made for either Figure 3.1-13 or Figure 3.1-14; therefore, no statistical data can be given to substantiate or disprove the feeling that the former provides the better correlation. A hand-fitted curve from Figure 3.1-13, together with values of D_c from Table 3.1-3, have been used to generate the dotted lines shown in Figure 3.1-12.

The results discussed above should be regarded with caution until similar approaches can be tested against other sets of data. Some validating evidence is afforded by curves of the dependence of the critical velocity V_c (below which no erosion takes place) on the jet diameter D (in a wheel-and-jet apparatus) presented by Vater.[13] He presented two curves, valid for materials of corrosion fatigue endurance limit of 2000 and 2200 kg/cm^2, which have been approximately averaged and reproduced here as the solid line in Figure 3.1-15. According to the above hypothesis, this relationship should be represented by $V_c^2D = G$ = constant, if the jet diameter can be regarded as analogous to drop diameter. The dotted line in Figure 3.1-15 shows such a relationship and follows very closely the experimental curve.

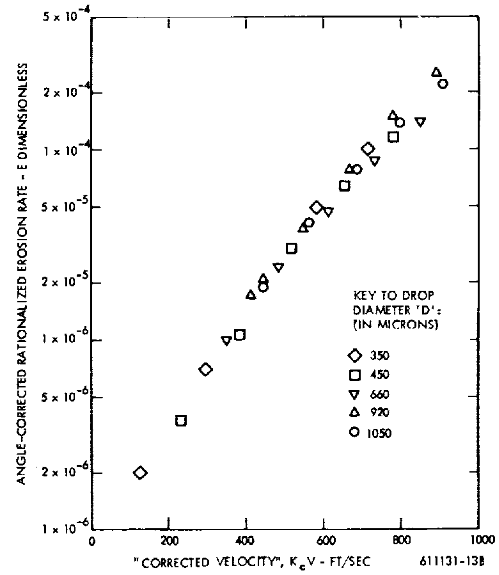

Figure 3.1-13 Correlation of Data of Figure 3.1-11 by Use of "Critical Factor" $K_c \equiv (1 - 10^8/V^2D)$

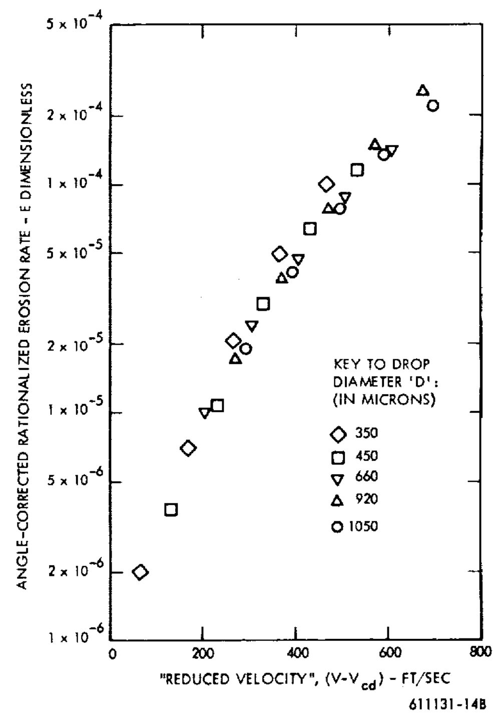

Figure 3.1-14 Correlation of Data of Figure 3.1-11 by Use of "Critical Velocity" $V_{cd} \equiv \sqrt{10^8/D}$

TABLE 3.1-3

CRITICAL VALUES OF V_{cd} AND D_c BASED ON $(V^2D)_c = 10^8$

D (μ):	350	450	660	920	1050
V_{cd}(ft/sec):	535	471	396	330	308
V(ft/sec):	600	700	800	900	1000
D_c(μ):	276	204	156	123	100

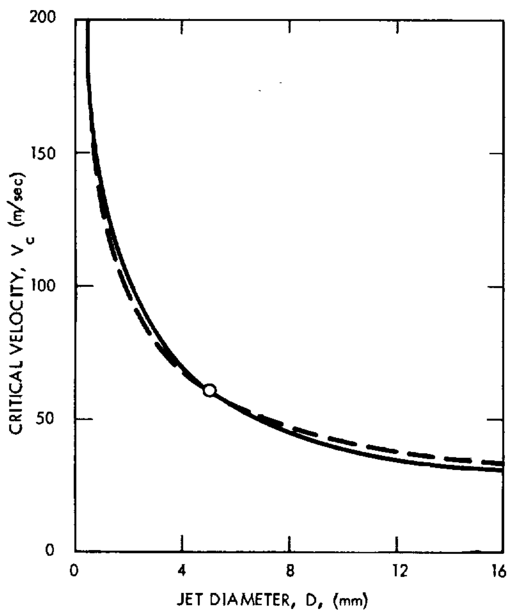

SOLID LINE: CURVE FROM REF. (13)
DOTTED LINE: V_c^2D = CONSTANT

Figure 3.1-15 Critical Velocity versus Jet Diameter

3.1.3.2 Physical Reasons for Drop Size Effect

Consider the question as to why there should be a drop size effect at all. The maximum pressure developed under the impinging drop is generally held to be on the order of the water hammer pressure, ρCV, where V is the impact velocity, ρ is the density of the liquid and C is the pressure wave velocity. This magnitude may be modified by factors which depend on the drop shape (e.g., Engel(14)); although Bowden and Field(15) hold that the maximum value of ρCV holds for spherical drops as well as flat-ended drops, and on the relative acoustic impedance of the target and drop materials (e.g., Vater(13)). None of these is explicitly a function of drop size.

It is now known, however, what the true criterion of erosion damage is. While some general correlations have been made between the ρCV value corresponding to the critical velocity and the endurance limit, it has also been shown(16) that surface deformation can occur at ρCV values far below the yield point.

When erosion does take place, there is no certainty that the rate of erosion is strictly a function of impact pressure levels. Thiruvengadam(17) has proposed that in cavitation damage the energy available from the collapsing bubbles is a criterion of the volume rate of material removal, so that the impact energy of impinging drops might be of interest.

The question to be asked is: What properties of the impacts, or of their effect on the target surface, vary when one reduces the size of droplets into which a given amount of water, impinging on a given target area in unit time, is subdivided?

The total impact area (as distinguished from target area) actually increases, since the number of drops increases as D^{-3} and the impact area per drop decreases as D^2 when the drop diameter D is reduced.

In other words, each target area element will be subjected to a greater number of stress pulses per unit time, if one can assume that the contact area of the impact bears a fixed relationship to the projected area of the drop. If this were a significant criterion, then the erosion would be expected to increase with decreasing drop size, which contradicts all experience.

However, another consequence of the increased impact area is that the total kinetic energy (which remains constant) of the impinging water is spread out over a greater area, and therefore the energy flux per unit area is reduced. A hypothesis based on this fact, led to the suggestion that the factor K_c (see Equation 2) represents the drop size effect.

Another factor which is of very likely significance is the duration of the pressure pulse on impact. Whatever precise reasoning is used to predict this duration (e.g., as in Reference 15), it is clear that for geometrically similar drops it must be proportional to drop diameter. Thus, the impulse per unit area is smaller in the impact of a smaller drop, and perhaps this is of consequence. Certainly the duration (microseconds) of the impact pressures are short enough so that strain rate effects, in those materials that exhibit them, may become significant. The smaller the drop, the higher the effective strain rate, therefore, the higher the effective yield point. The higher the effective yield point, the smaller the strain induced by the given applied stress which is determined by the impact pressure.

Finally, the impact areas may well be small enough where a size effect of the material itself becomes important. Particularly in the impact of a spherical drop (or sideways against a cylindrical jet), the impact area at the moment of peak pressure will be a small fraction of the projected area of the drop or jet. Size effects have been found in the values of endurance limits of notched specimens; this has been explained by Peterson[18] in the argument that for fatigue failure to occur, the endurance limit must be exceeded not merely at a point or line but across a dimension which is on the order of 0.002 to 0.003 inch, and may bear some relation to the grain size of the material. Since erosion damage, in the velocity domain now under consideration, is primarily a fatigue process and failure has been shown to occur initially by intergranular cracking, e.g., Marriott and Rowden[19], a similar size effect is very possible.

A physical or phenomenological picture of this kind of effect may be formed with reference to a fatigue model proposed by Weibull.[20] He points out that the fatigue process consists of two stages: crack initiation and crack propagation. A crack will initiate at a point in the material with a high damage factor, k, which can be regarded roughly as the ratio of the nominal applied stress magnified locally by stress raisers such as scratches or inclusions to the idealized strength of the material diminished locally by dislocations or other imperfections. The higher the local value of k, the smaller is the number of stress cycles N_o which are required to initiate a fracture at that point. Since the k values are dependent on local aberrations they vary statistically, and hence, N_o is a random variable with large scatter. Once a crack has been initiated, it raises the k-field in the vicinity so that adjacent points are brought more rapidly to the crack-initiation stage, and the crack thereby propagates.

As the drop size increases so does the surface area over which the impact pressure (assumed independent of drop size) extends, and so does (by elastic analysis) the depth to which a given stress level extends below the surface. Thus, the stress gradient into the material is reduced and the k-field under the surface is increased. Thus, not only is there a greater chance of initiating a sub-surface crack, by virtue of the fact that a greater volume is highly stressed, but the higher value of the k-field will result in more rapid and deeper crack propagation. In fact, if the depth of the stress field is less than some value characteristic of the grain size, it is unlikely that the cracks would ever propagate around the grain and no erosion would take place. This would establish the threshold drop size.

It is noteworthy that size effects have been found in other material removal processes: Backer, et al,[21] discovered a large increase in the shear energy required to remove a unit volume of material as the chip size (or depth of cut) decreases in turning, micro-milling and grinding operations; the depth of cut in these tests ranged from about 0.010 inch down to 2×10^{-5} inch. It is thought that, as the affected depth of material is reduced, the theoretical strength of the material is approached. These findings have been considered by Finnie[22] to be of relevance to erosion by solid particle impingement.

3.1.3.3 Effect of Drop Shape

The effect of the drop shape poses two questions; one is difficult to answer at the present, the other is relatively easy, at least qualitatively.

The first is the effect of the shape of the front surface of the drop that contacts the target. Some authors have stated that this shape affects the maximum contact pressure; others stated that it does not. In either case, however, the time rate of the pressure rise and fall and the variation in size of the actual contact area will definitely be affected. Both of these (and the interaction between them) will affect the damage produced, if the strain rate effect and material size effect are significant. Also, the shape of the front of the drop will affect the radial outflow velocity over the target surface after impact (see Bowden and Brunton[23] and Engel[14]), and this, in turn, is of importance at impact velocities high enough to cause single-impact damage. Complete theories or experimental data relating this geometry to the damage are lacking.

The second question is that of the tail surface of the drop, or its length perpendicular to the contact plane. Bowden's group and also DeCorso[24] have shown in single-impact tests that the length of the impinging mass of water is of significance. The duration of the high (water hammer) pressure is governed essentially by the time it takes pressure-release waves to move inward from the boundaries of the contact area and meet, or, in the case of an extremely short mass of liquid, the time it takes for the pressure wave to be reflected from its back end as a release wave and return to the contact face. Thereafter, the contact pressure is only the stagnation pressure $\rho V^2/2$, and the mass of liquid arriving then is relatively harmless.

Thus, the effective mass of an impinging drop or mass of liquid may be hypothesized to be approximately that mass through which the pressure release waves must travel before the water-hammer pressure is completely relieved at the contact face.

A test result with some bearing on this was given by Brandenberger and de Haller[1]. An elongated jet cross section was used in a wheel-and-jet apparatus and when impacted by the specimens on its broad side resulted in far more rapid erosion than when impacted on its narrow side. Quantitative conclusions cannot be drawn, because in the latter case the second stage of erosion was not reached, so that a reliable comparison of erosion rates is not possible; and further because the actual dimensions of the jet cross section are not given (although the proportions are suggested by a sketch), the size effect and the shape effect cannot be distinguished. Additional experiments of this type might be of value in helping to establish the significant criteria of a drop's damage potential, even though drop shapes may be of fairly uniform shape.

3.1.4 Dependence on Impact Velocity

3.1.4.1 Some Simple Empirical Equations for Velocity Dependence

The literature contains a considerable body of data relating erosion to velocity, but the usefulness of much of these data is limited by the considerations discussed in Section 3.1.1.

There are various functional forms to which one can attempt to fit such data; the most obvious ones are discussed below. Here, E = erosion rate and V = velocity:

$$E = a V^n \tag{3}$$

This represents a simple power relationship, and implies that some erosion will take place no matter how low the velocity. Usually, however, it is thought that there is a critical or threshold velocity, V_c, below which erosion is absent for all practical purposes. An obvious type of relationship to reflect this is

$$E = a (V - V_c)^n \tag{4}$$

$$= a_1 \left(\frac{V}{V_c} - 1 \right)^n \tag{4a}$$

This implies that erosion is proportional to a power of the velocity in excess of the critical or threshold velocity V_c. Pearson's equation is of that type. It has been used by a number of authors to express their results.

Another type of relationship involving a critical velocity is

$$E = a V^n - b \qquad (5)$$

which implies $\quad V_c = (b/a)^{1/n}$

and can be rewritten

$$E = \left[a_1 \left(\frac{V}{V_c} \right)^n - 1 \right] \qquad (5a)$$

Clearly both Equations (4) and (5) have the property that

$$\text{when} \left(V/V_c \right)^n >> 1, \; E \rightarrow a_1 \left(\frac{V}{V_c} \right)^n \qquad (6)$$

$$\text{and when} \quad V/V_c \rightarrow 1, \quad E \rightarrow 0$$

3.1.4.2 Some Physical Considerations Relating to Velocity Effect

3.1.4.2.1 Analogy with Fatigue S-N Data

Which among equations (3), (4) and (5) is a more logical choice depends to some extent on what physical reasoning--if any--is used to account for the influence of velocity. One physical argument can lead to yet another type of relationship: Vater[13, 25] noted that since erosion is a fatigue phenomenon, and the applied stress is proportional to (or at least a function of) velocity, the relation between velocity and erosion lends itself to a treatment analogous to the relation between stress and cycles to failure in fatigue. He presented curves in which velocity is plotted versus the number of impacts to obtain a given weight loss (Figure 3.1-16a), or versus the reciprocal of the weight loss obtained after a given number of impacts (Figure 3.1-16b). (The latter is, however, once more an example of doubtful comparisons, since after a given number of impacts, different stages of the erosion-time curve may have been reached.)

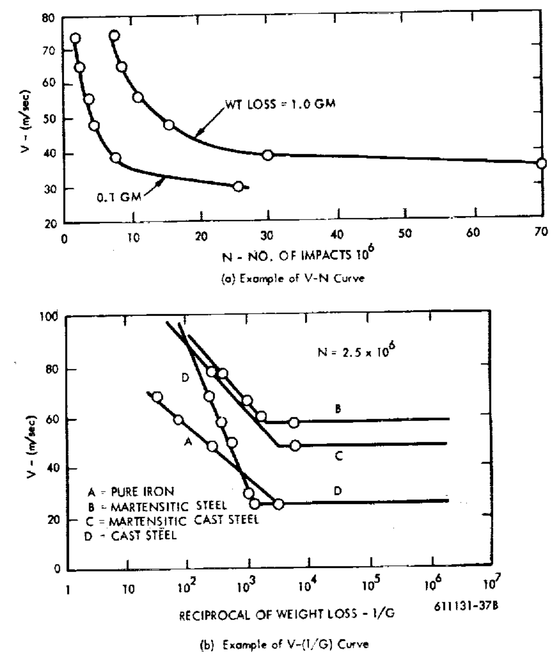

Figure 3.1-16 Erosion-Velocity Relationships Plotted in the Manner of Fatigue Data

Some caution should be exercised in making direct analogies between S-N fatigue curves and velocity versus erosion curves. If erosion takes place as a steady-state process and the mean size of erosion fragments is independent of V, then the volume rate of erosion E would be proportional to 1/N, where N is the mean number of impacts required to generate a loose erosion fragment. In turn, N could be assumed to be related to the impact stress and hence to the velocity V in a manner similar to the relation between cycles to failure and stress in conventional fatigue tests.

If these assumptions are correct, a V - (1/E) curve should exhibit similar characteristics to a S-N fatigue curve. If erosion is not a steady-state process, then the number of impacts to obtain a given cumulative volume loss (as plotted in Figure 3.1-16a) should be a valid analogy, provided that there are no variations in the initial target surface conditions which could affect the life-times of the original surface layer elements. (It might be pointed out that one implication of the erosion-rate-time model proposed in Section 3.2 is that the erosion process during the period of maximum erosion rate is generally not a steady-state process; rather this peak in the rate-time curve can occur as a result of a deluge of erosion fragments being loosened at about the most probable value of the number of impacts to failure, as measured from the time the impingement attack was initiated. It is only because of scatter in the sizes and the impacts-to-failure of the erosion fragments that there is a tendency towards a steady-state value.)

Fatigue S-N data are often depicted as an approximately straight line on a semi-log plot for intermediate values of N, as follows:

$$S = S_o - b \log N$$

with a leveling off to $S = S_y$ at low values of N, and a transition to $S = S_E$ at high values of N where

- S = stress corresponding to N cycles
- S_o = intercept of straight line on stress axis ($S_o > S_y$)
- S_y = yield stress
- S_E = endurance limit

Consequently, one might expect some analogous relationship such as

$$V = a - b \log \left(\frac{1}{E}\right)$$

or, in a form which is equivalent but more consistent with the previous types of equations listed,

$$E = a\ e^{nV} \qquad (7)$$

where e is the base of the logarithm chosen. This equation does not predict a critical velocity and must be combined with the separate condition that there is a transition to $E \rightarrow 0$ at some value $V = V_c$.

This relation, even for conventional fatigue data, is valid only within a limited range. A number of more complicated equations have been proposed for representing S-N data over the full range of values; these are surveyed on pages 174-178 of Reference 26. Such equations would predict a critical velocity. It does not seem profitable to attempt to use these, partly because of the computational difficulty involved and partly because one of the previously mentioned assumptions inherent in this direct analogy is almost certainly unjustified; that is, the assumption that the mean erosion fragment size is independent of impact velocity. Since a higher velocity generates a greater impact pressure in turn producing a larger stress-field in the target, i.e., a greater volume of material is highly stressed, it seems very likely that the mean fragment size increases with velocity. A velocity relationship could be postulated from this fact alone, as will be shown below.

3.1.4.2.2 Approach Based on Size of Stress-Field Under Impact

The approach will be demonstrated with reference to a two-dimensional model, which would apply to the wheel-and-jet type of apparatus: It is assumed that the contact pressure between the jet whose side impinges against the target, or vice versa, and the target surface can be reasonably represented by a belt of uniform pressure over the surface of a semi-infinite solid; furthermore that the effective width "2a" of this belt is a function of jet size and shape and is independent of impact velocity.

(This assumption seems more reasonable than a Hertzian contact stress distribution which would imply that the liquid behaves as an elastic solid on impact.) This corresponds to Case No. 11 on page 322 of Roark[27] where formulae are given for the compressive and shear stresses anywhere within the solid. Since the shear stress is surely a better criterion for failure than the compressive stress, consider the locus of a constant value of shear stress, S, as a function of the contact pressure, p, and the semi-width of the pressure belt, a. The formula given by Roark is

$$S = 0.318\, p \sin \alpha \qquad (8)$$
$$= (1/\pi)\, p \sin \alpha$$

where α is the angle subtended, at the point in question, by the boundaries of the pressure belt on the surface. It can easily be shown that the locus defined by Equation (8) consists of two circular arcs of radius, r, where

$$\frac{r}{a} = \frac{1}{\pi} \frac{p}{S},$$

whose centers lie a distance d, respectively, below and above the solid surface, where

$$\frac{d}{a} = \sqrt{\left(\frac{r}{a}\right)^2 - 1}$$

This is shown in Figure 3.1-17. The region stressed to values greater than S lies between the two arcs. Figure 3.1-18 shows these loci for a number of values of p/S; the highest value of the shear stress is of course $S = p/\pi$, and its region reduces to a semi-circular locus of radius, $r = a$.

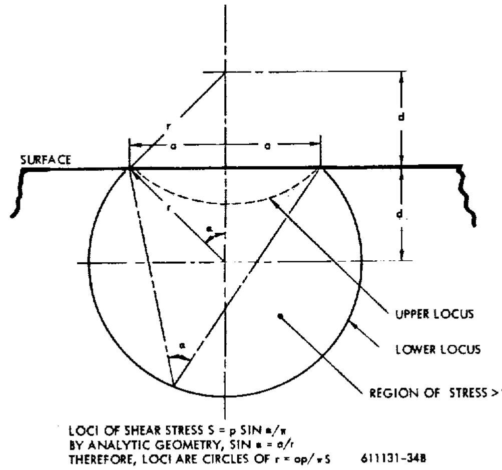

Figure 3.1-17 Loci of Constant Shear Stress S in Semi-Infinite Solid with Belt of Uniform Pressure P

Figure 3.1-18 can be regarded in two ways. It can represent the loci of various shear stresses in a given stress field, if the contact pressure p is assumed to be a fixed quantity. On the other hand, assuming the shear stress S to be the independent fixed quantity, then the lines on Figure 3.1-18 represent the spreading of the boundaries of the region bounded by that stress, as the contact pressure p is increased. It is the latter point of view which we adopt for our argument.

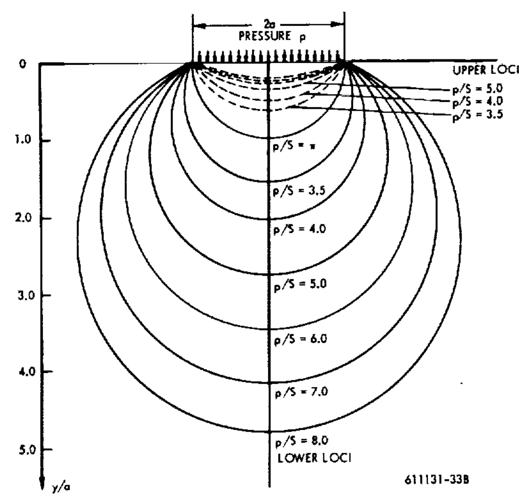

Figure 3.1-18 Upper and Lower Loci for Various Values of Pressure/Shear Stress Ratios

For the purpose of this argument it is assumed that if a reference stress S is selected exceeding an appropriate critical value or endurance limit, then the reference time (or number of impacts) required for fracture to have occurred all around the locus of S is independent of the length of that locus, since a greater length represents a proportionately greater number of crack initiation points. At this fixed reference time, all of the material between the original surface and the lower locus will have been lost. Therefore, a lower limit to the change in the erosion rate with contact pressure, and hence with velocity, is provided by the change in the area, A_S, which lies between the original surface and the lower locus of a given value of S, as p is increased.

The non-dimensionalized area A_S/a^2 has been computed as a function of p/S and is plotted on log-log scales in Figure 3.1-19, which therefore should represent an approach to a velocity-erosion rate relationship. Note that the slope begins at a high value and gradually approaches the value of 2.

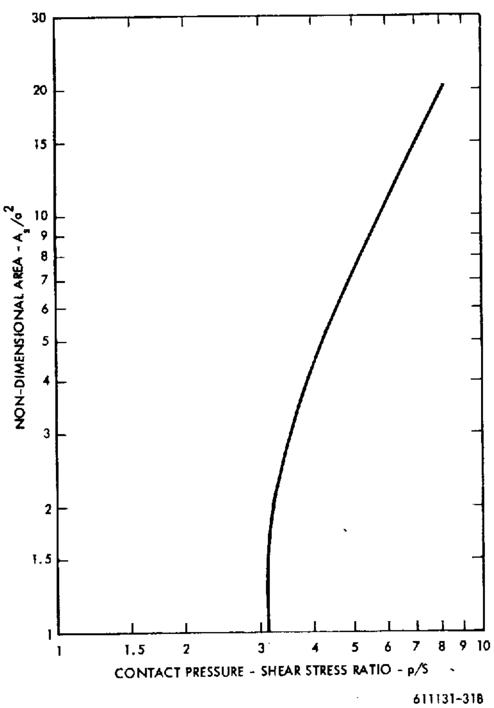

Figure 3.1-19 Area Between Surface and Lower Stress Locus

One should not, of course, take this model so literally as to infer from it that fracture actually occurs by cracks following along these loci. Moreover, it clearly gives a lower limit to the erosion rate because it ignores the fact that earlier fractures will occur above the reference stress locus because of the higher stresses there, thus altering the geometry and causing the locus of S to progress further down into the solid. In particular, this model predicts that when the pressure reaches $p = \pi S$, the erosion jumps from zero to a value corresponding to an area, $A_S/a^2 = \pi/2 = 1.57$.

In actuality, if the "reference stress" S is chosen to be above the endurance limit S_e so that the reference time is not infinite, then for all values of p, such that $p > \pi S_e$, there will still exist stresses high enough to cause material loss, though not within the same reference time. The model does show, however, that some quantitative conclusions may be drawn from a fatigue point of view, without any reference to specific S-N relationships. It also serves to emphasize that the extent of the stress field under the impact must be taken into account in any analytical approach to predicting the erosion-velocity relationship, whether that approach is based on stress or energy concepts.

3.1.4.2.3 Energy Considerations

An energy approach was described in pages 167-174 of Reference 11, that sought to predict effects both of velocity and drop size on the erosion. It was based on the assumption that the volume of material removed per unit area per impact, is proportional to, or a function of, the impact energy per unit area in excess of some energy threshold per unit area characteristic of the material surface. This resulted in the following relationship, expressed in non-dimensional terms:

$$E = f\left\{k_2\left[\frac{\frac{1}{2}\rho_L V^2}{S_o}\right]\left[1 - \frac{e_o}{k_3\left(\frac{1}{2}\rho_L V^2 D\right)}\right]\right\} \quad (9)$$

where

E = rationalized erosion rate $\left(\frac{\text{volume of eroded material}}{\text{volume of impinged liquid}}\right)$

V = impact velocity

D = characteristic dimension of droplet

ρ_L = density of liquid

k_2 = ratio of "effective" volume to total volume of drop

k_3 = ratio of "effective volume" to "effective impact area" times drop dimension

s_o = characteristic strength or elastic modulus of material

e_o = "threshold energy" per unit area of material surface

f = functional relationship or factor of proportionality

In a simplified form, and to bring out the "threshold conditions" implicit in it, Equation 9 can be rewritten as:

$$E = f_1 \left[V^2 \left(1 - \frac{G}{V^2 D} \right) \right] \qquad (9a)$$

where G represents a "critical value" such that if $V^2D < G$ no erosion takes place. (The relationship is of the type of Equation 5.) This critical value has proved quite successful, in one or two instances, of correlating drop-size effect data, as was shown in the previous section. In particular, it was shown that the data of Pearson in Reference 12 correlated well in the form

$$E = f_2 \left[V \left(1 - \frac{G}{V^2 D} \right) \right] \qquad (10)$$

However, the difference between Equations (9a) and (10) indicates that the energy threshold concept - at least in its present form - is still deficient.

A number of authors recently have sought to predict both erosion strength and erosion attack severity in terms of energy concepts (e.g., Thiruvengadom[17, 28, 29, 30], Hoff, et al,[6]; Shalnev, et al[31]) there are problems to be solved. The energy balance involved in a droplet impact is complex and has not yet been examined in sufficient depth. Part of the kinetic energy of the impinging drop will remain as the kinetic energy of the radial outflow velocities; part will be dissipated in the shock or pressure waves passing through the drop, and part in the shearing associated with the change of direction of the liquid flow; part will be dissipated in the target material; here too, the energy dissipation associated with stress waves should be examined as well as the quasi-static plastic strain hysteresis energy associated with each impact stress cycle. The picture is further complicated by the rather large amount of energy that will be stored temporarily as elastic strain energy in the target and will reappear in one of the previously-mentioned forms.

The energy dissipated in the target material is that energy associated with fracture, and therefore, with erosion. But it is not correct to assume that the volume of material removed is proportional to that energy. Two reasons account for this: One is that (at least in the case of larger drops at moderate velocities) erosion fragments produced by the random linking-up of fatigue-like cracks (see Reference 19) are not likely to be deformed to the fracture point throughout their volume; therefore, the accumulated plastic strain energy may be more related to the surface area of the fragment than to its volume, or at the least, be non-uniformly distributed within the volume. The other is that in fracture due to the repeated stressing, the total energy input increases greatly with the number of cycles to failure. This is evident in McAdams' results for impact fatigue tests,[32] and has been documented for a large collection of fatigue data by Halford[33]. Even if one postulates that the damaging energy is the same in all cases and the excess hysteresis energy is dissipated through non-damaging processes, the fact remains that all of the dissipated energy is supplied by the impinging droplets and even if the energy absorption by the target material is known, that in itself will not establish the erosion rate. The crudest broad conclusion one can draw from the above is that the erosion is likely to vary with the velocity to a power higher than 2, since the impinging energy is proportional to velocity squared, and the total energy to failure decreases with increasing velocity (i.e., with increasing stress and decreasing number of impacts to failure).

3.1.4.2.4 Relation Between Impact Pressure and Velocity

A final note of relevance to this subject concerns the relationship between the impact velocity and the contact pressure generated.

Let us first review one-dimensional approximations, and then discuss the three-dimensional effects introduced in the impact of a rounded drop or jet.

When a body has its velocity changed by means of an impact, a shock (or pressure, or stress) wave emanates from the initial impact interface and propagates into the body, progressively imparting the change of velocity to each particle "layer" through which the wave presses. The applicable pressure relationship is

$$p = \rho C V \qquad (11)$$

where

p = pressure rise across shock wave

ρ = density of unshocked material

C = velocity of propagation of shock wave

V = change in particle velocity across shock wave.

If we consider the low speed impact of a liquid against a rigid target, then the above takes the form of the well known "water hammer" equation:

$$p = \rho_o C_o V_i \qquad (11a)$$

where

ρ_o = density of undistrubed liquid

V_i = impact velocity

C_o = acoustic velocity of the liquid.

When target elasticity must be taken into account, then one may write two simultaneous equations (11), for the liquid and for the target material respectively: the pressures must be equal for both, and the two particle velocity changes must add up to the impact velocity. This leads to an equation sometimes attributed to deHaller:

$$p = \frac{\rho_o C_o V_i}{1 + \dfrac{\rho_o C_o}{\rho_T C_T}} \qquad (12)$$

where

ρ_T = density of undisturbed target material

C_T = stress wave velocity or acoustic velocity in the target.

Note that equations (12) and (11a), besides being one-dimensional approximations, both assume fixed values of the propagation velocities C_o and C_T. This makes them quite inaccurate for high-speed impact calculations, because the propagation velocity of a shock wave itself depends strongly on the shock pressure (or the particle velocity change across the shock).

Various studies have shown that for many materials, both liquid and solid, the relationship between shock velocity, C, and particle velocity change across the shock, V, is a nearly linear one and can be approximated by

$$C = C_o + kV \qquad (13)$$

where C_o is the acoustic velocity in the material and k is a constant for the particular material.

Heymann[34] gave a non-rigorous explanation of this relationship, demonstrating that for water $k \cong 2$ (in the range $0 \leq V \leq 1.2\ C_o$), and derived the following equations for one-dimensional impact between a liquid and a target.

If the target is rigid, $V = V_i$, and substitution of (13) into (11) gives

$$p = \rho_o C_o V_i (1 + k M_o) \qquad (14a)$$

where

$$M_o = V_i / C_o = \text{"Impact Mach Number"}$$

and

k_o is the "shock velocity constant" for liquid, as defined by equation (13).

If the target is elastic, but its shock velocity is assumed constant, it is not correct simply to substitute equation (13) into equation (12), although the error is generally less than 20 percent. The exact expression, derived in Reference 34, can be written in dimensionless form as:

$$\frac{p}{\rho_o C_o V_i} = u\,(1 + k_o M_o u) \qquad (14b)$$

where

$$u \equiv \left[\left(\frac{1+x}{2 k_o M_o}\right)^2 + \frac{x}{k_o M_o}\right]^{\frac{1}{2}} - \left[\frac{1+x}{2 k_o M_o}\right]$$

and

$$X \equiv \rho_T C_T / \rho_o C_o$$

(u is the ratio of particle velocity change in the liquid to impact velocity, and x is the acoustic impedance ratio between target and liquid.)

The assumption of a constant shock velocity C_T in the target can be justified when $x \ll 1$, which is generally true for metallic targets. In that case, the ratio of particle velocity change in the target to its acoustic velocity is so small that the difference between the true stress wave velocity and the acoustic velocity is negligible.

Curves of $p/\rho_o C_o V_i$ versus M_o, for several values of x, are given in Figure 3.1-20. These curves apply to $k = 2$, as for water.

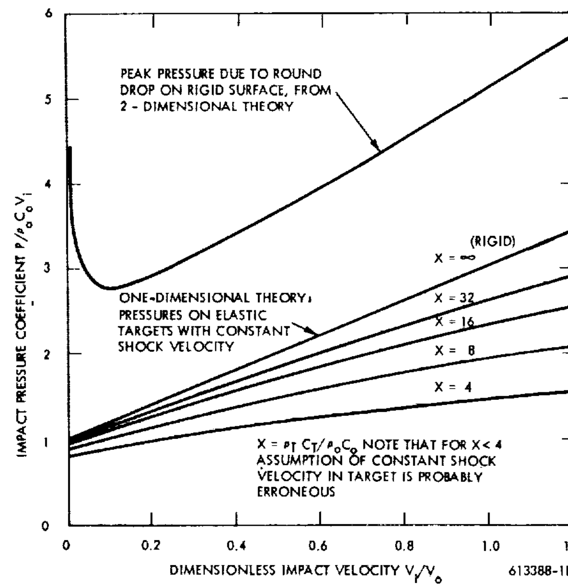

TO CALCULATE FOR WATER, WITH V_i IN FT/SEC AND P IN LBS/IN^2 USE FOLLOWING CONVERSIONS:

$$C_o = 4900$$

$$P = \left(\frac{P}{\rho_o C_o V_i}\right) \times V_i \times 65.4$$

Figure 3.1-20 Impact Pressure Versus Velocity

When $x \gg 1$, as say in the impact between water and an elastomeric target, then the greater particle velocity change will occur in the target. Such a case can be treated by exchanging the meanings of the subscripts (e.g., ρ_o, C_o, k_o now refer to the target material), provided k for the target material is known or determined.

Unfortunately, values of k are not easily found in the literature. The following is a partial list:

Material	C_o (km/sec)	k	Source
Water	1.5	2.0	Heymann, Ref. 34 (Deduced from Cole, R.H: "Underwater Explorious", Princeton Univ. Press, 1948)
Sodium	2.563	1.242	Rice, M.H: J. Phys. Chem. Solids, 26, 1965 pp. 483-492
Potassium	1.930	1.188	
Lithium	4.589	1.154	
Rubidium	1.232	1.184	
Gold	3.0	1.56	Jones, A.H., et al: J. Appl. Phys., 37, 1966, pp. 3493-3499
Tungsten	4.0	1.28	
"Fansteel 77"	3.9	1.355	
K Br	2.33	1.546	Ruoff, A.L: J. Appl. Phys., 38, 1967, pp. 4976-4980
Cs I	1.66	1.41	
Sodium	2.706	1.22	

Equations 14a and 14b still apply strictly only to one-dimensional impact (i.e., two semi-infinite bodies colliding). An exact analysis of a liquid sphere impacting against a plane surface has not yet been achieved. However, a qualitative picture of the sequence of events, based on various contributions relevant to this problem, has been given by Heymann.[35] [75] According to this picture, the impact pressure at the first instant of contact is equal to the one-dimensional pressure. As the contact area grows, the pressure distribution becomes more and more non-uniform. The pressure at the expanding boundary of the contact area increases, while the pressure at the center of the contact area decreases, from the one-dimensional value.

A "critical condition" is reached when the shock front expands faster than the contact boundary, and lateral "jetting" outflow begins. Soon thereafter, the contact pressures may be assumed to decrease everywhere.

Heymann[35] also presented an approximate two-dimensional analysis for the impact of a round liquid body onto a rigid plane, which permits the calculation of the pressure at the boundary of the contact area, from the moment of initial contact until the "critical condition" is reached. The numerical results support the previously described qualitative picture. The peak impact pressure is that at the critical condition, and if this "critical pressure" p_c is plotted in nondimensional terms, $p_c / \rho_o C_o V_i$ against nondimensional impact velocity M_o, for water, one finds that the lowest value of $p_c/\rho_o C_o V_i$ is about 2.8, at $M_o \cong 0.1$; at higher and lower values of M_o the value of $p_c/\rho_o C_o V_i$ increases rapidly. Thus, the simple one-dimensional water hammer equation (11a) underestimates the peak pressure by at least a factor of about 3. The curve applicable to water is shown on Figure 3. 1-20. Similar results are obtained for sodium and potassium.

These results are true only for impact on a rigid plane; the analysis has not yet been extended to an elastic target, on which the peak pressures presumably are smaller. The results did show, however, that the pressure at the contact boundary rises only slowly during the first half of the growth of the contact zone, so that one may conclude that a considerable portion of the eventual contact area is subjected to little more than the one-dimensional pressure. This conclusion may perhaps be extended to elastic targets as well. It could well be that this pressure is more significant in determining target material response than the more localized and fleeting "critical pressures", but this should not be assumed without further evidence. In any case, it would be desirable to have analytical results for the contact pressures developed by impacting rounded drops on elastic targets, on rough targets, on film-covered targets, and at oblique angles. This still remains to be accomplished.

3.1.4.3 Empirical Data from the Literature Search

3.1.4.3.1 Preliminary Remarks

In attempting to fit a simple equation to experimental data, equations like (3), (4), (5) or (7) would be selected. Equation (4) would form a straight line on log-log paper if plotted versus $(V - V_c)$, but one does not know V_c ahead of time. Equation (7) would form a straight line on semi-log paper, with V along the linear scale.

Figure 3.1-21 shows examples of these various relationships on a log-log plot. The upper portion represents equations of types (4) and (5) with V/V_c plotted against E, and the lower portion equations of types (3) and (7) with V plotted against E. For consistency, the constants, a, have been chosen so that all curves pass through the point E = 1, V or $V/V_c = 2$. A plot of this kind may be of help in deciding what type of relationship to try to fit to experimental data points when these are plotted on a log-log graph. A corresponding plot of these families of curves could be constructed on semi-log paper, with E as the log coordinate; in that case the equations of type (7) would plot as straight lines.

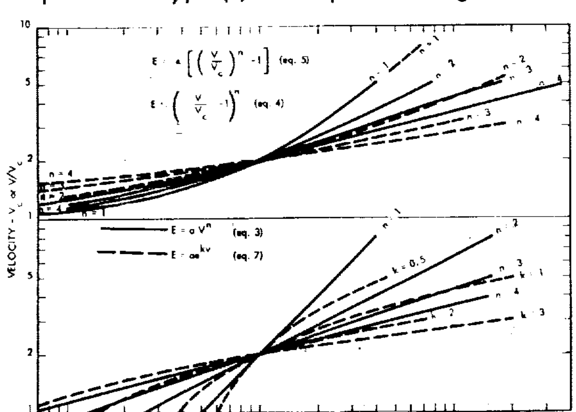

Figure 3.1-21 Families of Hypothetical Erosion Versus Velocity Curves, According to Equations (3) through (7)

A number of problems arise when attempting to establish an equation of these types for experimental data, either by plotting the data points on log or semi-log paper, or directly by numerical methods.

One of the problems is that much of the data is obtained at velocities not much greater than the critical velocity (seldom at more than $V/V_c = 2$). Therefore, one is probably examining that portion of the curve in which a transition is taking place, or in which even in a log-log plot, the curvature is greatest. Consequently, small errors in the data points, or small differences in the manner in which a smooth curve is fitted to them, will have a great effect on the values of the exponent n and the critical velocity deduced.

This difficulty is compounded because the scatter in erosion data is inevitably great, that in many of the test series no more than three velocities have been investigated, and that the ratio of the highest to the lowest of these is often small, about 1.5. This covers a very short span of the velocity axis on log-log paper. In short, a problem exists in which:

a) In the velocity range investigated the true relationship will not appear as a straight line.

b) There are too few data points and these cover too short a velocity range to allow a curved line to be fitted with the necessary accuracy.

If testing could be done at much higher velocities, then in theory the influence of V_c on the apparent exponent, i.e., the slope of the curve on a log-log plot, would be reduced and a more accurate determination could be made of n. In practice, however, at velocities much above $V/V_c = 2$ one gets into the region of single-impact damage, whose velocity dependence may not be the same as that for fatigue damage, and so, one may well be in another transition region.

3.1.4.3.2 Examination of the Better Test Data

One of the earliest comprehensive sets of test data at various velocities was given by Honegger[2]. His conclusion was that while the behavior of the various materials differs considerably, the rate of erosion may be generally expressed as:

$$E \propto (V-125)^2 \qquad (15)$$

where V is the impact velocity in m/sec. The above relationship was evidently deduced from his Figure 7, on which was plotted the specific loss in weight (weight loss per impact, hence a measure of erosion rate E) after 215,000 impacts, versus velocity. This type of comparison is not valid.

Also, the equation fits a mean curve drawn through the band of experimental curves; but some individual curves suggest exponents that are much higher. Thus, the curve for Specimen No. 26 is well described by $E \propto (V-110)^{3.3}$.

For a more valid basis of comparison, the rate-time curves presented for various materials and for the speeds of 175, 200, and 225 m/sec should be reviewed. From these, one can deduce characteristic erosion rates which fulfill the criteria specified in Section 3.1.1 of this report. This has been done as an approximation and the results are plotted on log-log coordinates in Figure 3.1-22. Their shape is not unlike what is predicted by Figure 3.1-19, at velocities close to the threshold value, but it would be unwise to fit any empirical equation to these data.

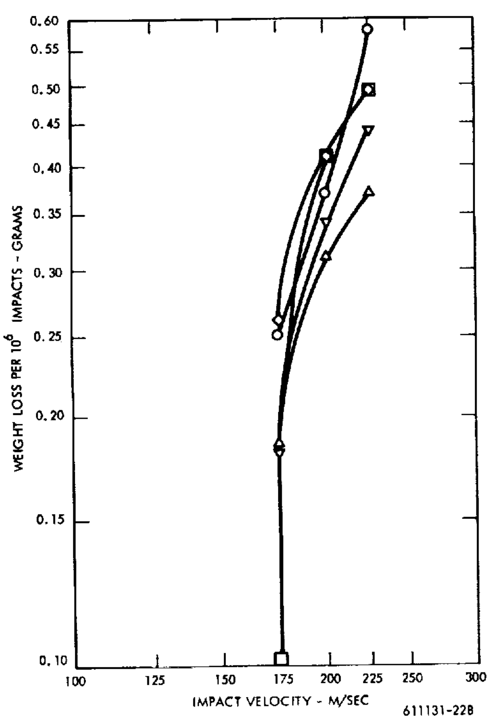

Figure 3.1-22 Erosion versus Velocity Curves, Computed from Data in Reference 2

An interesting set of results on one material was reported by Brandenberger & DeHaller[1], which was discussed in Section 3.1.2 with reference to the angle-effect. The rationalized erosion rates deduced from Reference 1 were plotted in Figure 3.1-7, and the data points of Figure 3.1-7b have been replotted on semi-log coordinates on Figure 3.1-23. They fall into a straight line, giving some support to the simple fatigue model of velocity dependence represented by equations of type 3.1-7. It should be pointed out, however, that the determination of the best values of E, from the irregular slopes of the very small graphs shown in Reference 1, involved a certain amount of judgment and some extrapolation for the u = 31 m/sec data. In preliminary attempts, with fewer pretensions to accuracy, the results were such as to fit equations of types 3.1-4 or 3.1-5 better than type 3.1-7.

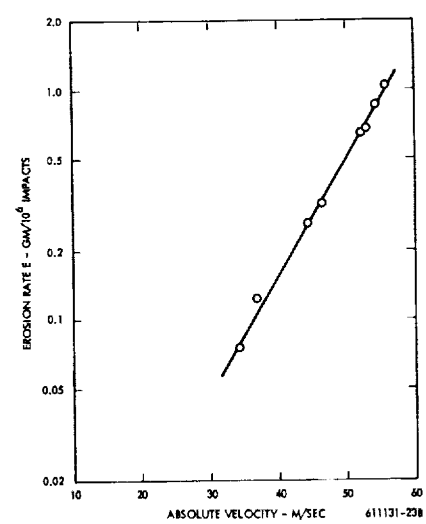

Figure 3.1-23 The Data of Figure 3.1-7b Plotted on Semi-Log Paper

The following equations have been fitted to the data of Reference 1 during these several attempts:

$$E \propto (V-20)^{3.5}$$

$$E \propto (V-25)^{2.6}$$

$$E \propto \frac{V^4}{31} - 1.0 \qquad (16)$$

$$E \propto e^{0.126V}$$

$$E \propto V^6$$

And yet these data are among the better in the literature, in that the velocity range covered was almost 2:1 and there were 8 data points in that range. This, again, demonstrates the (near) futility of applying a purely empirical approach and hoping to deduce therefrom some useful generalizations.

Another set of data covering an even larger velocity range was given by Hobbs in his discussion to a paper by Leith and Thompson[36], although no information was given on the material tested. The data were plotted on linear coordinates, labeled rate of weight loss, mg/sec, and impact velocity, ft/sec. From the units in which the erosion rate is given, one must infer that these data are not rationalized; therefore, the erosion rates should be divided by a factor proportional to the corresponding velocities to put them on a rationalized basis, i.e., on the basis of equal rates of impinging water. The actual data points from Hobbs' graph, and the values of E computed therefrom, are given in Table 3.1-4. The values of E have been plotted on log-log scales in Figure 3.1-24, both against actual velocity V (Curve "a"), and also against $(V-V_c)$ with V_c taken as 270 ft/sec (Curve "b"). Smoothly fitted curves are drawn as solid lines, and straight-line approximations as broken lines. These latter suggest that the results can be represented over a certain range by

$$E \propto V^{4.4}, \text{ or by} \qquad (17)$$
$$E \propto (V-270)^{2.4}$$

TABLE 3.1-4

DATA OF HOBBS IN REFERENCE 36

V ft/sec	Erosion Rate, R gm/sec	Rationalized Rate, E_3 (2×10^3 R/V)	Reduced Velocity (V-270) ft/sec
270	0	0	0
330	0.02	0.122	60
385	0.03	0.156	115
440	0.06	0.272	170
495	0.11	0.444	225
570	0.32	1.12	300
620	0.40	1.29	350
680	0.85	2.50	410
735	1.01	2.75	465
775	1.28	3.30	505
825	1.58	3.83	555

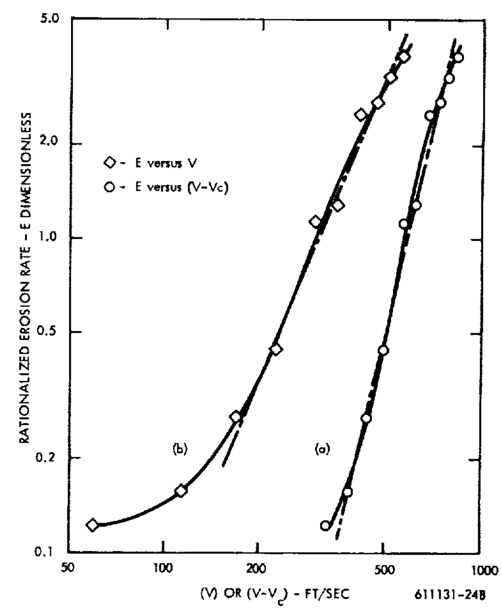

Figure 3.1-24 Data of Hobbs in Reference 36, Plotted both versus V, (Curve "a"), and versus (V-270), (Curve "b")

The latter may result in less scatter, but is valid over a more restricted range. The same data are shown plotted on semi-log coordinates in Figure 3. 1-25. A straight line fits the data well in the lower velocity range, but a distinct breakaway from it occurs at about 700 ft/sec. Thus, these results, too, provide no evidence pointing toward any particular simple type of empirical formulation.

The most comprehensive body of test data recently made available is that of Pearson(8, 10, 12). These data have already been discussed in relation to angle effects in Section 3. 1. 2 and drop size effects in Section 3. 1. 3; in the latter section there was success in collapsing the data for different drop sizes into a single curve by two different methods as shown in Figures 3. 1-13 and 3. 1-14. No actual curves were drawn in those figures so as not to obscure the data points themselves. Curves fitted by hand to these points are shown in Figure 3. 1-26. Curve (a) represents Figure 3. 1-13 and Curve (b) Figure 3. 1-14. The same curves, transposed onto log-log coordinates, are shown in Figure 3. 1-27, and straight lines (dot-dashed) are shown which coincide with the curves

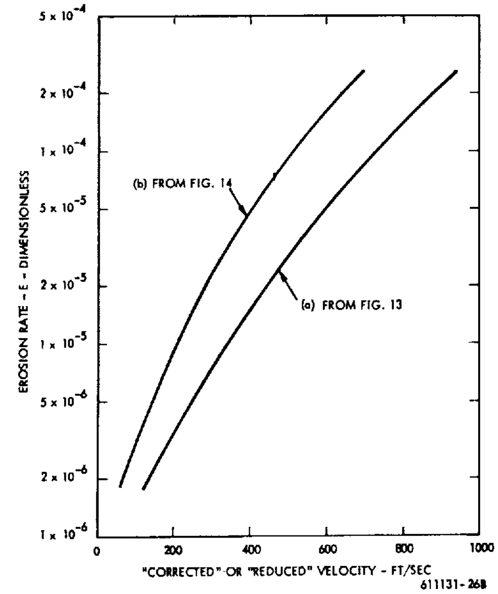

Figure 3. 1-26 Curves Based on the Data Points of Figures 3-1-13 and 14. Original Data from Reference 12

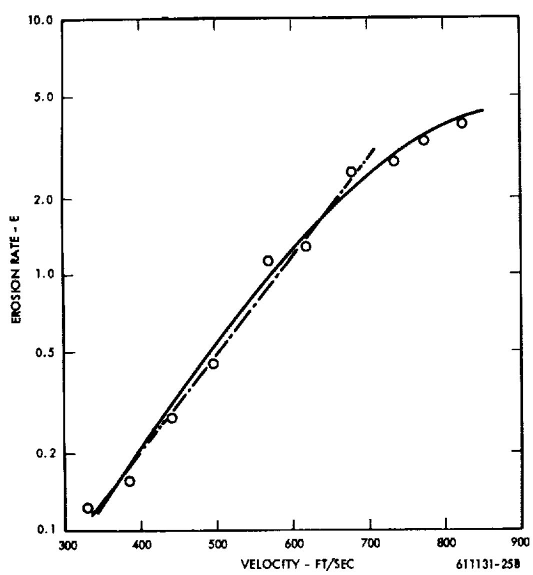

Figure 3. 1-25 Data of Figure 3. 1-24a on Semi-Log Paper

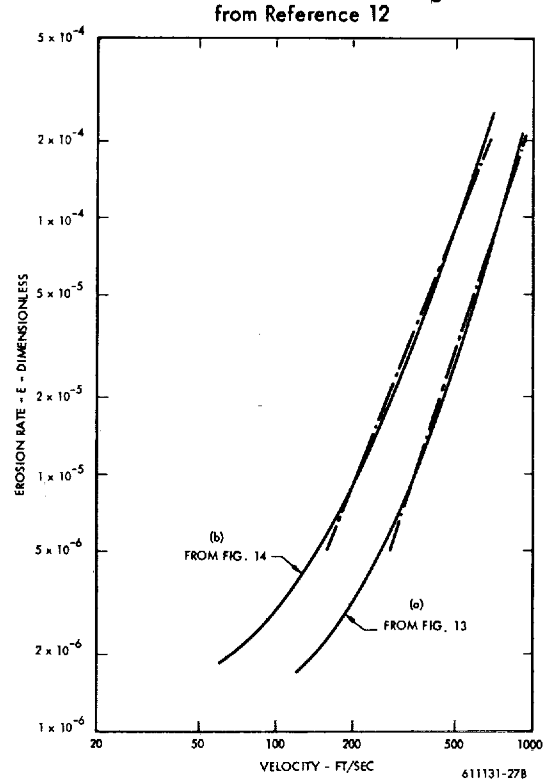

Figure 3. 1-27 Curves of Figure 3. 1-26 on Log-Log Plot

themselves at the values $E = 10^{-5}$ and $E = 10^{-4}$. They are reasonably valid approximations for the range from $E = 5 \times 10^{-6}$ to $E = 2 \times 10^{-4}$. These lines represent relationships as follows:

$$\text{Curve (a):} \quad E \propto (K_c V)^{3.05}$$
$$\text{Curve (b):} \quad E \propto (V - V_{cd}) \qquad (18)$$

where K_c and V_{cd} have been defined in Section 3.1.3 and in Figures 3.1-13 and 3.1-14.

Note that the latter has an exponent fairly close to the expression deduced by Pearson[10] for a single drop size:

$$E \propto (V-390)^{2.6} \qquad (19)$$

Note also that the general appearance of the curves of Figure 3.1-27 is similar to those of Figure 3.1-24 (except for the curvature at the highest velocities), and that the general appearance of those in Figure 3.1-26 is not unlike that of Figure 3.1-25. In particular, Curve 3.1-26a could reasonably be approximated by a straight line below about 600 ft/sec with a breakaway above that. (It must be remembered, however, that in Figure 3.1-25 the horizontal scale is actual velocity, whereas in Figure 3.1-26a it is a "corrected velocity" which is not a linear function of the actual velocity.)

3.1.4.3.3 Conclusions

About the only conclusion which seems justifiable, at this stage, is that even the best available erosion-versus-velocity data do not follow exactly any law such as represented by equations of types 3.1-3 through 3.1-7, but can, over limited ranges, be approximated by any of them. Equations of type 3.1-4 have seemed intuitively to be the most rational and have been adopted by many authors, including Honegger (see Equation 3.1-15), Pearson (Equation 3.1-19), and Fyall, et al[3] who present the following equation for the erosion rate of "perspex":

$$\text{Weight Loss Rate} \propto (V-208)^{3.37}$$

This, however, refers to the velocity of a target within a given rainfall. Thus the rate of water impingement increases linearly with velocity and the rationalized erosion rate would be given by

$$E \propto (V-208)^{2.37} \qquad (20)$$

The preceding comparison of various equations of the form of equation (3.1-4) suggests that when data can be represented in this manner, the value of the exponent will be not too far from 2.5.

Comparison of Figures 3.1-23 through 27 suggests that equations of the form of equation (3.1-7) tend to fit better in the lower velocity region (although there must also be transition to the critical velocity), whereas equations of the form of equation (4) fit best in the intermediate velocity region.

If a direct power law of the form of equation (3.1-3) is used to represent the results, the exponents tend to range from 4 to 6; though for brittle materials, such as glass, exponents as high as 13 have been quoted by Langbein[5].

In no case does it appear justifiable to use any of these curve-fitting equations for the purpose of extrapolating out of the test range.

3.1.5 <u>Dependent Parameters Other Than Rate</u>

3.1.5.1 The Incubation Period

All of the correlations discussed in the previous three sections have related to the slope of the second-stage or steady-state region of the erosion versus time curve, and minor attention has been given to the incubation-period or first-stage of erosion, which may be defined as the duration to the intercept of the steady-state or second-stage erosion line when that is extended to cross the zero-erosion axis. A proper understanding of the effect of velocity, and the other variables discussed, must eventually predict their effect on the incubation period as well as on the subsequent erosion rate, since the incubation period may under some conditions be a substantial portion of the effective life of the component being eroded. Figure 3.1-2 defined the incubation period as the term is used in this section and by the authors cited herein.

Pearson[8, 10, 12] has plotted incubation periods for different velocity drop sizes and impingement angles, and has found more scatter in these data than in the corresponding erosion rate data.
Figure 3.1-28 reproduces this data for different drop sizes in Reference 12, including the average curve drawn by Pearson, because "the amount of scatter . . . obscures the effect of drop diameter." It is nevertheless instructive to draw the best curves for each drop size separately, as is done in Figure 3.1-29, from the data points in Figure 3.1-28. From these points one can see a trend for the curvature of the lines to increase with decreasing drop size; this one would expect if the critical velocity increases with decreasing drop size, since near the critical velocity W_o would tend to infinity. In particular, the 350 micron curve seems consistent with the prediction from Table 3.1-3 that the critical velocity for this drop size is 535 ft/sec.

The simplified fatigue analogy which led to Equation (7) also implies that the incubation period should be proportional, or analogous, to the number of cycles to obtain fatigue failure. Some evidence supporting this has been given by Ripken, et al, 1965[37]. For one material, Ripken has measured the number of impacts corresponding to the incubation period as previously defined, and the resulting impact stress assumed to be given by 1/2 CV. He super-imposed these points on a standard S-N fatigue

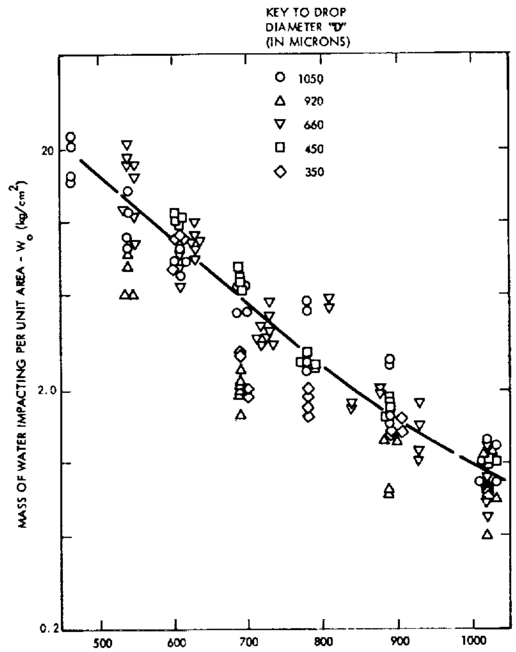

Figure 3.1-28 Rationalized Incubation Periods at Various Drop Diameters and Velocities (Copy of Figure 7 of Reference 12)

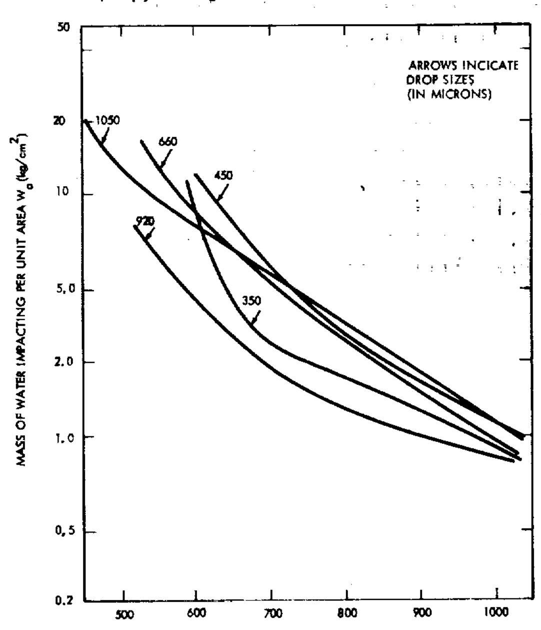

Figure 3.1-29 Individual Curves for Different Drop Sizes, Based on Data Points of Figure 3.1-28.

so-called incubation time. The data on incubation times are too sparse and exhibit too much scatter to allow any conclusions beyond the very broad and obvious one that as the impingement conditions (velocity and drop size) decline toward the threshold value, the incubation time increases.

The erosion rate-time model to be developed, in Section 3.2 of this report, implies that both the incubation time and the maximum erosion rate are strongly influenced by the statistical variations in the sizes and lifetimes of the erosion fragments formed. These, in turn, are influenced by the scatter in drop sizes and velocities as well as the scatter inherent in fatigue properties themselves. Consequently, it suggested that future correlations should be attempted on the basis of the time required to attain specified damage levels rather than on the arbitrarily-defined incubation and rate parameters.

The view that erosion is a form of fatigue leads directly to a number of corollaries:

a) There is little likelihood of finding one specific independently measurable material property which will predict erosion resistance, since none has been found to predict fatigue strength uniquely, and far more research has been done on fatigue than on erosion.

b) In fatigue, the relation between stress and endurance is determined by a test for each material, and cannot be stated in simple analytical form. Similarly, the relation between impact velocity and erosion very likely does not follow any universal law but must be established empirically, perhaps in graphic form, for each material.

c) In erosion, as in fatigue, the condition of the surface is likely to be of considerable importance.

d) Although erosion is the result of many failures, and some of the statistical scatter found in fatigue data may well average out in an erosion test, yet to obtain valid results (or results with calculable confidence limits) many more data points must be taken and many more replications must be run than have been done to date. Related to this is the need, often emphasized in this report, to establish accurately the erosion versus exposure curve, and to carry out all tests to the same degree of cumulative erosion damage if one wants to draw any quantitative comparisons. The amount of testing required and the validity of results should be optimized by proper statistical design of the experiment. This has seldom been done in erosion testing.

A final suggestion to those generating erosion test data is that with the results they should give all the pertinent information--material identification and preparation, physical and mechanical properties, surface preparation, size and shape of specimen, area exposed to erosion, amount of water impinging, and if possible, the drop size or drop size distribution, impact velocity, etc., -- necessary for computing the rationalized erosion and duration parameters and making meaningful correlations between these and the impingement and material parameters.

3.2 THE VARIATION OF EROSION RATE WITH EXPOSURE TIME*

3.2.1 Observed Rate-Time Patterns

The latest literature on the resistance of materials to impingement and cavitation erosion is concerned that the rate of material loss is not uniform in time. While this has been noted for many years, some of its consequences have only lately been emphasized. Thus, as Thiruvengadam and Preiser(50) have pointed out, the comparison of test results can be very misleading if not based on corresponding phases of the rate-time curve; therefore, the rather common practice of the earlier literature, to test all specimens for the same length of time is subject to criticism. The authors of Reference 50 proposed that characteristic erosion-time curves could be described in terms of four zones: an incubation zone with no weight loss, an accumulation zone with loss rate increasing to a peak, an attenuation zone with decreasing loss rate, and finally, a

* F. J. Heymann, Senior Engineer, Development Engineering Department, Westinghouse Steam Divisions, Westinghouse Electric Corp., Lester, Pa.

steady-state zone with constant loss rate, Figure 3.2-1. They do not attempt any detailed explanation of these zones, but suggest that the first three zones are influenced by the initial condition of the surface and that only the final zone is truly characteristic of the material itself and that it should be used for comparison or correlation purposes. This particular suggestion is disputed by Plesset and Devine[51], who showed photographically that in a magnetostrictive oscillator the attenuation zone is associated with a cavitation cloud of much reduced intensity, attributed to hydrodynamic damping effects due to the heavily roughened specimen surface. Moreover, the authors of Reference 51 stated that the accumulation zone and the attenuation zone are connected by a period of essentially uniform high loss rate persisting for some time, rather than by the narrow peak described by Reference 50, and that there is no real indication of any final steady-state zone. (See Figure 3.2-2.) Similar observations have been made bv a number of recent investigators.

Thus, both Hobbs,[38] using a magnetostrictive oscillator cavitation test, and Pearson,[8,12] using a drop impingement erosion rig, have called the region of maximum erosion rate the "steady-state" period, and have based their correlations of erosion with material properties and test conditions (such as oscillation amplitude or impingement velocity) on this maximum loss rate. Both have associated the declining loss-rate of final period with heavy surface damage, as did Reference 51, and feel that it is not a practicable measure of the erosion resistance. This, for practical reasons, has also been the approach adopted in Section 3.1 of this report.

All of the previously mentioned results exhibited what may be called the conventional pattern or some minor variation thereof. (For an actual example, see Figure 3.2-3.) However, there are erosion results which do not follow this pattern at all. Thus, Lichtman, et al,[52] presented loss-time curves many of which exhibit no apparent incubation or acceleration stages, but rather begin with a maximum rate which declines thereafter (See Figure 3.2-4.) These results were obtained in a rotating disc cavitation device.

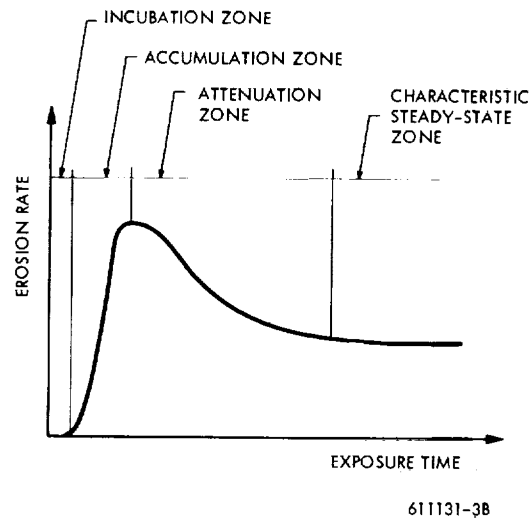

Figure 3.2-1 Characteristic Rate-Time Curve According to Thiruvengadam

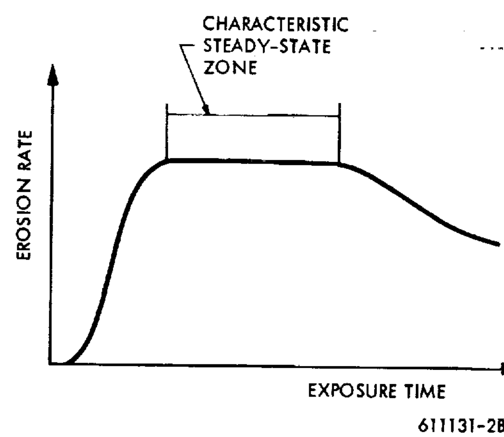

Figure 3.2-2 Characteristic Rate-Time Curve According to Plesset, Hobbs, and Pearson

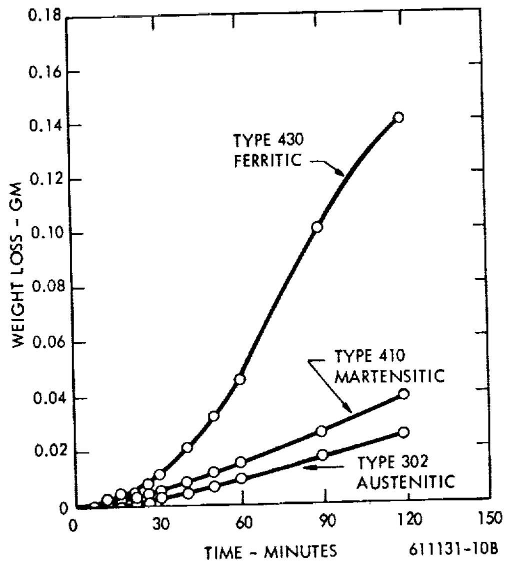

Figure 3.2-3 Typical Cumulative Erosion-Time Curves from Cavitation Tests, Adapted from Figure 7 of Reference 36. (Magnetostriction Device, in Distilled Water)

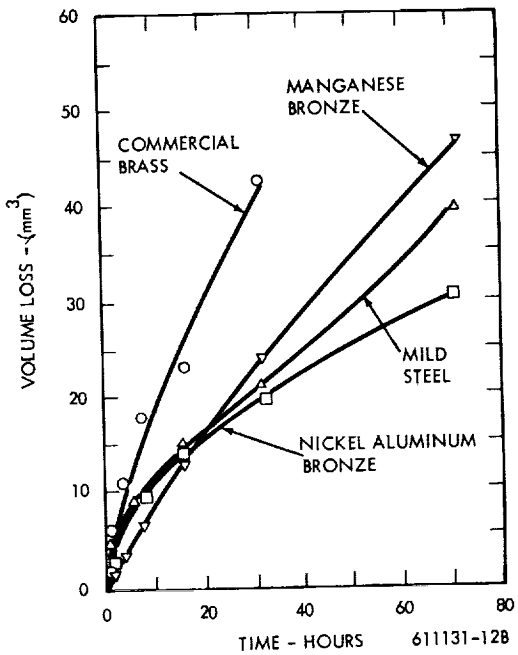

Figure 3.2-4 Cumulative Cavitation Erosion-Time Curves Which Begin at Maximum Rate, Adapted from Figure 24 of Reference 52. (Rotating Disc Device at 150 ft/sec)

Exactly the same type of result has been obtained in the spray impingement erosion test facility at the Westinghouse Steam Divisions Development Laboratory. Erosion rates invariably seem to begin at a maximum value and then decrease - rapidly at first, and then more gradually leading into or approaching a lower steady-state value. Figure 3.2-5 shows some characteristic erosion rate curves obtained by curve fitting through points obtained from several specimens for each material. One might suspect that incubation and acceleration stages lie in the region to the left of the curves as shown, and were simply missed because initial weight loss readings were generally not taken until after about two hours of exposure. To check this, the weight loss of one specimen - a titanium alloy of fairly good erosion resistance - was measured after five minutes of exposure and several more times during the first hour of testing. The result is shown in Figure 3.2-6 and suggests that the erosion rate does in fact begin at a maximum value, or, if there is an

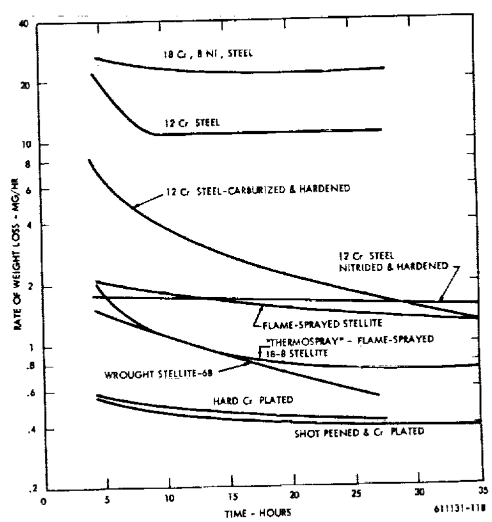

Figure 3.2-5 Typical Erosion Rate-Time Curve Obtained in Westinghouse Steam Division Spray Impingement Facility During 1956-1959

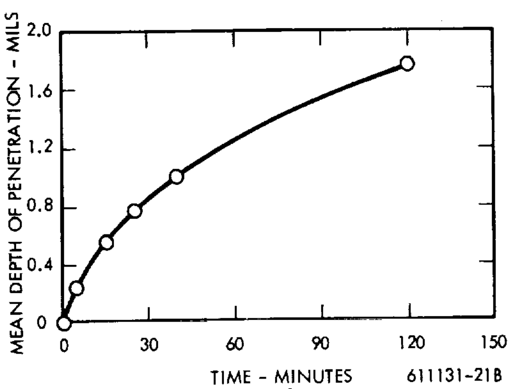

Figure 3.2-6 Early Loss Measurements for a Titanium (6% Al, 4% V) Alloy Tested in the Westinghouse Steam Division Facility)

incubation stage, it occurred within the first minute. The latter alternative is supported by the analytic model to be described. In all of the titanium specimens that were tested the erosion rate has continued to decrease for at least 30 hours. It may, however, be worth noting that Thiruvengadam[28] has shown the rotating disc to be the most intensive cavitation damage device, and that the Westinghouse test facility produces impingement of probably rather small droplets at a high velocity, probably exceeding 2000 ft/sec. Thus, single-impact damage may be occurring in both cases, contributing to the de-emphasis or lack of an incubation period.

The object of this section of the report is to show that a simple statistical model of the erosion process, which regards erosion as a multiplicity of fatigue failures, can predict characteristic rate-time curves of most observed types. Further, this section discusses some of the implications of this model in relation to the measurement and correlation problem.

3.2.2 Effect of Material Removal Mechanisms on Rate-Time Pattern

The spectrum of erosion mechanisms in a ductile material may be divided into several regimes as a function of impact intensity, or in the case of droplet impingement, as a function of impact velocity if drop size is held constant. These regimes merge one into the other; there are no sudden transitions between them.

For very low velocities below some first threshold value, no measurable damage or material loss will occur during any practical exposure time, or material loss is confined to isolated weak spots. Such threshold velocities, empirically deduced from test or operating experience or arbitrarily derived from the endurance limit of the material by some safety factor, have been used as design guides in some phases of steam turbine and condenser design. It is not fully established whether there actually is a velocity below which erosion will never occur: Honegger[2] doubted it; and Vater,[25] who suggested that the dependence of erosion on velocity could be regarded and plotted analogously to the dependence of fatigue life on applied stress, regarded the erosion process as one somewhat similar to corrosion fatigue (in which there is no endurance limit). He, therefore, stated that the threshold velocity has to be defined as that velocity below which no measurable weight loss occurred after some specified number of impacts. In any case, one might say that in this first regime the erosion, if any, corresponds to that in the incubation stage of the conventional rate-time pattern, i.e., it will be low, possibly gradually increasing with some random fluctuations, and will be highly influenced by the initial surface conditions and by the possibility of simultaneous corrosion as shown by Wheeler.[53]

As the velocity exceeds the first threshold, something akin to fatigue failure becomes the predominant failure mechanism. Metallurgical observations substantiating this, and descriptions of the probable sequence of events leading to failure and the formation of loose fragments, have been provided by many investigators including Vater,[25] von Schwartz, et al,[54] Brunton,[10] and Marriott and Rowden.[19]

Some investigators have found more plastic deformation in the surface than might be expected. Thus, Thomas[16] noted small plastic depressions in the surface during the early stages of exposure at velocities whose presumed impact pressures were less than the yield point of the material. Brandenberger and De Haller,[1] on the basis of extensive radiographic studies, concluded that fracture in erosion is neither like static fracture no like fatigue fracture, but is accompanied by a degree of damage to the crystal structure which is intermediate between that associated with those failure modes. It must be remembered, though, that the stress-geometry condition - at least when the surface is still relatively smooth - is not of such a nature as to make static rupture easily possible: thus, the general regime of predominant fatigue or repeated-impact rupture will extend well into the velocity range where each drop could be expected to produce noticeable plastic deformation. As the velocity increases, the regions of plastic deformation presumably spread from the immediate vicinity of the fracture surface toward a general deformation of the eventually-produced erosion fragments. In this regime one may expect to find rate-time curves exhibiting the conventional pattern, i.e., an incubation stage related to the fact that a certain number of impacts are required before fatigue failures occur, an acceleration stage, possibly a steady-state stage, an attenuation stage, and possibly a final steady-state stage, though probably no generalizations should be made about the behavior when gross surface damage has set in. The possibility of relating these phases in the erosion rate-time curve more specifically to the fatigue properties of the material will be explored in the following sections of this report.

A second threshold velocity may be associated with that velocity at which the material loss due to single-impact damage process becomes significant. This is probably related to the visible damage threshold described by DeCorso and Kothmann,[24,43] above which a single impact leaves a distinct crater in a smooth material surface. This regime eventually must merge into the regime of hypervelocity impact. The exact determination of the second threshold velocity from the point of view of material removal is difficult, because in single-impact experiments - such as those performed by DeCorso,[24] and also by Brunton,[10] Engel[39,40] and others - the actual amount of material removed from the surface could not be reliably established, although crater depths or crater profiles were measured. From two curves given in Reference 56, one can deduce that for hypervelocity impact of 1/16 inch diameter aluminum spheres on an aluminum surface, the ratio of target volume loss to crater volume is approximately 0.15 at a velocity of 7 km/sec (23,000 ft/sec), reducing to about 0.09 at 4 km/sec (13,000 ft/sec). One may cautiously infer from this that at the velocities of interest, say 1000-4000 ft/sec, the corresponding ratio will be very much smaller yet. (This inference should be valid qualitatively although the actual material removal mechanism in the hypervelocity regime is a liquid-like flow of the target material accompanied with some splashing out, whereas that in the regime of interest is related to the shear effect of radial outflow.) Of course, this must be balanced by the fact that such loss occurs with each impinging drop, whereas many repeated impacts over some finite area are required to generate one erosion fragment by the fatigue failure mechanism. For any quantitative estimate of the relative significance of the two mechanisms, more data are needed on each.

Qualitatively, one may say that as single-impact erosion becomes significant, the incubation period can no longer be a zero-weight loss period, but rather will begin by exhibiting an erosion rate corresponding to the single-impact erosion. This rate increases in time as additional fatigue-type erosion sets in. Fatigue in this instance probably corresponds more to low-cycle fatigue due to strain cycling than to high-cycle fatigue due to stress-cycling. The geometry of the eroded surface will now be affected by the heavy plastic deformation due to each drop as well as the breaking away of larger erosion fragments due to fatigue fractures. Eventually, as single-impact erosion becomes the predominant mechanism, one would expect to find little or no evidence of any incubation period, and the surface geometry should rapidly approach a steady-state condition, so that one might expect relatively little change of erosion rate with time.

3.2.3 An Analytic Model of the Erosion Rate-Time Relationship

3.2.3.1 Qualitative Description of Proposed Model

As seen in the previous section, the conventional erosion-rate versus time pattern is that associated with a predominant fatigue mechanism for material removal. It is in this regime that most of the test data and the practical experience lie. As is well known, fatigue is intrinsically a statistical process exhibiting a considerable scatter, and this fact will be utilized in developing an analytical model for the erosion rate-time pattern applicable to this regime. The qualitative results have interesting implications with reference to the previously reviewed findings and to previously-attempted correlations between erosion and fatigue data. The approach to be described, though numerical in nature, can at this time predict no more than qualitative trends and should be considered as exploratory.

The basic reasoning of the model is as follows:

It is assumed that each small element of surface is subjected to an impact fatigue environment and that after a certain time (i.e., a certain number of impacts) it will be detached from the surface as an erosion fragment, due to sub-surface fatigue failure. The time-to-failure distribution function for these newly-exposed surfaces will probably not be the same as that for the original surface. Unlike the original surface the newly-exposed surfaces will have been subjected to some sub-surface stress condition even before being exposed to direct impingement, and the surface geometry will no longer be a plane but a series of pits. Further, it is assumed that when many such surface elements are considered, the individual times required for their removal would be described by some statistical distribution function, much as the number of cycles to failure of a large number of fatigue specimens (stressed to the same level) can be described by a distribution function. When erosion fragments are removed and expose fresh surface to impingement attack, the time to remove elements of this new surface will likewise be described by a distribution function, and so on.

In the case of conventional fatigue specimens, the distribution occurs primarily as a result of the statistical nature of the fatigue process itself. In the case of erosion fragments it must ultimately reflect the variations in the concentration and the severity of impacts (i.e., droplet velocities and sizes), variations in the local surface geometry and properties, and variations in the size of fragments formed. At present, however, one arbitrary distribution curve is assumed to represent all of these sources of scatter.

Qualitatively, it can be seen that if these distributions had very little scatter or dispersion, i.e., if the lifetimes of all surface elements were about equal, then the erosion rate would be zero until that lifetime was reached; at this instant a very high rate would be exhibited while all of the original surface flaked off, to be followed by another interval of zero rate until the second layer flaked off, etc.

If, however, these distributions have a significant dispersion, one can predict that this will result in a rate-time curve which up to a first peak looks somewhat like the distribution curve, but in which subsequent peaks and valleys are attenuated and a steady-state rate is approached. An incubation period will exist if the dispersion is not excessive. One might think of the variation in the surface element lifetimes as dispersing the periodicity associated with one layer being removed after another.

The preliminary mathematical formulation and computer program considered one distribution function applicable to the original surface, and one other applicable to each of the subsequently exposed surfaces. Both were specified as normal distributions truncated and normalized over a finite time span. Thus the significant input parameters were the nominal mean lifetime (M_F) and standard deviation (σ_F) for the original surface, and the corresponding values (M_G and σ_G) for the undersurfaces. Figure 3.2-7 shows some rate-time curves obtained by this program, with the distribution parameters as indicated. Note that the attaining of a steady-state rate is hastened both by increasing the dispersion of the functions, and by specifying a shorter mean lifetime for the undersurfaces as compared to the original surface.

Fluctuations such as shown in Figure 3.2-7 have occasionally been observed, as illustrated by Figure 3.2-8 which shows rate-time curves computed from experimental cumulative erosion curves presented by Kent.[57] Moreover, fluctuations which would appear quite prominent in rate-time curves are not nearly as evident if the same data are plotted as cumulative erosion versus time - which is how the data are actually obtained. Therefore, it seems quite conceivable that in many cases such fluctuations would barely have been noted and would have been smoothed out of the raw data, or might have been lost entirely through the data points being too far apart in time.

The fluctuations, however, are by no means an inevitable consequence of this model if non-symmetrical distribution functions are used, as will be seen in the results obtained from the elaborated formulation of the model, described below.

3.2.3.2 Description and Results of Elaborated Model

In the elaborated analysis we have chosen to use log-normal distribution functions, since — as shown by References 58 and 59 — these provide a reasonable representation of fatigue life data. For added flexibility one can adopt a delayed log-normal, i.e., one which would appear as a normal distribution if the frequency of failures were plotted versus log $(t-T_0)$, where T_0 represents a delay time introduced to ensure that no failures occur prior to time $t = T_0$.

The distribution, when plotted on a $\log_{10}$ scale, is then described by its mean (m) and its standard deviation (σ). But one must use the distribution as transformed onto arithmetic or real-time scales. An important point to note is that while in a symmetrical distribution the mean, median, and mode values coincide, that is not true for a skew distribution such as the log-normal. The real-time values

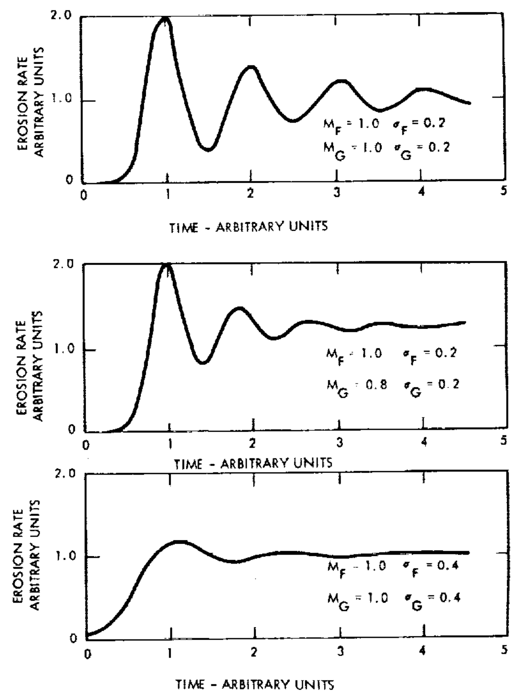

Figure 3.2-7 Typical Computed Erosion Rate-Time Curves from Preliminary Statistical Model, Using Normal Distribution Functions

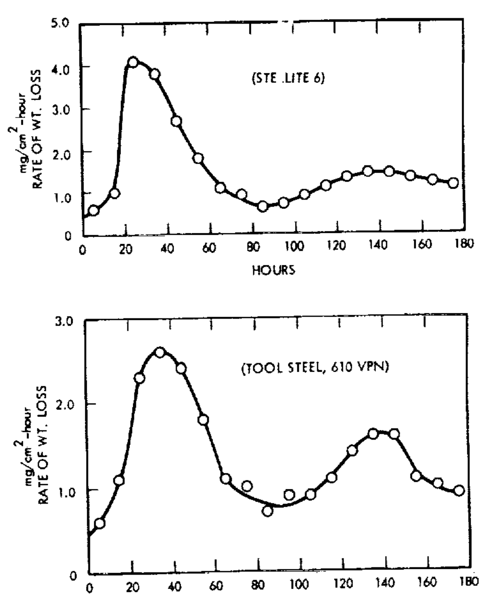

Figure 3.2-8 Experimental Erosion Rate-Time Curves, Computed from Cumulative Erosion Curves Given in Reference 32

corresponding to m, which is denoted by $T_m = 10^m$, establishes the median value of the log-normal distribution — i.e., that value of t at which half of the specimens (or surface elements) will have failed. This is the value generally used to establish a point of an engineering S-N curve. In the delayed log-normal, the median value is given by $M = T_o + T_m$. The mode, or peak in the distribution curves, will occur at a time value less than M. The mean value, or arithmetic average of all life-times, will occur at a time value greater than M, or specifically at a time $E = T_o + T_m \times 10^{1.15\sigma^2}$. For purposes of discussion, all distributions can be characterized by their values of T_o, σ, and either M or E.

The elaborated model permits the specifying of a different distribution function for each level below the original surface, and of two different functions for the original surface: one for the unaffected surface, in which erosion takes place by the initiation of new pits, and one for the affected surface, which is that surrounding existing pits and in which erosion is presumed to take place by the lateral growth of these pits. The program computes the rate of erosion, the cumulative erosion, and the exposed area at each level, from which in turn, it can compute an average surface roughness at selected time points.

The number of variations which could be investigated with this program is unlimited, and all that can be demonstrated here are some of the important effects. The most significant of these is the effect of the dispersion parameter σ. References 49 and 59 suggest that in conventional fatigue tests, σ, on a $\log_{10}$ scale, ranges approximately from 0.15 to 0.40, and for erosion fragment lifetimes even higher dispersions may be expected. Figure 3.2-9 shows computed erosion time curves for various values of σ from 0.15 to 080, with the median (M) held constant; Figure 3.2-10 shows a corresponding set of curves with the mean (E) held constant. In each case $T_o = 0$, and the same distribution is assumed for all surfaces and levels. Since in such cases the eventual steady-state erosion rate must be proportional to the reciprocal of the mean lifetime, all curves in Figure 3.2-10 approach the same steady-state rate.

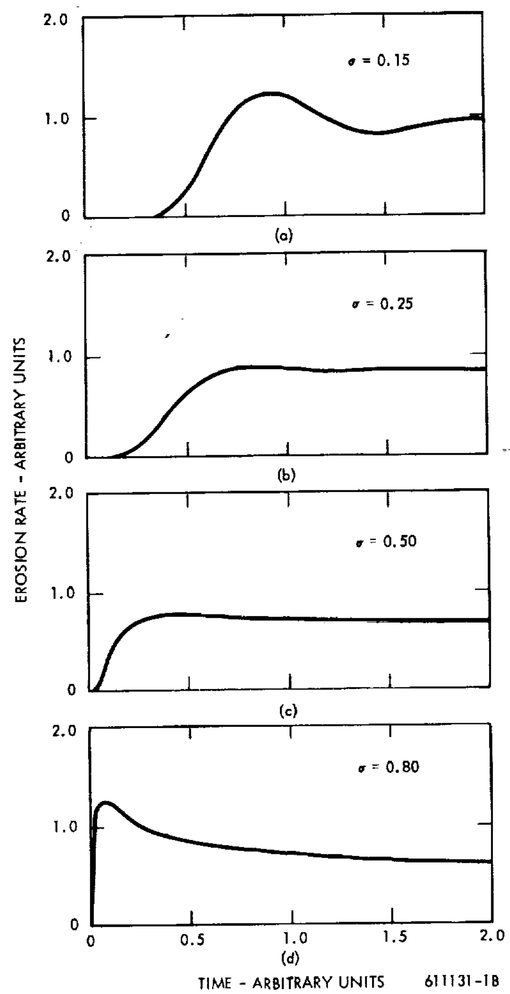

Figure 3.2-9 Computed Rate-Time Curves Based on Log-Normal Distributions, Showing Effect of Varying Dispersion, σ, with Median at Constant, M = 1.0

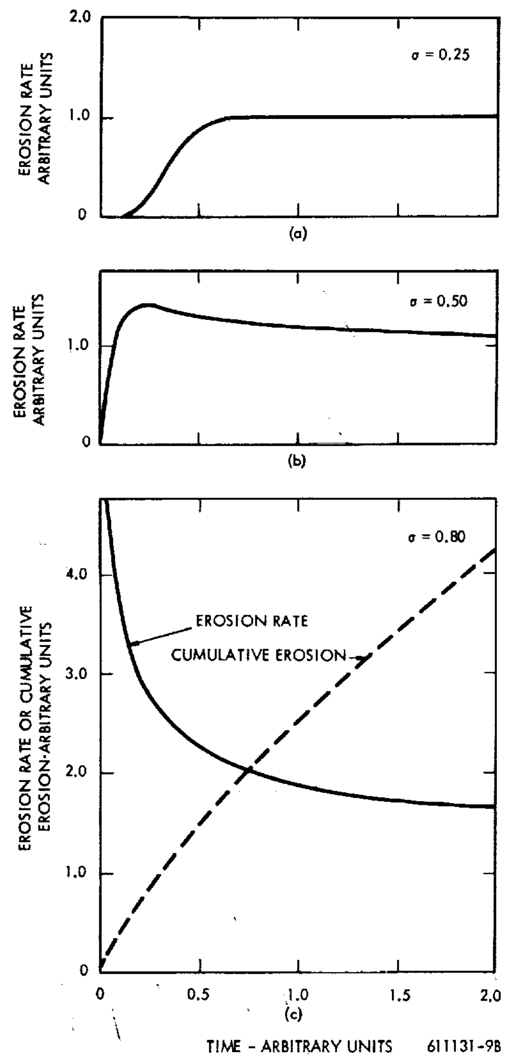

Figure 3.2-10 Computed Curves Based on Log-Normal Distributions, Showing Effect of Varying Dispersion, σ, with Mean at Constant, E = 1.0

Two striking results appear from these curves: First, the maximum erosion rates vary considerably. Second, almost all of the experimentally-found rate-time patterns can be at least qualitatively generated by proper choice of the dispersion parameter σ. When σ is small, the curves exhibit damped fluctuations similar to those of Figure 3.2-7. When σ is increased, the fluctuations die out and the steady-state rate is attained quite quickly. When σ is further increased, a single peak appears in the curve, and at very high values of σ this peak may occur so early that the time resolution is just not fine enough to show the acceleration stage of the rate-time curve, and the curve therefore appears to begin at its maximum value. The same is probably true for experimental data like that of Figures 3.2-4, 5 and 6. It does not seem unreasonable to suppose that erosion due to very small droplets, where each impact stresses only a minute portion of the surface area, would be characterized by a high dispersion in the fragment lifetimes.

In many of the curves of Figures 3.2-9 and 10 the ratio of the erosion peak to the expected steady-state value is not as great as sometimes found in practice — but it should be recognized that at times values greater than the median, the surface has suffered heavy erosion damage and one may therefore expect that geometric effects, such as suggested by References 2, 8, and 51, may have set in by this time and have caused an additional diminution of the erosion rate and possibly suppression of further fluctuations. Certainly one would expect the results predicted by this analysis to be at least modified by the geometric effects. Thus, Figures 3.2-9 and 3.2-10 may correspond to experimental results of the type of Figures 3.2-1 and Figures 3.2-9 and 3.2-10 to results of the type of Figure 3.2-2. It is possible, however, that some appropriate combination of distribution functions for the different surfaces could result in a plateau such as in Figure 3.2-2, which then again would not correspond to a steady-state value.

Figure 3.2-11 shows an example of slowing down the loss rate from the unaffected surface as compared to that of all other surfaces — which are presumed to be more susceptible to erosion because of the irregular geometry. This case is identical to that of Figure 3.2-9 except that for the unaffected surface the median lifetime has been increased to 3.0. Note that the shape of the rate curve has been made more similar to that typified by Figure 3.2-1; the cumulative loss rate is also shown and is quite similar to typical curves such as Figure 3.2-3.

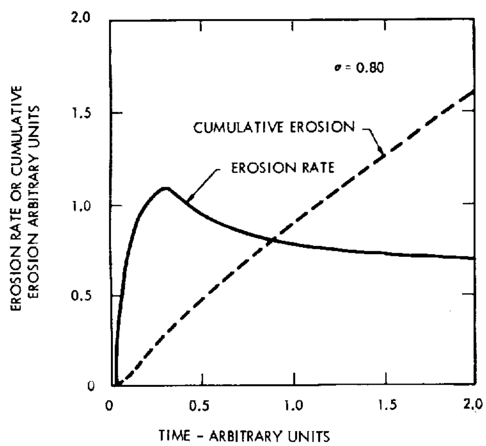

Figure 3.2-11 Effect of Higher Median Value for " Unaffected " Surface ($M_U = 3.0$) than for Other Surfaces ($M = 1.0$). (Compare with Figure 3 2-9 Note Difference in Vertical Scale)

Figure 3.2-12 shows surface profile curves, at various values of time T, for some of the previous cases. The ordinates indicate the surface level, with 0 representing the original surface. The abscissas represent the area not yet eroded away at each level. The difference in abscissa between adjacent levels represents the area exposed at the lower of the two levels. Note that in Figure 3.2-12, a case of low dispersion value ($\sigma = 0.25$), the erosion is shallower and more evenly distributed than

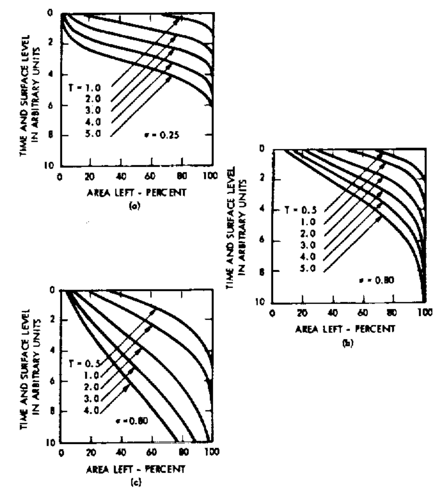

Figure 3.2-12 Examples of Computed "Surface Profile" Curves (Showing the Uneroded Area as a Function of Level Below the Original Surface, at Various Values of Time:

(a) - Corresponding to Figure 3.2-9

(b) - Corresponding to Figure 3.2-11

(c) - Corresponding to Figure 3.2-10

in the other two cases which represent high dispersion values ($\sigma = 0.8$). This suggests that the geometric effects which tend to reduce the erosion rate — i.e., those due to high roughness — are delayed in the former case; this may explain why the maximum erosion rate in such a case may persist for some time and give rise to rate curves typified by Figure 3.2-2. Figure 3.2-13 shows the computed surface roughness versus computed mean depth of penetration, for the same three cases, confirming the lower roughness associated with a lower dispersion value.

3.2.3.3 Discussion and Conclusions

Now to examine the implications of this model with respect to correlations of incubation times and erosion rates. Since the incubation time seems related to the fatigue nature of erosion, several investigators have attempted correlations reflecting this. Thus, Leith and Thompson(36) correlated the incubation times of several materials with the corrosion fatigue limit for 10^7 cycles of these materials.

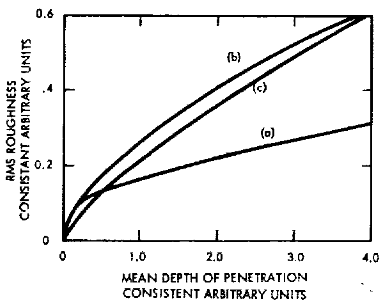

Figure 3.2-13 Computed rms Surface Roughness versus Mean Depth of Penetration (Cumulative Erosion) for Figure 3.2-12. The letters (a) (b) and (c) Correspond to the Similarly-Designated Cases in Figure 3.2-12

Mathieson and Hobbs[60] made a similar correlation with the conventional endurance limit for several aluminum alloys. In both cases the results were reasonably consistent, but the approach is hardly logical since the incubation time in erosion surely should be related to a finite-lifetime to failure, rather than to a stress value at which no failure occurs. Thus, the success of these correlations depended on a second, implicit correlation between the finite fatigue lives at the test stress, and the endurance limits valid for the group of materials compared. Ripken, et al,[37] have used a more logical approach, and have correlated the number of impacts corresponding to the incubation time at a given impact velocity, with the number of cycles to failure in bending fatigue at an equivalent stress level. The stress level was assumed to be given by the waterhammer pressure (ρ CV). The incubation period was defined by the intercept, on the time axis of the cumulative weight loss curve, of the straight line approximating the high erosion rate stage.

If the previously developed model is valid, this procedure is still not quite correct. The statistical model implies that the apparent incubation period depends not only on the mean lifetime of the erosion fragments but also on the scatter or dispersion in these lifetimes. The erosion-rate becomes non-zero when the first element fails, and continues to increase until approximately the mode or most probable value of the lifetime is reached on the top surface. But it is the mean value — which may occur later yet if the distribution is skewed — which corresponds to the nominal lifetime at the appropriate stress as obtained from a conventional S-N fatigue curve. Whether either the median lifetime or the associated scatter in erosion fragments corresponds to that of full-scale bending or pull-type fatigue specimens is at present a moot question. However, the discrepancies in the correlations of Reference 37 are in the direction which the above argument would predict.

If one stipulates a steady-state erosion process, then the erosion rate would certainly be inversely proportional to the mean lifetime of erosion fragments (provided their size distribution remained constant). This is the basis from which one can draw the analogy between the (loss rate)$^{-1}$ versus impact velocity in erosion, and cycles to failure versus stress level in fatigue, as proposed by Reference 25. This appears to provide a rational basis for attempting to predict an erosion-speed relationship on the basis of known fatigue data for the material, although to our knowledge this attempt has not been made. But here, again, the statistical model suggests that the obvious approach is not quite correct. It implies that the maximum erosion rate — which many investigators have linearized and used in correlations, for good and valid practical reasons — does not necessarily represent a steady-state erosion process at all, but rather the deluge of erosion fragments from the top surface layer which takes place in the vicinity of the most probable fragment lifetime from the beginning of exposure. Thus again, the maximum instantaneous erosion rate is not merely a function of the average fatigue life of the surface elements but also of the scatter in lifetimes. Consequently, any external or internal effect which influences that scatter will influence the maximum erosion rate, even though it may not affect the eventual hypothetical steady-state rate.

Finally, what can this model contribute toward the resolution of the dispute referred to in Section 3.2.1. First, it implies that Reference 50 is correct in claiming that the erosion rates during the stages encompassing the first peak in the rate-time curve are not characteristic merely of the material under test, since the shape of this curve depends on the shape of distribution functions which, in turn, depends in part on characteristics of the test method such as the distribution of bubble or droplet sizes, etc. Secondly, it implies that while the erosion rate would, in the absence of other influences tend toward a steady-state value as postulated by Reference 50, this generally occurs only after most of the original surface has eroded away, by which time the surface damage will be so severe as to make the erosion conditions susceptible to geometry effects such as described in Reference 51. In short, the instantaneous erosion rate may never be characteristic of only the material, and for valid correlations it will become necessary to standardize the test method very carefully, or to use properly chosen cumulative erosion measurements, such as the time required to attain some specified value of the rationalized erosion (MDP) of practical significance.

3.2.4 Mathematical Formulation of Model

3.2.4.1 First Simplified Formulation

Let any surface exposed to erosion be thought of as consisting of elementary areas (or volumes, if their thickness is considered) whose lifetimes under the erosion attack can be described by a normalized distribution function f (t). Thus by definition

$$\int_{\infty}^{\infty} f\,(t)\;dt = 1.0 \tag{21}$$

and the distribution function for a specific area A, exposed to erosion from time t = 0, is therefore

$$F_A\,(t) = A\;f\,(t) \tag{22}$$

Since a surface element is lost from the surface when its lifetime is reached, Equation 22 can equally well be regarded as a loss rate function for the area A.

Equation 22 may be further generalized by stating that the loss rate from an area A_1, first exposed to erosion at time $t = T_1$, is thereafter given by

$$F_1\,(t) = A_1\;f\,(t-T_1) \tag{23}$$

Let us now consider the original or top surface of a body exposed to erosion. One may take its area to be unity, and every portion of its area is simultaneously exposed to erosion at time t = 0. Thus f (t) adequately describes the loss rate from the top surface. As surface area is eroded, or lost from the top surface, an equal area is created or exposed at the second level located at distance h below the surface, where h is assumed as the thickness of erosion fragments. For convenience, the thickness h will also be assigned a numerical value of unity on some appropriate scale. In turn, the second level surface will be eroded to expose a third level surface and so on. But in computing the actual loss rates from all of the undersurfaces one must recognize that the lifetimes of surface elements must be measured from the time they were first exposed, and the total loss rate from all surface elements which were first exposed during a time increment dT at time T depends on the total area which was first exposed during that time interval.

Let Y(t) be the total rate of erosion, from all levels, at time t. This is what one desired to compute. But Y(t) is also equal to the rate at which new surface area is exposed, at all levels below the top surface, at time t. (Strictly speaking, it is proportional to it, but with h = 1.0 it is numerically equal.)

Thus, the total surface area first exposed during increment dT at time T, is Y(T) dT, and the loss rate from this area at time t is, by Equation 23,

$$F_T\,(t) = f\,(t-T)\;Y(T)\;dT \tag{24}$$

The total loss rate at time t, from all undersurfaces, is composed of contributions from all undersurface areas first exposed during all time increments from T = 0 to T = t, or

$$\int_0^t f\,(t-T)\;\;Y(T)\,dT$$

The total loss rate or erosion rate, $Y(t)$, is the sum of that from the top surface and that contributed by all undersurfaces, or

$$Y(t) = f(t) + \int_0^t f(t-T)\ Y(T)\ dT \tag{25}$$

The fact that the contributions from the undersurfaces and from the top surface form two distinct terms in Equation 25 makes it convenient to assign a different distribution function for the top surfaces as compared to all undersurfaces. This is desirable if one wants to reflect the fact that the tip surface has, in many ways, a different nature and history than the undersurfaces exposed as a result of erosion. Finally, one can state

$$Y(t) = f(t) + \int_0^t g(t-T)\ Y(T)\ dT \tag{26}$$

where

$f(t)$ = distribution function for top surface
$g(t)$ = distribution function for undersurfaces

It is worth noting that Equation 26 is a well-known integral equation having a convolution integral as its last term. A Laplace transformation yields

$$y(s) = f(s) + g(s)\ y(s)$$

By ordinary algebra

$$y(s) = f(s) \Big/ \left[1 - g(s)\right] \tag{27}$$

or

$$Y(t) = L^{-1} \left\{ f(s) \Big/ \left[1 - g(s)\right] \right\} \tag{28}$$

This solution may be useful if Equation 26 has Laplace transform and Equation 27 has an easy inverse transform. Ordinarily, numerical methods are required.

For the initial explorations Equation 26 was computer-programmed directly, using normal distributions for functions $f(t)$ and $g(t)$, normalized over specified time spans rather than between the limits of plus and minus infinity as suggested by Equation 21.

3.2.4.2 Formulation of Elaborated Model

In further explorations of this approach, it is desirable not only to keep track of the area exposed at each level as a function of time, so that an average surface profile or surface roughness can be computed, but it also may be desirable to assign different distribution functions for all levels. An analytical continuity approach to this becomes very cumbersome, and since the final evaluation is in any case a numerical one by computer, it becomes advantageous to develop the model as a step-wise process in time, and to have the computer program compute the processes occurring in each time interval, one after the other. In a sense, the computer program becomes a digitalized analog of the physical process.

The crux of the approach is that the program maintains, and up-dates for each time interval, the array $S_{L,J}$, in which each value represents the surface area presently existing at level L and dating back to time interval J during which it was first exposed as a result of loss from the next-higher level. Thus the total surface area presently existing at level L would be given by

$$\sum_{J=1}^{N-1} S_{L,J}, \text{ where N is the present time interval}$$

at which the evaluating is being done.

Let us now define a modified rate or quotient function $q(t)$, which represents the loss rate as a proportion of the remaining area at time t. In terms of the previously used distribution function $f(t)$, this is

$$q(t) = \frac{f(t)}{1.0 - \int_0^t f(t)\ dt} \tag{29}$$

For computation purposes the continuous function $q(t)$ is replaced by a loss quotient Q_I representing the finite amount of loss during the I^{th} time interval after the surface has first been exposed. This can be represented by

$$Q_I = q(I\Delta t)\quad \Delta t$$

where Δt is the length of a time interval. The program computes and stores all values of $Q_{L,J}$, where the additional subscript L refers to the level; thus a different distribution function f(t) can be specified for each level.

The total erosion from all levels during time interval N, Y_N, will then be composed of all contributions of the type

$$R_{L,J} = S_{L,J}\, Q_{L,N-J} \tag{30}$$

where $R_{L,J}$ represents the loss rate from that area at level L which was first created during time interval J. The total erosion rate is therefore approximated by

$$Y_N = \frac{\sum_{L=L}^{M} h_L \sum_{J=1}^{N-1} R_{L,J}}{\Delta t} \tag{31}$$

where h_L = thickness of erosion fragments lost from the L^{th} level
M = total number of levels considered

Using the $R_{L,J}$ values computed from the $S_{L,J}$ array which was valid for the beginning of the N^{th} time interval, one can readily compute the new values of $S_{L,J}$ which are valid for the end of the N^{th} interval, i.e., for the beginning of the (N + 1)th interval:

$$\left[S_{L,J}\right]_{N+1} = \left[S_{L,J}\right]_N - \left[R_{L,J}\right]_N \tag{32a}$$

for all values of $J < N$, and

$$\left[S_{L,N}\right]_{N+1} = \left[\sum_{J=1}^{N-1} R_{L-1,J}\right]_N \tag{32b}$$

for $J = N$.

The manner in which the cumulative erosion, surface profile and surface roughness can be computed from the above-mentioned quantities is straightforward.

The log-normal frequency distribution function as programmed is of the form

$$f(t) = \frac{1}{\sigma(t-T_o)\sqrt{2\pi}} \exp\left\{\frac{-\left[\log_e(t-T_o)-m\right]^2}{2\sigma^2}\right\} \tag{33}$$

This function has the following properties:

The mean, or expected value, is

$$E = T_o + e^{m+(1/2)\sigma^2} \tag{34}$$

The median value is

$$M = T_o + e^m \tag{35}$$

The mode, or most probable value, is

$$P = T_o + e^{m-\sigma^2} \tag{36}$$

The input may be prescribed in terms of T_o, m, and σ directly; the latter two may also be prescribed in terms of the equivalent logarithms to base 10, or in terms of the equivalent real-time quantities $T_m = e^m$ and $R = e^\sigma$.

3.2.4.3 Discrete Pit Formation and "Affected" Surface

In order to model the probable progress of erosion damage more faithfully, a further elaboration has been introduced for the top surface only. This is based on the observation that erosion tends to proceed by the formation and growth of discrete pits — which may extend to a considerable depth while the adjacent top surface is still intact - rather than by a randomly-distributed depth.

To approach this condition, the top surface is considered as consisting of two kinds of surface: affected areas and unaffected areas. Affected areas are defined as those areas of the top surface immediately surrounding existing erosion pits, whose resistance to erosion may be assumed to be influenced by this fact. Therefore, one distribution function, $f_a(t)$, is provided for the affected area, and another, $f_u(t)$ for the unaffected area which is the remainder of the still existing top surface. (In general one would suppose that f_a is such as to result in more rapid erosion than f_u, but the program does not make this a requirement.) The actual amount of area considered as affected is computed as follows: Let w be a characteristic dimension of erosion fragments which must be prescribed in the program input. Then the affected area A_a associated with a pit of surface area A_p is defined as the area of an annulus of width w surrounding a circle of area A_p. In other words, all of the potential erosion fragments bounding upon an existing pit are considered affected area. To carry this calculation through, it is necessary to know the number and size distribution of all pits. This is done as follows: During any time interval N, the loss from the existing unaffected surface, based on the f_u distribution function, is divided into an integral number of values A_o (where A_o is the area of a circle of diameter w). Thus a known number of new pits — all of area A_o — are said to be initiated. For the subsequent time interval, the new pits are assigned their annulus of affected area. Further enlargement of each of this generation of pits takes place by erosion from the affected area surrounding it, requiring the transformation of additional surrounding area to maintain the previously specifiec relationship between affected area and pit area. Thus, the number and present size of each generation of pits, and extent of affected area surrounding them, can be established and updated.

The rate of loss from the affected areas is based on the f_a distribution function, but not in a simple manner. Let us for the moment talk in terms of the continuous functions, though the actual calculations are carried through in terms of stepwise loss quotients. Consider an area which existed as unaffected area until time T_T, at which time it becomes transformed into affected area. Up until T_T the loss from this area was governed by f_u; henceforth, it is to be governed by f_a. Upon reflection it can be seen that our purpose would not be served in any realistic way by simply saying that at $t = T_T$ the loss rate jumps from $f_u(T_T)$ to $f_a(T_T)$, and henceforth is given by $f_a(t)$. (In an extreme case, $f_a(t)$ may represent such rapid erosion that T_T is well beyond the mean or mode value and $f_a(T_T)$ is already sensibly zero. Thus no further erosion, rather than more rapid erosion, would result from this switch.) A wholly rigorous approach would have to be based on cumulative fatigue damage theory, but a device which is adequate for our purpose is to require that the f_a distribution function be entered at an effective time T_E, such that the cumulative loss due to f_a at T_E is equal to the cumulative loss due to f_u at T_T, or

$$\int_0^{T_E} f_a(T)dT = \int^{T_T} f_u(T)dT \qquad (37)$$

If T_E is defined by Equation 37, then the loss rate from the area under consideration, at any time t subsequent to $t = T_T$, is given by $f_a(t - T_T + T_E)$. This device will at least ensure that if a given area is transformed at any time T_T whatever, then 100 percent of it -- no more and no less -- will have been lost at time $t = \infty$, which is the minimum logical requirement of any realistic approach. For some types of distribution functions, it is possible to express T_E in terms of T_T and the function constants. Thus, for the simple case of (normalized) exponential functions, where

$$f_u(t) = p_u e^{-p_u t} \text{ and } f_a(t) = p_a e^{-p_a t}$$

It is easy to show that

$$T_E = T_T (p_a/p_u)$$

An analytical expression can also be obtained for the log-normal distribution, but in many other cases, including the normal distribution, T_E would have to be computed by trial-and-error procedures from the relationship of Equation 37.

A consequence of this approach is that not only must the total affected area associated with each generation of pits be known, but so must each generation of affected area, since the rate of loss from any portion of the affected area depends on when it had been transformed from the unaffected to affected status. The number of pertinent computations required during the N^{th} time interval is therefore N^2, and the number of memory locations required for the affected area array is M^2, where M is the maximum number of time intervals to be computed. This is a compelling argument for making M reasonably small (100 in our program), which makes for a rather coarser time grid than one would otherwise desire.

The details of the computation method would require too much space to present here, but are generally analogous to the method described for the undersurfaces by Equations 30 through 32.

It should be emphasized merely that the concept of erosion by discrete particles of specified size is applied only to the initiation of new pits in the unaffected surface, and that the loss rates from the second and lower layers do not concern themselves with whether the second layer surface was exposed as a result of loss from unaffected or affected surface. This distinction is only made for the loss rates from the top surface itself.

The program in its present form has provision for using either log-normal distributions (to represent fatigue damage), or exponential distributions (to represent single-impact damage).

3.3 HYDRODYNAMIC MODEL OF CORRELATION OF METAL REMOVAL RATES FROM REPETITIVE DROP IMPACT *

3.3.1 Background

This section establishes numerical relationships between materials properties and the external variables and drop impingement loss rates. This is done through the use of a hydrodynamic model of correlation of metal removal rates from repetitive drop impacts applied to empirical information. This empirical information is that on metal removal by water drops impacting on steam turbine blade materials made available by the Central Electricity Generating Board (CEGB) of the United Kingdon[61, 62].

The CEGB results are from multiple impact tests. In these tests, samples of metals to be eroded are mounted around the rim of a wheel. Once each revolution of the wheel, each sample intersects a curtain of water drops of relatively uniform size at a known relative velocity. It seems likely that after a small number of impacts the water wets the sample and a film of water develops on the surface. In principle, this can change the maximum impact pressure and duration of impact from that resulting from the impact of a water drop on a dry surface.

Many have objected to this hypothesis on the basis that this is contrary to their experience with splashing water. They say splashing water does not form thin films, it runs from surfaces as drops or rivulets. However, this drop-rivulet behavior is probably true for contaminated surfaces. The contaminated surface is the type ordinarily seen, even if the contamination is only from fingerprints. In this connection it has been pointed out, to the author, by A. P. Fraas[63] that it is next to impossible to maintain dropwise-condensation in condensing water systems for useful lengths of times. The scrubbing action of the condensing water removes the surface contaminants and the process changes from drop-type condensation to film condensation. The scrubbing should be even more thorough in a repetitive drop impact situation. Therefore, observation of water runoff from casually prepared fresh surfaces is likely to be completely misleading as to the nature of this runoff after many impacts.

The basic approach used is that of dimensional analysis. The virtue of dimensionless analysis is its mathematical simplicity. The drawback is that its use to correlate data is valid only where it is reasonably sure the data exhibit similitude over the range of the data and the pertinent variables are known.

In the area of drop impact erosion there is very little in the way of established definitions, conventions, or theories by which conditions of similitude or selection of pertinent variables can be established. For this reason, the bulk of this section is concerned with establishing a reasonable presumption that the variables selected are the pertinent ones and that a condition of similitude exists between the correlated data.

3.3.2 Review of Some Observations on Drop Impact Material Removal

3.3.2.1 Single Impact Removal

As has been pointed out by several investigators[64, 65], there are at least two mechanisms of material removal operative during single liquid impact on metal surfaces. The first of these is the loss of material as the direct result of a hammer blow of a liquid drop or jet on the solid surface. The

* W. D. Pouchot, Advisory Engineer, Systems and Technology Dept., Astronuclear Laboratory, Westinghouse Electric Corp.

second is that small projections of metal are removed by the fluid squirting out of the region of liquid compression created and maintained momentarily by the liquid-solid impact. For the first of these mechanisms, at least for single impact damage, there is much evidence that the extent of the damage is directly proportional to the size of the drop or jet causing the damage (64, 66). There is more limited evidence that the same is true for single-impact lateral outflow damage (65) as well. It may be concluded from experimental evidence, that the damage done by single liquid impacts on dry metal surfaces is proportionally the same for small and large drops. De Corso and Kothman (66) in reporting results of their single-impact tests conclude that larger jets require a lower impact velocity than smaller jets to cause visible damage. Their data were taken at velocities greatly above a visibility threshold. The data also have a large scatter. Extrapolation of this data back to a visible threshold is a very doubtful procedure. In at least one of these cases such extrapolation will lead to a conclusion opposite to the one drawn.

- A General Description After Hancox and Brunton (65)

With multiple impact metal removal as with single impact metal material removal, there is loss of material as a result of the lateral flow of liquid along the surface of the liquid compressed by the primary impact. Paraphrasing Hancox and Brunton, erosion of metals begins with a roughening of the surface due to the appearance of small surface depressions and tilted grains. The larger projections in the roughened surface are later sheared by the flow to give surface pits. The pits grow and erosion continues either by a ductile tearing action or by the propagation of brittle fractures from the bottom of the pits. The erosion of metals depends entirely on the initial formation of small regions of plastic deformation. If a metal surface can be kept smooth by preventing roughening due to depressions and grain boundaries, then erosive action due to outward flow cannot take place. It seems, however, that in plastically deforming materials a few areas can be deformed at stress levels considerably below the average flow stress. As soon as this happens, the change in the shape of the surface leads to stress concentration at projections and depressions, the impact stresses increase, and ductile or brittle fracture brings about erosion. The final stage of erosion in metals is the growth of pits throughout the specimen -- a stage which is accompanied by appreciable weight loss. In metals prone to brittle fracture there is the formation of a network of cracks which fan out from the initial pits. With more ductile metal erosion proceeds by shear fractures in the metal around the pits.

The author interprets these preceding statements of Hancox and Brunton as saying that (1) the initial deformations which lead to erosion are caused by the primary impact of the drops working on weak spots in the surface, but (2) the major source of actual material removal is the secondary impacts from the outflow liquid working on the deformations produced by the primary impact.

- The Stages of Erosion as Defined by Pearson (67)

Usually there are several stages of erosion evidenced in multiple impact erosion tests carried out at constant liquid impingement rates, impinging drop diameter, and normal velocity of impingement. These are illustrated in Figure 3.3-1 and are as follows: (1) an incubation period during which the surface is deformed but there is no metal loss from the surface, (2) a period when surface metal loss rises rapidly to a maximum, (3) a period of maximum metal loss rate, and (4) a period when the metal loss rate falls toward or oscillates about an apparent steady-state value.

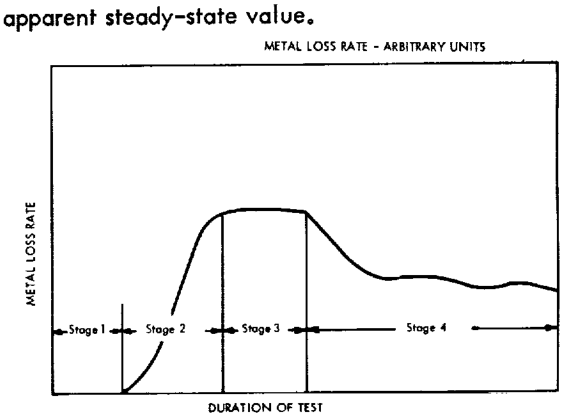

Figure 3.3-1 Model of Stages of Erosion After Pearson

- CEGB Data

The most extensive tabulations from the CEGB on material removal from steam turbine blade metals by impinging water drops record only the incubation period (stage 1) and the maximum rate of erosion (stage 3). Pearson[67] of the CEGB has examined and reported on an extensive set of these experiments carried out using a 12 percent chrome stainless steel.

The stage 1 stainless steel data is shown in Figure 3.3-2. This is a plot of the measured amount of impacting water per unit area required to incubate erosion at various normal impact velocities using a succession of constant diameter drops of the diameters indicated in the figure.

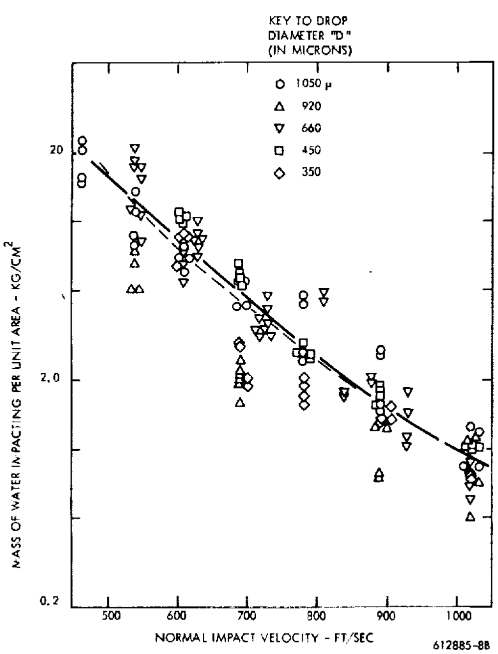

Figure 3.3-2 CEGB 12% Chrome Incubation (Stage 1) Data

The data scatter considerably. It has been noted by Heymann, in section 3.1, that there is no apparent trend to the data with respect to the diameter of drops impacted except at the lower limit of the test range of normal impact velocity.

For both jet impact and drop impact tests, if it is assumed that the duration of an individual impact is directly proportional to jet or drop diameter; the total impulse per unit area to which a particular surface location is subjected can be expressed as:

$$\Sigma p_i t_i :: p_i D N_i$$

It may also be noted that the mass of water impacted on a particular site per unit area has the same proportionality as Σt_i :

for drops

$$m/A :: \frac{D^3 N_i}{D^2} :: D N_i$$

for cylindrical jets

$$m/A :: \frac{D^3 L N_i}{D L} :: D N_i$$

That is, the measurement of the mass of water impacted per unit area to incubate erosion is a direct measure of the total impulse per unit area to incubate erosion at constant impact pressure. Therefore, since the stainless steel data, as plotted in Figure 3.3-2, does not evidence any consistent trend with drop diameter over most of the test range of normal impact velocities, it suggests that the important parameter during stage 1 erosion is the total impulse per unit area and not the number of blows per unit area. This is interpreted to mean that the end of the incubation period is signaled by a buildup to a certain level of permanent strain and that it is unimportant whether this strain is occasioned by many little blows or a few big ones. This conclusion also seems consistent with the previously paraphrased Hancox and Brunton description of surface distortions during stage 1 of erosion.

The stage 3 stainless steel erosion data of Pearson(67) is shown in Figure 3.3-3.* The marked separation of that data by drop diameter is quite apparent. Pearson found that the data could be correlated by an equation of the form:

$$\frac{m_m}{m_\ell} :: (U \sin\theta - U_{cd})^n \operatorname{cosec}\theta$$

Heymann in Section 3.1 showed that for Pearson's data:

$$U_{cd} :: \frac{1}{\sqrt{d}}$$

As stated by Pearson, since all the testing was carried out above the apparent threshold velocity, U_{cd} is only a convenient mathematical parameter and may not represent an absolute lower limit on normal impact velocity to cause erosion.

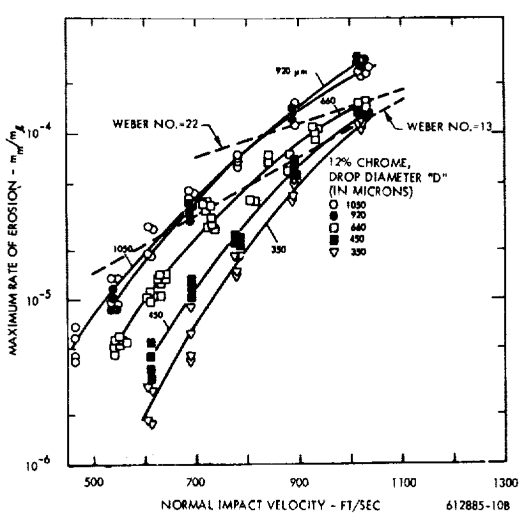

Figure 3.3-3 Stage 3 Erosion of 12% Chrome Steel (CEGB Data)

* The Weber No. lines will be discussed later.

In correlating the CEGB data on a hydrodynamic basis, it is important that there be similarity of eroded surface at corresponding points in the erosion cycle. This is what the CEGB found. Quoting from Reference 61, "In general, the topographical examination (of the eroded stainless steel) showed the following features:

a) The average distance between adjacent peaks in the surface increases as the mass loss increases. This is probably associated with the intersection of widening pits which tends to eliminate, progressively, the narrowest of the escarpments remaining between them.

b) Within the duration of the longest tests carried out, the average depth of the erosion pits continually increases.

c) There is no observable topographical difference between specimens which have suffered the same mass loss produced by water droplets of the same size but different impact velocities.

d) For corresponding positions on the curves of mass loss against mass of impacting water, the coarseness of the surface increases with drop size and the distance between adjacent erosion peaks is proportional to, and of the same order as, the droplet diameter."

3.3.3 Possible Reasons For Drop Size Effects

That Erosion Rates are drop diameter sensitive and that the erosion peaks and valleys are proportional to drop diameter has been noted by others (68, 69, 70), in addition to the CEGB. Various explanations of the drop diameter effect on erosion rates have been offered. Some of these are: (1) increase in local material fatigue limit as effective impact lengths become smaller with smaller drops as suggested by Heymann in Section 3.1, (2) smaller drops create more surface area per unit volume of material removed than do larger drops and it has been suggested that this means that more energy is required per volume of material removed with small drops than large drops (70), (3) smaller drops are more easily deflected by gas forces before impact than larger drops and therefore do not hit with as high an actual normal impact velocity, (4) the impacting drops become unstable aerodynamically and start to break up before impact, and (5) the test samples retain a film of water which attenuates the blow from smaller drops more than that of larger drops.

3.3.3.1 Size Effects in Fatigue Failure

Size effects in fatigue failure as related to multiple-impact erosion have been discussed in Section 3.1. In this discussion Heymann concludes after Peterson that for fatigue failure to occur the endurance limit must be exceeded not merely at a point or line but across a dimension which is on the order of 50 to 75 microns. Heymann then goes on to point out that, for an impact of a spherical drop or sideways impact of a cylindrical jet the impacted cross-sectional length is only a fraction of the projected drop cross-sectional length during the time of peak pressure. Hence, for drops of small effective impact length (less than 50 to 75 microns), an apparent increased erosion resistance of the material would be observed.

Some measure of the ratio of this effective impact length for dry surfaces can be obtained by reference to the work of Hancox and Brunton (65). These investigators impacted jets of mercury on polymethyl methacrylate specimens. They found values of interface angle β where vigorous outflow begins (see nomenclature for definition of β) as given in Table 3.3-1.

TABLE 3.3-1

VALUES OF THE INTERFACE ANGLE β FOR WHICH FLOW FIRST DEFORMS THE SURFACE

Jet Diameter (mm)	Velocity of Impact (m/s)	Angle
Mercury Jet 1	183	17° 15'
	169	16° 45'
	154	17° 0'
	152	16° 45'

Making the logical conclusion that there cannot be much release of impact pressure until there is substantial lateral liquid flow, the effective impact length must be on the order of 0.3 times the projected impacting jet diameter or larger. This value should also be a measure of the effective length ratio in drops impacted normal to a surface since the impact is axisymmetric. If this 0.3 value is applied to the drop diameters of the CEGB data (Figure 3.3-3), all effective length values are greater than 75 microns, some considerably so. It seems unlikely, that a material size effect is an adequate explanation of the evidenced drop size effect in terms of impacts on dry surfaces.

As seen by Table 3.3-1, Hancox and Brunton found that the angle β at which vigorous outflow began in their tests was about 17 degrees. They point out, from elementary considerations, that such outflow should have begun when the lateral velocity of impact of the jet on the solid surface fell below the compression wave velocity in the liquid. From geometric considerations, Hancox and Brunton find that the theoretical angle β is given by

$$\beta = \sin^{-1}\left(\frac{U_n}{C}\right)$$

where C is the compression wave velocity in the liquid, and U_n is the normal impact velocity.

As seen in Table 3.3-1, Hancox and Brunton found no such velocity dependence for β. In addition, the theoretical value of β is, in all cases, much less than the observed value. They attribute the observed delay in outflow to friction at the solid surface. (It should also be noted, however, that a jet is not necessarily a cylindrical object but may be varicose. In this case, the actual effective diameter of the jet might be considerably greater than the cylinder from which it originated. Hancox and Brunton's measurements may be misleading.) This is interpreted here to mean that vigorous outflow is delayed until the effective depth of compressed liquid is large enough for the dynamic forces to swamp the viscous forces.

A liquid film over the impact surface will give a lubricating effect such that lateral outflow (release of peak impact pressure) can begin much sooner than for a dry surface. In correlating the CEGB data, the assumption is made that such a film existed on the CEGB test pieces and that the angle β is a function of U_n/C.

Perhaps the most telling reason, however, for supposing that local material effects do not explain the drop diameter effect is that the dimensions of the peaks and valleys of the eroded surface are characteristically proportional to the drop size. It seems unlikely that such behavior would be observed if local material factors are a dominant influence. It seems likely that the area of impact of even smallest drops used by the CEGB is too great to bring local material strengthening factors into prominence.

3.3.3.2 Surface Area Effect

If the sizes of the peaks and valleys in an eroded surface are proportional to the diameter of the drops impinging, then more surface area is created per volume of metal removed with small drops than large drops. It has been argued that this greater surface to volume ratio of small versus large drops implies a greater energy requirement of small drops to remove the same volume of material as large drops. For this argument to be valid, erosion of metals would have to be a two-dimensional skin effect like atomization of liquid where the new surface is created by stretching the old surface and

$$E = \sigma(\Delta A)$$

All reported observations reviewed by this author clearly indicated that new surface is produced during erosion, not by stretching of old surface but by breakage of solid material. A stress level is, therefore, the appropriate strength of materials criterion. By the logic of dimensions then:

$$E = SV$$

or the energy of creation of new surface is proportional to the volume of material removed. The energy per unit volume removed is the same whether the removal is by many small pieces or a few big pieces.

3.3.3.3 Hydrodynamic Effects

In the CEGB tests, deflection of the smaller drops relative to the larger drops can almost certainly be ruled out. The CEGB could observe the impact of the drops and in fact had to make substantial modifications in the rig as originally designed to remove such deflections[71].

However, the impinging drops might have been aerodynamically unstable. It takes a finite time for a drop to disrupt even when unstable. For a considerable portion of that time period, it is difficult to observe any marked distortions indicating that the drop is in the process of disruption[72]. Assuming that the velocity of the vapor at the radius of the target in the CEGB apparatus was the same as the target velocity, calculations of drop Weber Number during the CEGB tests have been carried out, using Gardner's[73] (or if you prefer Hinze's [74]) water drop instability range of Weber Number 13 $\longleftrightarrow$ 22. These lines are plotted on Figure 3.3-3. The author interprets this range as: We < 13 - drops almost certainly stable, We > 22 - drops almost certainly unstable. From this it would appear that for most, but not all, of Figure 3.3-3 the impacting drops were aerodynamically stable. The 1050 and 920 micron drops may have been breaking up before impact at the higher test velocities. This may explain the crossover anomaly in the data.

If the drop diameter effects evident in the CEGB data for stage 3 erosion are not numerically feasible, in terms of local materials effects or aerodynamic effects before impact, they must be caused by the hydrodynamics of the impact itself. These might be due to frictional effects within the drop (either from surface tension or viscosity of the liquid) or to films of liquid on the surface. Numerically, the impact pressure forces over the range of drop sizes and impact velocities of the CEGB data are so great that surface tension cannot be a factor. This is also true for the mercury jet impacts of Hancox and Brunton, even though the surface tension of mercury is considerably higher than that of water, because the acoustic impedance of mercury is also markedly higher than that of water.

If the observed drop diameter effect is solely a result of internal hydrodynamics in the impacting drop, a viscosity-like effect must be the cause. Superficially, one might say in this connection, that such is the cause. The surface to volume ratio increases with decreasing drop diameter and the flow of liquid out of the impingement zone will be impeded and the violence of outward flow reduced. Reduced outward flow violence then can be equated with less erosion. This kind of reasoning, however, implies a steady-state continuity of impinging flow and outward flow which need not and probably does not exist during the most damaging period of impact. Over the entire period of impact there must be continuity of flow into and out of the impact, but this does not have to be true instantaneously except at one instant during the entire process. If, because of viscous effects, the liquid cannot initially flow out of the impact as fast as it is flowing in, the maximum pressure of the impact will have to be prolonged until it can. Otherwise, overall continuity of flow will not be preserved. This means that if internal viscous effects are a major cause of the drop diameter effect, the period of maximum impact pressure will be longer for smaller drops than larger drops. Smaller drops should inflict a more severe impact than larger drops and therefore cause proportionally greater damage. Since this is obviously not the case, one is left with the hydrodynamic interaction of the impacting drop with a film of liquid as the most probable cause for the observed drop diameter effect.

An obvious effect of a water layer would be to cushion the impact between the drop and the metal surface. The effective cushioning from a given thickness of surface water will be greater for smaller drops than for larger drops. This is a possible reason that for equal amounts of impacting water, the finer the division of the water and the lower the impact damage. This is one aspect of the water film. Another and perhaps more important aspect is that such a water film will provide a lubricated surface for lateral flow or a path for dissipation of the impact as a compression wave moving radially away from the impact through the film. This aspect of a liquid film is most important since it allows a postulation that the duration of drop impact during the CEGB tests was a function of normal impact velocity even though the Hancox and Brunton mercury jet single impact tests indicated no change in size of impact with change in normal impact velocity. The tests were carried out with dry surfaces and the results (even if taken at face value) are not applicable to a wet surface.

3.3.4 Correlation Model

It is assumed that because of the presence of the liquid film, the duration of the pressure pulse, liquid outflow, etc., correspond to the hypothetical model of Hancox and Brunton [65] as implied by their statement:

$$\beta = \sin^{-1}\left(\frac{U_n}{C}\right)$$

At the moment of impact between the water drop and liquid film, compression waves start into the film and the drop at or near the velocity of sound in the liquid. Initially, this compression wave is maintained at full liquid to liquid impact value by the crashing of successive segments of the drop on the surface at a rate in excess of the compression wave velocity. If during this period, the compression wave in the liquid film is reflected from on the solid surface, the average pressure exerted on the solid surface will be that of the full water hammer level. The pressure rise over the wave is equal to the water-to-water impact, $1/2\rho_\ell CU_n$, to which must be added the change in momentum of the liquid following the wave at velocity $U_n/2$, causing an additional pressure rise at the solid surface of $1/2\rho_\ell CU_n$.

Sometime later, the rate at which liquid crashes on the surface is reduced (because of the geometry of a sphere) to a level where a compression wave can outdistance the disturbance, reach a free surface, and be reflected back as a rarefaction wave. At this time, liquid outflow from the compressed region begins. The area of average maximum pressure then dwindles to nothing as the rarefaction wave progresses to the center of impact.

3.3.4.1 Forces of Impingement

There are two force or pressure levels of concern. The first of these is the pressure level of the initial impact, and the second is the impingement pressures generated by the liquid squirting laterally from the impacted area.

The first of these is taken to be the water hammer pressure. (Throughout this section, it will be assumed that the impact velocity levels and the strength of the metal surfaces are such that the metal can be considered rigid with little loss in accuracy.):

$$P_1 = \rho_\ell \, C U_n$$

Heymann has shown that the shock wave velocity, C, in water is to a first approximation, a simple function of C_o, the acoustic velocity in the uncompressed liquid, and the normal impact velocity, U_n, so that pressure, p_1, becomes, using Heymann's relation:

$$P_1 = \rho_\ell \, C_o U_n \left(1 + 2 \frac{U_n}{C_o}\right)$$

The maximum secondary impingement pressures are similarly assumed to be the water hammer pressure from impingement on a rigid projection at maximum lateral velocity. These maximum lateral velocities have been experimentally observed to be approximately:

$$U_2 = \sqrt{2 U_n C}$$

or

$$p_2 = \rho_\ell C_2 \sqrt{2 U_n C} = \rho_\ell C_o \left(1 + \frac{2}{C_o} \sqrt{2 U_n C_o \left(1 + 2 \frac{U_n}{C_o}\right)}\right) \sqrt{2 U_n C_o \left(1 + 2 \frac{U_n}{C_o}\right)}$$

For water drops impacting with normal velocities in the range of the CEGB experiments, this reduces in numerical approximation to:

$$p_2 \sim 9.5 \, \rho_\ell \, C_o U_n$$

That p_2 is numerically first order linear in $\rho_\ell C_o U_n$ simplifies the correlation problem with the CEGB water drop data since it may be assumed that the dimensionless ratio, p_1/p_2, is nearly constant.

3.3.4.2 Impingement Process, Duration, Total Impulse, and Total Energy

Assuming the geometry of the situation as illustrated in Figure 3.3-4, at time t after impact,

$$U_n t = r - y$$

or

$$\frac{dy}{dt} = -U_n \qquad (1)$$

Making use of the equation of a circle, $\frac{dy}{dx} = -\frac{x}{y}$, the rate of progression of the disturbance along the surface is

$$\frac{dx}{dt} = \frac{\sqrt{r^2 - x^2}}{x} U_n \qquad (2)$$

At a time defined as t_β, the rate of progression of the disturbance will fall to the velocity of the compression wave in the liquid along this same surface, or

$$\left(\frac{dx}{dt}\right)_\beta = C = \frac{\sqrt{r^2 - x_\beta^2}}{x_\beta} U_n,$$

and

$$x_\beta = \frac{r}{\sqrt{\left(\frac{C}{U_n}\right)^2 + 1}} \qquad (3)$$

In the regime of interest to turbines,

$$\left(\frac{C}{U_n}\right)^2 >> 1,$$

or

$$x_\beta \simeq r \frac{U_n}{C}$$

This model is identical to that of the hypothesis of Hancox and Brunton, since

$$\sin \beta = \frac{x_\beta}{r} = \frac{U_n}{C}$$

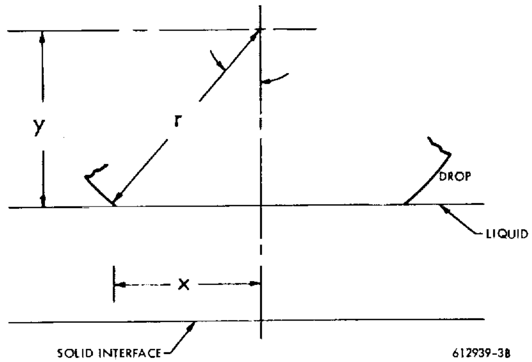

Figure 3.3-4 Configuration Diagram

Similarly, by integrating Equation 1 from zero to x_β and approximating,

$$t_\beta \simeq \frac{r}{2}\left(\frac{U_n}{C^2}\right) \quad (4)$$

This t_β is the time at which liquid outflow begins, and the compressed zone covers the maximum area. The complete time of the pressure pulse t_β is the time t_β plus the time for the rarefaction wave to travel to the point of initial impact from its radius of origin x_β. Thus,

$$t_b = t_\beta + \frac{x_\beta}{C} \quad (5)$$

In approximate terms for $\left(\frac{C}{U_n}\right)^2 >> 1$,

$$t_b \simeq 3/2\ \frac{r\,U_n}{C^2} \quad (6)$$

The average area over which the pressure pulse acts during t_b is then, approximately,

$$A = \frac{7\pi}{18} r^2 \left(\frac{U_n}{C}\right)^2 \quad (7)$$

The total impulse exerted by single drop on the surface during the maximum pressure phase of impact is (neglecting the time to compress the liquid film) given by:

$$I_i = \rho_\ell\, C\, U_n \sum A_i\, t_i = \rho_\ell\, C\, U_n \left(\frac{7\pi}{96}\right) D^3 \left(\frac{U_n^3}{C^4}\right)$$

$$= \rho_\ell\, C \left(\frac{U_n}{C}\right)^4 \left(\frac{7\pi}{96}\, D^3\right) \quad (8)$$

The total impulse per unit of surface area in terms of total water impacted per unit of surface area in the form of drops of diameter D is then:

$$\frac{\Sigma I_i}{A} = \frac{7}{16}\ \frac{m_\ell}{A}\ U_n \left(\frac{U_n}{C}\right)^3 \quad (9)$$

By observation earlier in this section, the quantity of total impulse per unit area that a given material can endure should be a constant of the material, or the amount of water to cause incubation is:

$$\left(\frac{m_\ell}{A}\right) = \frac{\Sigma I_i/A}{\frac{7}{16}\, U_n \left(\frac{U_n}{C}\right)^3} :: \frac{1}{U_n^4} \quad (10)$$

Referring to Figure 3.3-2, the dashed line shown is drawn for a $(m_\ell/A) :: 1/U_n^4$ dependence. The solid line is that drawn through the data by the original investigators.

The energy used in deforming a single drop, during this maximum pressure stage of impact, is the energy flux across the liquid solid interface required to maintain the compressive shock moving through the liquid or

$$E_i = C\, U_n^2\ \Sigma A_i\, t_i = I_i\, U_n \quad (11)$$

Hence, the total energy available per unit area to cause erosion from deformation of impinging drops (neglecting the time to compress the liquid film) is:

$$\frac{E_\ell}{A} = \frac{7}{16}\ \frac{m_\ell}{A} \left(\frac{U_n}{C}\right)^3 U_n^2 \quad (12)$$

or

$$\frac{E}{A} :: U_n^5$$

It has been observed by several investigators (76,77) that the rate of erosion of metals changes approximately as the fifth power of the normal impact velocity.

3.3.4.3 Liquid Film Thickness During the CEGB Tests

As stated previously, it is assumed that the CEGB test pieces were covered with a water film. At each revolution of the test sample this film is replenished as it passes through the curtain of water drops. This water then drains from the test piece under the centrifugal force field, gradually thinning the film until the next collision with the water drops.

Assuming that the surface of the sample is smooth and plane, that the flow from the sample is viscous and only in the radial direction, neglecting the low order terms in the Navier-Stokes equation, neglecting all external forces except centrifugal force and specifying a parabolic velocity distribution of the liquid film, a straightforward derivation of an approximate average film thickness at the moment of impact of the drops results. (See Section 3.3.8.)

$$\delta = \sqrt{\frac{3\,\mu\,D_s}{4\pi\rho_\ell\,U_s}} \qquad (13)$$

Calculated film thicknesses as a function of erosion sample velocity are shown in Figure 3.3-5. As can be seen, these calculated films are quite thin. It has been pointed out to the author by Professor D. E. Elliott, that the foregoing film thicknesses would, at best, apply only during the initial stage of an erosion test before the surface has become roughened. After the surfaces become roughened, the liquid film thickness will increase. This offers a possible explanation as to why the CEGB data show drop diameter segregation for stage 1 erosion not only at the lowest test velocities but over the entire range of test velocities for stage 3 erosion.

For correlation purposes, it is not necessary to know the absolute value of the film thickness so long as this thickness for a particular stage of erosion is the same multiple of the minimum thickness for all impinging drop diameters. This is apparently the case for the CEGB data since the characteristic size of the roughness, as previously quoted from Reference 61, is proportional to the drop diameter. If the film flow remains of a viscous character and follows the roughness of the surface, then the film thickness would be proportional to the square root

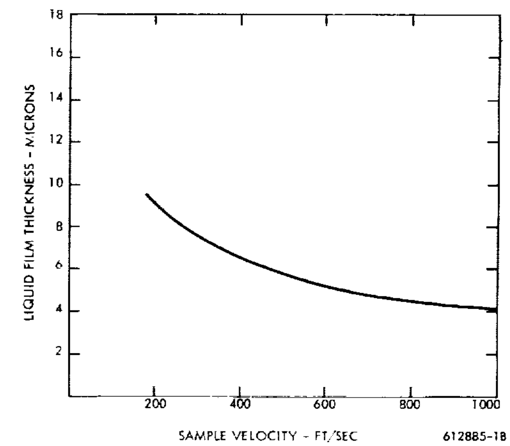

Figure 3.3-5 Calculated Film Thicknesses, CEGB Apparatus

of the path length. For geometrically similar roughness, the path length would be independent of the characteristic size so long as the characteristic size is much smaller than the total path length. This is not to say that the surface roughness level does not change from stage to stage, but rather that surface similitude with respect to impinging drop diameter prevails at any particular stage of erosion. Therefore, dimensional analysis based on minimum film thickness is a rational procedure so long as the stage of erosion is constant and the character of the film flow does not change.

The character of the film flow could change above and below the point where the pits or distortions of the surface retain water by capillarity. If the effective diameters of the pits are greater than some critical diameter, the pits would not retain water. If the effective pit diameters are less than this critical diameter, the pits would retain water. Equating surface tension forces and centrifugal forces, the order of the critical pit diameter should be:

$$D_c = 4\sqrt{\frac{\sigma R}{\rho_\ell\,U_s^2}} \qquad (14)$$

Characteristic numbers for the CEGB apparatus using Equation (13) are given in Table 3.3-2

TABLE 3.3-2

CRITICAL PIT DIAMETERS FOR CAPILLARY WATER RETENTION

U_s ft/sec	D_c microns
328.	253
492.	169
656.	127
984.	84

According to the CEGB investigators (61), the distances between erosion peaks tend to be of the order of the drop diameters. Since almost all the CEGB test data is for velocities greater than 600 ft/sec, and the minimum drop diameter used was 350 microns, it is unlikely that capillary retention of water was much of a factor.

In conclusion then, excluding the data taken using the 900, 1050 micron diameter drops above about 600 ft/sec, as these may have been unstable under the aerodynamic forces present, the CEGB data can be taken as a set of fluid-dynamic similitudes for a particular stage of erosion.

3.3.4.4 Impact Damage Threshold Velocity Correlation

It has been determined that the CEGB data may be expected to exhibit fluid-dynamic similitude for any particular stage of erosion. The film flow will be assumed to be always in the viscous flow regime. Its thickness for any particular stage of erosion may be assumed to be a simple multiple of a plane surface film thickness for any of the tests using stable drops. The unattenuated pressure of drop impact is numerically, to a good approximation, a simple multiple of the water hammer pressure for either the primary impact or secondary impacts from liquid squirting from the impact zone. It has also been found by Pearson(67) that the CEGB data for the third stage of erosion exhibits an apparent threshold velocity for damage which can be used to correlate the erosion material rates above this threshold. As observed by Heymann this apparent threshold velocity varies inversely as the square root of the drop diameter.

On the basis of these foregoing considerations, it is reasonable to assume that for relatively non-viscous fluids such as water and potassium, the only variables of importance are: (1) the threshold water hammer pressure to cause damage($\rho_\ell C U_{cd}$), (2) some strength of material criterion (S), (3) the liquid film thickness at threshold condition (δ_{cd}) over the uneroded surface, and (4) the diameter of the impinging drop (D). These variables may be related by dimensional analysis to give:

$$\frac{\rho_\ell C U_{cd}}{S} = \varphi \left(\frac{\delta_{cd}}{D}\right)$$

Ignoring the relatively small change in shock wave velocity, C, with threshold normal impact velocity, U_{cd}, gives:

$$\frac{\rho_\ell C_o U_{cd}}{S} = \varphi \left(\frac{\delta_{cd}}{D}\right)$$

3.3.4.5 Stage 3 Threshold Velocity Correlation

The summary of CEGB data (62) reports tests on three different materials where both the impinging drop diameter and normal impact velocity are varied. The materials are a Stellite 6, a 12 percent chrome steel, and a maraging steel.

From this information, it is possible to establish approximate relations between the dimensionless quantities of Equation (14), provided that a material strength criterion is selected. The criterion selected is the hardness of the material as measured in terms of the Vickers VPN. It is felt that none of the usual strength of materials quantities will be a universal criterion of the erosion strength of materials. From a cursory review of various available erosion test results, it is concluded that all suggested criteria are fallible. Among these usual criteria, hardness appears to be one of the best. In addition, it has also been observed by the CEGB (61) that it provides a reasonably good indicator with respect to the CEGB data.

The averaged results of examining the CEGB data in terms of Equation (14) are shown in Figure 3.3-6. In Figure 3.3-6, the factor $2.08(10^5)$ is used to convert the Vickers Hardness Number from metric to English units. The dimensions used are: ρ_ℓ in slugs/ft^3, C_o in ft/sec, VPN in kg/mm^2, δ in ft, D in ft, and U_{cd} in ft/sec. On an averaged basis there seems to be a clear separation between the materials. A data point by data point plot would somewhat obscure this separation, since the data scatter in the 12 percent chrome information (the only substantial body of data) is greater than the span between Stellite and the maraging steel. The separation by materials is hardly unexpected since it is well known that the erosion resistance of Stellite-like materials is almost always superior to that of other materials of similar physical property values. Similarly, the high hardness steels almost always show poorer erosion resistance than would be expected from a review of physical property values. It might be added that the vertical spread in Figure 3.3-6 is of the same order as that likely to be reported from a series of tests for the common strength of materials criteria for a single material.

3.3.4.6 State 1 Threshold Velocity

Because during the incubation period the impacted surface is smooth and not pitted as in the third stage of erosion, the liquid film covering the surface is, by this model, thinner than during the third stage. This means that the threshold velocity to incubate damage will be lower than the threshold velocity necessary to continue damage.

That the threshold velocities to cause incubation are lower than those required to continue erosion is evidenced by the less marked segregation by drop diameter of the incubation period data (see Figure 3.3-2). However, as pointed out by Heymann, at normal impact velocities below 700 ft/sec such segregation with drop diameter is present. Unfortunately, the data do not extend to low enough velocity levels to make an empirical correlation of the data practical.

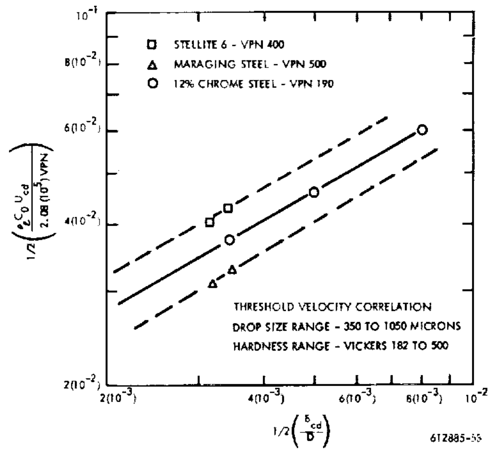

Figure 3.3-6 Threshold Velocity Correlation

Assuming that the basic rate controlling cause of damage and its mitigation by a liquid film does not change between the first and third stage of erosion, the correlation of Figure 3.3-6 can be used to estimate threshold velocities for incubation by accounting for the ratio in average film thicknesses between Stage 3 and Stage 1. To a first approximation, the ratio will be proportional to the square root of the ratio of the respective flow path lengths. From pictures in reference (61), it would appear that the flow path length during Stage 3 erosion is approximately three times the length of the original or incubation path length, or the film thicknesses in Stage 3 erosion are about 1.8 times the film thicknesses during the incubation period. On this basis, division of the calculated value of (δ_{cd}/D) by 1.8 before entering Figure 3.3-6 provides an estimate of Stage 1 erosion threshold velocities where δ_{cd} is calculated by Equation (13). In approximate terms, this yields a Stage 1 threshold velocity of about 70 percent of the Stage 3 threshold velocity.

3.3.4.7 Damage Rates Above the Threshold Velocity

It has been hypothesized by observers, that the ability of a material to resist erosion should be proportional to its ability to absorb the energy of impact above some threshold pressure level necessary to start erosion. Therefore, it will be assumed that the energy which must be absorbed by the impacted solid is proportional to the energy being expended in compression of the drops. Also, it will be assumed that the energy represented by that above the level necessary to produce a threshold pressure level $P_{cd} = \rho_\ell C U_{cd}$ is that available to produce erosion damage.

The total compression energy has already been given in Equation (12). Subtracting the energy below the threshold and rearranging terms yields:

$$E = \frac{7}{16}\, m_\ell\, U_n^2 \left(\frac{U_n}{C}\right)^3 \left(1 - \frac{U_{cd}}{U_n}\right) \qquad (15)$$

By dimensional considerations, energy E must be equal to a product of volume of metal eroded, V_m, and a material strength level, S, divided by an efficiency of removal. Further, $V_m = \frac{m_m}{\rho_m}$. Application of these relations to Equation (15) and rearranging of terms gives:

$$\frac{m_m}{m_\ell} = \frac{7}{16}\, \frac{\epsilon \rho_m U_n^2}{S} \left(\frac{U_n}{C}\right)^3 \left(1 - \frac{U_{cd}}{U_n}\right) \qquad (16)$$

Substitution for C in terms of C_o and U by use of Heymann's[75] relationship for water, introduction of the liquid density, and grouping of the variables in convenient dimensionless groups yields:

$$\frac{m_m}{m_\ell} = \frac{7}{8}\, \epsilon \left(\frac{\rho_m}{\rho_\ell}\right) \left(\frac{\rho_\ell U_n^2}{2 S}\right) \left(\frac{U_n}{C_o}\right)^2 \left(\frac{\frac{U_n}{C_o}}{\left[1 + \frac{2 U_n}{C_o}\right]^3}\right) \left(1 - \frac{U_{cd}}{U_n}\right) \qquad (17)$$

For the CEGB data on steels, the minimum test impact velocity is approximately 500 ft/sec. The maximum is approximately 1050 ft/sec. That is, the minimum value of U_n/C_o is slightly greater than 0.1 and the maximum is somewhat greater than 0.2. Values for the quantity

$$\frac{U_n/C_o}{\left(1 + \frac{2 U_n}{C_o}\right)^3}$$

are given in the following as a function of $\frac{U_n}{C_o}$

$\frac{U_n}{C_o}$	$\frac{U_n/C_o}{\left(1 + \frac{U_n}{C_o}\right)^3}$
0.01	0.9 (10^{-2})
0.05	3.8 (10^{-2})
0.10	5.8 (10^{-2})
0.15	6.8 (10^{-2})
0.20	7.3 (10^{-2})
0.30	7.3 (10^{-2})
0.40	6.9 (10^{-2})

It would seem, therefore, that for most of the CEGB data, Equation (17) might well be applied as

$$\frac{m_m}{m_\ell} \simeq \left(\frac{\epsilon}{17}\right) \left(\frac{\rho_m}{\rho_\ell}\right) \left(\frac{\rho_\ell U_n^2}{2 S}\right) \left(\frac{U_n}{C_o}\right)^2 \left(1 - \frac{U_{cd}}{U_n}\right) \qquad (18)$$

It will be noted that the proportionality terms in Equation (18) relating the materials loss ratio to the impingement velocity are a function of both the liquid and material properties.

Equation (18) can be written as

$$\frac{m_m}{m_\ell} :: \left(\frac{U_n}{U_{cd}}\right)^4 \left(1 - \frac{U_{cd}}{U_n}\right) \qquad (19)$$

This analytic expression for the erosion rate is compared with the CEGB data in Figure 3.3-7. The data points shown are taken from the 600 micron drop curve of Figure 3.3-3 for which U_{cd} was established as 390 ft/sec. The dotted lines shown in Figure 3.3-7 represent Equation (19) with a suitably chosen constant of proportionality. Figure 3.3-7 then illustrates the excellent agreement of Equation (19) with the experimental 660 micron drop data.

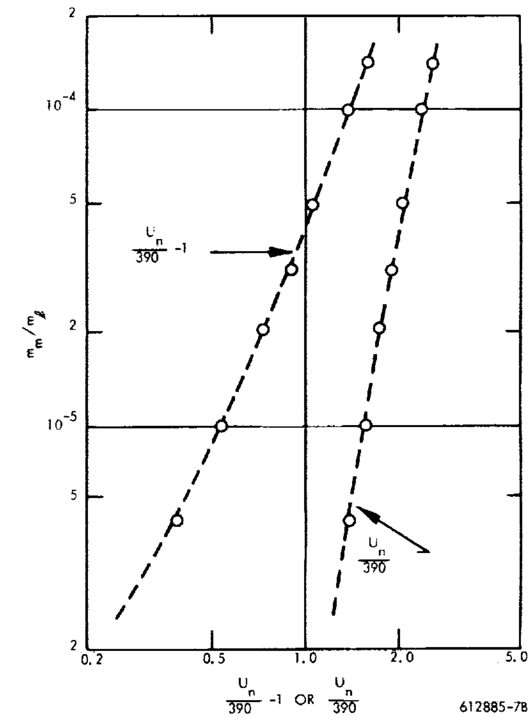

Figure 3.3-7 Correlation of CEGB Data by Means of Equation 19

3.3.4.8 Summary of Model Equations and Empirical Constants

The correlating relations of the model in equation form for Stage 3 erosion under water impingement conditions at or near CEGB test velocities are:

$$\frac{m_m}{m_\ell} = \left(\frac{\epsilon}{17}\right) \left(\frac{\rho_m}{\rho_\ell}\right) \left(\frac{\rho_\ell U_n^2}{2S}\right)\left(\frac{U_n}{C_o}\right)^2\left(1 - \frac{U_{cd}}{U_n}\right)$$

$$U_{cd} = K\left(\frac{S}{\rho_\ell C_o}\right) \left(\frac{\delta_{cd}}{D}\right)^n$$

where for the particular CEGB apparatus the correlating film thickness δ is given by:

$$\delta = \sqrt{\frac{3\mu D_s}{4\pi\rho_\ell U_s}}$$

Empirical coefficients for the maraging steel of VPN—500, the Stellite 6 of VPN—400, and the 12 percent chrome steel of VPN —190 are given below

Material	K	n	ϵ	(m_m/m_ℓ)*
Maraging steel	1.14	0.57	0.46	26 (10^{-6})
12% chrome steel	1.31	0.57	0.43	147 (10^{-6})
Stellite 6	1.52	0.57	0.12	8 (10^{-6})

* At U_n = 1020 ft/sec, D = 660 microns

It will be noted that even though the hardness of the two steels varies by a factor of 2.5 and the erosion rate by 5.5 at 1020 ft/sec impact velocity, the empirical coefficients are about the same. The threshold velocity constants for Stellite are similar to those for the steels but the constant ϵ, which is a measure of the effectiveness of the erosion process, is much lower. As is already known, Stellites are generally somewhat more erosion resistant in relation to surface hardness than are steels.

3.3.5 Temperature Effect In Drop Impingement Material Removal

In cavitation erosion tests there is a strong temperature effect on the measured erosion rates when materials and other conditions are held constant. A large amount of this effect can be ascribed to hydrodynamic causes [79].

Between cavitation erosion and impingement erosion there are often analogous effects. This is not to say that the detail causes are necessarily the same or that there is a quantitative correspondence, but in gross terms the two types of erosion exhibit a similar kind of behavior.

The possibility of a temperature linked hydrodynamic effect in drop impingement erosion sample testing in potassium has been investigated using the impingement correlation equations. The circumstances are analogous to a whirling arm drop impingement test using potassium drops of uniform size impinging on an erosion material sample mounted on the arm. The tests are such that the velocity of impact and the test temperature are the independent variables under investigation.

The behavior of the dependent variable, mass loss rate at temperature (T_o), has been investigated in terms of the independent parameters T and $U_n/U_{cd}(T_o)$. The results are shown in Figure 3.3-8 where ratio $m_m(T)/m_m(T_o)$ is on the y-axis, temperature is on the x-axis, and $U_n/U_{cd}(T_o)$ is the parameter. The base temperature has been taken as 350°K.

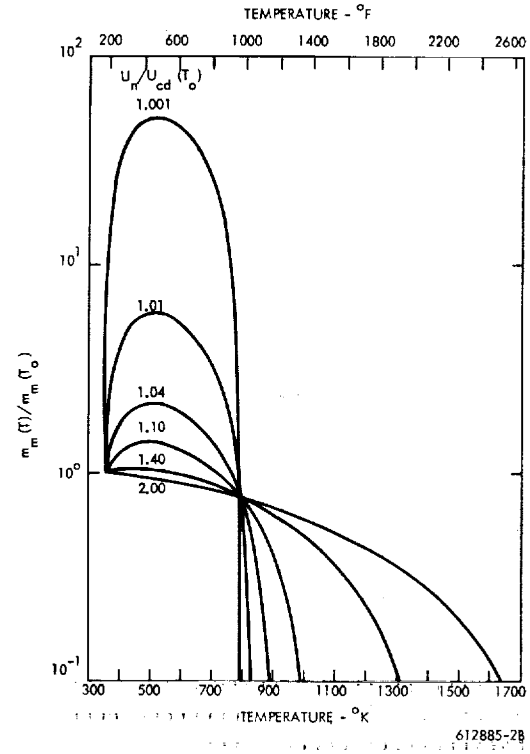

Figure 3.3-8 Referred Erosion Rates

As can be seen, there is a substantial change in the referred erosion rates with temperature. For low values of $U_n/U_{cd}(T_o)$ there is a marked erosion peak at 400-500°F. A low value of $U_n/U_{cd}(T_o)$ implies that at T_o, the reference temperature, the erosion conditions are only a little above a threshold condition to cause erosion. It is to be noted that: (1) the values plotted are referred values and that absolute values of material removal would be higher, the higher $U_n/U_{cd}(T_o)$; and (2) the supposed conditions are for a whirling arm materials test and no conclusion relative to actual turbine blade erosion should be drawn. The situation leading to turbine blade erosion is more complex and involves variation in drop sizes, amount of liquid impinging, etc.

integrated and manipulated, subject to specification of a parabolic velocity distribution in the liquid film and continuity of flow, * to give:

$$\frac{dm}{dt} = \frac{\rho U^2 \delta t^3}{3R} \left(\frac{\rho \Delta Z}{\mu}\right) \qquad (2)$$

At any time t after passing through the water curtain, the amount of liquid contained in a segment of length D and Width Δ Z is

$$m = \varrho D \Delta Z \delta \ , \qquad (3)$$

and the rate of change of this mass is

$$\frac{dm}{dt} = \varrho D \Delta Z \frac{d\delta}{dt} \ . \qquad (4)$$

Because this film is very thin it is reasonable to assume that $\delta_t \sim \delta$, and on substituting Eq. (4) in Eq. (2) on the basis that $\delta_t = \delta$ and integrating, the result is

$$\frac{\delta}{\delta_o} = \sqrt{\frac{3 \mu DR}{2 \varrho U^2 \delta_o^2 \Delta t + 3 \mu RD}} \qquad (5)$$

The time Δt between impacts or replenishing of the water film is given by

$$\Delta t = \frac{2 \pi R}{U} \ , \qquad (6)$$

which upon substitution in Eq. (5) yields

$$\frac{\delta}{\delta_o} = \sqrt{\frac{3 \mu D}{4 \pi \varrho U \delta_o^2 + 3 \mu D}} \qquad (7)$$

When the film thickness after a complete circuit of the wheel is substantially less than its initial value, the term 3 μ D in the denominator of Eq. (7) may be neglected relative to the other term $4 \pi \varrho U \delta_o^2$, or

$$\delta \approx \sqrt{\frac{3 \mu D}{4 \pi \varrho U}} \qquad (8)$$

*Refer to Section 2.5.3 of WANL-TME-1977

If the film thickness added at each pass through the water spray is of the same order as the final film thickness after a turn of the wheel, Eq. (8) is still a reasonable numerical approximation to Eq. (7) after enough revolutions that a steady state of operation is approached. This is illustrated by the following numerical example: the assumptions are (1) at the start of each revolution the initial film thickness is the residual film thickness plus an instantaneously deposited 4 microns (2) viscosity of water - 0.0114 poises, (3) density of water - 1 gm/cm^3, (4) erosion sample velocity - $3(10^4)$ cm/sec, and (5) erosion sample diameter - 2 cm.

The calculated residual film thicknesses as a relation of the number of revolutions after startup are given in the following table:

Revolution No.	Initial Film Thickness (cm)	Residual Film Thickness (cm)
1	$4 (10^{-4})$	$2.92 (10^{-4})$
2	$6.92 (10^{-4})$	$3.64 (10^{-4})$
3	$7.64 (10^{-4})$	$3.68 (10^{-4})$
4	$7.68 (10^{-4})$	$3.73 (10^{-4})$
5	$7.73 (10^{-4})$	$3.74 (10^{-4})$

Using Eq. (8), the value of residual film thickness is $4.25 (10^{-4})$ cm, not too different from the values in the table.

Thus, the thickness of water film impacted by the water drops is largely independent of the past history of the film and depends mainly on the liquid properties, the velocity of the sample (which is also the velocity of impact), and the size of the test sample.

3.4 TURBINE BLADE DISSOLUTION IN LIQUID METALS

3.4.1 Background

3.4.1.1 Discussion of Potassium Tests Involving Erosion

Table 3.4-1 lists some coupon and turbine tests where wet potassium vapor impinged on metal coupons or turbine surfaces. In all these tests there was some material removal.

In tests such as Nos. 1 and 5, where the oxygen content of the potassium is reported or suspected to have been high (high not defined quantitatively by authors), the rates of material or damage are substantial in 100 to 2000 hours for TZM material. It may be concluded that TZM is oxygen sensitive.

In tests such as Nos. 2, 3, 4, 7, 10, and 13, where the oxygen content of the potassium is reported to be low and impinging particle diameters are most probably submicronic, regardless of the theoretical moisture level or impact velocity or material tested, the loss rates observed were the order of 1 mil per 1000 hours or less. It may be concluded that where, because of the sub-micronic size of the impinging particles, impingement effects can be definitely assumed to be absent, material removal rates by material dissolution are quite low.

During the General Electric two-stage turbine tests, in tests such as Nos. 8 and 9, material losses were substantial for U-700 material. Calculated impinging drop velocities are of the order of 770 ft/sec and calculated impinging particle diameters are in the range of 30 to 100 microns. (Losses were massive during test No. 6, but for this test an estimate of the liquid particle diameters could not be made on the basis of the information examined and the particle diameters may have been very large.) Neither the impingement erosion model nor the dissolution model formulated hereafter would predict the substantial degree of material removal experienced during tests Nos. 8 and 9 on U-700 material. It may be concluded that there was a combined interaction of chemical (dissolution) removal and mechanical (impingement erosion) removal taking place in the U-700 material. The Westinghouse erosion analysis model treats dissolution and mechanical removal as independent processes with no interaction. However, under identical conditions (and at the same time actually) as test No. 8, TZM inserts, test No. 11, did not show this interaction. This observation is a justification for the formulation of a non-interaction erosion model.

The General Electric three-stage turbine tests, tests No. 12, 13 and 14, resulted in substantial material removal from the three stage rotor blades and damage to erosion (coupons) inserts aft of the third stage. This material removal may have been caused by liquid or it may have been mechanical damage from some blade retainer clips or pieces of third stage shrouding which broke loose during the course of the tests. It is Westinghouse opinion that most of the damage was caused by these broken pieces. It must be added, however, that informed opinion of NASA and its contractors is divided with respect to the causes of this material removal and the significance of this test.

3.4.1.2 Chemical Dissolution

The chemical dissolution of various materials into alkali and heavy liquid metals has been extensively investigated. Results, particularly with alkali metal systems, have been scattered. This scatter occurs because many difficulties arise when working with alkali liquid metals. Dissolution rates, besides varying with the standard parameters of temperature, material, flow rates, and temperature gradients, are also strongly influenced by alkali metal purity (small ppm concentrations of oxygen, carbon, or nitrogen contribute to increased corrosion), by dissimilar metal couples within the system, hot trap and getter efficiency, etc. Also, as experimental techniques and controls improve, the comparison of recent experimental results with earlier data further contributes to the problem.

TABLE 3.4-1

EXPERIENCE ON MATERIAL REMOVAL BY LIQUID POTASSIUM

Agency	No.	& Type of Test	Y %	V ft/sec	D Microns	Materials	Oxygen Content ppm	Test Duration hr.	Material Removal	Remarks		Ref.
ORNL	1	Coupon	17	~2000	D < 1	TZM	Unknown, high	1000-2000	High	Material removal attributed to oxygen attack		80
ORNL	2	Coupon	17	~2000	D < 1	TZM	Unknown, low	1000	Small			80
ORNL	3	Coupon	17	~2000	D < 1	Cb-1Zr	Unknown, low	3000	1-7 mils	Dissolution or corrosion attack		80
ORNL	4	1 stage turbine	15	~2000	D < 1	TZM	Unknown, low	2700	Unknown	No visual damage		80
Philco-Aeronautics	5	1 stage turbine	15	~2000	D < 1	TZM	Unknown, high	100	Several mils	Liquid jet cut groove in rotors Liquid collected in stator flow separation		80
General Electric	6	2 stage turbine No. 1	10-15	~500	Large Unknown	U-700	Unknown	< 50	Massive	Liquid sprayed into turbine inlet to increase wetness		81
General Electric	7	2 stage turbine No. 2	4-5	~500	D < 1	U-700	< 20 ppm	2000-3000	Nil	Rotor blades		80
General Electric	8	2 stage turbine	4-5	>700	30<D<100	U-700	< 20 ppm	2000-3000	8-10 mils	Erosion inserts (coupon test	Simul-taneous	80
General Electric	9	2 stage turbine No. 2	4-5	>700	30<D<100	U-700	< 20 ppm	2000-3000	Some	Shrouds, clips	experi-ments during	80
General Electric	10	2 stage turbine No. 2	4-5	<700	D<1	TZM	< 20 ppm	2000-3000	2.8 mils	Rotor blades	2 stage turbine test.	80
General Electric	11	2 stage turbine No. 2	4-5	>700	30>D>100	TZM	< 20 ppm	2000-3000	Nil	Erosion inserts (coupon test)		80
General Electric	12	3 stage turbine	8-12	~500	70>D>150	U-700 TZM, TZC	< 20 ppm	1300	20-40 mils	Leading edges 3rd stage rotor blades, not clearly liquid removal	Simul-taneous	82
General Electric	13	3 stage turbine	8-12	~500	D < 1	U-700 TZM, TZC	< 20 ppm	1300	1-2 mil rivulations	Rotor blades	experi-ments during 3 stage	82
General Electric	14	3 stage turbine	8-12	>850	20<D<30	U-700 TZM, TZC	< 20 ppm	1300	Substantial	Erosion inserts (coupon test) Not clearly liquid removal	turbine	82

Y - Theoretical moisture content of bulk flow (reported values)
V- Liquid impingement velocity (Westinghouse estimates)
D- Liquid particle diameter (Westinghouse estimates)

Most liquid metal corrosion data, either from refluxing capsules, natural convection loops, or pumped loops, have been of a qualitative nature. General surface dissolution, grain boundary penetration, and general mass transfer have been noted. However, the vast number of variables involved in most systems has not permitted the mathematical approaches expressed by Epstein in Reference 83 or Gill in Reference 84 to be extended to these more complex systems. Thus, experience with materials and systems has been relied upon to designate the materials and their properties most compatible to the system in which they are to be incorporated.

Within the last few years improved experimental techniques and equipment have permitted investigators to reduce some of the variables (especially oxygen contamination) to less influential levels. The quantitative data being generated today can, with due consideration of its source and system, be extrapolated to other similar systems for rough, predictive comparisons.

In this section the chemical dissolution of a turbine blade material into the thin stream of condensed potassium that flows radially outward along the blade is considered. Epstein's static dissolution equation in Reference 4 was solved with dynamic dissolution parameters from Gill in Reference 84.

3.4.2 Analytical Model

To repeat, a fraction of the condensed moisture present in the wet vapor will be collected by the stator blades and will carry over to the subsequent rotor row in the form of atomized drops.

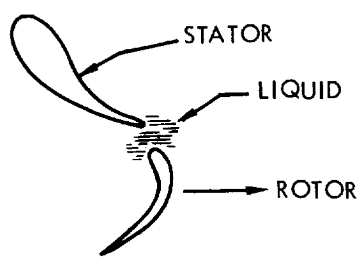

612752-4B

This liquid impacts the rotor blades along a relatively narrow portion of the leading edge of the convex surface and then flows in a nearly radial direction to discharge at the tips of the blades. It is assumed that the impacted moisture forms a continuous film and that the fluid impinges uniformly along the blade impaction zone. The concern of this analysis is the chemical dissolution of the blade material associated with the flow of this film.

Because the film of liquid formed on the rotor blades is at most a few micrometers thick and is violently stirred by the incoming drops, it is assumed that the rate controlling step in the dissolution process is that of the rate of dissolution for the blade material into the liquid at the liquid-solid interface.

This is different than for dissolution of solids into liquids in pipe flow. In pipe flow, the rate controlling step is often the rate of diffusion of the dissolved solute across the solvent boundary layer into the bulk flow of solvent in the pipe.

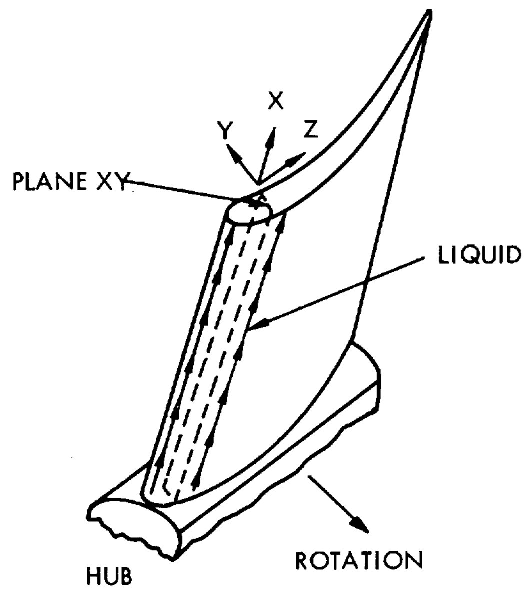

ROTOR BLADE 612752-5B

For a turbine operating at some steady-state condition, rates of flow are a function only of position. Hence at any location (see drawing below) x, z

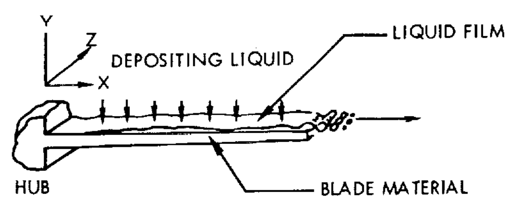

PLANE XY 612752-6B

measured from the hub and nose, respectively, of the rotor blade the rate flows of solute and solvent in the liquid film are time independent and the concentration, S, of solute in the solvent at location s, z is the ratio of the rate flow of solute to rate flow of solvent at this location or

$$S = \rho_\ell \frac{\dot{V}_m}{\dot{m}_\ell} \quad (1)$$

where

$\dot{V}_m$ is the rate flow of solute in the x direction per unit width of film (z direction) — cm^2/sec

$\dot{m}_\ell$ is the rate of solvent in the x direction per unit width of film— gm/sec/cm

ρ_ℓ is the solvent density — gm/cm^3

According to Epstein (83), the rate of dissolution of a pure metal into a pure liquid solvent at the metal - liquid interface is given by:

$$S = S_o \left[1 - \exp\left(-\frac{\alpha A t}{V_\ell}\right)\right] \quad (2)$$

where

A	is the surface area in contact with the liquid	—cm^2
S_o	is the saturation solubility of material in the solvent	—dimensionless
S	is the solute concentration in the solvent at time t	—dimensionless
V_ℓ	is the volume of liquid in contact with the metal for time t	—cm^3
t	is the contact time between liquid and metal along surface A	— sec
α	is the solution rate constant	—cm/sec

From Equation D-2 the following differential equations may be inferred:

$$\frac{dS}{dt} = \frac{\alpha}{V_\ell} (S_o - S) A \quad (3)$$

and since

$$d S = \frac{1}{V_\ell} \, d V_m$$

$$\frac{d V_m}{dt} = \dot{V}_m = \alpha (S_o - S) A \quad (4)$$

In the case of the rotor blade film of unit width at location x, Eq. (4) may be written:

$$\dot{V}_m = \int_o^x \alpha (S_o - S) \, dx \quad (5)$$

By the assumption of uniform deposition of liquid along the rotor blade impaction zone:

$$\dot{m}_\ell = \dot{m}_a x \quad (6)$$

where m_a is the rate of deposition per unit area per unit time —$gm/cm^2/$ sec.

Substitutions from Eq. (5) and (6) into Eq. (1) yield, after some rearranging of terms:

$$S_x = \frac{\rho_\ell}{\dot{m}_a} \int \alpha (S_o - S) \, dx \quad (7)$$

Differentiation of Eq. (7) and rearrangement of terms gives:

$$\frac{d S}{\frac{\rho_\ell \alpha}{\dot{m}_a} S_o - \left(1 + \frac{\rho_\ell \alpha}{\dot{m}_a}\right) S} = \frac{dx}{x} \quad (8)$$

Equation (8) is readily integrated to give:

$$S = \frac{\dot{m}_a}{\dot{m}_a + \rho_\ell \alpha} \left[\frac{\rho_\ell \alpha}{\dot{m}_a} S_o - \frac{C}{x^{\left(1 + \frac{\rho_\ell \alpha}{\dot{m}_a}\right)}}\right] \quad (9)$$

where C is a constant of integration.

Now, it may be noted that when $x = 0$ in Eq. (9) that $S = -\infty$ unless $C = 0$ (in which case S is indeterminate). However, a C taken equal to zero is the only reasonable physical interpretation, since the physical concentration S must fall with the limits:

$$0 \geq S \leq S_o$$

and the equation:

$$S = \frac{\dot{m}_a}{\dot{m}_a + \rho_\ell \alpha}\left[\frac{\rho_\ell \alpha}{\dot{m}_a} S_o - \frac{(0)}{x^{\left(1 + \frac{\rho_\ell \alpha}{\dot{m}_a}\right)}}\right] \tag{10}$$

satisfies these limits as $x \longrightarrow 0$.

Equation (9), therefore, reduces to:

$$S = \frac{\rho_\ell \alpha}{\dot{m}_a + \rho_\ell \alpha} S_o \tag{11}$$

It will be noted that the concentration S is not only time independent but is constant throughout the liquid flow zone along the rotor blades leading edge.

S in terms of S_o from Equation (11) may be substituted into Equation (5) to give:

$$\dot{V}_m = \int_o^x \alpha S_o \left(1 \frac{\rho_\ell \alpha}{\dot{m}_a + \rho_\ell \alpha}\right) dx = \alpha S_o \left(\frac{\dot{m}_a}{\dot{m}_a + \rho_\ell \alpha}\right) x \tag{12}$$

The rate of material thickness removal, δ_m, therefore is:

$$\dot{\delta}_m = \frac{\dot{V}_m}{x} = \alpha S_o \left(\frac{\dot{m}_a}{\dot{m}_a + \rho_\ell \alpha}\right) \tag{13}$$

This Eq. (13) presents a reasonable physical picture. If $\dot{m}_a >> \rho_\ell \alpha$, this implies that $S \longrightarrow 0$ or the rate of material thickness removal is:

$$\dot{\delta}_m = \alpha (S_o - (0)) = \alpha S_o$$

The thickness removal rate is dissolution rate constant controlled and is independent of liquid flow rate. If $\dot{m}_a$ is low, $\dot{m}_a << \rho \alpha$, this implies that $S \longrightarrow S_o$ and

$$\dot{\delta}_m = S_o \frac{\dot{m}_a}{\rho_\ell}$$

The thickness removal rate is then directly proportional to the liquid flow rate and independent of the dissolution rate constant.

In between these extremes the thickness removal rate is affected by both dissolution rate constant and liquid flow rate.

The discussion so far has assumed a pure metal dissolving into a pure liquid. The latter assumption, pure liquid, is probably reasonable since turbine system operators go to some length to keep a pure liquid in the system. However, turbine blade materials are alloys composed of materials of differing solubility and probably chemical activity. In advanced high temperature Rankine cycle liquid metal systems, the turbine blade materials are likely to be refractory alloys such as TZM and TZC. These are molybdenum alloys with small amounts of titanium, carbon, and zirconium. The alloying materials such as Ti and Zr are more soluble than the base material and while present in concentrations of only 1 percent to 2 percent, tend to collect at the alloy grain boundaries where they may be more readily leached from the surface than if they were uniformly mixed. In addition, if there is preferential leaching at the grain boundaries, this may so weaken the material that a considerably greater amount of material may be lost than that which simply dissolved.

At the present time there are insufficient experimental results or theory to judge these factors adequately. Nonetheless, it seems worthwhile to delineate these areas of uncertainty by the application of multiplicative correction factors to Equation (13), as:

$$\dot{\delta}_s = k_1 \dot{\delta}_m = k_1 \; k \; a \; \alpha \; S_o \left(\frac{\dot{m}_a}{\dot{m}_a + \rho_\ell \, k \, a \, \alpha} \right) \tag{14}$$

where

- a is the activity level of a readily dissolvable constituent of the alloy in the alloyed form relative to the constituents dissolvability in pure form
- k is ratio of the effective surface area from which the constituent is dissolving to the total surface area of the alloy
- k_1 is the ratio of total alloy removal rate to dissolving constituent removal rate
- $\dot{\delta}_s$ is the thickness removal rate for the alloy surface as a whole

In the numerical example given hereafter, it has been assumed that

$$k = 1/k_1 \text{ and } a \sim 1.$$

Hence,

$$\dot{\delta}_s = \alpha \, S_o \, \frac{\dot{m}_a}{\dot{m}_a + \rho_\ell \, k\alpha} \tag{15}$$

In addition, it has been assumed that k (the effective surface area ratio) is equal to the ratio of dissolving constituent volume to total alloy volume.

3.4.3 Analysis of Last Rotor of a Potassium Turbine Design

Using the previously derived equations, a numerical analysis of possible dissolution of metal from the last rotor blades of a potassium turbine design was performed. The numerical analysis was done by Westinghouse at the request of the AiResearch Manufacturing Company as a part of a study of Potassium Turbine-Alternator designs, for NASA Lewis Research Center, under Contract NAS 3-10934, and has been previously reported in reference 85. It is repeated here to give the reader an idea of the numerical levels that result from application of the model to potassium turbine designs.

To our knowledge there are no experimental values of dissolution rate constant (α) available for TZM, TZC constituents dissolving into potassium. There are values for Fe dissolving in Na[83] and 304 SS dissolving in Li[84]. The values for 304 SS dissolving in Li are used. (See Figure 3.4-1.) The saturation solubilities of the various materials are taken to be:

Material	S_o
Mo	0.2 ppm
Zr	58 ppm
Ti	68 ppm

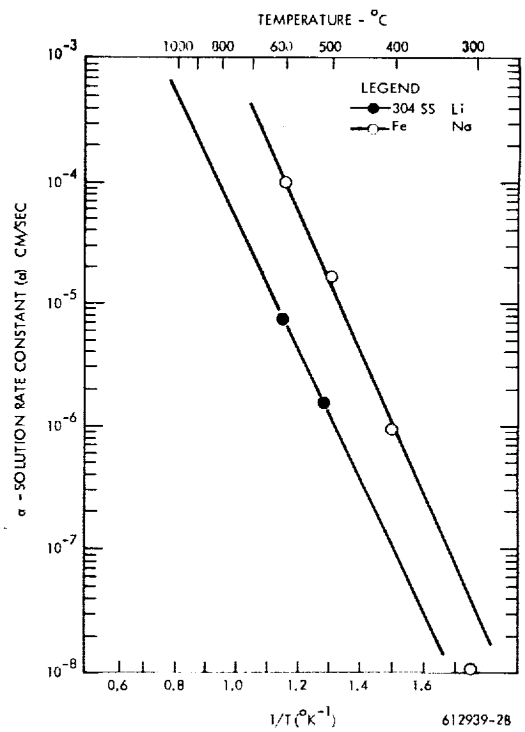

Figure 3.4-1 Temperature Dependence of α

The saturation solubilities of Zr and Ti are most uncertain [85] and may be as low as 10 ppm at analyzed rotor conditions. The values used are near the maximum values reported in the literature at the analyzed rotor temperature. The rotor blade material is assumed to be TZM of the following composition [86]:

Constituent	Volume Fraction
Carbon	0.0009
Titanium	0.0110
Zirconium	0.0014
Molybdenum	0.9867

The fluid and geometric conditions along the leading portion of the convex surface of the rotor blades are taken to be as follows: [85]

Rotor Blade Conditions

Total liquid flow	17.8 gm/sec
No. of rotor blades	59
Liquid flow/blade	0.302 gm/sec
Blade height	4.03 cm
Temperature	670° C
Liquid density	0.685 gm/cc
Liquid film width	0.25 cm
Liquid film area	1. cm^2

The information from Figure 3.4-1 and the previous three tables on material solubilities, the composition of TZM, and the rotor blade conditions were used to calculate material removal rates using Equation 15. The results of this calculation follow:

Rotor Blade Dissolution Results

$\dot{m}_a$ —liquid deposi-rate/unit area	0.302 $gm/cm^2/sec$
a solution rate constant	$2(10^{-5})$ cm/sec
k effective surface area ratio of Ti + Zr	0.012 dimensionless
S_o average saturation solubility of Ti and Zr	$63(10^{-6})$ ppm
ρ_ℓ a k dissolution factor	$1.65\ (10^{-7})\ gm/cm^2/sec$
$\dot{\delta}_s$ material thickness	$1.26\ (10^{-8})$ mm/sec
Thickness removed in 2000 hr	0.0036 in.
Thickness removed in 20,000 hr	0.0356 in.

It will be noted from the tabulation of results that the liquid deposition rate, $\dot{m}_a$, is some 2 million times greater than the dissolution factor, ρ ak. Therefore, the material loss rate is independent of the rate of liquid flow and deposition. By this model of material removal by dissolution, the liquid flow rate will have to be reduced to about 10^{-6} of the level used here to effect a substantial reduction in material loss rate. It will also be noted that the calculated removal of material in 20,000 hours is substantial in terms of a 4 cm(1.575 in.) high blade. Hopefully, the model and empirical coefficients used are overly conservative.

3.4.4 References

1. Brandenberger, E., and P. DeHaller, "Untersuchungen über Tropfenschlagerosion," Schweitzer Archiv-Annales Suisses, Vol. 10; n. 11, pp. 331 - 341, November 1944; and n. 12, pp 379 - 386, December 1944.

2. Honegger, E., "Tests on Erosion Caused by Jets," The Brown Boveri Review, Vol. 14, n. 4, pp. 95 - 104, April 1927.

3. Fyall, A. A., R. B. King and R. N. C. Strain, "Rain Erosion Aspects of Aircraft and Guided Missiles," J. Roy Aero. Soc., Vol. 66, pp. 447 - 453, July 1962.

4. King, R. B., "Rain Erosion Testing at Supersonic Speeds Using Rocket-Propelled Vehicles," Paper presented at Rain Erosion Conference, Meersburg, Germany, May 1965.

5. Langbein, G., "The Dependence of Rain Erosion on the Velocity and the Angle of Incidence of Drops," Paper presented at Rain Erosion Conference, Meersburg, Germany, May 1965.

6. Hoff, G., G. Langbein and H. Rieger, "Investigations of Material Destruction due to Liquid Impact," Paper to be presented at ASTM Symposium on Erosion by Impingement and Cavitation, Atlantic City, June 1966.

7. Baker, D. W. C., K. H. Jolliffe and D. Pearson: "The Resistance of Materials to Impact Erosion Damage," Paper No. 13 at Discussion on the Deformation of Solids by the Impact of Liquids, The Royal Society, London, May 27, 1965. To be published in Phil. Trans. Roy. Soc., 1966.

8. Pearson, D., "Some Factors Influencing the Erosion of a Stainless Steel," Central Electricity Generating Board (of Gt. Britain), Report RD/M/N 100, June 1964.

9. Busch, H. and G. Hoff, "Rain Erosion in High-Speed Flight," Interavia, Vol. 20, pp. 675-676, May 1965.

10. Brunton, J. H., "Deformation of Solids by Impact of Liquids at High Speeds," Symposium on Erosion and Cavitation, ASTM STP-307, Am. Soc. Testing Mats., pp. 83 - 89, 1962.

11. "Second Quarterly Progress Report; October 1, 1965 through January 15, 1966; Basic Investigation of Turbine Erosion Phenomena; Contract NAS 7-390," WANL-PR (DD)-077, Westinghouse Astronuclear Laboratory, February 1966.

12. Pearson, D., "The Effect of Drop Size on the Erosion of a Stainless Steel," Central Electricity Generating Board (of Gt. Britain) Report RD/M/N 128, December 1964.

13. Vater, M., "Prüfung und Verhalten metallischer Werkstoffe gegen Tropfenschlag und Kavitation," Korrosion and Metallschutz, Vol. 20, n. 6, pp. 171 - 179, June 1944.

14. Engel, Olive G., "Waterdrop Collisions with Solid Surfaces," J. Research NBS, Vol. 54, Vol. 54, n. 5, pp. 281-298, May 1965.

15. Bowden, F. P., and J. E. Field, "The Brittle Fracture of Solids by Liquid Impact, by Solid Impact, and by Shock," Proc. Roy. Soc. A, Vol. 282, pp. 331-352, 1964.

16. Thomas, G. P., "Multiple Impact Experiments and Initial Stages of Deformation," Discussion on the Deformation of Solids by the Impact of Liquids, The Royal Society, London, 1955. (To be published, Phil. Trans. Roy, Soc., 1966).

17. Thiruvengadam, A., "A Unified Theory of Cavitation Damage," ASME Trans. (J. Basic Engrg), Vol. 85D, pp. 365-376, September 1963.

18. Peterson, R. E., "Application of Stress Concentration Factors in Design," Experimental Stress Analysis (Proc. SESA), Vol. 1, n. 1, pp. 118-127,

19. Marriott, J. B., and G. Rowden, "The Deformation of Steam Turbine Blade Materials by Liquid Impact," Discussion on the Deformation of Solids by the Impact of Liquids, The Royal Society, London, 1965. (To be published, Phil. Trans. Roy. Soc., 1966).

20. Weibull, W., "Basic Aspects of Fatigue," IUTAM Colloquium on Fatigue (Stockholm, 1955), Springer-Verlag, Berlin, pp. 289-298, 1956.

21. Backer, W. R., E. R. Marshall, and M. C. Shaw, "The Size Effect in Metal Cutting," Trans. ASME, Vol. 74, pp. 61-72, 1952.

22. Finnie, I., "The Mechanism of Erosion of Ductile Materials," Proc. 3rd National Congress Applied Mechanics, pp. 527-532, 1958.

23. Bowden, F. P., and J. H. Brunton, "The Deformation of Solids by Liquid Impact at Supersonic Speeds," Proc. Roy. Soc. A, Vol. 263, pp. 433-450, October 1961.

24. DeCorso, S. M., and R. E. Kothmann, "Erosion by Liquid Impact," Symposium on Erosion and Cavitation, ASTM STP-307, Am. Soc. Testing Mats., pp. 32-45, 1962.

25. Vater, M., "Das Verhalten metallischer Werkstoffe bei Beanspruchung durch Flüssigkeitsschlag," Z. VDI, Vol. 81, n. 45, pp. 1305-1311, November 6, 1937.

26. Weibull, W., "Fatigue Testing and Analysis of Results," Oxford, Pergamon Press, 1961. (Published for and on behalf of AGARD).

27. Roark, R. J., "Formulas for Stress and Strain," New York, McGraw-Hill, 4th Edition, 1965.

28. Thiruvengadam, A., "A Comparative Evaluation of Cavitation Damage Test Devices," ASME Symposium on Cavitation Facilities and Techniques, 1964, pp. 157-164. (Also Hydronautics, Inc., Tech. Rept. No. 233-2, November 1963).

29. Thiruvengadam, A., and S. Waring, "Mechanical Properties of Metals and their Cavitation Damage Resistance," Hydronautics, Inc. Tech. Rept. No. 233-5, Contract Nonr-3755(00)FBM, June 1964.

30. Thiruvengadam, A., "The Concept of Erosion Strength," Hydronautics, Inc. Technical Report 233-9, December 1965. (Also to be presented at ASTM Symposium on Erosion, Atlantic City, June 1966.)

31. Shalnev, K. K., J. J. Varga and G. Sebestyen, "Verification of Energy Parameter for Cavitation Damage," Paper to be presented at ASTM Symposium on Erosion by Impingement and Cavitation, Atlantic City, June 1966.

32. McAdam, J. D., Jr., "Endurance Properties of Steel: Their Relation to Other Physical Properties and to Chemical Composition," ASTM Proc., Vol. 23, pp. 56-105, 1923.

33. Halford, G. R., "The Energy Required for Fatigue," Journal of Materials, Vol. 1, No. 1, pp. 3-18, March 1966.

34. Heymann, F. J., "On the Shock Wave Velocity and Impact Pressure in High-Speed Liquid-Solid Impact," Trans. ASME, J. Basic Engrg., Vol. 90D, Sept. 1968, pp. 400-402.

35. Heymann, F. J., "High-Speed Impact Between a Liquid Drop and a Solid Surface," J. Appl. Phys., Vol. 40, Dec. 1969, pp. 5113-5122.

36. Leith, W. C., and A. L. Thompson, "Some Corrosion Effects in Accelerated Cavitation Damage," ASME Trans., (J. Basic Engrg.), Vol. 82D, pp. 795-807, 1960.

37. Ripken, J. F., et al, "A New Facility for Evaluation of Materials Subject to Erosion and Cavitation Damage," Univ. of Minn., St. Anthony Falls Hydro. Lab., Project Report No. 77, Contract Nonr 710(56), March 1965.

38. Hobbs, J. M., private communication. (See also L. Hays, "Turbine Research in Great Britain," Informal trip report in connection with NAS 7-390 and NAS 7-391. Jet Propulsion Laboratory, November 11, 1965.)

39. Engel, O. G., "Pits in Metals Caused by Collision with Liquid Drops and Soft Metal Spheres," J. Research NBS, Vol. 62, n. 6, pp. 229-246, June 1959.

40. Engel, O. G., "Pits in Metals Caused by Collision with Liquid Drops and Rigid Steel Spheres," Journal of Research, National Bureau of Standards, Vol. 64A, pp. 61-72, 1960.

41. Jenkins, D. C., J. D. Booker, and J. W. Sweed, "An Experimental Method for the Study of the Impact Between a Liquid Drop and a Surface Moving at High Speed," Ministry of Supply (Gt. Britain), R & M 3203; Obtainable from NASA as N62-10146.

42. Jenkins, D. C., and J. D. Booker, "The Impingement of Water Drops on a Surface Moving at High Speed," in "Aerodynamic Capture of Particles", Pergamon Press, pp. 97-103, 1960.

43. DeCorso, S. M., "Erosion Tests of Steam Turbine Blade Materials," Proc. ASTM, Vol. 64, pp. 782-796, 1964.

44. International Conference on Rain Erosion Problems. Held in Meersburg/Bodensee, Germany, May 1965. Proceedings in English to be published by the Royal Aircraft Establishment, edited by A. A. Fyall.

45. Discussion on the Deformation of Solids by the Impact of Liquids, held at the Royal Society, London, England, May 27, 1965. To be published in Phil. Trans. Roy. Soc., 1966.

46. Symposium on Erosion by Cavitation and Impingement. (To be held during ASTM Annual Meeting), Atlantic City, N. J., June 1966. Proceedings will probably be published in 1967 as a "Special Technical Publication" by ASTM.

47. Heymann, F. J., "On the Time Dependence of the Rate of Erosion due to Liquid Impact or Cavitation," Westinghouse Steam Division Report E-1448, June 1966. (Also Paper No. 136, ASTM Annual Meeting, Atlantic City, June 1966.)

48. Busch, H., G. Hoff, and G. Langbein, "General View on Rain Erosion Tests in Germany," Discussion on the Deformation of Solids by the Impact of Liquids, The Royal Society, London, 1965. (To be published, Phil. Trans., Roy. Soc., 1966).

49. Freudenthal, A. M., "Physical and Statistical Aspects of Cumulative Damage," IUTAM Colloquium on Fatigue (Stockholm, 1955), Springer-Verlag, Berlin, pp. 53-62, 1956.

50. Thiruvengadam, A., and H. S. Preiser, "On Testing Materials for Cavitation Damage Resistance," Technical Report 233-3, Hydronautics, Inc., December 1963.

51. Plesset, M. S., and R. E. Devine, "Effect of Exposure Time on Cavitation Damage," Paper No. 65-WA/FE-23, Am. Soc. Mechanical Engrs, 1965.

52. Lichtman, J. Z., D. H. Kallas, C. K. Chatten and E. P. Cochran, Jr., "Study of Corrosion and Cavitation-Erosion Damage," Transactions, Am. Soc. Mechanical Engrs., Vol. 80, pp. 1325-1341, 1958.

53. Wheeler, W. H., "Mechanism of Cavitation Erosion," Cavitation in Hydrodynamics, (National Physical Laboratory Symposium, Teddington, England, 1955), Philosophical Library, New York, 1957.

54. von Schwarz, M., W. Mantel and H. Steiner, "Tropfenschlaguntersuchungen zur Feststellung des Kavitationswiderstandes (hohlsog), "Zeitschrift fur Metallkunde, Vol. 33, pp. 236-244, 1941.

55. See 10.

56. Eichelberger, R. J., "Hypervelocity Impact," Behavior of Materials Under Dynamic Loading, Am. Soc. Mechanical Engrs., pp. 155-187, 1965.

57. Kent, R. P., "Some Aspects of Metallurgical Research and Development Applied to Large Steam Turbines," Parsons Journal, Vol. 10, pp. 285-295, Christmas 1964.

58. Roeloffs, R., and F. Garofalo, "A Review of Methods Employed in the Statistical Analysis of Fatigue Data," Proceedings, Am. Soc. Testing Mats., Vol. 56, pp. 1081-1090, 1956.

59. Epremiam, E., and R. F. Mehl, "The Statistical Behavior of Fatigue Properties and the Influence of Metallurgical Factors," Symposium on Fatigue with Emphasis on Statistical Approach, ASTM STP-137, Am. Soc. Testing Mats., pp.25-27, 1953.

60. Mathieson, R., and J. M. Hobbs, "Cavitation Erosion: Comparative Tests," Engineering, Vol. 188, pp. 136-137, January 22, 1960.

61. Baker, D. W. C., K. H. Jolliffee, and D Pearson, "The Resistance of Materials to Impact Erosion," Phil. Trans. Roy. Soc. London, Series A, No. 1110, Vol. 260, pp. 193-204, 28 July 1966.

62. Pearson, D., "A Summary of the M. E. L. Experimental Data on Erosion," Marchwood Engineering Laboratories, CEGB, RDD/M/M18, Job. No. 30023, November 1964.

63. Fraas, A. P., loc. cit. Oak Ridge National Laboratories.

64. Engel, Olive G., "Mechanism of Rain Erosion; Part XIV, Pits in Metals Caused by Collision with Liquid Drops and Rigid Steel Spheres," WADC TR 53-192, U. S. National Bureau of Standards, May 1960.

65. Hancox, N. L. and J. H. Brunton, "The Erosion of Solids by the Repeated Impact of Liquid Drops," Phil. Trans. Roy. Soc. London, Series A, No. 1110, Vol. 260, pp. 121-140, 28 July 1966.

66. DeCorso, S. M., and R. E. Kothmann, "Erosion by Liquid Impact," Symposium on Erosion and Cavitation, ASTM STP-307, Am. Soc. Testing and Matls., pp. 32-45, 1962.

67. Pearson, D., "The Effect of Drop Size on the Erosion of a Stainless Steel," CEGB Report RD/M/N128, December 1964.

68. Honegger, E., "Tests on Erosion Caused by Jets," The Brown Boveri Review, Vol. 14, n. 4, pp. 95-104, April 1927.

69. Brandenberger, E., and P. DeHaller, "Untersuchungen über Tropfenschlagerosion," Schweitzer-Archiv-Annales Suisses, Vol. 10; n. 11, pp. 331-341, November 1944 and n. 12, pp. 379-386, December 1944.

70. Herbert, W., "Behavior of Iron and Hardened Steels Towards Drop Impact," Proc. Second Meersburg Conf. Rain Erosion and Allied Phenomena, August 16-18, 1967, Vol. I, Sect. 4.4.4, Published by RAE, Farnborough, England, Ed. by A. A. Fyall and R. B. King.

71. Pearson, D., "Turbine Blade Erosion Rig Research and Development Work Carried Out at Brighton," CEGB Report RD/M/N41, Job No. 43123, December 1962.

72. Wolfe, H. E. and W. H. Anderson, "Kinetics, Mechanism and Resultant Droplet Sizes of the Aerodynamic Breakup of Liquids," Report 0395-04-18SP, Aerojet-General Corp., April 1964.

73. Gardner, G. C., "Events Leading to Erosion in the Steam Turbine," Proc. Inst. Mech. Engrs., Vol. 178, Part I: Nor. 23, pp. 593-623, 1963-1964.

74. Hinze, J. O., "Fundamentals of the Hydrodynamic Mechanism of Splitting in Dispersion Processes," A. I. ChE. Journal, Vol. I, No. 3, P. 289 ff; September 1955.

75. Heymann, F. J., "A Survey of Clues to the Relationship between Erosion Rate and Impact Parameters, " Proceedings of the Second Meersburg Conference on Rain Erosion and Allied Phenomena", Vol. 2, pp. 655-682. (Issued by Royal Aircraft Establishment, Faruborough, England, 1968.)

76. Hobbs, J. M., Discussion of Paper of Leith and Thompson, ASME Trans., (J. Basic Engrg.) Vol. 82D, pp. 795-807, 1960.

77. Thiruvengadam, A. and S. L. Rudy, "Experimental and Analytical Investigations of Multiple Liquid Impact Erosion, " Hydronautics, Inc. Tech. Report 719/1, June 1968 Contract NAS W-1608.

78. Elliott, D. E., Private Communication, 4 September 1968.

79. Thiruvengadam, A., S. L. Rudy and H. S. Preiser, "Cavitation Damage in Liquid Metals, " Hydronautics Inc., TR 607, Contract NAS 3-8506, April 1968.

80. Hays, Lance G. (Ed.), Summary of Turbine Erosion Meeting Held at Jet Propulsion Laboratory, Dec. 29-30, 1966, NASA, JPL. Tech. Memo 33-354, June 15, 1967.

81. Schnetzer, E. (Ed.), "Two Stage Potassium Test Turbine, " Quarterly Progress Report No. 15, Period: Nov. 8, 1964 through Feb. 8, 1965, NASA-CR-54392, Contract NAS 5-1143.

82. Loc. cit., Potassium test turbine review meeting on October 15, 1968 at General Electric Co., Cincinnati, Ohio.

83. Epstein, L. F., "Static and Dynamic Corrosion and Mass Transfer in Liquid Metal Systems, " Chem. Engr. Prog. Symp. Series, Vol. 53, No. 20, p. 67 (1957).

84. Gill, W. N., et al, "Mass Transfer in Liquid-Lithium Systems, " A.I.Ch.E. Journal, Vol. 6, No. 1, p. 139 (1960).

85. Pouchot, W. D., "Technical Support for the Aerothermodynamic Design of the Potassium Turboalternator (KTA), " Westinghouse Astronuclear Laboratory, WANL-TME-1886, January 3, 1969, AiResearch Contract P711340 Final Report.

86. Climax Molybdenum Co., Spec No. CMX-WB-TZM-2, May 1964.

SECTION 4

LOW SPEED CASCADE TESTS *

ABSTRACT

Low speed cascade tests run on a turbine blade section, with various trailing edge thicknesses and shapes, investigated the downstream trailing edge wake. The blade section was modeled after a 3rd stator blade of the three stage potassium test turbine of NASA Contract NAS3-8520.

The wake velocity profiles were recorded by pressure traverse measurements at five different downstream positions. With these measurements, the mixing of the boundary layer and the vorticity associated with the trailing edge based drag of the wake were investigated. This investigation compared the traverse measurements with theoretical models for viscous and vortex flow.

4.1 BACKGROUND

Moisture erosion studies have been conducted by Westinghouse for the past four years under the sponsorship of NASA. These investigations have been largely analytical and have been performed on a number of liquid metal and steam turbines.

An important factor in each of these investigations has been the trailing edge wake downstream of the stator blade row. It is within the environment of this downstream wake that the moisture drops exist from the time of their discharge from the trailing edge to the time of their impingement on the downstream rotor. Hence, the properties of the wake, such as vorticity and velocity profile, have an important effect on the size and trajectory of the moisture drops.

The wake traverse tests investigated the effect of the trailing edge thickness and shape on the properties of the blade wake. The wake properties include the change in velocity profile with downstream distance and the nature of the wake flow. The latter property is influenced by whether the wake flow is predominantly viscous or vortex.

The wake flow associated with zero trailing edge thickness and the momentum mixing of the boundary layer should be viscous. On the other hand, the flow associated with large trailing edge thickness would be expected to resemble the separated vortex flow downstream of a circular cylinder.

* W. K. Fentress, Senior Engineer and K. A. Desai, Engineer, Development Engineering Dept., Westinghouse Steam Divisions, Lester, Pa.

Data on the wake profiles and the wake decay were supplied by the pressure traverse measurements. Information on the wake vorticity was obtained from the traverse measurements by comparing the downstream loss by test with the downstream loss by theoretical models. These models gave the theoretical downstream loss with viscous mixing and vortex flow. These comparisons indicated whether the downstream flow was largely viscous or vortex.

The tests were run on the third stage, stator blade section, of the three stage potassium test turbine of Contract NAS3-8520, with various trailing edge configurations. This blade was selected because of the association of the three-stage turbine with the NASA liquid metal program. Also, this blade was typical of those used in liquid metal and steam turbines.

A literature survey was conducted at the start of the program and a number of survey reports are listed in the reference section. However, not all of these reports are cited as references.

4.2 SYMBOLS

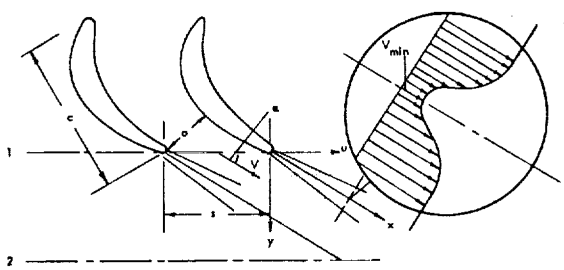

a^*	critical velocity
c	projected chord length of blade
C_D	trailing edge drag coefficient based on the trailing edge thickness T.
CF	energy loss coefficient, Eq. 2
CFD	increase in loss coefficient due to trailing edge thickness at position 2; i.e., $CF_{2,T} - CF_2$
CF_T	loss coefficient, finite trailing edge thickness
CF_1	loss coefficient, zero trailing edge thickness, at position 1
CF_2	loss coefficient, zero trailing edge thickness, at position 2
$CF_{1,T}$	loss coefficient, finite trailing edge thickness, at position 1
$CF_{2,T}$	loss coefficient, finite trailing edge thickness, at position 2
h	blade height
o	throat dimension
p_i	inlet stagnation pressure
p_s	downstream static pressure
p_t	downstream stagnation pressure
s	blade pitch
T	trailing edge thickness, temperature. See Table 4.3-1.
u	distance from blade trailing edge in the tangential direction
u/s	referred distance from blade trailing edge in the tangential direction
V	downstream velocity
V'	downstream velocity based on isentropic expansion from the inlet stagnation condition
V_r	Referred downstream velocity, Eq. 1
$V_{r,min}$	minimum, referred velocity in core of wake
$\dot{w}$	flow rate
x	distance along streamline downstream of the trailing edge

x/c	referred distance along streamline downstream of the trailing edge
y	distance in axial direction downstream of the trailing edge, inches
α	flow angle with respect to the tangential direction
α'	blade exit angle, with respect to tangential direction, based on the average of the suction and pressure surface angle at the trailing edge
γ	specific heat ratio, 1.4

Subscripts and Superscripts

1,2	downstream position at blade trailing edge, at position of uniform flow
D	drag
i	inlet stagnation
s	static
t	downstream stagnation
T	finite trailing edge thickness
r	referred
min	minimum
'	isentropic, blade

4.3 TEST APPARATUS AND PROCEDURE

4.3.1 Blade Description

The test blade is a 2 times full size model of the blade section from the three stage potassium test turbine of Contract NAS3-8520, e/4 blade height from the inner diameter position, third stator blade row.

There are nine separate configurations of the test blade which differ in trailing edge thickness and shape. These configurations consist of three different trailing edge thicknesses, 0.028 inch, 0.106 inch, and three different trailing edge shapes, round, square, and tapered (Table 4.3-1). The thin, round trailing edge configuration is an exact scale of the turbine blade section. The medium and thick trailing edge configurations differ slightly in the trailing edge suction surface region, but the gauging dimension and blade pitch are the same in all blades. Due to the constant gauging with change in thickness, the blade exit angle, α', varies from 21 to 27 degrees.

Three sets of blades with thin, medium and thick trailing edge thickness were used. The blades had a round trailing edge shape and were changed from round to square and from square to tapered, by machining the trailing edge. Details of the trailing edge shapes are given in Table 4.3-1.

The calculated boundary layer properties at the trailing edge of the blade follow:

	MOMENTUM THICKNESS-INCHES	DISPLACEMENT THICKNESS-INCHES	FULL THICKNESS-INCHES	EXPONENT
PRESSURE SURFACE	0.00164	0.00207	0.0179	7.68
SUCTION SURFACE	0.00763	0.0120	0.0540	3.51

These boundary layer properties were calculated by the methods in Reference 2 and are for a blade Reynolds number of 3.4×10^5. The exponent is used in the velocity profile equation.

Trip wires of 0.018 inch diameter were installed on the suction and pressure side of the blade approximately 0.45 inch from the leading edge.

4.3.2 Test Rig

The low speed cascade rig is illustrated in Figure 4.3-1. The cascade consisting of six blades was mounted between the circular end walls. The height of the test blade was set by the three inch space between the end walls.

The traversing probe was accessible to the region downstream of the blades by a slot in the end walls. This provided an approximate two inch travel in the axial direction and an approximate eight inch travel in the tangential, pitchwise direction.

TABLE 4.3-1

TEST BLADE SPECIFICATIONS

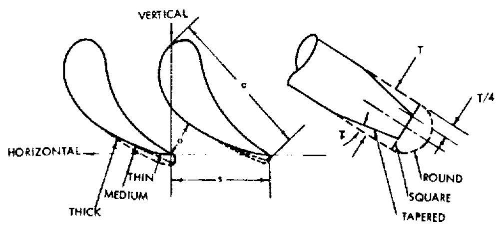

	c in.	o in.	s in.	T in.	τ deg.	h in.
Thin	2.14	.524	1.41	.028	4.5	3.0
Medium	2.20	.524	1.41	.106	12.4	3.0
Thick	2.24	.524	1.41	.160	18.4	3.0

HORIZONTAL INCHES	VERTICAL (INCHES) Thin	Medium	Thick
0.000	0.000	-0.035	-0.147
0.100	0.032	-0.142	-0.096
0.200	0.062	+0.001	-0.045
0.300	0.096	0.046	+0.008
0.400	0.130	0.093	0.062
0.500	0.168	0.141	0.116
0.600	0.208	0.190	0.172
0.700	0.252	0.242	0.229
0.800	0.300	0.295	0.287
0.900	0.350	0.350	0.346
1.000	0.406	0.406	0.406
1.100	0.472	0.472	0.472
1.200	0.552	0.552	0.552
1.292	0.650	0.650	0.650
1.370	0.750	0.750	0.750
1.426	0.850	0.850	0.850
1.470	0.950	0.950	0.950
1.495	1.050	1.050	1.050
1.506	1.150	1.150	1.150
1.510	1.250	1.250	1.250
1.504	1.350	1.350	1.350
1.484	1.450	1.450	1.450
1.440	1.550	1.550	1.550
1.350	1.638	1.638	1.638
1.250	1.674	1.674	1.674
1.150	1.656	1.656	1.656
1.050	1.582	1.582	1.582
0.994	1.500	1.500	1.500
0.948	1.400	1.400	1.400
0.922	1.300	1.300	1.300
0.902	1.200	1.200	1.200
0.882	1.100	1.100	1.100
0.855	1.000	1.000	1.000
0.824	0.900	0.900	0.900
0.780	0.800	0.800	0.800
0.726	0.700	0.700	0.700
0.664	0.600	0.600	0.600
0.592	0.500	0.500	0.500
0.500	0.388	0.388	0.388
0.400	0.288	0.288	0.288
0.300	0.206	0.206	0.206
0.200	0.138	0.138	0.138
0.100	0.082	0.082	0.082
0.012	0.026	0.026	0.026

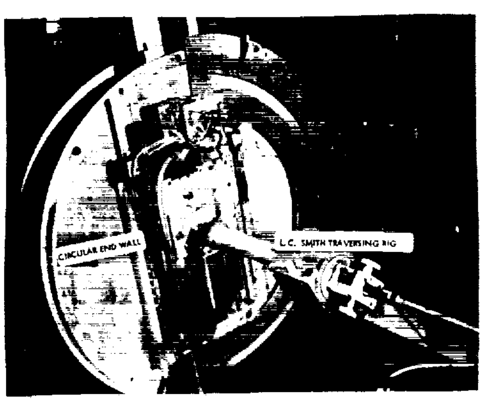

Figure 4.3-1 Cascade Test Rig

While there are circular end walls at the end of the blade span, there is a slot in each of these end walls and there are no end walls at the ends of the cascade in the axial-tangential direction. Thus the flow is not confined along the boundaries of the jet.

4.3.3 Instrumentation

A Kiel total pressure probe operated by the L. C. Smith traversing rig was used for traversing downstream of the cascade. The overall shield diameter of the probe was 1/16 inch. This probe measures the total pressure over a wide angle range and thus does not require point adjustment for yaw.

A total pressure cylindrical probe and thermocouple were located at the inlet to the cascade.

The probes were connected to pressure transducers. The electrical signals from the transducers and from the traversing rig were fed to the computerized data acquisition system.

4.3.4 Data Logging and Calculation

The data logging system, which is capable of accepting up to 300 channels of analog signals, digitizes the information and records the data on computer magnetic tape. In addition, the Hewlett Packard 2116A computer was coupled to a teletype printer which gave a continuous printout of the wake velocity. This made it possible to continuously monitor the data as they were acquired.

The L. C. Smith traversing rig was adjusted for traverse readings in 0.005 inch steps, approximately 10 seconds per step. Thus, each downstream traverse across the 1.41 inch blade pitch consisted of approximately 282 points and required approximately 50 minutes time.

The data from the magnetic tape were fed to the CDC 6400 computer. Calculations were made to determine the point by point referred velocity and the flow weight average loss coefficient by the following equations:

$$V_r = V_r(u,y) = V/V' = \left(\frac{1-(P_s/P_t)^{(\gamma-1)/\gamma}}{1-(P_s/P_i)^{(\gamma-1)/\gamma}}\right)^{1/2} \qquad \text{Eq. 1}$$

$$CF = CF(y) = \frac{\int_0^S (1-V_r^2)\, d\dot{w}}{\int_0^S d\dot{w}}$$

$$= \frac{\int_0^S V_r^2 P_t T^{-1/2} ((P_s/P_t)^{2/\gamma} - (P_s/P_t)^{(\gamma+1)/\gamma})^{1/2}\, du}{\int_0^S P_t T^{-1/2} ((P_s/P_t)^{2/\gamma} - (P_s/P_t)^{(\gamma+1)/\gamma})^{1/2}\, du} \qquad \text{Eq. 2}$$

The computer output included Cal Comp plots of the referred velocity across the pitch of the blade.

4.3.5 Checkout Procedure

A number of tests were run to determine the most suitable type of probe for the traverse tests and to establish the measurements. At the time it was not known how sharp the wake profile would be in the region of the trailing edge, how many points it would take to specify the profile, how the size of the probe would affect the measurements, or how quickly the profile would change with downstream distance.

Tests were performed with a number of probes: the 1/8 inch total-static cylindrical probe, 1/16 inch total-static Cobra probe, 1/16 inch total pressure pitot tube, and 1/8 inch total pressure Kiel probe. It was found that the Cobra probe and the Kiel probe gave a clear definition of the blade wake and gave wake profile plots that were nearly identical. However the Cobra probe required adjustment for yaw in each pitchwise traverse, particularly in the region of the trailing edge, while the Kiel probe required no adjustment. Also, the measured static pressure by the Cobra probe was particularly the same as atmospheric and gave essentially the same referred velocity except in the region 1/16 to 1/8 inch downstream of the trailing edge. Here the static pressure readings were erratic. It was therefore decided to use the

Kiel total pressure probe, consider the static pressure as atmospheric, and disregard the flow angle measurement.

In addition, tests were run to check on the downstream entrainment, the use of end walls, and the necessary number of blades for undisturbed flow in the center of the cascade. It was found that the six blade cascade was adequate. The wake profiles from the two center blades were practically identical and there was little change with respect to the wakes from the two center blades and the adjacent blades. This was true at all downstream positions. Measurements also were made at several blade span positions with similar results. Thus, it was not considered that the entrainment had an important effect on the flow in the center of the cascade or that it was necessary to have additional blades or end walls at the ends of the cascade in the axial-tangential direction. Further, it was feared that these end walls would restrict the downstream angle adjustment associated with the trailing edge thickness and invalidate the atmospheric pressure assumption.

Traverse measurements in the pitchwise direction were taken in 0.050 inch steps and in 0.005 inch steps. The 0.005 inch measurements gave much sharper profiles in the region of the blade trailing edge. As the traverse rig only provides for adjustment by factors of 10, and as it requires considerable time to make the adjustment, it was decided to take all the measurements in steps of 0.005 inch.

Finally, tests were run with and without the 0.018 inch trip wires. Although the wake profiles were apparently unaffected, it was decided to traverse with trip wires. This was to assure a turbulent boundary layer along the length of the blade as in turbine operation.

4.3.6 Wake Traverse Tests

Traverse tests were run on eight trailing edge configurations at zero incidence. These configurations were with thin, medium, and thick trailing edge thickness and with round, square, and tapered trailing edge shape. In addition, incidence angle tests were run on two of these configurations at ± 12 degrees incidence and Reynolds number tests on one of the configurations at 1.8×10^5 and 4.24×10^5 blade Reynolds number. Table 4.3-2 gives a list of the tests and the test conditions are listed below:

Tests	$p_i - p_s'$ (inches of water)	V/a^*	Reynolds No. ($\times 10^5$)
0° incidence	26.	0.33	3.4
± 12° incidence	26.	0.33	3.4
Reynolds No.	42.	0.41	4.2
	7.	0.17	1.8

The blade Reynolds number is based on the blade exit conditions and the projected chord length.

Traverse measurements were taken in 0.005 inch steps, across one blade pitch in the center of the cascade, and at five axial downstream positions. The order of tests on each of the three blade thicknesses was with round, square, and tapered trailing edge shape. Change in the original trailing edge shape, from round to square to tapered, was made by removing the blades from the cascade and machining the trailing edge. The blades were numbered and provided with positioning pins to provide for the same setting in each assembly.

Hot wire measurements of the downstream wake gave no indication of immediate results and were abandoned. It was felt that more could be gained by detailed analysis of the data.

4.4 RESULTS AND DISCUSSION

4.4.1 Theoretical Models of Flow

By comparing the traverse results with theoretical models of the downstream flow, it is possible to tell how nearly the various models conform to the actual process. Thus, it is shown whether the wake flow is associated with a viscous or a vortex process.

TABLE 4.3-2

LIST OF TESTS

BLADE TRAILING EDGE THICKNESS (INCHES)	TRAILING EDGE THICKNESS PITCH T/S	BLADE TRAILING EDGE SHAPE	0° INCIDENCE ANGLE TESTS	+12° and -12- INCIDENCE ANGLE TESTS	REYNOLDS NUMBER TESTS
THIN	0.0198	ROUND	X		
0.028	0.0198	SQUARE	X	X	
MEDIUM	0.0751	ROUND	X		
0.106	0.0751	SQUARE	X		X
	0.0751	ROUND	X		
THICK	0.1134	SQUARE	X		
0.160	0.1134	ROUND	X	X	
	0.1134	TAPERED	X		

The following models were used in the comparison.

1) Lieblein Model - Eq. 3 of reference 6 gives the referred velocity in the core of the wake as:

$$V_{r,\ min} = 1 - 0.13\ (x/c + 0.025)^{-1/2}$$

As the empirical equation is based on theory and test results for airfoils with zero trailing edge thickness, it associates the downstream wake with the viscous mixing of the boundary layer. This model is of particular interest as it was used in the moisture erosion calculations.

2) Viscous Model - This model associates the downstream loss with the mixing of the viscous boundary layer and with the filling of the dead space downstream of the trailing edge. The equations are specified by continuity, momentum, and energy relations; see reference 12. The equations are with respect to the positions at the trailing edge and at the downstream point of uniform flow, assume incompressibility, and assume constant static pressure in the pitchwise direction at the trailing edge position. The exponent in the boundary layer equations was taken as 5.5, corresponding to the calculated average for the suction and pressure surface. The constant pressure assumption implies no base drag at the trailing edge, i.e., that the trailing edge drag coefficient is zero.

3) Viscous Model with Trailing Edge Drag - This is the same as the viscous model, but without the constant static pressure assumption at the trailing edge position. The trailing edge drag coefficient would be expected to be approximately 0.41 for the round trailing blade as for a circular cylinder. The equations are the same as for the viscous model except for the addition of the C_D term in the axial momentum equation to allow for the base drag at the trailing edge, e.g., equation C3 of Reference 12:

$$gp_{s,1} + \sin^2 a_1 \left[1 - \delta^* - \delta_{te} - \theta^*\right] \left[\rho (v')^2\right]_1 = gp_{s,2} + \sin^2 a_2 \left[\rho v^2\right]_2$$

after the addition of the base drag term appears as:

$$\left[gp_{s,1}\right]^{-1/2} \left[\rho (v')^2\right]_1 \delta_{te} C_D + \sin^2 \alpha \left[1 - \delta^* - \delta_{te} - \theta^*\right] \left[\rho (v')^2\right]_1 = gp_{s,2} + \sin^2 a_2 \left[\rho v^2\right]_2$$

where g, ρ, δ^*, δ_{te}, and θ^* are in the symbols of the reference report (α is with respect to the tangential). Trailing edge drag implies vortex flow similar to the separated flow downstream of a circular cylinder.

4.4.2 Test Results

Figure 4.4-1 gives the Cal Comp plots of the traverse results. Bear in mind that the traverse was made in the pitchwise direction rather than normal to the wake. Thus, the traverse curves are at an approximate angle of 21 degrees to the blade wake rather than 90 degrees. The pressure and suction side of the wake are to the left and right of the trough and, due to the angularity, the pressure side of the wake is farther downstream in the streamline direction. This probably accounts for the fact that the wake appears to be thicker on the pressure side than on the suction side of the trough. $V_{r, min}$ does not occur at exactly the same value of u/s because of the impracticality of aligning the traversing rig in the pitchwise direction with respect to the center of the wake. Finally, all of the Figure 4.4-1 curves are for 3.4×10^5 Reynolds number.

Figure 4.4-2 compares the traverse results with the Lieblein model. This curve is a plot of the referred velocity at the core of the wake with downstream, streamline distance. While the cascade results for the thin trailing edge blade agree with the model, the discrepancy increases with trailing edge thickness; in particular, the thick trailing edge blade shows a slower rate of decay than specified by the Lieblein model. This is probably due to the increase in vorticity, with increase in trailing edge thickness, for which reason the wake does not attenuate as rapidly as with viscous flow. Also, the tapered trailing edge shape agrees better with theory in the medium thickness blade. Probably this is due to the lower effective thickness at which the boundary layer breaks away from the trailing edge. Allowing that the thin trailing edge is a direct scale of the turbine blade section, it appears that the Lieblein model gives a good account of the process.

The Figure 4.4-3 curves give the energy loss coefficient with respect to the downstream distance. These curves specify the loss coefficient at the trailing edge position and at the downstream point of uniform flow. The loss coefficients at the trailing edge and downstream positions are used in constructing Figure 4.4-4 and 5.

The Figure 4.4-4 and 5 curves compare the increase in downstream loss with respect to the downstream and trailing edge positions, and the increase in loss with trailing edge thickness, by test and theory. The theoretical curves are for the viscous model with trailing edge drag corresponding to $C_D = 0.$, 0.20, and 0.41. Generally, the tapered trailing edge blades conform to the model with C_D of 0. to 0.1, the round trailing edge blade to the model with C_D of roughly 0.2, and the square trailing edge blade to the model with C_D of roughly 0.3. Note that all trailing edge shapes, including the square trailing edge, exhibit less drag than the equivalent drag of a circular cylinder with separated flow. This corresponds to approximately $C_D = 0.41$. Perhaps this is due to the reduction in effective thickness caused by the blanketing effect of the boundary layer beyond the end of the blade or, in the tapered blade, due to the lower effective thickness at the point where the boundary layer breaks away from the trailing edge. As the T/s for the 3 stage blade is 0.02, it appears that the model with C_D of 0.2 is in good agreement with the flow.

Traverse tests at high and low blade Reynolds numbers of 4.2×10^5 and 1.8×10^5 did not show any distinguishable difference compared to those at 3.4×10^5 Reynolds numbers. Tests at higher and lower Reynolds numbers were limited by the capacity of the equipment and the accuracy of the instrumentation.

Also, tests at +12 and -12 degrees angle of incidence did not show any notable difference compared to those at zero incidence; see Figures 4.4-1 a, b, g, and i. This ± 12 degree incidence range is as large as that usually encountered in turbines.

Bear in mind that the magnitude of the theoretical trailing edge loss depends on the blade exit angle, increasing with α', e.g., CFD given by Figure 4.4-5 for $\alpha' = 21.$ degrees would be 12 percent greater for $\alpha' = 30$ degrees at $0. < T/s < 0.08$ and $C_D = 0.2$. It is probable that the test loss would correspond to this trend.

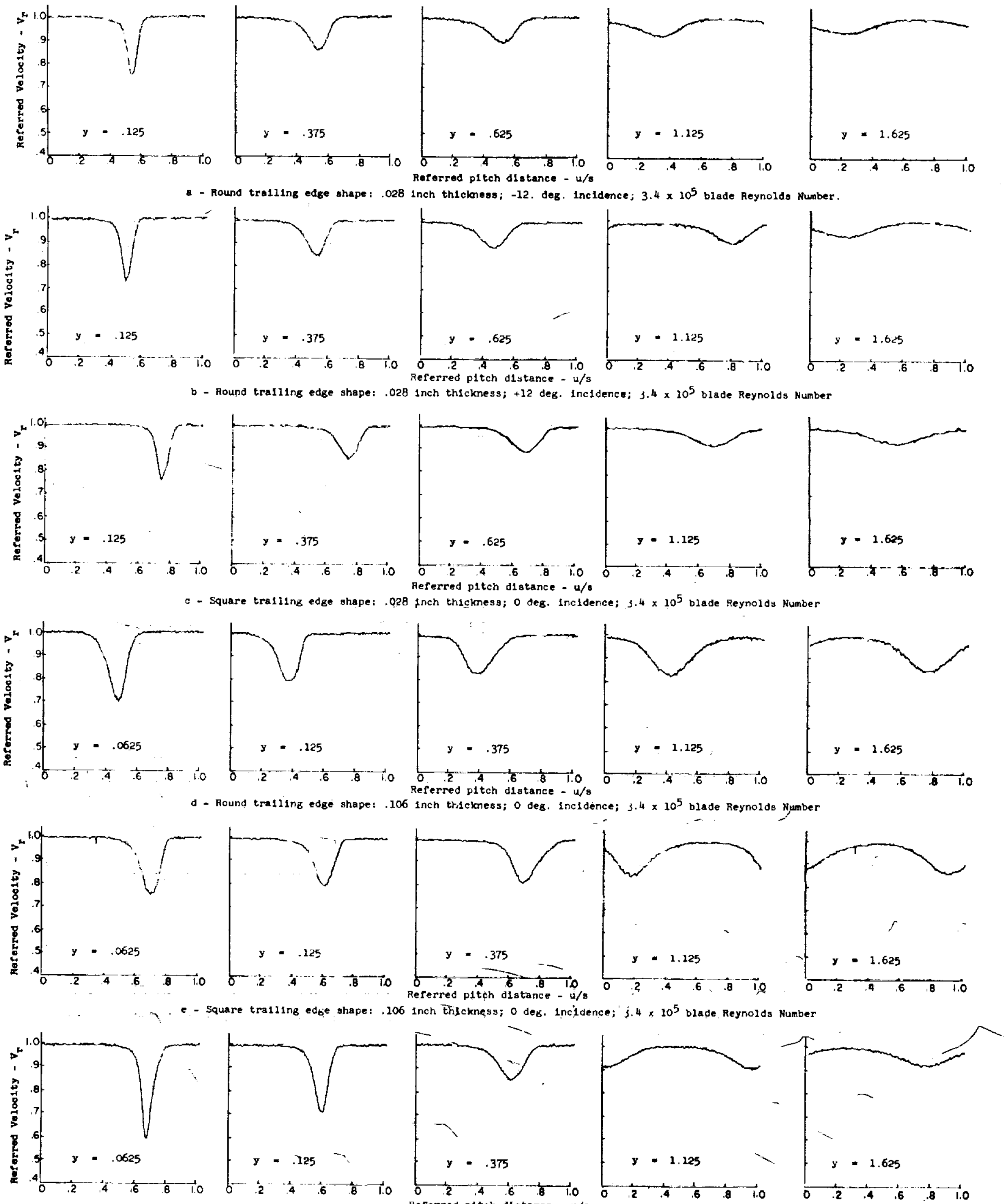

a - Round trailing edge shape: .028 inch thickness; -12. deg. incidence; 3.4 x 10^5 blade Reynolds Number.

b - Round trailing edge shape: .028 inch thickness; +12 deg. incidence; 3.4 x 10^5 blade Reynolds Number

c - Square trailing edge shape: .028 inch thickness; 0 deg. incidence; 3.4 x 10^5 blade Reynolds Number

d - Round trailing edge shape: .106 inch thickness; 0 deg. incidence; 3.4 x 10^5 blade Reynolds Number

e - Square trailing edge shape: .106 inch thickness; 0 deg. incidence; 3.4 x 10^5 blade Reynolds Number

f - Tapered trailing edge shape: .106 inch thickness; 0 deg. incidence; 3.4 x 10^5 blade Reynolds Number

Figure 4.4-1 Wake Velocity Profiles at Various Downstream Positions

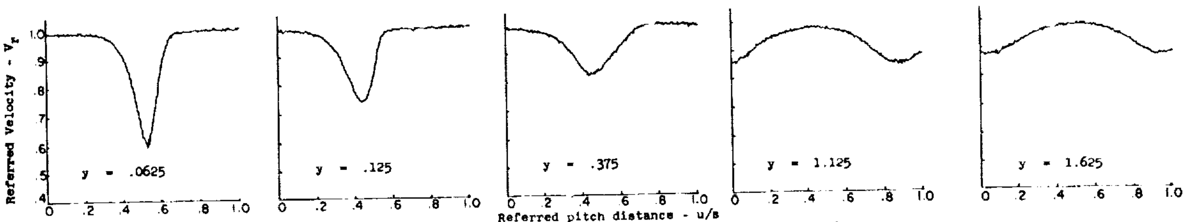

g - Round trailing edge shape: .160 inch thickness; +12 deg. incidence; 3.4×10^5 blade Reynolds Number

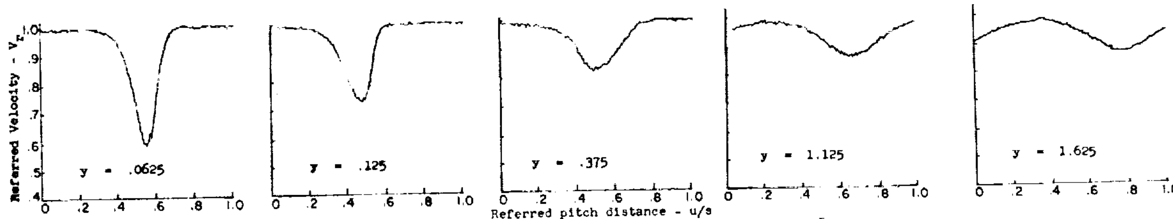

h - Round trailing edge shape: .160 inch thickness; 0 deg. incidence; 3.4×10^5 blade Reynolds Number

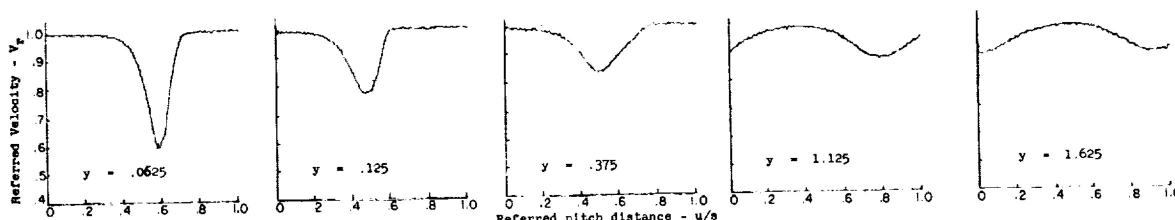

i - Round trailing edge shape: .160 inch thickness; -12 deg. incidence; 3.4×10^5 blade Reynolds Number

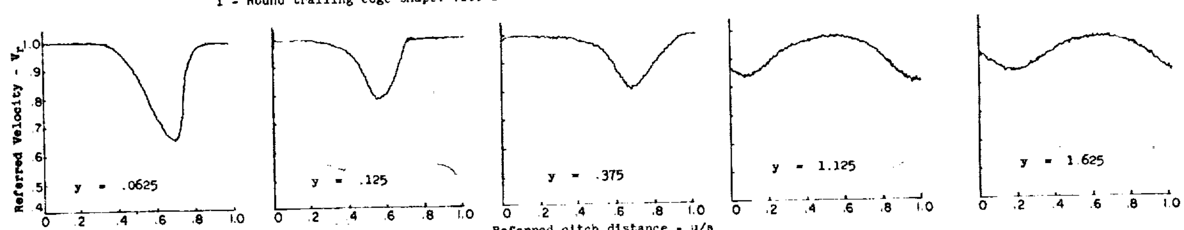

j - Square trailing edge shape: .160 inch thickness; 0 deg. incidence; 3.4×10^5 blade Reynolds Number

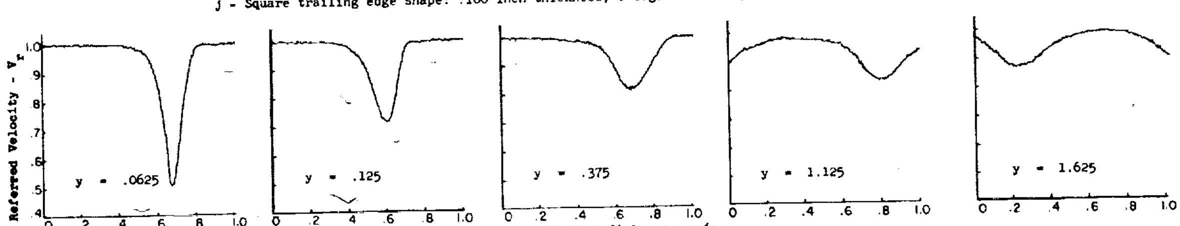

k - Tapered trailing edge shape: .160 inch thickness; 0 deg. incidence; 3.4×10^5 blade Reynolds Number

Figure 4.4-1 Wake Velocity Profiles at Various Downstream Positions

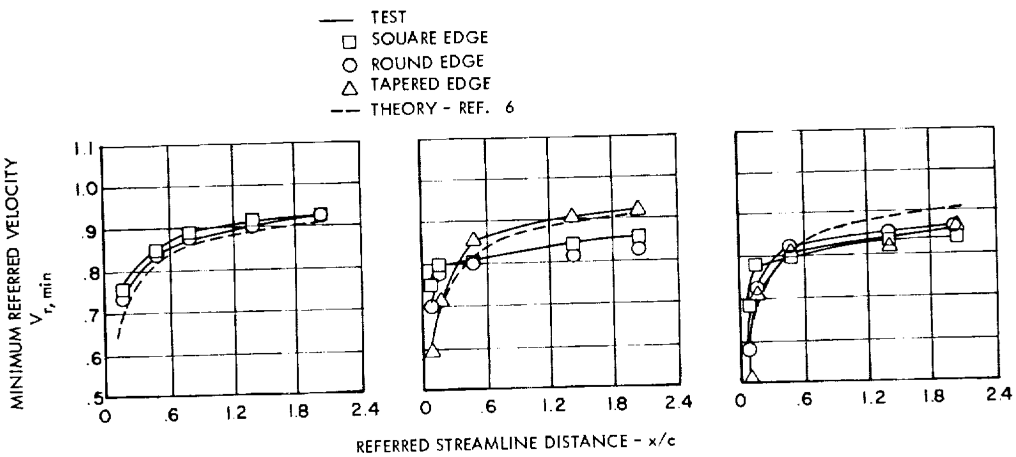

TRAILING EDGE THICKNESS

a) T = 0.028 in.

b) T = 0.106 in.

c) T = 0.106 in.

Figure 4.4-2 Change in Velocity in Core of Wake with Downstream Distance 0 Deg. Incidence; 3.4×10^5 Reynolds Number

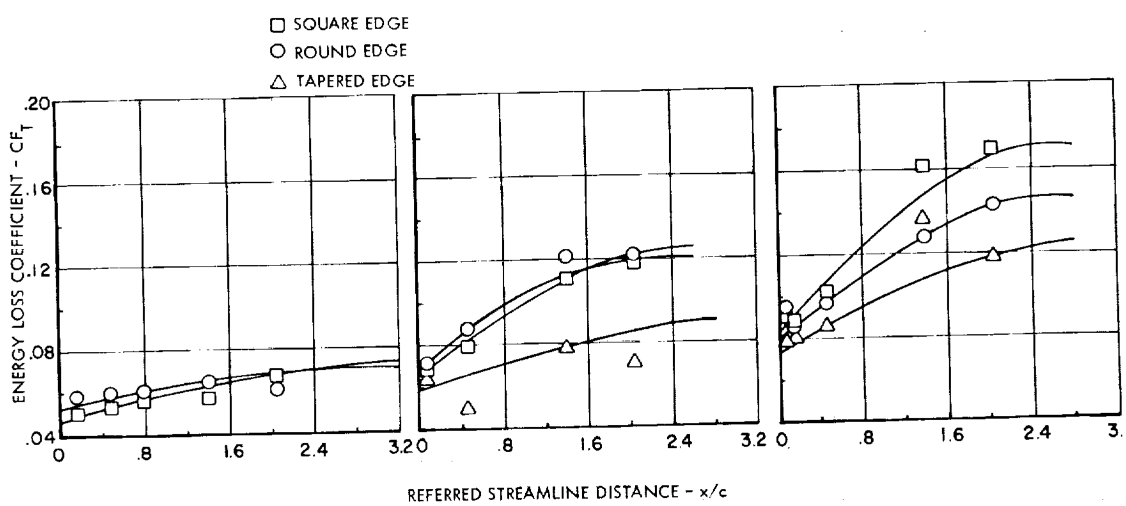

TRAILING EDGE THICKNESS

a) T = 0.028 in.

b) T = 0.160 in.

c) T = 0.160 in.

Figure 4.4-3 Increase in Wake Mixing Loss with Downstream Distance; 0 Deg. Incidence; 3.4×10^5 Reynolds Number

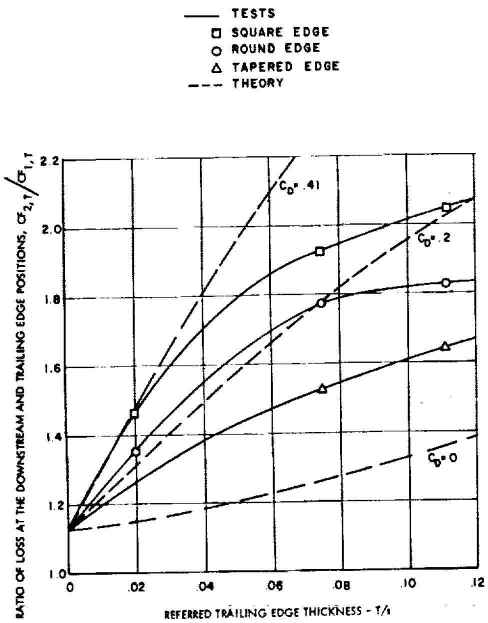

Figure 4.4-4 Increase in Wake Mixing Loss with Trailing Edge Thickness. 0 Deg. Incidence; 3.4×10^5 Reynolds Number

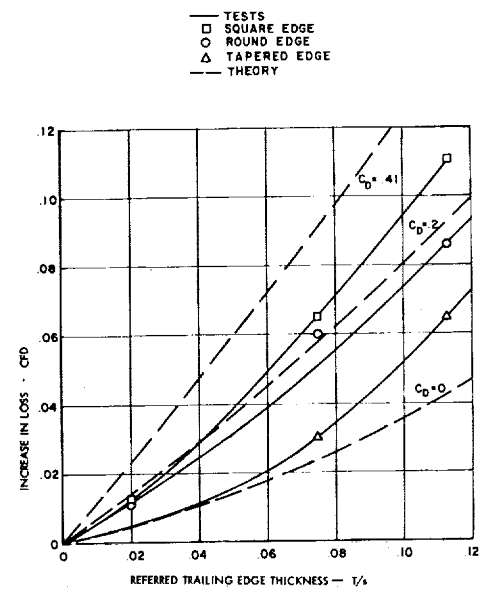

Figure 4.4-5 Increase in Loss Coefficient with Trailing Edge Thickness. 0 Deg. Incidence; 3.4×10^5 Reynolds Number

4.5 SUMMARY OF RESULTS

The Lieblein empirical equation gives a good account of the wake decay for the thin trailing edge configurations, T/s = 0.02. At large trailing edge thickness, T/s = 0.075 and T/s = 0.113, the rate of decay is less than specified by the equation due to the increase in the vorticity. Generally, the tapered trailing edge more nearly agrees with the model due to the reduction in effective thickness.

From a more detailed analysis: The wake flow is associated with the viscous mixing of the boundary layers shed from the suction and pressure side of the blade and with the vortex flow due to the base drag at the trailing edge of the blade. Generally, the base drag and vorticity increases with the trailing edge thickness and with the bluntness of the trailing edge. In the case of the round trailing edge, the wake flow is approximated by a theoretical model based on the momentum mixing of the boundary layer and a base drag corresponding to $C_D = 0.2$.

Blade Reynolds number in the range of 1.8×10^5 to 4.2×10^5 and blade incidence in the range of ± 12 degrees did not have a distinguishable effect on the properties of the wake.

4.6 REFERENCES

1. Bearman P.W., "On Vortex Street Wakes," J. Fluid Mech. (1967), Vol. 28, part 4, pg. 625-641.

2. Fentress, W. K., "A Computer Program for Calculating the Boundary Layer Properties Along the Surface of Turbomachinery Blades.," Astronuclear Laboratory, Westinghouse Electric Corporation, WANL-TME-1689, Nov. 1, 1967.

3. Heskestad, G. and Olberts, D.R., "Influence of Trailing-Edge Geometry on Hydraulic-Turbine-Blade Vibration Resulting from Vortex Excitation," J. or Eng. for Power, Trans. ASME 82A, 1960, pg. 103-110.

4. Hoerner, S.F., "Fluid-Dynamic Drag," Published by Author, Midland Park, N.J., 1958.

5. Johnston, I.H., Dransfield, D.C., and Fullbrook, D.J., "Experiments Concerning the Effect of Trailing-Edge Thickness on Blade Loss and Turbine Stage Efficiency," ARC - R&M 3459, 1964.

6. Lieblein, S. and Roudebush, W.H.,"Low-Speed Wake Characteristics of Two-Dimensional Cascade and Isolated Airfoil Sections," NACA TN 3771, 1956.

7. Markov, N.M., "Calculation of the Aerodynamic Characteristics of Turbine Blading," Translated and Published by Associated Technical Services, Glen Ridge, N.J., 1958.

8. Nash, J.F.,"An Analysis of the Subsonic Flow Past Symmetrical Blunt-Trailing-Edge-Aerofoil Sections at Zero Incidence, in the Absence of a Vortex Street," ARC R&M 3436, 1966.

9. Reeman, J. and Simonis, E.A., "The Effect of Trailing Edge Thickness of Blade Loss," RAE TN 116, 1943. (NASA Sc. and Tech. Info. Fac. Accession no. X65 - 81166.)

10. Rossbach, R.J., Wesling, G.C. and Lemond, W.F., "Three Stage Potassium Test Turbine - Final Design - Vol. 1 - Fluid Design," NASA - CR - 72249.

11. Schlichting, H., "Boundary Layer Theory," Pergamon Press, New York, 1955.

12. Stewart, W.L., "Analysis of Two-Dimensional Compressible-Flow Loss Characteristics Downstream of Turbomachine Blade Rows in Terms of Basic Boundary-Layer Characteristics," NACA TN 3515, 1955.

13. Toebes, G. H. and Eagleson, P.S., "Hydroelastic Vibrations of Flat Plates Related to Trailing Edge Geometry," J. of Basic Eng., Trans. ASME 83D, 1961, pg. 671 - 678.

NASA-Langley, 1971 — 15
Coml., Birmingham, Ala.